

University of Southampton Research Repository
ePrints Soton

Copyright © and Moral Rights for this thesis are retained by the author and/or other copyright owners. A copy can be downloaded for personal non-commercial research or study, without prior permission or charge. This thesis cannot be reproduced or quoted extensively from without first obtaining permission in writing from the copyright holder/s. The content must not be changed in any way or sold commercially in any format or medium without the formal permission of the copyright holders.

When referring to this work, full bibliographic details including the author, title, awarding institution and date of the thesis must be given e.g.

AUTHOR (year of submission) "Full thesis title", University of Southampton, name of the University School or Department, PhD Thesis, pagination

UNIVERSITY OF SOUTHAMPTON
FACULTY OF PHYSICAL SCIENCES AND ENGINEERING
SCHOOL OF ELECTRONICS AND COMPUTER SCIENCE

Coherent Versus Differential Multiple-Input Multiple-Output Systems

by

Peichang Zhang

B. Eng., MSc.

A doctoral thesis report submitted in partial fulfilment of
the requirements for the award of Doctor of Philosophy
at the University of Southampton

January 2015

SUPERVISORS:

Professor Lajos Hanzo

FREng, FIEEE, FIEE, DSc, EIC IEEE Press

Chair of Southampton Wireless Group

and

Professor Sheng Chen

FREng, FIEEE, FIET, CEng, DSc

Department of Electronics and Computer Science

University of Southampton

Southampton SO17 1BJ

United Kingdom

Dedicated to my family

UNIVERSITY OF SOUTHAMPTON

ABSTRACT

FACULTY OF ENGINEERING AND APPLIED SCIENCE
School OF ELECTRONICS AND COMPUTER SCIENCE

Doctor of Philosophy

Coherent Versus Differential Multiple-Input Multiple-Output Systems

by Peichang Zhang

In recent years, Multiple-Input-Multiple-Output (MIMO) techniques have attracted substantial attention due to their capability of providing spatial diversity and/or multiplexing gains. Inspired by the concept of Spatial Modulation (SM), the novel concept of Space-Time-Shift-Keying (STSK) was recently proposed, which is considered to have the following advantages: 1) STSK constitutes a generalized shift keying architecture, which is capable of striking the required trade-off between the required spatial and time diversity as well as multiplexing gain and includes SM and Space Shift Keying (SSK) as its special cases. 2) Its high degree of design-freedom, the above-mentioned flexible diversity versus multiplexing gain trade-off can be achieved by optimizing both the number and size of the dispersion matrices, as well as the number of transmit and receive antennas. 3) Similar to the SM/SSK schemes, the Inter-Antenna-Interference (IAI) may be eliminated and consequently, the adoption of single-antenna-based Maximum Likelihood (ML) detection becomes realistic in STSK schemes.

In this report, our investigation can be classified into two major categories, Coherent STSK (CSTSK) and Differential STSK (DSTSK) schemes. For CSTSK, since Channel State Information (CSI) is required for data detection, Channel Estimation (CE) techniques become necessary. To be more explicit, we first briefly review the conventional Training Based CE (TBCE) and Semi-Blind CE (SBCE) schemes for the CSTSK MIMO schemes. In addition, we develop a Block-of-Bits Selection Based CE (BBSBCE) algorithm for CSTSK schemes for increasing the overall system's throughput, while improving the accuracy of the CE. Additionally, it has been widely recognised that MIMO schemes are capable of achieving a diversity and/or multiplexing gain by employing multiple Antenna Elements (AEs) at the transmitter and/or the receiver. However, it should also be noted that since MIMO systems utilize multiple RF chains, their power consumption and hardware costs become substantial. Against this background, we introduce the concept of (Antenna Selection) AS and propose a simple yet efficient AS algorithm, namely the Norm-Based Joint Transmit and Receive AS (NBJTRAS) for assisting MIMO systems.

For DSTSK, since no CSI is required for differential detection schemes, it also draws our attention. However, in the absence of CE, the Conventional Differential Detection (CDD) schemes usually suffer from a 3 dB performance degradation and may exhibit an error-flow when Doppler frequency is excessive. In order to mitigate this problem, we investigate Multiple-Symbol Dif-

ferential Sphere Detection (MSDSD) scheme and adopt it in our DSTSK scheme to improve the system performance, while reducing the detection complexity. Furthermore, based on our MS-DSD detected DSTSK scheme, we propose a DSTSK aided Multi-User Successive Relaying aided Cooperative System (MUSRC), which is capable of supporting various number of users flexibly, while covering the conventional 50% throughput loss due to the half-duplex transmit and receive constraint of practical transceivers.

Declaration of Authorship

I, Peichang Zhang, declare that the thesis entitled Coherent Versus Differential Multiple-Input Multiple-Output Systems and the work presented in it are my own and has been generated by me as the result of my own original research. I confirm that:

- This work was done wholly or mainly while in candidature for a research degree at this University;
- Where any part of this thesis has previously been submitted for a degree or any other qualification at this University or any other institution, this has been clearly stated;
- Where I have consulted the published work of others, this is always clearly attributed;
- Where I have quoted from the work of others, the source is always given. With the exception of such quotations, this thesis is entirely my own work;
- I have acknowledged all main sources of help;
- Where the thesis is based on work done by myself jointly with others, I have made clear exactly what was done by others and what I have contributed myself;
- Parts of this work have been published.

Signed:

Date:

Acknowledgements

Firstly, I would like to express my sincere gratitude to my supervisors, Professor Lajos Hanzo and Professor Sheng Chen for their insightful guidance and extraordinary support. They have provided me a lot of suggestions and directions throughout my research. They also have encouraged me to work with our excellent research colleagues on many interesting research areas and topics, which have made me well settle down into my research.

I would also like to show my grateful thanks to all my colleagues in the Southampton Wireless Group for their help and advice. Specially, I would like to thank Chao Xu, Li Li, Shaoshi Yang, Chen Dong, Junyi Jiang and Fan Jin for their valuable support and advice throughout my research.

Finally, I would like to express my truthful thanks to my parents and my wife for their unselfish and unconditional love and support.

List of Publications

Journal Papers (7):

1. **P. Zhang, S. Chen, and L. Hanzo**, “Differential space-time shift-keying aided successive-relaying-assisted decode-and-forward cooperative multiuser CDMA”, *IEEE Transactions on Vehicular Technology*, vol. 62, pp. 2156-2169, June. 2013.
2. **P. Zhang, S. Chen, and L. Hanzo**, “Reduced-complexity near-capacity joint channel estimation and three-stage turbo detection for coherent space-time shift keying”, *IEEE Transactions on Communications*, vol. 61, pp. 1902-1913, May. 2013.
3. **P. Zhang, S. Chen, and L. Hanzo**, “Embedded iterative semi-blind channel estimation for three-stage-concatenated MIMO-aided QAM turbo-transceivers”, *IEEE Transactions on Vehicular Technology*, vol. 63, pp. 439-446, August. 2013.
4. **P. Zhang, S. Chen, and L. Hanzo**, “Two-tier channel estimation aided near-capacity MIMO transceivers relying on norm-based joint transmit and receive antenna selection”, *IEEE Transactions on Wireless Communications*, vol. 14, pp. 122-137, January. 2015.
5. **P. Zhang, S. Sugiura, S. Chen, and L. Hanzo**, “Single- versus multiple-RF spatial modulation”, *IEEE Communications Surveys & Tutorials*, to be submitted.
6. **P. Zhang, S. Chen, C. Xu, J. Jiang, F. Jin, and L. Hanzo**, “Joint transmit and receive antenna selection aided differential space-time shift keying systems”, *To be submitted to IEEE Transactions on Vehicular Technology*.
7. **J. Jiang, P. Zhang, R. Zhang, S. Chen, and L. Hanzo**, “Three-stage ACO-OFDM aided MIMO system relying on norm-based joint transmit/receive aperture selection for FSO turbulence channel”, *Submitted to IEEE Transactions on Vehicular Technology*.

Conference Papers (4):

1. **P. Zhang, S. Chen, and L. Hanzo**, “Near-capacity joint channel estimation and three-stage turbo detection for MIMO systems”, in *Proceedings of IEEE Wireless Communications and Networking Conference (WCNC 2013)*, Shanghai, China, pp. 1-6, 7-10 April 2013.
2. **P. Zhang, S. Chen, C. Dong, L. Li, and L. Hanzo**, “Norm-based joint transmit/receive antenna selection aided and two-tier channel estimation assisted STSK systems”, in *Proceedings of IEEE International Conference on Communications (ICC 2014)*, Sydney, Australia, pp. 1-6, 10-14 June 2014.
3. **P. Zhang, I. Dey, S. Sugiura, and S. Chen**, “Semi-blind adaptive space-time shift keying systems based on iterative channel estimation and data detection”, in *Proceedings of IEEE*

Vehicular Technology Conference (VTC-2011 Spring), Budapest, Hungary, pp. 1-5, May 2011.

4. **P. Zhang, S. Sugiura, S. Chen, and L. Hanzo**, “Adaptive space-time shift keying systems”, *at The UK-China Science Bridges: UC4G 2010 Beijing Workshop*, BUPT, Beijing, China, August 2010.

Contents

Abstract	ii
Declaration of Authorship	iv
Acknowledgements	v
List of Publications	vi
Glossary	xv
List of Symbols	xix
1 Introduction	1
1.1 Co-Located Multiple-Input Multiple-Output Systems	1
1.1.1 Diversity Techniques	2
1.1.2 Multiplexing Techniques	5
1.1.3 Multiple-Access Techniques	6
1.1.4 Beamforming Techniques	7
1.2 MIMO Channel Estimation	8
1.2.1 Training Based Channel Estimation	8
1.2.2 Blind Channel Estimation	10
1.2.3 Semi-Blind Channel Estimation	10
1.3 Antenna Selection	11
1.3.1 Receive Antenna Selection	13

1.3.2	Transmit Antenna Selection	14
1.3.3	Joint Transmit and Receive Antenna Selection	14
1.4	Differential Detection and Cooperative Communications	16
1.4.1	Differential Detection	16
1.4.2	Cooperative Communications	18
1.5	Novel Contributions	19
1.6	Thesis Outline	20
2	SDM/V-BLAST and Space-Time Shift Keying MIMO Review	24
2.1	Uncoded SDM/V-BLAST Systems	25
2.1.1	System Overview	25
2.1.2	Simulation Results	26
2.2	Three-Stage Serial-Concatenated Turbo Coded SDM/V-BLAST Systems	31
2.2.1	System Overview	31
2.2.2	Simulation Results	33
2.2.2.1	MIMO(2, 2, BPSK)	33
2.2.2.2	MIMO(4, 2, 4-QAM)	37
2.2.2.3	MIMO(4, 4, 4-QAM)	40
2.3	Uncoded Coherent STSK	41
2.3.1	System Overview	41
2.3.2	Computational Complexity	44
2.3.3	Maximum Achievable Diversity Order of CSTSK Systems	45
2.3.4	Dispersion Matrix Generation	46
2.3.5	Maximum Minimum-Determinant Based Configuration Selection	47
2.3.6	Simulation Results	49
2.3.6.1	Effects of Conventional Modulation Constellation Size \mathcal{L}	50
2.3.6.2	Effects of Number of Dispersion Matrices Q	51
2.3.6.3	Effects of Antenna Configurations	55
2.3.6.4	Maximum Minimum-Determinant Based Configuration Selection for CSTSK Systems	56

2.4	Three-Stage Serial-Concated Turbo Coding Aided CSTSK Systems	58
2.4.1	CSTSK Soft-Demapper	58
2.4.2	Simulation Results	60
2.4.2.1	CSTSK(4,2,2,4,QPSK)	60
2.4.2.2	CSTSK(4,4,2,4,16-QAM)	61
2.5	Chapter Summary and Conclusions	63
3	Channel Estimation for Coherent MIMO Systems	67
3.1	Introduction	67
3.2	Training Based Channel Estimation for MIMO Systems	68
3.2.1	System Model	68
3.2.2	Simulation Results	70
3.2.2.1	Uncoded TBCE Aided CSTSK	71
3.2.2.2	Three-stage Serial-Concated Turbo Coded and TBCE Aided CSTSK	75
3.3	Semi-Blind Channel Estimation for MIMO Systems	77
3.3.1	System Model	77
3.3.2	Simulation Results	78
3.3.2.1	CSTSK(2,2,2,4,QPSK) associated with $R = 2$ bits/symbol	79
3.3.2.2	CSTSK(4,2,2,4,QPSK) associated with $R = 2$ bits/symbol	81
3.3.2.3	CSTSK(4,4,2,4,16-QAM) associated with $R = 3$ bits/symbol	84
3.4	Joint Channel Estimation and Three-Stage Turbo Detection for MIMO Systems	86
3.4.1	Conventional Iterative Channel Estimation and Turbo Detection MIMO	86
3.4.2	Joint BBSBCE and Three-Stage Turbo Demapping/Decoding for MIMOs	88
3.4.2.1	System Model	89
3.4.3	Cramér-Rao Lower Bound	96
3.4.4	Simulation Results	98
3.4.4.1	CSTSK(4,2,2,4,QPSK) having a normalized throughput of $R = 2$ bits/symbol	99
3.4.4.2	CSTSK(4,4,2,4,16-QAM) having a normalized throughput of $R = 3$ bits/symbol	104

3.5	Soft-Decision Aided Channel Estimation for MIMO-Aided Turbo Transceivers . . .	108
3.5.1	Semi-Blind Soft-Decision Aided and Three-Stage Turbo Coded MIMO Transceiver	111
3.5.1.1	Soft Symbol Estimation	111
3.5.1.2	BBSB Soft Channel Estimation	115
3.5.1.3	Computational Complexity of the BBSB-SCE Based MIMO System	118
3.5.2	Simulation Results and Discussions	118
3.5.2.1	Example One	118
3.5.2.2	Example Two	124
3.5.2.3	Example Three	127
3.6	Chapter Summary and Conclusions	128
4	Norm-Based Joint Transmit/Receive Antenna Selection Aided MIMO Systems	133
4.1	Introduction	133
4.1.1	Two Antenna Selection Optimization Criteria	133
4.1.1.1	Capacity-Based Antenna Selection	134
4.1.1.2	Norm-Based Antenna Selection	135
4.1.2	Antenna Selection Classifications	136
4.1.2.1	Transmit Antenna Selection	136
4.1.2.2	Receive Antenna Selection	138
4.1.2.3	Transmit/Receive Antenna Selection	138
4.1.3	Channel Estimation for AS aided MIMO Systems	139
4.2	NBJTRAS Aided MIMO System Based on Perfect CSI	140
4.2.1	System Description	140
4.2.1.1	NBJTRAS Algorithm	141
4.2.1.2	An Example of NBJTRAS	142
4.2.1.3	Complexity Analysis	144
4.2.1.4	Additional Diversity Order Attained	145
4.2.2	Simulation Results	145
4.2.2.1	Uncoded NBJTRAS Aided CSTSK Systems	146

4.2.2.1.1	$\text{CSTSK}(M, N; 2, 2; 2, 4, \text{QPSK})$ associated with $R = 2$ bits/symbol	146
4.2.2.1.2	$\text{CSTSK}(M, N; 4, 2; 2, 4, \text{QPSK})$ associated with $R = 2$ bits/symbol	151
4.2.2.1.3	$\text{CSTSK}(M, N; 4, 4; 2, 4, 16\text{-QAM})$ associated with $R = 3$ bits/symbol	151
4.2.2.2	Three-Stage Turbo Coded and NBJTRAS Aided SDM/V-BLAST MIMO Systems	151
4.2.2.2.1	$\text{MIMO}(M, N; 2, 2; \text{BPSK})$ associated with $R = 2$ bits/symbol under Independent Fading Environments	152
4.2.2.2.2	$\text{MIMO}(M, N; 2, 2; \text{BPSK})$ associated with $R = 2$ bits/symbol under Spatially Correlated Fading Environments	155
4.2.2.2.3	$\text{MIMO}(M, N; 4, 2; 4\text{-QAM})$ associated with $R = 8$ bits/symbol under Independent Fading Environments	157
4.2.2.2.4	$\text{MIMO}(M, N; 4, 2; 4\text{-QAM})$ under Spatially Correlated Fading Environments	159
4.3	Channel Estimation for NBJTRAS	160
4.3.1	Conventional TBCE for NBJTRAS	161
4.3.1.1	System Description	161
4.3.1.2	Simulation Results	163
4.3.1.2.1	TBCE for NBJTRAS Aided Uncoded CSTSK Systems	163
4.3.1.2.2	TBCE for NBJTRAS Aided Three-Stage Turbo Coded SDM/V-BLAST Systems	167
4.3.2	TTCE for NBJTRAS	170
4.3.2.1	System Description	171
4.3.2.1.1	Tier One	172
4.3.2.1.2	Tier Two	172
4.3.2.2	Simulation Results and Discussions	173
4.3.2.2.1	TTCE for NBJTRAS Aided Uncoded CSTSK System	173
4.3.2.2.2	TTCE for NBJTRAS Aided Three-Stage Turbo Coded SDM/V-BLAST MIMO System	175

4.4 Chapter Summary and Conclusions	178
5 Multiple-Symbol Differential Sphere Detection Aided Differential Space-Time Shift Keying	184
5.1 Introduction	184
5.1.1 Differential MIMO Systems	184
5.1.2 Cooperative Communication Systems	185
5.1.3 Novel Contributions	186
5.2 MSDSD for DSTSK	186
5.2.1 DSTSK Transmitter Structure	187
5.2.2 Hard-Decision Aided MSDSD	188
5.2.3 Soft-Decision Aided MSDSD	190
5.2.4 Simulation Results	191
5.2.4.1 Uncoded Hard-Decision aided MSDSD for DSTSK	192
5.2.4.2 Soft-Decision aided MSDSD for DSTSK	195
5.3 DSTSK aided MUSRC System	197
5.3.1 System Model	197
5.3.1.1 System Operation Overview	198
5.3.1.2 Relay Architecture Overview	199
5.3.1.3 Source Nodes	201
5.3.1.4 Relay Nodes	202
5.3.1.5 Destination Node	206
5.3.2 DSTSK Configuration Selection	206
5.3.3 Simulation Results	207
5.3.3.1 DBPSK for SR transmission and DSTSK($2, 1, 2, Q, \mathcal{L}$) for RD transmission	210
5.3.3.2 DQPSK for SR transmission and DSTSK($2, 2, 2, Q, \mathcal{L}$) for RD transmission	215
5.4 Chapter Summary and Conclusions	218
6 Conclusions and Future Research	221

6.1	Summary and Conclusions	221
6.2	Design Guidelines	229
6.3	Future Research	232
6.3.1	Particle Swarm Optimisation for Antenna Selection Schemes	232
6.3.2	Antenna and Relay Selection in Cooperative Communications	233
6.3.3	Millimetre-Wave Mobile Broadband Systems	233
	Bibliography	235
	Subject Index	251
	Author Index	254

Glossary

1G	First generation
2G	Second generation
3G	Third generation
4G	Fourth generation
5G	Fifth generation
ACO	Ant Colony Optimization
AEs	Antenna Elements
AF	Amplified-and-Forwarded
AS	Antenna Selection
ASCs	AS criteria
AWGN	Additive White Gaussian Noise
BBSB	Block-of-Bits Selection Based
BBSB-SCE	BBSB Soft-decision aided CE
BBSBCE	Block-of-Bits Selection Based CE
BCE	Blind CE
BCH	Bose-Chadhuri-Hocquenghem
BER	Bit Error Ratio
BLAST	Bell Labs Layered Space-Time
BLER	Block Error Ratio
BPB	Bits Per Transmission Block
BPSK	Binary PSK
BS	Base Station
CBAS	Capacity-Based AS
CDD	Conventional Differential Detection
CE	Channel Estimation

CIR	Channel Impulse Responses
COAS	Capacity Optimised AS
CRLB	Cramér-Rao Lower Bound
CSI	Channel State Information
CSTSK	Coherent STSK
D-BLAST	Diagonal BLAST
DD-LSCE	decision-directed-LSCE
DDCE	Decision-Directed CE
DDSBCE	Decision-Directed SBCE
DF	Decoded-and-Forwarded
DLDC	Differential LDC
DN	Destination Node
DPSK	Differential Phase Shift Keying
DS-CDMA	Direct-Sequence Code-Division Multiple-Access
DSTM	Differential Space-Time Modulation
DSTSK	Differential STSK
EDAS	Euclidean Distance Optimised AS
EGC	Equal Gain Combining
EXIT	EXtrinsic Information Transfer
FEC	Forward-Error-Correction
FH	Frequency-Hopping
FIM	Fisher Information Matrix
IAS	Inter-Antenna Synchronization
ICI	Inter-Channel Interference
IMT-2000	International Mobile Telecommunications 2000
ISSA	Incremental Successive Selection Algorithm
IVI	Inter-VAA-Interference
JTRAS	Joint Transmit and Receive AS
LDCs	Linear Dispersion Codes
LLRs	Log Likelihood Ratios
LS	Least Squares
LS-MIMO	large-scale MIMO

LSCE	Least Squares CE
MAI	Multiple Access Interference
MCEE	Mean CE Error
MIMO	Multiple-Input Multiple-Output
ML	Maximum-Likelihood
ML-MSDD	ML MSDD
MMB	Millimetre-wave Mobile Broadband
MMBCS	Maximum Minimum-Determinant Based Configuration Selection
MMSE	Minimum Mean Square Error
MRC	Maximal-Ratio Combining
MSDD	Multiple-Symbol Differential Detection
MSDSD	Multiple-Symbol Differential Sphere Detection
MSE	Mean Square Error
MUSRC	Multi-User Successive Relaying assisted Cooperative
NBAS	Norm-Based AS
NBJTRAS	Norm-Based Joint Transmit and Receive Antenna Selection
OF	Objective Function
OFDM	Orthogonal Frequency-Division Multiplexing
OFDMA	Orthogonal Frequency-Division Multiple Access
PED	Partial Euclidean distance
PEP	Pairwise Error Probability
PO	Pilot Overhead
PSAM	Pilot Symbol Assisted Modulation
PSEP	Pairwise Symbol Error Probability
PSK	Phase Shift Keying
PSO	Particle Swarm Optimisation
QoS	Quality of Service
QPSK	Quadrature PSK
RAs	Receive Antennas
RF	Radio Frequency
RLS	Recursive Least Squares
RNs	Relay Nodes

RSC	Recursive Systematic Convolutional
RWBS	Repeated Weight Boosting Search
Rx	Receive
RxAS	Receive AS
SBCE	Semi-Blind CE
SC	Selection Combining
SD	Sphere Decoding
SDM	Spatial Division Multiplexing
SDMA	Space Division Multiple Access
SIMO	Single-Input-Multiple-Output
SISO-MSDSD	Soft-Input Soft-Output MSDSD
SM	Spatial Modulation
SN	Source Node
SNR	signal-to-noise ratio
SSK	Space-Shift Keying
STBC	Space-Time Block Codes
STC	Space-Time Codes
STSK	Space-Time Shift Keying
STTCs	Space-Time Trellis Codes
SwC	Switched Combining
TAs	Transmit Antennas
TB-LSCE	Training-Based LSCE
TBCE	Training Based CE
TTCE	Two-Tier CE
TVCE	Time-Varying Channe's Estimation
Tx	Transmit
TxAS	Transmit AS
URC	Unity-Rate-Code
V-BLAST	Vertical BLAST
VAA	Virtual Antenna Array
ZF	Zero-Forcing

List of Symbols

Special Symbols

\mathcal{L} :	Constellation size.
H :	MIMO channel state information (CSI) matrix.
M :	Number of transmit antennas.
N :	Number of receive antennas.
y :	Received signal vector.
s :	A transmitted symbol.
s :	Transmitted signal vector.
S :	Transmitted signal matrix.
v :	Complex-valued AWGN vector.
V :	Complex-valued AWGN matrix.
N_0 :	Variance of an AWGN noise.
E_s :	Average transmitted symbol energy.
b :	Value of a binary bit.
Π :	The interleaver.
Π^{-1} :	The deinterleaver.
L_a :	The <i>a priori</i> log likelihood ratios (LLRs).
L_e :	The <i>extrinsic</i> LLRs.
L_p :	The <i>a posteriori</i> LLRs.

I_A :	The <i>a priori</i> information.
I_E :	The <i>extrinsic</i> information.
G_{RSC} :	Feedforward generator polynomial of an RSC encoder.
G_{RSC}^r :	Feedback generator polynomial of an RSC encoder.
G_{URC} :	Feedforward generator polynomial of a URC encoder.
G_{URC}^r :	Feedback generator polynomial of a URC encoder.
I_{in} :	Number of inner iterations of three-stage turbo decoder.
I_{out} :	Number of outer iterations of three-stage turbo decoder.
Q :	Number of dispersion matrices.
A :	A dispersion matrix.
T :	Number of time slots of space-time codes.
R :	Normalized throughput.
π :	The circular constant.
Y :	Received signal matrix.
I_T :	Identity matrix associated with size of $(T \times T)$.
d_{min} :	Minimum determinant value.
$d_{max-min}$:	Maximum minimum determinant value.
M_T :	The number of training symbols available for channel estimation (CE).
Y_{tM_T} :	Received training data.
S_{tM_T} :	Transmitted training symbols.
$Y_{d\tau}$:	Observation data for MIMO detector.
$\widehat{S}_{d\tau}$:	Detected data.
\widehat{H} :	Estimate of MIMO channel matrix H .
J_{MCE} :	Mean channel error.
J_{MSE} :	Mean square error.
C_{loss} :	Effective throughput loss.

\mathbf{l}_p :	<i>a posteriori</i> information vector.
\mathbf{L}_p :	<i>a posteriori</i> information matrix.
\hat{s} :	Estimate of a symbol s .
T_h :	Block-of-bits selection threshold.
τ_{sel} :	Maximum number of detected symbol blocks imposed for CE.
τ_s :	Number of detected symbol blocks imposed for CE.
\mathbf{F} :	Fisher information matrix.
K_{run} :	Number of channel realizations.
I_{ce} :	Maximum number of iterations of a semi-blind iterative CE scheme.
C_{ML} :	Computational complexity of ML detection.
d_e :	Soft-symbol estimation error.
f_d :	Normalized Doppler frequency.
L_F :	Frame length in bits.
L_T :	Number of selected transmit antennas.
L_R :	Number of selected receive antennas.
\mathbf{H}_{sub} :	Optimal subset channel matrix selected from the full channel matrix \mathbf{H} .
$\tilde{\mathbf{H}}_{sub}$:	A subset channel matrix selected from the full channel matrix \mathbf{H} .
$\hat{\mathbf{H}}_{sub}$:	Estimate of \mathbf{H}_{sub} .
C_k^n :	Combinations of selecting n members from a group of size k .
f_{AS} :	Antenna selection (AS) loading factor.
\mathbf{M}_{Norm} :	Norm metric matrix of norm-based transmit and receive AS (NBJTRAS) algorithm.
\mathbf{m}_{max} :	Max-norm metric vector of NBJTRAS algorithm.
C_{ES} :	Computational complexity of exhaustive search.
$C_{NBJTRAS}$:	Computational complexity of NBJTRAS algorithm.
C_{MIMO} :	MIMO channels' throughput.
N_w :	Observation window size of multiple-symbol joint detection algorithms.

D :	Accumulated information matrix of multiple-symbol differential sphere detection (MSDSD) algorithm.
R_{YY} :	Correlation matrix of Y .
L :	Lower triangular matrix.
U :	Upper triangular matrix.

Special Operations

$\ \cdot\ ^2$:	The Euclidean norm operation.
$(\cdot)^H$:	The Hermitian transpose of a matrix.
$(\cdot)^T$:	The transpose of a matrix.
$(\cdot)^*$:	The conjugate of a complex symbol/vector/matrix.
$\lfloor \cdot \rfloor$:	Rounding a numerical value to its nearest integer.
$\lceil \cdot \rceil$:	Rounding a numerical value to its nearest higher integer.
$\lfloor \cdot \rfloor$:	Rounding a numerical value to its nearest lower integer.
Σ :	The summation of all elements.
Π :	The product of all elements.
\forall :	For all elements within a certain range.
\int :	The integration function.
$\det[\cdot]$:	The determinant operation.
$E[\cdot]$:	The expectation operation.
$\exp(\cdot)$:	The exponential operation.
$\log(\cdot)$:	The logarithm operation.
$\ln(\cdot)$:	The natural logarithm.
$\max[\cdot]$:	The maximum value of a vector/matrix.
$\min[\cdot]$:	The minimum value of a vector/matrix.
$\text{tr}[\cdot]$:	The trace operation of a matrix.
$\text{vec}(\cdot)$:	The vertical stacking of the columns of a matrix.
\otimes :	The Kronecker product.

Chapter 1

Introduction

1.1 Co-Located Multiple-Input Multiple-Output Systems

Recently, Multiple-Input Multiple-Output (MIMO) wireless communication systems, where both the transmitters and receivers are equipped with multiple Antenna Elements (AEs) [1], have attracted substantial attention due to their potential of providing spatial diversity and/or multiplexing gains [2–5]. Explicitly, since in MIMO systems the signals are transmitted by a number of AEs and are processed at each receive antenna, the transmission reliability and/or the data rate may be significantly increased [6–8], resulting in a higher Quality of Service (QoS) and potentially increased revenues. Depending on the specific performance gain sought, co-located MIMO techniques may be classified into four categories, which are summarized in Fig. 1.1 [6].

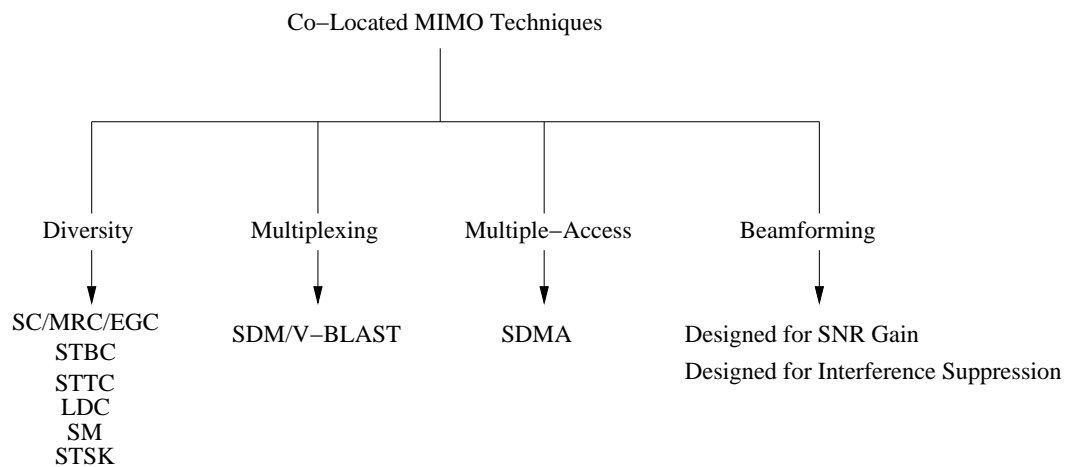


Figure 1.1: Classification of co-located MIMO systems.

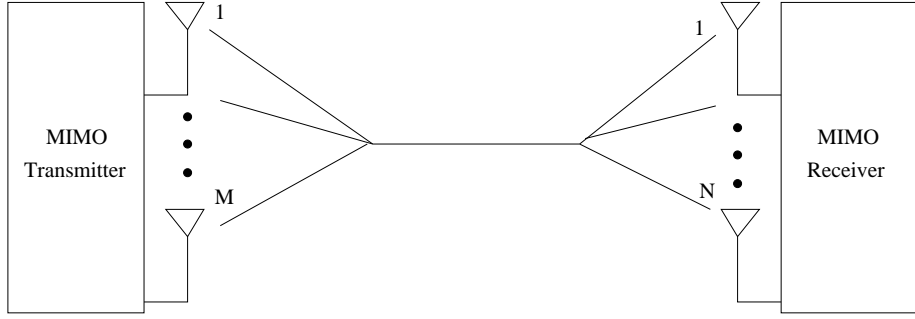


Figure 1.2: Block diagram of a spatial diversity technique [6].

1.1.1 Diversity Techniques

It has been widely recognized that in wireless communications, the wireless channel may be gravely faded and this may result in detection errors. A typical way of combating the fading effects is constituted by the adoption of diversity techniques, which are designed to provide the receiver with several independently faded replicas of the same transmitted symbols. In this way, diversity gains may be attained.

Generally, the diversity gains may be achieved in three domains, namely in the time-, frequency- and spatial-domain. The classic Forward-Error-Correction (FEC) coding may be viewed as a typical example of a time diversity oriented scheme [1, 9]. More specifically, in FEC coding schemes, redundant bits are introduced into the original information bits sequence, therefore the redundant bits may experience independent fading at different time slots. The basic idea of frequency diversity is to activate different transmit frequencies at different time slots, for example by using a Frequency-Hopping (FH) technique [10]. Since these activated frequencies are often separated by more than the coherence bandwidth, independent fading is experienced by each frequency at different time instances, hence exhibiting frequency diversity [11].

As another type of diversity, the main idea of spatial diversity techniques is to employ multiple antennas at the MIMO transmitter and/or receiver in order to enhance the reliability of the wireless links, whilst relying on the condition that each link experiences independent fading. Fig. 1.2 shows the block diagram of spatial diversity techniques, where it may be seen that multiple copies of the signals may be transmitted and/or received through multiple transmit and/or receive antennas. In this way, if some wireless links are deeply faded, the others may not be, hence a spatial diversity gain may be achieved for improving the system's Bit Error Ratio (BER) performance compared to conventional single link systems. Additionally, it has been mentioned that time diversity is achieved by introducing redundancy in the time domain, while frequency diversity is achieved by using sufficiently distant frequency bands and activating a single frequency band at a time. However, it may be observed that both of these diversity techniques may impose a reduction in bandwidth efficiency, which is one of the most important issues to be considered in any wireless system design. On the

other hand, spatial diversity is achieved by adding more AEs at the transmitter and/or receiver in order to create several independently fading channels, and therefore, no bandwidth efficiency reduction is experienced. Moreover, in order to create independent fading channels, the AEs at the transmitter and/or receiver should be sufficiently separated, ideally by multiples of the wavelength [9]. In this case, the maximum achievable spatial diversity order that may be achieved is $(M \times N)$, where M and N correspond to the number of transmit and receive AEs, respectively.

Usually the spatial diversity order may be further classified into two types, namely receive diversity and transmit diversity. Generally, receive diversity may be achieved by a Single-Input-Multiple-Output (SIMO) system, which is more practical for the mobile uplink rather than for the downlink due to the limited physical size of mobile handsets. More specifically, the family of receive diversity combining techniques contains selection-, switched-, maximal-ratio-combining, and equal gain combining, just to mention a few [6, 12]. The main idea of the Selection Combining (SC) technique is to select the received signal associated with the largest power to be demodulated. Even though this technique is relatively easy to implement, it is obviously not optimal, since only one out of N receive antennas is utilised. Another selection based combining technique is Switched Combining (SwC), or scanning diversity. Unlike the already mentioned SC, SwC does not monitor the status of all the branches all the time, it only combines a single branch until its signal-to-noise ratio (SNR) falls below the threshold. Therefore, compared to the SC techniques, SwC is even easier to implement at the cost of a modest performance loss [9]. When narrow-band frequency-flat fading is considered, the well-known Maximal-Ratio Combining (MRC) achieves the optimal performance by maximizing the receive SNR. This is accomplished by appropriately weighting the individual signals from N branches according to their own branch SNRs and then summing the weighted signals. However, a critical aspect of MRC is that of estimating the channel's fading amplitudes. To circumvent this high-complexity operation, the Equal Gain Combining (EGC) was proposed, which is suboptimal, but it is often more attractive due to its reduced complexity compared to optimal MRC [12].

Transmit diversity, as another type of spatial diversity technique, which employs multiple AEs at the transmitter, implying that this type of diversity is mainly beneficial in a downlink scenario, since the Base Station (BS) usually has enough room for sufficiently separated AEs. One of the earliest transmit diversity schemes was proposed by Wittneben in 1991 [13], where multiple BSs were employed for achieving transmit antenna diversity. It was shown that in the context of antenna diversity, the diversity gain is improved as the number of transmit antennas increased. Alamouti's Space-Time Codes (STC), namely the Space-Time Block Codes (STBC) scheme, was proposed in 1998 [4], which was shown to be capable of achieving the maximum attainable diversity order using a MRC receiver, despite its low complexity. However, it should also be mentioned that the maximum spectral efficiency of the full-rate orthogonal STBCs is limited to one bit per symbol duration [5]. Roughly at the same time as Alamouti proposed STBC, Space-Time Trellis Codes (STTCs) were proposed by Tarokh *et al.* in 1998 [14], where multiple copies of a trellis

code or a convolutional code were transmitted via a number of transmit antennas. Compared to Alamouti's STBC, STTC provides both a spatial diversity gain and a coding gain, at the cost of a higher decoding complexity. Furthermore, for the sake of achieving a flexible tradeoff between the achievable diversity and multiplexing gains, Hassibi and Hochwald proposed the unified space-time transmission architecture of Linear Dispersion Codes (LDCs), which includes both the V-BLAST and Alamouti's STBC scheme in its ultimate form [15]. Additionally, the differentially encoded counterpart of LDCs was developed in order to make non-coherent detection at the receiver feasible, when in the absence of Channel State Information (CSI), which is referred to as Differential LDC (DLDC) [16].

As a more recent concept of MIMO systems, Spatial Modulation (SM) [3, 17, 18] and Space-Shift Keying (SSK) [19] were proposed, where the basic idea is to activate one of M AEs during the transmission of each symbol. This leads to an additional way of conveying source information, potentially increasing the overall spectrum efficiency. Furthermore, since only a single antenna is activated at each symbol period, the Inter-Channel Interference (ICI) is eliminated and the Inter-Antenna Synchronization (IAS) specification can be relaxed. As a result, compared to the high decoding complexity imposed by the ICI mitigation in V-BLAST, low-complexity single-antenna-based Maximum-Likelihood (ML) detection becomes feasible in SM/SSK systems. Additionally, since only a single RF-chain is employed in SM, it is considered to be a promising transmission concept for the large-scale (or massive) MIMO family [20]. However, since SM/SSK is designed to achieve a multiplexing gain, instead of diversity gain, combating the effects of fading channels has to rely on the employment of multiple AEs at the receiver [5], which becomes extremely challenging in downlink scenarios due to the limited size of mobile devices. In addition, even though SM/SSK is capable of conveying additional source information, this throughput increase relies on 2^M transmit antennas, implying that the number of transmit antennas has to be increased exponentially for a linear increase in transmission rate [5].

Inspired by the above-mentioned MIMO systems, the novel concept of Space-Time Shift Keying (STSK) was introduced in [5], which is considered to have the following advantages over conventional SM/SSK schemes:1) In STSK schemes, one of Q appropriately indexed space-time dispersion matrices is activated within each STSK signal block duration, as opposed to one of M antennas in SM/SSK schemes. As a result, STSK fully exploits both the spatial- and time-dimensions.2) Due to the high degree of design-freedom, a flexible diversity versus multiplexing gain tradeoff can be realized by STSK scheme, which is achieved by optimizing both the number and size of the dispersion matrices as well as the number receive antennas. Moreover, according to [5,21], STSK is capable of achieving both transmit and receive diversity gains, which is different from conventional SM/SSK schemes, where only receive diversity gain can be attained.3) Similar to the family of SM/SSK schemes, the ICI in STSK schemes is also completely eliminated and consequently, the adoption of single-antenna-based ML detection becomes realistic.

We have summarized the above-mentioned types of spatial diversity techniques in Table 1.1.

Table 1.1: A brief summary of major contributions on spatial diversity techniques.

Year	Author(s)	Contributions
1959	Brennan [22]	Introduced three linear receive diversity techniques, namely SC, MRC and EGC.
1991	Wittneben [13]	Proposed a transmit diversity scheme for digital simulcast systems, where multiple transmit antennas were utilised for transmitting the same signal.
1998	Alamouti [4]	Proposed the STBC scheme associated with $M = 2$ transmit antennas, which was demonstrated to be capable of achieving the maximum attainable diversity order using a MRC aided reception.
1998	Tarokh <i>et al.</i> [14]	Proposed the STTC scheme, which transmitted multiple, redundant copies of a trellis code or a convolutional code via a number of transmit antennas.
2006	Mesleh <i>et al.</i> [3]	Proposed SM which only activated one of M AEs during the transmission of each symbol.
2009	Jeganathan <i>et al.</i> [19]	Proposed SSK, where only the antenna activation index m conveys source information.
2010	Sugiura <i>et al.</i> [5]	Proposed the novel STSK concept, which included SM/SSK as its special cases and was demonstrated to be capable of striking an arbitrary trade-off amongst the attainable spatial-, time-, and multiplexing gains.
2011	Sugiura <i>et al.</i> [21]	Proposed the novel generalized STSK architecture, acts as a unified MIMO framework.
2013	Xu <i>et al.</i> [23]	Proposed a pair of hard-decision and soft-decision aided SM/STSK detectors at a reduced complexity.
2014	Kadir <i>et al.</i> [24]	Provided a survey and tutorial on the subject of MIMO multicarrier systems based on STSK approach.

1.1.2 Multiplexing Techniques

The spatial diversity techniques reviewed in Section 1.1.1 mainly aim for improving the system's achievable BER performance by achieving diversity gains. However, this BER performance improvement is often achieved at the cost of reducing the system's overall throughput, since multiple copies of the signals may be transmitted and/or received through multiple transmit and/or receive antennas. On the other hand, as another type of co-located MIMO techniques, the multiplexing MIMO scheme was designed for improving the system's achievable throughput. The schematic

of multiplexing-type MIMOs is shown in Fig. 1.3, where it may be seen that the improvement of the system's throughput is achieved by transmitting independent symbol streams via different transmit antennas at the same frequency band and time. In this way, the overall throughput of the multiplexing MIMO schemes is linearly proportional to the number of transmit antennas, and the corresponding performance gain is referred to as the multiplexing gain.

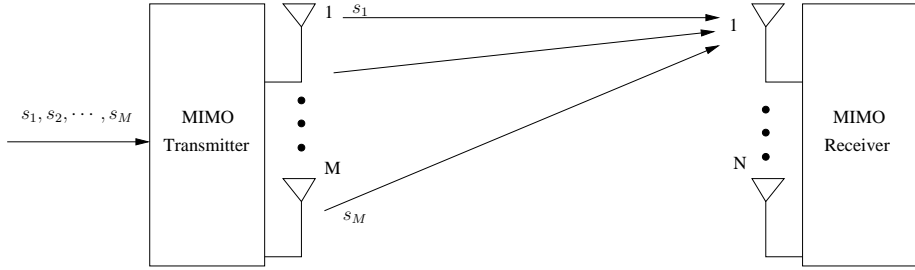


Figure 1.3: Block diagram of a multiplexing MIMO technique.

A typical family of multiplexing MIMO schemes may be referred to as the class of Spatial Division Multiplexing (SDM) schemes, which may be represented by the Bell Labs Layered Space-Time (BLAST) schemes [2, 25]. More specifically, the Diagonal BLAST (D-BLAST) scheme was proposed by Foschini [25] in 1996, which utilized multiple antennas for transmitting symbols in a diagonally layered coding structure. However, it was recognized by Wolniansky *et. al* that the implementation of D-BLAST may impose a high computational complexity. Therefore, the Vertical BLAST (V-BLAST) scheme was proposed for mitigating its complexity [2]. In V-BLAST scheme, at the transmitter, each antenna transmits an independent symbol stream in the same frequency band and at the same time. As a result, the multiplexed signals have to be decomposed at the receivers. The optimal ML detector may be invoked for the sake of achieving the highest possible performance at the cost of an exponentially increased detection complexity, as the number of transmit antennas or the number of bits per symbol conveyed by the modulation scheme increases. On the other hand, if the number of receive antennas is higher than or equal to the number of transmit antennas, low-complexity linear detectors, such as Minimum Mean Square Error (MMSE) [26] and Zero-Forcing (ZF) detectors [6], may be adopted for the sake of reducing the detection complexity at the expense of a certain performance loss. Additionally, some near-optimal detection schemes, such as sphere detection schemes were proposed [27], which are capable of attaining a near-ML performance at a moderate complexity. Additionally, it should be mentioned that a major limitation of BLAST systems is that the diversity gain may only be achieved by employing multiple receive antennas, since all transmit antennas are utilized for achieving a multiplexing gain.

1.1.3 Multiple-Access Techniques

From the discussions in Section 1.1.1 and 1.1.2 it may be seen that multiple antennas may be employed for achieving spatial diversity and/or multiplexing gains, in a single-user scenario. By

contrast, multiple-access MIMO techniques are designed for supporting multiple spatially separated users, which can be achieved by for example Space Division Multiple Access (SDMA) [28]. In an SDMA multi-user MIMO system, each single-antenna user simultaneously transmits his/her own signals to the BS in the same frequency band, and their unique user-specific Channel Impulse Responses (CIR) may be used for user identification at the BS. In this way, the network's overall throughput may be increased. Note that the overall structure of SDMA is equivalent to that of the BLAST-style SDM schemes introduced in Section 1.1.2, except that SDM aims for increasing the overall capacity of point-to-point wireless links, while SDMA exploits its multiplexing gain for supporting more users.

1.1.4 Beamforming Techniques

Apart from the above three types of co-located MIMOs, beamforming also constitutes an important MIMO technique, which may be designed either for enhancing the system's SNR or for achieving angularly selective interference suppression in a multi-user scenario [6, 29, 30]. The block diagram of the beamforming technique is shown in Fig. 1.4, where it may be seen that the basic idea of beamforming is to focus the transmit/receive beam pattern in the direction of the intended antenna(s) or user. In this way, the transmit power may be concentrated on the specific users or antennas, whilst less power will be dispersed in other directions and the corresponding SNR can be enhanced. Additionally, since the data is transmitted through a directional beam, less interference will be spread to other users, and in this way, the interference may be suppressed by beamforming in multi-user scenarios.

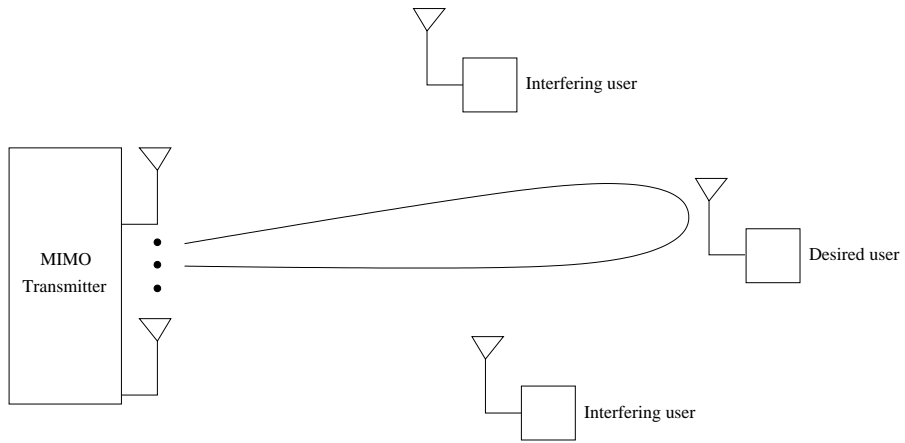


Figure 1.4: Block diagram of a beamforming system.

1.2 MIMO Channel Estimation

In Section 1.1, the concept of MIMO systems has been briefly introduced, where it has been shown that various types of MIMO schemes may be capable of significantly increasing the reliability and/or capacity of wireless communication systems. However, it has been widely recognized that accurate knowledge of the CSI is required in coherent MIMO systems for the sake of achieving the above-mentioned MIMO advantages. As a result, the system's ability to approach its capacity strongly depends on the accuracy of CSI and Channel Estimation (CE) becomes a core component in a coherent MIMO communication system [31, 32]. Additionally, CE schemes designed for MIMO systems may be classified into three types, namely the Training Based CE (TBCE), Blind CE (BCE), and Semi-Blind CE (SBCE).

1.2.1 Training Based Channel Estimation

The TBCE schemes excel in terms of their simplicity [33–36], where a specific training symbol sequence may be employed for estimating the CSI for coherent communications systems. Fig. 1.5 illustrates the general transmit frame structure of a TBCE scheme, where it may be seen that pilot symbols are attached to each frame and transmitted prior to the data at the transmitter. At the receiver side, the CSI is firstly estimated relying on the received training pilots and then used for coherent data detection.



Figure 1.5: General transmit frame structure of TBCE.

More specifically, as one of the earliest contributions on TBCE scheme, the Pilot Symbol Assisted Modulation (PSAM) was proposed in 1991 [37] for conventional QAM/PSK modulation schemes. Then the PSAM scheme was also applied for estimating doubly selective fading channels in [38]. The ML method based TBCE scheme designed for BLAST MIMO systems was proposed in [39], where it was pointed out that the length of training sequences has to be as high as half of the frame length for the sake of achieving the maximum possible effective throughput. Moreover, a Least Squares (LS) method based TBCE scheme was conceived for MIMO-aided Orthogonal Frequency-Division Multiplexing (OFDM) systems by Li in 2000 [40], where an optimum training sequence design was proposed, and the channel estimator was simplified by avoiding any matrix inversion operation, at the cost of a modest performance degradation. It was recognized that the optimal training sequences must have impulse-like auto correlation and zero cross correlation. This may impose a problem, since usually multiple training sequences are required for the estimation of multiple wireless channels. A simplified optimal training sequence generation was proposed for STCs in [35], where the problem of requiring multiple training sequences was solved by designing a

single training sequence with impulse-like auto correlation. The Least Squares CE (LSCE) scheme was conceived for the recent MIMO concept of STSK in [32], where it was shown that TBCE was capable of achieving accurate CSI by employing a high number of training pilots. Additionally, the effects of MMSE based TBCE on SM was analyzed in [41].

Even though the TBCE scheme is capable of acquiring accurate MIMO CSI as long as the training overhead is large enough, the system's effective throughput may be significantly reduced. Again, as it has been mentioned in [39] that ML-based TBCE scheme designed for BLAST MIMO systems requires half of the frame to be training symbols, which reduces the system's effective throughput by 50%. Therefore, this throughput reduction problem has become the major limitation of the TBCE scheme.

We have summarized the above-mentioned TBCE schemes in Table 1.2.

Table 1.2: A brief summary of major contributions on TBCE schemes.

Year	Author(s)	Contributions
1991	Cavers [37]	Proposed the PSAM scheme for conventional PSK/QAM modulations.
1999	Marzetta [39]	Proposed a ML method based TBCE scheme for a BLAST MIMO system.
2000	Li [40]	Proposed the LS method based TBCE scheme for a MIMO-OFDM system, along with a simplified CE scheme by avoiding the high-complexity channel matrix inversion.
2003	Ma <i>et al.</i> [38]	Applied PASM for estimating doubly selective fading channels.
2003	Fragouli <i>et al.</i> [35]	Proposed a simplified optimal training sequence generation for STCs.
2011	Zhang <i>et al.</i> [32]	Proposed TBCE scheme for STSK MIMO scheme, pointing out that TBCE was capable of achieving accurate CSI by employing a high number of training pilots, at the cost of reduced system's throughput.
2012	Sugiura <i>et al.</i> [41]	Studied the effects of MMSE based TBCE on SM MIMO schemes.
2014	Nasir <i>et al.</i> [42]	Proposed a TBCE scheme for assisting an amplify-and-forward two way relaying network.

1.2.2 Blind Channel Estimation

It has been mentioned in the Section 1.2.1 that TBCE schemes are capable of achieving accurate MIMO CSI estimation provided that the training overhead is large enough, which will obviously lead to a reduction in the overall system throughput. As a result, in order to eliminate this throughput reduction problem, another category of CE algorithms referred to as BCE schemes was introduced in [43–46], where no training sequence will be needed and therefore, no throughput loss will be imposed.

Even though the concept of blind identification had long been studied, in the fields of statistics and economics, it was only introduced into the wireless communication area by Tong *et al.* as late as 1991 [43], where a fundamental mathematical structure of blind identification was developed. Later a BCE scheme was proposed for STBC by Stoica *et al.* in [44], where the minimization of the ML metric with respect to both of the channel and source data was carried out in an iterative fashion. Then a closed-form BCE-aided STBC scheme was further proposed by Shahbazpanahi *et al.* [45], which was capable of estimating the CSI by exploiting the orthogonality of the STBCs. Additionally, a subspace based approach was conceived for BCE aided MIMO OFDM systems in [46], which unified and generalized the existing single-input single-output OFDM BCE to the case of MIMO OFDM scenarios. However, it is widely recognized that the BCEs impose a high complexity and slow convergence, whilst suffering from unavoidable estimation and decision ambiguities [47, 48]. This significantly limits the applications of BCE schemes.

1.2.3 Semi-Blind Channel Estimation

It may be seen from the discussions in Section 1.2.1 and 1.2.2 that the low-complexity TBCE scheme may significantly reduce the system’s effective throughput, while the BCE, which does not require training, may not only impose a high complexity and slow convergence, but also suffers from unavoidable estimation and decision ambiguities. As a more recent concept, SBCE schemes were proposed for solving these problems [31, 32, 36, 48–59], where only a small number of training symbols is employed for generating an initial CE. Initial data detection is then carried out based on this initial LSCE. Then the channel estimator and data detector iteratively exchange their information for updating the channel estimates.

One of the earliest contributions on SBCE may be referred to as the SBCE scheme proposed for spatial multiplexing systems by Medles *et al.* in 2001 [50], which exploited both training and blind principles. Stoica *et al.* proposed an SBCE scheme for STBC MIMO schemes, demonstrating that compared to the TBCE scheme, SBCEs always achieved a better BER performance at the same data rate. As an appealing compromise, SBCE achieves a much better BER performance than BCE at the cost of a slightly lower effective data rate [44]. Then the performance of the SBCE scheme proposed in [44] was analyzed in [51] in both single- and multiple-antenna scenarios.

ios, where closed-form formulas were given for both MMSE and LS channel estimators. An SBCE scheme was proposed for a BLAST MIMO system in [52], where the Repeated Weight Boosting Search (RWBS) was employed for identifying MIMO channel, while the reduced-complexity ML sphere detector was employed for the ensuring data detection. Another SBCE solution was proposed for BLAST MIMOs in [53], where the RWBS global search utilised in [52] was replaced by a low-complexity Particle Swarm Optimisation (PSO) aided CE. The decision-directed LSCE and the low-complexity single-stream ML data detector form an iterative loop of joint CE and data detection for the uncoded Coherent STSK (CSTSK) system of [31] and for the coded CSTSK system of [32]. A similar joint CE and data detection strategy was employed for the coded Direct-Sequence Code-Division Multiple-Access (DS-CDMA) system of [54]. An outer iterative loop involving a channel estimator and a turbo detector/decoder was introduced in [55–59] to form a joint CE and turbo detection/decoding scheme for MIMO aided OFDM systems.

In all the above-mentioned existing contributions, joint CE and turbo (or non-turbo) detection/decoding was carried out within an extra outer iterative loop, which may require a number of additional iterations to achieve convergence and therefore imposes a considerable extra computational complexity. Additionally, all these contributions employ all the detected bits for updating the channel estimate, which has the following effects. Firstly, the sequence of transmitted bits is usually long and this may impose an unnecessarily high complexity on the CE. Secondly and more profoundly, some of the detected bits may be erroneous, which will inflict a performance degradation, particularly under low SNR conditions.

We have summarized the above-mentioned SBCE schemes in Table 1.3.

1.3 Antenna Selection

Recently, the large-scale MIMOs have attracted significant attention owing to their capability of further increasing the reliability and/or bandwidth efficiency of MIMO systems [1, 63]. However, conventional MIMO systems usually activate all the antennas all the time. Since each data stream requires an individual Radio Frequency (RF) chain, multiple RF chains are necessitated by these MIMO systems. This may lead to grave implementation issues in terms of both power consumption and hardware costs. More specifically, in wireless communications systems, each RF chain contains a certain number of circuit components, such as power amplifiers, mixers, synthesizers, filters, etc, which may lead to substantial power consumption and hardware costs. Moreover, for large-scale MIMO systems and particularly for millimetre-wave based MIMO systems [63–65], the number of available antenna array elements that can be accommodated in a limited space increases massively [66, 67], while in practice the number of fiscally affordable RF chains is typically limited.

As a remedy, Antenna Selection (AS) offers a low-cost, low-complexity technique of reducing the number of RF chains utilized at the transmitter and/or receiver, while retaining the significant

Table 1.3: A brief summary of major contributions on SBCE schemes.

Year	Author(s)	Contributions
2001	Medles <i>et al.</i> [50]	Proposed the SBCE concept for spatial multiplexing systems, which exploited both training and blind information.
2002	Stoica <i>et al.</i> [44]	Proposed an SBCE scheme for STBC MIMO schemes and concluded that the SBCE struck a better compromise in terms of BER vs complexity trade-off than TBCE and BCE.
2004	Buzzi <i>et al.</i> [51]	Provided closed-form formulas for both MMSE and LS channel estimators invoked in SBCE scheme.
2007	Jiang <i>et al.</i> [55]	Introduced turbo codes into the SBCE scheme for the sake of achieving an improved BER performance.
2008	Abuthinien <i>et al.</i> [52]	Combined RWBS and reduced-complexity ML sphere detector for joint CE and data detection.
2009	Palally <i>et al.</i> [53]	Modified the SBCE of [52] by replacing RWBS with PSO for the sake of achieving a reduced complexity.
2010	Chen <i>et al.</i> [31]	Proposed a decision-directed LSCE and a low-complexity single-stream ML data detector to form an iterative loop of joint CE and data detection for the uncoded CSTSK.
2011	Zhang <i>et al.</i> [32]	Improved the performance of the SBCE scheme of [31] by employing a channel coding scheme.
2013	Zhang <i>et al.</i> [60]	Proposed a low-complexity joint Block-of-Bits Selection Based CE (BBSBCE) and three-stage iterative demapping-decoding scheme for near-capacity CSTSK systems, which does not impose an extra iterative loop between the channel estimator and the three-stage turbo detector.
2014	Zhang <i>et al.</i> [61]	Further extended BBSBCE scheme of [60] to the BBSB Soft-decision aided CE (BBSB-SCE) scheme.
2014	Abdallah <i>et al.</i> [62]	Proposed a SBCE aided two-way relaying networks, where both transmitted pilots and received data samples were utilized for CE.

advantages of MIMO systems. In AS aided MIMO systems, we only active a subset of antennas associated with the optimal or near-optimal channel conditions (e.g. a subset associated with the highest equivalent SNR) from the entire antenna set to form the actual MIMO communication system, which therefore provides significant performance gains for MIMO systems [68]. Generally, AS may be classified into three categories, namely Transmit AS (TxAS), Receive AS (RxAS) as well as Joint Transmit and Receive AS (JTRAS) [68].

1.3.1 Receive Antenna Selection

Table 1.4: A brief summary of major contributions on RxAS schemes.

Year	Author(s)	Contributions
1959	Brennan [22]	Introduced the SC receive diversity technique, which may be viewed as one of the earliest RxAS scheme utilising a single RF chain at the receiver.
2002	Govokhov [69]	Proposed a low-complexity RxAS scheme for maximizing the system capacity by removing the antennas associated with the lowest capacity contribution.
2004	Gharavi-Alkhansari <i>et al.</i> [70]	Modified Govokhov's method by incorporating new antennas associated with the highest capacity contribution.
2008	Hiwale <i>et al.</i> [71]	Proposed an optimal SNR based receive AS scheme for STTCs, which selected the receive antennas associated with the highest instantaneous SNR.
2009	Liu <i>et al.</i> [72]	Proposed a performance based RxAS scheme for V-BLAST MIMO systems.
2009	Xu <i>et al.</i> [73]	analyzed the effects of spatial channel correlation on the RxAS aided MIMO systems and provided a closed-form expression for both the outage probability and for an upper bound for the average capacity.
2011	Hussaibi <i>et al.</i> [74]	Proposed a RxAS scheme for uplink SDMA systems communicating over correlated Rayleigh fading channels.
2013	Yang <i>et al.</i> [75]	Proposed the BER analysis for RxAS aided multiuser relaying networks, where users were equipped multiple antennas, while source and relays were equipped with single antenna.
2013	Stephen <i>et al.</i> [76]	Proposed a Markov decision theoretic approach aided RxAS scheme.

The basic idea of RxAS is to select the Rx antenna(s) to maximize either the system's SNR or the system's capacity [69–74]. The history of RxAS scheme may be traced back to 1959, when Brennan introduced the SC scheme of [22], where the main idea was to select one out of N receive antennas associated with highest receive SNR. Then the SC scheme was expanded to the case, where the receiver was equipped with multiple RF chains. In this situation, a subset of the receive antennas had to be selected. More specifically, a low-complexity RxAS scheme was proposed in [69]. The algorithm explores the full channel matrix, and every step of its operation it removes one antenna associated with the lowest contribution to the overall system capacity. This algorithm was

demonstrated to achieve a lower computational complexity than that of the full-search algorithm. This algorithm was further improved in [70], where instead of commencing from a full matrix and gradually removing antennas, the improved algorithm begins with an empty matrix and incorporates one antennas per step. The authors of [71] proposed an optimal RxAS scheme for STTCs, which selected receive antennas having the highest instantaneous SNR. The philosophy of RxAS was proposed for V-BLAST MIMO systems in [72], where it was shown that the system's performance was improved with the aid of AS in terms of its Block Error Ratio (BLER). Additionally, it has been widely recognized that encountering spatial correlation between the AEs may reduce the diversity gain, hence the performance of AS schemes may be degraded in the presence of spatial correlation. The effects of spatial channel correlation on the RxAS aided MIMO system's capacity was analyzed in [73], where a closed-form expression was derived for both the outage probability and for an upper bound of the average capacity. Additionally, a RxAS scheme was proposed for uplink SDMA systems communicating over correlated Rayleigh fading channels [74], where it was shown that RxAS provided an efficient solution for SDMA in correlated MIMO channel environments.

We have summarised the above-mentioned RxAS schemes in Table 1.4.

1.3.2 Transmit Antenna Selection

Similar to the idea of RxAS algorithms, the main idea of TxAS based on the norm of the channel matrix is to select the transmit antenna(s) associated either with the highest SNR or maximizing the system capacity [77–80]. More specifically, a TxAS scheme was proposed in [77] for assisting the family of spatial multiplexing systems equipped with linear receivers, where it was shown that the performance of low complexity linear receivers was significantly improved at the cost of employing a modest number of extra transmit antennas. Two TxAS techniques were proposed and compared in [78] for SM systems by Rajashekhar *et al*, where it was shown that the proposed Capacity Optimised AS (COAS) scheme outperformed the Euclidean Distance Optimised AS (EDAS) scheme. Additionally, three AS criteria (ASCs) were proposed for SSK systems in [79], which were max-norm based AS (ASC1), maximum norm difference based AS (ASC2) and the hybrid scheme combining ASC1 and ASC2. The corresponding simulation results showed that AS techniques improved the performance of SSK-based MIMO systems, and ASC1 outperformed both ASC2 and the hybrid design. Moreover, it should be noted that since the knowledge of the CSI is usually needed for AS and it is often only available at the receiver side, TxAS relies on the CSI to be fed back to transmitter side in order to carry out AS, while no feedback is required in RxAS scheme [68].

1.3.3 Joint Transmit and Receive Antenna Selection

In Section 1.3.1 and 1.3.2, the RxAS and TxAS schemes have been introduced, where the AS only takes place at either the receiver or the transmitter side. However, often we have multiple antennas at both the transmitter and the receiver. In this case, a hybrid version of TxAS and

RxAS, namely the JTRAS may be applied for selecting both transmit and receive antennas. Diverse JTRAS schemes were investigated in [81–88], where it was observed that MIMO systems employing JTRAS were capable of improving the achievable system performance, while maintaining a low hardware complexity compared to the conventional MIMO systems employing the same number of RF chains and operating without JTRAS.

Table 1.5: A brief summary of major contributions on JTRAS schemes.

Year	Author(s)	Contributions
2004	Sanayei <i>et al.</i> [81]	Proposed a reduced-complexity sub-optimal JTRAS scheme based on a two-step Incremental Successive Selection Algorithm (ISSA).
2006	Kim <i>et al.</i> [82]	Improved Sanayei's ISSA [81] by selecting the specific antennas associated with the largest gap between the maximum and minimum values in the same column/row of the channel matrix.
2006	Wei <i>et al.</i> [83]	Invoked Sanayei's two-step selection algorithm [81] in correlated fading environments.
2007	Gucluoglu <i>et al.</i> [86]	Proposed a sub-optimal two-step successive selection algorithm for STCs, which separately selected only a single receive antenna and multiple transmit antennas.
2008	Gucluoglu <i>et al.</i> [88]	Analyzed the performance of JTRAS in the context of the STCs of [86] in flat fading channel environments and derived the PEP.
2009	Naeem <i>et al.</i> [85]	Proposed a reduced-complexity near-optimal JTRAS algorithm adopting Ant Colony Optimization (ACO).
2010	Yilmaz <i>et al.</i> [87]	Proposed a JTRAS scheme for two-hop amplify-and-forward relaying systems.
2013	Chakravarti <i>et al.</i> [89]	Analyzed the transmit diversity of Alamouti's STBC with the aid of a sub-optimal JTRAS scheme.
2015	Zhang <i>et al.</i> [90]	Proposed a simple yet efficient norm-based JTRAS algorithm for MIMO systems.

Generally, there are two major types of AS algorithms – Capacity-Based AS (CBAS) and Norm-Based AS (NBAS) [68]. The main idea of CBAS is to select those antennas that can maximize the MIMO channel capacity [1]. However, it is well-known that the optimal CBAS requires exhaustive search over all the possible subsets of the full channel matrix, which becomes impractical for systems having a large number of Transmit Antennas (TAs) and/or Receive Antennas (RAs) [70]. Diverse sub-optimal CBAS techniques were developed in [82–85], which were capable of reduc-

ing the AS complexity at the cost of a performance loss. As another efficient yet low-complexity category of AS algorithms, a range of NBAS techniques were studied in [81, 86–88], which aim for selecting those specific antennas that are capable of maximizing the system’s SNR. It was shown that the family of NBAS algorithms is capable of approaching the performance of CBAS techniques, while imposing a lower AS complexity. More specifically, Sanaye *et al.* [81] proposed a reduced-complexity norm-based two-step sub-optimal JTRAS scheme, where the receive antennas were firstly selected via norm-based ranking, and then the transmit antennas were selected using incremental successive selection. A near-optimal JTRAS method was presented in [86], which first selects the particular RA having the maximum receive SNR and then selects some of the TAs that are related to the selected RA. A major limitation of this near-optimal AS method is that it is restricted to select a single RA. Then the performance of JTRAS schemes designed for STCs [86] operating in flat fading channels was analyzed in [88], where a Pairwise Error Probability (PEP) was derived, and it was demonstrated that the NBAS scheme was indeed capable of achieving the maximum attainable diversity gain, provided that the STC matrix had a fullrank. An enhanced JTRAS algorithm was proposed for two-hop amplify-and-forward relaying systems in [87], where only a single TA/RA pair is selected in each phase of relay communication.

We have summarized the above-mentioned JTRAS schemes in Table 1.5.

1.4 Differential Detection and Cooperative Communications

1.4.1 Differential Detection

In coherent MIMO schemes, accurate knowledge of the CSI is required for performing data detection. In this case, the accuracy of CE may have a significant impact on the performance of coherently detected MIMO systems. Since CE techniques [43, 45–47] exploit the fact that the consecutive time-domain samples of each of the CIR taps are correlated, obeying a Doppler-frequency-dependent correlation, which is commensurate with the velocity of the vehicle. Naturally, both the pilot symbol overhead and the CE complexity increase, as the vehicular speed increases. This implies having more rapidly fluctuating CIR taps. Additionally, for a MIMO system associated with M Tx antennas and N Rx antennas, a total of $(M \times N)$ MIMO channels have to be estimated, which may also lead to an excessive CE complexity, as the number of Tx and Rx antennas increases.

By contrast to classic coherent detectors, the family of differentially encoded non-coherent detectors requires no CSI at the receivers, hence they constitute an attractive design alternative [104, 105]. It is widely recognized that Conventional Differential Detection (CDD) schemes, where the decision of a single symbol/block is based on as few as two ($N_w = 2$) adjacent received symbols/blocks, usually suffer from a 3 dB performance loss. Additionally, Doppler frequency also affects the performance of CDD schemes. To be more explicit, when the Doppler

Table 1.6: A brief summary of major contributions on MSDD.

Year	Author(s)	Contributions
1990	Divsalar <i>et al.</i> [91]	Proposed a MSDD scheme for MPSK in AWGN channel using the ML sequence estimation of the transmitted symbols.
1992	Ho <i>et al.</i> [92]	Analyzed the performance of MSDD designed for PSK for transmission over correlated Rayleigh fading channels and found that MSDD was an effective strategy of eliminating the irreducible error floor associated with CDD.
1994	Divsalar <i>et al.</i> [93]	Derived metrics for ML-MSDD of both uncoded and trellis coded MPSK and QAM modulation for transmission over both Rayleigh and Rician fading channels.
1994	Mackenthun [94]	Proposed a reduced-complexity MSDD conceived for MPSK, which only imposed a complexity of order $N_w \cdot \log(N_w)$ per N_w symbol blocks.
2001	Fan [95]	Applied the MSDD algorithm to differential G2 STC operating in slow fading channels.
2001	Simon [96]	Employed multiple receive antennas in an MSDD scheme designed for DPSK and derived its performance bound.
2002	Schober <i>et al.</i> [97]	Proposed MSDD for DSTM operating in Rayleigh fading channels.
2005	Lampe <i>et al.</i> [98]	Designed MSDSD for DPSK, which introduced the SD algorithm into MSDD schemes for the sake of reducing the computational complexity.
2005	Pauli <i>et al.</i> [99]	Proposed soft-decision aided MSDSD for the sake of incorporating turbo codes.
2007	Pauli <i>et al.</i> [100]	MSDSD was conceived for DSTM based on the algorithm of [98].
2011	Xu <i>et al.</i> [101]	Extended MSDSD to DSTBC using QAM constellations.
2013	Zhang <i>et al.</i> [102]	Proposed a MSDSD aided Multi-User Successive Relaying assisted Cooperative (MUSRC) system.
2014	Kadir <i>et al.</i> [103]	Proposed a soft-decision aided MSDSD for OFDM-aided multicarrier Differential STSK (DSTSK) systems.

frequency increases, the system performance will be significantly degraded, leading to an error floor in CDD schemes [106]. As a result, Multiple-Symbol Differential Detection (MSDD) was proposed in [91–94, 96, 107, 108] for differential symbol detections, which was then extended to G2 STCs and to Differential Space-Time Modulation (DSTM) in [95, 97]. In MSDD schemes, more

than two ($N_w \geq 2$) consecutive received symbols/blocks are utilized for simultaneously making a joint decision on ($N_w - 1$) symbols/blocks as opposed to symbol-by-symbol detection [96]. This will lead to a narrower performance discrepancy between the coherent and noncoherent schemes. Additionally, for ML MSDD (ML-MSDD) the BER performance improves monotonically as the observation window size N_w increases. However, the detection complexity increases exponentially with N_w [98].

In order to conceive low-complexity ML-MSDD for Rayleigh fading channels, Multiple-Symbol Differential Sphere Detection (MSDSD) was designed for Differential Phase Shift Keying (DPSK) in [98], which introduces the concept of Sphere Decoding (SD) [27] into MSDD schemes for the sake of reducing the computational complexity from the order of L^{N_w-1} in case of MSDD to an order of $L(N_w - 1)$. Then the MSDSD scheme was extended to DSTM in [100] and to space-time block codes in [101]. Moreover, Soft-Input Soft-Output MSDSD (SISO-MSDSD) was proposed in [99], which was designed for accepting the *a priori* information to achieve power-efficient digital communications, while maintaining the low-complexity of MSDSD schemes.

We have summarized the evolution of differential detection in Table 1.6.

1.4.2 Cooperative Communications

It has been discussed in Section 1.1 that employing multiple transmit antennas is a beneficial method for combating the effects of fading by providing diversity gains. Transmit diversity is capable of improving the BER performance, if the channels spanning from transmit antennas to the receive antenna(s) experience independent fading, which can be achieved by arranging the transmit antennas to be sufficiently far apart—much farther than the carrier’s wavelength. However, due to the limited size of hand-held mobile devices, it becomes impractical to separate the transmit antennas far enough to experience independent fading [6]. Therefore, the received signals may suffer from considerable correlation and hence both the BER performance and the achievable capacity may be degraded. In order to mitigate this problem, the concept of distributed MIMOs, constituted by cooperating single-antenna mobiles, was introduced in [109–113].

Generally speaking, the cooperative communication model consists of a Source Node (SN), some Relay Nodes (RNs) and a Destination Node (DN). To be more explicit, in the broadcast phase, the source information is transmitted from the SN, which is received by the RNs and/or the DN. The data received at RN will be either Amplified-and-Forwarded (AF) [104, 114, 115] or Decoded-and-Forwarded (DF) [105, 116] to the DN during the relaying phase. As a result, the DN will receive multiple copies of the source information. Furthermore, since in mobile communication systems the RNs can be carefully selected by the resource allocation to be sufficiently separated, each copy of the source information received by the DN experiences an independent fading channel. Hence the system benefits from a spatial diversity gain, therefore improving the system’s BER performance. The concept of Virtual Antenna Array (VAA) was conceived by Dohler *et al.* in

[117], which relies on mutual communication amongst spatially separated RNs forming a virtual MIMO channel. This special form of ad-hoc networks realizes distributed STCs in cooperative communication networks, such as Alamouti’s STBC [4] and the recently proposed STSK schemes [21].

1.5 Novel Contributions

The novel research aspects provided by this report are summarized as follows:

- We propose a low-complexity joint BBSBCE and three-stage iterative demapping-decoding scheme for near-capacity CSTSK systems, which does not impose an extra iterative loop between the channel estimator and the three-stage turbo detector. Specifically, in order to maintain a high system throughput, only a low training overhead is utilized for obtaining an initial CE. Naturally, the number of training blocks is related to the number of transmit antennas [31]. Then the low-complexity single-antenna based ML soft-demapping of [5] is carried out and the soft decisions are exchanged between the Unity-Rate-Code (URC) decoder and CSTSK soft-demapper within the inner turbo loop, before they are forwarded to the outer Recursive Systematic Convolutional (RSC) decoder. Moreover, the “high quality” or “more reliable” blocks-of-bits are selected based on the *a posteriori* information produced by the CSTSK soft-demapper within the original inner turbo loop of the URC decoder and CSTSK soft-demapper, which are re-modulated concurrently with each outer iteration of the original outer turbo loop for the sake of facilitating decision-directed-LSCE (DD-LSCE) updates. Since the CE is naturally embedded into the original iterative three-stage demapping-decoding scheme, no extra iterative loop is required between the CE and the three-stage CSTSK demapper-decoder. Moreover, since our proposed BBSBCE scheme only selects a sufficient number of high-quality decisions for CE, the complexity of our channel estimator is dramatically lower than any existing Decision-Directed CE (DDCE) scheme which employs the entire frame of the detected symbols. All these features result in a low system complexity. In other words, the proposed joint BBSBCE and three-stage turbo demapping-decoding scheme has a similar computational complexity to that of the original three-stage turbo demapping-decoding scheme with the known CSI. Furthermore, the proposed semi-blind joint CE and turbo detection-decoding scheme is capable of fully exploiting the “turbo effects” of the joint CE and three-stage demapping-decoding for approaching the optimal performance obtained by the idealised three-stage turbo demapping-decoding receiver furnished with the perfect CSI, despite using the same low number of turbo iterations as the latter. **- These novel contributions were proposed in paper “Journal No.2” in the publication list.**
- We further extend our propose BBSBCE scheme to the BBSB-SCE scheme. In our BBSB-

SCE scheme, only a ‘just-sufficient-number’ of the high-quality soft-estimated symbols are utilised for CE. By contrast to the existing state-of-the-art solutions, it does not suffer from the usual performance degradation imposed by erroneous decisions. Furthermore, this measure dramatically reduces the complexity of the DD-LSCE. - **These novel contributions were detailed in papers “Journal No.3” and “Conference No.1” in the publication list.**

- Additionally, we propose a Norm-Based Joint Transmit and Receive Antenna Selection (NBJ-TRAS) aided MIMO system relying on the assistance of a novel two-tier channel estimation scheme. Specifically, a rough estimate of the full MIMO channel matrix is first generated by a low-complexity, low-training-overhead based TBCE scheme, which relies on reusing a modest number of RF chains. NBJTRAS is then carried out based on this initial CE. The NBJTRAS aided MIMO system is capable of significantly outperforming conventional MIMO systems equipped with the same modest number of RF chains, while dispensing with the idealised simplifying assumption of having perfectly known CSI. Moreover, the initial subset channel estimate associated with the selected subset MIMO channel matrix is then used for activating a SBCE scheme, in which the channel estimate may be refined by BBSB-SCE embedded in the iterative detection and decoding process. The joint channel estimation and turbo detection-decoding scheme operating with the aid of the BBSB-SCE channel estimator is capable of approaching the performance of the near-capacity ML turbo transceiver associated with perfect CSI. This is achieved without increasing the complexity of the ML turbo detection and decoding process. - **These novel contributions were detailed in papers “Journal No.4” and “Conference No.2” in the publication list.**
- We propose a DSTSK aided MUSRC system. By exploiting the flexibility of the DSTSK concept, our system becomes capable of supporting different number of users by appropriately adjusting the constellation size of the Phase Shift Keying (PSK) modulation scheme employed by DSTSK, and we opt for using Binary PSK (BPSK), Quadrature PSK (QPSK), 8-PSK, etc., in conjunction with a variable number of dispersion matrices. Additionally, our system is capable of activating a different number of relays by adjusting the dimensions of each dispersion matrix. Since we apply the successive relaying philosophy in our system, the 50% throughput loss of conventional two-phase relaying is recovered at the cost of supporting less users. Finally, the DS-CDMA concept is adopted for suppressing the Multiple Access Interference (MAI). - **These novel contributions were detailed in paper “Journal No.1” in the publication list.**

1.6 Thesis Outline

Let us now highlight the outline of this thesis, which is organized as shown in Figure 1.6.

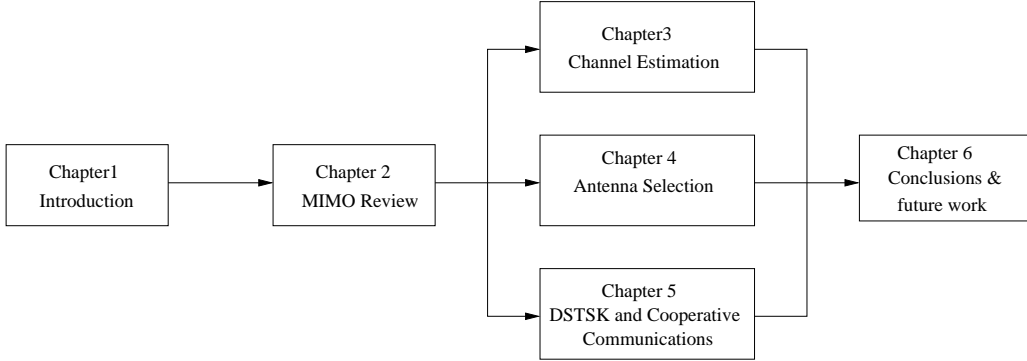


Figure 1.6: Organization of the thesis.

In Chapter 2, two MIMO systems, namely the SDM/V-BLAST and the STSK, will be briefly reviewed. More specifically, the system model and performance of uncoded SDM/V-BLAST are introduced and investigated in Section 2.1, where it will be demonstrated that a diversity gain may only be achieved by increasing the number of receive antennas at the receiver side, while a multiplexing gain may be achieved by increasing the number of transmit antennas. For the sake of achieving near-capacity performance, the powerful three-stage serial-concatenated turbo coded SDM/V-BLAST MIMO scheme is introduced in Section 2.2, where it may be seen that with the aid of three-stage turbo coding scheme, the MIMO systems are capable of achieving a near-capacity performance. In Section 2.3, the novel concept of CSTSK scheme is introduced in terms of its system model, computational complexity, maximum achievable diversity order, and dispersion matrix generation. We also propose a novel Maximum Minimum-Determinant Based Configuration Selection (MMBCS) algorithm, which is capable of selecting the best STSK configuration, while avoiding the time-consuming Monte-Carlo simulation based approach. The uncoded CSTSK MIMO system's performance is then intensively investigated based on various CSTSK configurations. By analysing the results obtained, it may be concluded that the proposed CSTSK scheme is capable of striking a flexible tradeoff between the MIMO's diversity and multiplexing gains, while facilitating the low-complexity single-antenna-based ML detection owing to the elimination of ICI. Finally, a three-stage serial-concatenated turbo coding aided CSTSK MIMO systems is developed in Section 2.4 for the sake of achieving a near-capacity performance.

Chapter 3: Channel Estimation for Coherent MIMO Systems

In Chapter 2, the family of coherent MIMO systems represented by the classic SDM/V-BLAST and the recent CSTSK is reviewed under the idealized simplifying assumption of perfectly known CSI. It has been widely recognized that the ability of a coherent MIMO system to approach its attainable capacity heavily relies on the accuracy of the CSI. In order to dispense with the assumption of perfectly known CSI, in Chapter 3, CE schemes for MIMO systems will be discussed. We first briefly review the conventional TBCE and SBCE

schemes based on the CSTSK MIMO scheme in Section 3.2 and Section 3.3, respectively. It will be demonstrated that the conventional TBCE scheme is capable of achieving accurate CE by employing a high Pilot Overhead (PO), at a cost of reduced effective throughput. On the other hand, the SBCE may acquire accurate CE in an iterative joint CE and data detection fashion associated with a low PO. Section 3.4 is dedicated to develop the SBCE aided and three-stage serial-concatenation turbo coded scheme for near-capacity CSTSK MIMO systems. More specifically, the novel BBSBCE scheme is proposed, which utilizes a low PO for generating an initial CE. Most significantly, unlike the existing methods, the proposed BBSBCE scheme does not require an extra iterative loop between the CE and the turbo detector-decoder, since the BBSB iterative CE was naturally embedded into the original iterative three-stage demapping-decoding turbo loop. This novel arrangement enables us to maintain a low system complexity. Furthermore, since only high-confidence decision blocks are selected in the BBSBCE based scheme, the error propagation problem existed in conventional SBCE schemes is mitigated. Additionally, the novel BBSBCE scheme is further developed into a soft version in Section 3.5, namely BBSB-SCE. The corresponding simulation results demonstrate that the proposed BBSB-SCE based scheme is capable of achieving the optimal ML performance bound associated with the perfect CSI, while maintaining a high system throughput without imposing an excessive computational complexity.

Chapter 4: Norm-Based Joint Transmit/Receive Antenna Selection Aided MIMO Systems

In Chapter 4 we mainly focus on the AS scheme for MIMO systems. It has been discussed in Chapter 2 that MIMO schemes are capable of achieving a diversity and/or multiplexing gain by employing multiple AEs at the transmitter and/or the receiver. However, it should also be noted that since MIMO systems utilize multiple RF chains, their power consumption and hardware costs become substantial. Against this background, we introduce the concept of AS in Section 4.1 and propose a simple yet efficient AS algorithm, namely the NBJTRAS in Section 4.2. The corresponding simulation results based on perfect CSI demonstrate that the proposed NBJTRAS is capable of improving both the BER performance and throughput of the MIMO systems, compared to the conventional MIMO systems utilizing the same number of RF chains. We also propose a novel TTCE scheme for NBJTRAS aided MIMO systems, which exploits the facts that the AS is relatively less sensitive to the CE errors than the data detection. The corresponding simulation results demonstrate that the proposed TTCE scheme is capable of achieving both high CE accuracy and a high system throughput.

Chapter 5: Multiple-Symbol Differential Sphere Detection Aided DSTSK

In this chapter, we focus on the MSDSD aided DSTSK scheme. Section 5.2 reviews the MSDSD aided DSTSK systems, where it will demonstrate that first, MSDSD is capable of mitigating the error floor exhibited by CDD in DSTSK schemes, especially when the fading rate is relatively high, i.e. normalized Doppler frequency $f_d = 0.03$ in the simulation. Addition-

ally, in relatively fast fading environments, the performance of MSDSD may be improved by expanding the window size N_w , at the cost of the increased computational complexity. Since in differentially encoded systems CSI is no longer required, it is natural to consider applying differential schemes in cooperative communications. Consequently, the DSTSK aided MUSRC system is proposed in Section 5.3. We demonstrate that by exploiting the flexibility of the concept of DSTSK schemes, our system is capable of supporting different number of users by appropriately adjusting the constellation size of the PSK modulation scheme employed by DSTSK, we opted for using BPSK, QPSK, 8-PSK, etc., conceived with a variable number of dispersion matrices. Additionally, our system is capable of activating a different number of relays by adjusting the dimensions of each dispersion matrix.

Chapter 6: Conclusions and Future Research

In this chapter, we summarize the major findings and contributions of this thesis. Specific design guidelines are listed in Section 6.2 to show the rational of our design decisions, and to provide further insights of the advanced technologies invoked in this thesis. We further outline a range future research topics in Section 6.3.

Chapter 2

SDM/V-BLAST and Space-Time Shift Keying MIMO Review

In this chapter, two MIMO systems that are used in this thesis are reviewed. It has been widely recognised that MIMO systems are capable of achieving a multiplexing gain and/or diversity gain by employing multiple antennas at the transmitters and/or receivers. To be more explicit, the family of SDM/V-BLAST [2] MIMO systems is capable of achieving a multiplexing gain by employing multiple Transmit (Tx) antennas. However, the SDM/V-BLAST MIMO system is only capable of achieving a diversity gain by employing multiple Receive (Rx) antennas.

Unlike the above mentioned conventional SDM/V-BLAST MIMO systems, the recently proposed STSK scheme [5,21] is capable of achieving both a Tx and a Rx diversity gain by employing multiple Tx antennas and Rx antennas. Additionally, in STSK-aided MIMO systems, one of the Q appropriately indexed space-time dispersion matrices is activated within each STSK signal block duration and therefore, STSK fully exploits both the spatial- and time- dimensions. Moreover, due to its high degree of design-freedom, a flexible diversity versus multiplexing gain tradeoff can be realized by the STSK scheme, which is achieved by appropriately optimizing both the number and size of the dispersion matrices as well as the number of transmit and receive antennas. Additionally, the ICI encountered in STSK MIMO systems is also completely removed and consequently, the adoption of single-antenna-based ML detection becomes realistic.

The rest of this chapter is organised as follows. Section 2.1 reviews the system model and the achievable system performance of the conventional uncoded SDM/V-BLAST MIMO systems. For the sake of achieving near-capacity performance, the powerful three-stage serial-concatenated turbo coded SDM/V-BLAST MIMO system is introduced in Section 2.2. Additionally, the powerful tool of EXtrinsic Information Transfer (EXIT) charts is adopted for predicting the BER performance of turbo coded MIMO systems in this section. The system's overview and the achievable performance of both uncoded and three-stage serial-concatenated turbo coded coherent STSK systems are pro-

vided in Section 2.3 and Section 2.4, respectively. Finally, Section 2.5 provides the summary of this chapter. Since the objective of this chapter is to benchmark the achievable performance of the SDM/V-BLAST and STSK MIMO systems, we assume that the MIMO CSI is known at receiver. In the later chapters, we will dispense this idealised assumption.

2.1 Uncoded SDM/V-BLAST Systems

2.1.1 System Overview

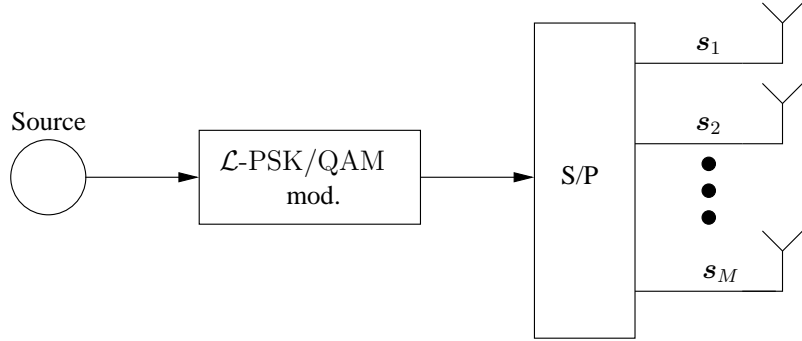


Figure 2.1: Transmitter structure of uncoded SDM/V-BLAST MIMO scheme.

In this section, we consider an uncoded SDM/V-BLAST MIMO system relying on M Tx antennas and N Rx antennas for communication in a frequency-flat Rayleigh fading environment. Given a bits per \mathcal{L} – PSK/QAM symbol throughput of $\text{BPS} = \log_2(\mathcal{L})$, the number of Bits Per Transmission Block (BPB) may be expressed as $\text{BPB} = M \cdot \text{BPS}$. The corresponding transmitter structure of a SDM/V-BLAST MIMO system is shown in Fig. 2.1, where it may be seen that a block of BPB binary source bits is firstly mapped into an \mathcal{L} – PSK/QAM modulation scheme. Then the modulated symbols are serial-to-parallel converted and mapped to a total number of M Tx antennas. This MIMO system model may be equivalently expressed as

$$\mathbf{y}(i) = \mathbf{H}\mathbf{s}(i) + \mathbf{v}(i), \quad (2.1)$$

where i denotes the symbol index, $\mathbf{s}(i) = [s_1 \ s_2 \ \dots \ s_M]^T$ is the transmitted \mathcal{L} -PSK/QAM symbol vector with $(\cdot)^T$ denoting the transpose operator and the MIMO channel matrix is given by

$$\mathbf{H} = \begin{bmatrix} h_{11} & h_{12} & \cdots & h_{1M} \\ h_{21} & h_{22} & \ddots & \vdots \\ \vdots & \ddots & \ddots & \vdots \\ h_{N1} & h_{N2} & \cdots & h_{NM} \end{bmatrix},$$

while $\mathbf{y}(i) = [y_1 \ y_2 \ \dots \ y_N]^T$ denotes the received signal vector and $\mathbf{v}(i) = [v_1 \ v_2 \ \dots \ v_N]^T$ represents the noise vector, whose elements obey the complex-valued zero-mean Gaussian distribution of $\mathcal{CN}(0, N_0)$, with a variance of $N_0/2$ per dimension. The system's SNR is defined as

$\text{SNR} = E_s/N_0$, where E_s is the average symbol energy. The corresponding normalized throughput R per time-slot of the SDM/V-BLAST MIMO system is given by

$$R = M \cdot \log_2(\mathcal{L}) \text{ [bits/symbol].} \quad (2.2)$$

For instance, if a SDM/V-BLAST MIMO system adopts a MIMO setup of $M = 2$ Tx antennas and QPSK as the modulation scheme, the corresponding normalized throughput may be expressed as $R = 2 \cdot \log_2(4) = 4$ bits/symbol.

At the receiver, since the multiple symbols of a transmitted symbol vector $\mathbf{s}(i)$ have to be decomposed, both the achievable performance and the detection complexity of SDM/V-BLAST MIMO systems significantly depend on the detection algorithm employed. To be more explicit, employing the well-known ML detection algorithm is capable of achieving the optimal performance, albeit at a cost of exponentially increased computational complexity upon increasing the number of symbols multiplexed in the transmitted symbol vector $\mathbf{s}(i)$. More specifically, the corresponding computational complexity of the optimal ML detection algorithm to detect a block of BPB bits, which is evaluated by the number of real-valued multiplications, may be formulated as:

$$C_{\text{ML}} = (4MN + 2N) \mathcal{L}^M. \quad (2.3)$$

Generally speaking, the conditional probability of $P(\mathbf{y}(i)|\mathbf{s}(i), \mathbf{H})$ in MIMO systems may be expressed as

$$P(\mathbf{y}(i)|\mathbf{s}(i), \mathbf{H}) = \frac{1}{(\pi N_0)^N} \exp\left(-\frac{\|\mathbf{y}(i) - \mathbf{H}\mathbf{s}(i)\|^2}{N_0}\right), \quad (2.4)$$

where $\|\cdot\|$ denotes the norm operator. Then, assuming that the CSI is known at the receiver, the ML estimate [118] of a multiplexed symbol sequence $\mathbf{s}(i)$ may be expressed as

$$\hat{\mathbf{s}} = \arg \min_{\mathbf{s}_l \in \mathcal{S}} \|\mathbf{y}(i) - \mathbf{H}\mathbf{s}_l\|^2, \quad (2.5)$$

where $\mathcal{S} = \{\mathbf{s}_l\}_{l=1}^{\mathcal{L}^M}$ represents the set of the legitimate transmitted symbol vectors.

As it has been mentioned above that even though the ML detector is capable of achieving the optimal performance, its complexity increases exponentially with the total number of Tx antennas, which may become excessive particularly when large-scale MIMO systems are considered. Therefore, the family of classic linear detectors, such as the ZF and MMSE detectors, may be adopted for the sake of maintaining low detection complexity, which is achieved at the expense of a certain performance loss. Additionally, some near-optimal detection schemes, such as sphere detection schemes [27], have also been proposed, which are capable of attaining a quasi-optimal performance at a moderate complexity.

2.1.2 Simulation Results

In this section, the achievable performance of the uncoded SDM/V-BLAST MIMO system of Fig. 2.1 is presented. A frequency-flat Rayleigh fading environment was considered. The average transmitted symbol energy E_s was normalised to unity and, therefore, the SNR was given as $\frac{1}{N_0}$, with N_0

being the AWGN power. A SDM/V-BLAST MIMO system associated with M Tx antennas, N Rx antennas and employing \mathcal{L} – PSK/QAM may be represented as $\text{MIMO}(M, N, \mathcal{L} - \text{PSK/QAM})$. The well-known ML detection algorithm of Eq. (2.5) was adopted here for the sake of achieving the optimal performance. The system parameters of uncoded SDM/V-BLAST MIMO system of Fig. 2.1 are summarized in Table 2.1.

Table 2.1: System parameters of the uncoded SDM/V-BLAST MIMO system of Fig. 2.1.

Number of Tx antennas	M
Number of Rx antennas	N
Modulation	\mathcal{L} -QAM or \mathcal{L} -PSK
Channels	Frequency-flat Rayleigh fading
Detector	ML detector of Eq. (2.5)

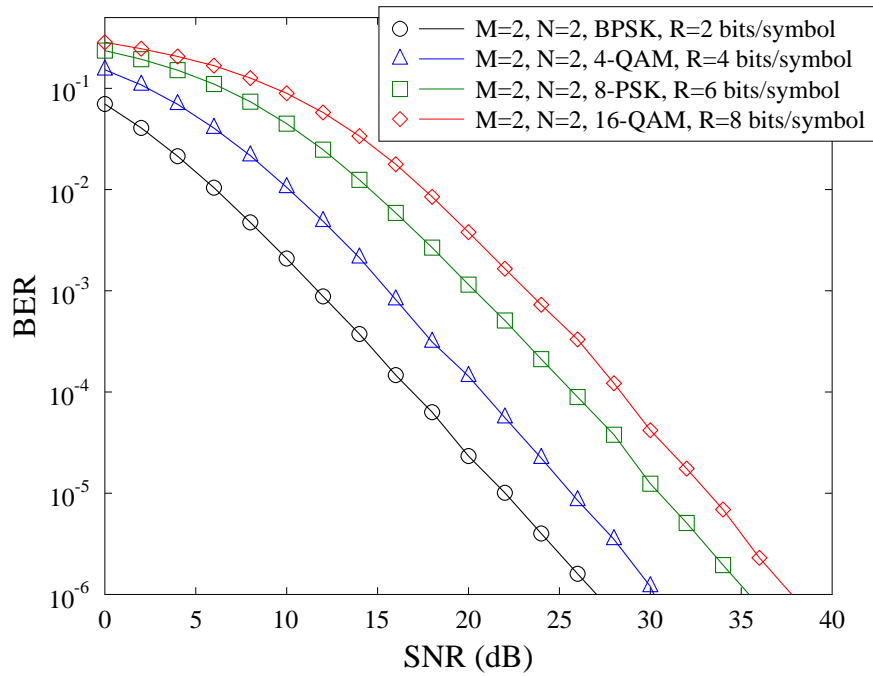


Figure 2.2: Achievable BER performance of a SDM/V-BLAST MIMO system of Fig. 2.1 associated with $M = 2$ Tx antennas, $N = 2$ Rx antennas and various throughputs. All other system parameters were summarized in Table 2.1.

Fig. 2.2 shows the achievable BER performance of the uncoded SDM/V-BLAST MIMO system $\text{MIMO}(2, 2, \mathcal{L} - \text{PSK/QAM})$. It may be seen that when the BPSK modulation scheme is adopted, the system achieved the best BER performance, reaching a BER of 10^{-6} at about $\text{SNR} = 27$ dB, associated with a corresponding throughput of $R = 2$ [bit/symbol]. When 4-QAM is adopted, the normalized throughput increases to $R = 4$ [bit/symbol], with a corresponding SNR loss of about

3 dB at the BER of 10^{-6} compared to the performance of the BPSK modulation scenario. Similarly, when the throughput becomes higher, namely when 8-PSK and 16-QAM are used, the corresponding normalized throughput increases to $R = 6$ and 8 [bits/symbol], respectively. The corresponding BER performance is degraded by about 8 and 11 dB, respectively, compared to that of the BPSK performance benchmark. Therefore, we may see that in SDM/V-BLAST MIMO systems, the normalized throughput may be increased by adopting higher-order modulation schemes, at the expense of a BER performance loss. However, it has been mentioned that SDM/V-BLAST MIMO systems mainly aim for achieving a multiplexing gain at the transmitter, whilst a diversity gain may only be achieved at the receiver by employing multiple Rx antennas. Therefore, it may be seen in Fig. 2.2 that all the BER curves of various normalized throughputs share the same slope, implying that the same diversity gain may be achieved in all scenarios, since the number of antennas employed at MIMO receiver is the same, namely $N = 2$ in this example.

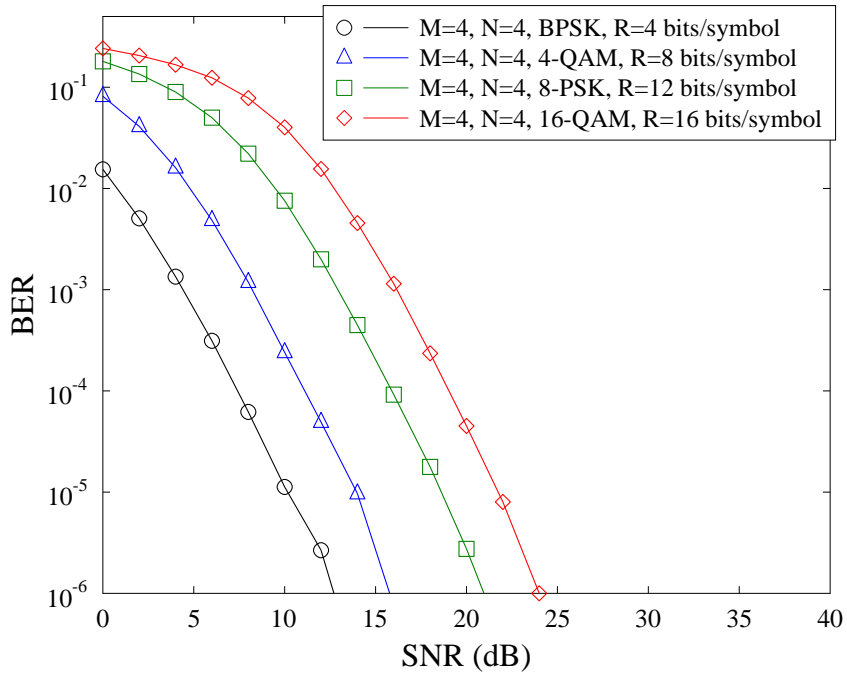


Figure 2.3: Achievable BER performance of a SDM/V-BLAST MIMO system of Fig. 2.1 associated with $M = 4$ Tx antennas, $N = 4$ Rx antennas and various throughputs. All other system parameters were summarized in Table 2.1.

The performance of the uncoded SDM/V-BLAST MIMO system MIMO(4,4, \mathcal{L} – PSK/QAM) is depicted in Fig. 2.3, where it may be seen that similar to the performance shown in Fig. 2.2, in the case of using BPSK signalling, the system achieves the best BER performance, associated with the lowest normalized throughput of $R = 4$ [bits/symbol]. As the order of the modulation scheme increases, the corresponding normalized throughput increases as well, but naturally, at the expense of a degraded BER performance. However, it may also be seen that due to using the same MIMO antenna setup, i.e. the same number of Rx antennas, the diversity gains are identical in all the four

scenarios.

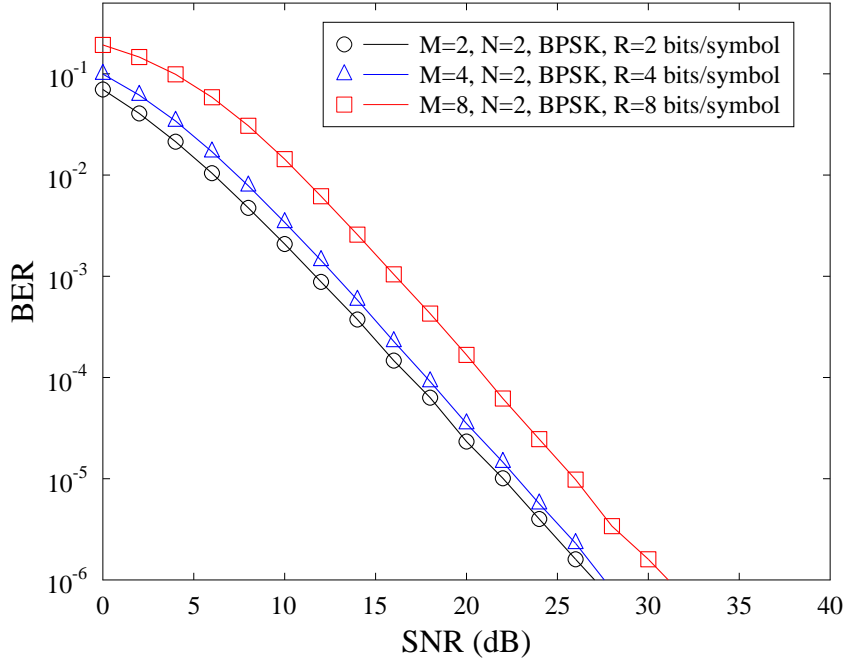


Figure 2.4: Achievable BER performance of a SDM/V-BLAST MIMO system of Fig. 2.1 associated with $N = 2$ Rx antennas and $M = 2, 4$ and 8 Tx antennas. BPSK signalling is adopted. All other system parameters were summarized in Table 2.1.

Fig. 2.4 shows the effects of increasing the number of Tx antennas on the system's BER performance associated with the specific system configuration of MIMO($M, 2$, BPSK). It may be seen from Fig. 2.4 that as the number of Tx antennas increases, the throughput increases at the expense of a BER performance degradation. However, we may also find that even though the BER performances are different for the three different configurations, the slopes of their BER curves are the same, implying that the same diversity gain may be achieved by these three configurations. Therefore, we may confirm that in SDM/V-BLAST MIMO systems, increasing the number of Tx antennas has no effects on the attainable diversity gain of the system.

As it has been mentioned before that in SDM/V-BLAST MIMO systems, a diversity gain may only be achieved at receiver side by employing multiple Rx antennas. Fig. 2.5 shows the effects of employing various numbers of Rx antennas on the performance of the MIMO associated with the configuration of MIMO($2, N$, BPSK), with $N \in \{2, 4, 8\}$ and at a throughput of $R = 2$ [bits/symbol]. It may be seen from Fig. 2.5 that as the number of Rx antennas increases, the slope of the BER curve becomes sharper, implying that a higher diversity gain may be achieved. However, it may also be observed that the performance gain becomes smaller, as the number of Rx antennas keeps on increasing. To be more explicit, by changing the number of Rx antennas from $N = 2$ to $N = 4$, the system's diversity gain is significantly increased and an SNR gain of over 15 dB

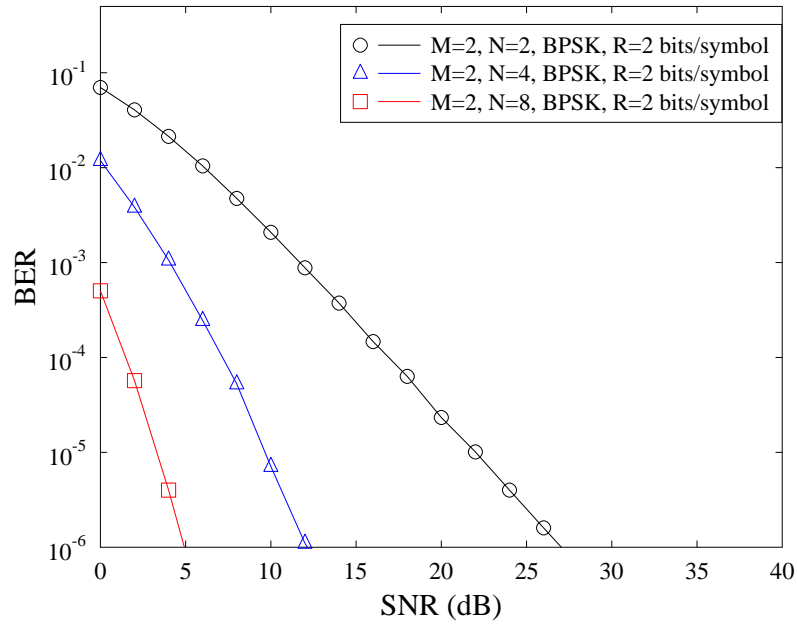


Figure 2.5: Achievable BER performance of a SDM/V-BLAST MIMO system of Fig. 2.1 associated with $M = 2$ Tx antennas and $N = 2, 4$ and 8 Rx antennas. BPSK signalling is adopted. All other system parameters were summarized in Table 2.1.

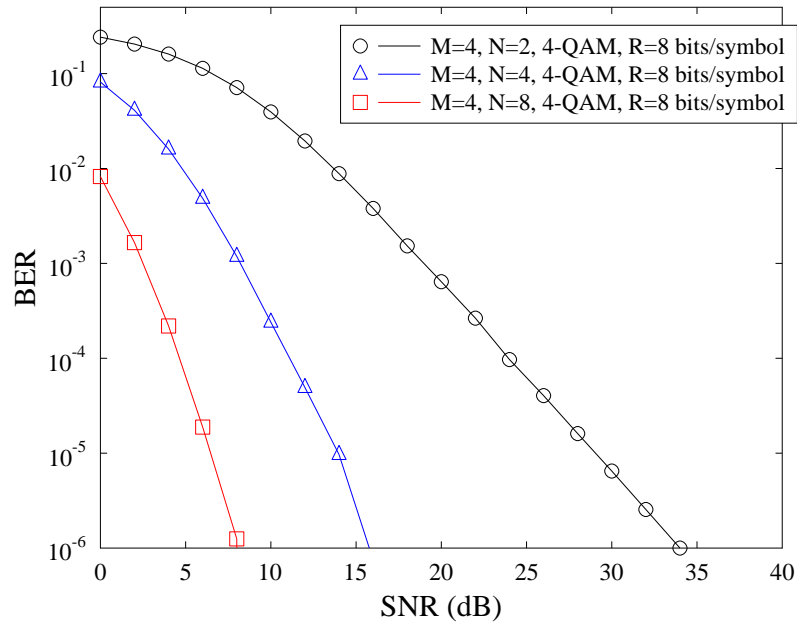


Figure 2.6: Achievable BER performance of a SDM/V-BLAST MIMO system of Fig. 2.1 associated with $M = 4$ Tx antennas and $N = 2, 4$ and 8 Rx antennas. 4-QAM signalling is adopted. All other system parameters were summarized in Table 2.1.

is achieved at the BER of 10^{-6} . However, when the number of Rx antennas is further increased to $N = 8$, the diversity gain improvement becomes less obvious and the SNR gain is reduced to less than 8 dB. Additionally, the effects of increasing the number of Rx antennas at receiver on the diversity gain of the MIMO system MIMO(4, N , 4-QAM) are shown in Fig. 2.6, where it may also be seen that increasing the number of Rx antennas may achieve an improved receive diversity gain, while imposing a higher hardware complexity, including an increased detection complexity.

2.2 Three-Stage Serial-Concatenated Turbo Coded SDM/V-BLAST Systems

2.2.1 System Overview

In Section 2.1.1, uncoded SDM/V-BLAST MIMO systems were introduced. However, it may be seen that without the aid of a channel coding scheme, SDM/V-BLAST MIMO systems fail to achieve a near-capacity performance. As a result, in this section, a powerful three-stage serial-concatenated turbo coding scheme is invoked for improving the performance of SDM/V-BLAST MIMO systems. The corresponding structure of this three-stage serial-concatenated turbo encoder and decoder invoked for a SDM/V-BLAST MIMO system is shown in Fig. 2.7. We consider a frequency-flat Rayleigh fading environment. Let i denote the SDM/V-BLAST symbol vector index. At the transmitter, the binary source information bits $\{b\}$ are firstly encoded by a half-rate RSC outer encoder and interleaved by a random interleaver Π_1 . Then the interleaved bits $\{u_1\}$ are encoded by a low-complexity memory-1 URC encoder [6], resulting in the bit sequence $\{x_2\}$, which are further interleaved by a second random interleaver Π_2 . Here, the reason for incorporating a URC is to allow the system to beneficially spread the *extrinsic* information across the iterative decoder components. As a benefit, a vanishingly low BER may be attained [1, 119]. At the SDM/V-BLAST modulator, the RSC-URC encoded bits $\{u\}$ are modulated, mapped and transmitted, which may be expressed by the equivalent MIMO system model formulated in Eq. (2.1).

The structure of the three-stage serial-concatenated turbo coding aided SDM/V-BLAST receiver is illustrated in Fig. 2.7, where it may be seen that the soft-input soft-output decoders and symbol-to-bit demapper of the receiver iteratively exchange soft extrinsic information in the form of Log Likelihood Ratios (LLRs). To be more explicit, the operations of the iterative three-stage serial-concatenated decoder/demapper may be divided into two parts, namely, the inner iterations and outer iterations. Within an inner iteration, the SDM/V-BLAST soft demapper shown in Fig. 2.7 firstly receives the transmitted signals over the MIMO channel and then combines the signals with the extrinsic information output by the URC decoder. Meanwhile, the URC decoder of Fig. 2.7 receives the extrinsic information both from the MIMO soft-demapper and from the RSC decoder, and also generates the extrinsic information for its neighbour blocks, i.e. for both the MIMO soft-demapper and for the RSC decoder. On the other hand, within each outer iteration, the RSC decoder

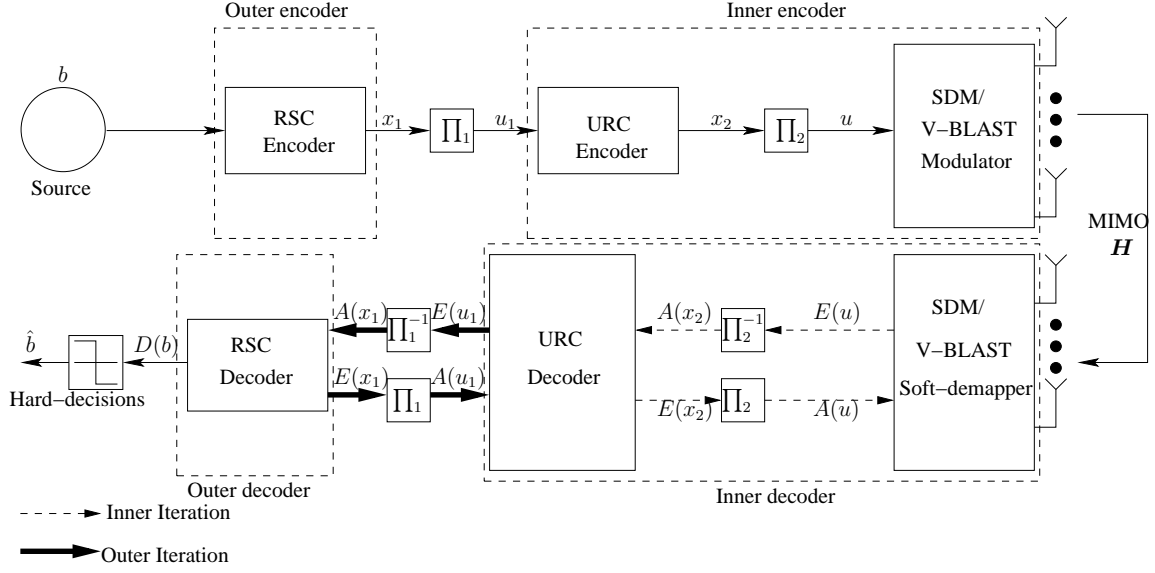


Figure 2.7: The structure of three-stage serial-concatenated turbo encoder/decoder for a SDM/V-BLAST MIMO system.

of Fig. 2.7 receives its extrinsic information from the URC decoder of Fig. 2.7 and generates the estimates of the decoded information bits after all the outer iterations have been completed. Here, let us denote the numbers of inner iterations and outer iterations as I_{in} and I_{out} , respectively. Since I_{in} iterations occur per outer iteration, the total number of iterations implemented by the three-stage serial-concatenated receiver becomes $I_{in} \cdot I_{out}$.

Again, we consider the SDM/V-BLAST MIMO system of Fig. 2.7 relying on M Tx antennas and N Rx antennas for communication in a frequency-flat Rayleigh fading environment. Given that the number of bits per \mathcal{L} – PSK/QAM symbol is $BPS = \log_2(\mathcal{L})$, the number of bits per block may be expressed as $BPB = M \cdot BPS$. At the MIMO soft-demapper of Fig. 2.7, upon obtaining the *a priori* LLRs $\{L_a(u_k)\}_{k=1}^{BPB}$ from the URC decoder, where $\{u_k\}_{k=1}^{BPB}$ indicates the corresponding bits that are mapped to the symbol vector $s(i)$, the *a posteriori* LLRs produced by the ML MIMO soft-demapper¹ are expressed as [122]

$$L_p(u_k) = L_p(k) = \ln \frac{\sum_{s^n \in \{s_{u_k=1}\}} \exp(p_n)}{\sum_{s^n \in \{s_{u_k=0}\}} \exp(p_n)}, \quad (2.6)$$

where $\{s_{u_k=1}\}$ and $\{s_{u_k=0}\}$ represent the \mathcal{L} -QAM/PSK symbol vector sets associated with the corresponding bit $u_k = 1$ and $u_k = 0$, respectively. The probability metrics $\{p_n\}_{n=1}^{\mathcal{L}^M}$ for the legitimate \mathcal{L} -QAM/PSK symbol vectors $\{s^n\}_{n=1}^{\mathcal{L}^M}$ are given as

$$p_n = -\frac{\|\mathbf{y}(i) - \mathbf{H}s^n\|^2}{N_0} + \sum_{k=1}^{BPB} \tilde{u}_k L_a(u_k), \quad (2.7)$$

¹For large MIMO systems, we may opt for using reduced-complexity near-optimum detection schemes, e.g. the K-best sphere detector [120, 121], to avoid the exponentially increasing complexity imposed by the ML detector.

where $\{\tilde{u}_k\}_{k=1}^{\text{BPP}}$ indicates the corresponding bits that are mapped to the specific symbol vector s^n .

2.2.2 Simulation Results

In this section, the achievable performance of the three-stage serial-concatenated turbo coding aided SDM/V-BLAST MIMO system of Fig. 2.7 is presented. Again, a frequency-flat Rayleigh fading environment was considered. An interleaver length of 10^6 bits was used by the pair of random interleavers in the three-stage serial-concatenated turbo encoder/decoder of Fig. 2.7. The binary generator polynomials of the RSC encoder were $G_{RSC} = [1, 0, 1]_2$ and $G_{RSC}^r = [1, 1, 1]_2$, while those of the URC encoder were $G_{URC} = [1, 0]_2$ and $G_{URC}^r = [1, 1]_2$, where G_{RSC}^r and G_{URC}^r indicated the feedback polynomials of the RSC and URC encoders, respectively. The average transmitted symbol energy was normalised to unity. Therefore, the SNR was given by $\frac{1}{N_0}$, with N_0 being the AWGN power. A SDM/V-BLAST MIMO system associated with M Tx antennas, N Rx antennas, and employing \mathcal{L} -PSK/QAM may be represented as $\text{MIMO}(M, N, \mathcal{L}-\text{PSK/QAM})$. Three configurations were considered in this section, which were MIMO(2, 2, BPSK), MIMO(4, 2, 4-QAM) and MIMO(4, 4, 4-QAM). The system parameters of the three-stage serial-concatenated turbo coding aided SDM/V-BLAST MIMO system of Fig. 2.7 are summarized in Table 2.2.

Table 2.2: System parameters of the three-stage serial-concatenated turbo coding aided SDM/V-BLAST MIMO system of Fig. 2.7.

Number of Tx antennas	M
Number of Rx antennas	N
Modulation	\mathcal{L} -QAM or \mathcal{L} -PSK
Channels	Frequency-flat Rayleigh fading
Detector	ML MIMO soft-demapper of Eq. (2.6)
Interleaver block-length	10^6 bits
Outer channel code	Half-rate RSC
Generator polynomials	$(G_{RSC}^r, G_{RSC}) = (7, 5)_8$
Precoder	URC
Number of inner iterations	I_{in}
Number of outer iterations	I_{out}

2.2.2.1 MIMO(2, 2, BPSK)

The EXIT chart [1] is adopted as a tool for predicting the convergence behaviour of the iterative decoder. This is achieved by examining the evolution of the input/output mutual information between the inner and outer decoders [123]. To be more explicit, an EXIT chart is said to have a closed tunnel when the EXIT curves of the inner and outer decoders intersect each other. For example, in

Fig. 2.8, when we have $\text{SNR} = -3.8 \text{ dB}$, the EXIT curves of the half-rate RSC decoder and of the MIMO Demapper-URC decoder are intersected, hence a closed tunnel is experienced. In this case, a high BER is expected, because the iterative decoding trajectory is prevented from reaching the point of perfect convergence to the $(1.0, 1.0)$ at the top-right-hand corner of the EXIT chart. This may be seen from the corresponding BER performance shown in Fig. 2.9, where at $\text{SNR} = -3.8 \text{ dB}$, we observe that almost no iteration gain is achieved and a BER in excess of 0.1 is obtained. By contrast, if an open tunnel exists between the EXIT curves of the inner and outer decoders, the decoding trajectory is capable of reaching the point of perfect convergence at $(1.0, 1.0)$ in the EXIT chart, where a vanishingly low BER may be achieved. This may be seen from the EXIT chart shown in Fig. 2.8, where at $\text{SNR} = -3.2 \text{ dB}$, an open tunnel exists between the EXIT curves of the half-rate RSC decoder and the MIMO Demapper-URC decoder of Fig. 2.7, and the Monte-Carlo simulation based decoding trajectory is capable of reaching the $(1.0, 1.0)$ point within $I_{out} = 9$ outer iterations, implying that a vanishingly low BER can be achieved and any potential error flow can be eliminated [1]. This may be confirmed by the corresponding BER performance shown in Fig. 2.9, where a vanishingly low BER is observed at $\text{SNR} = -3.2 \text{ dB}$. Additionally, in order to clearly show the effects of SNR on the EXIT chart characteristics of the three-stage serial-concatenated turbo coding aided SDM/V-BLAST MIMO system, Fig. 2.10 is provided, which shows that as the

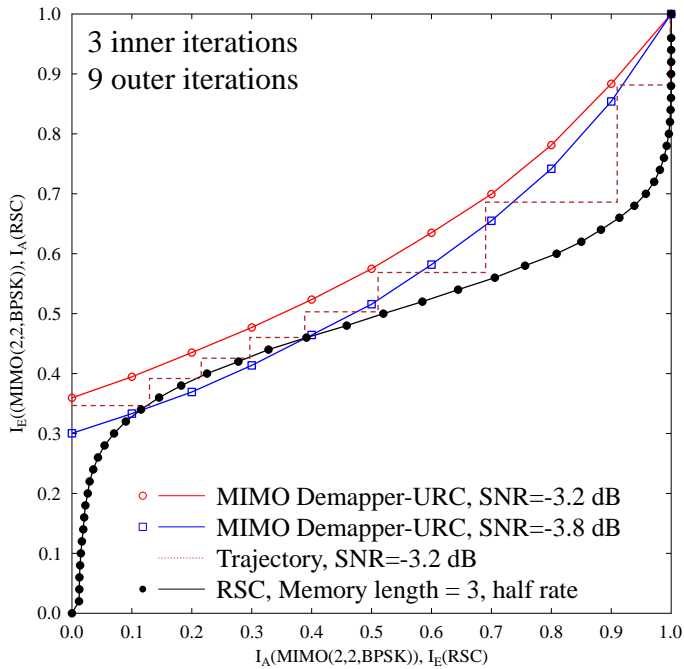


Figure 2.8: EXIT chart of the three-stage serial-concatenated turbo coding aided SDM/V-BLAST MIMO system of Fig. 2.7 associated with the configuration of $\text{MIMO}(2, 2, \text{BPSK})$ at an effective throughput of $R = 2$ bits/symbol. All other system parameters were summarized in Table 2.2. The corresponding BER curves are seen in Fig. 2.9.

SNR increases, the open tunnel between the half-rate RSC decode and the MIMO Demapper-URC decoder becomes wider.

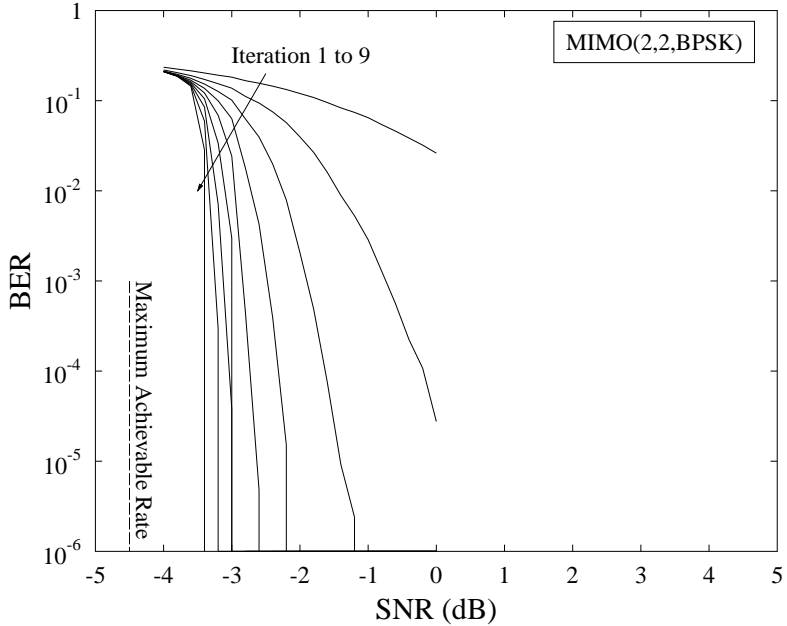


Figure 2.9: Achievable BER convergence of the three-stage serial-concatenated turbo coding aided SDM/V-BLAST MIMO system of Fig. 2.7 associated with the configuration of MIMO(2, 2, BPSK) at an effective throughput of $R = 2$ bits/symbol. All other system parameters were summarized in Table 2.2. The corresponding EXIT chart is seen in Fig. 2.8.

Fig. 2.9 depicts the corresponding achievable BER performance of the three-stage serial-concatenated turbo coding aided SDM/V-BLAST MIMO system associated with the configuration of MIMO(2, 2, BPSK), where it is seen that the system's BER performance improves, as the number of iterations increases. Additionally, when the number of iterations reaches $I_{out} = 9$, a 'turbo cliff' appears at approximately $\text{SNR} = -3.2$ dB, where a 'near-error-free' performance is achieved. This is in line with the conclusions obtained from the EXIT chart seen in Fig. 2.8. Furthermore, the maximum achievable rate² of MIMO(2, 2, BPSK) is provided in Fig. 2.9, where it may be seen that the SNR gap is about 1 dB between the SNR value required to attain an infinitesimally low BER by the system and the SNR value required for reaching the maximum achievable rate, implying that the system is indeed capable of attaining a near-capacity performance.

Our comparison between the achievable BER performance of both the uncoded and three-stage serial-concatenated turbo coded SDM/V-BLAST systems is shown in Fig. 2.11, where it may be seen that by employing the three-stage turbo coding scheme, the BER performance of

²The maximum achievable rate here is referred to as a SNR value where the corresponding EXIT curve of MIMO Demapper-URC decoder covers a lower region associated with an area that equals to coding rate of RSC codes [6].

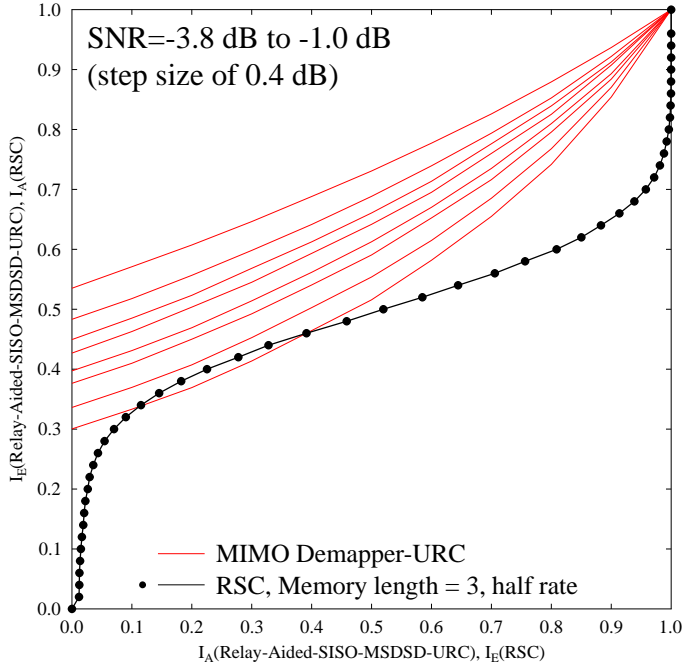


Figure 2.10: Effects of SNR on the EXIT chart characteristics of the three-stage serial-concatenated turbo coding aided SDM/V-BLAST MIMO system of Fig. 2.7 associated with the configuration of MIMO(2,2,BPSK) at an effective throughput of $R = 2$ bits/symbol. All other system parameters were summarized in Table 2.2.

MIMO(2,2,BPSK) is dramatically improved, although at the expense of a decreased bandwidth efficiency due to the redundancy introduced by the channel coding scheme as well as at the cost of imposing an increased receiver complexity. For example, the uncoded MIMO system is capable of achieving a BER of 10^{-6} at about SNR = 27 dB, while the three-stage turbo coded MIMO system is capable of attaining a vanishingly low BER at about SNR = -3.2 dB. Therefore, a performance gain of more than 30 dB is achieved by the latter. However, due to the 1/2 coding rate of the RSC code adopted, in order to convey the same number of information bits, the frame length of the coded MIMO system should be twice as long as that of the uncoded scenario. Additionally, it may also be noticed that the BER performance curves of the uncoded system and of the corresponding coded system exhibit a crossover (threshold) at about SNR = -3.6 dB. This phenomenon is in fact quite often observed in the performance comparison between channel coded and uncoded systems. The reason for a crossover is that a channel coding scheme may be deemed to have a time-diversity gain, which results in an improved error correction capability. However, when the number of errors within a block becomes higher than the number of errors that can be corrected, the channel decoder will be overwhelmed by these errors. In this case, the channel coding scheme makes an erroneous detection, which results in erroneous ‘corrected’ bits and in an increased BER. However, it may be worth mentioning that compared to the conventional channel coding schemes, such as Bose-Chaudhuri-Hocquenghem (BCH) and convolutional codes [9], the three-stage serial-concatenated

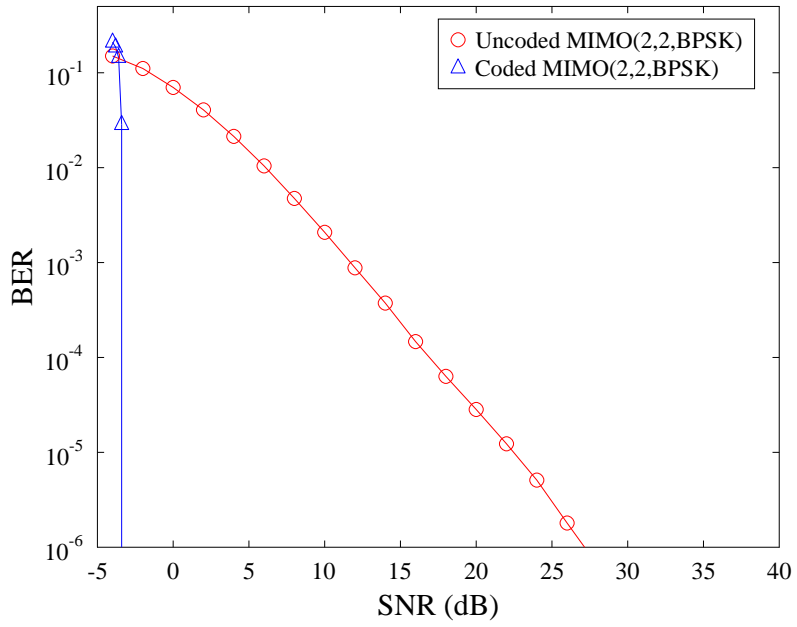


Figure 2.11: Achievable BER performance of the three-stage serial-concatenated turbo coding aided SDM/V-BLAST MIMO system of Fig. 2.7 associated with the configuration of MIMO(2,2,BPSK), in comparison to that of the corresponding uncoded system of Fig. 2.1. The throughputs of both systems are $R = 2$ bits/symbol. All other system parameters were summarized in Table 2.2.

turbo codes employed in this section exhibit a reduced crossover probability, hence implying an error correction improvement at low SNRs.

2.2.2.2 MIMO(4,2,4-QAM)

Our investigations of the three-stage serial-concatenated turbo coding aided SDM/V-BLAST MIMO system of Fig. 2.7 relying on the configuration of MIMO(4,2,4-QAM) were commenced with its EXIT chart analysis and further results are also depicted in Fig. 2.12. It may be seen that an open tunnel exists between the EXIT curves of the inner MIMO soft-demapper-URC decoder and the RSC outer decoder at about SNR= 4 dB. Additionally, the Monte-Carlo simulation based staircase shaped decoding trajectory, which closely matches the EXIT chart curves, was also provided at the same SNR= 4 dB. The trajectory shows that the three-stage serial-concatenated turbo coding aided MIMO(4,2,4-QAM) system is capable of reaching the point of perfect convergence of (1.0, 1.0) at about SNR= 4 dB, with the aid of $I_{in} = 3$ inner iterations and $I_{out} = 5$ outer iterations.

Fig. 2.13 illustrates the achievable BER performance of the three-stage serial-concatenated turbo coding aided SDM/V-BLAST MIMO system of Fig. 2.7 associated with the configuration of MIMO(4,2,4-QAM), where it can be seen that as the number of outer iterations increases from 1 to

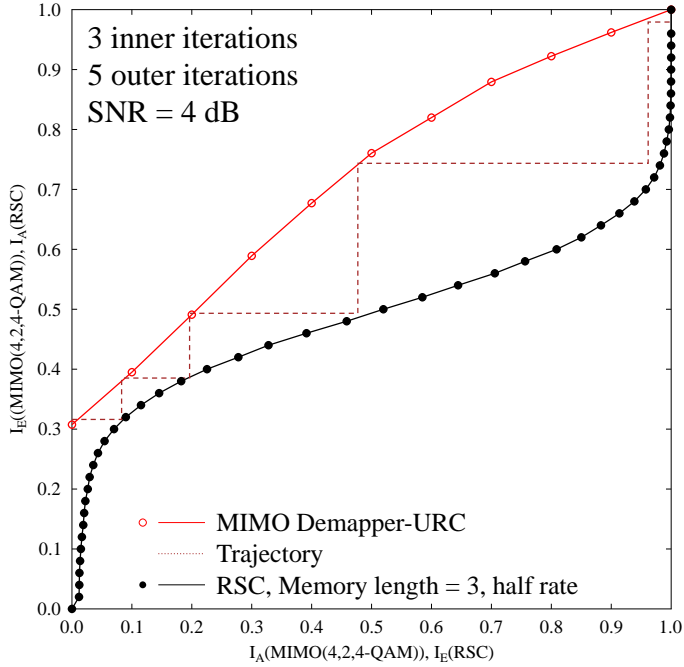


Figure 2.12: EXIT chart of the three-stage serial-concatenated turbo coding aided SDM/V-BLAST MIMO system of Fig. 2.7 associated with the configuration of MIMO(4, 2, 4-QAM) at an effective throughput of $R = 8$ bits/symbol. All other system parameters were summarized in Table 2.2. The corresponding BER curves are seen in Fig. 2.13.

5, the system's BER performance is substantially improved. To be more explicit, when the number of iterations reaches $I_{out} = 5$, a ‘turbo cliff’ appears at about SNR = 4 dB, where an infinitesimally low BER is achieved. This is in line with the characteristics of the EXIT chart shown in Fig. 2.12. Furthermore, the maximum achievable rate of MIMO(4, 2, 4-QAM) is also provided in Fig. 2.13, where it can be seen that the SNR gap between the SNR value required by the system to attain an infinitesimally low BER and that needed for approaching the maximum achievable rate is just over 3 dB, implying that the system is indeed capable of achieving a near-capacity performance.

Fig. 2.14 compares the achievable BER performance of both the three-stage turbo coded and uncoded MIMO(4, 2, 4-QAM) systems, where it is seen that similar to the case of MIMO(2, 2, BPSK), the three-stage turbo coding scheme significantly improves the achievable BER performance, achieving a SNR gain of more than 30 dB at the BER of 10^{-6} , at a cost of a reduced bandwidth efficiency and an increased computational complexity. Additionally, the classic crossover point for the coded and uncoded BER curves may be found at about SNR = 3.2 dB.

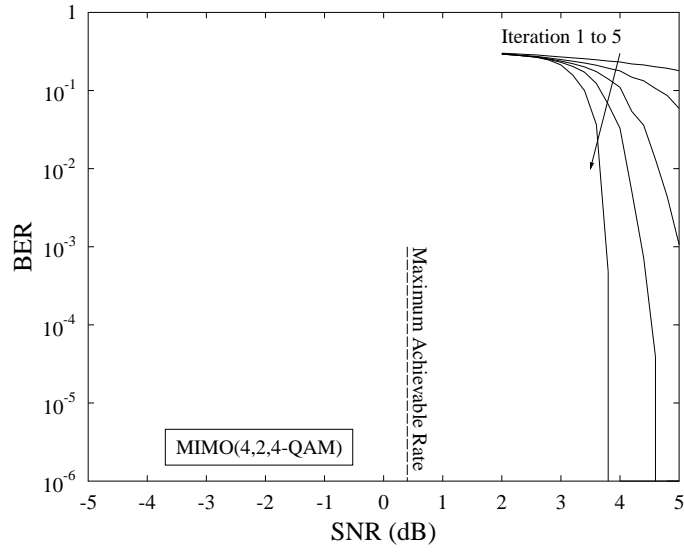


Figure 2.13: Achievable BER convergence of the three-stage serial-concatenated turbo coding aided SDM/V-BLAST MIMO system of Fig. 2.7 associated with the configuration of MIMO(4,2,4-QAM) at an effective throughput of $R = 8$ bits/symbol. All other system parameters were summarized in Table 2.2. The corresponding EXIT chart is seen in Fig. 2.12.

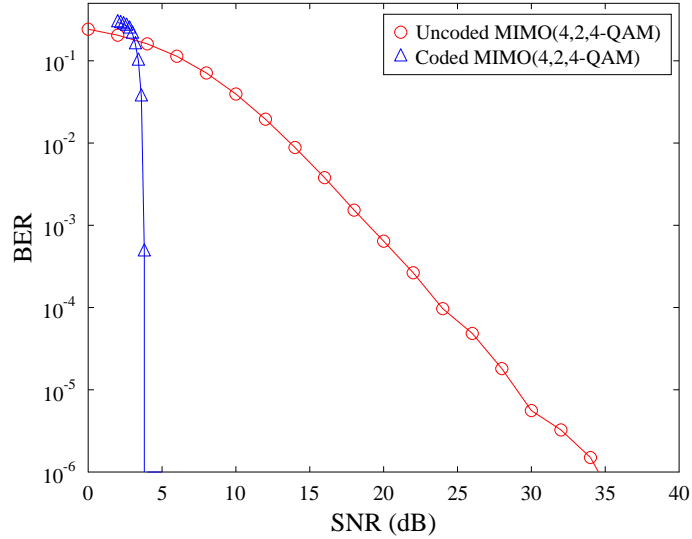


Figure 2.14: Achievable BER performance of the three-stage serial-concatenated turbo coding aided SDM/V-BLAST MIMO system of Fig. 2.7 associated with the configuration of MIMO(4,2,4-QAM), in comparison to that of the corresponding uncoded system of Fig. 2.1. The throughputs of both systems are $R = 8$ bits/symbol. All other system parameters were summarized in Table 2.2.

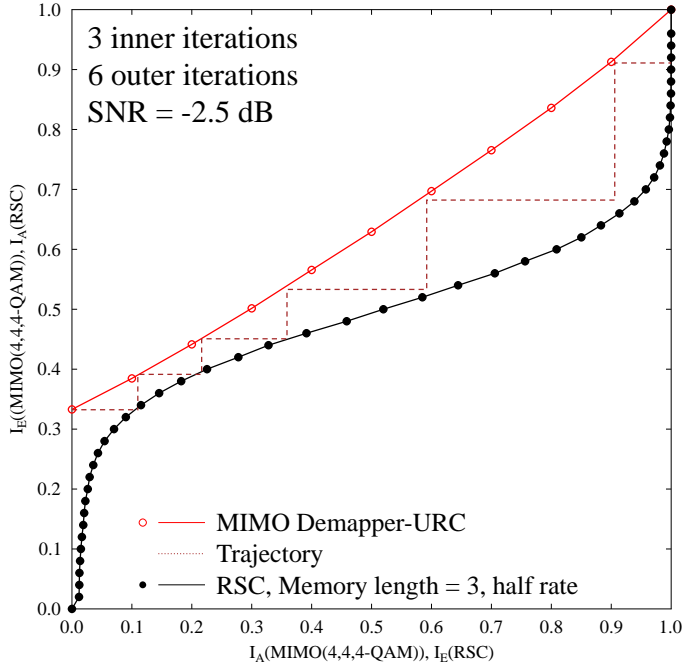


Figure 2.15: EXIT chart of the three-stage serial-concatenated turbo coding aided SDM/V-BLAST MIMO system of Fig. 2.7 associated with the configuration of MIMO(4,4,4-QAM) at an effective throughput of $R = 8$ bits/symbol. All other system parameters were summarized in Table 2.2. The corresponding BER curves are seen in Fig. 2.16.

2.2.2.3 MIMO(4,4,4-QAM)

The EXIT chart of the three-stage serial-concatenated turbo coding aided MIMO(4,4,4-QAM) scheme is depicted in Fig. 2.15. It may be seen that an open tunnel exists between the EXIT curves of the inner MIMO soft-demapper-URC decoder and the RSC outer decoder at about $\text{SNR} = -2.5$ dB. Additionally, the Monte-Carlo simulation based staircase shaped decoding trajectory, which closely matches the EXIT chart curves, is also provided at about $\text{SNR} = -2.5$ dB. The trajectory shows that the three-stage serial-concatenated turbo coding aided MIMO(4,4,4-QAM) system is capable of reaching the point of perfect convergence of $(1.0, 1.0)$ at about $\text{SNR} = -2.5$ dB, with the aid of $I_{in} = 3$ inner iterations and $I_{out} = 6$ outer iterations.

Fig. 2.16 presents the achievable BER performance of the three-stage serial-concatenated turbo coding aided SDM/V-BLAST MIMO system of Fig. 2.7 associated with the configuration of MIMO(4,4,4-QAM), where it may be seen that as the number of outer iterations increases from 1 to 6, the system's BER performance may be improved. More explicitly, when the number of iterations reaches $I_{out} = 6$, a ‘turbo cliff’ appears at about $\text{SNR} = -2.5$ dB, where an infinitesimally low BER may be achieved. This is in line with the characteristics of the EXIT chart shown in Fig. 2.15. Furthermore, the maximum achievable rate of the MIMO(4,2,4-QAM) is also depicted

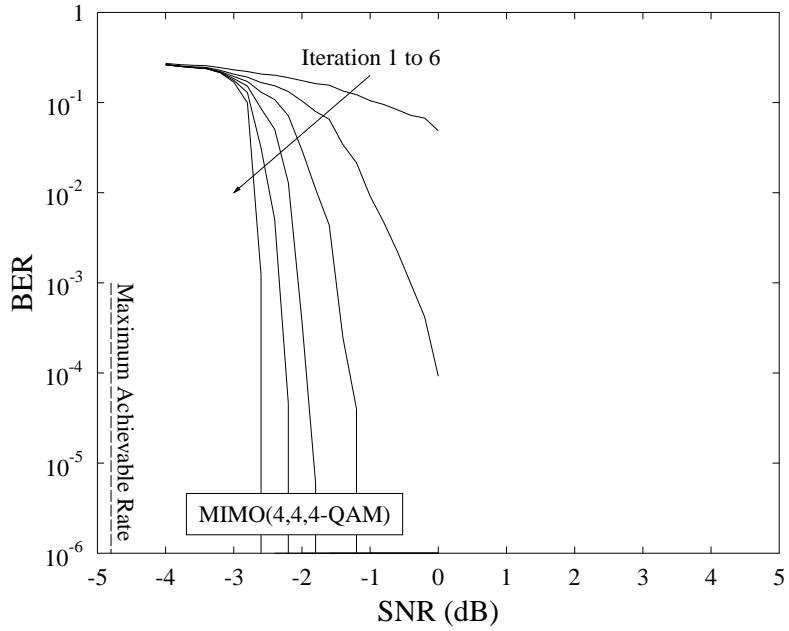


Figure 2.16: Achievable BER convergence of the three-stage serial-concatenated turbo coding aided SDM/V-BLAST MIMO system of Fig. 2.7 associated with the configuration of MIMO(4,4,4-QAM) at an effective throughput of $R = 8$ bits/symbol. All other system parameters were summarized in Table 2.2. The corresponding EXIT chart is seen in Fig. 2.15.

in Fig. 2.16, which shows that the SNR gap between the SNR value required by the system to attain an infinitesimally low BER and the SNR value required for approaching the maximum achievable rate is just over 2 dB, again implying that this system is indeed capable of achieving a near-capacity performance.

2.3 Uncoded Coherent STSK

2.3.1 System Overview

In the previous section, the classic SDM/V-BLAST MIMO system has been reviewed, where it has been recognised that this type of MIMO systems are mainly designed for achieving a multiplexing gain. In this section, a novel coherent MIMO scheme, known as the Coherent STSK (CSTSK) MIMO system is introduced, which is capable of achieving both a multiplexing gain and a diversity gain, as well as offering a high degree of design freedom. Let us define the configuration of the generic CSTSK MIMO system as $\text{CSTSK}(M, N, T, Q, \mathcal{L} - \text{PSK/QAM})$, where M and N indicate the number of Tx antennas and Rx antennas, respectively, while T denotes the number of time slots occupied by the CSTSK signal block and Q is the number of dispersion matrices employed. Let i

denote the CSTSK block index. Again, a frequency-flat Rayleigh fading environment is considered.

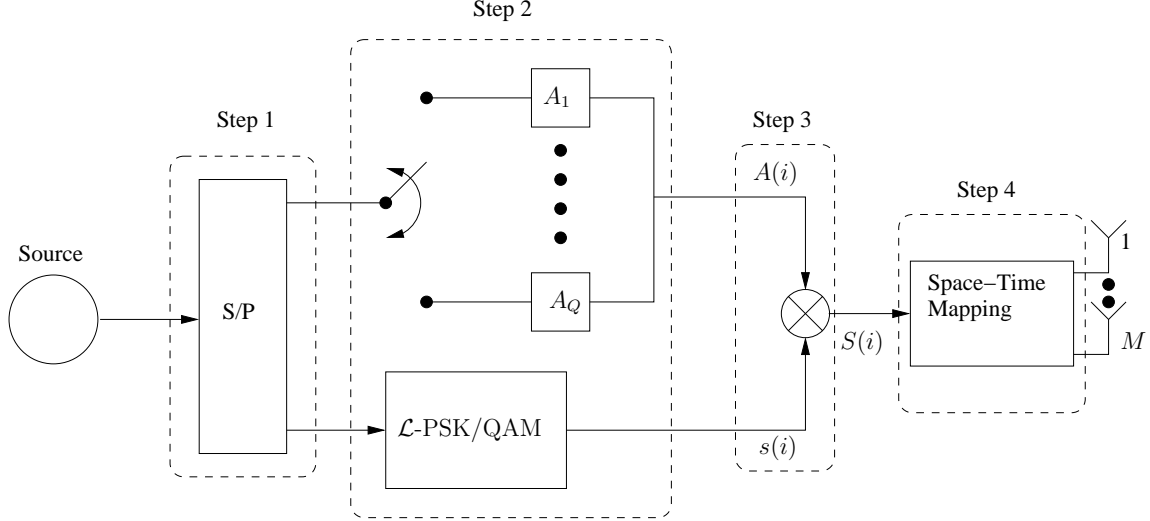


Figure 2.17: Transmitter structure of the CSTSK based MIMO scheme [5].

The structure of a CSTSK transmitter is shown in Fig. 2.17, where it can be seen that the STSK encoding process may be divided into four steps:

Step 1) The sequence of source bits is firstly converted to two parallel bit sequences. Specifically, every $\text{BPB} = \log_2(Q) + \log_2(\mathcal{L})$ source bits of Fig. 2.17 is divided into a pair of parallel sub-blocks, containing $\log_2(Q)$ source bits and $\log_2(\mathcal{L})$ source bits, respectively.

Step 2) For the i th block, the first $\log_2(Q)$ bits are used for choosing a single dispersion matrix $A(i)$ from the Q pre-assigned dispersion matrices $\{A_q \in \mathbb{C}^{M \times T}, 1 \leq q \leq Q\}$, while the remaining $\log_2(\mathcal{L})$ bits are mapped to a complex-valued symbol $s(i) \in \{s_l, 1 \leq l \leq \mathcal{L}\}$ of a conventional modulation scheme, such as \mathcal{L} -PSK/QAM [5, 21].

Step 3) A total number of $\log_2(Q \cdot \mathcal{L})$ source bits are thus mapped to a single STSK signalling block $S(i) \in \mathbb{C}^{M \times T}$, which may be expressed as

$$S(i) = s(i)A(i). \quad (2.8)$$

Step 4) Finally, the STSK signalling blocks are mapped to the corresponding Tx antennas and time slots by the space-time mapper of Fig. 2.17. More explicitly, the m th row of $S(i)$ is transmitted through the m th Tx antenna, and the t th column of $S(i)$ is transmitted during the t th time slot.

In a STSK based MIMO system, each block of signal is transmitted within T time slots, and the average transmission power in each time slot is normalized to unity. Therefore, the dispersion matrices are designed to obey the power constraints of $\text{tr}[A_q^H A_q] = T$ for $1 \leq q \leq Q$ [5, 21], where $(\cdot)^H$ and $\text{tr}[\cdot]$ denote the conjugate transpose and trace operators, respectively, while the normalized throughput R per time-slot of this STSK system is given by

$$R = \frac{\log_2(Q \cdot \mathcal{L})}{T} \text{ [bits/symbol].} \quad (2.9)$$

For instance, if the CSTSK MIMO system of Fig. 2.17 employs a signalling block size of $\text{BPB} = \log_2(Q \cdot \mathcal{L}) = 3$ bits and uses $T = 2$ time slots for transmitting one signalling block, then the corresponding normalized throughput is given by $R = 1.5$ bits/symbol. A range of legitimate combinations of the number of dispersion matrices Q and the constellation size \mathcal{L} are listed in Table 2.3, given the normalized throughput of $R = 1.5$ bit/symbol. Let us now consider the CSTSK system associated with the configuration of CSTSK(2, 2, 2, 4, BPSK), implying that we have $Q = 4$ and $\mathcal{L} = 2$. Then, if the i th block of input source bits are “011”, according to Table 2.3, the resultant CSTSK signalling block becomes $\mathbf{S}(i) = s(i)\mathbf{A}(i) = e^{j\pi} \cdot \mathbf{A}_2$.

Input Bits	$Q = 1, \mathcal{L} = 8$		$Q = 2, \mathcal{L} = 4$		$Q = 4, \mathcal{L} = 2$		$Q = 8, \mathcal{L} = 1$	
	$\mathbf{A}(i)$	$s(i)$	$\mathbf{A}(i)$	$s(i)$	$\mathbf{A}(i)$	$s(i)$	$\mathbf{A}(i)$	$s(i)$
000	\mathbf{A}_1	1	\mathbf{A}_1	1	\mathbf{A}_1	1	\mathbf{A}_1	1
001	\mathbf{A}_1	$e^{j\frac{\pi}{4}}$	\mathbf{A}_1	$e^{j\frac{\pi}{2}}$	\mathbf{A}_1	$e^{j\pi}$	\mathbf{A}_2	1
010	\mathbf{A}_1	$e^{j\frac{2\pi}{4}}$	\mathbf{A}_1	$e^{j\frac{2\pi}{2}}$	\mathbf{A}_2	1	\mathbf{A}_3	1
011	\mathbf{A}_1	$e^{j\frac{3\pi}{4}}$	\mathbf{A}_1	$e^{j\frac{3\pi}{2}}$	\mathbf{A}_2	$e^{j\pi}$	\mathbf{A}_4	1
100	\mathbf{A}_1	$e^{j\frac{4\pi}{4}}$	\mathbf{A}_2	1	\mathbf{A}_3	1	\mathbf{A}_5	1
101	\mathbf{A}_1	$e^{j\frac{5\pi}{4}}$	\mathbf{A}_2	$e^{j\frac{\pi}{2}}$	\mathbf{A}_3	$e^{j\pi}$	\mathbf{A}_6	1
110	\mathbf{A}_1	$e^{j\frac{6\pi}{4}}$	\mathbf{A}_2	$e^{j\frac{2\pi}{2}}$	\mathbf{A}_4	1	\mathbf{A}_7	1
111	\mathbf{A}_1	$e^{j\frac{7\pi}{4}}$	\mathbf{A}_2	$e^{j\frac{3\pi}{2}}$	\mathbf{A}_4	$e^{j\pi}$	\mathbf{A}_8	1

Table 2.3: Example of the CSTSK modulation scheme of Fig. 2.17 with Q dispersion matrices and the constellation size of \mathcal{L} , where $Q \cdot \mathcal{L} = 8$ and \mathcal{L} -PSK signalling is adopted as the conventional modulation scheme [5].

At the receiver, the received signal block $\mathbf{Y}(i) \in \mathbb{C}^{N \times T}$ of this CSTSK system may be expressed as [5, 21]

$$\mathbf{Y}(i) = \mathbf{H}\mathbf{S}(i) + \mathbf{V}(i), \quad (2.10)$$

where $\mathbf{H} \in \mathbb{C}^{N \times M}$ is the corresponding MIMO channel matrix, whose elements obey the complex-valued Gaussian distribution of zero mean and unit variance $\mathcal{CN}(0, 1)$, while $\mathbf{V}(i) \in \mathbb{C}^{N \times T}$ is the Additive White Gaussian Noise (AWGN) matrix, whose components obey $\mathcal{CN}(0, N_0)$ with N_0 being the corresponding AWGN variance.

Let us now introduce the detection scheme of the CSTSK scheme of Fig. 2.17. As one of the most popular signal detection algorithms, the basic idea of the ML detection algorithm is to choose the most probably transmitted symbol block by comparing the Euclidean distances between the received signal block and every legitimate transmitted symbol blocks in the entire legitimate transmitted symbol block set. By applying the vector stacking operation $\text{vec}(\cdot)$, to the received signal block $\mathbf{Y}(i)$ in Eq. (2.10), the equivalent system model can be expressed as [5, 21]

$$\bar{\mathbf{y}}(i) = \bar{\mathbf{H}}\mathbf{Y}\mathbf{k}(i) + \bar{\mathbf{v}}(i), \quad (2.11)$$

where we have:

$$\bar{\mathbf{y}}(i) = \text{vec}(\mathbf{Y}(i)) \in \mathbb{C}^{NT \times 1}, \quad (2.12)$$

$$\bar{\mathbf{H}} = \mathbf{I}_T \otimes \mathbf{H} \in \mathbb{C}^{NT \times MT}, \quad (2.13)$$

$$\mathbf{Y} = [\text{vec}(\mathbf{A}_1) \text{vec}(\mathbf{A}_2) \cdots \text{vec}(\mathbf{A}_Q)] \in \mathbb{C}^{MT \times Q}, \quad (2.14)$$

$$\bar{\mathbf{v}}(i) = \text{vec}(\mathbf{V}(i)) \in \mathbb{C}^{NT \times 1}, \quad (2.15)$$

in which \mathbf{I}_T is the $(T \times T)$ -element identity matrix and \otimes represents the Kronecker product, while the equivalent transmitted signal vector $\mathbf{k}(i) \in \mathbb{C}^{Q \times 1}$ may be formulated as

$$\mathbf{k}(i) = [\underbrace{0 \cdots 0}_{q-1} s(i) \underbrace{0 \cdots 0}_{Q-q}]^T. \quad (2.16)$$

Explicitly, the q th element of $\mathbf{k}(i)$ in Eq. (2.16) is the conventionally modulated signal $s(i)$ and its remaining elements are zero, where q indicates the corresponding dispersion matrix that is activated for the i th STSK block. Since the constellation size is \mathcal{L} and the number of the dispersion matrices is Q , the total number of the legitimate transmit signal vectors $\mathbf{k}(i)$ is $\mathcal{L} \cdot Q$. Therefore, we have

$$\mathbf{k}(i) \in \mathbb{K} = \{\mathbf{k}_{q,l}, 1 \leq q \leq Q, 1 \leq l \leq \mathcal{L}\} \quad (2.17)$$

with

$$\mathbf{k}_{q,l} = [\underbrace{0 \cdots 0}_{q-1} s_l \underbrace{0 \cdots 0}_{Q-q}]^T, \quad (2.18)$$

where s_l denotes the l th symbol in the \mathcal{L} -point constellation of the conventional \mathcal{L} -PSK/QAM modulation scheme.

Similar to the SM based system of [18], the ICI has been completely eliminated in the above CSTSK system, as clearly seen from Eq. (2.11). Thus, the receiver complexity can be significantly reduced [18] and single-antenna-based ML detection can be adopted at a low complexity [5]. Let us consider a generic fading environment, where the channel matrix changes for every signal block, and the channel matrix during the i th signal block period is denoted by $\bar{\mathbf{H}}(i)$. Then the corresponding ML estimates (\hat{q}, \hat{l}) may be formulated as

$$(\hat{q}, \hat{l}) = \arg \min_{1 \leq q \leq Q, 1 \leq l \leq \mathcal{L}} \|\bar{\mathbf{y}}(i) - \bar{\mathbf{H}}(i)\mathbf{Y}\mathbf{k}_{q,l}\|^2 \quad (2.19)$$

$$= \arg \min_{1 \leq q \leq Q, 1 \leq l \leq \mathcal{L}} \|\bar{\mathbf{y}}(i) - s_l (\bar{\mathbf{H}}(i)\mathbf{Y})_q\|^2, \quad (2.20)$$

where $(\bar{\mathbf{H}}(i)\mathbf{Y})_q$ represents the q th column of the matrix $\bar{\mathbf{H}}(i)\mathbf{Y}$.

2.3.2 Computational Complexity

In this section, the computational complexity of the CSTSK scheme of Fig. 2.17 is analyzed in terms of the number of real-valued multiplications required. The computational complexity imposed by the ML detection in the CSTSK scheme for both fast and slow fading may be expressed

by [5]

$$NTQ(4MT + 6\mathcal{L})/\log_2(Q \cdot \mathcal{L}) \quad (\text{fast fading}), \quad (2.21)$$

$$NTQ[(4MT + 4\mathcal{L})/\tau + 2\mathcal{L}]/\log_2(Q \cdot \mathcal{L}) \quad (\text{slow fading}), \quad (2.22)$$

where τ is referred to as an integer factor that quantifies the coherence time as $\tau \cdot T$ in slow fading environments [5]. Furthermore, if the value of τ equals to 1, the complexity becomes identical to that of the fast fading case, implying that we assume $\tau > 1$ in slow fading environments. More explicitly, according to Eq. (2.19), in fast fading environments, the ML detector of the CSTSK scheme is required to calculate $\bar{H}(i)\mathbf{Yk}_{q,l}$, $1 \leq q \leq Q$ and $1 \leq l \leq \mathcal{L}$, for each CSTSK block, with the corresponding complexity of $NTQ(4MT + 4\mathcal{L})/\log_2(Q \cdot \mathcal{L})$ out of the total ML detection complexity expressed in Eq. (2.21). However, in a slow fading situation, since the associated calculation can be reused within the channel's coherence time, the complexity may be reduced to $NTQ[(4MT + 4\mathcal{L})/\tau]/\log_2(Q \cdot \mathcal{L})$ out of the total ML detection complexity that is given in Eq. (2.22) [5]. Additionally, the complexity expressions of the SM/SSK scheme are also provided in [5], which are given by

$$6MN\mathcal{L}/\log_2(M \cdot \mathcal{L}) \quad (\text{fast fading}), \quad (2.23)$$

$$(4/\tau + 2)MN\mathcal{L}/\log_2(M \cdot \mathcal{L}) \quad (\text{slow fading}). \quad (2.24)$$

By comparing the above four equations, namely Eq. (2.21) to Eq. (2.24), it may be concluded that the SM/SSK scheme usually has a lower complexity than the CSTSK scheme. However, compared to the classic MIMO systems, such as SDM/V-BLAST, the complexity of the CSTSK MIMO system is significantly lower, because just like the SM/SSK scheme, it also benefits from the elimination of ICI [5]. Additionally, the ratio of the CSTSK's complexity in Eq. (2.21) over that of the SM/SSK shown in Eq. (2.23) is expressed by $TQ(4MT + 4\mathcal{L})/6M\mathcal{L}$. Based on this ratio, it can be seen that as the number of time slots T in the CSTSK scheme increases, the complexity ratio also increases. However, this also increases the attainable transmit diversity gain of the CSTSK MIMO system [5]. The SM/SSK scheme is of course still unable to attain any transmit diversity.

2.3.3 Maximum Achievable Diversity Order of CSTSK Systems

Generally, for a CSTSK MIMO system model, the maximum achievable diversity order can be formulated as [5]

$$N \cdot \min(M, T), \quad (2.25)$$

where $\min(M, T)$ corresponds to the achievable transmit diversity gain. This implies that as the CSTSK block duration T increases, the relative transmit diversity order will increase, assuming that the number of transmit antennas M is higher than or equal to the block duration T . In other words, increasing T beyond the value of M does not help achieve a higher diversity at all. On the

other hand, if the CSTSK block duration T is lower than M , the increase of M does not result in any improvement of the diversity gain. Moreover, according to Eq. (2.25), a smaller T may lead to a lower transmit diversity order, but it also results in a lower computational complexity and a high transmission rate, which constitutes an important trade-off for any communication system and further demonstrates the design flexibility of CSTSK [5].

2.3.4 Dispersion Matrix Generation

It can be seen from Fig. 2.17 that the choice of the dispersion matrix set $\{A_q, 1 \leq q \leq Q\}$ may have significant effects on the system's achievable performance [5,21]. In this section, we discuss how to generate the STSK dispersion-matrix set. We assume that the number of Tx and Rx antennas M and N as well as the number of time slots T have been fixed by hardware implementation considerations as well as according to other design requirements, such as the desired transmit diversity order.

Given the size Q of the dispersion matrix set, the design or generation of a near-optimum STSK dispersion matrix set was proposed in [5], which is based on a carefully conducted random search using the Objective Function (OF) of minimizing the so-called Pairwise Symbol Error Probability (PSEP). To elaborate a little further, the dispersion matrices $A_q, 1 \leq q \leq Q$, are first randomly generated as unitary matrices, which obey the power constraint of

$$\text{tr} [A_q^H A_q] = T, \quad 1 \leq q \leq Q, \quad (2.26)$$

hence leading to a unity average transmission power for each STSK symbol duration. Then these initial dispersion matrices are optimized using a random search algorithm to minimize the PSEP expressed as [124]

$$p(\mathbf{X} \rightarrow \hat{\mathbf{X}}) \leq \frac{1}{\det \left[\mathbf{I}_{TN} + \frac{E_s}{4N_0} \mathbf{R}_X \otimes \mathbf{I}_N \right]}, \quad (2.27)$$

where \mathbf{X} and $\hat{\mathbf{X}}$ are an arbitrary pair of the legitimate ‘codewords’ selected from the STSK ‘symbol’ set $\{s_l A_q, 1 \leq l \leq \mathcal{L}, 1 \leq q \leq Q\}$ having a size of $Q \cdot \mathcal{L}$. Furthermore, E_s denotes the symbol energy and N_0 the AWGN power, while we have $\mathbf{R}_X = (\mathbf{X} - \hat{\mathbf{X}})^H (\mathbf{X} - \hat{\mathbf{X}})$ and $\det[\cdot]$ denotes the matrix determinant operator.

We further propose the following alternative criterion for designing a near-optimum STSK dispersion matrix set. To be more specific, if \mathbf{R}_X has full rank in the PSEP expression, the error probability is determined by the minimum value of the determinant of \mathbf{R}_X [125]. As a result, by ensuring that \mathbf{R}_X has full rank, the STSK dispersion-matrix set may be optimized by maximizing the minimum-determinant d_{\min} of \mathbf{R}_X for any pair of legitimate codewords, where d_{\min} is the function of $A_q, 1 \leq q \leq Q$, and \mathcal{L} , which can be expressed as

$$d_{\min}(A_q, 1 \leq q \leq Q; \mathcal{L}) = \min \{ \det[\mathbf{R}_X], \forall \mathbf{R}_X \}. \quad (2.28)$$

In other words, given a legitimate configuration Q and \mathcal{L} that meets the throughput requirement of $R \cdot T$, the set of near-optimum STSK dispersion matrices can be determined by solving the following optimization

$$d_{\max-\min}(Q, \mathcal{L}) = \max_{\substack{A_q, 1 \leq q \leq Q \\ \log_2(Q \cdot \mathcal{L}) = R \cdot T}} d_{\min}(A_q, 1 \leq q \leq Q; \mathcal{L}). \quad (2.29)$$

According to the above minimum-determinant design criterion, for example, the dispersion matrices designed for CSTSK(2,2,2,4) are obtained as

$$\begin{aligned} A_1 &= \begin{bmatrix} 0.0002 + j0.1810 & 0.8053 + j0.0538 \\ -0.1065 - j0.3093 & -0.2929 + j0.0047 \end{bmatrix} \\ A_2 &= \begin{bmatrix} -0.0945 + j0.9968 & -0.6147 + j0.0826 \\ 0.1045 - j0.1268 & -0.7007 - j0.3077 \end{bmatrix} \\ A_3 &= \begin{bmatrix} -0.8263 - j0.2239 & 0.2992 + j0.6753 \\ 0.0804 - j0.0062 & -0.8362 + j0.1261 \end{bmatrix} \\ A_4 &= \begin{bmatrix} -0.4286 - j0.1219 & -0.4714 - j0.2877 \\ -0.5521 - j0.5868 & -0.0195 + j0.9203 \end{bmatrix}, \end{aligned} \quad (2.30)$$

where according to [5], 100,000 random dispersion-matrix sets were tentatively generated.

2.3.5 Maximum Minimum-Determinant Based Configuration Selection

It can readily be seen from Section 2.3.1 that a STSK MIMO system may achieve a required normalized throughput R by various combinations of the number of dispersion matrices Q and of the size of the conventional modulation scheme \mathcal{L} . For example, for a CSTSK MIMO system associated with the configuration of CSTSK(4, 2, 2, Q, \mathcal{L} – PSK/QAM), given a normalized throughput of $R = 2$ bits/symbol, there are three possible combinations of Q and \mathcal{L} , which are $(Q, \mathcal{L}) = (2, 8)$, $(Q, \mathcal{L}) = (4, 4)$ and $(Q, \mathcal{L}) = (8, 2)$. Table 2.4 list all the legitimate CSTSK configuration combinations (Q, \mathcal{L}) that are capable of achieving the four different normalized throughput requirements

$R = 1$ bit/symbol	$R = 1.5$ bits/symbol	$R = 2$ bits/symbol	$R = 2.5$ bits/symbol
$Q = 2, \mathcal{L} = 2$	$Q = 2, \mathcal{L} = 4$	$Q = 2, \mathcal{L} = 8$	$Q = 2, \mathcal{L} = 16$
N/A	$Q = 4, \mathcal{L} = 2$	$Q = 4, \mathcal{L} = 4$	$Q = 4, \mathcal{L} = 8$
N/A	N/A	$Q = 8, \mathcal{L} = 2$	$Q = 8, \mathcal{L} = 4$
N/A	N/A	N/A	$Q = 16, \mathcal{L} = 2$

Table 2.4: Combinations of Q and \mathcal{L} selected for achieving various normalized throughputs of $R = 1, 1.5, 2$ and 2.5 [bits/ symbol], with the number of time slots fixed to $T = 2$.

R , assuming that the number of time slots is fixed to $T = 2$. Since the different configurations of (Q, \mathcal{L}) selected for achieving the same throughput R may have different values of $d_{\max-\min}(Q, \mathcal{L})$ defined in Eq. (2.29), the resultant BERs may be different as well. It is therefore highly desired to select the most appropriate STSK configuration (Q, \mathcal{L}) that yields the best BER performance. One way to choose the best configuration is to perform the Monte-Carlo simulation based BER calculations for all the legitimate configurations of the STSK system for a fixed throughput R . However, the associated Monte-Carlo simulations are extremely time-consuming, hence this approach should be avoided if possible. Below we propose an effective MMBCS algorithm for selecting the most appropriate STSK configuration for the given throughput requirement R . Here, we again assume that the other configuration parameters such as M , N and T have been determined based on other considerations.

	$Q = 2$	$Q = 4$	$Q = 8$	$Q = 16$
$\mathcal{L} = 2$	$d_{\max-\min}(2, 2)$ = 1.99846 [1 bit/symbol]	$d_{\max-\min}(4, 2)$ = 1.70468 [1.5 bits/symbol]	$d_{\max-\min}(8, 2)$ = 0.424595 [2 bits/symbol]	$d_{\max-\min}(16, 2)$ = 0.092138 [2.5 bits/symbol]
$\mathcal{L} = 4$	$d_{\max-\min}(2, 4)$ = 1.94413 [1.5 bits/symbol]	$d_{\max-\min}(4, 4)$ = 1.54174 [2 bits/symbol]	$d_{\max-\min}(8, 4)$ = 0.21126 [2.5 bits/symbol]	N/A
$\mathcal{L} = 8$	$d_{\max-\min}(2, 8)$ = 0.343146 [2 bits/symbol]	$d_{\max-\min}(4, 8)$ = 0.40317 [2.5 bits/symbol]	N/A	N/A
$\mathcal{L} = 16$	$d_{\max-\min}(2, 16)$ = 0.15224 [2.5 bits/symbol]	N/A	N/A	N/A

Table 2.5: The maximum minimum-determinant $d_{\max-\min}(Q, \mathcal{L})$ of different combinations of (Q, \mathcal{L}) for achieving various normalized throughputs of $R = 1, 1.5, 2$ and 2.5 bits/symbol, associated with the CSTSK configuration of CSTSK(4, 2, 2, Q, \mathcal{L} – PSK).

More explicitly, given a throughput requirement R , for each of the legitimate STSK configurations (Q, \mathcal{L}) , the near-optimum set of dispersion matrices is generated by solving the optimization problem formulated in Eq. 2.29, which also records the corresponding maximum minimum-determinant value $d_{\max-\min}(Q, \mathcal{L})$. The optimal STSK configuration $(Q_{\text{opt}}, \mathcal{L}_{\text{opt}})$ is then simply the solution of the following optimization problem:

$$(Q_{\text{opt}}, \mathcal{L}_{\text{opt}}) = \arg \max_{Q, \mathcal{L}: \log_2(Q \cdot \mathcal{L})=R \cdot T} d_{\max-\min}(Q, \mathcal{L}). \quad (2.31)$$

Table 2.5 lists the maximum minimum-determinant values of $d_{\max-\min}(Q, \mathcal{L})$ for the various STSK configurations (Q, \mathcal{L}) that are capable of meeting the throughput requirements of $R = 1, 1.5,$

$R = 1$ bit/symbol	$R = 1.5$ bits/symbol	$R = 2$ bits/symbol	$R = 2.5$ bits/symbol
$(Q_{\text{opt}}, \mathcal{L}_{\text{opt}}) = (2, 2)$	$(Q_{\text{opt}}, \mathcal{L}_{\text{opt}}) = (2, 4)$	$(Q_{\text{opt}}, \mathcal{L}_{\text{opt}}) = (4, 4)$	$(Q_{\text{opt}}, \mathcal{L}_{\text{opt}}) = (4, 8)$

Table 2.6: Optimal combinations $(Q_{\text{opt}}, \mathcal{L}_{\text{opt}})$ for achieving the various normalized throughputs of $R = 1, 1.5, 2$ and 2.5 bits/ symbol, associated with the CSTSK configuration of $\text{CSTSK}(4, 2, 2, Q, \mathcal{L} - \text{PSK})$.

2 and 2.5 bits/symbol and are associated with the CSTSK configuration of $\text{CSTSK}(4, 2, 2, Q, \mathcal{L} - \text{PSK})$. From Table 2.5, we arrive at the optimal STSK configurations $(Q_{\text{opt}}, \mathcal{L}_{\text{opt}})$ capable of achieving the normalized throughputs of $R = 1, 1.5, 2$ and 2.5 bits/ symbol, respectively, which are summarized in Table 2.6. In the following simulation study, we will demonstrate that the most appropriate STSK configuration selected by our proposed MMBCS algorithm is capable of outperforming other STSK configurations in terms of their BER performance.

2.3.6 Simulation Results

In this section, the BER performance of the uncoded $\text{CSTSK}(M, N, T, Q, \mathcal{L} - \text{PSK/QAM})$ scheme of Fig. 2.17 was evaluated. A frequency-flat Rayleigh fading environment associated with the coherence time of T was considered, implying that the channels have a constant envelope over a CSTSK block duration, but fade independently between consecutive CSTSK blocks [5]. The transmitted signal power of all the simulated systems was normalized to unity and, therefore, the SNR was defined as $\frac{1}{N_0}$, with N_0 being the AWGN power. The ML detector of Eq. (2.19) was employed for the sake of achieving the optimal performance. The system parameters of the uncoded CSTSK scheme of Fig. 2.17 are summarized in Table 2.7.

Table 2.7: System parameters of the uncoded CSTSK scheme of Fig. 2.17.

Number of Tx antennas	M
Number of Rx antennas	N
Symbol durations per block	T
Number of dispersion matrices	Q
Modulation	\mathcal{L} -QAM or \mathcal{L} -PSK
Channels	Frequency-flat Rayleigh fading
Channel's coherence time	T
Detector	ML detector of Eq. (2.19)

2.3.6.1 Effects of Conventional Modulation Constellation Size \mathcal{L}

Since the size of conventional modulation alphabet \mathcal{L} directly affects the achievable performance of a CSTSK system, our study commenced with an investigation of the effects of \mathcal{L} , while fixing the number of dispersion matrices Q . Specifically, the configurations of CSTSK(2,2,2,4, \mathcal{L} – PSK/QAM), CSTSK(4,2,2,4, \mathcal{L} – PSK/QAM), and CSTSK(4,4,2,4, \mathcal{L} – PSK/QAM) were considered.

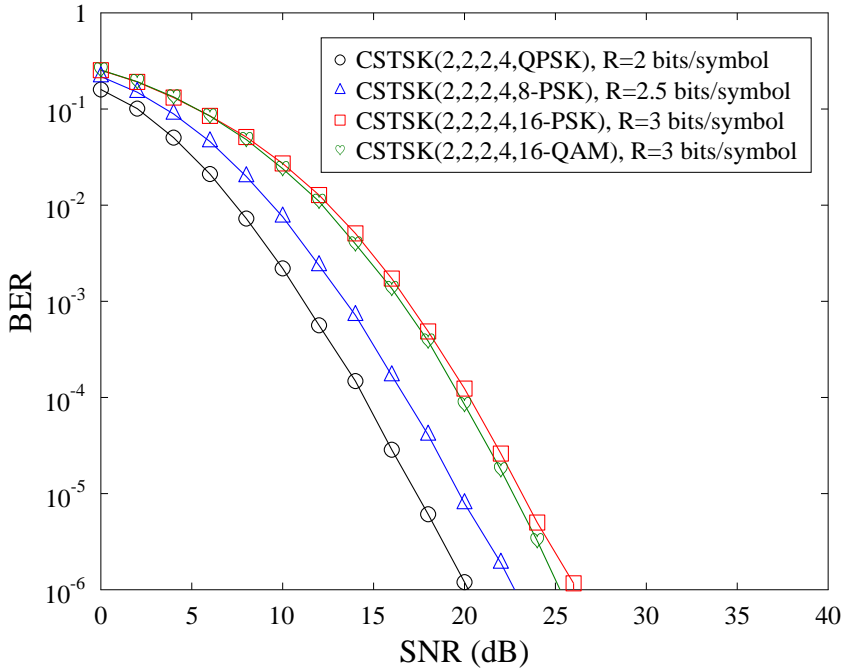


Figure 2.18: Achievable BER performance comparison of CSTSK(2,2,2,4, \mathcal{L} – PSK/QAM) of Fig. 2.17 associated with conventional modulations of QPSK, 8-PSK, 16-PSK and 16-QAM. The corresponding normalized system throughputs are $R = 2, 2.5, 3$ and 3 bits/symbol, respectively. All other system parameters were summarized in Table 2.7.

Fig. 2.18 compares the achievable BER performances of the CSTSK(2,2,2,4, \mathcal{L} – PSK/QAM) systems, associated with four conventional modulation schemes. According to the normalized throughput of Eq. (2.9), the corresponding normalized throughputs of these four systems associated with QPSK/4-QAM and 8-PSK are $R = 2$ bits/symbol, $R = 2.5$ bits/symbol, respectively, while for 16-PSK and 16-QAM it is $R = 3$ bits/symbol. As expected, by increasing the size of conventional modulation scheme \mathcal{L} , the normalized throughput is increased, but at the cost of a BER degradation. For example, at the BER of 10^{-6} , the CSTSK system associated with the configuration of CSTSK(2,2,2,4, 8-PSK) is capable of achieving a SNR gain of about 3 dB compared to that of CSTSK(2,2,2,4, 16-QAM). Moreover, observe in Fig. 2.18 that all the BER curves associated with various values of \mathcal{L} generally share the same slope, implying that same diversity gain may

be achieved. Therefore, we may conclude that as expected, changing the value of the conventional modulation level \mathcal{L} directly affects the system's normalized throughput and BER performance, while the diversity gain may remain the same. Interestingly, the CSTSK(2,2,2,4,16-QAM) system slightly outperforms CSTSK(2,2,2,4,16-PSK) in terms of its BER, despite the fact that these two systems have the same normalized throughput.

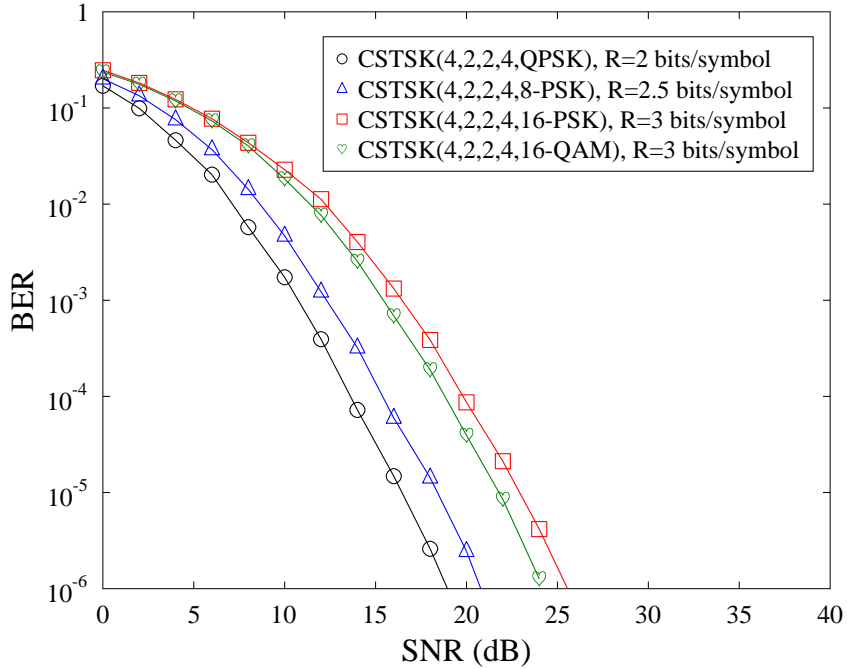


Figure 2.19: Achievable BER performance comparison of CSTSK(4,2,2,4, \mathcal{L} - PSK/QAM) of Fig. 2.17 associated with conventional modulations of QPSK, 8-PSK, 16-PSK and 16-QAM. The corresponding normalized system throughputs are $R = 2, 2.5, 3$ and 3 bits/symbol, respectively. All other system parameters were summarized in Table 2.7.

Additionally, the achievable BER performances of the CSTSK(4,2,2,4, \mathcal{L} - PSK/QAM) and CSTSK(4,4,2,4, \mathcal{L} - PSK/QAM) systems are depicted in Figs. 2.19 and 2.20, respectively. Similar to the simulation results for the various CSTSK(2,2,2,4, \mathcal{L} - PSK/QAM) systems, a smaller value of \mathcal{L} leads to a better BER performance, but at the cost of a lower system throughput. Additionally, we also find that the systems' diversity gain remains unaffected by \mathcal{L} . Moreover, with all the other configuration parameters kept identical, the CSTSK configuration associated with 16-QAM outperforms that associated with 16-PSK in terms of its achievable BER performance.

2.3.6.2 Effects of Number of Dispersion Matrices Q

The effects of the number of dispersion matrices Q on the system BER performances were also investigated, while fixing the size \mathcal{L} of the conventional modulation alphabet. The system configu-

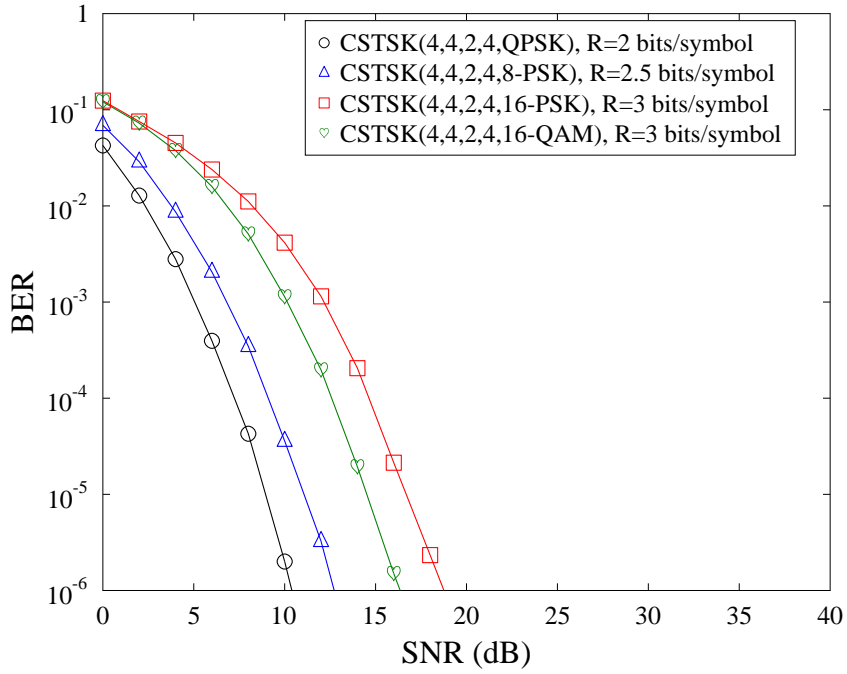


Figure 2.20: Achievable BER performance comparison of $\text{CSTSK}(4,4,2,4, \mathcal{L} - \text{PSK/QAM})$ of Fig. 2.17 associated with conventional modulations of QPSK, 8-PSK, 16-PSK and 16-QAM. The corresponding normalized system throughputs are $R = 2, 2.5, 3$ and 3 bits/symbol, respectively. All other system parameters were summarized in Table 2.7.

rations of $\text{CSTSK}(2,2,2,Q, \text{QPSK})$, $\text{CSTSK}(4,2,2,Q, \text{QPSK})$ and $\text{CSTSK}(4,4,2,Q, 16\text{-QAM})$ associated with various throughputs were studied in this section.

The BER performance of the $\text{CSTSK}(2,2,2,Q, \text{QPSK})$ systems of Fig. 2.17 associated with $Q = 4, 8$ and 16 having throughputs of $R = 2, 2.5$ and 3 bits/symbol are shown in Fig. 2.21, where it may be seen that changing Q while fixing \mathcal{L} produces similar effects as changing \mathcal{L} while fixing Q . Specifically, increasing the number of dispersion matrices employed by the system increases the system's throughput, but degrades the achievable BER performance. The reason for this phenomenon is that as Q increases, the minimum value of the determinant of codeword difference matrix $\mathbf{R}_X = (X - \hat{X})^H(X - \hat{X})$ will decrease, where X and \hat{X} are an arbitrary pair of the legitimate codewords. According to the expression of the PSEP in Eq. (2.27), a higher minimum value of this determinant will result in a better BER performance and vice versa. The corresponding minimum determinant values d_{\min} of the $\text{CSTSK}(2,2,2,Q, \text{QPSK})$ systems associated with $Q = 4, 8$ and 16 dispersion matrices are shown in Table 2.8, where it can be seen that as the value of Q increases, the value of d_{\min} decreases which leads to a degradation in the system's BER performance as shown in Fig. 2.21.

The BER performance of the $\text{CSTSK}(4,2,2,Q, \text{QPSK})$ systems for the three different values of

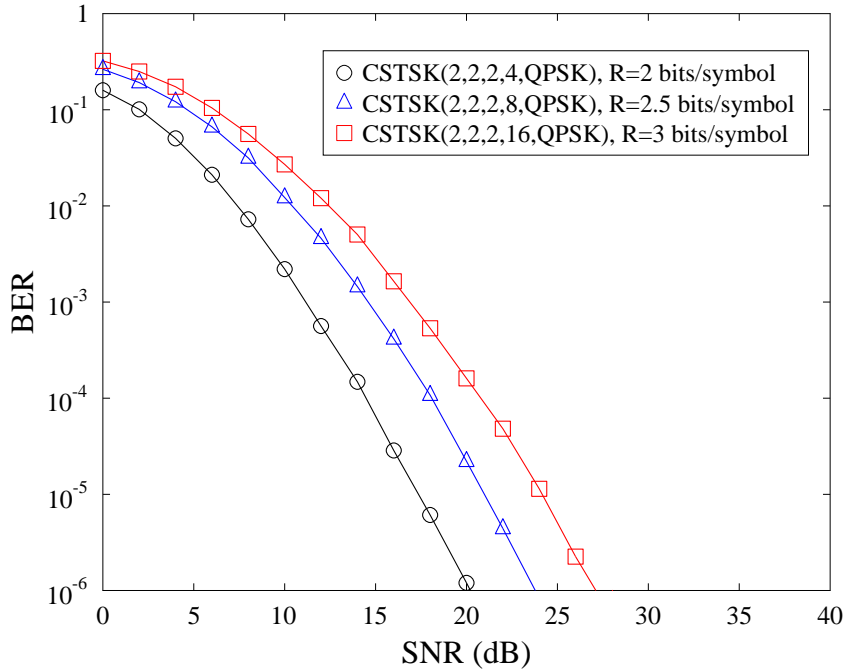


Figure 2.21: Achievable BER performance comparison of CSTSK(2,2,2,Q,QPSK) of Fig. 2.17 associated with $Q = 4, 8$ and 16 . The corresponding normalized system throughputs are $R = 2, 2.5$ and 3 bits/symbol, respectively. All other system parameters were summarized in Table 2.7.

Table 2.8: Minimum determinant values of the CSTSK(2,2,2,Q,QPSK) systems associated with $Q = 4, 8$ and 16 dispersion matrices.

CSTSK(2,2,2,4,QPSK)	CSTSK(2,2,2,8,QPSK)	CSTSK(2,2,2,16,QPSK)
$d_{\min} = 0.807703$ [2 bits/symbol]	$d_{\min} = 0.276201$ [2.5 bits/symbol]	$d_{\min} = 0.064366$ [3 bits/symbol]

$Q = 4, 8$ and 16 having throughputs of $R = 2, 2.5$ and 3 bits/symbol are shown in Fig. 2.22, where the same conclusions to those observed from Fig. 2.21 can be drawn. Explicitly, given the same conventional modulation scheme, as the number of dispersion matrices employed by the system increases, the system's throughput increases, but the corresponding BER performance degrades. The minimum determinant values d_{\min} of the CSTSK(4,2,2,Q,QPSK) systems associated with $Q = 4, 8$ and 16 dispersion matrices are listed in Table 2.9, where it may also be seen that as the value of Q increases, the corresponding d_{\min} decreases. Additionally, the BER performance and minimum determinant values d_{\min} of the CSTSK(4,4,2,Q,16-QAM) associated with $Q = 4, 8$ and 16 dispersion matrices are shown in Fig. 2.23 and Table 2.10, respectively.

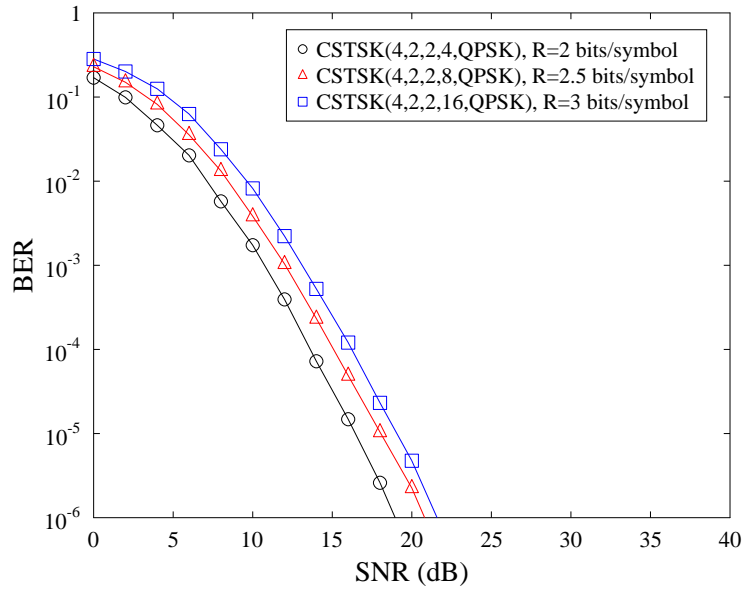


Figure 2.22: Achievable BER performance comparison of $\text{CSTSK}(4, 2, 2, Q, \text{QPSK})$ of Fig. 2.17 associated with $Q = 4, 8$ and 16 . The corresponding normalized system throughputs are $R = 2, 2.5$ and 3 bits/symbol, respectively. All other system parameters were summarized in Table 2.7.

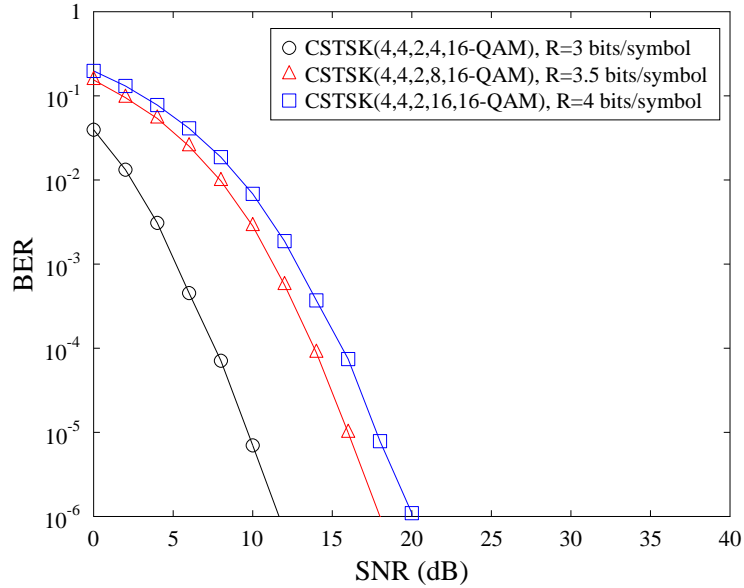


Figure 2.23: Achievable BER performance of $\text{CSTSK}(4, 4, 2, Q, 16\text{-QAM})$ of Fig. 2.17 associated with $Q = 4, 8$ and 16 . The corresponding normalized system throughputs are $R = 3, 3.5$ and 4 bits/symbol, respectively. All other system parameters were summarized in Table 2.7.

Table 2.9: Minimum determinant values of the CSTSK($4, 2, 2, Q$, QPSK) systems associated with $Q = 4, 8$ and 16 dispersion matrices.

CSTSK($4, 2, 2, 4$, QPSK)	CSTSK($4, 2, 2, 8$, QPSK)	CSTSK($4, 2, 2, 16$, QPSK)
$d_{\min} = 1.54174$ [2 bits/symbol]	$d_{\min} = 0.241162$ [2.5 bits/symbol]	$d_{\min} = 0.067764$ [3 bits/symbol]

Table 2.10: Minimum determinant values of the CSTSK($4, 4, 2, Q$, 16-QAM) systems associated with $Q = 4, 8$ and 16 dispersion matrices.

CSTSK($4, 4, 2, 4$, 16-QAM)	CSTSK($4, 4, 2, 8$, 16-QAM)	CSTSK($4, 4, 2, 16$, 16-QAM)
$d_{\min} = 0.0352915$ [3 bits/symbol]	$d_{\min} = 0.00862591$ [3.5 bits/symbol]	$d_{\min} = 0.0023994$ [4 bits/symbol]

2.3.6.3 Effects of Antenna Configurations

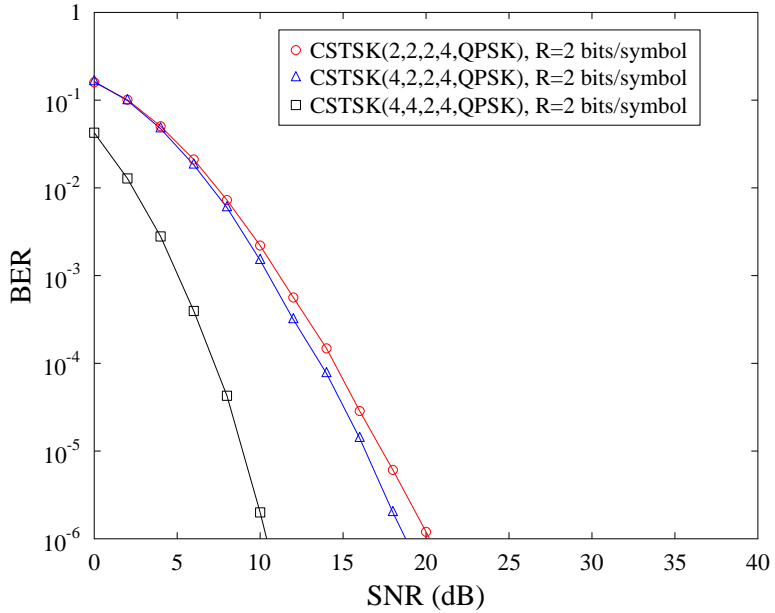


Figure 2.24: Achievable BER performance of the CSTSK($M, N, 2, 4$, QPSK) systems associated with different antenna configurations of $(M, N) = (2, 2)$, $(4, 2)$ and $(4, 4)$, having a normalized throughput of $R = 2$ bits/symbol. All other system parameters were summarized in Table 2.7.

In this section, the effects of different antenna configurations on the system's BER performance was investigated, while fixing the other configuration parameters. Specifically, for $T = 2$ and $Q = 4$, the corresponding results are shown in Fig. 2.24 associated with QPSK and in Fig. 2.25 associated with 16-QAM. According to Eq. (2.25), the maximum achievable diversity orders of $(M, N) = (2, 2)$, $(4, 2)$ and $(4, 4)$ associated with $T = 2$ are 4, 4 and 8, respectively. It can

be seen from Figs. 2.24 and 2.25 that the configuration of $(M, N) = (4, 2)$ slightly outperforms the configuration of $(M, N) = (2, 2)$, although both systems have the same maximum achievable diversity order. The configuration of $(M, N) = (4, 4)$ achieves the best BER performance and has the sharpest BER curve slope, because it has the highest diversity order.

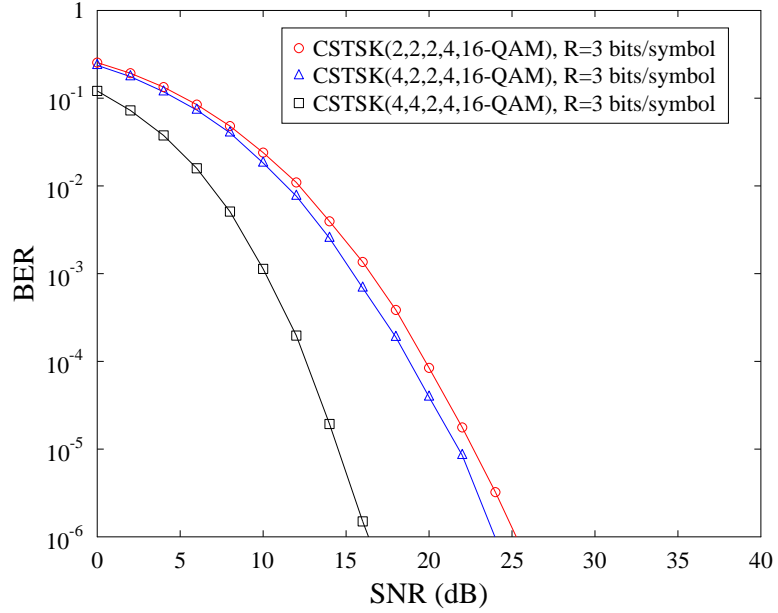


Figure 2.25: Achievable BER performance comparison of the CSTSK($M, N, 2, 4, 16$ -QAM) systems associated with different antenna configurations of $(M, N) = (2, 2)$, $(4, 2)$ and $(4, 4)$, having a normalized throughput of $R = 3$ bits/symbol. All other system parameters were summarized in Table 2.7.

2.3.6.4 Maximum Minimum-Determinant Based Configuration Selection for CSTSK Systems

In this section, we investigated the performance of the MMBCS algorithm of Section 2.3.5 for selecting the CSTSK configuration parameters (Q, \mathcal{L}) . The CSTSK systems associated with the configuration of CSTSK($4, 2, 2, Q, \mathcal{L}$ – PSK/QAM) and having the normalized system's throughputs of $R = 1.5$ bits/symbol and $R = 2$ bits/symbol were chosen in the study.

Our analysis commenced with the CSTSK($4, 2, 2, Q, \mathcal{L}$ – PSK/QAM) systems associated with a normalized throughput of $R = 1.5$ bits/symbol. According to the details listed in Table 2.5, there are two combinations of the number of dispersion matrices Q and of the conventional PSK/QAM modulation alphabet \mathcal{L} for this CSTSK scheme, which are the systems of CSTSK($4, 2, 2, 2$, QPSK) and CSTSK($4, 2, 2, 4$, BPSK), associated with the minimum-determinant values of $d_{\max-\min}(2, 4) = 1.94413$ and $d_{\max-\min}(4, 2) = 1.70468$, respectively. Since $d_{\max-\min}(2, 4) > d_{\max-\min}(4, 2)$, CSTSK($4, 2, 2, 2$, QPSK) is expected to outperform CSTSK($4, 2, 2, 4$, BPSK), and our MMBCS algorithm selects CSTSK($4, 2, 2, 2$, QPSK) as the optimal configuration. The corresponding BER

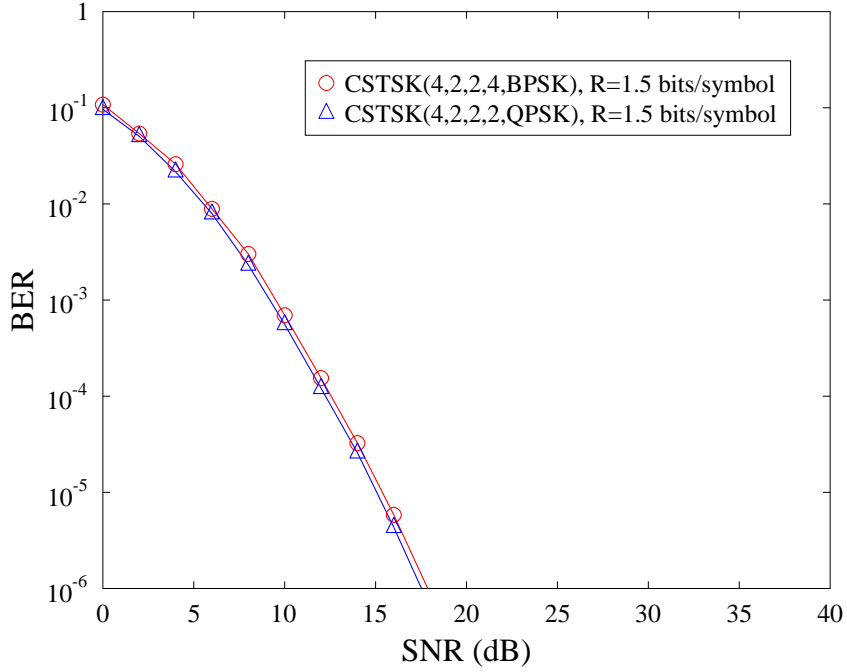


Figure 2.26: Achievable BER performance comparison of the $\text{CSTSK}(4, 2, 2, Q, \mathcal{L} - \text{PSK/QAM})$ systems associated with a normalized throughput of $R = 1.5$ bits/symbol. All other system parameters were summarized in Table 2.7.

performance comparison shown in Fig. 2.26 confirms that the $\text{CSTSK}(4, 2, 2, 2, \text{QPSK})$ system outperforms the $\text{CSTSK}(4, 2, 2, 4, \text{BPSK})$ system by about 0.5 dB in SNR at the BER of 10^{-6} . This demonstrates the power of our MMBCS algorithm in selecting the optimal configuration parameters (Q, \mathcal{L}) .

For the $\text{CSTSK}(4, 2, 2, Q, \mathcal{L} - \text{PSK/QAM})$ scheme to achieve a normalized throughput of $R = 2$ bits/symbol, there are three combinations, namely scheme $(Q, \mathcal{L}) = (2, 8)$, $(Q, \mathcal{L}) = (4, 4)$ and $(Q, \mathcal{L}) = (8, 2)$, which correspond to the three systems of $\text{CSTSK}(4, 2, 2, 2, 8\text{-PSK})$, $\text{CSTSK}(4, 2, 2, 4, \text{QPSK})$ and $\text{CSTSK}(4, 2, 2, 8, \text{BPSK})$. From Table 2.5, since we have

$$d_{\max-\min}(4, 4) = 1.54174 > d_{\max-\min}(8, 2) = 0.424595 > d_{\max-\min}(2, 8) = 0.343146,$$

we conclude that the $\text{CSTSK}(4, 2, 2, 8, \text{BPSK})$ system outperforms $\text{CSTSK}(4, 2, 2, 2, 8\text{-PSK})$, while $\text{CSTSK}(4, 2, 2, 4, \text{QPSK})$ attains the lowest BER among the three configurations and hence it is the optimal configuration selected by our proposed MMBCS algorithm. The BER comparison of these three systems depicted in Fig. 2.27 confirms the above conclusions. To be more explicit, the optimal configuration of $\text{CSTSK}(4, 2, 2, 4, \text{QPSK})$ outperforms the configurations of $\text{CSTSK}(4, 2, 2, 8, \text{BPSK})$ and $\text{CSTSK}(4, 2, 2, 2, 8\text{-PSK})$ by about 1 dB and 3 dB in SNR, respectively, at the BER of 10^{-6} .

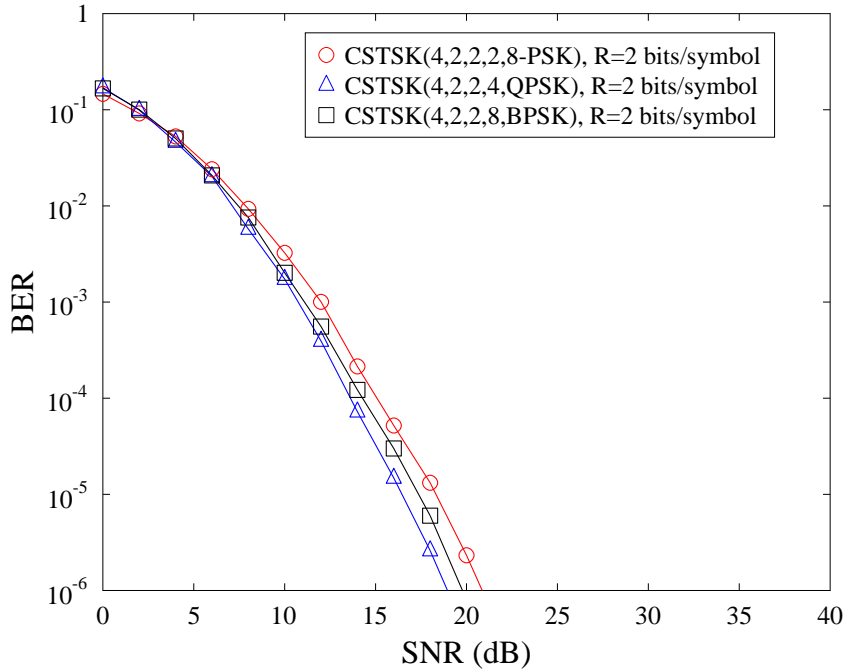


Figure 2.27: Achievable BER performance comparison of the $\text{CSTSK}(4, 2, 2, Q, \mathcal{L} - \text{PSK/QAM})$ systems associated with a normalized throughput of $R = 2$ bits/symbol. All other system parameters were summarized in Table 2.7.

2.4 Three-Stage Serial-Concatenated Turbo Coding Aided CSTSK Systems

In Fig. 2.7 of Section 2.2, the structure of a three-stage turbo coding aided MIMO scheme has been introduced for the classic SDM/V-BLAST MIMO. For the sake of achieving near-capacity performance, in this section the three-stage iterative turbo coding scheme is also applied to the novel CSTSK MIMO discussed in Section 2.3. The three-stage serial-concatenated turbo coding aided CSTSK MIMO scheme is depicted in Fig. 2.28, where we observe that its structure is identical to the one shown in Fig. 2.7, except that the modulator of the transmitter and the soft-demapper at the receiver in the SDM/V-BLAST system are replaced by the modulator and soft-demapper of the CSTSK system. Since the CSTSK modulation process has been introduced in Section 2.3.1, in this section we will mainly focus on the soft-demapper of the CSTSK MIMO system.

2.4.1 CSTSK Soft-Demapper

As discussed in Section 2.3.1, the CSTSK MIMO scheme is free from ICI, hence a low-complexity single-stream ML detector/demapper can be employed [5, 21]. Additionally, since we incorporate a three-stage serial-concatenated turbo coding scheme for the sake of achieving a near-capacity performance, a CSTSK soft-demapper is required. According to Eq. (2.11), the conditional probability

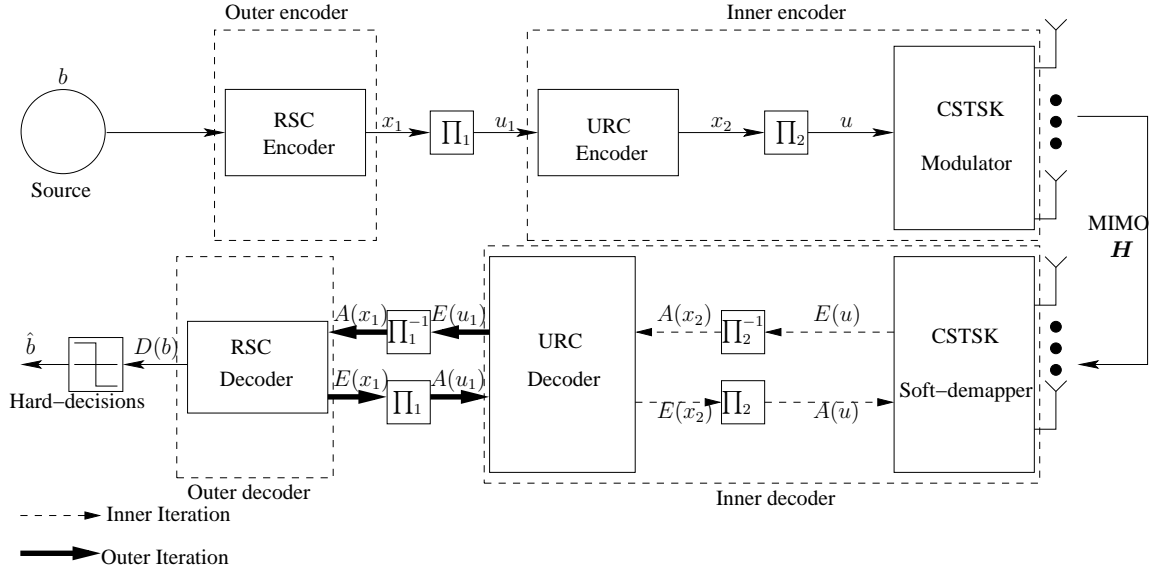


Figure 2.28: The structure of three-stage serial-concatenated turbo encoder/decoder for CSTSK MIMO system. Note that different to Fig. 2.7, the modulator of the transmitter and the soft-demapper at the receiver in the SDM/V-BLAST system are replaced by the modulator and soft-demapper of the CSTSK system.

$p(\bar{y}|k_{q,l})$ is given by [1,21]

$$p(\bar{\mathbf{y}}|\mathbf{k}_{q,l}) = \frac{1}{(\pi N_0)^{NT}} \exp\left(-\frac{\|\bar{\mathbf{y}} - \bar{\mathbf{H}}\mathbf{Y}\mathbf{k}_{q,l}\|^2}{N_0}\right). \quad (2.32)$$

The total number of channel-coded bits carried by the received signal vector \bar{y} is $N_c = \log_2(Q \cdot \mathcal{L})$, and the extrinsic LLR value of bit u_n , $n \in \{1, 2, \dots, N_c\}$, may be expressed as

$$\begin{aligned}
L_e(u_n) &= \ln \frac{\sum_{k_{q,l} \in \mathbb{K}_1^n} p(\bar{y}|k_{q,l}) \cdot \exp \left(\sum_{j \neq n} u_j L_a(u_j) \right)}{\sum_{k_{q,l} \in \mathbb{K}_0^n} p(\bar{y}|k_{q,l}) \cdot \exp \left(\sum_{j \neq n} u_j L_a(u_j) \right)} \\
&= \ln \frac{\sum_{k_{q,l} \in \mathbb{K}_1^n} \exp \left(-\|\bar{y} - \bar{H}\mathbf{Y}k_{q,l}\|^2/N_0 + \sum_{j \neq n} u_j L_a(u_j) \right)}{\sum_{k_{q,l} \in \mathbb{K}_0^n} \exp \left(-\|\bar{y} - \bar{H}\mathbf{Y}k_{q,l}\|^2/N_0 + \sum_{j \neq n} u_j L_a(u_j) \right)}, \tag{2.33}
\end{aligned}$$

where $L_a(u_n)$ represents the *a priori* information expressed in terms of the LLR of the corresponding bit u_n , $\mathbb{K}_1^n = \{k_{q,l} \in \mathbb{K} | u_n = 1\}$ and $\mathbb{K}_0^n = \{k_{q,l} \in \mathbb{K} | u_n = 0\}$ are the sub-sets of the legitimate equivalent signals, when the corresponding bits are $u_n = 1$ and $u_n = 0$, respectively.

Upon applying the max-log approximation [1], Eq. (2.33) can be simplified to

$$L_e(u_n) = \max_{k_{q,l} \in \mathbb{K}_1^n} \left\{ -\|\bar{\mathbf{y}} - \bar{\mathbf{H}}\mathbf{Y}k_{q,l}\|^2/N_0 + \sum_{j \neq n} u_j L_a(u_j) \right\} \\ - \max_{k_{q,l} \in \mathbb{K}_0^n} \left\{ -\|\bar{\mathbf{y}} - \bar{\mathbf{H}}\mathbf{Y}k_{q,l}\|^2/N_0 + \sum_{j \neq n} u_j L_a(u_j) \right\}, \quad (2.34)$$

and the *a posteriori* information output by the CSTSK demapper is then given by

$$L_p(u_n) = L_e(u_n) + L_a(u_n). \quad (2.35)$$

2.4.2 Simulation Results

A frequency-flat Rayleigh fading environment was considered. An interleaver length of 10^6 bits was used by the three-stage serial-concatenated turbo encoder/decoder of Fig. 2.28. The binary generator polynomials of the RSC encoder were $G_{RSC} = [1, 0, 1]_2$ and $G_{RSC}^r = [1, 1, 1]_2$, while these of the URC encoder were $G_{URC} = [1, 0]_2$ and $G_{URC}^r = [1, 1]_2$, where G_{RSC}^r and G_{URC}^r are the feedback polynomials of the RSC and URC encoders, respectively. The transmitted signal power of all the simulated systems was normalized to unity, therefore, the SNR was defined as $\frac{1}{N_0}$, with N_0 being the AWGN power. The system parameters of the three-stage serial-concatenated turbo coding aided CSTSK system of Fig. 2.28 are summarized in Table 2.11.

Table 2.11: System parameters of the three-stage serial-concatenated turbo coding aided CSTSK system of Fig. 2.28.

Number of Tx antennas	M
Number of Rx antennas	N
Symbol durations per block	T
Number of dispersion matrices	Q
Modulation	\mathcal{L} -QAM or \mathcal{L} -PSK
Channels	Frequency-flat Rayleigh fading
Channel's coherence time	T
Detector	ML max-log soft-demapper of Eq. (2.34)
Interleaver blocklength	10^6 bits
Outer channel code	Half-rate RSC
Generator polynomials	$(G_{RSC}^r, G_{RSC}) = (7, 5)_8$
Precoder	URC
Number of inner iterations	I_{in}
Number of outer iterations	I_{out}

2.4.2.1 CSTSK(4, 2, 2, 4, QPSK)

We first considered the CSTSK(4, 2, 2, 4, QPSK) system having a normalized throughput of $R = 2$ bits/symbol. Our investigations commenced with the EXIT chart analysis and the corresponding results are depicted in Fig. 2.29, where it may be seen that an open tunnel exists between the EXIT curves of the inner CSTSK soft-demapper-URC decoder and the RSC outer decoder at about

SNR = 0 dB. Additionally, the Monte-Carlo simulation based staircase shaped decoding trajectory, which closely matches the EXIT chart curves, was also provided at SNR = 0 dB. The trajectory shows that the three-stage serial-concatenated turbo coding aided CSTSK(4,2,2,4,QPSK) system of Fig. 2.28 is capable of reaching the point of perfect convergence at about SNR = 0 dB with the aid of $I_{in} = 3$ inner iterations and $I_{out} = 10$ outer iterations.

The corresponding BER performance of this three-stage serial-concatenated turbo coding aided CSTSK(4,2,2,4,QPSK) system of Fig. 2.28 is shown in Fig. 2.30. It can be seen that the system's BER performance was improved as the number of iterations increased and a 'turbo cliff' appeared at about SNR = -0.1 dB, indicating that a 'near-error free' performance is achieved. This is in line with the conclusions drawn from the EXIT chart of Fig. 2.29. Furthermore, the maximum achievable rate of this system is also included to prove that the system is capable of achieving a near-capacity performance.

2.4.2.2 CSTSK(4,4,2,4,16-QAM)

Fig. 2.31 shows the EXIT chart characteristics of the CSTSK(4,4,2,4,16-QAM) system, indicating that an open tunnel appears at about SNR = -1.2 dB, with the aid of $I_{in} = 3$ inner iterations and $I_{out} = 9$ outer iterations. Since the Monte-Carlo simulation based staircase shaped decoding trajectory closely matches the EXIT chart curves at SNR = -1.2 dB, a vanishingly low BER performance may be achieved by this CSTSK(4,4,2,4,16-QAM) scheme at about

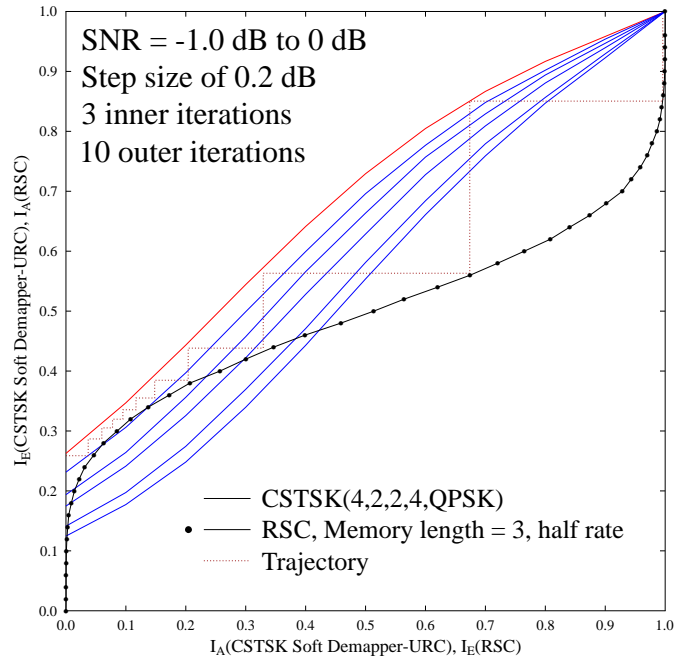


Figure 2.29: EXIT charts of the three-stage serial-concatenated turbo coding aided CSTSK(4,2,2,4,QPSK) system of Fig. 2.28 associated with various SNR values. The corresponding BER curves are seen in Fig. 2.30.

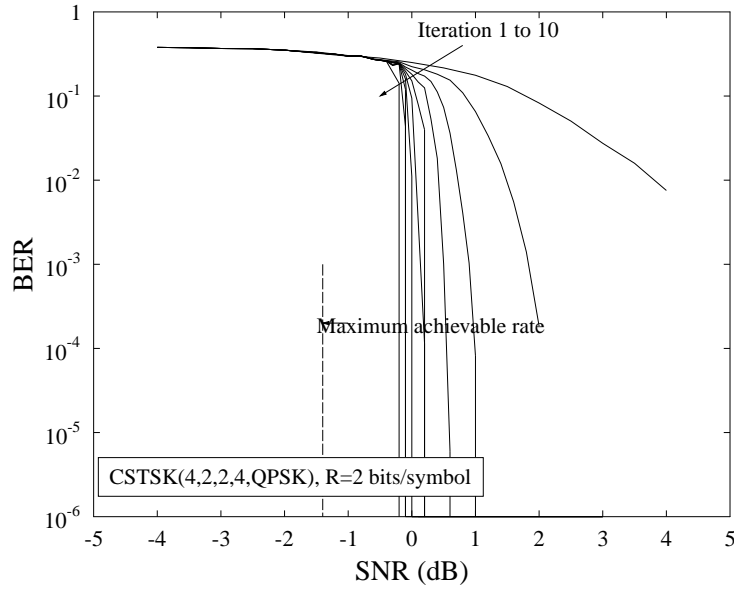


Figure 2.30: Achievable BER performance of the three-stage serial-concatenated turbo coding aided CSTSK(4,2,2,4,QPSK) system of Fig. 2.28 and the system's maximum achievable rate. The system normalized throughput is $R = 2$ bits/symbol. All other system parameters were summarized in Table 2.11. The corresponding EXIT chart is seen in Fig. 2.29.

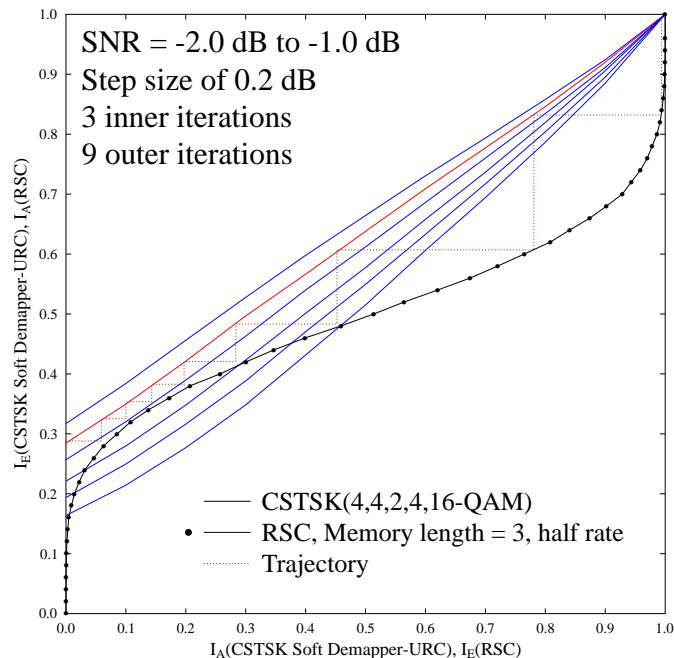


Figure 2.31: EXIT charts of the three-stage serial-concatenated turbo coding aided CSTSK(4,4,2,4,16-QAM) system of Fig. 2.28 associated with various SNR values. The corresponding BER curves are seen in Fig. 2.32.

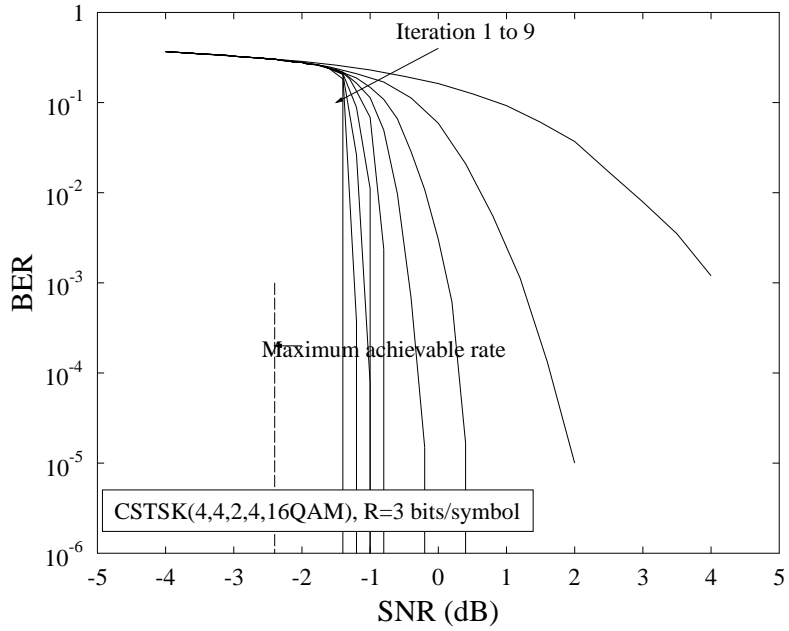


Figure 2.32: Achievable BER performance of the three-stage serial-concatenated turbo coding aided CSTSK(4,4,2,4,16-QAM) systems of Fig. 2.28 and the system's maximum achievable rate. The system normalized throughput is $R = 3$ bits/symbol. All other system parameters were summarized in Table 2.11. The corresponding EXIT chart is seen in Fig. 2.31.

SNR = -1.2 dB. This may also be inferred from the Monte-Carlo simulation based BER performance shown in Fig. 2.32, where it may be seen that a ‘near-error free’ performance is achieved at about SNR = -1.2 dB. Additionally, the maximum achievable rate of this system is also provided in Fig. 2.32 to demonstrate that the system is capable of achieving a near-capacity performance.

2.5 Chapter Summary and Conclusions

In this chapter, we have reviewed two MIMO systems, namely the conventional SDM/V-BLAST and the novel CSTSK MIMO systems.

Our discussion related to the uncoded classic SDM/V-BLAST MIMO system of Fig. 2.1 were provided in Section 2.1. To be more explicit, the uncoded SDM/V-BLAST MIMO was described in Section 2.1.1, where it was pointed out that employing the well-known ML detector is capable of achieving the optimal performance at the cost of an exponentially increasing computational complexity along with an increased number of multiplexed symbols in the transmitted symbol vector $s(i)$. For the sake of achieving a lower detection complexity, the family of classic linear detectors, such as the ZF and MMSE detectors may be adopted, although at the expense of a certain performance loss. Additionally, some near-optimal detection schemes, such as sphere detection schemes,

Table 2.12: Performance summary of SDM/V-BLAST systems at $\text{BER} = 10^{-6}$. Their complexity is on the order of $(4MN + 2N)\mathcal{L}^M$.

MIMO Scheme	Throughput [bits/symbol]	SNR (Uncoded) [dB]	SNR (Coded) [dB]	Figure
MIMO(2,2,BPSK)	2	27	-3.2	Fig. 2.2 and 2.9
MIMO(2,4,BPSK)	2	12		Fig. 2.5
MIMO(2,8,BPSK)	2	5		Fig. 2.5
MIMO(2,2,4-QAM)	4	30		Fig. 2.2
MIMO(4,2,BPSK)	4	27.5		Fig. 2.4
MIMO(4,4,BPSK)	4	12.5		Fig. 2.3
MIMO(2,2,8-PSK)	6	35		Fig. 2.2
MIMO(2,2,16-QAM)	8	37.5		Fig. 2.2
MIMO(4,2,4-QAM)	8	34	4	Fig. 2.6 and 2.13
MIMO(8,2,BPSK)	8	31		Fig. 2.4
MIMO(4,4,4-QAM)	8	16	-2.5	Fig. 2.3 and 2.16
MIMO(4,8,4-QAM)	8	8		Fig. 2.6
MIMO(4,4,8-PSK)	12	21		Fig. 2.3
MIMO(4,4,16-QAM)	16	24		Fig. 2.3

are capable of attaining a near-optimal performance at a moderate complexity. The performance of the uncoded SDM/V-BLAST system was investigated in Section 2.1.2, where it was demonstrated that in the SDM/V-BLAST system, a diversity gain may only be achieved by increasing the number of Rx antennas, while increasing the number of Tx antennas is capable of improving the multiplexing gain.

The three-stage serial-concatenated turbo coding aided SDM/V-BLAST MIMO of Fig. 2.7 was introduced in Section 2.2 for the sake of achieving near-capacity performance, where a URC is employed for the sake of beneficially spreading the *extrinsic* information across the iterative decoder components to avoid the well-known error-floor of the conventional two-stage turbo schemes [1]. The corresponding simulation results of the three-stage serial-concatenated turbo coding aided SDM/V-BLAST system were portrayed in Fig. 2.8, Fig. 2.10, Fig. 2.12, and Fig. 2.15 of Section 2.2.2, where EXIT chart was introduced as an efficient tool for predicting the convergence behaviour of the iterative decoder. Additionally, the BER performance of the coded SDM/V-BLAST was investigated in Fig. 2.9, Fig. 2.11, Fig. 2.13, Fig. 2.14, and Fig. 2.16, where it was shown that with the aid of the powerful three-stage serial-concatenated turbo coding scheme, the MIMO systems were capable of achieving a near-capacity performance. We have summarized the performance of uncoded SDM/V-BLAST MIMO system of Fig. 2.1 and the three-stage serial-concatenated turbo coding aided SDM/V-BLAST MIMO of Fig. 2.7 in Table 2.12, including the

throughput, required SNR for achieving $\text{BER} = 10^{-6}$ and complexity order.

Table 2.13: Performance summary of CSTSK systems at $\text{BER} = 10^{-6}$. Their complexity is on the order of $NTQ(2MT + 4\mathcal{L})$.

MIMO Scheme	Throughput [bits/symbol]	SNR (Uncoded) [dB]	SNR (Coded) [dB]	Figure
CSTSK(4,2,2,4,BPSK)	1.5	17.5		Fig. 2.26
CSTSK(4,2,2,2,QPSK)	1.5	17		Fig. 2.26
CSTSK(4,2,2,2,8-PSK)	2	21		Fig. 2.27
CSTSK(2,2,2,4,QPSK)	2	20		Fig. 2.18
CSTSK(4,2,2,8,BPSK)	2	19.7		Fig. 2.27
CSTSK(4,2,2,4,QPSK)	2	18.8	0	Fig. 2.19 and 2.30
CSTSK(4,4,2,4,QPSK)	2	10.5		Fig. 2.20
CSTSK(2,2,2,8,QPSK)	2.5	23.5		Fig. 2.21
CSTSK(2,2,2,4,8-PSK)	2.5	22.5		Fig. 2.18
CSTSK(4,2,2,4,8-PSK)	2.5	21		Fig. 2.19
CSTSK(4,2,2,8,QPSK)	2.5	20.5		Fig. 2.22
CSTSK(4,4,2,4,8-PSK)	2.5	12.5		Fig. 2.20
CSTSK(2,2,2,16,QPSK)	3	27		Fig. 2.21
CSTSK(2,2,2,4,16-PSK)	3	26		Fig. 2.18
CSTSK(4,2,2,4,16-PSK)	3	25.5		Fig. 2.19
CSTSK(2,2,2,4,16-QAM)	3	25		Fig. 2.18
CSTSK(4,2,2,4,16-QAM)	3	24		Fig. 2.19
CSTSK(4,2,2,16,QPSK)	3	21.5		Fig. 2.22
CSTSK(4,4,2,4,16-PSK)	3	18		Fig. 2.20
CSTSK(4,4,2,4,16-QAM)	3	16	-1.2	Fig. 2.20 and 2.32
CSTSK(4,4,2,8,16-QAM)	3.5	18		Fig. 2.23
CSTSK(4,4,2,16,16-QAM)	4	20		Fig. 2.23

In Section 2.3, the novel concept of CSTSK modulation was introduced in terms of its system model, computational complexity, maximum achievable diversity order, and dispersion matrix generation. We also proposed a novel MMBCS algorithm in Section 2.3.5, which is capable of selecting the best STSK configuration, while avoiding the time-consuming Monte-Carlo simulation based approach. The uncoded CSTSK MIMO system's performance was then intensively investigated in Fig. 2.18, Fig. 2.19, Fig. 2.20, Fig. 2.21, Fig. 2.22, Fig. 2.23, Fig. 2.24, Fig. 2.25, Fig. 2.26 and Fig. 2.27 of Section 2.3.6 based on various CSTSK configurations. By analysing the results obtained, it was concluded that the proposed CSTSK scheme is capable of striking a

flexible tradeoff between the MIMO's diversity and multiplexing gains, while facilitating the low-complexity single-antenna-based ML detection owing to the elimination of ICI. In particular, it was found that the system's throughput can be increased by either increasing the size of conventional modulation alphabet \mathcal{L} or by increasing the number of dispersion matrices Q , at the expense of a degraded BER performance. Moreover, the simulation results also confirmed that the proposed MMBCS of Section 2.3.5 algorithm was capable of selecting the optimal CSTSK configuration at a given throughput.

Finally, the three-stage serial-concatenated turbo coding aided CSTSK MIMO systems of Fig. 2.28 was developed in Section 2.4 for the sake of achieving a near-capacity performance. The corresponding simulation results confirmed that with the aid of the powerful three-stage serial-concatenated turbo coding scheme, the CSTSK MIMO system became capable of achieving near-capacity performance. We have summarized the performance of uncoded CSTSK system of Fig. 2.17 and the three-stage serial-concatenated turbo coding aided CSTSK of Fig. 2.28 in Table 2.13, including the throughput, required SNR for achieving $\text{BER} = 10^{-6}$ and complexity order.

This chapter has characterized the attainable performance of the coherently-detected SDM/V-BLAST and CSTSK MIMO systems in both uncoded and three-stage serial-concatenated turbo coded scenarios, assuming that the MIMO CSI is perfectly known at the receivers. However, in practice, the challenge is to acquire accurate CSI estimates without imposing excessive complexity and substantial pilot overhead. Therefore, in the next chapter, we will discuss the family of various CE schemes for coherent MIMO schemes and propose an efficient yet low complexity semi-blind CE scheme.

Chapter **3**

Channel Estimation for Coherent MIMO Systems

3.1 Introduction

In Chapter 2, the family of coherent MIMO systems represented by the classic SDM/V-BLAST and the recent CSTSK have been reviewed under the idealized simplifying assumption of perfectly known CSI. It has been widely recognised that the ability of a coherent MIMO system to approach its attainable capacity heavily relies on the accuracy of the CSI. In order to dispense with the assumption of perfectly known CSI, in this chapter, CE schemes for MIMO systems will be discussed.

As one of the most commonly used CE algorithms, the conventional TBCE schemes [33–36] will be firstly reviewed. In this kind of CE schemes, training pilots are firstly sent for the receiver to acquire the CSI, which are followed by the actual data transmission. However, It may be noticed that the TBCE schemes are capable of achieving accurate MIMO CSI as long as the training overhead is sufficiently large, which will inevitably lead to a large reduction in the overall system throughput [31]. A possible solution may be the BCE schemes, where no training pilots are needed and, therefore, no throughput loss may be induced. However, the BCE schemes not only impose high complexity and slow convergence, but also suffer from unavoidable estimation and decision ambiguities [47, 48]. Against this background, another category of CE schemes, known as SBCE algorithms [31, 32, 36, 48–59, 126], will be discussed in this chapter, where only a small number of training symbols is employed for generating an initial TBCE. Data detection is initially carried out based on this initial CE, and the data detector and the channel estimator iteratively exchange their information for updating the channel estimate and improving the data detection accuracy. In this way, the number of training symbols utilized for initial TBCE may be reduced, while acquiring an accurate CE and achieving an accurate data detection.

In particular, based on the SBCE approach, we propose a low-complexity BBSBCE and three-stage turbo detection-decoding scheme for near-capacity coherent MIMO systems. In the proposed scheme, only a minimum number of MIMO training blocks are employed for generating an initial TBCE, which is then used for initial data detection. As usual, the detected soft information is first exchanged a number of times within the inner turbo loop between the URC decoder and the MIMO soft-demapper, and the information gleaned from the inner URC decoder is then iteratively exchanged with the outer decoder in the outer turbo loop. Unlike the existing SBCE based schemes, however, our channel estimation scheme is naturally embedded in the outer turbo loop of the three-stage turbo detector and decoder, which exploits the *a posteriori* information produced by the MIMO soft-demapper. In other words, our scheme does not impose an additional iterative loop for exchanging information between the decision-directed channel estimator and the three-stage turbo detector-decoder. Hence, the computational complexity of our joint channel estimation and three-stage turbo detection remains similar to that of the three-stage turbo detection-decoding scheme. Moreover, our proposed low-complexity BBSBCE scheme is capable of approaching the optimal ML turbo detection performance attained with the aid of perfect CSI, as confirmed by our simulation results. Additionally, it has been recognised that the effects of “bad” decisions may be mitigated to certain extent and the system performance and robustness may be improved by employing the so-called soft CE schemes [127–131]. Therefore, we further propose a novel BBSB-SCE scheme for MIMO systems.

The rest of this chapter is organised as below. Section 3.2 introduces the conventional TBCE scheme for MIMO systems in both uncoded and three-stage serial-concatenated turbo coded scenarios. The system model and achievable performance of efficient SBCE scheme are provided in Section 3.3 in the uncoded scenario. Then based on the novel BBSBCE approach, the reduced-complexity joint channel estimation and three-stage iterative demapping-decoding scheme for near-capacity coherent MIMO systems is proposed in Section 3.4. Additionally, the BBSB-SCE is discussed in Section 3.5 and its performance is investigated based on the SDM/V-BLAST MIMO system. Finally, the chapter summary and conclusions are given in Section 3.6.

3.2 Training Based Channel Estimation for MIMO Systems

3.2.1 System Model

In this section, the performance of classic TBCE is characterized in the context of the CSTSK MIMO system discussed in Chapter 2 associated with the configuration of CSTSK(M, N, T, Q, \mathcal{L} -PSK/QAM), where M and N indicate the number of Tx and Rx antennas, respectively, while T denotes the number of time slots occupied by the CSTSK signal block and Q is the number of dispersion matrices employed. Let i denote the CSTSK transmission block index. As in Chapter 2, a quasi-static frequency-flat Rayleigh fading environment is considered.

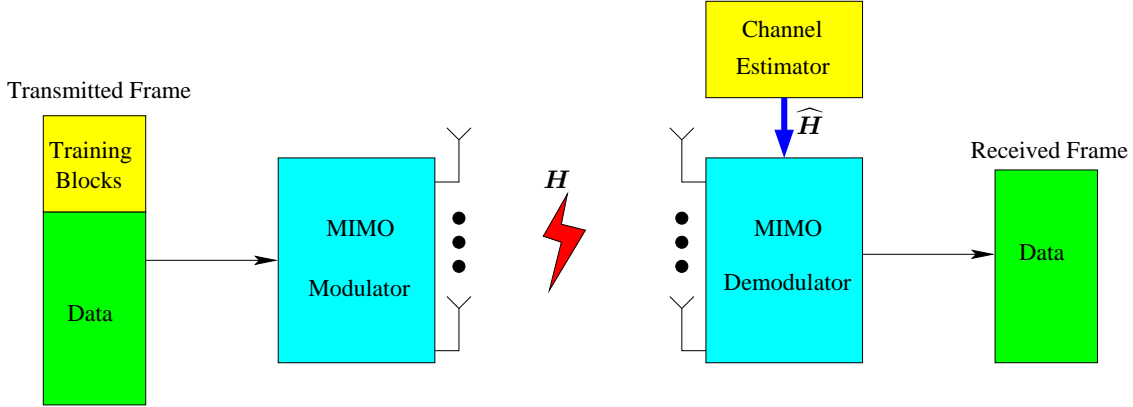


Figure 3.1: Structure of a TBCE aided MIMO system.

The schematic diagram of the TBCE aided CSTSK system is shown in Fig. 3.1, where it may be seen that at the CSTSK transmitter, the transmitted frame is formulated by two parts, namely, the training blocks and the data. Both the training blocks and the data are modulated by the CSTSK MIMO modulator and transmitted through the wireless channel H . The received signal block $\mathbf{Y}(i) \in \mathbb{C}^{N \times T}$ of the CSTSK system was given in Eq. (2.10), which is quoted below

$$\mathbf{Y}(i) = \mathbf{H}\mathbf{S}(i) + \mathbf{V}(i). \quad (3.1)$$

Assume that the number of available training blocks is M_T and if we arrange the training data as

$$\mathbf{Y}_{tM_T} = [\mathbf{Y}(1) \ \mathbf{Y}(2) \cdots \mathbf{Y}(M_T)], \quad (3.2)$$

$$\mathbf{S}_{tM_T} = [\mathbf{S}(1) \ \mathbf{S}(2) \cdots \mathbf{S}(M_T)], \quad (3.3)$$

the training based LSCE of the MIMO channel matrix H is then given by

$$\hat{\mathbf{H}} = \mathbf{Y}_{tM_T} \mathbf{S}_{tM_T}^H (\mathbf{S}_{tM_T} \mathbf{S}_{tM_T}^H)^{-1}, \quad (3.4)$$

associated with a complexity order of $\mathcal{O}(M_T^3)$. In order to ensure that $\mathbf{S}_{tM_T} \mathbf{S}_{tM_T}^H$ has the full rank of M , it is necessary to guarantee that we have $M_T \cdot T \geq M$ and this leads to a lower bound on the number of training blocks, which is

$$M_T \geq \left\lceil \frac{M}{T} \right\rceil, \quad (3.5)$$

where $\lceil \cdot \rceil$ denotes the integer ceiling operator. For instance, if we have $M = 4$ and $T = 2$, then the lower bound is $M_T = 2$ and we may choose to use as few as two CSTSK training blocks for TBCE. However, it may be expected that with such a low number of training blocks, the accuracy of the LSCE of Eq. (3.4) will be poor and hence the achievable BER performance based on this channel estimate will also remain poor. The accuracy of TBCE may be improved by increasing the number of training blocks M_T , at the expense of reducing the effective throughput of the system.

Table 3.1: System parameters of the TBCE aided CSTSK system of Fig. 3.1.

Number of Tx antennas	M
Number of Rx antennas	N
Symbol durations per block	T
Number of dispersion matrices	Q
Modulation	\mathcal{L} -QAM or \mathcal{L} -PSK
Channels	Frequency-flat Rayleigh fading
Detector	ML detector
Number of training blocks	M_T
Number of signal blocks per frame	$\tau = 250$
Pilot overhead	O_p of Eq. (3.7)
Interleaver blocklength	10^6 bits
Outer channel code	Half-rate RSC
Generator polynomials	$(G_{RSC}^r, G_{RSC}) = (7,5)_8$
Precoder	URC
Number of inner iterations	I_{in}
Number of outer iterations	I_{out}

3.2.2 Simulation Results

In this section, the performance of the TBCE aided CSTSK scheme is investigated in both the uncoded scenario of Fig. 2.17 and three-stage serial-concatenated turbo coded scenario of Fig. 2.28. A quasi-static Rayleigh fading environment was considered. In the uncoded scenario, the block-length was set to $\tau = 250$ STSK symbol-blocks per frame. An interleaver length of 10^6 bits was used by the three-stage serial-concatenated turbo encoder and decoder of Fig. 2.28. The binary generator polynomials of the RSC encoder were $G_{RSC} = [1, 0, 1]_2$ and $G_{RSC}^r = [1, 1, 1]_2$, while these of the URC encoder were $G_{URC} = [1, 0]_2$ and $G_{URC}^r = [1, 1]_2$. The transmitted signal power of all the simulated systems was normalized to unity and, therefore, the SNR was defined as $\frac{1}{N_0}$, with N_0 being the AWGN power. Two metrics were used for assessing the achievable performance, namely the BER and the Mean CE Error (MCEE) defined by

$$J_{\text{MCEE}}(\hat{\mathbf{H}}) = \frac{1}{N \cdot M} \|\mathbf{H} - \hat{\mathbf{H}}\|^2, \quad (3.6)$$

where $\hat{\mathbf{H}}$ represents the estimate of the channel matrix \mathbf{H} . All the results were averaged over 10,000 channel realizations. We define the PO as

$$O_p = \frac{M_T}{\tau} \times 100\%, \quad (3.7)$$

for quantifying the throughput efficiency of the TBCE aided system. More specifically, a higher value of O_p leads to a lower effective throughput and vice versa. The system parameters of the

TBCE aided CSTSK system of Fig. 3.1 are summarized in Table 3.1.

3.2.2.1 Uncoded TBCE Aided CSTSK

This section characterizes the BER and MCEE performance of the uncoded TBCE aided CSTSK systems associated with the configurations of CSTSK(2, 2, 2, 4, QPSK), CSTSK(4, 2, 2, 4, QPSK) and CSTSK(4, 4, 2, 4, 16-QAM), which have normalized throughputs of $R = 2, 2$ and 3 bits/symbol, respectively, as seen in Table 3.5.

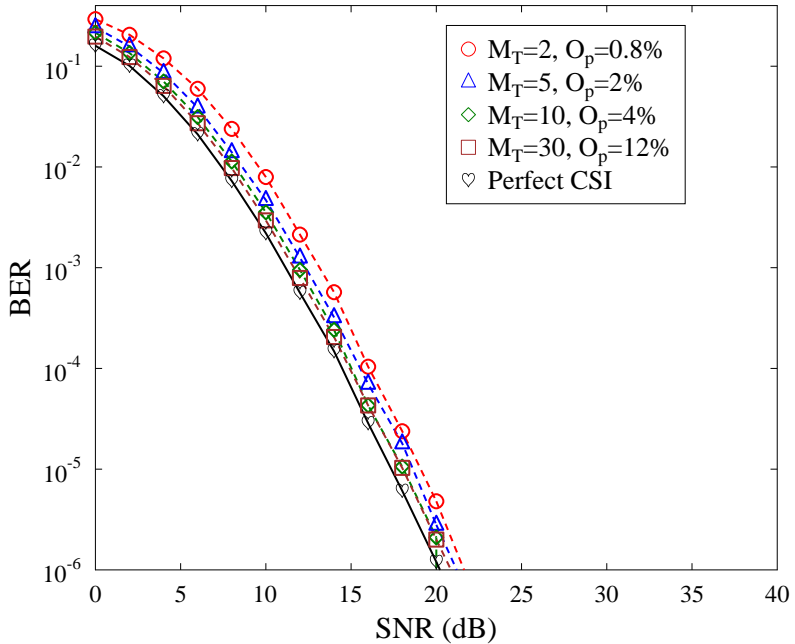


Figure 3.2: Achievable BER performance of the TBCE aided CSTSK(2, 2, 2, 4, QPSK) system of Fig. 3.1 having a normalized throughput of $R = 2$ bits/symbol, associated with different numbers of the STSK training blocks of $M_T = 2, 5, 10$ and 30 , and the corresponding POs of $O_p = 0.8\%, 2\%, 4\%$ and 12% , in comparison to the performance of the perfect CSI. All other system parameters were summarized in Table 3.1.

Fig. 3.2 shows the BER performance of the TBCE aided CSTSK(2, 2, 2, 4, QPSK) system of Fig. 3.1, associated with the number of STSK training blocks $M_T \in \{2, 5, 10, 30\}$, corresponding to the POs of $O_p = 0.8\%, 2\%, 4\%$ and 12% , respectively. The system's normalized throughput is $R = 2$ bits/symbol. The BER performance based on the perfect CSI is also depicted as the benchmark. It may be seen from Fig. 3.2 that as the PO increases, the BER performance is improved, although at the expense of a reduced effective system's throughput. For example, when the number of training blocks is set to $M_T = 2$, the SNR gap between the perfect CSI case and the TBCE based system is about 1.5 dB at the BER level of 10^{-6} , and the PO is $O_p = 0.8\%$. However, when the number of training blocks is increased to $M_T = 30$, the SNR gap between the perfect CSI based system and the TBCE based system is reduced to a value below 0.8 dB, while the PO is increased

to $O_p = 12\%$.

As expected, the results of Fig. 3.2 confirm that in the TBCE assisted MIMO scheme, increasing the number of training blocks, i.e. having a higher PO, improves the BER performance. This BER performance gain is the consequence of the improved CE accuracy owing to the increased PO, which may be quantified by the MCEE defined in Eq. (3.6). The corresponding MCEE performance of the TBCE aided CSTSK(2, 2, 2, 4, QPSK) system of Fig. 3.1 is depicted in Fig. 3.3 at the SNR values of 6 dB, 12 dB and 18 dB, respectively. It may be seen that as the PO increases, the CE accuracy is improved. For example, at SNR = 6 dB, the MCEE is approximately $J_{\text{MCEE}} = 0.1257$ when the number of training blocks is $M_T = 2$ ($O_p = 0.8\%$), while in the case of $M_T = 30$ ($O_p = 12\%$), the MCEE becomes approximately $J_{\text{MCEE}} = 0.0084$, implying that a higher CE accuracy may be achieved by increasing the number of STSK training blocks, i.e. having a higher PO, at the expense of a reduced system's effective throughput. In particular, the MCEE performance associated with the case of $M_T = \tau = 250$ STSK training blocks is also depicted in Fig. 3.3, which corresponds to the best achievable MCEE performance, where all the symbol blocks within a frame are used as training blocks, implying that the PO becomes $O_p = 100\%$. Moreover, it may also be found that when the PO increases beyond a certain value, almost no further CE quality improvement is attained. For example, for the case of SNR = 6 dB, when the PO increases from $O_p = 0.8\%$ to $O_p = 12\%$, the absolute MCEE reduction is about $\Delta J_{\text{MCEE}} = 0.117$. However, when PO further

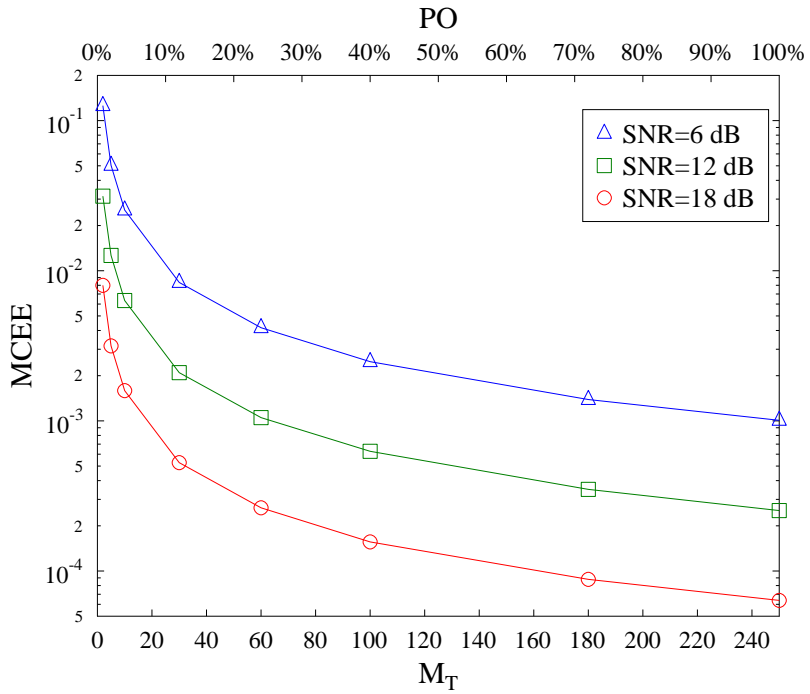


Figure 3.3: Achievable MCEE performance of the TBCE aided CSTSK(2, 2, 2, 4, QPSK) system of Fig. 3.1 as a function of the PO, at various SNR values. The system's normalized throughput is $R = 2$ bits/symbol. All other system parameters were summarized in Table 3.1.

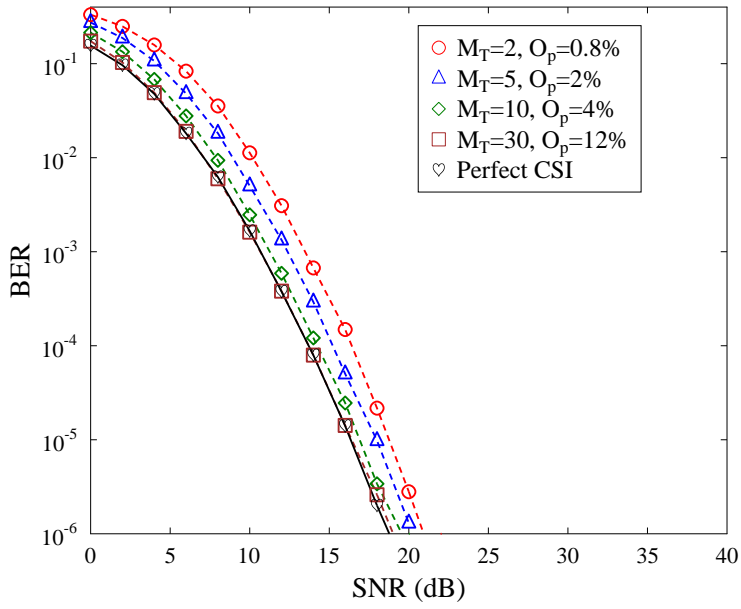


Figure 3.4: Achievable BER performance of the TBCE aided CSTSK(4, 2, 2, 4, QPSK) system of Fig. 3.1 having a normalized throughput of $R = 2$ bits/symbol, associated with different numbers of the CSTSK training blocks of $M_T = 2, 5, 10$ and 30 , and the corresponding POs of $O_p = 0.8\%, 2\%, 4\%$ and 12% , in comparison to the performance of the perfect CSI. All other system parameters were summarized in Table 3.1.

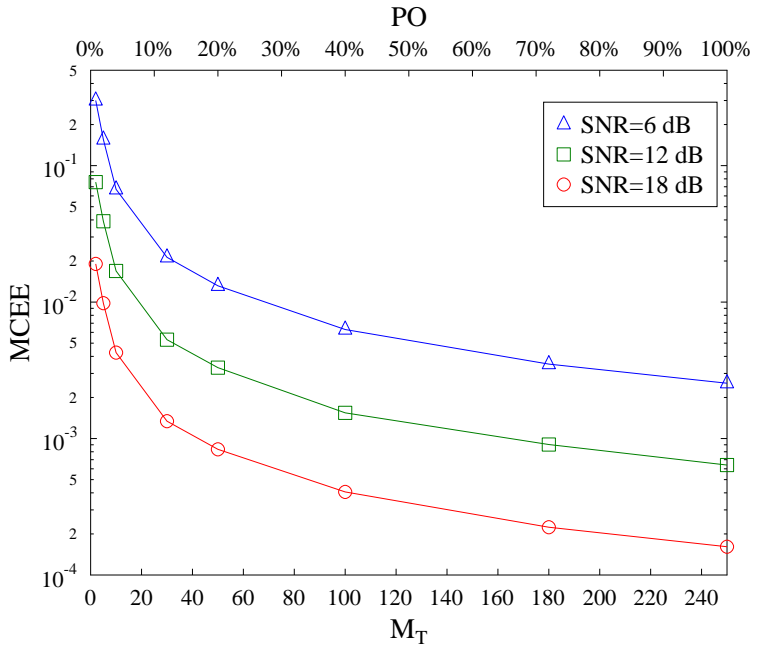


Figure 3.5: Achievable MCEE performance of the TBCE aided CSTSK(4, 2, 2, 4, QPSK) system of Fig. 3.1 as a function of the PO, at various SNR values. The system's normalized throughput is $R = 2$ bits/symbol. All other system parameters were summarized in Table 3.1.

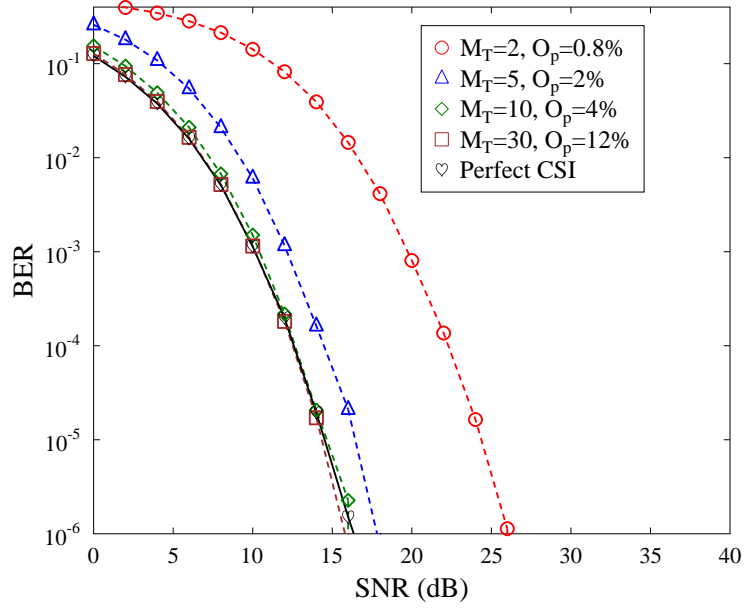


Figure 3.6: Achievable BER performance of the TBCE aided CSTSK(4,4,2,4,16-QAM) system of Fig. 3.1 having a normalized throughput of $R = 3$ bits/symbol, associated with different numbers of the STSK training blocks of $M_T = 2, 5, 10$ and 30 , and the corresponding POs of $O_p = 0.8\%, 2\%, 4\%$ and 12% , in comparison to the performance of the perfect CSI. All other system parameters were summarized in Table 3.1.

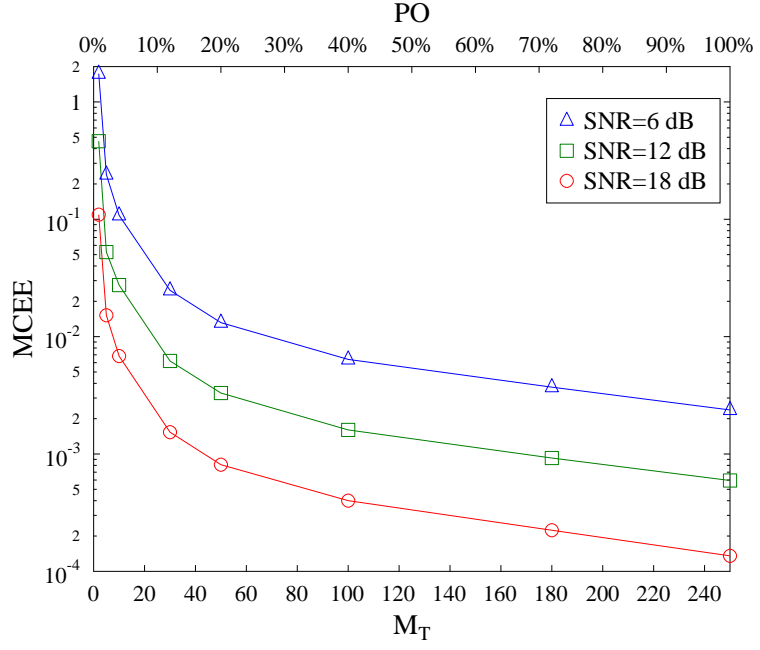


Figure 3.7: Achievable MCEE performance of the TBCE aided CSTSK(4,4,2,4,16-QAM) system of Fig. 3.1 as a function of the PO, at various SNR values. The system's normalized throughput is $R = 3$ bits/symbol. All other system parameters were summarized in Table 3.1.

increases from $O_p = 12\%$ to $O_p = 24\%$, the absolute MCEE reduction becomes insignificant, which is just about $\Delta J_{\text{MCEE}} = 0.004$. This implies that increasing the PO over a certain range, say $O_p = 12\%$, may not be helpful in terms of improving the system's performance, despite reducing the system's effective throughput. Additionally, it may also be seen from Fig. 3.3 that given a PO, as the SNR increases, the accuracy of CE is improved. For example, given the PO of $O_p = 12\%$, at the SNR = 6 dB, the MCEE is about $J_{\text{MCEE}} = 0.0084$, while at the SNR = 12 dB, the MCEE is reduced to $J_{\text{MCEE}} = 0.0021$.

Fig. 3.4 depicted the achievable BER performance of the TBCE aided CSTSK(4, 2, 2, 4, QPSK) system of Fig. 3.1, having a throughput of $R = 2$ bits/symbol. Similar to the BER performance of the TBCE aided CSTSK(2, 2, 2, 4, QPSK), as the PO increases, the BER performance is improved, albeit at the expense of a reduced effective system throughput. When the PO is increased to $O_p = 12\%$, i.e. having a number of training blocks of $M_T = 30$, the BER performance of the TBCE based system becomes capable of approaching the performance bound associated with the perfect CSI scenario. The corresponding MCEE performance of the TBCE aided CSTSK(4, 2, 2, 4, QPSK) is shown in Fig. 3.5, where it can also be seen that as PO increases, the CE accuracy is improved.

The BER and MCEE performance of the TBCE aided CSTSK(4, 4, 2, 4, 16-QAM) are shown in Figs. 3.6 and 3.7, respectively, where the same conclusions may be gleaned as those drawn from the above discussions on the CSTSK(2, 2, 2, 4, QPSK) and CSTSK(4, 2, 2, 4, QPSK) systems.

3.2.2.2 Three-stage Serial-Concatenated Turbo Coded and TBCE Aided CSTSK

This section provides the BER performance of the three-stage serial-concatenated turbo coded and TBCE aided CSTSK systems of Fig. 2.28 associated with the configurations of CSTSK(4, 2, 2, 4, QPSK) and CSTSK(4, 4, 2, 4, 16-QAM), relying on the system parameters of Table 3.1, having normalized throughputs of $R = 2$ and 3 bits/symbol, respectively.

The BER performance based on the CSTSK(4, 2, 2, 4, QPSK) scheme of Fig. 2.28 is depicted in Fig. 3.8, where it may be seen that as the PO increases, the BER performance of the TBCE based system gets closer to the performance bound associated with perfect CSI. For example, when the PO is $O_p = 0.8\%$, the system becomes capable of achieving an infinitesimally low BER at approximately SNR = 3.1 dB, with a performance gap of about 3.3 dB compared to the perfect CSI scenario. However, when the PO is increased to $O_p = 12\%$, the performance gap between the TBCE assisted scheme and the perfect CSI case is reduced to 1.2 dB. Furthermore, when a PO of $O_p = 20\%$ utilized, the performance gap is further reduced to about 0.2 dB. However, it is worth mentioning again that although increasing the PO improves the system's BER performance, it also reduces the system's effective throughput. Additionally, even with a high PO of $O_p = 20\%$, the three-stage serial-concatenated turbo coded and TBCE aided scheme of Fig. 2.28 still fails to approach the optimal performance bound associated with perfect CSI.

Fig. 3.9 shows the BER performance of the TBCE aided CSTSK(4, 2, 2, 4, QPSK) system of

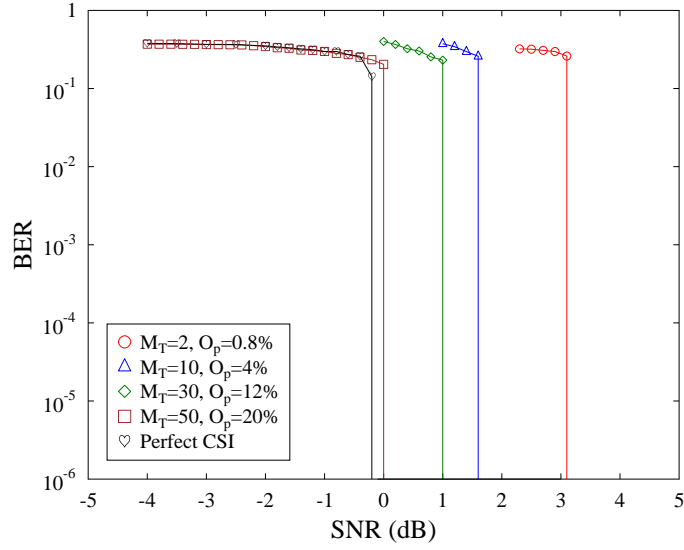


Figure 3.8: Achievable BER performance of the three-stage serial-concatenated turbo coding aided and TBCE assisted CSTSK(4,2,2,4,QPSK) system of Fig. 2.28, having a normalized throughput of $R = 2$ bits/symbol, associated with the POs of $O_p = 0.8\%$, 4% , 12% and 20% , in comparison to the performance of the perfect CSI. The number of inner and outer iterations is $I_{in} = 3$ and $I_{out} = 10$. All other system parameters were summarized in Table 3.1.

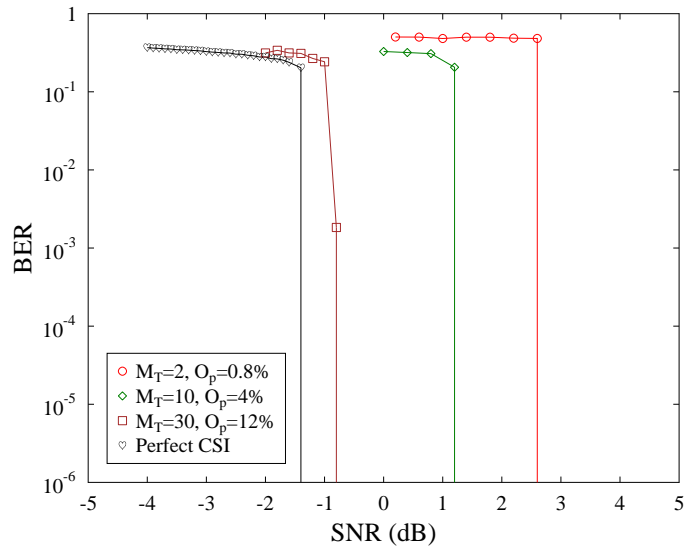


Figure 3.9: Achievable BER performance of the three-stage serial-concatenated turbo coding aided and TBCE assisted CSTSK(4,4,2,4,16-QAM) system of Fig. 2.28, having a normalized throughput of $R = 3$ bits/symbol, associated with the POs of $O_p = 0.8\%$, 4% and 12% , in comparison to the performance of the perfect CSI. The number of inner and outer iterations is $I_{in} = 3$ and $I_{out} = 9$. All other system parameters were summarized in Table 3.1.

Fig. 2.28. Similar to the performance of the TBCE aided CSTSK(4, 2, 2, 4, QPSK) depicted in Fig. 3.8, it may also be seen in Fig. 3.9 that as the PO increases, the BER performance of the TBCE aided system gets closer to the performance bound associated with perfect CSI. To be more explicit, when the PO is $O_p = 0.8\%$, the system becomes capable of achieving an infinitesimally low BER at about SNR = 2.6 dB, where there exists a performance gap of about 4 dB compared to the perfect CSI case. However, when the PO is increased to $O_p = 12\%$, the performance gap between the TBCE assisted scheme and the perfect CSI case is reduced to approximately 0.5 dB.

3.3 Semi-Blind Channel Estimation for MIMO Systems

3.3.1 System Model

It may be seen from the discussions provided in Section 3.2 that the conventional TBCE aided system is capable of achieving an accurate CE at the cost of reducing the system's effective throughput. For example, from the BER performance of the uncoded CSTSK(2, 2, 2, 4, QPSK) system depicted in Fig. 3.2, it may be seen that when the PO is $O_p = 0.8\%$, an SNR gap in excess of 2 dB is observed between the perfect CSI case and the TBCE aided system, while this gap is reduced to less than 0.5 dB when the PO is increased to $O_p = 12\%$. Naturally this PO leads to the system throughput loss increased from 0.8% to 12%. In order to alleviate this throughput loss problem, while achieving a high CE quality, semi-blind CE methods were proposed in [31, 32, 36, 48–59, 126]. The corresponding system's structure is shown in Fig. 3.10. It may be seen that unlike the conventional TBCE aided system of Fig. 3.1, an iteration loop is formed by the MIMO demodulator, data detector, MIMO modulator and channel estimator. To be more explicit, at the receiver, only a low PO, i.e. a small number of training blocks, is utilized for providing an initial TBCE. Then data detection is carried out based on this initial CE. The detected information bits are then re-modulated and fed into the CE for performing further DDCE. The data detector and CE iterate a number of times, until the DDCE converges.

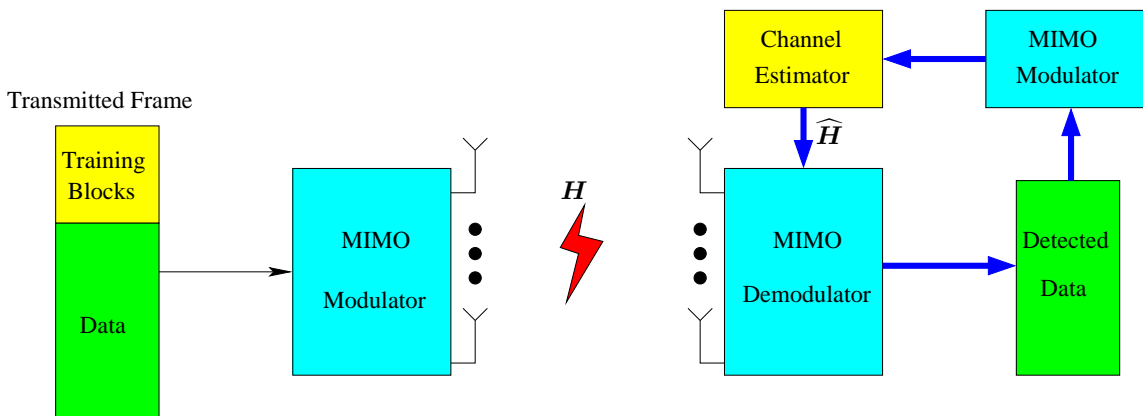


Figure 3.10: Structure of a SBCE aided CSTSK system.

Let us now discuss the iterative channel estimation and data detection scheme in more detail based on the CSTSK MIMO system of Section 2.3 of Chapter 2. For the CSTSK MIMO model of Eq. (3.1) and with the number of data blocks per frame τ , the observation data for the MIMO ML detector may be formulated as

$$\mathbf{Y}_{d\tau} = [\mathbf{Y}(1) \mathbf{Y}(2) \cdots \mathbf{Y}(\tau)]. \quad (3.8)$$

Furthermore let us denote the maximum number of iterations between the channel estimator and MIMO detector by I_{ce} . Then, given the initial TBCE $\hat{\mathbf{H}}$, the semi-blind iterative algorithm may be summarized as below:

Step 1) Set the iteration index to $t = 0$ and the initial CE as $\hat{\mathbf{H}}^{(t)} = \hat{\mathbf{H}}$;

Step 2) Given the CE of $\hat{\mathbf{H}}^{(t)}$, perform ML MIMO detection on $\mathbf{Y}_{d\tau}$. The corresponding detected information bits are re-modulated to yield

$$\hat{\mathbf{S}}_{d\tau}^{(t)} = [\hat{\mathbf{S}}_{d\tau}^{(t)}(1) \hat{\mathbf{S}}_{d\tau}^{(t)}(2) \cdots \hat{\mathbf{S}}_{d\tau}^{(t)}(\tau)]; \quad (3.9)$$

Step 3) Update the CE with

$$\hat{\mathbf{H}}^{(t+1)} = \mathbf{Y}_{d\tau} \left(\hat{\mathbf{S}}_{d\tau}^{(t)} \right)^H \left(\hat{\mathbf{S}}_{d\tau}^{(t)} \left(\hat{\mathbf{S}}_{d\tau}^{(t)} \right)^H \right)^{-1}; \quad (3.10)$$

Step 4) Set the iteration index to $t = t + 1$: if $t < I_{ce}$, go back to Step 2); otherwise, stop.

The total complexity of this semi-blind iterative channel estimation and data detection process is on the order of $I_{ce} \cdot (\mathcal{O}(\tau^3) + C_{ML})$, with $\mathcal{O}(\tau^3)$ and C_{ML} being the complexity order of CE and ML MIMO detection. Our empirical results show that a small number of iterations is often sufficient for the iterative procedure to converge, and typically $I_{ce} \leq 5$. For medium to high SNR values, this iterative procedure is capable of converging to the optimal ML detection performance obtained under perfect CSI. In fact, if the initial TBCE $\hat{\mathbf{H}}^{(0)}$ can yield a relatively low BER, e.g. BER below 0.1, the DDCE of Step 3) is capable of improving the accuracy of the CE. This in turn significantly enhances the BER of the ML data detection in Step 2) of next iteration. Therefore, a few iterations are sufficient to attain the optimal ML solution. For low SNR values, however, some degradation from the optimal ML performance may be expected, particularly when the initial BER is higher than 0.1. In such a situation, increasing the minimum training blocks M_T of Eq. (3.5) by a few blocks will often ensure the convergence to the ML solution.

3.3.2 Simulation Results

In this section, the performance of the SBCE aided CSTSK scheme was simulated in uncoded scenarios. Again a quasi-static Rayleigh fading environment was considered. All the results were averaged over 100 channel realisations. The transmitted signal power of all the simulated systems was normalized to unity and, therefore, the SNR was defined as $\frac{1}{N_0}$, with N_0 being the AWGN

power. The BER and the MCEE defined in Eq. (3.6) were used as two metrics. The length of STSK data blocks for performing ML detection was $\tau = 250$. The system parameters of the SBCE aided CSTSK system of Fig. 3.10 are summarized in Table 3.2.

Table 3.2: System parameters of the SBCE aided CSTSK system of Fig. 3.10.

Number of Tx antennas	M
Number of Rx antennas	N
Symbol durations per block	T
Number of dispersion matrices	Q
Modulation	\mathcal{L} -QAM or \mathcal{L} -PSK
Channels	Frequency-flat Rayleigh fading
Detector	ML detector
Number of training blocks	M_T
Number of signal blocks per frame	$\tau = 250$
Pilot overhead	O_p of Eq. (3.7)
Number of CE iterations	I_{ce}

3.3.2.1 CSTSK(2, 2, 2, 4, QPSK) associated with $R = 2$ bits/symbol

The achievable BER performance of the SBCE aided CSTSK(2, 2, 2, 4, QPSK) scheme of Fig. 3.10 associated with the PO of $O_p = 0.8\%$ is compared to those of the TBCE aided system associated with POs of $O_p = 0.8\%$ and $O_p = 12\%$, corresponding to $M_T = 2$ and 30 in Fig. 3.11, with the BER performance obtained given the perfect CSI as the benchmark. The system's normalized throughput is $R = 2$ bits/symbol. It can be seen that for the TBCE based system, using only $M_T = 2$ CSTSK training blocks, i.e. a PO of $O_p = 0.8\%$, is inadequate and, to approximate the true ML performance, more than 30 CSTSK training blocks are required, which corresponds to a PO of over 12%. By contrast, the performance of the iterative SBCE based system with only $M_T = 2$ initial CSTSK training blocks, i.e. a PO of $O_p = 0.8\%$, is capable of outperforming the TBCE based system associated with $M_T = 30$ training blocks ($O_p = 12\%$) and is even capable of approaching the performance of the perfect CSI benchmark for $\text{SNR} > 14$ dB. Therefore, it may be concluded that given a sufficiently high SNR, the SBCE scheme is capable of approaching the optimal performance based on perfect CSI, while utilizing a low PO with the objective of maintaining a high system throughput.

The MCEE performance of the SBCE aided CSTSK(2, 2, 2, 4, QPSK) scheme of Fig. 3.10 associated with $M_T = 2$ initial training blocks and $O_p = 0.8\%$ is depicted in Fig. 3.12, in comparison to the MCEE performance of the TBCE based scheme associated with $M_T = 250$ training blocks and $O_p = 100\%$, at the SNRs of 6 dB, 12 dB and 18 dB. It may be seen that the

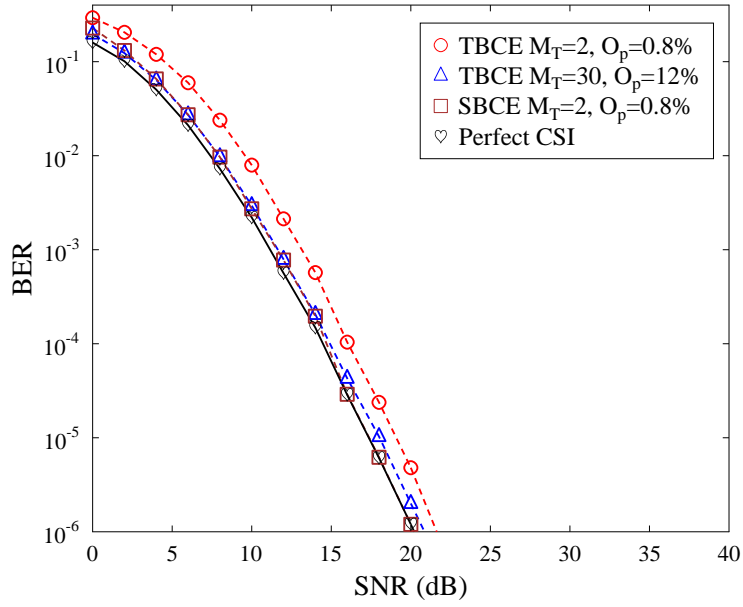


Figure 3.11: Achievable BER performance of the SBCE aided CSTSK(2,2,2,4, QPSK) system of Fig. 3.10 having a normalized throughput of $R = 2$ bits/symbol, associated with $M_T = 2$ initial training blocks and a PO of $O_p = 0.8\%$, in comparison to those of the TBCE aided system of Fig. 3.1 associated with $M_T = 2$ and 30 training blocks and the POs of $O_p = 0.8\%$ and $O_p = 12\%$, respectively. The perfect CSI scenario is also depicted as the benchmark. All other system parameters were summarized in Table 3.2.

MCEE of the SBCE based scheme is capable of reaching a steady state within $I_{ce} = 5$ iterations at all the SNR values investigated. Furthermore, as the SNR increases, fewer CE and data detection iterations may be required. More explicitly, given SNR = 6 dB, the steady state MCEE may be achieved by $I_{ce} = 5$ iterations. When the SNR increases to 12 dB, only $I_{ce} = 3$ iterations are required. Additionally, as expected, when the SNR increases, the MCEE value decreases. To be more explicit, given SNR = 6 dB, the steady state of the MCEE is $J_{MCEE} = 0.0038$. However, when the SNR is increased to 12 dB, the steady state of the MCEE becomes $J_{MCEE} = 0.00026$, which is significantly lower than that of the SNR = 6 dB scenario. Moreover, we also plot the MCEE performance of the TBCE scheme associated with $M_T = 250$ training blocks and $O_p = 100\%$ at the three SNRs seen in Fig. 3.12, for the sake of providing a pertinent benchmark performance for the SBCE aided CSTSK(2,2,2,4, QPSK) associated with $M_T = 2$ initial training blocks and $O_p = 0.8\%$. Note that in our simulations, we set the number of data blocks for performing the ML detection to $\tau = 250$. Therefore, if most decisions are correct at a certain SNR range, the DDCE associated with $\tau = 250$ detected data blocks will be capable of approaching the optimal CE accuracy of the TBCE associated with $M_T = 250$ training blocks and $O_p = 100\%$. It may be seen from Fig. 3.12 that given SNR = 6 dB, there exists an MCEE difference of approximately $\Delta J_{MCEE} = 0.0024$ between the optimal TBCE and the SBCE, whilst when the SNR is increased to 12 dB, the MCEE difference is reduced to less than $\Delta J_{MCEE} = 0.0001$. When the SNR is further

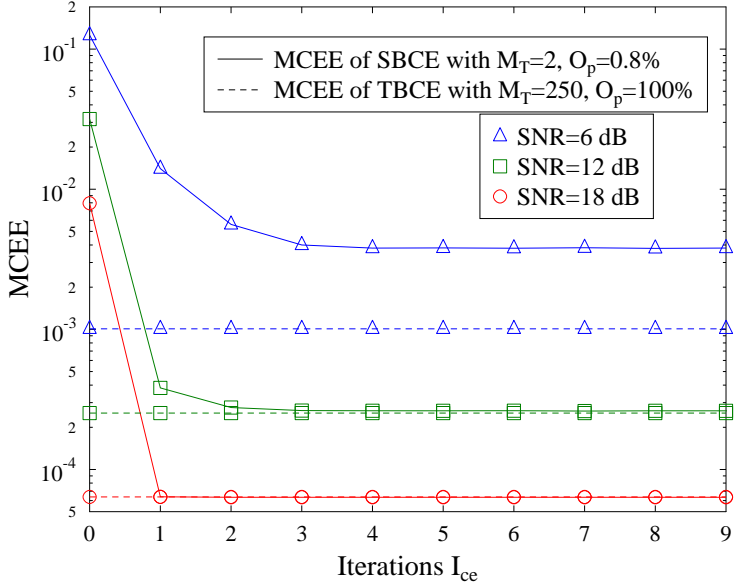


Figure 3.12: MCEE performance of the SBCE aided CSTSK(2,2,2,4, QPSK) system of Fig. 3.10 having a normalized throughput of $R = 2$ bits/symbol, associated with $M_T = 2$ initial training blocks and the PO of $O_p = 0.8\%$, in comparison to that of the TBCE aided system of Fig. 3.1 associated with $M_T = 250$ training blocks and the PO of $O_p = 100\%$, given SNR values of 6 dB, 12 dB and 18 dB. All other system parameters were summarized in Table 3.2.

increased to 18 dB, the steady-state MCEE of the SBCE scheme converges exactly to the optimal TBCE bound. Therefore, we may conclude that as the SNR increases, the difference between the steady-state MCEE of the SBCE scheme and the optimal MCEE of the TBCE scheme associated with $\tau = M_T$ decreases. Moreover, the steady-state MCEE of the SBCE scheme is capable of approaching to that of the optimal TBCE for sufficiently high SNR values, i.e. for SNRs over 12 dB for this example scenario.

3.3.2.2 CSTSK(4,2,2,4, QPSK) associated with $R = 2$ bits/symbol

Fig. 3.13 shows the achievable BER performance of the SBCE aided CSTSK(4,2,2,4, QPSK) scheme of Fig. 3.10 associated with $M_T = 2$ initial training blocks and $O_p = 0.8\%$, in comparison to those of the TBCE based system with $M_T = 2$ and 30 training blocks, having corresponding POs of $O_p = 0.8\%$ and $O_p = 12\%$, respectively. The system's normalized throughput is $R = 2$ bits/symbol. The BER performance based on perfect CSI is also provided as the benchmark. Similar to the performance for the CSTSK(2,2,2,4, QPSK) system, it can be seen that for the CSTSK(4,2,2,4, QPSK) arrangement, the TBCE scheme using only $M_T = 2$ CSTSK training blocks and $O_p = 0.8\%$ is also inadequate for approaching the true ML detection performance. On the other hand, the performance of the TBCE scheme associated with $M_T = 30$ training blocks

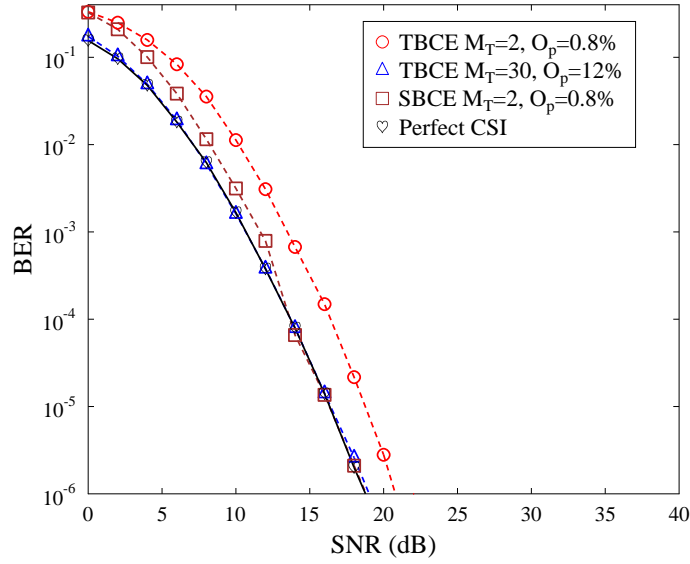


Figure 3.13: Achievable BER performance of the SBCE aided CSTSK(4, 2, 2, 4, QPSK) system of Fig. 3.10 having a normalized throughput of $R = 2$ bits/symbol, associated with $M_T = 2$ initial training blocks and a PO of $O_p = 0.8\%$, in comparison to those of the TBCE aided system of Fig. 3.1 associated with $M_T = 2$ and 30 training blocks and the POs of $O_p = 0.8\%$ and $O_p = 12\%$, respectively. The perfect CSI scenario is also depicted as the benchmark. All other system parameters were summarized in Table 3.2.

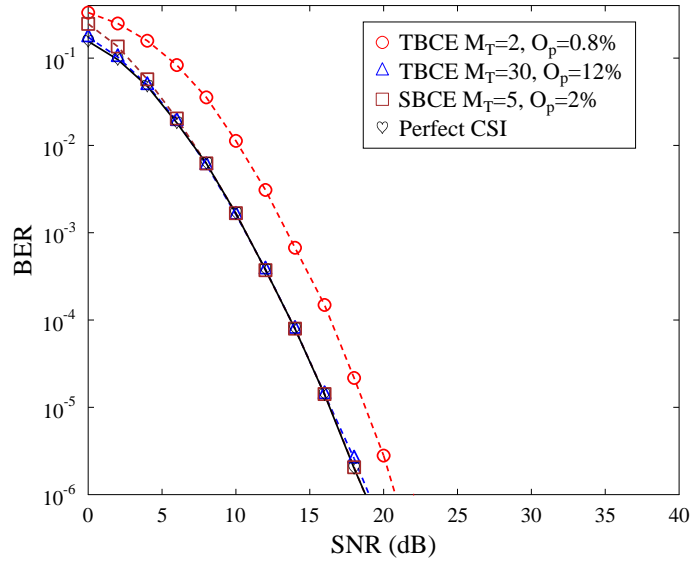


Figure 3.14: Achievable BER performance of the SBCE aided CSTSK(4, 2, 2, 4, QPSK) system of Fig. 3.10 having a normalized throughput of $R = 2$ bits/symbol, associated with $M_T = 5$ initial training blocks and a PO of $O_p = 2\%$, in comparison to those of the TBCE aided system of Fig. 3.1 associated with $M_T = 2$ and 30 training blocks and the POs of $O_p = 0.8\%$ and $O_p = 12\%$, respectively. The perfect CSI scenario is also depicted as the benchmark. All other system parameters were summarized in Table 3.2.

$(O_p = 12\%)$ is capable of reaching the optimal performance bound based on perfect CSI, but the system's throughput is significantly reduced. It may be seen from Fig. 3.13 that the SBCE scheme with $M_T = 2$ initial CSTSK training blocks and $O_p = 0.8\%$ is capable of achieving a similar performance to that of the SBCE based system associated with $M_T = 30$ training blocks and $O_p = 12\%$, and thus only capable of approaching the perfect CSI benchmark for $\text{SNR} \geq 14 \text{ dB}$. However, at low SNRs, the SBCE scheme fails to approach the optimal ML performance bound. This is because for this CSTSK(4, 2, 2, 4, QPSK) system, there are $M \cdot N = 8$ complex-valued channel taps. Two training blocks corresponds to 8 training bits and to $O_p = 0.8\%$, yielding a training overhead of 1 bit per channel use. The SBCE scheme under such a low training overhead and the condition of $\text{SNR} < 14 \text{ dB}$ suffers from some degradation with regard to the optimal BER performance. This performance degradation may be reduced by employing a slightly higher PO. The corresponding BER performance of employing $M_T = 5$ initial training blocks ($O_p = 2\%$) is depicted in Fig. 3.14, where it may be seen that the SBCE scheme now becomes capable of approaching the optimal BER performance for $\text{SNR} \geq 6 \text{ dB}$.

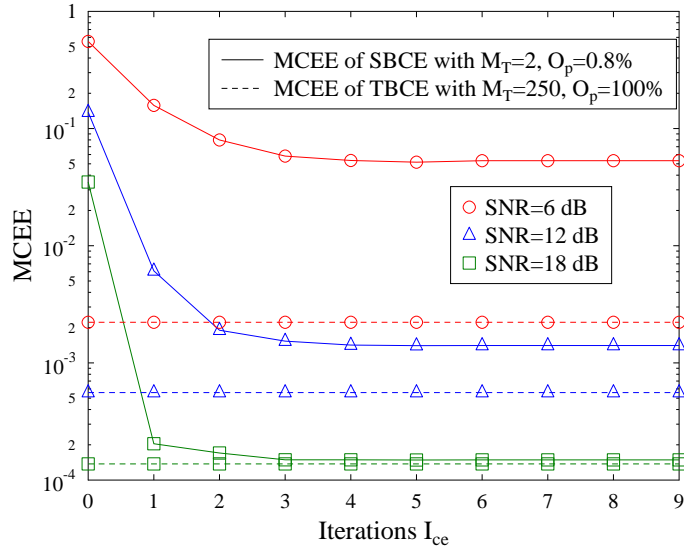


Figure 3.15: MCEE performance of the SBCE aided CSTSK(4, 2, 2, 4, QPSK) system of Fig. 3.10 having a normalized throughput of $R = 2$ bits/symbol, associated with $M_T = 2$ initial training blocks and the PO of $O_p = 0.8\%$, in comparison to that of the TBCE aided system of Fig. 3.1 associated with $M_T = 250$ training blocks and the PO of $O_p = 100\%$, given SNR values of 6 dB, 12 dB and 18 dB. All other system parameters were summarized in Table 3.2.

The MCEE performance of the SBCE aided CSTSK(4, 2, 2, 4, QPSK) scheme of Fig. 3.10 associated with $M_T = 2$ initial training blocks and $O_p = 0.8\%$ is depicted in Fig. 3.15, in comparison to the MCEE of the TBCE scheme associated with $M_T = 250$ training blocks and a PO of $O_p = 100\%$, at the SNRs of 6 dB, 12 dB and 18 dB. It may be seen from Fig. 3.15 that the MCEE of the SBCE scheme is capable of reaching a steady state within $I_{ce} = 5$ iterations at all the three

SNRs, and as expected, as the SNR increases, the steady-state MCEE value decreases. Additionally, we may also see that the steady-state MCEE of the SBCE scheme may converge to the optimal MCEE of the TBCE scheme associated with $M_T = 250$ ($O_p = 100\%$) at high SNRs, specifically, the case of SNR = 18 dB in Fig. 3.15 for this example. This agrees with the corresponding BER performance illustrated in Fig. 3.13.

3.3.2.3 CSTSK(4, 4, 2, 4, 16-QAM) associated with $R = 3$ bits/symbol

We also provide the achievable BER performance of the SBCE aided CSTSK(4, 4, 2, 4, 16-QAM) scheme of Fig. 3.10 associated with $M_T = 2$ ($O_p = 0.8\%$) and 3 ($O_p = 1.2\%$) initial training blocks in Fig. 3.16 and 3.17, respectively, in comparison to those of the TBCE based system with $M_T = 2$ and 30 training blocks, having POs of $O_p = 0.8\%$ and $O_p = 12\%$, respectively. It may be seen that despite using an extremely low training overhead of just $M_T = 2$ training blocks, the SBCE based scheme becomes capable of approaching the optimal ML performance based on perfect CSI for the $\text{SNR} \geq 12$ dB. However, by employing just one more training block, i.e. $M_T = 3$ and $O_p = 1.2\%$, the SBCE based scheme becomes capable of approaching the optimal ML performance bound for $\text{SNR} \geq 2$ dB. The MCEE convergence performance of the SBCE

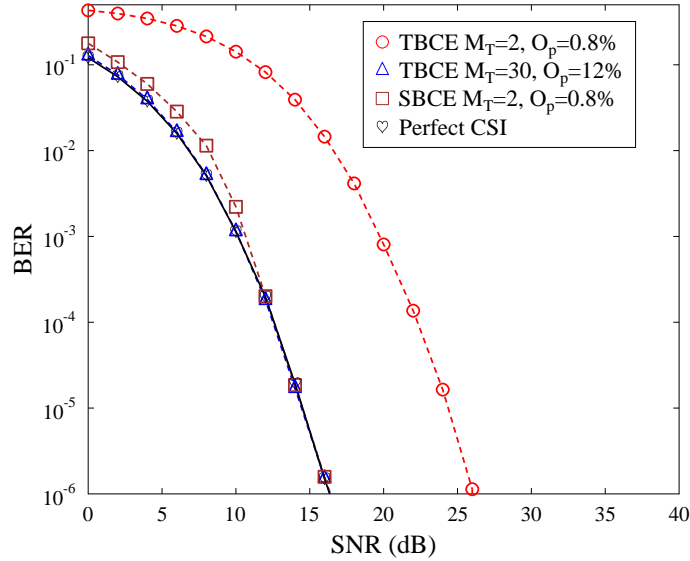


Figure 3.16: Achievable BER performance of the SBCE assisted CSTSK(4, 4, 2, 4, 16-QAM) system of Fig. 3.10 having a normalized throughput of $R = 3$ bits/symbol, associated with $M_T = 2$ initial training blocks and a PO of $O_p = 0.8\%$, in comparison to those of the TBCE aided system of Fig. 3.1 associated with $M_T = 2$ and 30 training blocks and the POs of $O_p = 0.8\%$ and $O_p = 12\%$, respectively. The perfect CSI scenario is also depicted as the benchmark. All other system parameters were summarized in Table 3.2.

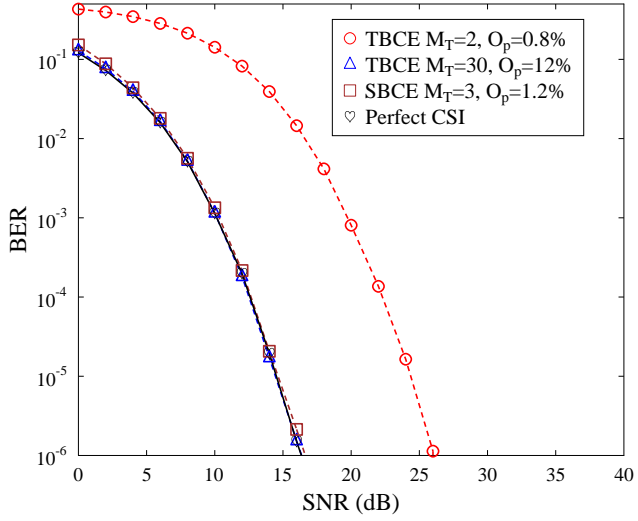


Figure 3.17: Achievable BER performance of the SBCE assisted CSTSK(4,4,2,4,16-QAM) system of Fig. 3.10 having a normalized throughput of $R = 3$ bits/symbol, associated with $M_T = 3$ initial training blocks and a PO of $O_p = 1.2\%$, in comparison to those of the TBCE aided system of Fig. 3.1 associated with $M_T = 2$ and 30 training blocks and the POs of $O_p = 0.8\%$ and $O_p = 12\%$, respectively. The perfect CSI scenario is also depicted as the benchmark. All other system parameters were summarized in Table 3.2.

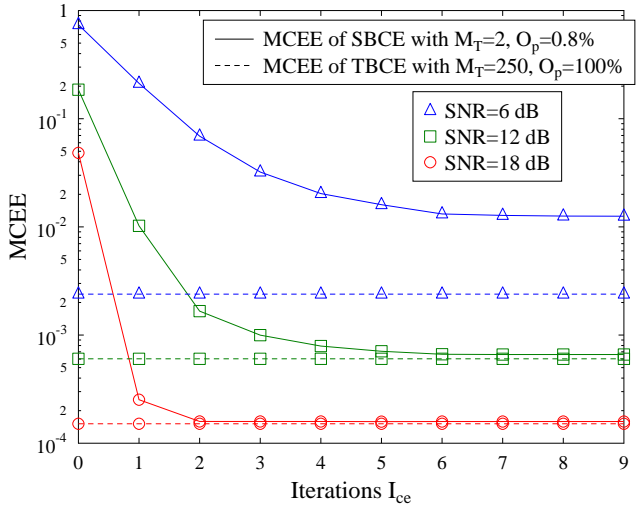


Figure 3.18: MCEE performance of the SBCE assisted CSTSK(4,4,2,4,16-QAM) system of Fig. 3.10 having a normalized throughput of $R = 3$ bits/symbol, associated with $M_T = 2$ initial training blocks and the PO of $O_p = 0.8\%$, in comparison to that of the TBCE aided system of Fig. 3.1 associated with $M_T = 250$ training blocks and the PO of $O_p = 100\%$, given SNR values of 6 dB, 12 dB and 18 dB. All other system parameters were summarized in Table 3.2.

aided CSTSK(4, 4, 2, 4, 16-QAM) associated with $M_T = 2$ ($O_p = 0.8\%$) initial training blocks is depicted in Fig. 3.18, in comparison to the MCEE of the TBCE scheme associated with $M_T = 250$ training blocks ($O_p = 100\%$), at the SNRs of 6 dB, 12 dB and 18 dB. It may be seen that the MCEE of the SBCE based scheme is capable of reaching a steady state within $I_{ce} = 5$ iterations at all the three SNRs, similar to the previous two systems, and as the SNR increases, the steady-state MCEE value decreases. Additionally, we may also see that the steady-state MCEE of the SBCE aided system may converge to that of the TBCE scheme associated with $M_T = 250$ at high SNRs, i.e. for the case of SNR = 12 dB in Fig. 3.18 for this example.

3.4 Joint Channel Estimation and Three-Stage Turbo Detection for MIMO Systems

In Section 3.3, the semi-blind iterative CE and data detection scheme for uncoded MIMO systems has been discussed, where the initial TBCE is carried out with the aid of a small number of MIMO training blocks in order to maintain a high system throughput. The channel estimate is then further refined within an iterative loop exchanging information between the DD channel estimator and the MIMO detector, which requires several iterations to converge. As discussed in Chapter 2, employing a three-stage serial-concatenated turbo coding scheme can significantly improve the system performance, achieving near-capacity performance. In this section, we will introduce the concept of three-stage serial-concatenated turbo coding scheme into our SBCE scheme discussed in the last section.

3.4.1 Conventional Iterative Channel Estimation and Turbo Detection MIMO

The state-of-the-arts [55–59, 127–137] can be represented by the conventional iterative CE and three-stage turbo detector-decoder structure¹ depicted in Fig. 3.19. As it has been discussed that in the SBCE scheme, the number of initial training blocks is usually low in order to maintain a high effective system throughput. Therefore, the accuracy of the initial TBCE is poor, and hence the achievable BER based on this initial channel estimate is also poor. However, the three-stage turbo detector-decoder is capable of improving the reliability of the detected bits for assisting the DDCE, which then provides a more accurate channel estimate. This iterative process results in an increasingly more reliable turbo detector-decoder output, which in turn further enhances the accuracy of the DDCE. Although the conventional iterative CE and three-stage turbo detector-decoder structure of Fig. 3.19 is very powerful, it has certain drawbacks.

Observe from Fig. 3.19 that since all the detected bits are used by the channel estimator, the DDCE update operation takes place after the convergence of the three-stage turbo detection-

¹Most of these schemes were originally designed for the two-stage turbo detector-decoder structure, but they can be readily extended to the three-stage turbo detector-decoder structure discussed here.

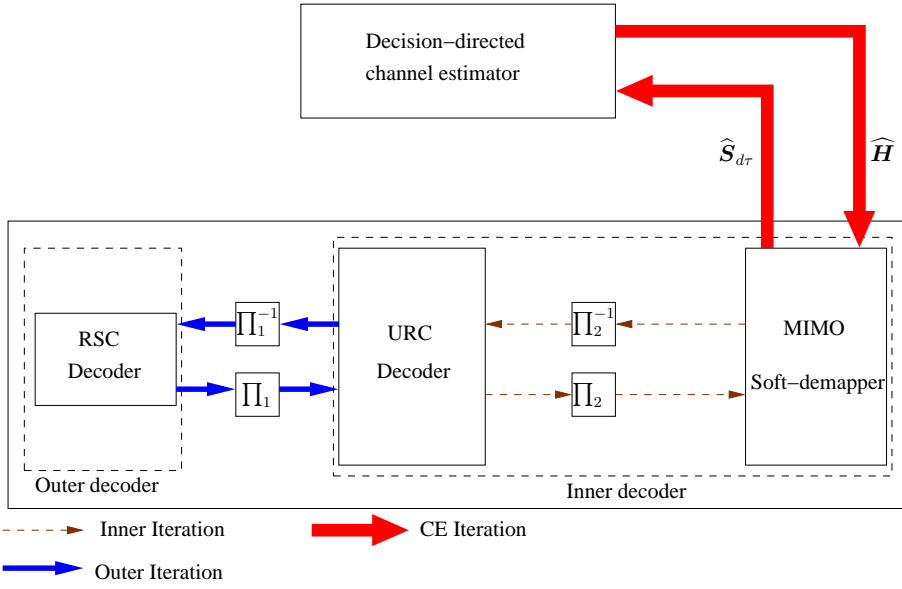


Figure 3.19: Conventional iterative CE and three-stage turbo detector-decoder. Note that all the detected bits are used by the decision-directed channel estimator. In order to benefit from the full error correction capability of the three-stage turbo detection and decoding, the updating of the DD channel estimate takes place after the convergence of the outer turbo loop.

decoding, in order to fully exploit the error correction capability of the three-stage turbo detector-decoder. This introduces the additional CE loop shown in Fig. 3.19, which requires I_{ce} iteration to converge. Furthermore, a turbo coded frame typically contains a very large number of data blocks τ , usually in thousands. Thus, the computational complexity of the LS based channel estimator is extremely high, in the order of $\mathcal{O}(\tau^3)$. Consequently, the turbo coding and CE structure shown in Fig. 3.19 requires extremely high computational complexity. To be more explicit, let C_{RSC} , C_{URC} and C_{ML} denote the computational complexity of the RSC decoder, the URC decoder, and the ML soft-demapper, respectively. Assume that given the CSI, the two-stage inner turbo loop requires I_{in} iterations, while the outer turbo loop requires I_{out} iterations. Then, given the CSI, the computational complexity of the three-stage turbo receiver can be formulated as

$$C_{\text{ideal}} = I_{out} \left(C_{RSC} + I_{in} (C_{ML} + C_{URC}) \right). \quad (3.11)$$

Given that the number of data blocks per frame is τ and the CE loop of Fig. 3.19 requires I_{ce} iterations to converge, the overall computational complexity of this conventional iterative CE and three-stage turbo receiver can be expressed as

$$C_{\text{conventional}} = I_{ce} \cdot \mathcal{O}(\tau^3) + I_{ce} \cdot C_{\text{ideal}}, \quad (3.12)$$

which is significantly higher than C_{ideal} . More importantly, the frame of the detected bits may contain a large percentage of erroneous decisions, particularly at the low SNRs, which will degrade the DDCE that utilize all the detected symbol blocks $\hat{S}_{d\tau}$ corresponding to the received data frame.

Therefore, the existing conventional iterative CE and three-stage turbo receivers fail to approach the optimal BER performance bound of the idealised three-stage turbo ML detector-decoder associated with the perfect CSI [127–129].

The above analysis of the disadvantages associated with this existing state-of-the-art motivates us to propose a novel iterative BBSBCE and three-stage turbo detector-decoder structure, which is capable of overcoming the drawbacks of the conventional iterative CE and three-stage turbo detector-decoder structure.

3.4.2 Joint BBSBCE and Three-Stage Turbo Demapping/Decoding for MIMOs

From the above discussion, it may be concluded that there exist two main limitations of the conventional joint CE and turbo detection based MIMO structures based on a low training overhead. Firstly, the conventional turbo coded CE scheme utilizes the entire detected data frame for DDCE and introduces an extra CE loop, all of these lead to significant increase in computational complexity. Secondly and more importantly, the detected frame contains erroneous or “bad” decisions, leading to potentially serious error propagation, particularly during the early turbo iterations under poor SNR conditions, which will degrade the system’s achievable performance. As a result, the conventional iterative CE and turbo detection based MIMO structures utilizing a low number of initial training blocks are incapable of matching the optimal performance bound associated with perfect CSI, despite of imposing a significantly higher complexity. In order for these iterative CE and turbo detection structures to approach the optimal performance bound associated with perfect CSI, it would be necessary to increase the training overhead, at the cost of reducing the effective system throughput considerably.

In order to overcome these two limitations, we propose a low-complexity joint BBSBCE and three-stage iterative demapping-decoding scheme for near-capacity CSTSK MIMO systems, which does not impose an extra iterative loop between the channel estimator and the three-stage turbo detector-decoder and which is capable of approaching the optimal performance bound associated with perfect CSI, while only imposing a minimum training overhead. Specifically, in order to maintain a high system throughput, only the minimum number of CSTSK training blocks is utilized for obtaining an initial TBCE. Naturally, the number of training blocks is related to the number of Tx antennas [31]. Then the low-complexity single-antenna based ML soft-demapping of [5] is carried out and the soft decisions are exchanged between the URC decoder and MIMO soft-demapper within the inner turbo loop, before they are forwarded to the outer RSC decoder. Moreover, the “high quality” or “more reliable” blocks-of-bits are selected based on the *a posteriori* information produced by the MIMO soft-demapper within the original inner turbo loop of the URC decoder and MIMO soft-demapper, which are re-modulated after each outer iteration of the original outer turbo loop for the sake of facilitating DDCE updates. Since the CE is naturally embedded into the original iterative three-stage demapping/decoding scheme, no extra iterative loop is required between

the CE and the three-stage MIMO demapper-decoder. This results in a low system complexity. In other words, the proposed joint BBSBCE and three-stage turbo demapping/decoding scheme has a similar computational complexity to that of the original three-stage turbo demapping-decoding scheme, which relies on the CSI-estimate of a dedicated training based channel estimator. Moreover, the proposed semi-blind joint CE and turbo detection-decoding scheme is capable of fully exploiting the “turbo effects” of the joint CE and three-stage demapping-decoding for approaching the optimal performance obtained by the idealised three-stage turbo demapping-decoding receiver furnished with perfect CSI, despite using only the same number of turbo iterations as the latter.

3.4.2.1 System Model

We begin by detailing the novel BBSBCE aided and three-stage serial-concatenated turbo coding assisted CSTSK, which has the configuration of $\text{CSTSK}(M, N, T, Q, \mathcal{L} - \text{PSK/QAM})$ discussed in Section 2.4, where M and N indicate the number of Tx antennas and Rx antennas, respectively, while T denotes the number of time slots occupied by the CSTSK signal block and Q is the number of dispersion matrices employed. Let i denote the CSTSK block index. A quasi-static frequency-flat Rayleigh fading environment is considered².

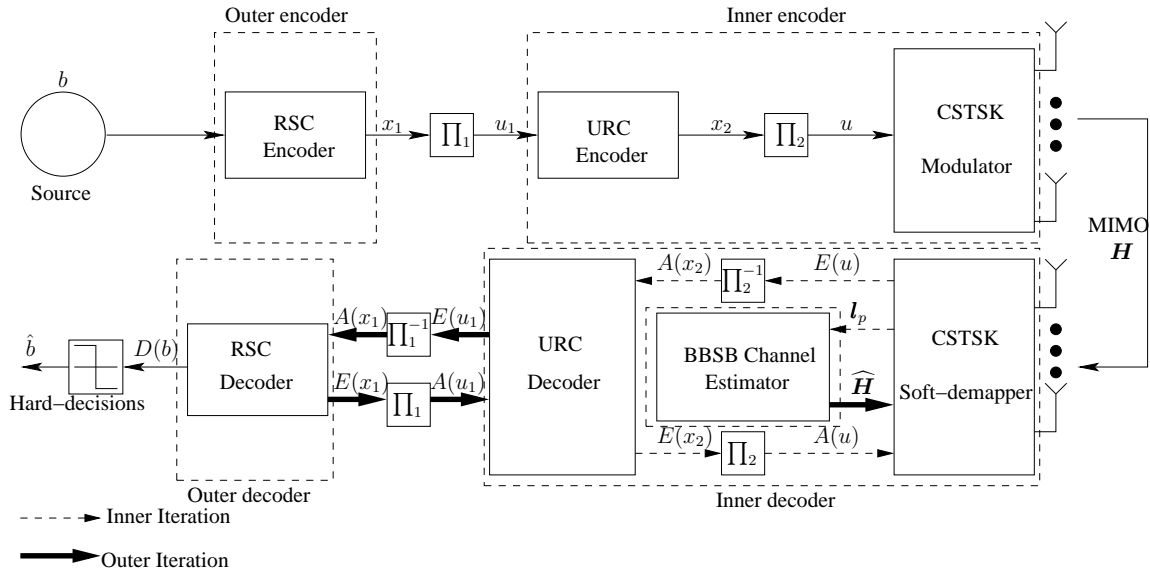


Figure 3.20: Joint BBSBCE aided and three-stage serial-concatenated turbo detection assisted CSTSK MIMO system.

The block diagram of our proposed BBSBCE aided and three three-stage serial-concatenated turbo coding assisted CSTSK system is shown in Fig. 3.20. It may be seen that the *a posteriori* information l_p output by the MIMO soft-demapper provides the confidence levels, i.e. the probabilities of binary 1s and binary 0s [1]. Therefore, based on this confidence level, we may opt for

²Note that the proposed BBSBCE scheme may be appropriately modified and applied in OFDM aided MIMO systems [24] for transmission over frequency-selective fading channels.

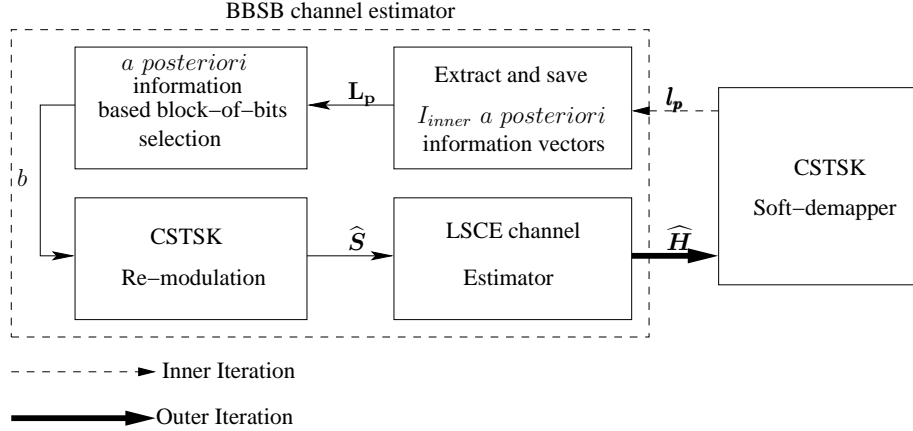


Figure 3.21: The proposed block-of-bits selection based blind channel estimator.

selecting reliable decisions from the MIMO soft-demapper's output sequence for the DDCE update. Note that in contrast to the existing joint CE and turbo detection-decoding schemes [55–59], as a benefit of selecting high-confidence decisions, the Block-of-Bits Selection Based (BBSB) blind channel estimator in our proposed scheme of Fig. 3.20 does not have to wait for the accurate final convergence of the turbo detector-decoder. Quite the contrary, our scheme updates the DDCE within the original outer loop of the three-stage turbo demapper-decoder, as explicitly emphasized in Figs. 3.20 and 3.21. In other words, unlike the existing schemes of [55–59], no additional iterative loop involving the CE and the three-stage turbo demapper-decoder is required. Consequently, the computational complexity of our joint scheme remains similar to that of the original three-stage turbo demapper-decoder, which is furnished with the CSI-estimate. Moreover, as it will be confirmed later in our simulation study, our joint BBSBCE and three-stage turbo demapper-decoder is capable of approaching the optimal near-capacity performance associated with perfect CSI. Let us now detail our proposed scheme further.

According to the CSTSK system model presented in Section 2.3, the received signal block can be expressed as

$$\mathbf{Y}(i) = \mathbf{H}\mathbf{S}(i) + \mathbf{V}(i), \quad (3.13)$$

where $\mathbf{H} \in \mathbb{C}^{N \times M}$ is the corresponding MIMO channel matrix, whose elements obey the complex-valued Gaussian distribution of zero-mean and unit variance $\mathcal{CN}(0, 1)$, while $\mathbf{V}(i) \in \mathbb{C}^{N \times T}$ is the AWGN matrix, whose components obey $\mathcal{CN}(0, N_0)$ with N_0 being the AWGN variance. Similar to the uncoded SBCE scheme discussed in Section 3.3, our proposed scheme also relies on a low number of training blocks. Let us assume that the number of available training blocks is M_T . If we arrange the training data as

$$\mathbf{Y}_{tM_T} = [\mathbf{Y}(1) \ \mathbf{Y}(2) \ \dots \ \mathbf{Y}(M_T)], \quad (3.14)$$

$$\mathbf{S}_{tM_T} = [\mathbf{S}(1) \ \mathbf{S}(2) \ \dots \ \mathbf{S}(M_T)], \quad (3.15)$$

the initial LSCE of the MIMO channel matrix \mathbf{H} is then given by

$$\hat{\mathbf{H}}_{LSCE} = \mathbf{Y}_{tM_T} \mathbf{S}_{tM_T}^H (\mathbf{S}_{tM_T} \mathbf{S}_{tM_T}^H)^{-1}. \quad (3.16)$$

For the sake of maintaining a high system throughput, only a small number of STSK training blocks should be used. On the other hand, in order to ensure for $\mathbf{S}_{tM_T} \mathbf{S}_{tM_T}^H$ to have the full rank of M , it is necessary to guarantee that $M_T \cdot T \geq M$ and this leads to a lower bound of the number of training blocks, which is given in Eq. (3.5). For instance, if we have $M = 4$ and $T = 2$, then the lower bound is $M_T = 2$ and we may choose to use as few as two STSK training blocks for initial CE. With such a low number of initial training blocks, the accuracy of the LSCE of Eq. (3.16) will be poor and hence the achievable BER performance based on the initial channel estimate will also remain poor. The task of the joint BBSBCE and three-stage turbo demapper-decoder is to iteratively refine the channel estimate for the sake of achieving a near-capacity BER performance, while imposing no excessive computational requirements.

Referring to Fig. 3.21, let the number of iterations in the two-stage inner turbo loop be I_{in} and the number of iterations in the outer turbo loop be I_{out} , respectively. Let us further denote the observation data at the output of the CSTSK soft-demapper of Fig. 3.21 as

$$\mathbf{Y}_{d\tau} = [\mathbf{Y}(1) \ \mathbf{Y}(2) \ \cdots \ \mathbf{Y}(\tau)], \quad (3.17)$$

where τ is referred to as the number of data blocks in a transmitted CSTSK frame. The joint BBSBCE and three-stage turbo demapper-decoder is described as follows.

Semi-Blind Iterative Algorithm

Step 1) Set the iteration index to $t = 0$ and the initial channel estimate to $\hat{\mathbf{H}}^{(t)} = \hat{\mathbf{H}}_{LSCE}$.

Step 2) Given the channel estimate $\hat{\mathbf{H}}^{(t)}$, perform the ML soft-demapping on the observation data $\mathbf{Y}_{d\tau}$ of Eq. (3.17). The CSTSK soft-demapper then exchanges its soft information with the URC inner decoder for I_{in} iterations, which yields the I_{in} vectors of the *a posteriori* information arranged as

$$\mathbf{L}_p = [l_p^1 \ l_p^2 \ \cdots \ l_p^{I_{in}}]^T, \quad (3.18)$$

where $\mathbf{L}_p \in \mathbb{C}^{I_{in} \times (\text{BPB} \cdot \tau)}$ is referred to as the equivalent *a posteriori* information matrix and $l_p^i = [l_p^i(1) \ l_p^i(2) \ \cdots \ l_p^i(\text{BPB} \cdot \tau)]^T \in \mathbb{C}^{(\text{BPB} \cdot \tau) \times 1}$ denotes the *a posteriori* information vector obtained by the CSTSK soft-demapper during the i th inner iteration with $l_p^i(k)$ defined in Eq. (2.6), while $\text{BPB} = \log_2(Q) + \log_2(\mathcal{L})$ represents the bits per CSTSK symbol block. Based on the fact that the n th column of \mathbf{L}_p represents the I_{in} soft decisions for the n th information bit, where $n \in \{1, 2, \dots, (\text{BPB} \cdot \tau)\}$, the n th bit decision may be regarded as correct and it is selected for CE in the following two cases:

Case 1: If the soft decisions in the same column share similar values, these soft decisions may result in a reliable bit decision, which may hence be invoked for CE. Specifically, the

criterion for the n th information bit to be selected is

$$\frac{|L_p^1(n) - L_p^2(n)| + |L_p^2(n) - L_p^3(n)| + \cdots + |L_p^{I_{in}-1}(n) - L_p^{I_{in}}(n)|}{|\mu|} \in (0, T_h), \quad (3.19)$$

where μ is the mean of the soft decisions in the n th column of the matrix L_p , while T_h denotes the block-of-bits selection threshold used.

Case 2: If the absolute values of the soft decisions in the n th column of L_p are in monotonically ascending order and these soft decisions share the same sign, namely, we have,

$$\begin{aligned} |L_p^1(n)| &< |L_p^2(n)| < \cdots < |L_p^{I_{in}}(n)| \text{ and} \\ \text{sign}\{L_p^1(n)\} &= \text{sign}\{L_p^2(n)\} = \cdots = \text{sign}\{L_p^{I_{in}}(n)\}, \end{aligned} \quad (3.20)$$

then the n th detected bit may be regarded as a correct one.

After checking through the columns of L_p , only “high confidence” decisions are selected and the corresponding STSK symbol block indices may be obtained by a sliding window based method using a window size of BPB. More explicitly, if BPB consecutive information bits are all regarded as correct, the corresponding information block will be selected for CE, while if a bit decision in a block of BPB consecutive bits is regarded as low quality, the process moves to examine the next block. This moving-window process yields a “high confidence” integer-valued index vector, which is denoted as $x^t = [x^t(1) \ x^t(2) \ \cdots \ x^t(\tau_s^t)]^T$, with the number of the selected elements τ_s^t varying within $\{0, 1, \dots, \tau_{\text{sel}}\}$, where $\tau_{\text{sel}} (\ll \tau)$ is the imposed maximum number of selected decision-based signal blocks. By using this index vector, the corresponding observation data can be selected from Eq. (3.17), and they are re-arranged and combined with the training data to form

$$\mathbf{Y}_{\text{sel}}^{(t)} = [\mathbf{Y}_{tM_T} \ \mathbf{Y}(x^t(1)) \ \mathbf{Y}(x^t(2)) \ \cdots \ \mathbf{Y}(x^t(\tau_s^t))]. \quad (3.21)$$

This sliding-window process used for selecting reliable detected symbol vectors is illustrated in Fig. 3.22. Note that whenever the number of selected blocks τ_s^t reaches the maximum limit τ_{sel} , the moving-window process will stop, leaving any remaining blocks unexamined. On the other hand, at some extreme situation, it may be possible although unlikely that no reliable detected symbol block is selected after examining all the columns of L_p , i.e. $\tau_s^t = 0$. To guard against this extreme case, we combine the training data with the detected data, as indicated in Eq. (3.21).

Step 3) By re-modulating the selected detected blocks-of-bits with the aid of x^t and combining them with the training data, we have

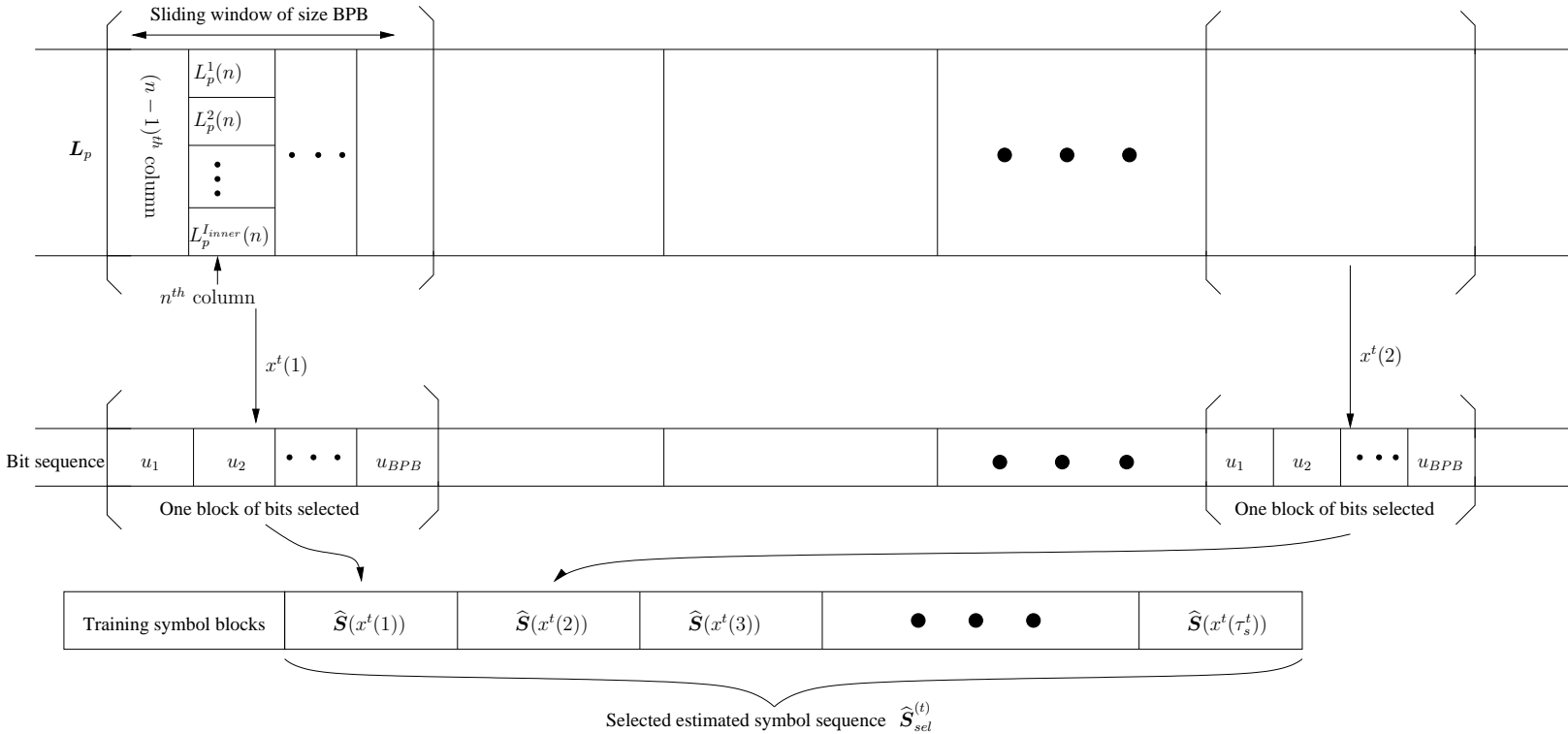
$$\widehat{\mathbf{S}}_{\text{sel}}^{(t)} = [\mathbf{S}_{tM_T} \ \widehat{\mathbf{S}}(x^t(1)) \ \widehat{\mathbf{S}}(x^t(2)) \ \cdots \ \widehat{\mathbf{S}}(x^t(\tau_s^t))]. \quad (3.22)$$

The resultant decision-directed LSCE update is then given by

$$\widehat{\mathbf{H}}^{(t+1)} = \mathbf{Y}_{\text{sel}}^{(t)} (\widehat{\mathbf{S}}_{\text{sel}}^{(t)})^H \left(\widehat{\mathbf{S}}_{\text{sel}}^{(t)} (\widehat{\mathbf{S}}_{\text{sel}}^{(t)})^H \right)^{-1}. \quad (3.23)$$

At the same time the corresponding soft information is further exchanged with the outer RSC decoder.

Figure 3.22: Illustration of the sliding-window process using a window-size of BPB bits to select reliable detected symbol vectors.



Step 4) Set $t = t + 1$. If $t < I_{out}$, repeat steps 2) and 3); otherwise, stop.

The idea behind Case 1 is that, if the decisions are relatively stable during several consecutive turbo iterations, it may be regarded as reliable decisions. This makes sense because a stable state may be achieved for turbo coding after a few iterations and the stable decisions may be high-quality ones. It can be seen that Case 1 mainly occurs during the later outer turbo iterations. With regard to Case 2, we note that if the soft values for a specific bit are in monotonically ascending order and share the same polarity in consecutive iterations, the corresponding bit decision may also be deemed reliable. This also makes sense, because the correct decisions may experience a gradual iteration gain and this will lead to increasing absolute values of the soft-decisions as the number of iterations increases, especially during the early turbo outer iteration stages.

Selecting the high-confidence detected blocks of bits is carried out within the inner turbo loop consisting of the CSTSK soft-demapper and the URC decoder of Fig. 3.20. This is because the selected $x^t(i)$ -th detected block of bits can be linked to the corresponding observation block $\mathbf{Y}(x^t(i))$ after it is re-modulated to generate the detected CSTSK signal block $\widehat{\mathbf{S}}(x^t(i))$. The selection cannot be carried out within the outer turbo loop of Fig. 3.20, since the RSC encoder will disperse the bits of the blocks. It is worth emphasising that the decision-directed LSCE update of Eq. (3.23) takes place concurrently, when the information is exchanged between the two-stage inner CSTSK soft-demapper/URC decoder and the outer RSC decoder. Therefore, no extra iterative loop is needed between the CE and the three-stage turbo demapper-decoder. It is also worth pointing out that our selection procedure is based on the information of the whole turbo detection-decoding process, not just relying on the single LLR $L_p^{I_{in}}(n)$ information. Therefore, it is capable of selecting only reliable detected symbol blocks for DDCE. This is crucial to ensure that our proposed BBSBCE aided and three-stage turbo demapping-decoding scheme is capable of approaching the optimal performance bound associated with perfect CSI, as will be demonstrated later in the simulation study.

The value of the block-of-bits selection threshold T_h employed in step 2) **Case 1** should be carefully chosen. Too small a value may lead to an insufficient number of blocks selected for CE even after examining the entire sequence of $\text{BPB} \cdot \tau$ bit decisions. By contrast, too large a value may result in an excessive number of selected blocks τ_s^t , potentially approaching the maximum affordable value τ_{sel} after only examining a small initial portion of the $\text{BPB} \cdot \tau$ bit decisions, and the selected blocks may contain many “low confidence” decisions. Both of these situations will result in a performance degradation. However, apart from these two extreme cases, there exists a relatively wide range of values for T_h , which allows our scheme to approach its optimal performance without increasing the numbers of turbo iterations I_{out} and I_{in} . Our experience suggests that within the appropriate range of threshold values, the performance of our semi-blind scheme is fairly insensitive to the value of T_h . Specifically, the limit τ_{sel} imposed on the number of data blocks selected in step 2) is to avoid imposing an unnecessary CE complexity. The appropriate value of τ_{sel} depends on the size of the MIMO channel matrix and for an $(N = 4) \times (M = 4)$ MIMO system, our empirical results show that $\tau_{\text{sel}} = 100$ is sufficient for converging to the optimal ML detection

performance associated with the perfect CSI.

Let us denote the complexity of the RSC decoder, the URC decoder and the CSTSK ML soft-demapper by C_{RSC} , C_{URC} and C_{ML} , respectively. The overall system complexity of the idealised three-stage turbo detector-decoder associated with the perfect CSI given in Eq. (2.11) is quoted below again

$$C_{\text{ideal}} = I_{\text{out}} \left(C_{\text{RSC}} + I_{\text{in}} (C_{\text{ML}} + C_{\text{URC}}) \right). \quad (3.24)$$

Typically, I_{in} and I_{out} are small, i.e. a few inner turbo iterations and a few outer iterations are often sufficient. Since our BBSBCE scheme selects no more than τ_{sel} data blocks for DDCE, our decision-directed LSCE of Eq. (3.23) has a complexity upper bound on the order of $\mathcal{O}(\tau_{\text{sel}}^3)$. Furthermore, as it will be confirmed later in our simulation study, our proposed amalgamated scheme approaches the perfect-CSI based performance bound with the same numbers of turbo iterations, I_{in} and I_{out} , while the decision-directed LSCE of Eq. (3.23) approaches the Cramér-Rao Lower Bound (CRLB) [138] associated with the τ_{sel} optimal training pilot blocks with the aid of I_{out} iterations. Therefore, the overall system complexity of our proposed joint BBSBCE and three-stage turbo demapping-decoding scheme can be expressed as

$$C_{\text{proposed}} \leq I_{\text{out}} \cdot \mathcal{O}(\tau_{\text{sel}}^3) + C_{\text{ideal}}. \quad (3.25)$$

By contrast, all the existing conventional schemes utilize the entire sequence of τ detected data blocks and, therefore, the complexity of the decision-directed LSCE in these conventional schemes is on the order of $\mathcal{O}(\tau^3)$. Moreover, these conventional schemes introduce an extra iterative loop between the channel estimator and the three-stage turbo detector-decoder, which takes I_{ce} iterations to converge³. Let us make an optimistic assumption that the three-stage turbo detector-decoder aided by these conventional DDCE schemes also requires I_{in} inner turbo iterations and I_{out} outer turbo iterations. Then the overall system complexity of these existing conventional joint CE and three-stage turbo detector-decoder structures is given in Eq. (3.12), which we quote below again

$$C_{\text{conventional}} = I_{\text{ce}} \cdot \mathcal{O}(\tau^3) + I_{\text{ce}} \cdot C_{\text{ideal}}. \quad (3.26)$$

By comparing Eq. (3.25) with Eq. (3.26), it becomes obvious that our proposed joint BBSBCE and three-stage turbo detector-decoder scheme requires a dramatically lower computational complexity than the existing conventional joint CE and three-stage turbo detector-decoder schemes. More specifically, since typically $C_{\text{ideal}} \gg I_{\text{out}} \cdot \mathcal{O}(\tau_{\text{sel}}^3)$, it is clear that our proposed joint BBSBCE and three-stage turbo demapping-decoding scheme has a complexity very close to that of the idealised three-stage turbo demapping-decoding scheme associated with perfect CSI. By contrast, the complexity of the existing conventional joint CE and three-stage turbo detector-decoder structures is dramatically higher than C_{ideal} .

³We would like to emphasize that since a conventional joint CE and turbo receiver utilizes all the symbol decisions of a transmitted frame in DDCE regardless whether they are reliable, it is necessary to wait until the turbo detector-decoder converges before the channel update can take place, in order to benefit from the error correction capability of the turbo detection-decoding.

Also note that the length τ of a turbo coded frame is typically in the thousands, while it is sufficient to set τ_{sel} to be 10% of τ in our scheme, i.e. τ_{sel} is typically in the hundreds. Consequently, the complexity of the DDCE in our proposed scheme is at least three orders of magnitude lower than that of the existing conventional schemes for the typical frame symbol block length in thousands. For $\tau = 100$ to 260 symbol blocks, Fig. 3.23 illustrates the complexity order comparison between the conventional DDCE which utilises all the τ detected symbol blocks and our proposed BBSBCE scheme which only utilises at most $\tau_{\text{sel}} = 100$ “high quality” detected symbol blocks, where as expected it can be seen that the complexity difference increases as the length of symbol blocks τ increases.

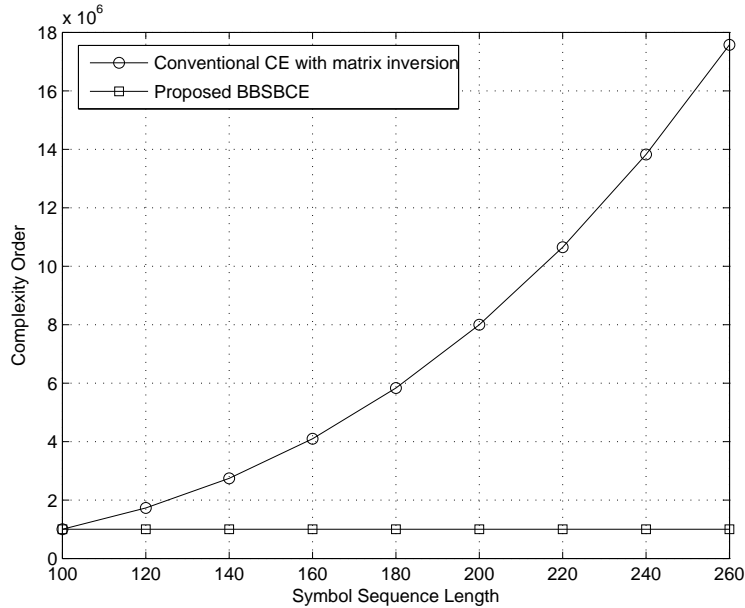


Figure 3.23: Channel estimation complexity order comparison between the conventional DDCE schemes which utilises all the τ detected symbol blocks and the proposed BBSBCE scheme which only utilises at most $\tau_{\text{sel}} = 100$ “high quality” detected symbol blocks.

3.4.3 Cramér-Rao Lower Bound

Since the CRLB provides the best attainable performance for an unbiased estimator [138–143], we can also evaluate the achievable performance of our joint BBSBCE and three-stage turbo demapping-decoding scheme by comparing the Mean Square Error (MSE) of its DD channel estimator with the CRLB. Let the number of available signal blocks invoked for TBCE be $\tilde{\tau} = \tau_{\text{sel}}$. Then the CSTSK model of Eq. (3.13) over the $\tilde{\tau}$ signal blocks can be written as

$$\mathbf{Y}_{t\tilde{\tau}} = \mathbf{H} \mathbf{S}_{t\tilde{\tau}} + \mathbf{V}_{t\tilde{\tau}}, \quad (3.27)$$

or equivalently

$$\tilde{\mathbf{y}}_{\tilde{\tau}} = \tilde{\mathbf{S}}_{\tilde{\tau}}^T \tilde{\mathbf{h}} + \tilde{\mathbf{v}}_{\tilde{\tau}}, \quad (3.28)$$

where $\mathbf{Y}_{t\tilde{\tau}} = [\mathbf{Y}(1) \ \mathbf{Y}(2) \cdots \mathbf{Y}(\tilde{\tau})]$, $\mathbf{S}_{t\tilde{\tau}}$ and $\mathbf{V}_{t\tilde{\tau}}$ are similarly defined, while

$$\tilde{\mathbf{y}}_{\tilde{\tau}} = \text{vec}(\mathbf{Y}_{t\tilde{\tau}}^T) \in \mathbb{C}^{NT\tilde{\tau} \times 1}, \quad (3.29)$$

$$\tilde{\mathbf{S}}_{\tilde{\tau}} = \mathbf{I}_N \otimes \mathbf{S}_{t\tilde{\tau}} \in \mathbb{C}^{NM \times NT\tilde{\tau}}, \quad (3.30)$$

$$\tilde{\mathbf{h}} = \text{vec}(\mathbf{H}^T) \in \mathbb{C}^{NM \times 1}, \quad (3.31)$$

$$\tilde{\mathbf{v}}_{\tilde{\tau}} = \text{vec}(\mathbf{V}_{t\tilde{\tau}}^T) \in \mathbb{C}^{NT\tilde{\tau} \times 1}. \quad (3.32)$$

Given the training signal matrix $\tilde{\mathbf{S}}_{\tilde{\tau}}$, the conditional probability $p(\tilde{\mathbf{y}}_{\tilde{\tau}}|\tilde{\mathbf{h}})$ is expressed as

$$p(\tilde{\mathbf{y}}_{\tilde{\tau}}|\tilde{\mathbf{h}}) = \frac{1}{(\pi N_0)^{NT\tilde{\tau}}} \exp\left(-\frac{\|\tilde{\mathbf{y}}_{\tilde{\tau}} - \tilde{\mathbf{S}}_{\tilde{\tau}}^T \tilde{\mathbf{h}}\|^2}{N_0}\right). \quad (3.33)$$

The Fisher Information Matrix (FIM) [138] is defined as

$$\mathbf{F}(\tilde{\mathbf{S}}_{\tilde{\tau}}) = -\mathbb{E}\left\{\frac{\partial^2 \log(p(\tilde{\mathbf{y}}_{\tilde{\tau}}|\tilde{\mathbf{h}}))}{\partial \tilde{\mathbf{h}} \partial \tilde{\mathbf{h}}^H}\right\} = -\mathbb{E}\left\{\frac{\partial}{\partial \tilde{\mathbf{h}}^H}\left(\frac{\partial \log(p(\tilde{\mathbf{y}}_{\tilde{\tau}}|\tilde{\mathbf{h}}))}{\partial \tilde{\mathbf{h}}^H}\right)^H\right\}, \quad (3.34)$$

where the expectation operation $\mathbb{E}\{\}$ is with respect to the noise $\tilde{\mathbf{v}}_{\tilde{\tau}}$. Substituting (3.33) into (3.34) results in

$$\mathbf{F}(\tilde{\mathbf{S}}_{\tilde{\tau}}) = \frac{1}{N_0} \tilde{\mathbf{S}}_{\tilde{\tau}} \tilde{\mathbf{S}}_{\tilde{\tau}}^H. \quad (3.35)$$

Let

$$\tilde{\mathbf{S}}_{\tilde{\tau}\text{opt}} = \arg \max_{\tilde{\mathbf{S}}_{\tilde{\tau}}} \text{tr}\{\mathbf{F}(\tilde{\mathbf{S}}_{\tilde{\tau}})\}. \quad (3.36)$$

The i th diagonal element of $\mathbf{F}^{-1}(\tilde{\mathbf{S}}_{\tilde{\tau}\text{opt}})$ provides a lower bound of the variance for the unbiased estimate of the i th element of $\tilde{\mathbf{h}}$ based on the training signal block length of $\tilde{\tau}$, and

$$\text{CRLB}(\tilde{\tau}) = \text{tr}\{\mathbf{F}^{-1}(\tilde{\mathbf{S}}_{\tilde{\tau}\text{opt}})\} \quad (3.37)$$

is the minimum MSE achievable by an unbiased estimator based on the training block length $\tilde{\tau}$.

Note that we have $\tilde{\mathbf{S}}_{\tilde{\tau}\text{opt}} = \mathbf{I}_N \otimes \mathbf{S}_{t\tilde{\tau}\text{opt}}$ with

$$N_0 \cdot \mathbf{S}_{t\tilde{\tau}\text{opt}} = \arg \max_{\mathbf{S}_{t\tilde{\tau}}} \text{tr}\{\mathbf{S}_{t\tilde{\tau}} \mathbf{S}_{t\tilde{\tau}}^H\}, \quad (3.38)$$

where

$$\text{tr}\{\mathbf{S}_{t\tilde{\tau}} \mathbf{S}_{t\tilde{\tau}}^H\} = \text{tr}\left\{\sum_{i=1}^{\tilde{\tau}} \mathbf{S}(i) \mathbf{S}(i)^H\right\}. \quad (3.39)$$

Since $\mathbf{S}(i) = \mathbf{s}(i)\mathbf{A}(i)$ with $\mathbf{s}(i) \in \{\mathbf{s}_l, 1 \leq l \leq \mathcal{L}\}$ and $\mathbf{A}(i) \in \{\mathbf{A}_q, 1 \leq q \leq \mathcal{Q}\}$, the determination of the “optimal” training signal matrix $\tilde{\mathbf{S}}_{\tilde{\tau}\text{opt}}$ is non-trivial. We therefore use the CRLB for the given training signal matrix $\tilde{\mathbf{S}}_{\tilde{\tau}}$, defined as

$$\text{CRLB}(\tilde{\mathbf{S}}_{\tilde{\tau}}) = \text{tr}\{\mathbf{F}^{-1}(\tilde{\mathbf{S}}_{\tilde{\tau}})\}, \quad (3.40)$$

to approximate $\text{CRLB}(\tilde{\tau})$. For a large block length of $\tilde{\tau}$, this approximation is accurate.

Let $\hat{\tilde{h}}$ be an unbiased estimate of \tilde{h} produced by our semi-blind scheme with the selected decisions limited to no more than τ_{sel} . The MSE of the channel estimate $\hat{\tilde{h}}$ is expressed as

$$J_{\text{MSE}}(\hat{\tilde{h}}) = \mathbb{E}\left\{\|\hat{\tilde{h}} - \tilde{h}\|^2\right\} \approx \frac{1}{K_{\text{run}}} \sum_{k=1}^{K_{\text{run}}} \|\hat{\tilde{h}}^{(k)} - \tilde{h}\|^2, \quad (3.41)$$

where K_{run} is the number of estimation experiments and $\hat{\tilde{h}}^{(k)}$ is the channel estimate obtained during the k th experiment. Clearly, we have

$$J_{\text{MSE}}(\hat{\tilde{h}}) \geq \text{CRLB}(\tilde{S}_{\tilde{\tau}}). \quad (3.42)$$

In the following simulation study, we will demonstrate that the MSE of the channel estimate produced by our proposed semi-blind joint BBSBCE and three-stage demapping-decoding algorithm associated with as few as $M_T = 2$ initial training blocks and with the limit of $\tau_{\text{sel}} = 100$ imposed on selected decision blocks attains the CRLB of $\text{CRLB}(\tilde{S}_{\tilde{\tau}})$ with $\tilde{\tau} = 100$.

3.4.4 Simulation Results

Table 3.3: System parameters of the BBSBCE aided and three-stage serial-concatenated turbo coding assisted CSTSK system of Fig. 3.20.

Number of Tx antennas	M
Number of Rx antennas	N
Symbol durations per block	T
Number of dispersion matrices	Q
Modulation	\mathcal{L} -QAM or \mathcal{L} -PSK
Channels	Frequency-flat Rayleigh fading
Detector	ML detector
Number of training blocks	M_T
Number of signal blocks per frame	$\tau = 1000$
Number of selected reliable STSK symbol blocks	$\tau_{\text{sel}} = 100$
Pilot overhead	O_p of Eq. (3.7)
Block-of-bits selection threshold	T_h
Interleaver blocklength	10^6 bits
Outer channel code	Half-rate RSC
Generator polynomials	$(G_{RSC}^r, G_{RSC}) = (7, 5)_8$
Precoder	URC
Number of inner iterations	I_{in}
Number of outer iterations	I_{out}

We investigated the achievable performance of our proposed BBSBCE and three-stage turbo demapping-decoding scheme of Fig. 3.20 under a quasi-static Rayleigh fading environment. An interleaver length of 10^6 bits was used by the three-stage serial-concatenated turbo encoder/decoder of Fig. 3.20. The binary generator polynomials of the RSC encoder were $G_{RSC} = [1, 0, 1]_2$ and $G'_{RSC} = [1, 1, 1]_2$, while these of the URC encoder were $G_{URC} = [1, 0]_2$ and $G'_{URC} = [1, 1]_2$. The number of inner iterations was set to $I_{in} = 3$. The transmitted signal power of all the simulated systems was again normalized to unity and, therefore, the SNR was defined as $\frac{1}{N_0}$ with N_0 being the AWGN power. The achievable performance was assessed in terms of three metrics: the MSE of the CE defined in Eq. (3.41), the achievable BER, and the EXIT charts [1]. All the results were averaged over $K_{\text{run}} = 100$ channel realisations. The maximum number of selected reliable detected STSK symbol blocks was set to $\tau_{\text{sel}} = 100$, which corresponded to 10% of a data frame, i.e. $\tau_{\text{sel}} = 0.1\tau$. The system parameters of the BBSBCE aided and three-stage serial-concatenated turbo coding assisted CSTSK scheme of Fig. 3.20 are summarized in Table 3.3.

3.4.4.1 CSTSK(4, 2, 2, 4, QPSK) having a normalized throughput of $R = 2$ bits/symbol

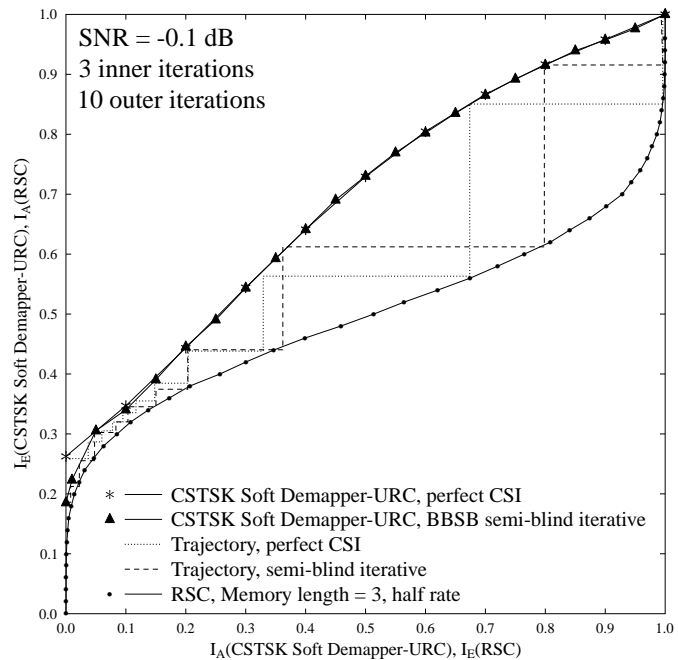


Figure 3.24: EXIT chart analysis of our proposed semi-blind BBSBCE and three-stage turbo demapping-decoding aided CSTSK(4, 2, 2, 4, QPSK) system of Fig. 3.20 having a normalized throughput of $R = 2$ bits/symbol, using $M_T = 2$ initial training blocks and a PO of $O_p = 0.2\%$. A block-of-bits selection threshold of $T_h = 0.2$ is used. The performance is compared to the perfect-CSI scenario. All other system parameters were summarized in Table 3.3. The corresponding BER curves are seen in Fig. 3.26.

We first considered the semi-blind BBSBCE and three-stage turbo demapping-decoding aided CSTSK(4, 2, 2, 4, QPSK) system of Fig. 3.20 associated with $\mathcal{L} = 4$. Our investigation com-

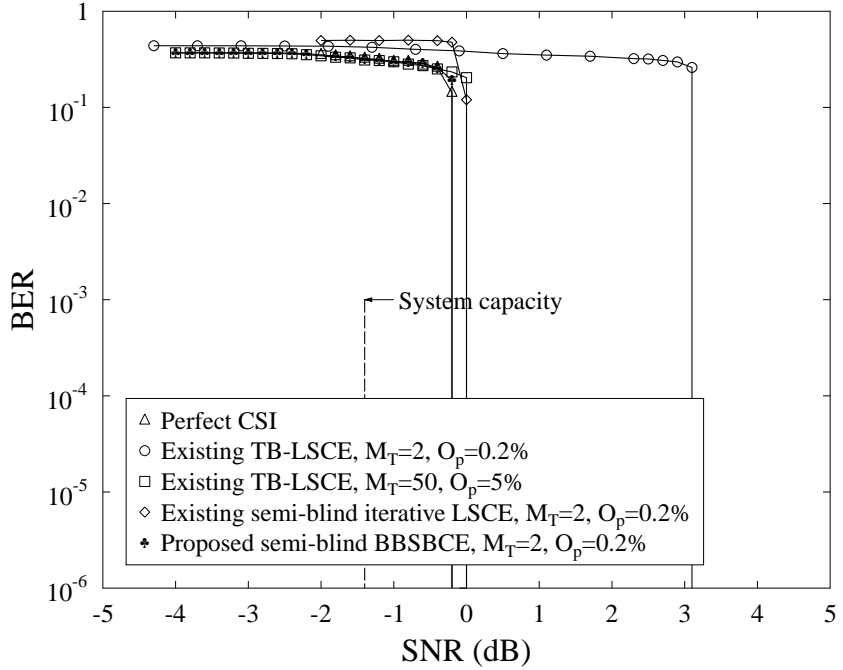


Figure 3.25: BER performance of our proposed semi-blind BBSBCE and three-stage turbo demapping-decoding aided CSTSK(4, 2, 2, 4, QPSK) system of Fig. 3.20 associated with a normalized throughput of $R = 2$ bits/symbol, using $I_{out} = 10$ outer turbo iterations, $M_T = 2$ initial training blocks ($O_p = 0.2\%$) and a block-of-bits selection threshold of $T_h = 0.2$, in comparison to a) the training-based cases using $M_T = 2$ ($O_p = 0.2\%$) and 50 ($O_p = 5\%$) training blocks, respectively, b) the existing conventional joint CE and three-stage turbo demapping-decoding scheme using $M_T = 2$ ($O_p = 0.2\%$) initial training blocks and utilizing all the detected signal blocks for the decision-directed LSCE, as well as c) the perfect-CSI case. All other system parameters were summarized in Table 3.3.

commenced with the EXIT chart analysis of the proposed semi-blind iterative scheme in conjunction with the block-of-bits selection threshold of $T_h = 0.2$, in comparison to the perfect-CSI scenario. It can be seen from the EXIT charts shown in Fig. 3.24 that open tunnels exist between the EXIT curves of the amalgamated inner CSTSK soft-demapper-URC decoder and the outer RSC decoder for both the proposed semi-blind scheme and the optimal ML detection based on the perfect CSI at $\text{SNR} = -0.1$ dB. The actual Monte-Carlo simulation based stair-case shaped decoding trajectories, which closely match the EXIT curves, are also provided at $\text{SNR} = -0.1$ dB. Both the trajectories show that the perfect convergence point at $(1.0, 1.0)$ can be reached with the aid of $I_{out} = 10$ iterations, implying that the proposed semi-blind scheme is capable of achieving the optimal ML detection performance at the same number of turbo iterations. Additionally, due to the poor-quality initial training based LSCE used during the first iteration, the starting point of the EXIT curve of the inner CSTSK soft-demapper-URC decoder of the semi-blind scheme is lower than that of the

optimal ML detection based on the perfect CSI. However, the *a priori* information is improved as the number of iterations increased, and the two curves gradually become overlapped. In other words, an accurate CE is obtained by the semi-blind BBSB iterative CE scheme, even though the initial LSCE based on $M_T = 2$ training blocks ($O_p = 0.2\%$) is very poor.

The BER performance achieved by the semi-blind BBSBCE and three-stage turbo demapping-decoding aided CSTSK(4, 2, 2, 4, QPSK) system of Fig. 3.20 relying on $M_T = 2$ initial training blocks and a PO of $O_p = 0.2\%$ is shown in Fig. 3.25, where the near-capacity optimal performance obtained with the aid of perfect CSI is also included as the benchmark. For the CSTSK(4, 2, 2, 4, QPSK) system, there are $M \cdot N = 8$ complex-valued channel taps. $M_T = 2$ initial training blocks correspond to 8 training bits, leading to an extremely low training overhead of 1 bit per channel. Observe that our semi-blind joint BBSBCE and three-stage turbo demapping-decoding scheme associated with $M_T = 2$ ($O_p = 0.2\%$) initial training blocks approaches the perfect-CSI based performance bound, as predicted by the EXIT chart analysis of Fig. 3.24, while maintaining a high system throughput and imposing no excessively additional complexity. The ML detection performance of the three-stage turbo demapping-decoding scheme operating with

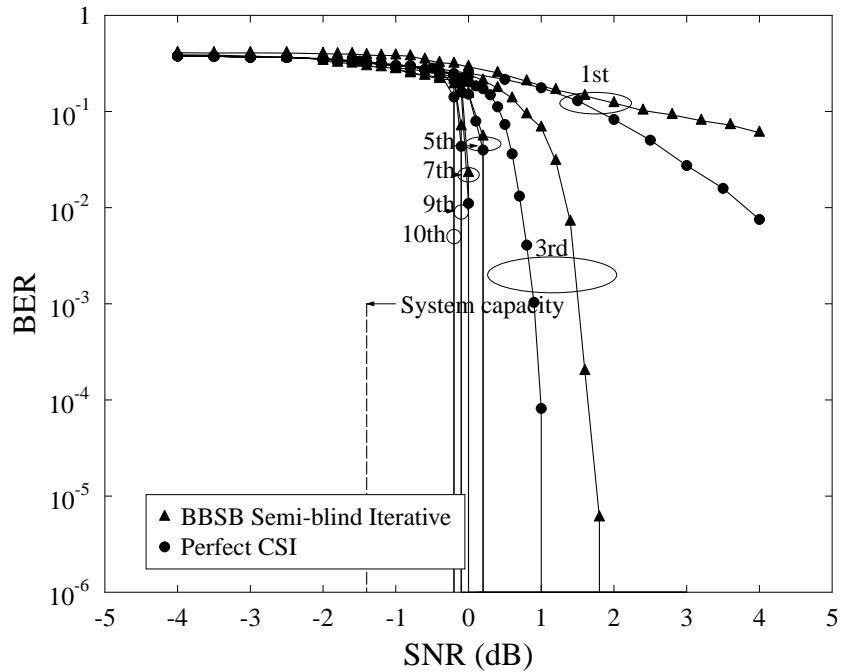


Figure 3.26: BER convergence performance of our proposed semi-blind BBSBCE and three-stage turbo demapping-decoding aided CSTSK(4, 2, 2, 4, QPSK) scheme of Fig. 3.20 associated with a normalized throughput of $R = 2$ bits/symbol, using $I_{out} = 10$ outer turbo iterations, $M_T = 2$ initial training blocks ($O_p = 0.2\%$) and a block-of-bits selection threshold of $T_h = 0.2$, in comparison to the perfect-CSI case. All other system parameters were summarized in Table 3.3. The corresponding EXIT chart is seen in Fig. 3.24.

the aid of the Training-Based LSCE (TB-LSCE) [144] as well as relying on 2 ($O_p = 0.2\%$) and 50 ($O_p = 5\%$) training blocks, respectively, are also depicted in Fig. 3.25. It can be seen that when using only 2 training blocks and $O_p = 0.2\%$, as expected, the performance of the TB-LSCE scheme is extremely poor. Even with 50 training blocks, the TB-LSCE scheme still suffers from a 0.2 dB SNR loss in comparison to the perfect-CSI based bound. Additionally, we also designed a convectional semi-blind joint CE and three-stage turbo demapping-decoding scheme using $M_T = 2$ ($O_p = 0.2\%$) initial training blocks as well as utilizing all the detected signal blocks for the decision-directed LSCE to represent the existing conventional approaches. The corresponding BER performance is portrayed in Fig. 3.25. Observe that unlike our proposed scheme, this conventional scheme cannot attain the perfect-CSI based performance bound, despite using the entire sequence of detected data blocks for DDCE and, therefore, imposing a substantially higher complexity than our scheme.

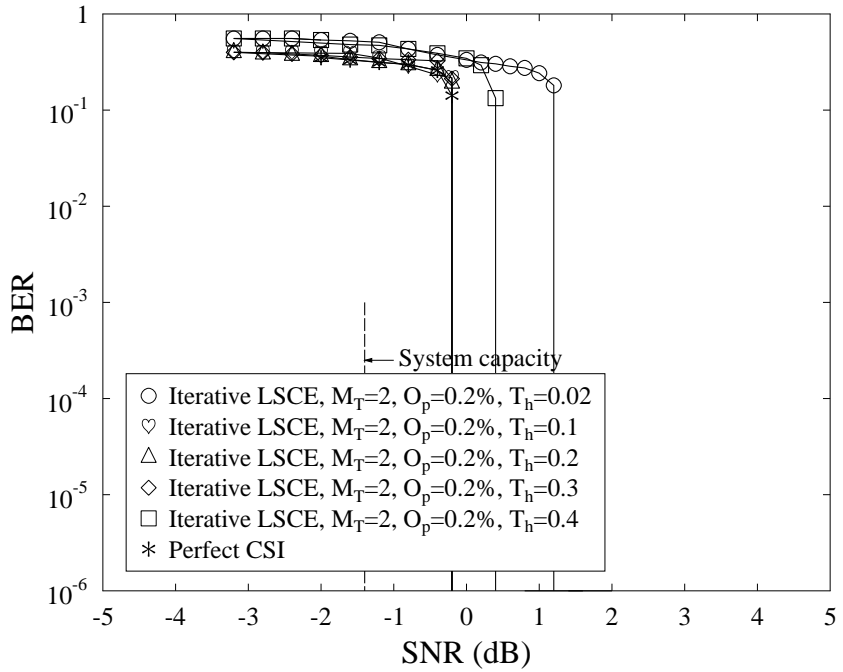


Figure 3.27: Effects of the block-of-bits selection threshold T_h on the BER performance of our proposed semi-blind joint BBSBCE and three-stage turbo demapping-decoding aided CSTSK(4, 2, 2, 4, QPSK) system of Fig. 3.20 associated with a normalized throughput of $R = 2$ bits/symbol, using $M_T = 2$ initial training blocks and $O_p = 0.2\%$. The number of outer turbo iterations is $I_{out} = 10$. All other system parameters were summarized in Table 3.3.

The BER convergence performance of the semi-blind BBSBCE and three-stage turbo demapping-decoding aided CSTSK(4, 2, 2, 4, QPSK) system of Fig. 3.20 is illustrated in Fig. 3.26, in comparison to that of the perfect-CSI scenario. Note that unlike all the other existing semi-blind schemes, our scheme does not impose an extra iterative CE loop, since our channel estimator is naturally em-

bedded into the original three-stage serial-concatenated turbo loop. It can be seen from Fig. 3.26 that for both the semi-blind and perfect CSI based cases, $I_{out} = 10$ outer iterations are sufficient for achieving near-capacity performance. In addition, it can be seen that the BER performance gap between the proposed semi-blind scheme and the optimal ML detection using the perfect CSI reduces, as the number of outer iterations increases. More specifically, during the third iteration, the SNR gap is still about 0.8 dB, but at the fifth iteration, the semi-blind iterative scheme has converged to the optimal ML detection performance. In other words, the decision-directed channel estimate in the semi-blind BBSBCE scheme has converged to the true channel within five iterations for this CSTSK(4, 2, 2, 4, QPSK) system.

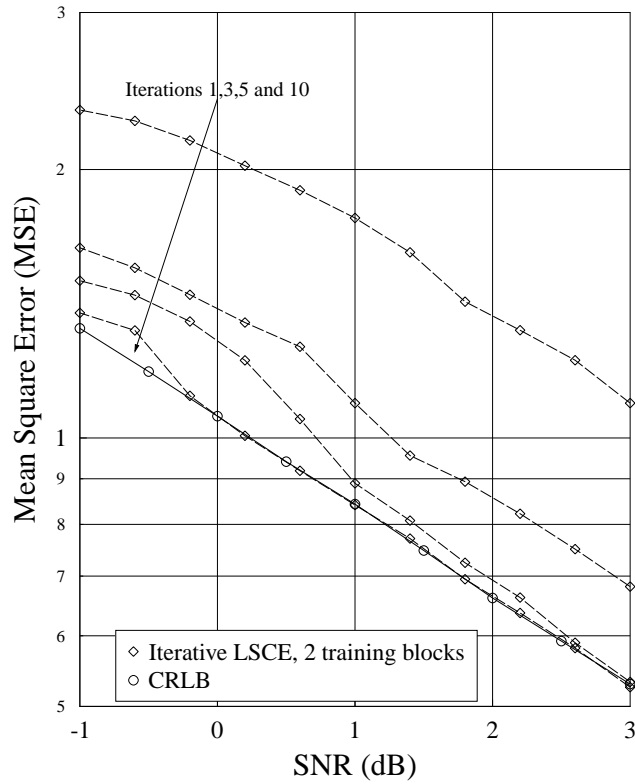


Figure 3.28: MSE convergence performance of the channel estimator in our proposed semi-blind joint BBSBCE and three-stage turbo demapping-decoding aided CSTSK(4, 2, 2, 4, QPSK) system of Fig. 3.20 associated with a normalized throughput of $R = 2$ bits/symbol, using $M_T = 2$ initial training blocks and $O_p = 0.2\%$, a block-of-bits selection threshold of $T_h = 0.2$ and the maximum number of selected decision blocks $\tau_{sel} = 100$, in comparison to the CRLB associated with the training block length $\tilde{\tau} = 100$. All other system parameters were summarized in Table 3.3.

The effects of the block-of-bits selection threshold T_h on the achievable BER performance were also investigated by varying the value of T_h in the set $\{0.02, 0.1, 0.2, 0.3, 0.4\}$ under the same system configuration. The corresponding results are shown in Fig. 3.27, where it can be seen that for $T_h = 0.1, 0.2$ and 0.3 , the BER performance of the proposed semi-blind iterative scheme all converge to that of the perfect-CSI case. However, for a threshold value of $T_h = 0.02$, a

performance degradation occurred, since the number of selected decision blocks for CE is probably insufficient for such a low threshold. On the other hand, given a relatively high value of $T_h = 0.4$, some unreliable decision blocks may have been selected for CE and this may lead to a performance degradation from the perfect-CSI case. The results of Fig. 3.27 clearly demonstrate that as long as the threshold value is not chosen to be too high or too low, the performance of the proposed semi-blind iterative scheme is not sensitive to the actual value of T_h . Indeed, there exists a wide range of values for T_h , which allow our scheme to approach the optimal performance of the perfect-CSI case even without the need of increasing the number of turbo iterations. For this system, $T_h \in [0.1, 0.3]$ are all appropriate.

The MSE performance of the channel estimator in the proposed semi-blind iterative scheme is depicted in Fig. 3.28 in comparison to the CRLB. It can be seen that the MSE of the DD channel estimate approaches the CRLB, once the number of iterations reaches $I_{out} = 10$ for $\text{SNR} \geq -0.2$ dB. This corresponds to the BER ‘‘turbo cliff’’ at $\text{SNR} = -0.2$ dB and $I_{out} = 10$ shown in Fig. 3.26, implying that the DDCE in our scheme is most efficient for $\text{SNR} \geq -0.2$ dB, since it approaches the CRLB. However, it can also be seen that for $\text{SNR} < -0.2$ dB, the MSE of the DDCE was slightly degraded. This is expected because for such low SNR values, the open EXIT tunnel shown in Fig. 3.24 becomes closed and hence the BER remains practically to be 50% even for the perfect-CSI case. Under such adverse conditions, the number of actually selected decision blocks τ_s^t may be far smaller than $\tau_{sel} = 100$ and, consequently, our DD channel estimator, although remaining most efficient, cannot converge to the $\text{CRLB}(\tilde{\tau} = 100)$. It is worth emphasizing that under such adverse conditions, any existing semi-blind DDCE scheme utilising the whole sequence of decision blocks would diverge, i.e. the MSE of its DD channel estimator would be even larger than the MSE of the initial TBCE, owing to the serious error propagation. By contrast, observe from Fig. 3.28 that under such low SNR conditions, our DD channel estimator is still capable of converging to a MSE value very close to the $\text{CRLB}(\tilde{\tau} = 100)$. This demonstrates the effectiveness of our proposed strategy of only selecting reliable decision blocks.

3.4.4.2 CSTSK(4, 4, 2, 4, 16-QAM) having a normalized throughput of $R = 3$ bits/symbol

We also considered the CSTSK(4, 4, 2, 4, 16-QAM) system of Fig. 3.20 with $\mathcal{L} = 16$ and a normalized throughput of $R = 3$ bits/symbol. Fig. 3.29 depicts our EXIT chart analysis, where it can be seen that an open tunnel existed at $\text{SNR} = -1.2$ dB. The stair-case shaped decoding trajectories recorded for the proposed semi-blind BBSBCE based iterative scheme using $M_T = 2$ ($O_p = 0.2\%$) initial training blocks and the optimal ML detection relying on perfect CSI are also plotted in Fig. 3.29 to show that for this CSTSK(4, 4, 2, 4, 16-QAM) system, the perfect convergence point (1.0, 1.0) may be reached by our proposed semi-blind iterative algorithm for the same $I_{out} = 9$ iterations as for the perfect-CSI case.

Fig. 3.30 shows the BER performance of our joint BBSBCE and three-stage turbo detection-

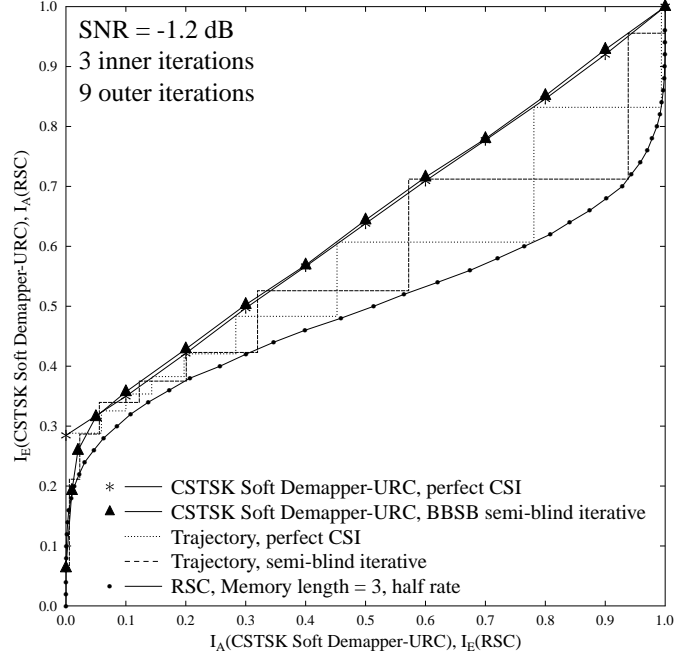


Figure 3.29: EXIT chart analysis of our proposed semi-blind BBSBCE and three-stage turbo demapping-decoding aided CSTSK(4,4,2,4,16-QAM) system of Fig. 3.20 having a normalized throughput of $R = 3$ bits/symbol, using $M_T = 2$ initial training blocks and a PO of $O_p = 0.2\%$. A block-of-bits selection threshold of $T_h = 0.2$ is used. The performance is compared to the perfect-CSI scenario. All other system parameters were summarized in Table 3.3. The corresponding BER curves are seen in Fig. 3.31.

decoding scheme using $M_T = 2$ ($O_p = 0.2\%$) initial training blocks and a block-of-bits selection threshold of $T_h = 0.2$, in comparison to those of the three-stage turbo detector-decoder algorithm relying on the TB-LSCE based on 2 and 50 training blocks, respectively. Fig. 3.30 also includes the performance of the existing conventional semi-blind joint CE and three-stage turbo detection-decoding scheme using $M_T = 2$ ($O_p = 0.2\%$) initial training blocks and invoking the entire detected data sequence for the decision-directed LSCE. It can be seen from Fig. 3.30 that the TB-LSCE scheme suffers from a performance loss of 0.4 dB in comparison to the perfect-CSI based bound even with $M_T = 50$ ($O_p = 5\%$) training blocks. By contrast, our semi-blind joint BBSBCE scheme using only 2 initial training blocks ($O_p = 0.2\%$) is capable of approaching the perfect-CSI based performance bound at the same number of turbo iterations. The results shown in Fig. 3.30 also confirm that the existing conventional semi-blind joint scheme suffers from a performance degradation of 0.2 dB with respect to the perfect-CSI based performance bound, despite of utilizing the entire detected data sequence for the DDCE and therefore imposing a considerably higher complexity than our proposed scheme.

The BER convergence performance of our semi-blind BBSB iterative scheme is depicted in Fig. 3.31, where it can be seen that a near-capacity performance may be achieved by our semi-blind BBSB iterative algorithm using the same $I_{out} = 9$ turbo iterations as the perfect-CSI case.

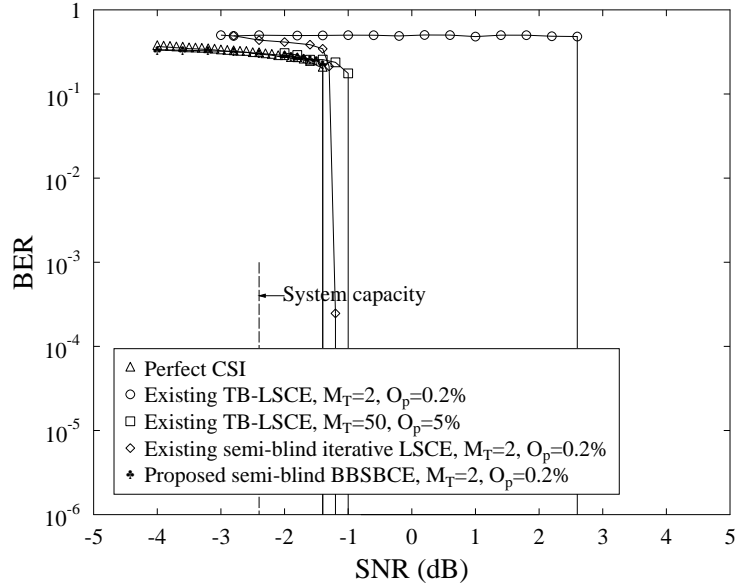


Figure 3.30: BER performance of our proposed semi-blind BBSBCE and three-stage turbo demapping-decoding aided CSTSK(4,4,2,4,16-QAM) system of Fig. 3.20 associated with a normalized throughput of $R = 3$ bits/symbol, using $I_{out} = 9$ outer turbo iterations, $M_T = 2$ initial training blocks ($O_p = 0.2\%$) and a block-of-bits selection threshold of $T_h = 0.2$, in comparison to a) the training-based cases using $M_T = 2$ ($O_p = 0.2\%$) and 50 ($O_p = 5\%$) training blocks, respectively, b) the existing conventional joint CE and three-stage turbo demapping-decoding scheme using $M_T = 2$ ($O_p = 0.2\%$) initial training blocks and utilizing all the detected signal blocks for the decision-directed LSCE, as well as c) the perfect-CSI case. All other system parameters were summarized in Table 3.3.

Additionally, Fig. 3.32 investigates the effects of the block-of-bits selection threshold T_h on the BER performance of our semi-blind BBSBCE and three-stage turbo demapping-decoding scheme. Similar to the results recorded for the CSTSK(4,2,2,4,QPSK) system, using $T_h \in [0.1, 0.3]$ enables our scheme with as few as $M_T = 2$ ($O_p = 0.2\%$) initial training blocks to approach the near-capacity performance of the perfect CSI case using the same $I_{out} = 9$ iterations. Finally, the MSE convergence of the CE used in our semi-blind scheme is portrayed in Fig. 3.33, in comparison to the CRLB for this CSTSK(4,4,2,4,16-QAM) system. The results of Fig. 3.33 confirm that the MSE of our DD channel estimator converges to the CRLB using $I_{out} = 9$ iterations over the range of $\text{SNR} \geq -1.2$ dB.

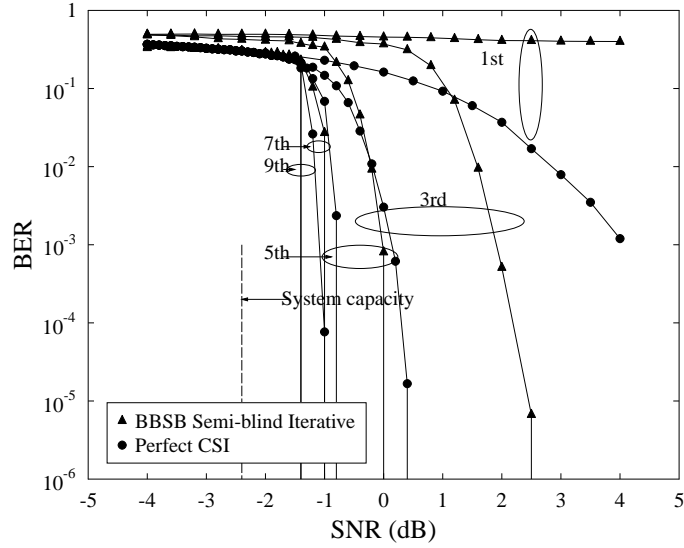


Figure 3.31: BER convergence performance of our proposed semi-blind BBSBCE and three-stage turbo demapping-decoding aided CSTSK(4,4,2,4,16-QAM) scheme of Fig. 3.20 associated with a normalized throughput of $R = 3$ bits/symbol, using $I_{out} = 9$ outer turbo iterations, $M_T = 2$ initial training blocks ($O_p = 0.2\%$) and a block-of-bits selection threshold of $T_h = 0.2$, in comparison to the perfect-CSI case. All other system parameters were summarized in Table 3.3. The corresponding EXIT chart is seen in Fig. 3.29.

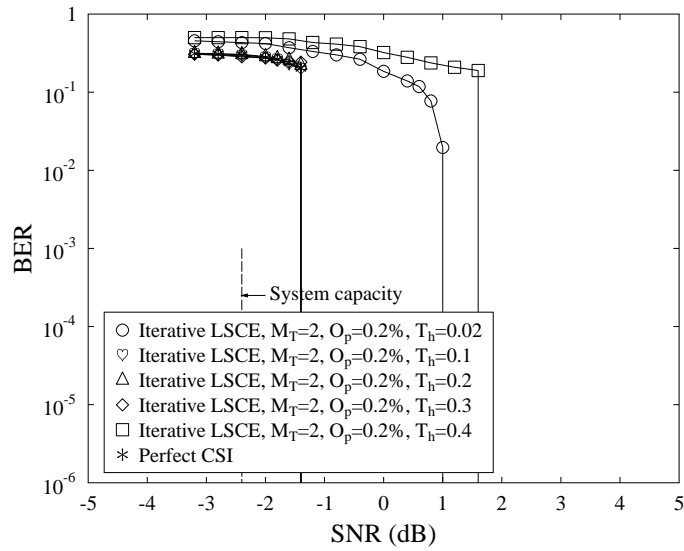


Figure 3.32: Effects of the block-of-bits selection threshold T_h on the BER performance of our proposed semi-blind joint BBSBCE and three-stage turbo demapping-decoding aided CSTSK(4,4,2,4,16-QAM) system of Fig. 3.20 associated with a normalized throughput of $R = 3$ bits/symbol, using $M_T = 2$ initial training blocks and $O_p = 0.2\%$. The number of outer turbo iterations is $I_{out} = 9$. All other system parameters were summarized in Table 3.3.

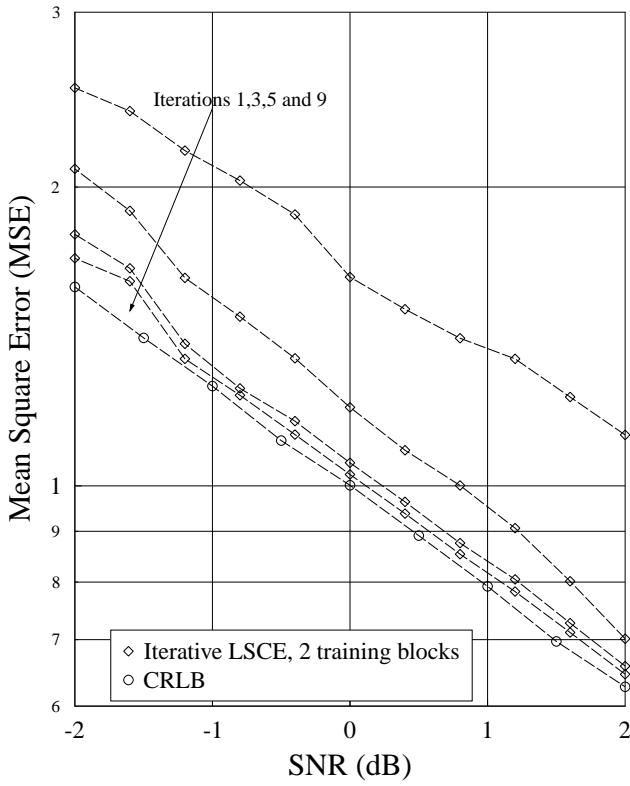


Figure 3.33: MSE convergence performance of the channel estimator in our proposed semi-blind joint BBSBCE and three-stage turbo demapping-decoding aided CSTSK(4,4,2,4,16-QAM) system of Fig. 3.20 associated with a normalized throughput of $R = 3$ bits/symbol, using $M_T = 2$ initial training blocks and $O_p = 0.2\%$, a block-of-bits selection threshold of $T_h = 0.2$ and the maximum number of selected decision blocks $\tau_{\text{sel}} = 100$, in comparison to the CRLB associated with the training block length $\tilde{\tau} = 100$. All other system parameters were summarized in Table 3.3.

3.5 Soft-Decision Aided Channel Estimation for MIMO-Aided Turbo Transceivers

In the previous section, an effective yet low-complexity BBSBCE scheme has been proposed for aiding three-stage serial-concatenated turbo coded CSTSK systems, which is capable of selecting just-sufficient reliable or high-quality *hard-decision* STSK data blocks for DDCE. In this way, the effects of erroneous decisions can be mitigated and, consequently, the system performance and robustness are improved. A well-known alternative way of reducing the effects of erroneous decisions in DDCE is to employ *soft-decision* based CE schemes [130], which are also known as turbo CE schemes. Instead of using hard-decision estimates of data symbols, this kind of channel estimators utilise the soft estimates of data symbols as the input of channel estimator. Additionally, due to the nature of soft-decision aided CE schemes, they are commonly incorporated with turbo coding schemes to form a joint soft CE and turbo detection-decoding structure. For example,

an iterative CE scheme using soft-decision feedback was proposed in [127], which weights the probabilities of decisions from the equalizer for aiding the channel estimator. In [128], a soft-input Kalman channel estimator and a weighted turbo Recursive Least Squares (RLS) channel estimator were proposed. In [129], a soft-decision aided iterative CE and symbol detection technique was proposed for coded CDMA systems. These existing works show that the soft DDCE schemes are capable of achieving better performance than the corresponding hard-decision aided DDCE schemes.

Against this background, it is natural to exploit employing the effective soft-decision aided scheme in DDCE for the CSTSK based MIMO system introduced in Section 3.4. However, it may be demonstrated that the soft-decision aided CE scheme may not be appropriate for CSTSK systems. Recall that in a CSTSK system, the symbol block is generated by the two parts, namely, the conventional \mathcal{L} -PSK/QAM symbol $s(i)$ and the activated dispersion matrix $A(i)$. More specifically, given the number of bits per block of $\text{BPB} = \log_2(Q) + \log_2(\mathcal{L})$, the first $\log_2(Q)$ bits are used to choose a single dispersion matrix $A(i)$ from the Q pre-assigned dispersion matrices $\{A_q \in \mathbb{C}^{M \times T}, 1 \leq q \leq Q\}$, while the remaining $\log_2(\mathcal{L})$ bits are mapped to a complex-valued symbol $s(i) \in \{s_l, 1 \leq l \leq \mathcal{L}\}$ of a conventional modulation scheme, such as \mathcal{L} -PSK/QAM [5]. Hence, the transmitted signal block is given by

$$S(i) = s(i)A(i), \quad (3.43)$$

which takes value from the set $\{S^n\}_{n=1}^{Q \cdot \mathcal{L}}$. According to [136], a soft estimated symbol block $\hat{S}(i)$ of the transmitted CSTSK symbol block $S(i)$ could be expressed as

$$\hat{S}(i) = \sum_{n=1}^{Q \cdot \mathcal{L}} S^n \Pr\{S(i) = S^n\}. \quad (3.44)$$

Let $\{\tilde{b}_j\}_{j=1}^{\text{BPB}}$ represent the bit mapping corresponding to the specific CSTSK symbol block $\{S^n\}_{n=1}^{Q \cdot \mathcal{L}}$ and $L_p(b_j)$ be referred to as the *a posteriori* information of bit b_j . Then the corresponding probability of $\Pr\{S(i) = S^n\}$ might be expressed as

$$\Pr\{S(i) = S^n\} = \frac{\exp\left(\sum_{j=1}^{\text{BPB}} \tilde{b}_j L_p(b_j)\right)}{\prod_{j=1}^{\text{BPB}} \{1 + \exp(L_p(b_j))\}}. \quad (3.45)$$

We now demonstrate that the soft estimate of Eq. (3.44) is inappropriate for DDCE.

In Fig. 3.30, we have the BER performance of the proposed BBSBCE and three-stage turbo demapping-decoding scheme as well as the conventional joint CE and three-stage turbo demapping-decoding scheme utilizing all the detected signal blocks for the CSTSK(4, 4, 2, 4, 16-QAM) system associated with a normalized throughput of $R = 2$ bits/symbol, both of these two schemes employing a hard-decision based channel estimator. We re-plot the BER performance of these two schemes in Fig. 3.34. For the same CSTSK system, we design a conventional joint CE and three-stage turbo demapping-decoding scheme utilizing all the soft detected signal blocks for the soft-decision based LSCE, which employs the soft estimate of the transmitted STSK symbol block given in Eq. (3.44).

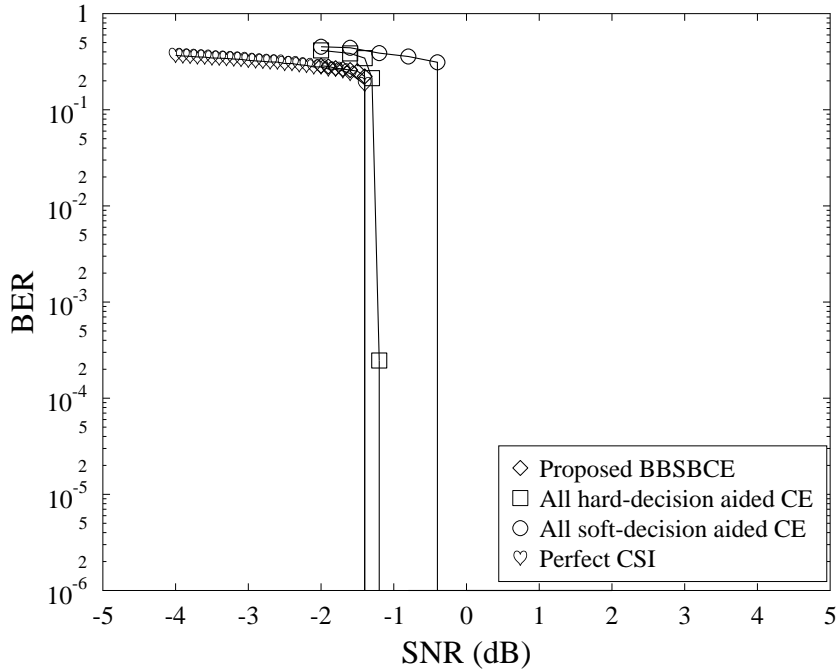


Figure 3.34: BER performance of the proposed hard-decision based BBSBCE and three-stage turbo demapping-decoding scheme using $M_T = 2$ ($O_p = 0.2\%$) initial CSTSK training blocks and a block-of-bits selection threshold of $T_h = 0.2$, in comparison to a) the conventional joint CE and three-stage turbo demapping-decoding scheme using $M_T = 2$ ($O_p = 0.2\%$) initial training blocks and utilizing all the hard detected signal blocks for the hard-decision based LSCE, and b) the conventional joint CE and three-stage turbo demapping-decoding scheme using $M_T = 2$ ($O_p = 0.2\%$) initial training blocks and utilizing all the soft detected signal blocks for the soft-decision based LSCE, for the CSTSK(4, 4, 2, 4, 16-QAM). All other system parameters were summarized in Table 3.3.

The corresponding BER performance obtained is also shown in Fig. 3.34, where it can be observed that both the hard-decision based schemes outperform this soft-decision aided scheme. The reason for this phenomenon is that in the soft-decision based channel estimator, the weighted CSTSK decisions of Eq. (3.44) cause the distortion to the dispersion matrix. To be more explicit, recall that the CSTSK transmit symbol block is generated by two parts – the dispersion matrix part and the conventional \mathcal{L} -PSK/QAM symbol part. The conventional \mathcal{L} -PSK/QAM symbol part may be weighted by Eq. (3.44), which in fact is designed specifically for conventional modulation. However, for the dispersion matrix part, it is the dispersion matrix index q that is used to represent the block of $\log_2(Q)$ bit values, and the soft-estimate of Eq. (3.44) is inappropriate for this part. For example, if we have a total number of $Q = 4$ dispersion matrices for a CSTSK system, then the matrix index may only take value of 1, 2, 3 or 4. Therefore, the soft-estimate of Eq. (3.44) is inappropriate for STSK systems.

3.5.1 Semi-Blind Soft-Decision Aided and Three-Stage Turbo Coded MIMO Transceiver

It has been demonstrated above that the soft-decision aided DDCE scheme is inappropriate for the CSTSK MIMO system due to its special bit mapping scheme. However, for many other MIMO schemes, such as the classic SDM/V-BLAST MIMO system, we can expect that appropriately weighting detected data symbols helps to alleviate the error propagation owing to erroneous decisions and, therefore to improve the attainable system performance. In this section, we develop a novel soft-decision aided CE and three-stage turbo detection-decoding based scheme for SDM/V-BLAST MIMO systems, which is capable of approaching the optimal perfect-CSI based MIMO performance bound with the aid of a very modest training overhead and without a significant increase in computational complexity. To be more explicit, we combine the highly effective BBSBCE strategy proposed in Section 3.4 with an appropriate soft-decision weighting method to form a soft-decision aided BBSBCE scheme, referred to as the BBSB-SCE, which selects a “just-sufficient” number of high-quality detected symbol blocks based on the *a posteriori* information produced by the MIMO soft-demapper within the original inner turbo loop of the URC decoder and MIMO detector. Since our proposed BBSB-SCE scheme only utilizes high-quality detected symbol blocks for soft-decision CE, in contrast to the existing state-of-the-art soft-decision CE solutions, it does not suffer from the usual performance degradation imposed by erroneous decisions. Furthermore, this measure dramatically reduces the complexity of the soft-decision CE.

3.5.1.1 Soft Symbol Estimation

Before we proceed with discussing the BBSB-SCE scheme, let us first elaborate a little further on the soft symbol estimation invoked for the conventional L -QAM/PSK modulation schemes utilized in the SDM/V-BLAST MIMO systems of Fig. 2.7.

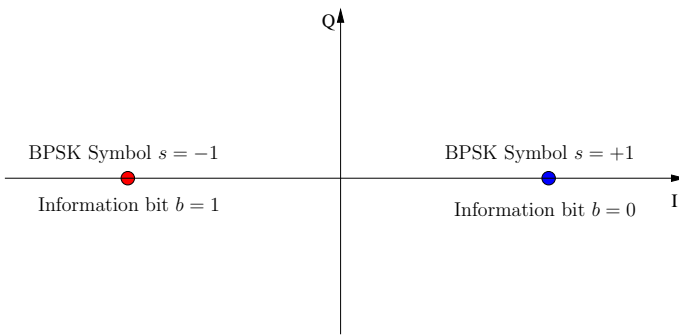


Figure 3.35: Conventional BPSK signalling constellation.

We commence by reviewing the basic soft symbol estimation procedure of BPSK symbols used in [145]. The constellation diagram of a BPSK modulation scheme is shown in Fig. 3.35. In the hard-decision turbo coded BPSK modulation scheme, an information bit is estimated on the basis of its *a posteriori* LLR output by the soft data detector, as introduced in Eq. (2.6) of Chapter 2.

Additionally, due to the specific “one bit per symbol” nature of BPSK, the *a posteriori* LLR L_p of a bit can be equivalently used for estimating the corresponding symbol s , and the nonlinear demapping operation is given by

$$s = \begin{cases} +1, & \text{if } L_p > 0, \\ -1, & \text{if } L_p \leq 0. \end{cases} \quad (3.46)$$

In this case, the demapped hard-decision of the BPSK symbol will fall exactly onto one of the two constellation points of Fig. 3.35. However, if soft-decisions of BPSK symbols are desired, the following operation may be needed

$$\hat{s} = \tanh\left(\frac{L_p}{2}\right). \quad (3.47)$$

The soft symbol estimation process of Eq. (3.47) is graphically illustrated in Fig. 3.36, where it may be seen that the estimate \hat{s} of a symbol s depends on the magnitude of its corresponding LLR L_p . This is plausible, because in view of turbo coding theory, a high LLR value indicates a high confidence level of the corresponding decision and vice versa [1]. In other words, if the magnitude of an LLR value is relatively small, the confidence level of the corresponding decision will be low. In this case, the position of soft-estimated symbol \hat{s} may be far away from the related reference constellation point s_r in the standard constellation map, causing a relatively large estimation error. On the other hand, if the magnitude of the LLR value is relatively large, the decision may have quite a high confidence level, and the corresponding soft-estimated symbol \hat{s} may be located close to the corresponding constellation point s_r , thus leading to a small estimation error. Naturally, the sign of the LLR L_p determines the sign of the soft estimate \hat{s} , namely, which of the two reference points of $s_r = \pm 1$ that \hat{s} is close to.

An example of how the LLR value affects the soft estimation of the corresponding BPSK symbol is illustrated in Fig. 3.37, where it may be seen that if we have an LLR of $L_p = -4$, which represents a high magnitude, then the soft estimation of this BPSK symbol is $\hat{s} = -0.9640$ according to Eq. (3.47), which is quite close to the reference constellation point of $s_r = -1$. If we define the soft symbol estimation error as the distance between the soft estimated symbol \hat{s} and its closest

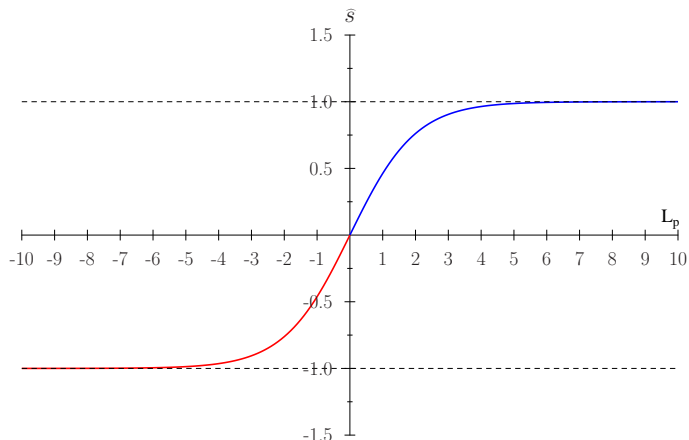


Figure 3.36: Soft symbol estimate according to the bit’s LLR for BPSK signalling.

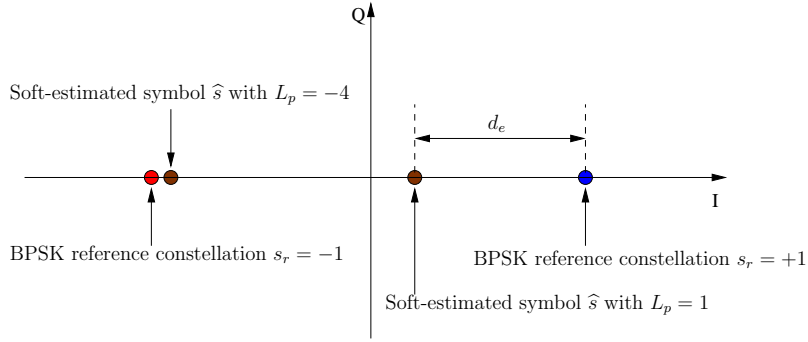


Figure 3.37: The effects of the LLR value to the soft-estimation of a BPSK symbol.

reference constellation point given by

$$d_e = \|s_r - \hat{s}\|^2, \quad (3.48)$$

then the soft symbol estimation error in this case is a relatively small value of $d_e = 1.296 \times 10^{-3}$. However, if we have an LLR associated with a small magnitude, say $L_p = 1$, the soft estimate of this BPSK symbol is $\hat{s} = 0.4621$, which is relatively far away from the reference constellation point of $s_r = +1$, leading to a relatively large estimation error of $d_e = 2.893 \times 10^{-1}$.

It may be seen from the above discussion that for the BPSK signalling, the soft estimation of a specific symbol may be obtained by the LLR of the corresponding information bit due to the “one bit per symbol” nature of BPSK signalling. For a high-order PSK/QAM signalling, however, the direct soft estimation operation of Eq. (3.47) no longer works because each symbol now contain more than one information bit. In this situation, an appropriate way of accomplishing soft estimation of a symbol must be considered. A close examination of the BPSK soft symbol estimate \hat{s} of Eq. (3.47) and its graphical illustration of Fig. 3.36 reveals that the magnitude $|\hat{s}|$ may be used as the estimated probability of \hat{s} belonging to the corresponding reference constellation point s_r . By extending this idea to high-order modulation, an efficient way of carrying out soft symbol estimation was proposed in [136], where the main idea is to estimate a soft symbol based on the probabilities of its legitimate reference constellation points. This soft symbol estimate based on the associated probabilities of all legitimate “constellation points” is in fact what we attempt to achieve in Eq. (3.44) for the STSK MIMO system. However, this is inappropriate for STSK systems because its bit mapping is not specified solely by the conventional modulation used for the other MIMO systems, which employ conventional modulation signalling, such as \mathcal{L} -PSK/QAM, the soft symbol estimation proposed in [136] is entirely appropriate.

To be more explicit, given the constellation size of \mathcal{L} and the bits per symbol of throughput of $BPS = \log_2 \mathcal{L}$, the soft symbol estimation can be accomplished within the following two steps.

Step 1) Calculate the probability P_l of each of the \mathcal{L} symbol points $\{s^l\}_{l=1}^{\mathcal{L}}$ in the constellation diagram based on the *a posteriori* LLRs $L_p(u_j)$ of each of the BPS information bits $\{\tilde{u}_j\}_{j=1}^{BPS}$ that

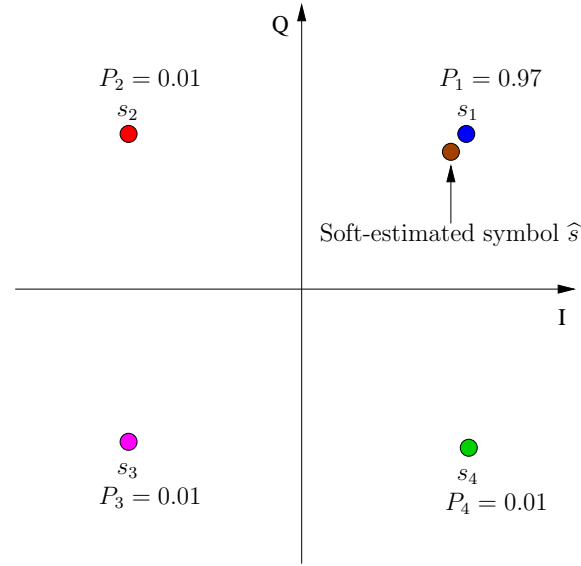


Figure 3.38: Soft estimation example of a QPSK symbol for Case 1: one constellation point has significantly higher probability than the others have.

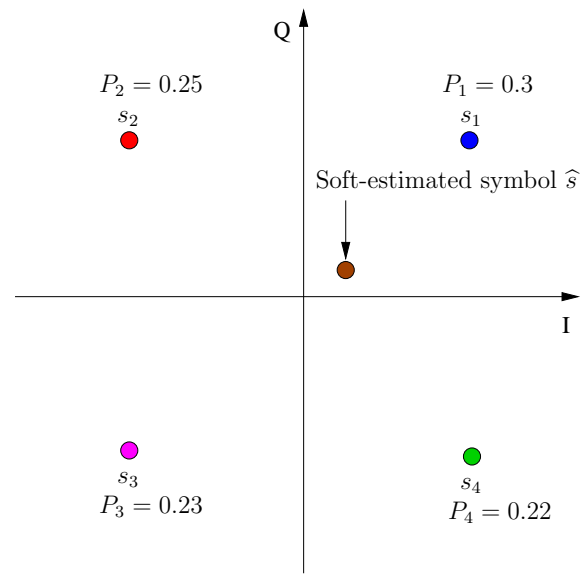


Figure 3.39: Soft estimation example of a QPSK symbol for Case 2: all constellation points share similar probabilities.

map to a symbol s^l , where we have $l = 1, 2, \dots, \mathcal{L}$. More specifically, P_l is calculated according to

$$P_l = \Pr\{s = s^l\} = \frac{\exp\left(\sum_{j=1}^{\text{BPS}} \tilde{u}_j L_p(u_j)\right)}{\prod_{j=1}^{\text{BPS}} \left(1 + \exp(L_p(u_j))\right)}. \quad (3.49)$$

Step 2) The soft-estimate of a symbol is then calculated by summing up the product of each of the

\mathcal{L} constellation points with its corresponding probability obtained from Eq. (3.49), yielding

$$\hat{s} = \sum_{l=1}^{\mathcal{L}} s^l P_l. \quad (3.50)$$

Figs. 3.38 and 3.39 show two examples of accomplishing soft symbol estimation for QPSK signalling: **Case 1**). One of the constellation points has significantly higher probability than the others, as exemplified by $P_1 = 0.97$, $P_2 = 0.01$, $P_3 = 0.01$, and $P_4 = 0.01$; and **Case 2**). All the constellation points share similar probabilities, specifically, $P_1 = 0.3$, $P_2 = 0.25$, $P_3 = 0.23$, and $P_4 = 0.22$, respectively. It may be seen from Fig 3.38 that in Case 1, the resultant soft-estimated symbol \hat{s} is dominated by s_1 due to its high probability of $P_1 = 0.97$, leading to an estimation error as small as $d_e = 0.0396$. This implies that the LLRs output from the soft data detector are relatively reliable. By contrast, it may be seen from Fig. 3.39 that when the \mathcal{L} constellation points have similar probability values, none of the constellation points could dominate the soft-estimated symbol \hat{s} , which leads to a large estimation error $d_e = 0.965$ between \hat{s} and its “reference” constellation point s_1 , which implies that the LLRs output by the soft data detector are less reliable.

3.5.1.2 BBSB Soft Channel Estimation

By understanding how the soft symbol estimator works, we can now detail our novel BBSB-SCE scheme for assisting classic SDM/V-BLAST MIMO systems. Again we consider a three-stage serial-concatenated turbo coded MIMO system discussed in Section 2.2 of Chapter 2, relying on M Tx antennas and N Rx antennas and employing high-order \mathcal{L} -PSK/QAM modulation for communicating over a frequency-flat Rayleigh fading environment.

The structure of our proposed BBSB-SCE and three-stage turbo detector-decoder is shown in Fig. 3.40, which looks similar to that of the BBSBCE based scheme proposed for CSTSK depicted in Fig. 3.20 of Section 3.4, except for that the “CSTSK Modulator”, “CSTSK Soft-demapper” and “BBSB Channel Estimator” are now replaced by “MIMO Modulator”, “MIMO Soft-demapper” and “Soft BBSB Channel Estimator”, respectively. Note that similar to the BBSBCE based scheme, in a BBSB-SCE scheme aided SDM/V-BLAST MIMO system, there is also no additional iterative loop involving the soft-decision CE and the three-stage turbo detector-decoder. In other words, our soft-decision aided channel estimator is embedded in the original outer loop of the three-stage turbo structure, and the soft-decision CE update occurs concurrently with the original outer turbo decoding iteration. Moreover, our CE does not use the entire frame of the detected bits. Rather, it only selects the high-quality or reliable decisions. Specifically, the *a posteriori* information output by the MIMO soft-demapper provides the confidence levels of binary 1s and 0s [1]. Therefore, based on this confidence level, we can select the reliable decisions from the MIMO soft-demapper’s output sequence for CE. Removing most of the erroneous decisions from the CE leads to a much more accurate channel estimate, which in turn enhances the performance of the three-stage turbo detection-decoding process. Additionally, by employing the soft symbol estimation scheme discussed in

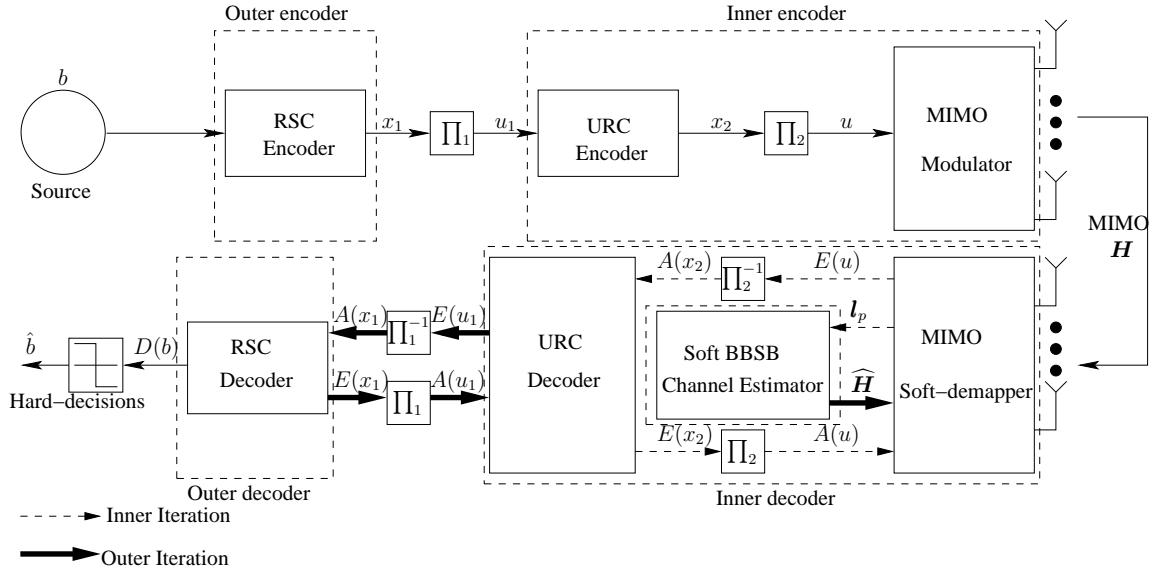


Figure 3.40: Joint BBSB-SCE aided and three-stage serial-concatenated turbo detection-decoding assisted MIMO system. Note that different to Fig. 3.20, the ‘BBSB Channel Estimator’ and ‘CSTSK Modulator’ of Fig. 3.20 have been replaced by ‘Soft BBSB Channel Estimator’ and ‘MIMO Modulator’ in Fig. 3.40.

Section 3.5.1.1, the effects of a few erroneous decisions that might have been selected mistakenly can further be reduced. Consequently, our joint BBSB-SCE and three-stage turbo detector-decoder is capable of attaining the optimal performance bound of the idealised three-stage turbo detector-decoder associated with perfect CSI, as will be confirmed in our simulation study. As a further benefit of only selecting reliable decisions, the complexity of our soft-decision aided LSCE is dramatically lower than that of the conventional soft-decision based LSCE scheme utilizing the whole data blocks. Let us now elaborate our scheme further.

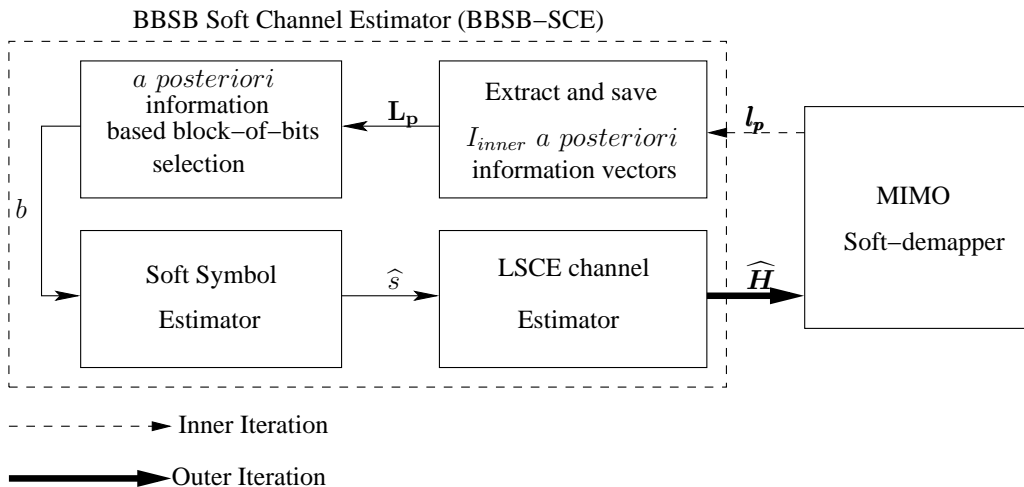


Figure 3.41: Block diagram of the proposed BBSB-SCE.

The details of the proposed BBSB-SCE procedure is illustrated in Fig. 3.41. Note that compared to Fig. 3.21 of Section 3.4, the main difference is that the ‘‘CSTSK Re-modulation’’ in Fig. 3.21 is replace by ‘‘Soft Symbol Estimator’’. This means that the proposed BBSB-SCE scheme for SDM/V-BLAST MIMO systems is exactly identical to the BBSBCE scheme for CSTSK presented in Section 3.4, except for that the only difference corresponding to Step 3) of the BBSBCE algorithm. To be more explicit, in Step 3) of the BBSBCE scheme for CSTSK systems, by only obtaining reliable decision block-of-bits, the selected CSTSK blocks of hard bits are re-modulated and further involved for DDCE. However, in the BBSB-SCE for SDM/V-BLAST MIMO systems, since soft symbol estimation is invoked for the sake of further reducing the effects of erroneous decisions, the soft symbol estimator introduced in Section 3.5.1.1 is employed instead. Therefore, the detailed Steps 1), 2) and 4) of the proposed BBSBCE adided and three-stage turbo detection-decoding assisted scheme are omitted here, since they are identical to Steps 1), 2) and 4) of the BBSBCE scheme which are detailed in Section 3.4.2.1, and only its Step 3) is described below.

For the notational consistency, denote the M_T blocks of the training data that are used to obtain the initial training-based LSCE of the MIMO channel matrix by $\mathbf{Y}_{tM_T} \in \mathbb{C}^{N \times M_T}$ and $\mathbf{S}_{tM_T} \in \mathbb{C}^{M \times M_T}$. Further denote the observation data to the MIMO receiver by

$$\mathbf{Y}_{d\tau} = [\mathbf{y}(1) \mathbf{y}(2) \cdots \mathbf{y}(\tau)], \quad (3.51)$$

where τ is the number of symbol blocks in a transmitted MIMO frame.

Step 3) By completing Steps 1) and 2), we have the selected symbol index vector $\mathbf{x}^t = [x^t(1) \ x^t(2) \ \cdots \ x^t(M_s^t)]^T$ in which $x^t(i)$ is the position or index of the i th selected symbol vector in the transmitted symbol vector sequence. The number of the selected symbol vectors M_s^t varies within $\{0, 1, \dots, M_{\text{sel}}\}$, where $M_{\text{sel}} \ll \tau$ is the maximum number of blocks imposed for CE. Specifically, whenever the number of selected reliable symbol vectors M_s^t reaches the limit M_{sel} , the sliding-window process ends; otherwise, the sliding-window process examines all the possible bit blocks and outputs the M_s^t selected symbol vectors. Then based on the selected high-confidence blocks of soft-decision bits, generate the soft-estimate of each symbol element as [136]

$$\hat{s}^m(x^t(n)) = \sum_{l=1}^{\mathcal{L}} s^l \Pr\{s^m(x^t(n)) = s^l\} = \sum_{l=1}^{\mathcal{L}} s^l \cdot \frac{\exp\left(\sum_{j=1}^{\text{BPS}} \tilde{u}_j L_p(u_j)\right)}{\prod_{j=1}^{\text{BPS}} (1 + \exp(L_p(u_j)))}, \quad (3.52)$$

for $1 \leq n \leq M_s^t$, where $\{s^l\}_{l=1}^{\mathcal{L}}$ denotes the \mathcal{L} -PSK/QAM symbol set, $m \in \{1, 2, \dots, M\}$ indicates the symbol index in the soft-estimated symbol vector $\hat{\mathbf{s}}(x^t(n))$, and $\{\tilde{u}_j\}_{j=1}^{\text{BPS}}$ represents the bit mapping corresponding to s^l . Combining the initial training input \mathbf{S}_{tM_T} with the soft-estimated symbol vectors $[\hat{\mathbf{s}}(x^t(1)) \ \hat{\mathbf{s}}(x^t(2)) \ \cdots \ \hat{\mathbf{s}}(x^t(M_s^t))]$ yields

$$\hat{\mathbf{S}}_{\text{sel}}^{(t)} = [\mathbf{S}_{tM_T} \ \hat{\mathbf{s}}(x^t(1)) \ \hat{\mathbf{s}}(x^t(2)) \ \cdots \ \hat{\mathbf{s}}(x^t(M_s^t))]. \quad (3.53)$$

Similarly, the symbol index vector \mathbf{x}^t allows us to select the corresponding observation blocks from $\mathbf{Y}_{d\tau}$ of Eq. (3.51), which are combined with \mathbf{Y}_{tM_T} to produce

$$\mathbf{Y}_{\text{sel}}^{(t)} = [\mathbf{Y}_{tM_T} \ \mathbf{y}(x^t(1)) \ \mathbf{y}(x^t(2)) \ \cdots \ \mathbf{y}(x^t(M_s^t))], \quad (3.54)$$

The soft decision-directed LSCE is readily given by

$$\widehat{\mathbf{H}}^{(t+1)} = \mathbf{Y}_{\text{sel}}^{(t)} (\widehat{\mathbf{S}}_{\text{sel}}^{(t)})^H \left(\widehat{\mathbf{S}}_{\text{sel}}^{(t)} (\widehat{\mathbf{S}}_{\text{sel}}^{(t)})^H \right)^{-1}. \quad (3.55)$$

This update occurs as the soft information is exchanged between the two-stage inner decoder and the outer RSC decoder, as indicated in Fig. 3.41. Then go to Step 4).

3.5.1.3 Computational Complexity of the BBSB-SCE Based MIMO System

The computational complexity of our soft-decision CE is upper bounded by $\mathcal{O}(M_{\text{sel}}^3)$ which is dramatically smaller than $\mathcal{O}(\tau^3)$. For example, considering a reasonable case of $\tau = 1000$ and $M_{\text{sel}} = 100$, the complexity of our CE is more than 1000 times smaller than that of the conventional scheme which utilizes the entire soft detected sequence of τ symbol blocks. The total complexity of our proposed BBSB-SCE aided and three-stage turbo detection-decoding based scheme satisfies

$$C_{\text{proposed}} \leq I_{\text{out}} \cdot \mathcal{O}(M_{\text{sel}}^3) + C_{\text{ideal}}, \quad (3.56)$$

where C_{ideal} represents the computational complexity of the idealised three-stage turbo receiver associated with perfect CSI, as expressed in Eq. (3.24). Since $I_{\text{out}} \cdot \mathcal{O}(M_{\text{sel}}^3) \ll C_{\text{ideal}}$, we have $C_{\text{proposed}} \approx C_{\text{ideal}}$. By contrast, the existing state-of-the-art soft-decision CE and three-stage turbo detection-decoding scheme has the computational complexity of

$$C_{\text{conventional}} = I_{\text{ce}} \cdot \mathcal{O}(\tau^3) + I_{\text{ce}} \cdot C_{\text{ideal}}, \quad (3.57)$$

because it utilizes the entire sequence of τ soft estimated symbol vectors for CE and, therefore, imposes an additional CE loop which requires I_{ce} iterations to converge.

3.5.2 Simulation Results and Discussions

3.5.2.1 Example One

A quasi-static Rayleigh fading MIMO system using $M = N = 4$ and 16-QAM was simulated. An interleaver length of $L_F = 16,000$ bits was used, yielding $\tau = 1000$ 16-QAM symbol vectors per frame. The binary generator polynomials of the half-rate RSC encoder were $G_{\text{RSC}} = [1, 0, 1]_2$ and $G_{\text{RSC}}^r = [1, 1, 1]_2$, while those of the URC encoder were $G_{\text{URC}} = [1, 0]_2$ and $G_{\text{URC}}^r = [1, 1]_2$. The transmitted signal power was normalised to unity and, therefore, the SNR was given as $\frac{1}{N_0}$. The number of initial training data blocks was chosen to be $M_T = 6$, yielding a PO of $O_p = 0.6\%$, while the maximum number of selected blocks for our BBSB-SCE was limited to $M_{\text{sel}} = 100$. At the beginning of each frame, a new MIMO channel matrix \mathbf{H} was generated by randomly drawing the channel taps according to the complex-valued Gaussian distribution $\mathcal{CN}(0, 1)$, and \mathbf{H} was kept constant in the frame duration. Two metrics were used to assess the achievable performance, namely, the BER and the MSE of the CE. The CRLB, which is known to provide the best attainable

performance for an unbiased estimator, was used for lower-bounding the MSE of a channel estimator. The system parameters of the joint BBSB-SCE and three-stage turbo receiver of Fig. 3.40 are summarized in Table 3.4.

Table 3.4: System parameters of the joint BBSB-SCE and three-stage turbo receiver of Fig. 3.40.

Number of Tx antennas	$M = 4$
Number of Rx antennas	$N = 4$
Modulation	16-QAM
Channels	Frequency-flat Rayleigh fading
Detector	ML detector
Number of training blocks	$M_T = 6$
Number of signal blocks per frame	τ
Number of selected reliable MIMO symbol blocks	$M_{\text{sel}} = 100$
Pilot overhead	$O_p = 0.6\%$
Block-of-bits selection threshold	T_h
Interleaver blocklength	L_F
Outer channel code	Half-rate RSC
Generator polynomials	$(G_{\text{RSC}}^r, G_{\text{RSC}}) = (7, 5)_8$
Precoder	URC
Number of inner iterations	$I_{in} = 3$
Number of outer iterations	$I_{out} = 5$

Fig. 3.42 shows the EXIT chart of our proposed joint BBSB-SCE and three-stage turbo receiver associated with a block-of-bits selection threshold of $T_h = 1.0$, in comparison to that of the perfect-CSI case. The corresponding system's throughput is $R = 16$ bits/symbol. It can be seen that open tunnels exist between the EXIT curves of the amalgamated inner MIMO soft-demapper-URC decoder and the outer RSC decoder for both the proposed semi-blind BBSB-SCE based scheme and the idealised optimal ML detection based on the perfect CSI, at SNR = 5.0 dB. The Monte-Carlo simulation based stair-case shaped decoding trajectories, which closely match the EXIT curves, are also provided at SNR = 5.0 dB. It is seen that the both trajectories are capable of reaching the perfect convergence point of (1.0, 1.0), implying that the proposed semi-blind BBSB-SCE based scheme with an initial training overhead of $M_T = 6$ ($O_p = 0.6\%$) is capable of achieving the optimal performance bound associated with the idealised three-stage receiver with the same number of turbo iterations. Additionally, it can also be seen that the starting point of the EXIT curve of the semi-blind BBSB-SCE based scheme is lower than that of the perfect CSI scenario. This is expected because a poor initial CE quality leads to a lower extrinsic information. However, as the *a priori* information value increases, the EXIT curve of the BBSB-SCE based scheme is capable of

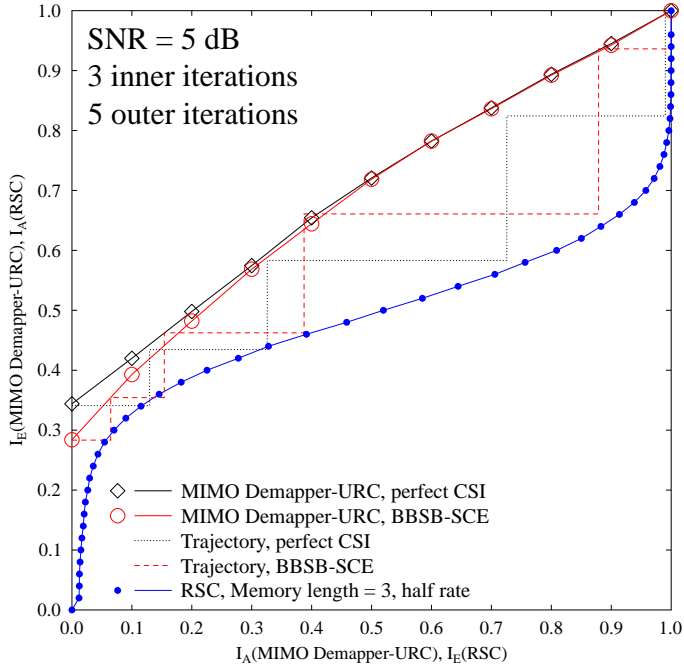


Figure 3.42: EXIT chart analysis of our proposed semi-blind joint BBSB-SCE and three-stage turbo receiver of **Example 1** quasi-static MIMO system of Fig. 3.40 having a throughput of $R = 16$ bits/symbol, using $M_T = 6$ initial training blocks and a PO of $O_p = 0.6\%$. A block-of-bits selection threshold of $T_h = 1.0$ is used. The performance is compared to the perfect-CSI scenario. All other system parameters were summarized in Table 3.4. The corresponding BER curves are seen in Fig. 3.44.

converging to that of the perfect CSI scenario, implying that an accurate channel estimate has been obtained.

The BER performance of the proposed joint BBSB-SCE and three-stage turbo receiver is shown in Fig. 3.43, in comparison to that of the perfect CSI bound and those of the conventional semi-blind joint CE and three-stage turbo schemes utilizing the entire detected data sequence for the soft and hard decision aided CE, respectively. Our semi-blind joint BBSB-SCE and three-stage turbo detector-decoder employed $I_{in} = 3$ inner turbo iterations and $I_{out} = 5$ outer turbo iterations, which were identical to those employed by the idealised three-stage turbo detector-decoder associated with perfect CSI. It can be seen from Fig. 3.43 that the proposed semi-blind BBSB-SCE scheme is capable of attaining the near-capacity optimal ML performance associated with the perfect CSI, with the same ‘turbo-cliff’ occurring before SNR = 5 dB. The conventional joint CE and three-stage turbo receiver combined with the soft-decision aided CE employing the entire detected data sequence cannot attain the perfect CSI performance bound, and there is a 2 dB gap between the BER turbo-cliffs of the two receivers. The conventional scheme employing the hard-decision aided CE based on the entire detected data sequence exhibits a further 1.5 dB degradation from its soft-decision assisted counterpart.

Fig. 3.44 illustrates the convergence behaviour of the proposed joint BBSB-SCE and three-

stage turbo scheme. It can be seen that the BER gap between the proposed BBSB-SCE based scheme and the perfect CSI case reduces, as the number of outer iterations increases. Specifically, after the initial iteration there is a large BER gap, while during the third iteration the BER gap is reduced to around 1 dB. Finally, at the fifth iteration there is no BER gap, indicating that the BBSB-SCE scheme has converged to the true MIMO CIR. This is very significant, since our semi-blind BBSB-SCE based scheme has as low a PO as 0.6% and yet it attains the optimal performance of the idealised three-stage turbo receiver associated with perfect CSI, while only imposing a complexity similar to the latter, as evidence by our complexity comparison given in (3.56).

The effects of the block-of-bits selection threshold T_h on the achievable performance of our proposed semi-blind scheme were investigated by varying the value of T_h in the set $\{0.2, 0.5, 1.0, 2.0, 3.0\}$. The results obtained are shown in Fig. 3.45, where it is seen that $T_h \in [0.5, 1.0]$ for this example allows our scheme to approach the perfect CSI performance bound.

The MSE performance of the channel estimator in our proposed scheme is compared to the CRLB associated with the optimal training sequence of length $M_T^{\text{opt}} = 100$ in Fig. 3.46, where it can be seen that the MSE of our DDCE approaches the CRLB, once the number of outer turbo iterations reaches $I_{\text{out}} = 5$ for $\text{SNR} \geq 5.0$ dB. This corresponds to the BER cliff at $\text{SNR} \approx 5.0$ dB and $I_{\text{out}} = 5$ shown in Fig. 3.43.

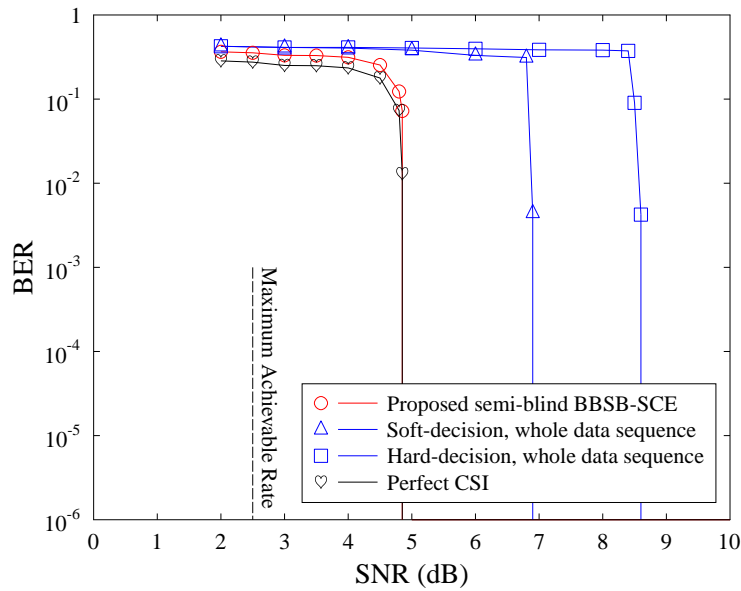


Figure 3.43: BER performance comparison: a) perfect CSI case, b) proposed joint BBSB-SCE and three-stage turbo receiver with $T_h = 1.0$, and c) conventional joint CE and three-stage turbo receivers employing the entire detected data sequence for the soft and hard decision aided channel estimators, respectively, for **Example 1** of quasi-static MIMO system. The number of initial training blocks for all the three CE schemes is $M_T = 6$, corresponding to a PO of $O_p = 0.6\%$. The system's throughput is $R = 16$ bits/symbol. All other system parameters were summarized in Table 3.4.

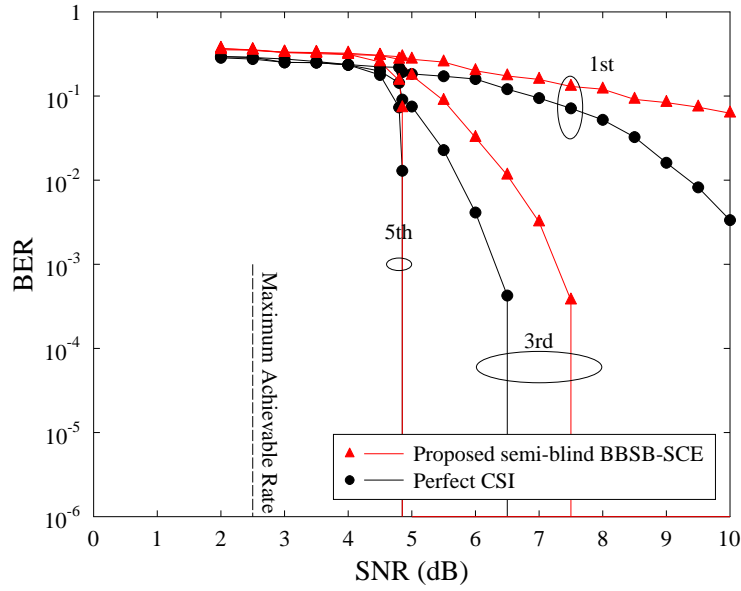


Figure 3.44: Convergence performance of the proposed joint BBSB-SCE and three-stage turbo detector-decoder with $T_h = 1.0$, in comparison to the perfect-CSI case, for **Example 1** of quasi-static MIMO system of Fig. 3.40 having a throughput of $R = 16$ bits/symbol, using $M_T = 6$ initial training blocks and a PO of $O_p = 0.6\%$. All other system parameters were summarized in Table 3.4. The corresponding EXIT chart is seen in Fig. 3.42.

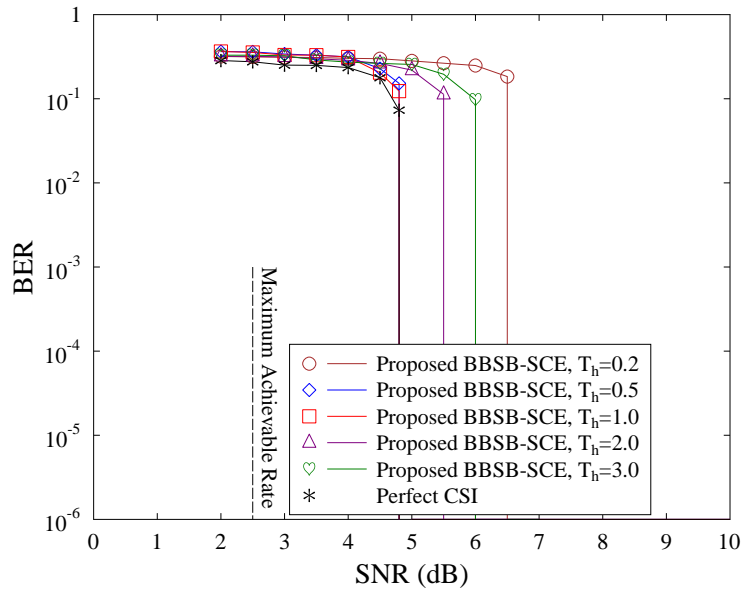


Figure 3.45: Effects of the block-of-bits selection threshold T_h on the achievable BER performance of our proposed BBSB-SCE and three-stage turbo scheme, for **Example 1** of quasi-static MIMO system of Fig. 3.40 having a throughput of $R = 16$ bits/symbol, using $M_T = 6$ initial training blocks and a PO of $O_p = 0.6\%$. All other system parameters were summarized in Table 3.4.

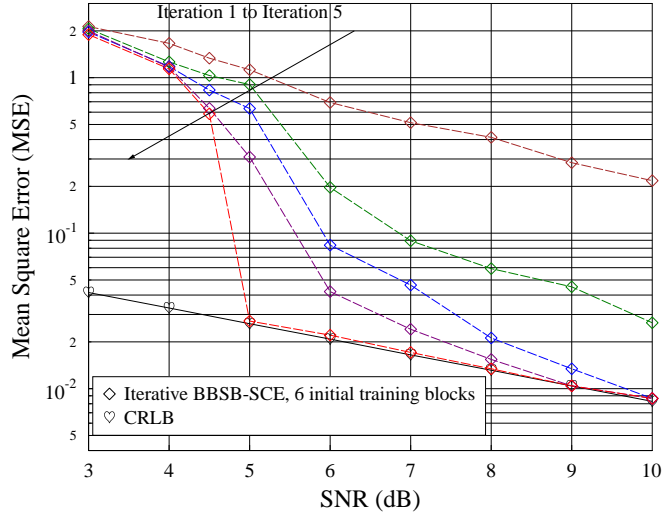


Figure 3.46: MSE convergence performance of the channel estimator in our semi-blind joint BBSB-SCE and three-stage turbo detection-decoding scheme using $M_T = 6$ initial training blocks, a block-of-bits selection threshold of $T_h = 1.0$ and the maximum number of selected blocks $M_{\text{sel}} = 100$, for **Example 1** of quasi-static MIMO system of Fig. 3.40 having a throughput of $R = 16$ bits/symbol, using $M_T = 6$ initial training blocks and a PO of $O_p = 0.6\%$. All other system parameters were summarized in Table 3.4.

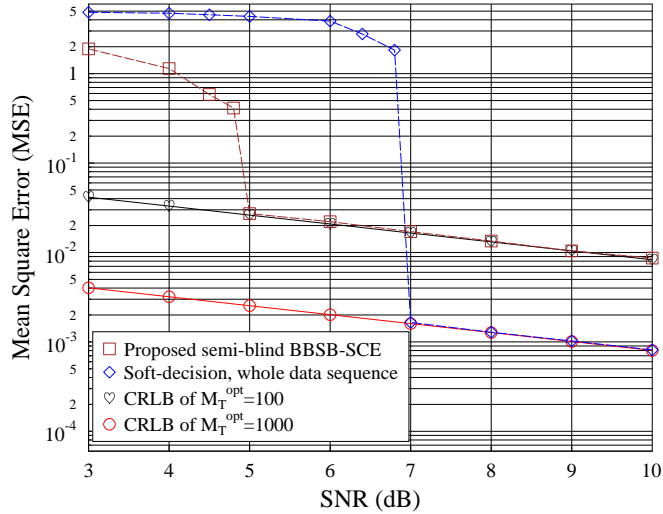


Figure 3.47: Comparison of the MSE performance of our joint BBSB-SCE and three-stage turbo detector-decoder, which selects $M_s^t \leq 100$ high-quality soft detected symbol vectors for the channel estimator, with that of the conventional joint CE and three-stage turbo detector-decoder, which uses all the $\tau = 1000$ soft detected symbol vectors for the channel estimator, for **Example 1** of quasi-static MIMO system of Fig. 3.40 having a throughput of $R = 16$ bits/symbol, using $M_T = 6$ initial training blocks and a PO of $O_p = 0.6\%$. All other system parameters were summarized in Table 3.4.

Fig. 3.47 compares the achievable MSE performance of our joint BBSB-SCE and three-stage turbo receiver, which only selects $M_s^t \leq 100$ high-quality soft detected symbol vectors for aiding the channel estimator, with that of the conventional joint CE and three-stage turbo receiver, which uses all the $\tau = 1000$ soft detected symbol vectors for the CE. Observe that for $\text{SNR} \geq 7.0$ dB, the soft-DDCE utilizing all the $\tau = 1000$ detected symbol vectors approaches the CRLB associated with the optimal training sequence of length $M_T^{\text{opt}} = 1000$, because at this level of SNR there exists no decision error and all the detected symbol vectors are correct. However, the operational SNR of this system is around 5 dB, and at the operational SNR region, the initial BER is practically 50%, which leads to the “failure” of the conventional joint CE and three-stage turbo receiver, as can be clearly seen from Figs. 3.43 and 3.47.

3.5.2.2 Example Two

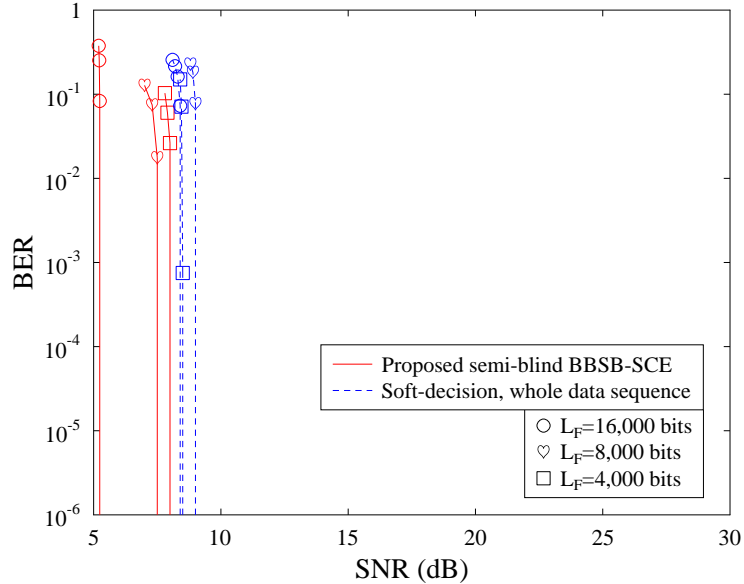


Figure 3.48: BER performance comparison: a) proposed joint BBSB-SCE and three-stage turbo receiver of Fig. 3.40 with $T_h = 1.0$, and b) conventional joint CE and three-stage turbo receiver employing the entire detected data sequence for the soft decision aided channel estimator, for **Example 2** of time-varying MIMO system with the normalised Doppler frequency $f_d = 10^{-5}$ as well as the interleaver lengths of $L_F = 16,000$ bits, 8,000 bits and 4,000 bits, yielding the POs of $O_p = 0.6\%$, 1.2% and 2.4%, respectively. The system’s throughput is $R = 16$ bits/symbol. All other system parameters were summarized in Table 3.4.

The system setup was identical to that of *Example 1* as shown in Table 3.4, except for that the MIMO channels were time-varying. Specifically, \mathbf{H} was faded at the symbol-rate during each

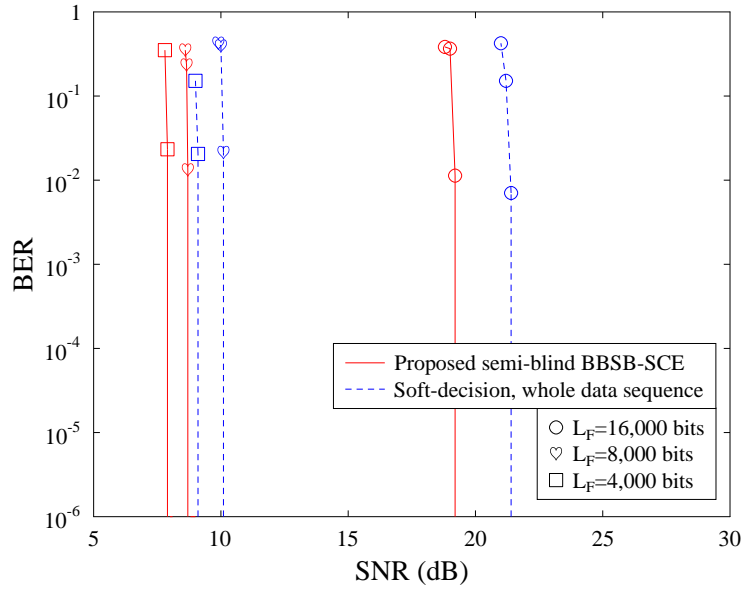


Figure 3.49: BER performance comparison: a) proposed joint BBSB-SCE and three-stage turbo receiver Fig. 3.40 with $T_h = 1.0$, and b) conventional joint CE and three-stage turbo receiver employing the entire detected data sequence for the soft decision aided channel estimator, for **Example 2** of time-varying MIMO system with the normalised Doppler frequency $f_d = 10^{-4}$ as well as the interleaver lengths of $L_F = 16,000$ bits, 8,000 bits and 4,000 bits, yielding the POs of $O_p = 0.6\%$, 1.2% and 2.4%, respectively. The system's throughput is $R = 16$ bits/symbol. All other system parameters were summarized in Table 3.4.

frame according to the normalized Doppler frequency of f_d , which may be formulated as

$$f_d = f_m \cdot T_s, \quad (3.58)$$

where T_s is the symbol period. Given the carrier frequency of f_c , the maximum Doppler frequency f_m is given by

$$f_m = \frac{v \cdot f_c}{c}, \quad (3.59)$$

where v and c are the velocity of mobile and the speed of light, respectively. For example, in the LTE standard, the carrier frequency is about $f_c = 2.5$ GHz and the symbol period is $T_s = 66.7 \mu s$. Then a normalized Doppler frequency of $f_d = 10^{-4}$ corresponds to a walking speed of about 0.5 m/s and hence slow fading is experienced. When the normalized Doppler frequency is $f_d = 10^{-2}$, the corresponding mobile velocity increases to 50 m/s, where fast fading is experienced. Note that for the time-varying MIMO channels, there exists a trade-off between the Time-Varying Channel's Estimation (TVCE) performance and the turbo channel decoder's performance. To be more explicit, for turbo channel coding, a long interleaver length L_F is preferred for the sake of achieving a near-capacity performance [1]. However, a short frame block length τ , i.e. a short interleaver length L_F ,

is preferred for the sake of achieving a good TVCE performance. In our simulations, we varied f_d and investigated the effect of different interleaver lengths to the achievable BER performance⁴.

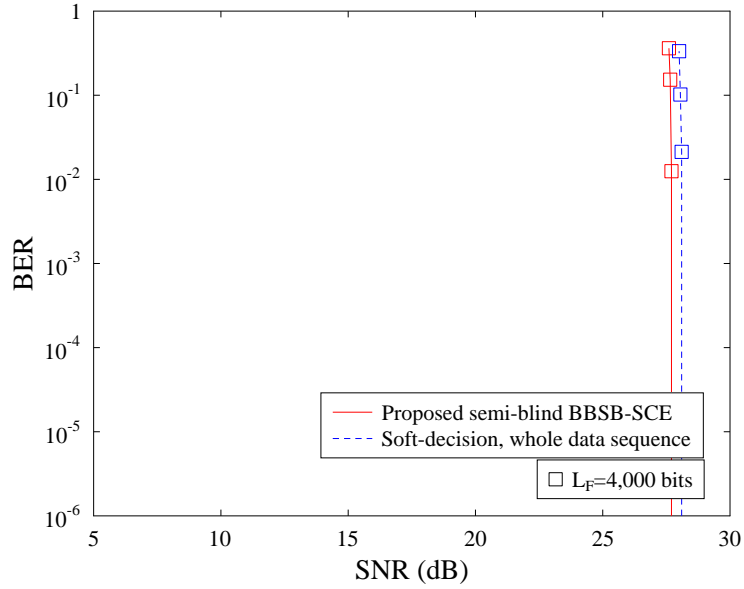


Figure 3.50: BER performance comparison: a) proposed joint BBSB-SCE and three-stage turbo receiver Fig. 3.40 with $T_h = 1.0$, and b) conventional joint CE and three-stage turbo receiver employing the entire detected data sequence for the soft decision aided channel estimator, for **Example 2** of time-varying MIMO system with the normalised Doppler frequency $f_d = 5 \times 10^{-4}$ and the interleaver length of $L_F = 4,000$ bits, yielding a PO of 2.4%. The system's throughput is $R = 16$ bits/symbol. All other system parameters were summarized in Table 3.4.

Fig. 3.48 shows the results obtained for the case of the normalised Doppler frequency $f_d = 10^{-5}$ with $L_F = 16,000$ bits, $8,000$ bits and $4,000$ bits, respectively, where it can be seen that for each given interleaver length L_F the proposed semi-blind joint BBSB-SCE and three-stage turbo receiver outperforms the conventional semi-blind joint CE and three-stage turbo scheme utilizing the entire detected data sequence. Specifically, our scheme achieves SNR gains of 3.1 dB, 1.5 dB and 0.5 dB over the conventional one for $L_F = 16,000$ bits, $L_F = 8,000$ bits and $L_F = 4,000$ bits, respectively. As expected, our proposed semi-blind BBSB-SCE scheme achieves its best BER performance for the long interleaver length of $L_F = 16,000$ bits. This is because the normalized Doppler frequency of $f_d = 10^{-5}$ represents a relatively slowly fluctuating channel. Hence the achievable system performance is dominated by the performance of iterative channel decoder which favours a high L_F value. Furthermore, as the interleaver length of our scheme reduces, the number of potential high-quality candidates may also be reduced, which may hence contribute to the degradation of the system's performance. A similar conclusion may be drawn for the conventional semi-blind CE scheme that utilises the entire soft detected data sequence from Fig. 3.48, where the

⁴In practice, Doppler spread may be estimated using the schemes proposed in [146–148].

performance of the conventional scheme is degraded by about 0.6 dB, when the interleaver length is reduced from 16,000 bits to 8,000 bits. However, unlike for our proposed semi-blind BBSB-SCE scheme, in this particular case, the performance of the conventional semi-blind CE based scheme recorded for $L_F = 4,000$ bits is better than that of the $L_F = 8,000$ -bit scenario.

Fig. 3.49 compares the achievable BER performance of our proposed scheme to that of the conventional scheme for the case of the normalised Doppler frequency $f_d = 10^{-4}$ with $L_F = 16,000$ bits, 8,000 bits and 4,000 bits, respectively. As seen from Fig. 3.49, the best performance is achieved with the interleaver length of $L_F = 4,000$ bits, while the worst performance is obtained for the interleaver length of $L_F = 16,000$ bits for both our proposed scheme and the conventional one. At the normalised Doppler frequency of $f_d = 10^{-4}$ the MIMO system's overall performance is dominated by the TVCE performance, which favours a short interleaver. Evidently, there exists a trade off between the turbo channel coding performance and the TVCE performance in choosing the best interleaver length. Observe furthermore in Fig. 3.49 that for a given interleaver length L_F , our proposed scheme always outperforms the conventional one.

When considering an even higher normalised Doppler frequency of $f_d = 5 \times 10^{-4}$, both our proposed semi-blind joint BBSB-SCE and three-stage turbo receiver as well as the conventional semi-blind joint CE and three-stage turbo scheme utilizing the entire detected data sequence for the soft-decision aided CE cannot converge (there exists no open tunnel between the EXIT curves of the inner and outer decoders) for the interleaver lengths of $L_F = 16,000$ bits and $L_F = 8,000$ bits associated with an SNR as high as 30 dB. Evidently, using $L_F = 16,000$ bits or $L_F = 8,000$ bits is excessively long, which degrades the TVCE performance to an unacceptable level. However, when the interleaver length was reduced to $L_F = 4,000$, both schemes become capable of achieving convergence, as seen from Fig. 3.50. Observe from Fig. 3.50 that the proposed semi-blind BBSB-SCE scheme outperforms the conventional semi-blind CE scheme by about 0.4 dB.

3.5.2.3 Example Three

We also considered a quasi-static Rayleigh fading BPSK MIMO system associated with $M = N = 2$. The system's throughput is $R = 2$ bits/symbol and a interleaver length of $L_F = 16,000$. The initial training block length was set to $M_T = 6$, yielding a PO of $O_p = 0.075\%$. The other system settings were the same as given in *Example 1*. The purpose of this simulation investigation was to compare our proposed BBSB-SCE based scheme to the decision selection scheme for soft CE proposed by Abe and Matsumoto [149]. The simulation results are shown in Fig. 3.51, where again the perfect CSI performance bound is used as the benchmark. It can be clearly seen from Fig. 3.51 that as expected, our BBSB-SCE scheme approaches the optimal performance bound associated with the perfect CSI and it outperforms the scheme proposed by Abe and Matsumoto by about 0.5 dB.

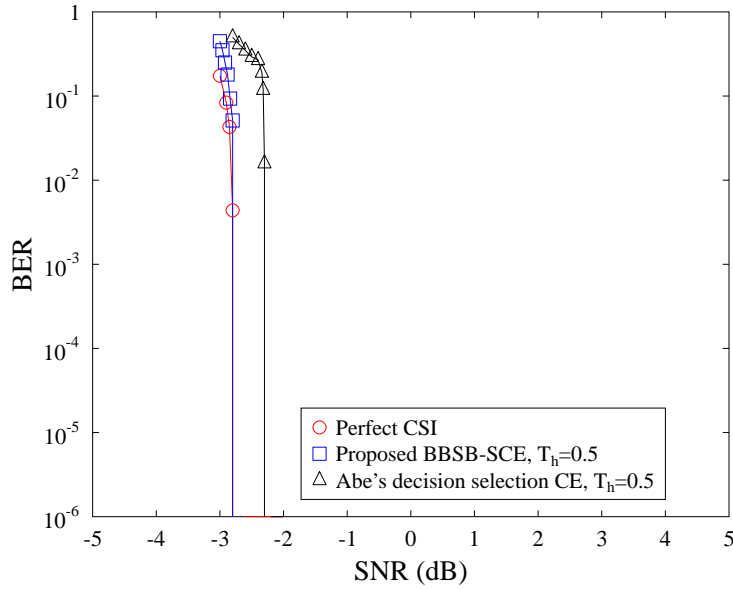


Figure 3.51: BER performance comparison: a) perfect CSI case, b) proposed joint BBSB-SCE and three-stage turbo receiver of Fig. 3.40 with $T_h = 0.5$, and c) Abe and Matsumoto's BPSK decision selection scheme based soft CE [149], for **Example 3** of quasi-static BPSK MIMO system with $M = N = 2$, having a system throughput is $R = 2$ bits/symbol. All other system parameters were summarized in Table 3.4.

3.6 Chapter Summary and Conclusions

In this chapter, we have discussed a pair of CE approaches designed for coherently detected MIMO systems, namely, the TBCE and SBCE. Our challenging objective has been to construct a CE based MIMO system that is capable of approaching the perfect CSI performance bound without implanting a substantial number of training pilots and without imposing a significant increase in computational complexity.

The widely used TBCE scheme designed for uncoded and three-stage serial-concatenated turbo coded MIMO systems was discussed in Section 3.2. To be more explicit, the system model of a TBCE aided MIMO system of Fig. 3.1 was introduced in Section 3.2.1, where the LSCE algorithm was discussed and the lower bound of the number of training blocks was given in Eq. (3.5). The performance of the TBCE scheme was investigated and the corresponding simulation results were portrayed in Fig. 3.2, Fig. 3.3, Fig. 3.4, Fig. 3.5, Fig. 3.6, Fig. 3.7, Fig. 3.8 and Fig. 3.9 of Section 3.2.2, based on the CSTSK MIMO system of Fig. 2.17, both in uncoded and three-stage serial-concatenated turbo coded scenarios. Two metrics, namely the BER and the MCEE of Eq. (3.6) were adopted for assessing the performance the CE based schemes. As expected, the simulation results confirmed that in order for the TBCE based scheme to approach the performance of the perfect CSI benchmark, a large number of training blocks are required, at the cost of a higher PO and substantially reducing the system's effective throughput. We have summarized the

Table 3.5: Performance summary of TBCE aided CSTSK systems of Fig. 3.1 at $\text{BER} = 10^{-6}$. Their CE complexity is on the order of $\mathcal{O}(M_T^3)$.

MIMO Scheme	Throughput [bits/symbol]	M_T	PO	SNR (Uncoded) [dB]	SNR (Coded) [dB]	Figure
CSTSK(2,2,2,4,QPSK)	2	2	0.8%	21.5		Fig. 3.2
		5	2%	21.2		
		10	4%	20.8		
		30	12%	20.7		
CSTSK(4,2,2,4,QPSK)	2	2	0.8%	21	3.1	Fig. 3.4 and Fig. 3.8
		5	2%	20	1.6	
		10	4%	19.5	1	
		30	12%	19	0	
CSTSK(4,4,2,4,16-QAM)	3	2	0.8%	26	2.6	Fig. 3.6 and Fig. 3.9
		5	2%	18		
		10	4%	16	1.2	
		30	12%	16	-0.8	

performance of TBCE scheme of Fig. 3.1 in Table 3.6, including the throughput, number of training blocks, PO, required SNR for achieving $\text{BER} = 10^{-6}$ and complexity order.

Table 3.6: Performance summary of SBCE aided uncoded CSTSK systems of Fig. 3.10 at $\text{BER} = 10^{-6}$. Their CE complexity is on the order of $\mathcal{O}(\tau^3)$.

MIMO Scheme	Throughput [bits/symbol]	M_T	PO	SNR [dB]	Figure
CSTSK(2,2,2,4,QPSK)	2	2	0.8%	20	Fig. 3.11
CSTSK(4,2,2,4,QPSK)	2	2	0.8%	18.8	Fig. 3.13
		5	2%	18.8	Fig. 3.14
CSTSK(4,4,2,4,16-QAM)	3	2	0.8%	16	Fig. 3.16
		3	1.2%	16	Fig. 3.17

In order to overcome the above-mentioned limitation of TBCE schemes, the SBCE scheme designed for MIMO systems of Fig. 3.10 was introduced in Section 3.3 for an uncoded scenario. In contrast to a TBCE scheme, a relatively accurate CE may be achieved by employing a low PO, i.e. just a few training blocks. The detailed system model of SBCE was provided in Section 3.3.1, where the iterative SBCE algorithm was detailed. The corresponding simulation results were discussed in Section 3.3.2, in terms of the BER and MCEE performance. It was found from the BER

simulation results of Fig. 3.11, Fig. 3.13, Fig. 3.14, Fig. 3.16 and Fig. 3.17 that the SBCE based scheme was capable of approaching the performance of the perfect CSI scenario at a low PO, hence substantially outperforming the TBCE scheme utilising the same PO. Additionally, it can be clearly seen from the MCEE simulations portrayed in Fig. 3.12, Fig. 3.15 and Fig. 3.18 that typically as few as $I_{ce} = 5$ iterations are sufficient for the MCEE to converge to its minimum. Furthermore, above a certain SNR threshold, the SBCE based scheme is capable of reaching the ultimate performance bound associated with perfect CSI. We have summarized the performance of SBCE scheme of Fig. 3.10 in Table 3.6, including the throughput, number of training blocks, PO, required SNR for achieving $\text{BER} = 10^{-6}$ and complexity order.

Section 3.4 was dedicated to developing the novel SBCE aided and three-stage serial-concatenated turbo coded scheme for near-capacity CSTSK MIMO systems. To be more explicit, Section 3.4.1 discussed the existing state-of-the-art semi-blind joint CE and three-stage turbo detection-decoding scheme of Fig. 3.19, which explored the entire frame of detected bits for DDCE. Its limitations were also characterized in Section 3.4.1. Specifically, it imposes an excessive computational complexity and it is incapable of approaching the optimal performance bound associated with perfect CSI. In order to overcome these limitations, the efficient yet low-complexity BBSBCE based scheme of Fig. 3.20 was proposed in Section 3.4.2. Observed in Fig. 3.20 and Fig. 3.21 that a high system throughput was maintained, since the proposed scheme only utilized a low PO for generating an initial CE. Most significantly, in contrast to the existing methods, the proposed BBSBCE scheme did not require an extra iterative loop between the CE and the turbo detector-decoder, since the BBSB iterative CE was naturally embedded into the original iterative three-stage demapping-decoding turbo loop. This novel arrangement enabled us to maintain a low system complexity. Furthermore, since only high-confidence decision blocks were selected in the BBSBCE based scheme, the error propagation problem of the conventional SBCE schemes was mitigated. Extensive simulation results provided in Fig. 3.24, Fig. 3.24, Fig. 3.25, Fig. 3.26, Fig. 3.27, Fig. 3.29, Fig. 3.30, Fig. 3.31 and Fig. 3.32 of Section 3.4.4 confirmed that the proposed semi-blind BBSBCE and three-stage turbo demapping-decoding scheme was capable of approaching the near-capacity performance bound of the idealised three-stage turbo detector-decoder at low number of turbo iterations. Additionally, the CRLB was also introduced to demonstrate the capability of the proposed BBSBCE scheme. The corresponding simulation results are depicted in Fig. 3.28 and Fig. 3.33. We have summarized the performance of BBSBCE based scheme of Fig. 3.20 in Table 3.7, including the throughput, number of training blocks, PO, block-of-bits selection threshold T_h , required SNR for achieving $\text{BER} = 10^{-6}$ and complexity order.

In Section 3.5, another effective way of reducing the effects of erroneous decisions in the soft-decision based CE scheme was introduced. Firstly, we demonstrated in Fig. 3.34 that the soft-decision aided CE was inappropriate for the STSK MIMO system owing to its specific signal block mapping scheme. Therefore, the novel semi-blind joint BBSB-SCE and three-stage turbo detection-decoding scheme was proposed for near-capacity SDM/V-BLAST MIMO systems in Section 3.5.1.

Table 3.7: Performance summary of BBSBCE aided CSTSK systems of Fig. 3.20 at $\text{BER} = 10^{-6}$. Their CE complexity is on the order of $\mathcal{O}(\tau_{\text{sel}}^3)$.

MIMO Scheme	Throughput [bits/symbol]	M_T	PO	T_h	SNR [dB]	Figure
CSTSK(4,2,2,4,QPSK)	2	2	0.2%	0.02	1.2	Fig. 3.27
				0.1	-0.1	
				0.2	-0.1	
				0.3	-0.1	
				0.4	0.4	
CSTSK(4,4,2,4,16-QAM)	3	2	0.2%	0.02	1	Fig. 3.32
				0.1	-1.2	
				0.2	-1.2	
				0.3	-1.2	
				0.4	1.6	

Table 3.8: Performance summary of BBSB-SCE aided SDM/V-BLAST systems of Fig. 3.40 in quasi-static channel environment at $\text{BER} = 10^{-6}$. Their CE complexity is on the order of $\mathcal{O}(M_{\text{sel}}^3)$.

MIMO Scheme	Throughput [bits/symbol]	M_T	PO	T_h	SNR [dB]	Figure
MIMO(4,4,16-QAM)	16	6	0.6%	0.2	6.5	Fig. 3.45
				0.5	5	
				1.0	5	
				2.0	5.5	
				3.0	6	

To be more explicit, the soft symbol estimation invoked for soft-decision based CE was first reviewed in Section 3.5.1.1. Then the system model of the BBSB-SCE aided scheme is detailed in Fig. 3.40 of Section 3.5.1.2 for near-capacity MIMO system. The corresponding simulation results were portrayed in Fig. 3.42, Fig. 3.43, Fig. 3.44, Fig. 3.45, Fig. 3.46 and Fig. 3.47 of Section 3.5.2, where it was confirmed that with the aid of selecting just-sufficient number of reliable decision blocks and by employing the soft-decision based CE of Section 3.5, the proposed BBSB-SCE based scheme was capable of achieving the optimal ML performance bound associated with perfect CSI, while maintaining a high effective throughput without imposing an excessive computational complexity. We have summarized the performance of the BBSB-SCE aided scheme of Fig. 3.40 in Table 3.8 and Table 3.9, under quasi-static and time-varying channel environment,

Table 3.9: Performance summary of BBSB-SCE aided SDM/V-BLAST systems of Fig. 3.40 in time-varying channel environment at $\text{BER} = 10^{-6}$. The number of initial training blocks is $M_T = 6$ and system's throughput is $R = 16$ bits/symbol. Their CE complexity is on the order of $\mathcal{O}(M_{\text{sel}}^3)$.

MIMO Scheme	CE Scheme	f_d	PO	L_F [bits]	SNR [dB]	Figure
MIMO(4,4,16-QAM)	BBSB-SCE	10^{-5}	0.6%	16,000	5.3	Fig. 3.48
			1.2%	8,000	7.6	
			2.4%	4,000	8.1	
	Whole sequence	10^{-5}	0.6%	16,000	8.4	
			1.2%	8,000	9.1	
			2.4%	4,000	8.6	
MIMO(4,4,16-QAM)	BBSB-SCE	10^{-4}	0.6%	16,000	19.2	Fig. 3.49
			1.2%	8,000	8.7	
			2.4%	4,000	8	
	Whole sequence	10^{-4}	0.6%	16,000	21.5	
			1.2%	8,000	10.2	
			2.4%	4,000	9.2	
MIMO(4,4,16-QAM)	BBSB-SCE	5×10^{-4}	2.4%	4,000	27.8	Fig. 3.50
	Whole sequence	5×10^{-4}	2.4%	4,000	28.2	

respectively.

This chapter focused on the design of CE schemes for assisting coherent MIMO systems in efficiently exploring the “MIMO advantages”, such as achieving diversity and/or multiplexing gains. However, it was also demonstrated that since MIMO systems rely on multiple RF chains at the transmitter and receiver, their power consumption and hardware costs are substantial. Moreover, for large-scale MIMO (LS-MIMO) systems and particularly for millimetre-wave based MIMO systems, the number of available antenna array elements increases massively, while in practice the affordable number of available RF chains is typically limited. As a remedy, AS offers a low-cost, low-complexity technique of reducing the number of RF chains utilised at the transmitter and/or receiver, while retaining the significant advantages of MIMO systems. Therefore, in the next chapter, AS designed for MIMO systems will be discussed and a simple yet efficient CE scheme will be proposed for AS aided MIMO systems.

Chapter **4**

Norm-Based Joint Transmit/Receive Antenna Selection Aided MIMO Systems

4.1 Introduction

Recently, MIMO concepts, especially LS-MIMO, have attracted significant attention owing to their capability of substantially increasing the reliability and/or bandwidth efficiency of communication systems substantially [1,63]. However, since MIMO systems utilize multiple RF chains, their power consumption and hardware costs are considerable. Moreover, for LS-MIMO systems and particularly for millimetre-wave based LS-MIMO systems [63–65], the number of antenna array elements that can be accommodated is increased [66, 67], but the affordable number of RF chains remains limited. As a remedy, AS offers a low-cost, low-complexity technique of reducing the number of RF chains utilized at the transmitter and/or receiver, while retaining the significant advantages of MIMO systems. In AS aided MIMO systems, a high number of AEs can be employed, which may be beneficially combined with AS techniques to select a specific subset of antennas associated with the best channel condition. Explicitly, this may be the particular subset associated with the highest equivalent SNR, carefully selected from the whole set of antennas to form a reduced-dimentional, yet improved-quality MIMO communication system, which therefore provides significant performance gains for MIMO systems [68].

4.1.1 Two Antenna Selection Optimization Criteria

Generally, there are two popular optimization criteria for AS algorithms, namely, the CBAS and NBAS [68].

4.1.1.1 Capacity-Based Antenna Selection

According to [1], a MIMO system with the channel matrix $\tilde{\mathbf{H}}_{sub} \in \mathbb{C}^{L_R \times L_T}$ and the channel noise power N_o has the channel capacity given by

$$C_{\text{MIMO}}(\tilde{\mathbf{H}}_{sub}, L_T, L_R; N_o) = \log \left(\det \left\{ \mathbf{I}_{L_R} + \frac{N_o}{L_T} \tilde{\mathbf{H}}_{sub} \tilde{\mathbf{H}}_{sub}^H \right\} \right), \quad (4.1)$$

where it may be seen that the overall channel capacity heavily relies on the product $(\tilde{\mathbf{H}}_{sub} \tilde{\mathbf{H}}_{sub}^H)$. Hence, the main idea of CBAS is to find the most appropriate channel matrix $\tilde{\mathbf{H}}_{sub}$ to maximize the channel capacity. More specifically, let M and N be the number of available Tx and Rx antennas, respectively, while the number of available Tx and Rx RF chains is denoted by L_T and L_R , respectively. Since we have $L_T < M$ and $L_R < N$, we can only select an $(L_R \times L_T)$ -element subset MIMO channel matrix $\tilde{\mathbf{H}}_{sub}$ from the full MIMO channel matrix $\mathbf{H} \in \mathbb{C}^{N \times M}$ for actual data transmission.

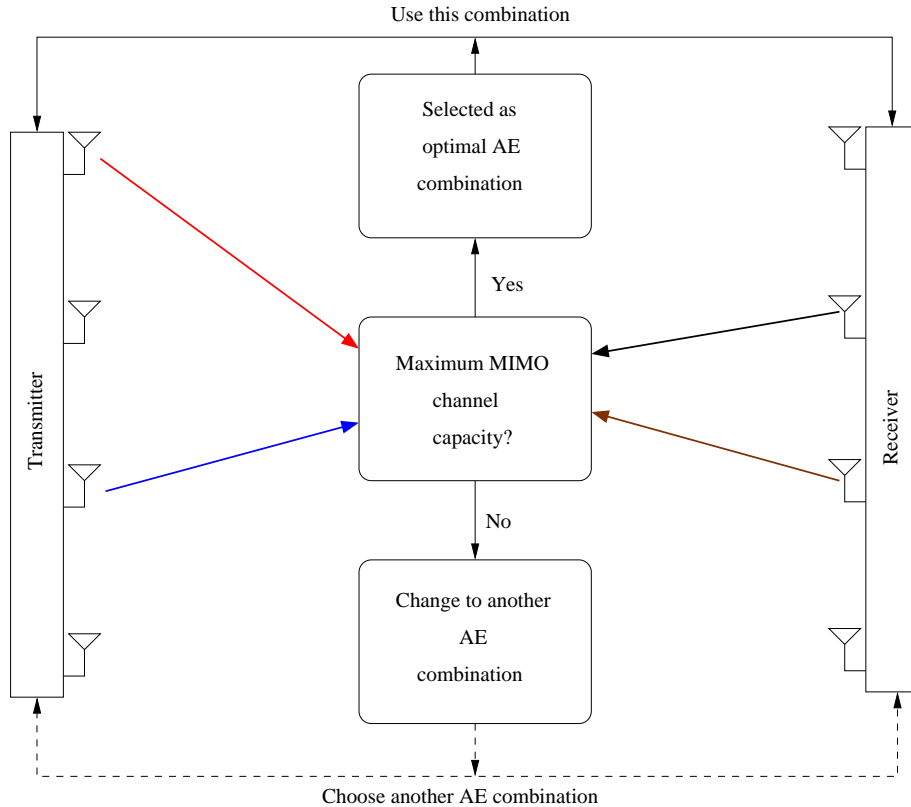


Figure 4.1: Capacity-based antenna selection.

The basic process of implementing the CBAS algorithm is illustrated in Fig. 4.1, where it can be seen that for a selected combination of Tx antennas and/or Rx antennas, the corresponding MIMO channel's capacity is calculated according to Eq. (4.1). After obtaining the MIMO capacity values of all the possible combinations of Tx antennas and/or Rx antennas, the specific combination associated with the highest MIMO capacity value is the optimal combination in terms of the CBAS criterion. However, this exhaustive search over all the possible subsets of the full channel matrix may become impractical for systems having a large numbers of Tx antennas and/or Rx antennas.

[70]. Diverse sub-optimal CBAS techniques have been developed in [68, 70], which are capable of reducing the AS complexity at the cost of a certain performance loss.

4.1.1.2 Norm-Based Antenna Selection

In contrast to the above-mentioned CBAS criterion, as an efficient yet low-complexity category of AS algorithms, NBAS techniques mainly focus on the BER performance of a MIMO system [86, 87]. Generally speaking, higher channel gains may reduce the influence of the channel noise, and in turn, they enhance the equivalent SNR. As a result, Tx and/or Rx antennas related to the subset of the full channel matrix, which has the highest norm, are selected in NBAS. The corresponding NBAS criterion may be formulated as

$$\mathbf{H}_{sub} = \arg \max_{\tilde{\mathbf{H}}_{sub} \in \mathbf{H}} \left\{ \sum_{n_t=1}^{L_T} \sum_{n_r=1}^{L_R} |\tilde{\mathbf{H}}_{sub}(n_r, n_t)| \right\}, \quad (4.2)$$

where $\tilde{\mathbf{H}}_{sub}(n_r, n_t)$ denotes the channel element at the n_r th row and n_t th column of $\tilde{\mathbf{H}}_{sub}$, where $|\cdot|$ represents the magnitude operator. The selected $\mathbf{H}_{sub} \in \mathbb{C}^{L_R \times L_T}$ has the highest channel norm among all the subset channel matrices and hence it is used for actual transmission. A conceptual illustration of the basic NBAS algorithm is given in Fig. 4.2. For the sake of clarity, only the direct links represented by the diagonal elements of the full channel matrix \mathbf{H} are shown. It may be seen from Fig. 4.2 that for the specific time slot, indicated by the vertical line the pair of channel links associated with the two highest power are selected. Since it has been shown that NBAS algorithms are capable of approaching the performance of CBAS techniques, while imposing a lower AS complexity [68], we will mainly consider the NBAS criterion in this chapter.

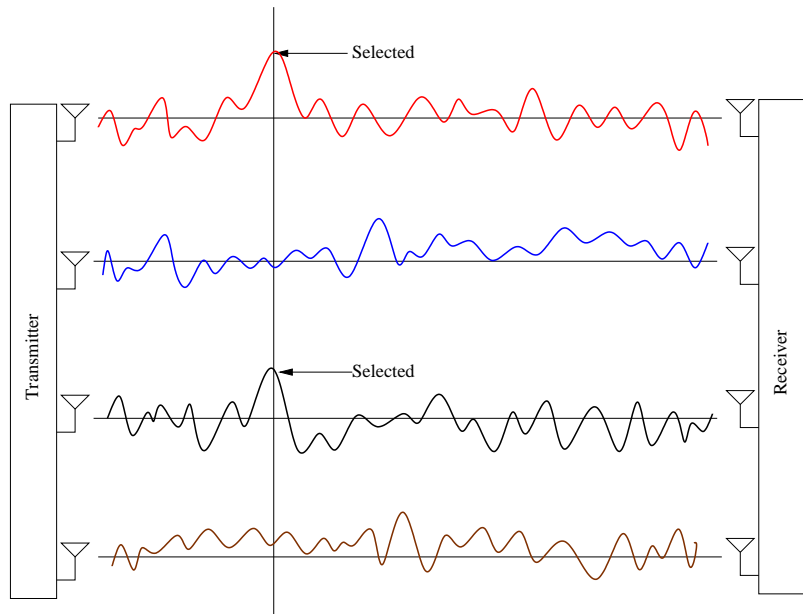


Figure 4.2: Norm-based antenna selection.

4.1.2 Antenna Selection Classifications

The family of AS techniques may be classified into one of three categories, namely, TxAS, RxAS and JTRAS, respectively, according to the corresponding antenna configurations [68].

4.1.2.1 Transmit Antenna Selection

The main idea of TxAS based on the channel's norm is to select the specific Tx antennas associated with the highest channel norm (or equivalently the highest channel power or the highest system SNR) [78–80]. The schematic of TxAS schemes conceived for MIMO systems is shown in Fig. 4.3, where it may be seen that AS only takes place at the transmitter of the MIMO system. Additionally, a feedback containing the index of the AE selected has to be fed back from the receiver to the transmitter, since the CSI is usually only known at the receiver. Fig. 4.4 shows an example of the

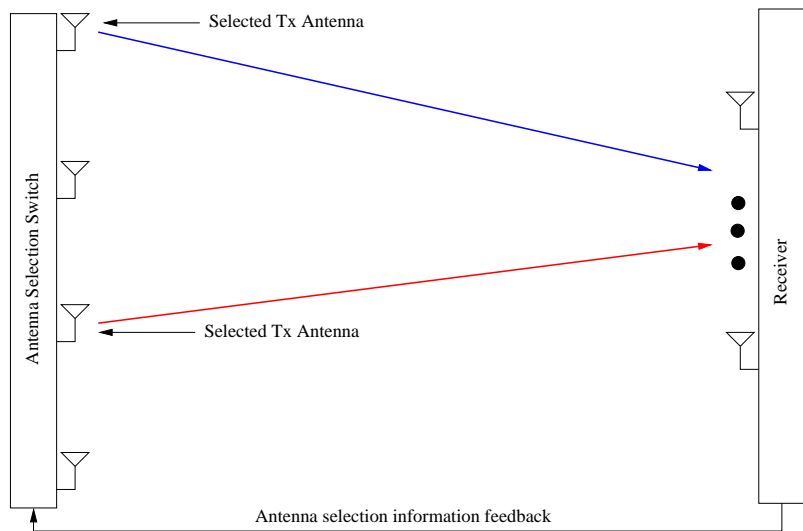


Figure 4.3: Transmit antenna selection, where the selected AE index is fed back from receiver to the transmitter.

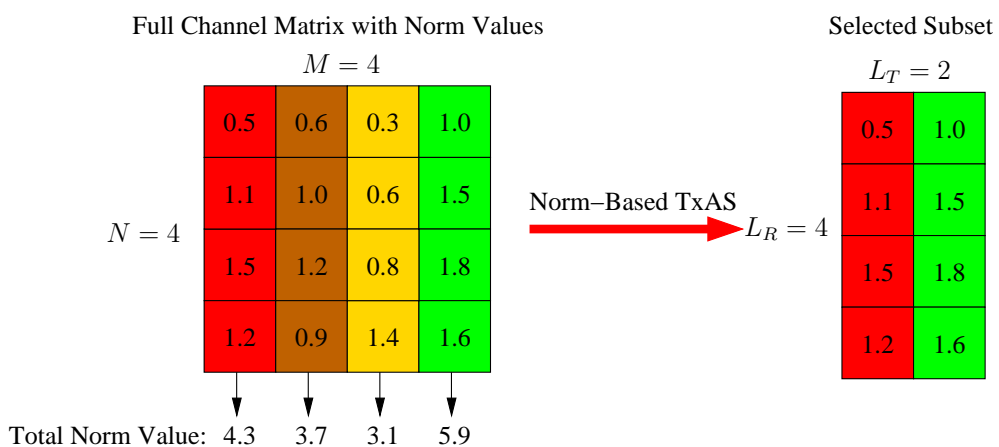


Figure 4.4: An example of the norm-based transmit antenna selection scheme.

norm-based TxAS scheme. Without loss of generality, we consider a full channel matrix associated with $M = 4$ Tx antennas as well as $N = 4$ Rx antennas and we select $L_T = 2$ Tx antennas, namely, two columns of the full channel matrix \mathbf{H} . More specifically, according to the NBAS criterion of Eq. (4.2), $L_T = 2$ columns associated with the highest total norm values of the full channel matrix are selected. It may be seen from Fig. 4.4 that the $L_T = 2$ highest accumulated column-norm values are 5.9 and 4.3, which correspond to the fourth and first column, respectively. Therefore, the first and fourth Tx antennas are selected, resulting in a selected subset channel matrix, as illustrated at the right hand side of Fig. 4.4. The corresponding full MIMO links and selected links of the example of Fig. 4.4 is illustrated in Fig. 4.5.

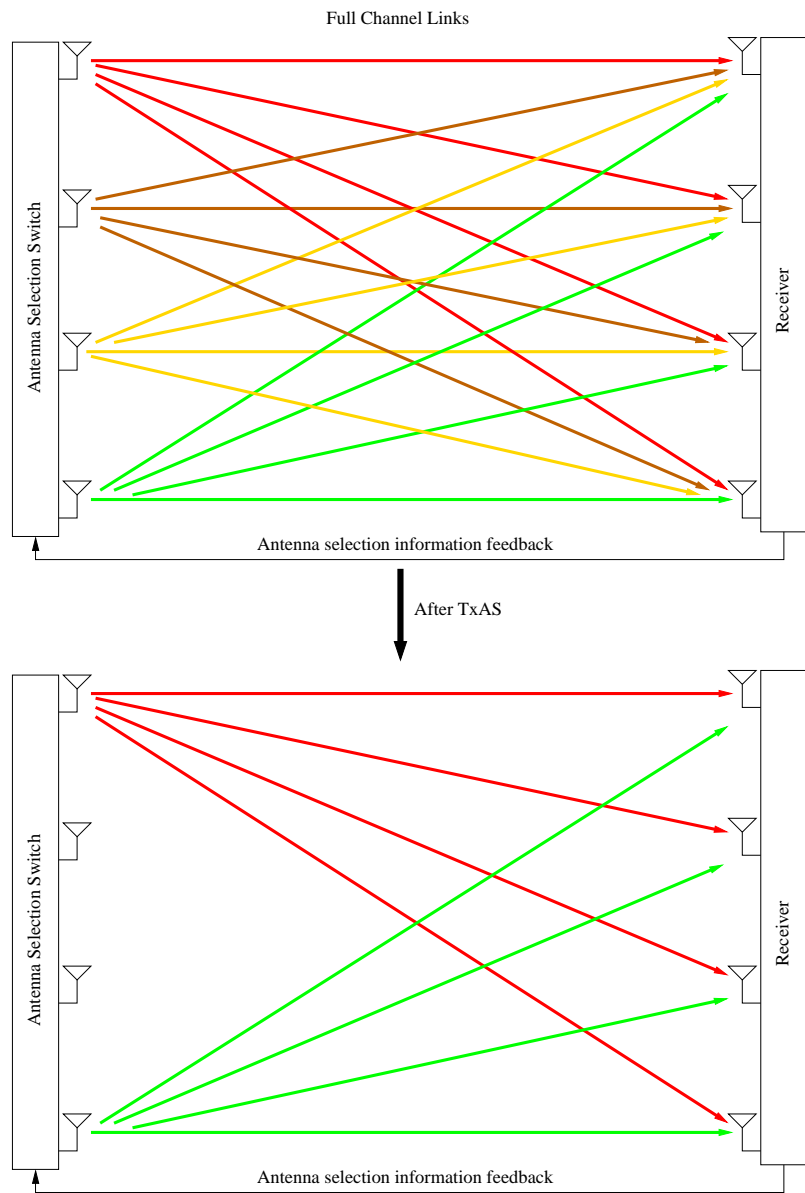


Figure 4.5: Selection of wireless links of the example shown in Fig. 4.4.

4.1.2.2 Receive Antenna Selection

Similar to the TxAS scheme based on the NBAS criterion, the idea of RxAS based on the NBAS criterion is to select the Rx antenna(s) associated with the highest channel norm (or equivalently the channel power) [71–74]. The corresponding block diagram of the RxAS schemes conceived for MIMO systems is shown in Fig. 4.6. It may be seen that unlike the TxAS scheme of Fig. 4.3, no feedback of AS information is required in RxAS aided MIMO systems. This is because AS only takes place at the receiver side of the MIMO system, and the CSI required for AS is usually available at the receiver as well.

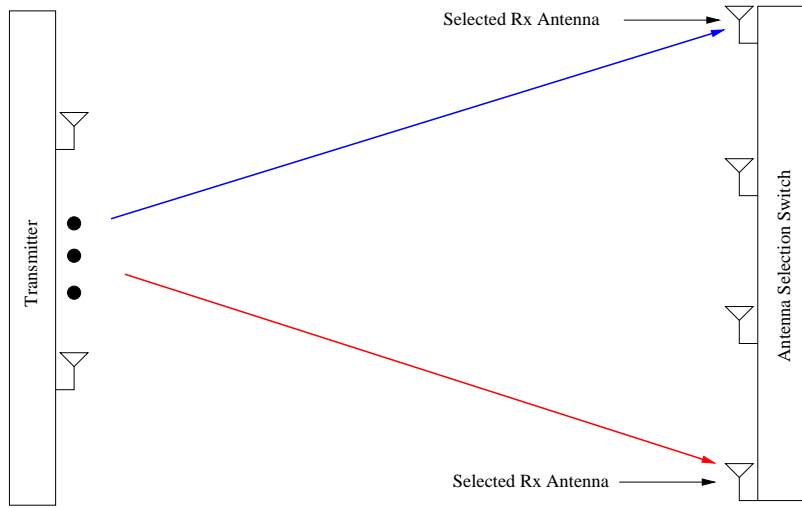


Figure 4.6: Receive antenna selection. In contrast to TxAS of Fig. 4.3, no antenna selection information feedback is required.

4.1.2.3 Transmit/Receive Antenna Selection

As a hybrid version of TxAS and RxAS, JTRAS schemes were proposed in [68, 70, 86, 87], where it was observed that MIMO systems employing JTRAS were capable of improving the achievable system performance, while maintaining a low hardware complexity compared to the family of conventional MIMO systems employing the same number of RF chains and operating without JTRAS. Unlike the above-mentioned TxAS and RxAS schemes, the JTRAS scheme jointly selects the Tx and Rx antenna(s). It has been recognised that the optimal JTRAS can be constructed with the aid of a full-search method, which however, may impose a high computational complexity. Therefore, in this chapter, we propose a low-complexity yet efficient NBJTRAS algorithm. The system is capable of significantly outperforming the non-AS aided conventional MIMO systems utilizing the same number of RF chains, both in terms of its BER and throughput. Additionally, the proposed NBJTRAS aided MIMO system is capable of achieving extra diversity gains over that of the conventional MIMO system relying on the same number of RF chains and operating without AS, albeit this gain is achieved at the cost of employing more AEs than the latter.

4.1.3 Channel Estimation for AS aided MIMO Systems

It has been widely recognised [68, 70–72, 78, 79, 86, 87] that AS techniques are capable of significantly improving the performance of coherently detected MIMO systems based on the assumption of perfectly known CSI, in comparison to the conventional MIMO systems equipped with the same number of RF chains. However, in practice, CSI has to be acquired, and a standard CE technique is the TBCE, where pilot symbols are used for acquiring an estimated CSI prior to actual data transmission. An analytical framework that enables the evaluation of the performance of multiple-branch diversity systems with the aid of TBCE was developed in [150], where the TBCE scheme was shown to be capable of preserving the diversity order of a MIMO system at the cost of a SNR penalty. The conventional TBCE channel estimator was employed in [151] for RxAS aided space-time coded MIMO systems communicating over Rayleigh flat fading channels, which however only considered selecting a single RA. The performance of the training-based channel estimator was investigated in [152] for employment in OFDM based MIMO systems using RxAS, where AS was simply performed based on the received signal power quantified prior to CE. However, the conventional TBCE schemes adopted in [151, 152] are capable of generating accurate MIMO CSI only at the cost of imposing a potentially excessive PO, which not only significantly erodes the system’s throughput, but also results in an excessive CE complexity. Additionally, it has been shown in [153, 154] that for AS aided MIMO systems, AS requires a less accurate CSI, while data detection must rely on a very accurate channel estimate. According to this observation, an efficient CE method was proposed for RxAS in [153], where just-sufficient training pilots are firstly sent for RxAS and then extra pilots are sent for further refining the channel estimate associated with the selected antennas. Similarly, a dual pilot-based training scheme was proposed in [154] for an AS aided multi-user Orthogonal Frequency-Division Multiple Access (OFDMA) system, where an uplink user firstly transmits a reference signal to the base station for acquiring the CSI for AS as well as for frequency-domain transmission scheduling. Then the uplink user sends a second reference signal for further refining the channel estimate for supporting data detection. Both these two novel schemes are capable of improving the attainable system performance at the cost of transmitting extra pilots. Therefore, the challenge here is also the acquisition of accurate MIMO CSI without imposing an excessive training overhead.

Against the above background, we propose a novel Two-Tier CE (TTCE) scheme relying on a low training overhead for assisting the NBJTRAS aided MIMO system to approach the near-capacity optimal MIMO performance bound associated with perfect CSI, which maintains a high system throughput, while imposing a low computational complexity. To be more explicit, in tier one of the proposed TTCE scheme, a low-complexity low-PO based TBCE scheme relying on RF chain reuse generates a coarse initial estimate of the full MIMO channel matrix using only a low number of training symbol blocks. Then NBJTRAS is carried out based on this rough CE, and the selected TAs and RAs are activated for actual data transmission. In tier two of the proposed scheme, a powerful semi-blind BBSB-SCE and three-stage turbo detection-decoding structure is employed. This

scheme relies on the selected subset channel matrix, obtained in the tier-one NBJTRAS stage, as the initial MIMO CE for activating the turbo detection and decoding process invoked for detecting the data as well as for refining the CE.

The rest of this chapter is organised as below. Section 4.2 provides the system model and achievable system performance of the NBJTRAS aided MIMO system, where perfectly known CSI is assumed. The CE schemes for NBJTRAS aided MIMO systems is discussed in Section 4.3. To be more explicitly, the conventional TBCE for NBJTRAS is introduced in Section 4.3.1, while the novel TTCE scheme for NBJTRAS is proposed in Section 4.3.2. Finally, Section 4.4 provides the chapter summary of this chapter.

4.2 NBJTRAS Aided MIMO System Based on Perfect CSI

We consider the MIMO system employing M Tx antennas and N Rx antennas, as well as L_T Tx RF chain and L_R Rx RF chains. If the hardware resources are affordable and we have $L_T = M$ and $L_R = N$, a full $(N \times M)$ -element MIMO system described in Chapter 2 may be realized. In practice, however, the number of affordable RF chains is often limited, and we have $L_T < M$ and $L_R < N$, particularly for large-scale MIMO systems. For a MIMO system of $L_T < M$ and $L_R < N$, the full MIMO system is ‘virtual’, i.e. the full channel matrix $\mathbf{H} \in \mathbb{C}^{N \times M}$ is ‘virtual’, since the communications only occur over an $(L_R \times L_T)$ -element subset channel matrix $\mathbf{H}_{sub} \in \mathbb{C}^{L_R \times L_T}$. The conventional MIMO system operating without the aid of AS refers to the MIMO system that only employs L_T Tx antennas and L_R Rx antennas. In the generic case of $L_T < M$ and $L_R < N$, in order to efficiently utilize the available hardware resources, it is desirable to choose the most appropriate L_T Tx antennas from the full set of M Tx antennas and the most appropriate L_R Rx antennas from the full set of N Rx antennas to form a desired $(L_R \times L_T)$ -element MIMO channel for actual data communications. Now let us detail our proposed NBJTRAS aided MIMO system.

4.2.1 System Description

Our proposed NBJTRAS aided MIMO system is depicted in Fig. 4.7, where we assume for the time being that the ‘virtual’ full channel matrix \mathbf{H} is perfectly known at both transmitter and receiver. Additionally, it may also be seen that electronic switches are required at both transmitter and receiver to connect the available RF chains to the activated antennas. RSC-URC channel encoder/decoder may be added to the proposed NBJTRAS aided MIMO system for the sake of achieving near-capacity performance. In this NBJTRAS aided MIMO system, our proposed NBJTRAS algorithm constructs a MIMO system where MIMO symbol blocks are transmitted over the activated subset channel matrix $\mathbf{H}_{sub} \in \mathbb{C}^{L_R \times L_T}$ with $\mathbf{H}_{sub} \subset \mathbf{H}$.

It has been mentioned previously that increasing the channel gain is equivalent to reducing the

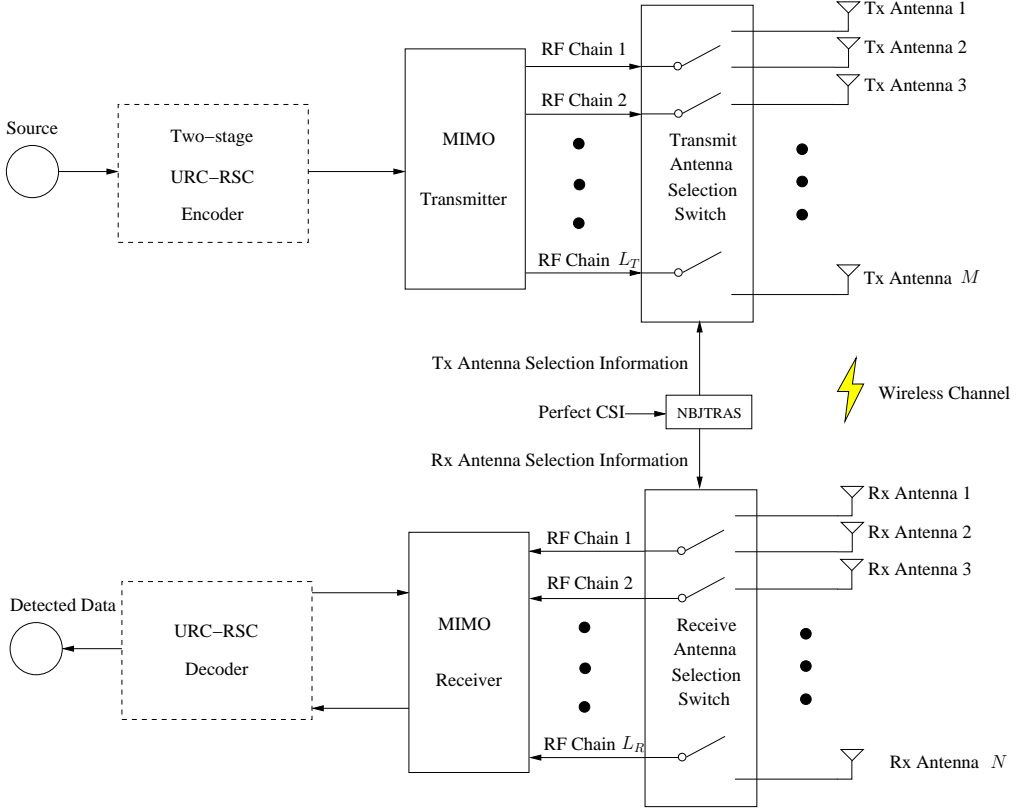


Figure 4.7: Proposed NBJTRAS aided MIMO system.

effects of noise, which yields an improved system performance. This motivates our NBAS approach that selects the specific Tx antennas and Rx antennas related to the subset channel matrix having the highest channel norm, which may be accomplished by solving the NBAS optimisation of Eq. (4.2). To be more explicit, solving this optimisation problem by exhaustive search requires us to evaluate the norms of the $\mathbf{C}_N^{L_R} \times \mathbf{C}_M^{L_T}$ candidate subset matrices, where $\mathbf{C}_k^n = \frac{k!}{n!(k-n)!}$, $\mathbf{C}_N^{L_R}$ and $\mathbf{C}_M^{L_T}$ are the row-dimension and column-dimension combinations of \mathbf{H}_{sub} , respectively. This will impose an extremely high computational complexity, particularly for large-scale MIMO systems associated with high M and/or N . We propose a novel NBJTRAS scheme for solving the optimisation problem of Eq. (4.2) at a substantially reduced complexity. We now detail our NBJTRAS scheme.

4.2.1.1 NBJTRAS Algorithm

Given the full channel matrix $\mathbf{H} \in \mathbb{C}^{N \times M}$, without loss of generality, we assume $\mathbf{C}_N^{L_R} \leq \mathbf{C}_M^{L_T}$. The algorithm accomplishes the optimisation of Eq. (4.2) in the following two steps.

Step 1): Row Dimension Operations.

Let $i_r \in \{1, 2, \dots, \mathbf{C}_N^{L_R}\}$ be the row combination index and let us denote the row indices

corresponding to the i_r th sub-matrix $\mathbf{H}_{i_r} \in \mathbb{C}^{L_R \times M}$ by $\mathbf{l}_{i_r} = [l_{i_r}^1 \ l_{i_r}^2 \ \cdots \ l_{i_r}^{L_R}]^T$. Then we have

$$\mathbf{H}_{i_r} = \begin{bmatrix} \mathbf{h}_{l_{i_r}^1}^T \\ \mathbf{h}_{l_{i_r}^2}^T \\ \vdots \\ \mathbf{h}_{l_{i_r}^{L_R}}^T \end{bmatrix} = \begin{bmatrix} \mathbf{H}_{i_r}\langle 1, 1 \rangle & \cdots & \mathbf{H}_{i_r}\langle 1, M \rangle \\ \mathbf{H}_{i_r}\langle 2, 1 \rangle & \cdots & \mathbf{H}_{i_r}\langle 2, M \rangle \\ \vdots & \cdots & \vdots \\ \mathbf{H}_{i_r}\langle L_R, 1 \rangle & \cdots & \mathbf{H}_{i_r}\langle L_R, M \rangle \end{bmatrix}, \quad (4.3)$$

where \mathbf{h}_x^T is the x th row of \mathbf{H} . The evaluation of

$$m_{i_r}^x = \sum_{j=1}^{L_R} |\mathbf{H}_{i_r}\langle j, x \rangle|, \quad 1 \leq x \leq M, \quad (4.4)$$

where $m_{i_r}^x$ represents the magnitude of the x th column in \mathbf{H}_{i_r} , yields the norm metric vector

$$\mathbf{m}_{i_r}^T = [m_{i_r}^1 \ m_{i_r}^2 \ \cdots \ m_{i_r}^M]. \quad (4.5)$$

Applying the operations of Eqs. (4.4) and (4.5) to all the $\mathbb{C}_N^{L_R}$ possible combinations leads to the norm metric matrix $\mathbf{M}_{Norm} \in \mathbb{C}^{\mathbb{C}_N^{L_R} \times M}$ given by

$$\mathbf{M}_{Norm} = \begin{bmatrix} \mathbf{m}_1^T \\ \mathbf{m}_2^T \\ \vdots \\ \mathbf{m}_{\mathbb{C}_N^{L_R}}^T \end{bmatrix} = \begin{bmatrix} m_1^1 & m_1^2 & \cdots & m_1^M \\ m_2^1 & m_2^2 & \cdots & m_2^M \\ \vdots & \vdots & \cdots & \vdots \\ m_{\mathbb{C}_N^{L_R}}^1 & m_{\mathbb{C}_N^{L_R}}^2 & \cdots & m_{\mathbb{C}_N^{L_R}}^M \end{bmatrix}. \quad (4.6)$$

Step 2): Column Dimension Operations.

Find the largest L_T elements in the i_r th row of \mathbf{M}_{Norm} and sum them up, which is denoted as $m_{\max}^{i_r}$, as well as record the column indices of these L_T elements in the index vector $\mathbf{l}_{i_c}(i_r) = [l_{i_c}^1(i_r) \ l_{i_c}^2(i_r) \ \cdots \ l_{i_c}^{L_T}(i_r)]^T$. This produces the max-norm metric vector

$$\mathbf{m}_{\max}^T = [m_{\max}^1 \ m_{\max}^2 \ \cdots \ m_{\max}^{\mathbb{C}_N^{L_R}}]. \quad (4.7)$$

Next find

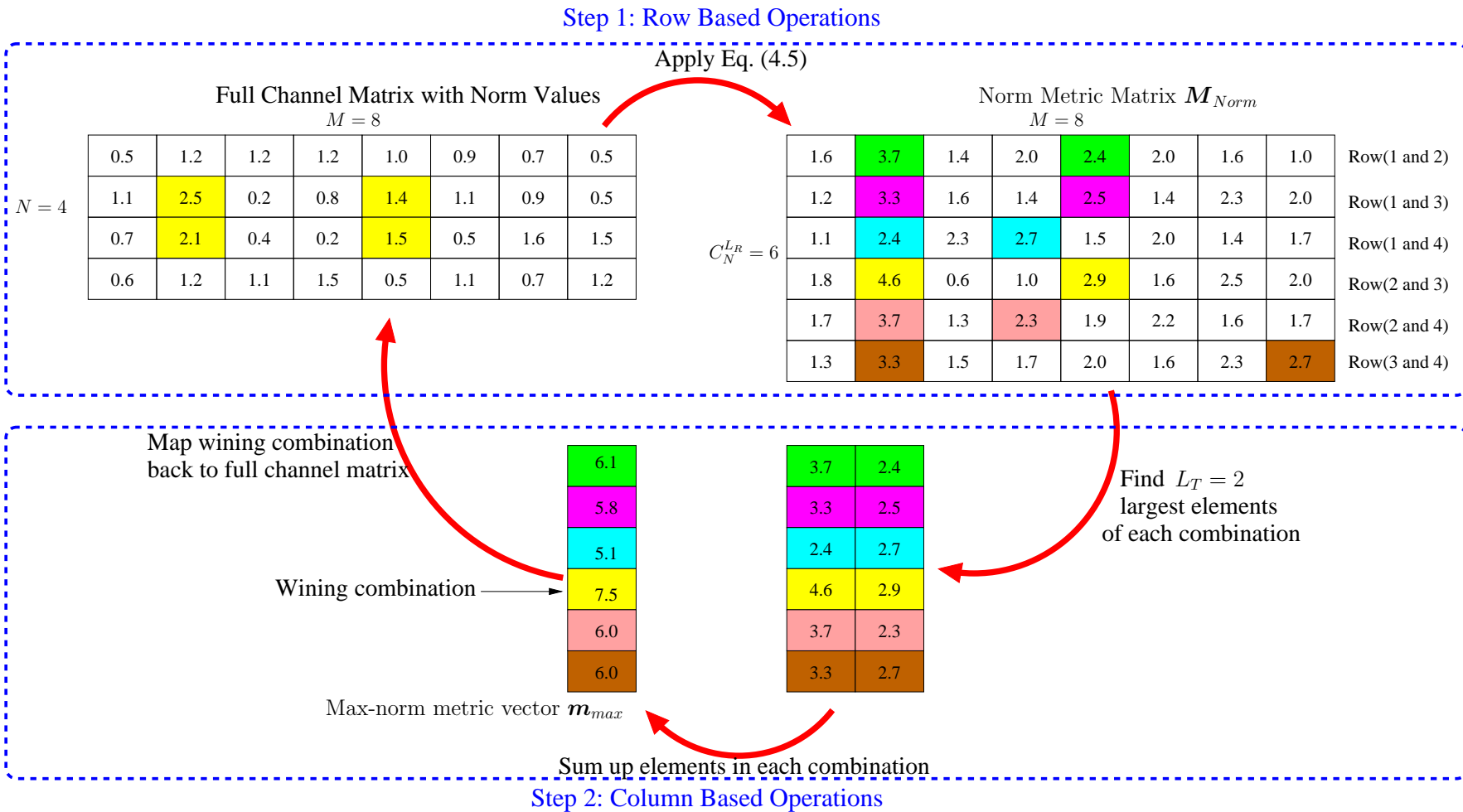
$$\bar{i}_r = \arg \max_{1 \leq i_r \leq \mathbb{C}_N^{L_R}} m_{\max}^{i_r}. \quad (4.8)$$

Then the selected TA and RA indices are specified by $\mathbf{l}_{i_c}(\bar{i}_r)$ and $\mathbf{l}_{\bar{i}_r}$, respectively, and the corresponding subset channel matrix \mathbf{H}_{sub} is the optimal solution of Eq. (4.2).

4.2.1.2 An Example of NBJTRAS

We use an example presented in Fig. 4.8 to illustrate how the proposed NBJTRAS algorithm works. We consider a full channel matrix \mathbf{H} associated with $M = 8$ Tx antennas and $N = 4$ Rx antennas. The number of Tx and Rx RF chains is set to $L_T = L_R = 2$. In this case, the number of row

Figure 4.8: An example of NBJTRAS algorithm.



combinations is $C_N^{L_R} = 6$, which is lower than the number of column combinations of $C_M^{L_T} = 28$. Therefore, our NBJTRAS commences with the row-based operations and followed by the column-based operations, as depicted in Fig. 4.8. Let us now describe the proposed NBJTRAS in more detail:

- In Step 1 of the row-based operations, by applying the norm operation, we have the full channel matrix with its associated norm values as shown in the top-left of Fig. 4.8.
- Then we apply Eq. (4.5) to each row combination, in order to form the norm metric matrix M_{Norm} of Eq. (4.6) in the top-right of Fig. 4.8, with each row of M_{Norm} representing a combination of $L_R = 2$ rows of the original full channel matrix. For instance, the first row of M_{Norm} represents the combination of the first and second rows of the full channel matrix, as indicated in Fig. 4.8.
- After obtaining the norm metric matrix M_{Norm} , we may start Step 2 of the column-based operations. First, we find the largest $L_T = 2$ elements in each row of M_{Norm} and sum them up, yielding the max-norm metric vector m_{max} of Eq. (4.7).
- Then we find the largest element in m_{max} which has a value of 7.5 of Fig. 4.8, and the corresponding combination is the winning combination. To be more explicit, the winning element is the fourth element of the max-norm metric vector, which corresponds to the second and fifth elements of the fourth row of the norm metric matrix of Fig. 4.8. Since the fourth row of the norm metric matrix corresponds to the combination of the second and third row of the original full channel matrix, we find that the combination of the second and fifth elements in the second and third rows of the original full channel matrix is the optimal combination, which are selected by our NBJTRAS algorithm for actual communication.

4.2.1.3 Complexity Analysis

In the case of $C_N^{L_R} \leq C_M^{L_T}$, the complexity of the above NBJTRAS algorithm can be shown to be on the order of

$$C_{NBJTRAS} \approx \mathcal{O} \left((M \cdot (L_R + 1) + 1) \cdot C_N^{L_R} \right). \quad (4.9)$$

Additionally, if $C_N^{L_R} > C_M^{L_T}$, our NBJTRAS algorithm starts with **Step 1**) of the Column Dimension Operations followed by **Step 2**) of Row Dimension Operations, and the complexity of this algorithm is given by

$$C_{NBJTRAS} \approx \mathcal{O} \left((N \cdot (L_T + 1) + 1) \cdot C_M^{L_T} \right). \quad (4.10)$$

By contrast, the complexity of the exhaustive search is given by

$$C_{ES} \approx \mathcal{O} \left((L_R \cdot L_T) \cdot (C_M^{L_T} \cdot C_N^{L_R}) \right). \quad (4.11)$$

Clearly C_{NBJTRAS} is much lower than C_{ES} . Consider the AS example of Section 4.2.1.2 again. The corresponding computational complexity order of NBJTRAS according to Eq. (4.9) is $C_{\text{NBJTRAS}} \approx 150$, while that of the exhaustive search of Eq. (4.11) is $C_{\text{ES}} \approx 672$.

Fig. 4.9 explicitly compares the complexity of the proposed NBJTRAS algorithm with that of the exhaustive search method, where without loss of generality, we assume that the numbers of Tx and Rx RF chains are $L_T = L_R = 2$. It can be clearly seen from Fig. 4.9 that C_{NBJTRAS} is significantly lower than C_{ES} , especially when the numbers of Tx and/or Rx antennas are large.

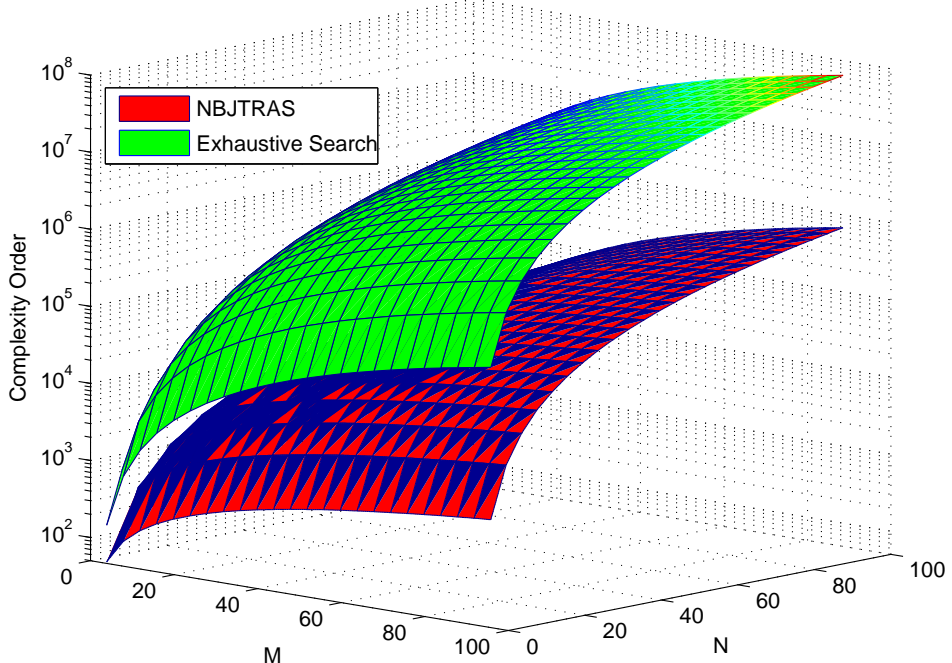


Figure 4.9: Complexity comparison of the proposed NBJTRAS and exhaustive search method, where the numbers of Tx and Rx RF chains are set to $L_T = L_R = 2$.

4.2.1.4 Additional Diversity Order Attained

Given L_R and L_T , the achievable multiplexing gain of the MIMO system is determined. We define the loading factor of AS as

$$f_{\text{AS}}(M, N) = \frac{M + N}{L_T + L_R}, \quad (4.12)$$

which determines the additional diversity order attainable by JTRAS schemes, such as our NBJTRAS algorithm, over the conventional MIMO system formed by employing L_T TAs and L_R RAs as well as operating without AS.

4.2.2 Simulation Results

This section provides the simulation results of the proposed NBJTRAS algorithm of Fig. 4.7. In our simulation study, the transmitted signal power was normalised to unity, and therefore the

SNR was given as $\frac{1}{N_o}$, with N_o being the power of the channel AWGN. Two MIMO systems were considered, which were the uncoded CSTSK system and the three-stage serial-concatenated turbo coded SDM/V-BLAST MIMO system. The CSTSK MIMO system, having M Tx antennas and N Rx antennas as well as employing L_T Tx RF chains and L_R Rx RF chains, was denoted by $\text{CSTSK}(M, N; L_T, L_R; T, Q, \mathcal{L} - \text{PSK/QAM})$, while the SDM/V-BLAST MIMO system, having the same antenna and RF chain configuration, was denoted as $\text{MIMO}(M, N; L_T, L_R; \mathcal{L} - \text{PSK/QAM})$. In order to keep both the hardware complexity and the power consumption at the same level, the numbers of RF chains employed, namely, L_T and L_R , were equal in both the NBJTRAS aided MIMO systems and in the conventional MIMO systems operating without AS, implying that the MIMO channel matrix activated for data communication had the same dimension of $\mathbf{H}_{sub} \in \mathbb{C}^{L_R \times L_T}$ for the both systems. More specifically, the conventional MIMO system operating without AS had the “ $M = L_T$ and $N = L_R$ ” arrangement, while the NBJTRAS aided MIMO system employed the “ $M > L_T$ and $N > L_R$ ” structure along with the AS loading factor of $f_{AS}(M, N)$ of Eq. (4.12). The achievable BER and the MIMO channel’s throughput were used as two main metrics of evaluating the performance of the proposed NBJTRAS algorithm. The MIMO channels’ throughput [1] is given in Eq. (4.1) and is quoted below again

$$C_{\text{MIMO}}(\mathbf{H}_{sub}, L_T, L_R; N_o) = E \left\{ \log \left(\det \left\{ \mathbf{I}_{L_R} + \frac{N_o}{L_T} \mathbf{H}_{sub} \mathbf{H}_{sub}^H \right\} \right) \right\}, \quad (4.13)$$

with $\mathbf{H}_{sub} \in \mathbb{C}^{L_R \times L_T}$ denoting the corresponding MIMO channel matrix for actual communication.

4.2.2.1 Uncoded NBJTRAS Aided CSTSK Systems

Three CSTSK configurations, $\text{CSTSK}(M, N; 2, 2; 2, 4, \text{QPSK})$, $\text{CSTSK}(M, N; 4, 2; 2, 4, \text{QPSK})$ and $\text{CSTSK}(M, N; 4, 4; 2, 4, 16\text{-QAM})$, were simulated in a quasi-static independent Rayleigh fading environment, having corresponding normalized throughputs of $R = 2, 2$ and 3 bits/symbol, respectively. We have summarized the system parameters of the NBJTRAS aided CSTSK system of Fig. 4.7 in Table 4.1.

4.2.2.1.1 CSTSK($M, N; 2, 2; 2, 4, \text{QPSK}$) associated with $R = 2$ bits/symbol

Let us first consider the $\text{CSTSK}(M, N; 2, 2; 2, 4, \text{QPSK})$ system, of which the numbers of Tx and Rx chains were $L_T = L_R = 2$. The corresponding system’s normalized throughput is $R = 2$ bits/symbol. The BER performance of the NBJTRAS aided $\text{CSTSK}(M, N; 2, 2; 2, 4, \text{QPSK})$ system of Fig. 4.7 is depicted in Fig. 4.10, in comparison to the performance of the conventional $\text{CSTSK}(2, 2; 2, 2; 2, 4, \text{QPSK})$ system of Fig. 2.17 operating without AS. It may be seen that with the aid of perfectly known CSI, the BER performance of the NBJTRAS aided CSTSK system is significantly improved, compared to that of the conventional CSTSK system. To be more explicit, the BER of the non-AS aided $\text{CSTSK}(2, 2; 2, 2; 2, 4, \text{QPSK})$ reaches the BER of 10^{-4} at approximately SNR of 14.5 dB, while the BER of the NBJTRAS aided $\text{CSTSK}(4, 4; 2, 2; 2, 4, \text{QPSK})$ system with

Table 4.1: System parameters of the NBJTRAS aided CSTSK system of Fig. 4.7.

Number of Tx antennas	M
Number of Rx antennas	N
Number of Tx RF chains	L_T
Number of Rx RF chains	L_R
Symbol durations per block	T
Number of dispersion matrices	Q
Modulation	\mathcal{L} -QAM or \mathcal{L} -PSK
AS loading factor	$f_{AS}(M, N)$ of Eq. (4.12)
Channels	Frequency-flat Rayleigh fading
Detector	ML detector of Eq. (2.19)

the AS loading factor of $f_{AS}(4, 4) = 2$ reaches the BER of 10^{-4} at approximately $\text{SNR} = 8.5 \text{ dB}$, yielding a significant SNR gain of about 6 dB. Additionally, it may also be seen that the NBJTRAS aided CSTSK(4, 4; 2, 2; 2, 4, QPSK) system associated with $f_{AS}(4, 4) = 2$ achieves a higher diversity gain (a steeper slope of the BER curve) than the conventional CSTSK system operating without AS. Moreover, as the value of the AS loading factor increases from 2 to 3, a further SNR gain of about 1.5 dB is obtained. However, when the AS loading factor increases from 3 to 11, only an additional SNR gain of 1.4 dB is achieved. Further increasing the value of the AS factor leads to negligible “diversity” gain attained.

The achievable MIMO channels’ throughput performance of the uncoded NBJTRAS aided CSTSK($M, N; 2, 2; 2, 4$, QPSK) system Fig. 4.7 recorded at three different AS loading factors are compared to that of the conventional CSTSK(2, 2; 2, 2; 2, 4, QPSK) operating without AS in Fig. 4.11. It may be seen that generally, the higher the AS loading factor, the larger the achievable throughput gain the proposed NBJTRAS scheme may have. This trend is similar to the BER performance enhancements attained by the NBJTRAS scheme depicted in Fig. 4.10. Specifically, given the AS loading factor of $f_{AS}(4, 4) = 2$ and the SNR value of 10 dB, the throughput obtained by the NBJTRAS aided MIMO system is approximately 2 [bits/symbol/Hz] higher than that of the conventional MIMO system operating without AS, while the gain becomes about 2.5 [bits/symbol/Hz] for the AS loading factor of $f_{AS}(6, 6) = 3$, yielding a further throughput gain of about 0.5 [bit/symbol/Hz]. However, when the AS loading factor further increases from $f_{AS}(6, 6) = 3$ to $f_{AS}(40, 4) = 11$, the further throughput gain is still about 0.5 [bit/symbol/Hz]. Therefore, it may be concluded that increasing the AS loading factor over a certain range may lead to negligible throughput gain.

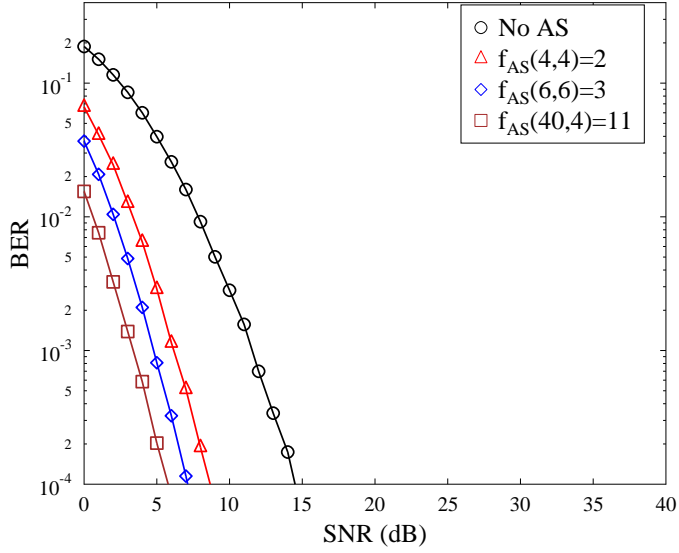


Figure 4.10: Achievable BER performance of the proposed NBJTRAS aided CSTSK($M, N; 2, 2; 2, 4$, QPSK) system of Fig. 4.7 associated with a system's throughput of $R = 2$ bits/symbol and various AS loading factors, in comparison to the performance of the conventional CSTSK($2, 2; 2, 2; 2, 4$, QPSK) system of Fig. 2.17 operating without AS. CSI is assumed to be perfectly known at both transmitter and receiver. All other system parameters were summarized in Table 4.1.

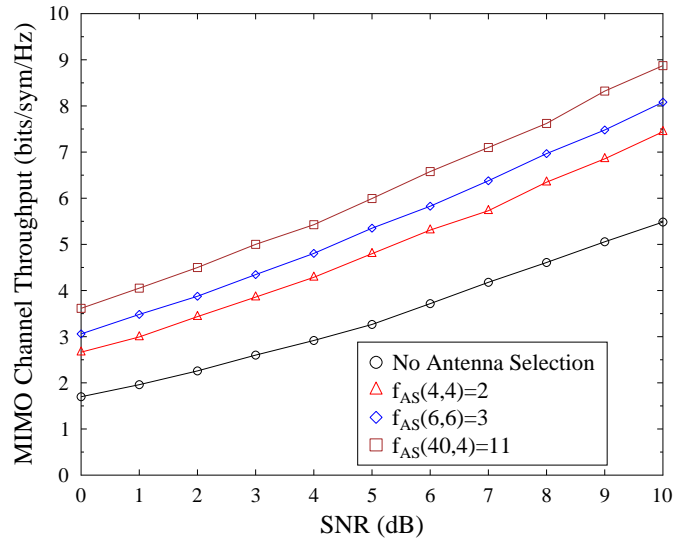


Figure 4.11: MIMO channels' throughput performance of our NBJTRAS aided CSTSK($M, N; 2, 2; 2, 4$, QPSK) system of Fig. 4.7 associated with a system's throughput of $R = 2$ bits/symbol and various AS loading factors, in comparison to the performance of the conventional CSTSK($2, 2; 2, 2; 2, 4$, QPSK) system of Fig. 2.17 operating without AS. CSI is assumed to be perfectly known at both transmitter and receiver. All other system parameters were summarized in Table 4.1.

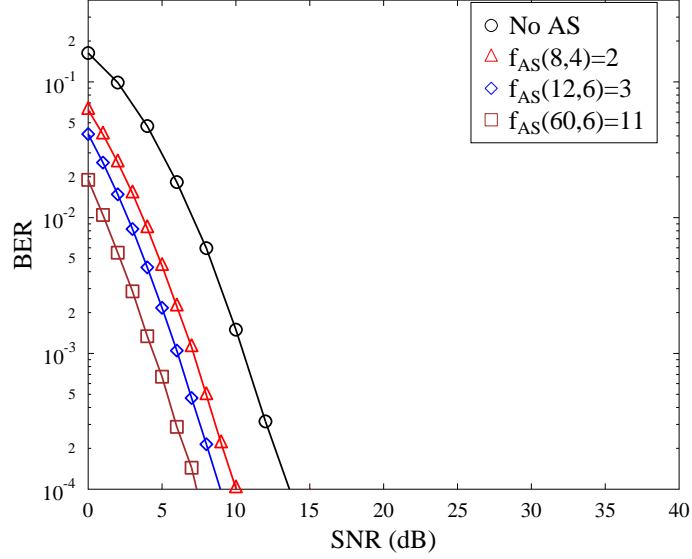


Figure 4.12: Achievable BER performance of the proposed NBJTRAS aided CSTSK($M, N; 4, 2; 2, 4$, QPSK) system of Fig. 4.7 associated with a system's throughput of $R = 2$ bits/symbol and various AS loading factors, in comparison to the performance of the conventional CSTSK($4, 2; 4, 2; 2, 4$, QPSK) system of Fig. 2.17 operating without AS. CSI is assumed to be perfectly known at both transmitter and receiver. All other system parameters were summarized in Table 4.1.

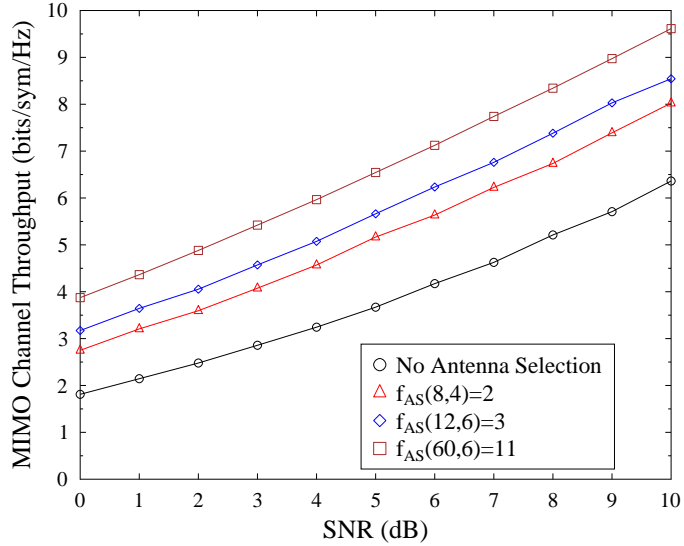


Figure 4.13: MIMO channels' throughput performance of our NBJTRAS aided CSTSK($M, N; 4, 2; 2, 4$, QPSK) system of Fig. 4.7 associated with a system's throughput of $R = 2$ bits/symbol and various AS loading factors, in comparison to the performance of the conventional CSTSK($4, 2; 4, 2; 2, 4$, QPSK) system of Fig. 2.17 operating without AS. CSI is assumed to be perfectly known at both transmitter and receiver. All other system parameters were summarized in Table 4.1.

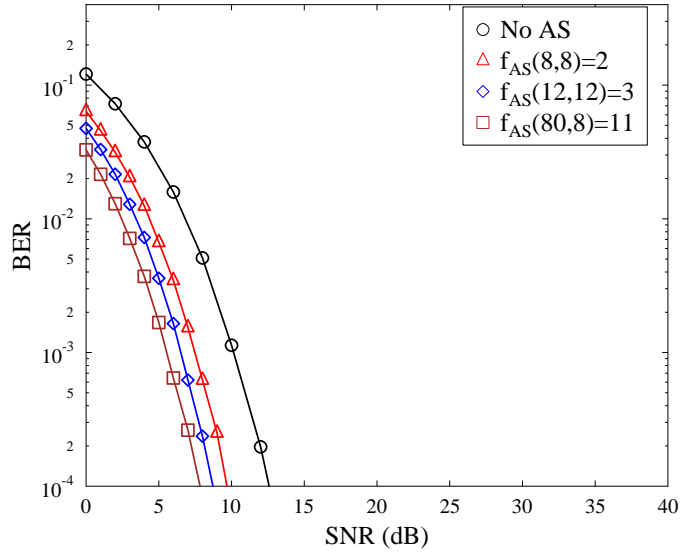


Figure 4.14: Achievable BER performance of the proposed NBJTRAS aided CSTSK($M, N; 4, 4; 2, 4, 16\text{-QAM}$) system associated with a system's throughput of $R = 3$ bits/symbol and various AS loading factors, in comparison to the performance of the conventional CSTSK($4, 4; 4, 4; 2, 4, 16\text{-QAM}$) system of Fig. 2.17 operating without AS. CSI is assumed to be perfectly known at both transmitter and receiver. All other system parameters were summarized in Table 4.1.

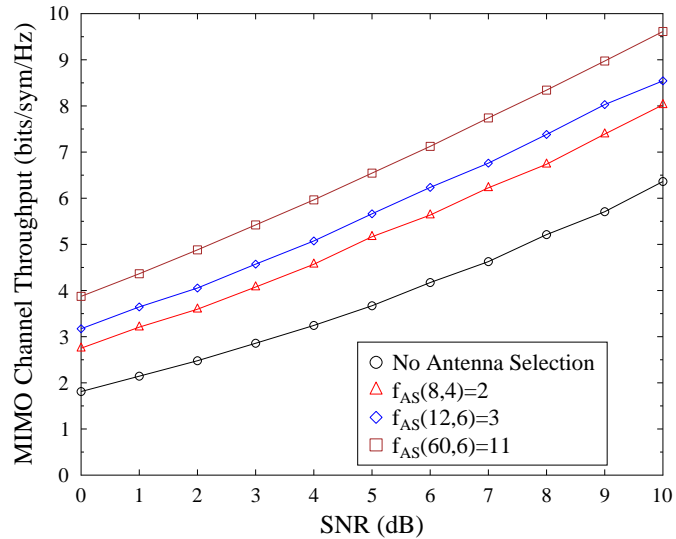


Figure 4.15: MIMO channels' throughput performance of our NBJTRAS aided CSTSK($M, N; 4, 4; 2, 4, 16\text{-QAM}$) system system of Fig. 4.7 system associated with a system's throughput of $R = 3$ bits/symbol and various AS loading factors, in comparison to the performance of the conventional CSTSK($4, 4; 4, 4; 2, 4, 16\text{-QAM}$) system of Fig. 2.17 operating without AS. CSI is assumed to be perfectly known at both transmitter and receiver. All other system parameters were summarized in Table 4.1.

4.2.2.1.2 CSTSK($M, N; 4, 2; 2, 4$, QPSK) associated with $R = 2$ bits/symbol

We also consider the NBJTRAS aided CSTSK($M, N; 4, 2; 2, 4$, QPSK) system with $L_T = 4$ Tx RF chains and $L_R = 2$ Rx RF chains, having a normalized throughput of $R = 2$ bits/symbol. The achievable BER performance of the proposed NBJTRAS aided CSTSK($M, N; 4, 2; 2, 4$, QPSK) system given three different AS loading factors are shown in Fig. 4.12, in comparison to the performance of the conventional CSTSK($4, 2; 4, 2; 2, 4$, QPSK) system operating without AS. Similar to the results shown in Fig. 4.10, it may be seen that with the aid of the NBJTRAS, the performance of the CSTSK system is significantly improved. To be more explicit, the BER of the conventional CSTSK reaches the BER level of 10^{-4} at approximately SNR = 13.5 dB, while the BER of the NBJTRAS aided CSTSK($8, 4; 4, 2; 2, 4$, QPSK) system with the AS loading factor of $f_{AS}(8, 4) = 2$ reaches the BER level of 10^{-4} at about SNR = 10 dB, yielding an SNR gain of over 3 dB. Moreover, as the value of the AS loading factor increases from 2 to 3, a further SNR gain of about 1 dB is obtained. However, when the AS loading factor increases from 3 to 11, only an additional SNR gain of 1.8 dB is achieved.

We provide the achievable throughputs of the NBJTRAS aided CSTSK($M, N; 4, 2; 2, 4$, QPSK) system associated with various AS loading factors and a normalized throughput of $R = 2$ bits/symbol in Fig. 4.13, in comparison to that of the non-AS aided conventional CSTSK($4, 2; 4, 2; 2, 4$, QPSK) system. Similar to the conclusions drawn from Fig. 4.11, the results in Fig. 4.13 also show that the proposed NBJTRAS is capable of significantly improving the MIMO channels' throughput.

4.2.2.1.3 CSTSK($M, N; 4, 4; 2, 4$, 16-QAM) associated with $R = 3$ bits/symbol

We also provide the achievable BER performance and the MIMO channels' throughput performance of the proposed NBJTRAS aided CSTSK($M, N; 4, 4; 2, 4$, 16-QAM) system having a normalized throughput of $R = 3$ bits/symbol in Figs. 4.14 and 4.15, respectively, in comparison to the performance of the conventional CSTSK system operating without AS. It can be seen again that with the aid of the NBJTRAS, both the BER and MIMO channels' throughput performance of the CSTSK MIMO system are improved significantly.

4.2.2.2 Three-Stage Turbo Coded and NBJTRAS Aided SDM/V-BLAST MIMO Systems

This section presents the performance of the three-stage serial-concatenated turbo coded and NBJTRAS aided SDM/V-BLAST MIMO systems. In the simulation, the generator polynomials of the half-rate RSC encoder were expressed in binary format as $G_{RSC} = [1, 0, 1]_2$ and $G_{RSC}^r = [1, 1, 1]_2$, while those of the URC encoder were $G_{URC} = [1, 0]_2$ and $G_{URC}^r = [1, 1]_2$, where G_{RSC}^r and G_{URC}^r denoted the feedback polynomials of the RSC and URC encoders, respectively. An interleaver length of 160,000 bits was used by the three-stage serial-concatenated turbo encoder-decoder. Two SDM/V-BLAST systems were considered, which were MIMO($M, N; 2, 2$; BPSK)

and $\text{MIMO}(M, N; 4, 2; 4\text{-QAM})$. Additionally, both the independent Rayleigh fading environment and spatially correlated environment¹ were considered. The channels' spatial correlation factor was set to $\rho = 0, 0.3, 0.6$ and 0.9 , where $\rho = 0$ implied fully independent fading and $\rho = 1$ indicated fully correlated fading. We have summarized the system parameters of the three-stage serial-concatenated turbo coded and NBJTRAS aided SDM/V-BLAST MIMO systems of Fig. 4.7 in Table 4.2.

Table 4.2: System parameters of the three-stage serial-concatenated turbo coded and NBJ-TRAS aided SDM/V-BLAST MIMO systems of Fig. 4.7.

Number of Tx antennas	M
Number of Rx antennas	N
Number of Tx RF chains	L_T
Number of Rx RF chains	L_R
Modulation	$\mathcal{L}\text{-QAM}$ or $\mathcal{L}\text{-PSK}$
AS loading factor	$f_{AS}(M, N)$ of Eq. (4.12)
Channels	Frequency-flat Rayleigh fading
Channel's spatial correlation factor	ρ
Detector	ML MIMO soft-demapper of Eq. (2.6)
Interleaver blocklength	160,000 bits
Outer channel code	Half-rate RSC
Generator polynomials	$(G_{RSC}^r, G_{RSC}) = (7, 5)_8$
Precoder	URC
Number of inner iterations	I_{in}
Number of outer iterations	I_{out}

4.2.2.2.1 MIMO($M, N; 2, 2$; BPSK) associated with $R = 2$ bits/symbol under Independent Fading Environments

We first considered the independent Rayleigh fading environment associated with a channel's spatial correlation factor of $\rho = 0$. Our investigations commenced with the EXIT chart analysis of the proposed three-stage serial-concatenated turbo coded and NBJTRAS aided MIMO($4, 4; 2, 2$; BPSK) system of Fig. 4.7 having a system's throughput of $R = 2$ bits/symbol, in comparison to that of the conventional three-stage serial-concatenated turbo coded MIMO($2, 2; 2, 2$; BPSK) system of Fig. 2.7, assuming again the CSI was perfectly known at both the transmitter and receiver. It can be seen from the EXIT charts shown in Fig. 4.16 that for the proposed NBJTRAS aided MIMO system having an AS loading factor of $f_{AS}(4, 4) = 2$, an open EXIT-tunnel exists between the

¹The generation of spatially correlated fading channels may be found in [155, 156].

EXIT curve of the amalgamated inner MIMO soft-demapper-URC decoder and the outer RSC decoder at $\text{SNR} = -6.6 \text{ dB}$. The actual Monte-Carlo simulation based stair-case shaped decoding trajectory, which closely matches the EXIT curves, is also shown at $\text{SNR} = -6.6 \text{ dB}$ for this NBJTRAS aided MIMO system. The trajectory shows that the point of perfect convergence at $(1.0, 1.0)$ may be reached with the aid of $I_{out} = 7$ outer iterations, implying that the proposed NBJ-TRAS aided MIMO scheme is capable of achieving a vanishingly low BER at $\text{SNR} = -6.6 \text{ dB}$. This is confirmed by the BER performance shown in Fig. 4.17, where it can be seen that for the case of $f_{AS}(4,4) = 2$, the ‘turbo-cliff’ of the BER curve is observed just before the point of $\text{SNR} = -6.6 \text{ dB}$. Fig. 4.16 also shows the EXIT curve of the conventional MIMO system operating without AS. Unlike the NBJTRAS aided MIMO system, the conventional MIMO system without AS fails to achieve an open tunnel between the EXIT curve of the amalgamated inner MIMO soft-demapper-URC decoder and the outer RSC decoder. This implies that the conventional MIMO system operating without AS cannot attain a vanishingly low BER at $\text{SNR} = -6.6 \text{ dB}$, which is confirmed by its BER performance shown in Fig. 4.17, where the actual convergence point of this conventional MIMO system using no AS is near $\text{SNR} = -3 \text{ dB}$.

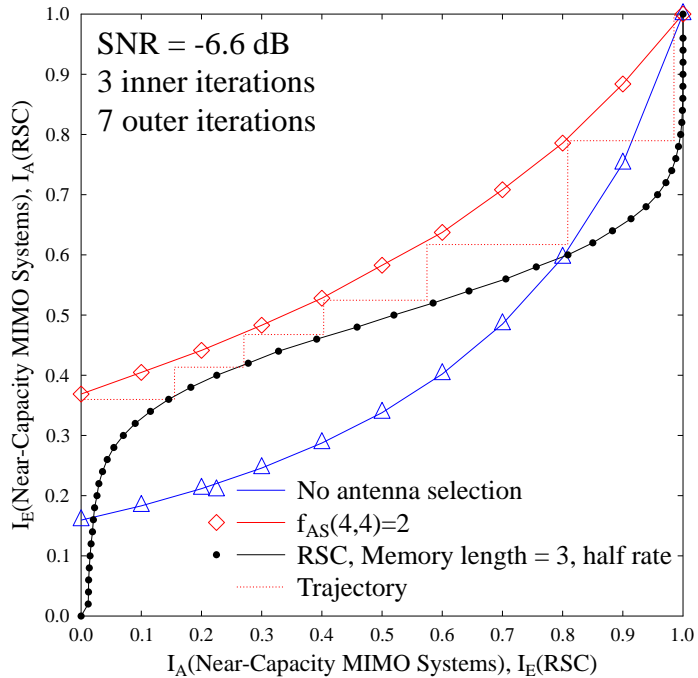


Figure 4.16: EXIT chart analysis of the NBJTRAS aided MIMO(4,4;2,2;BPSK) system of Fig. 4.7 relying on the three-stage turbo detection-decoding scheme under the independent Rayleigh fading environment, in comparison to that of the conventional MIMO(2,2;2,2;BPSK) system of Fig. 2.7 operating without AS. The systems’ throughput is $R = 2$ bits/symbol. All other system parameters were summarized in Table 4.2. The corresponding BER curves are seen in Fig. 4.17.

The BER performance of our NBJTRAS aided three-stage turbo MIMO($M, N; 2, 2; \text{BPSK}$) system of Fig. 4.7 having a system’s throughput of $R = 2$ bits/symbol is depicted in Fig. 4.17

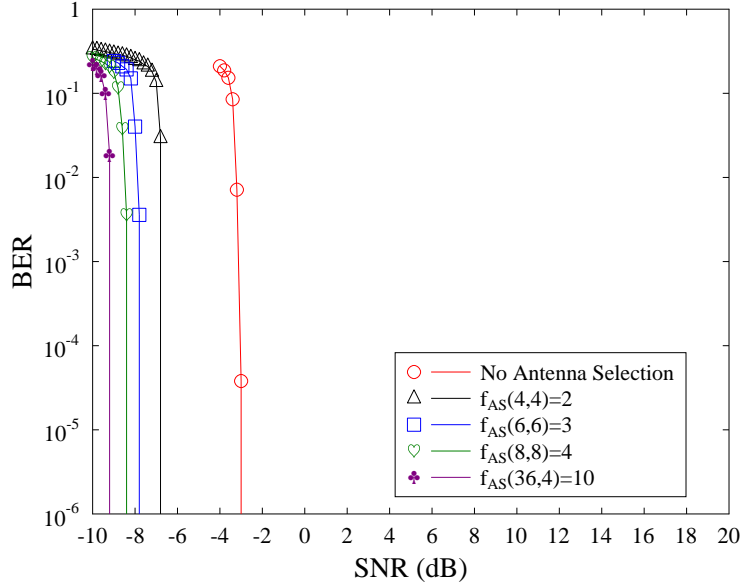


Figure 4.17: Achievable BER performance of the proposed NBJTRAS aided MIMO($M, N; 2, 2$; BPSK) system of Fig. 4.7 associated with various AS loading factors under the independent Rayleigh fading environment, in comparison to that of the conventional MIMO($2, 2; 2, 2$; BPSK) system of Fig. 2.7 operating without AS. The systems' throughput is $R = 2$ bits/symbol. All other system parameters were summarized in Table 4.2. The corresponding EXIT chart is seen in Fig. 4.16.

associated with various AS loading factors, in comparison to the performance of the conventional three-stage turbo MIMO($2, 2; 2, 2$; BPSK) system of Fig. 2.7 operating without AS. It can be seen from Fig. 4.17 that the BER performance of the NBJTRAS aided MIMO system is significantly better than that of the conventional MIMO system operating without AS. More specifically, the BER of the conventional MIMO system operating without AS achieves an infinitesimally low BER at about $\text{SNR} = -3$ dB, while the BER of the NBJTRAS aided MIMO system using $f_{\text{AS}}(4, 4) = 2$ reaches the same infinitesimally low BER at about $\text{SNR} = -6.6$ dB, representing an SNR gain of 3.6 dB. The BERs of our NBJTRAS aided MIMO system associated with the AS loading factors of $f_{\text{AS}}(6, 6) = 3$, $f_{\text{AS}}(8, 8) = 4$ and $f_{\text{AS}}(36, 4) = 10$ are also shown in Fig. 4.17, which converge to a vanishingly low BER at about $\text{SNR} = -7.7$ dB, -8.3 dB and -9.1 dB, achieving SNR gains of about 4.7 dB, 5.3 dB and 6.1 dB, respectively, compared to the conventional MIMO system operating without AS. It can be seen that for the NBJTRAS aided MIMO system, high performance gains are achieved by increasing the AS loading factor, at the cost of requiring more antennas. Most interestingly, although the rate of the gain enhancement does appear to slow down as the AS loading factor increases, further significant gains are achieved, as the AS loading factor tends to large values. This is dissimilar to the standard diversity order trends, where the achieved gain tends to saturate upon increasing the diversity order to large values.

4.2.2.2.2 MIMO($M, N; 2, 2$; BPSK) associated with $R = 2$ bits/symbol under Spatially Correlated Fading Environments

The investigations carried out so far assumed an independent fading channel environment, an assumption that is commonly made in the literature of AS techniques. However, in practice, the MIMO channels are often spatially correlated, because the antenna spacing may not be sufficiently high to experience independently fading MIMO channels. Hence, we investigated the impact of spatial correlation on the BER performance of the proposed NBJTRAS algorithm.

The NBJTRAS aided MIMO($4, 4; 2, 2$; BPSK) system of Fig. 4.7 using $f_{AS}(4, 4) = 2$ was first considered associated with a throughput of $R = 2$ bits/symbol. Furthermore, a perfectly known full MIMO CSI was assumed and again all the results were averaged over 100 channel realisations. The simulation results obtained are shown in Fig. 4.18, in comparison to those of the conventional MIMO($2, 2; 2, 2$; BPSK) system of Fig. 2.7 operating without AS. As expected, the BER performance of both the NBJTRAS aided MIMO system and the conventional MIMO degrade, as the spatial correlation between the MIMO channels increases, because increasing the channel's spatial correlation is expected to reduce the diversity gain of the MIMO system. It can also be observed that the NBJTRAS aided MIMO system is capable of outperforming the conventional MIMO system operating without AS in a spatially correlated channel environment. To be more explicit, in the independent fading environment, an SNR gain of about 3.6 dB is achieved by the NBJTRAS aided MIMO system over the conventional MIMO system operating without AS. At the spatial correlation value of $\rho = 0.3$, the NBJTRAS aided MIMO still outperforms the conventional MIMO by approximately 3.2 dB in the SNR gain. As the spatial correlation value is increased to $\rho = 0.6$ and $\rho = 0.9$, the SNR gain is reduced to approximately 2.1 dB and 1.6 dB, respectively. Based on these results, we may conclude that at a low spatial correlation level of say $\rho < 0.3$, the NBJTRAS aided MIMO system is capable of achieving the same performance gain over the conventional MIMO system without AS as in the independent fading environment, while in the highly correlated channel environment of say $\rho > 0.6$, the NBJTRAS aided MIMO is still capable of outperforming the conventional MIMO, but provides a smaller SNR gain.

We also provided the BER performance of NBJTRAS aided MIMO($8, 8; 2, 2$; BPSK) system of Fig. 4.7 associated with a throughput of $R = 2$ bits/symbol and $f_{AS}(8, 8) = 4$ in Fig. 4.19, in comparison to those of the conventional MIMO($2, 2; 2, 2$; BPSK) system of Fig. 2.7 operating without AS. Comparing Fig. 4.19 with Fig. 4.18, it may be seen that in the spatially correlated fading environment, the performance gain of the NBJTRAS aided MIMO system can be further enhanced by increasing the AS loading factor, at the cost of employing more AEs.

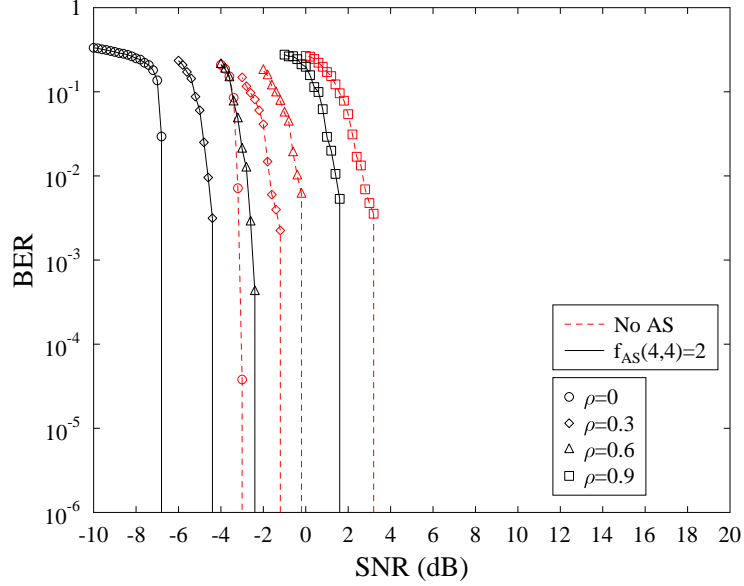


Figure 4.18: Achievable BER performance of the proposed NBJTRAS aided MIMO(4,4;2,2;BPSK) system of Fig. 4.7 associated with $f_{AS}(4,4) = 2$ and a throughput of $R = 2$ bits/symbol, in comparison to those of the conventional MIMO(2,2;2,2;BPSK) system of Fig. 2.7 operating without AS, under various spatially correlated channel environments. All other system parameters were summarized in Table 4.2.

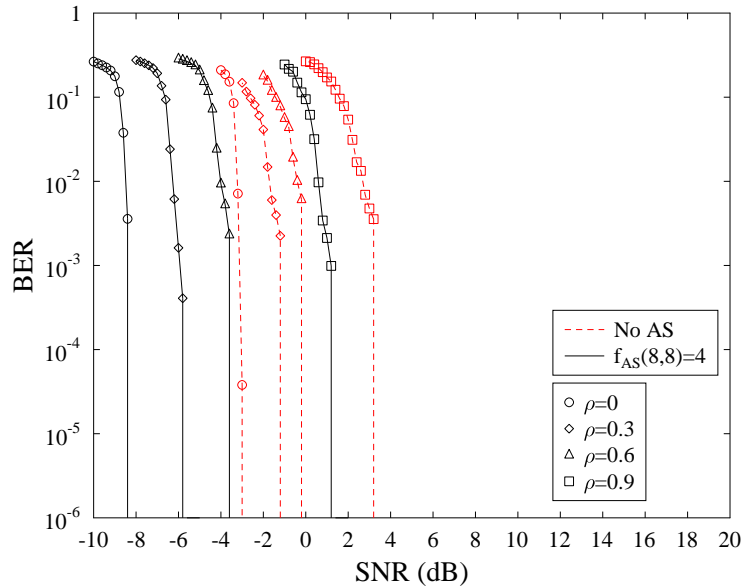


Figure 4.19: Achievable BER performance of the proposed NBJTRAS aided MIMO(8,8;2,2;BPSK) system of Fig. 4.7 associated with $f_{AS}(8,8) = 4$ and a throughput of $R = 2$ bits/symbol, in comparison to those of the conventional MIMO(2,2;2,2;BPSK) system of Fig. 2.7 operating without AS, under various spatially correlated channel environments. All other system parameters were summarized in Table 4.2.

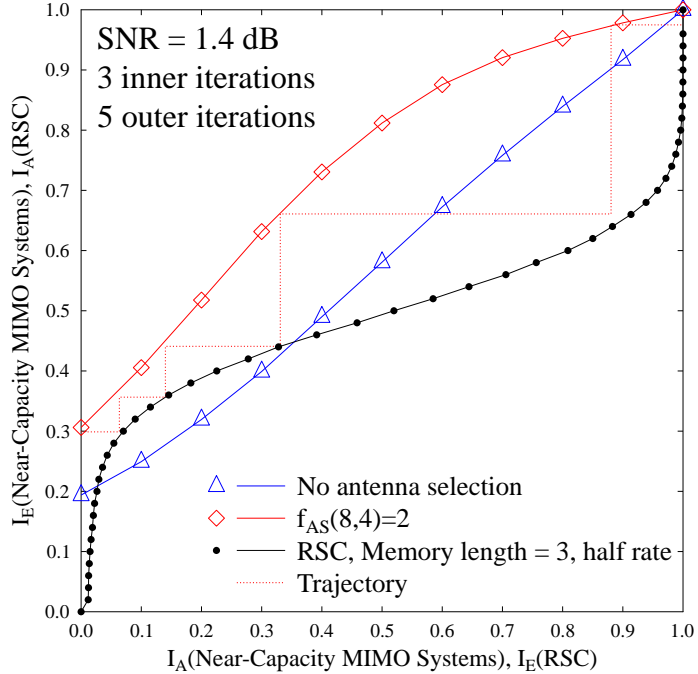


Figure 4.20: EXIT chart analysis of the NBJTRAS aided MIMO(8,4;4,2;4-QAM) system of Fig. 4.7 relying on the three-stage turbo detection-decoding scheme under the independent Rayleigh fading environment, in comparison to that of the conventional MIMO(4,2;4,2;4-QAM) system of Fig. 2.7 operating without AS. The systems' throughput is $R = 8$ bits/symbol. All other system parameters were summarized in Table 4.2. The corresponding BER curves are seen in Fig. 4.21.

4.2.2.3 MIMO($M, N; 4, 2; 4\text{-QAM}$) associated with $R = 8$ bits/symbol under Independent Fading Environments

We next focused on the EXIT chart analysis of our NBJTRAS aided MIMO(8,4;4,2;4-QAM) system of Fig. 4.7 associated with $f_{AS}(8,4) = 2$ and a system's throughput of $R = 8$ bits/symbol, under the independent Rayleigh fading environment, in comparison to that of the conventional MIMO(4,2;4,2;4-QAM) system of Fig. 2.7, assuming again that the CSI was perfectly known at both the transmitter and receiver. Similar to the EXIT chart results shown in Fig. 4.16 for the MIMO(4,4;2,2;BPSK) system, it can be seen from the EXIT charts shown in Fig. 4.20 that for the NBJTRAS aided MIMO(8,4;4,2;4-QAM) system having an AS loading factor of 2, an open EXIT-tunnel exists between the EXIT curve of the amalgamated inner MIMO soft-demapper-URC decoder and the outer RSC decoder at SNR = 1.4 dB. The actual Monte-Carlo simulation based stair-case shaped decoding trajectory, which closely matches the EXIT curves, is also shown at SNR = 1.4 dB for this NBJTRAS aided MIMO system. The trajectory shows that the point of perfect convergence at (1.0, 1.0) may be reached with the aid of $I_{out} = 5$ iterations, implying that the proposed NBJTRAS aided MIMO scheme is capable of achieving a vanishingly low BER at SNR = 1.4 dB. This is confirmed by the BER performance shown in Fig. 4.21, where it can be seen

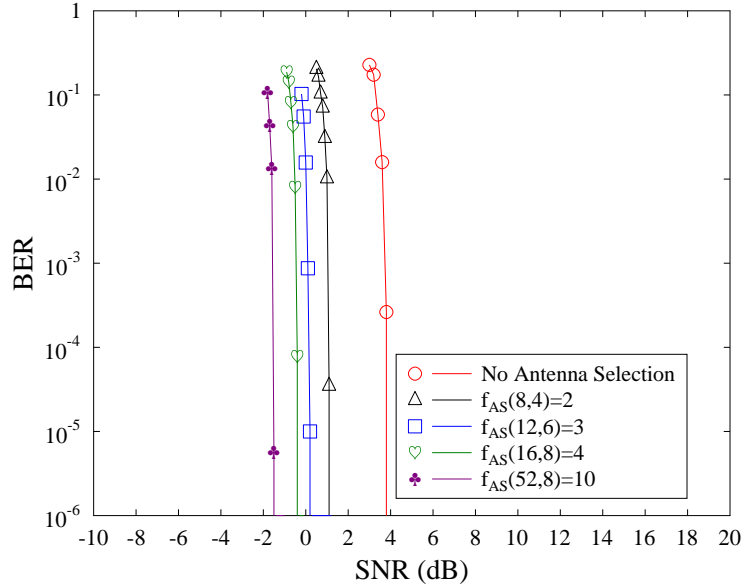


Figure 4.21: Achievable BER performance of the proposed NBJTRAS aided MIMO($M, N; 4, 2; 4\text{-QAM}$) system of Fig. 4.7 associated with various AS loading factors under the independent Rayleigh fading environment, in comparison to that of the conventional MIMO($4, 2; 4, 2; 4\text{-QAM}$) system of Fig. 2.7 operating without AS. The systems' throughput is $R = 8$ bits/symbol. All other system parameters were summarized in Table 4.2. The corresponding EXIT chart is seen in Fig. 4.20.

that for the case of $f_{AS}(8,4) = 2$, the ‘turbo-cliff’ of the BER curve is observed just before the point of $\text{SNR} = 1.4$ dB. Fig. 4.20 also shows the EXIT curve of the conventional MIMO system operating without AS. Unlike the NBJTRAS aided MIMO system, the conventional MIMO system dispensing with AS fails to achieve an open tunnel between the EXIT curve of the amalgamated inner MIMO soft-demapper-URC decoder and the outer RSC decoder. This implies that the conventional MIMO system operating without AS cannot attain a vanishingly low BER at $\text{SNR} = 1.4$ dB, which is confirmed by its BER performance shown in Fig. 4.21, where the actual convergence point of this conventional MIMO system using no AS is approximately at $\text{SNR} = 4$ dB.

The BER performance of our NBJTRAS aided three-stage turbo MIMO($M, N; 4, 2; 4\text{-QAM}$) system of Fig. 4.7 having a system’s throughput of $R = 8$ bits/symbol is depicted in Fig. 4.21, in comparison to the performance of the conventional three-stage turbo MIMO($4, 2; 4, 2; 4\text{-QAM}$) system of Fig. 2.7 operating without AS, where it can be seen that the BER performance of the NBJTRAS aided MIMO system is significantly improved compared to that of the conventional MIMO system without AS. More specifically, the conventional MIMO system operating without AS achieves an infinitesimally low BER at approximately $\text{SNR} = 4$ dB, while the NBJTRAS aided MIMO system using $f_{AS}(8,4) = 2$ reaches an infinitesimally low BER at about $\text{SNR} = 1.4$ dB, which represents a significant SNR gain of 2.6 dB. As also shown in Fig. 4.21, our NBJTRAS aided MIMO system associated with the AS loading factors of $f_{AS}(12,6) = 3$, $f_{AS}(16,8) = 4$ and $f_{AS}(52,8) = 10$ converge to a vanishingly low BER at approximately $\text{SNR} = 0.2$ dB, -0.4 dB

and -1.5 dB, respectively, achieving the SNR gains of about 3.8 dB, 4.4 dB and 5.5 dB, compared to the conventional MIMO system operating without AS.

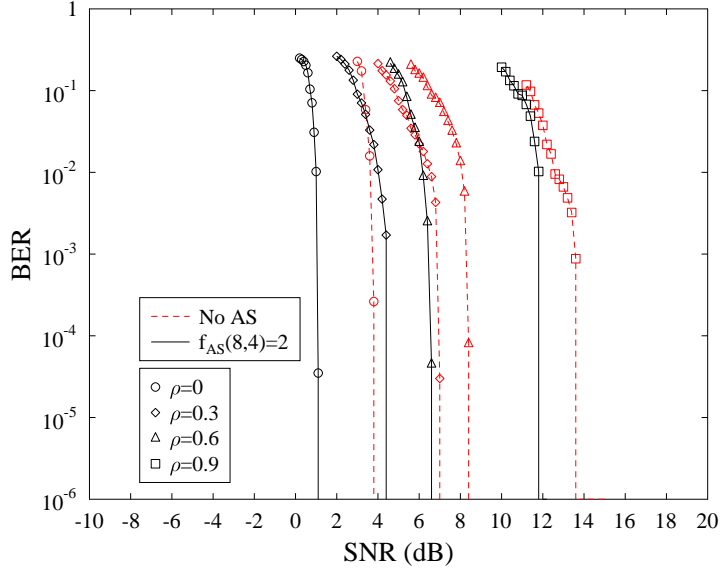


Figure 4.22: Achievable BER performance of the proposed NBJTRAS aided MIMO(8,4;4,2;4-QAM) system of Fig. 4.7 associated with $f_{AS}(8,4) = 2$ and a throughput of $R = 8$ bits/symbol, in comparison to those of the conventional MIMO(4,2;4,2;4-QAM) system of Fig. 2.7 operating without AS, under various spatially correlated channel environments. All other system parameters were summarized in Table 4.2.

4.2.2.2.4 MIMO($M, N; 4, 2; 4$ -QAM) under Spatially Correlated Fading Environments

Fig. 4.22 shows the achievable BER performance of the NBJTRAS aided MIMO(8,4;4,2;4-QAM) system of Fig. 4.7 associated with $f_{AS}(8,4) = 2$ and a system's throughput of $R = 8$ bits/symbol, in comparison to those of the conventional MIMO(4,2;4,2;4-QAM) system of Fig. 2.7 using no AS. Similar to the results shown in Fig. 4.18 for the MIMO(4,4;2,2;BPSK) system, the BER performance of both the NBJTRAS aided MIMO(8,4;4,2;4-QAM) and the conventional MIMO(4,2;4,2;4-QAM) degrade as the correlation between the MIMO channels increases. It can also be observed that the NBJTRAS aided MIMO system is capable of outperforming the conventional MIMO system operating without AS in a spatially correlated channel environment. To be more explicit, in the independent fading environment, an approximate SNR gain of 2.6 dB is achieved by the NBJTRAS aided MIMO system over the conventional MIMO system operating without AS. At the spatial correlation value of $\rho = 0.3$, the NBJTRAS aided MIMO still outperforms the conventional MIMO with an approximate SNR gain of 2.6 dB. As the spatial correlation value is increased to $\rho = 0.6$ and $\rho = 0.9$, respectively, the SNR gain achieved by the NBJTRAS aided MIMO over the conventional MIMO is reduced to approximately 1.8 dB.

We also provide the BER performance of the NBJTRAS aided MIMO(16,8;4,2;4-QAM) sys-

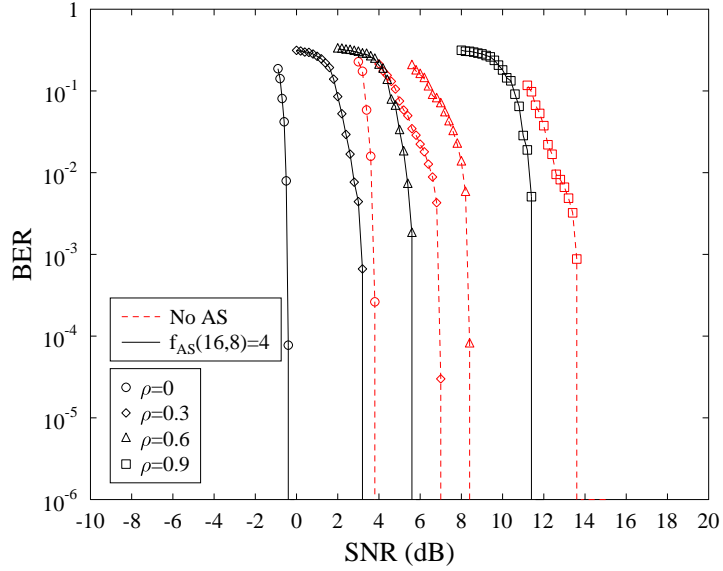


Figure 4.23: Achievable BER performance of the proposed NBJTRAS aided MIMO(16,8;4,2;4-QAM) system of Fig. 4.7 associated with $f_{AS}(16,8) = 4$ and a throughput of $R = 8$ bits/symbol, in comparison to those of the conventional MIMO(4,2;4,2;4-QAM) system of Fig. 2.7 operating without AS, under various spatially correlated channel environments. All other system parameters were summarized in Table 4.2.

tem of Fig. 4.7 associated with a $f_{AS}(16,8) = 4$ and a system's throughput of $R = 8$ bits/symbol in Fig. 4.23 under various spatially correlated fading environments, in comparison to the performance of the conventional MIMO(4,2;4,2;4-QAM) system of Fig. 2.7 operating without AS. By comparing Fig. 4.23 with Fig. 4.22, it can be seen again that the performance gain of the NBJTRAS aided MIMO system can be enhanced by increasing the AS loading factor, at the cost of employing more AEs.

4.3 Channel Estimation for NBJTRAS

In the previous section, we have assumed having a perfect knowledge of the CSI for the NBJTRAS aided MIMO system. However, in practice, the CSI required for both AS operation and data detection must be estimated. Additionally, it has been mentioned in Section 4.1.3 that AS operation may rely on a less accurate CSI estimate, while data detection must rely on a very accurate CSI estimate. Therefore, in this section let us focus on the CE schemes for our proposed NBJTRAS algorithm.

4.3.1 Conventional TBCE for NBJTRAS

4.3.1.1 System Description

The TBCE schemes of [151, 152] may be preferred for estimating the MIMO CSI owing to their algorithmic simplicity, albeit they impose a substantial PO. Fortunately, it has been shown in [157] that the achievable diversity order obtained under the assumption of perfect CSI is not reduced, when an imperfect CE is used for AS. In other words, AS is relatively insensitive to the CE error. Consequently, a simple TBCE scheme relying on a small to modest PO may be sufficient for assisting our proposed NBJTRAS aided MIMO system in its AS operation. However, the full MIMO channel matrix $\mathbf{H} \in \mathbb{C}^{N \times M}$ must be estimated by a MIMO channel estimator for the NBJTRAS algorithm to carry out AS, but we can only configure an $(L_R \times L_T)$ -element MIMO physically. Therefore, a way must be found to estimate the ‘virtual’ full MIMO channel matrix based on the limited affordable hardware resources. An attractive solution is to *reuse* the available RF chains for estimating all the $(L_R \times L_T)$ -element subset MIMO channel matrices and consequently to form the estimate of this full MIMO channel matrix based on these estimated subset channel matrices. The resultant full MIMO estimate can then be adopted for NBJTRAS. Moreover, the selected subset MIMO CE can be further employed in data detection. The equivalent system block diagram of this TBCE assisted NBJTRAS is shown in Fig. 4.24.

For the sake of simplicity and without loss of generality, we assume that the ratios $\frac{M}{L_T}$ and $\frac{N}{L_R}$ are both integers. Then the number of the subset channel matrices that have to be estimated is $\frac{M}{L_T} \times \frac{N}{L_R}$. More specifically, we have to estimate the subset channel matrices $\mathbf{H}^{(i,j)} \in \mathbb{C}^{L_R \times L_T}$ for $i \in \{1, 2, \dots, \frac{N}{L_R}\}$ and $j \in \{1, 2, \dots, \frac{M}{L_T}\}$ in order to form the full MIMO channel matrix $\mathbf{H} \in \mathbb{C}^{N \times M}$. For an illustrative purpose, we further assume that the MIMO system considered is the SDM/V-BLAST type, and the number of the training blocks available for TBCE is M_T . Then

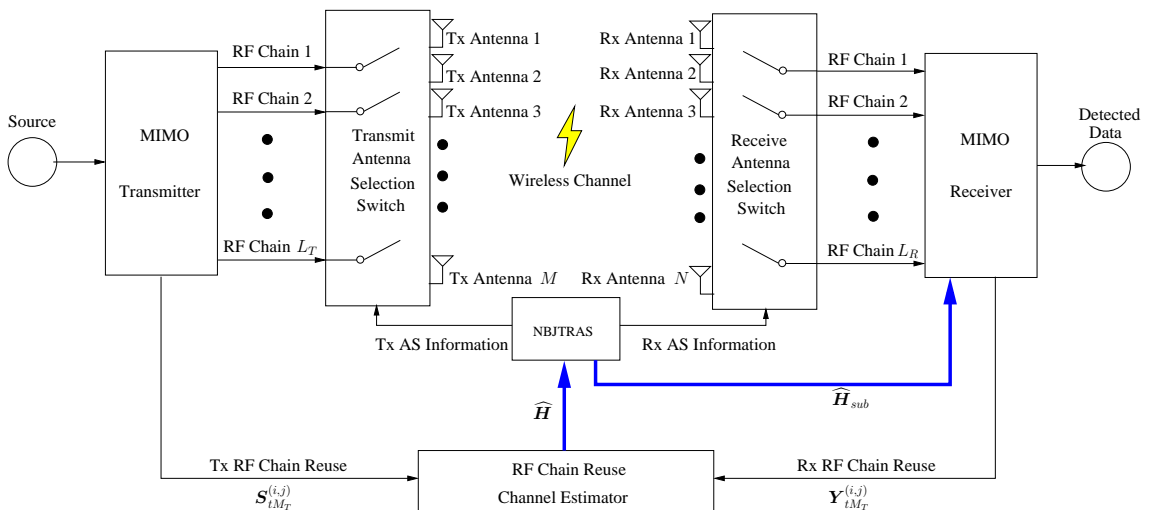


Figure 4.24: TBCE scheme relying on RF chain reuse for the NBJTRAS aided MIMO.

the training data for estimating $\mathbf{H}^{(i,j)}$ can be arranged as

$$\mathbf{Y}_{tM_T}^{(i,j)} = \left[\mathbf{y}^{(i,j)}(1) \mathbf{y}^{(i,j)}(2) \cdots \mathbf{y}^{(i,j)}(M_T) \right], \quad (4.14)$$

$$\mathbf{S}_{tM_T}^{(i,j)} = \left[\mathbf{s}^{(i,j)}(1) \mathbf{s}^{(i,j)}(2) \cdots \mathbf{s}^{(i,j)}(M_T) \right], \quad (4.15)$$

where $\mathbf{y}^{(i,j)}(q) \in \mathbb{C}^{L_R}$ is the received signal vector corresponding to the transmitted symbol vector $\mathbf{s}^{(i,j)}(q) \in \mathbb{C}^{L_T}$ for $1 \leq q \leq M_T$. The estimate of $\mathbf{H}^{(i,j)}$ based on the training data of Eqs. (4.14) and (4.15) is readily obtained as

$$\widehat{\mathbf{H}}^{(i,j)} = \mathbf{Y}_{tM_T}^{(i,j)} \left(\left(\mathbf{S}_{tM_T}^{(i,j)} \right)^H \mathbf{S}_{tM_T}^{(i,j)} + N_0 \cdot \mathbf{I}_{M_T} \right)^{-1} \left(\mathbf{S}_{tM_T}^{(i,j)} \right)^H, \quad (4.16)$$

and the estimate of the full channel matrix $\mathbf{H} \in \mathbb{C}^{N \times M}$ can be formed according to

$$\widehat{\mathbf{H}} = \begin{bmatrix} \widehat{\mathbf{H}}^{(1,1)} & \widehat{\mathbf{H}}^{(1,2)} & \cdots & \widehat{\mathbf{H}}^{(1, \frac{M}{L_T})} \\ \widehat{\mathbf{H}}^{(2,1)} & \widehat{\mathbf{H}}^{(2,2)} & \cdots & \widehat{\mathbf{H}}^{(2, \frac{M}{L_T})} \\ \vdots & \vdots & \cdots & \vdots \\ \widehat{\mathbf{H}}^{(\frac{N}{L_R}, 1)} & \widehat{\mathbf{H}}^{(\frac{N}{L_R}, 2)} & \cdots & \widehat{\mathbf{H}}^{(\frac{N}{L_R}, \frac{M}{L_T})} \end{bmatrix}. \quad (4.17)$$

Then the NBJTRAS described in Section 4.2 is carried out based on this estimated full channel matrix $\widehat{\mathbf{H}} \in \mathbb{C}^{N \times M}$, which also yields the estimate $\widehat{\mathbf{H}}_{sub} \in \mathbb{C}^{L_R \times L_T}$ of the subset channel matrix $\mathbf{H}_{sub} \in \mathbb{C}^{L_R \times L_T}$ for the selected subset MIMO system over which the actual data transmission will take place.

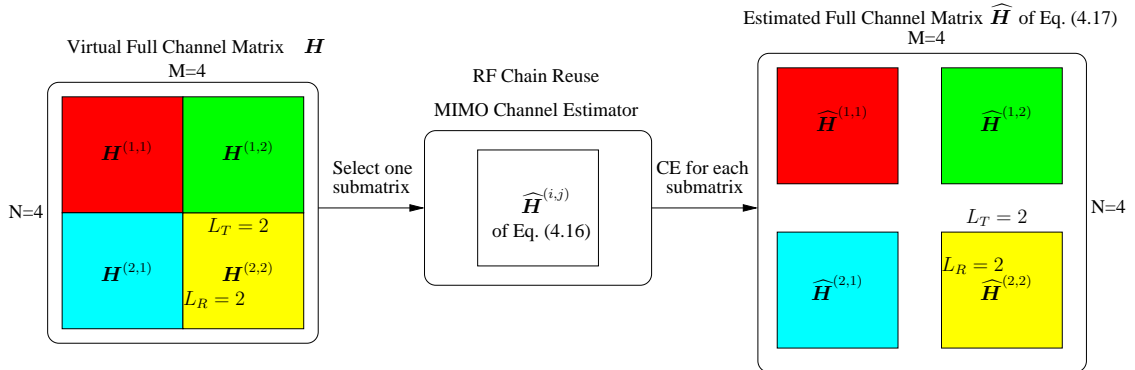


Figure 4.25: An example of the TBCE relying on RF chain reuse, which is related to the “RF Chain Reuse Channel Estimator” component of Fig. 4.24.

Fig. 4.25 shows an example of the TBCE for NBJTRAS relying on RF chain reuse. Without loss of generality, we consider a full channel matrix \mathbf{H} associated with $M = 4$ Tx antennas and $N = 4$ Rx antennas. The number of Tx and Rx RF chains is set to $L_T = L_R = 2$, respectively. In this case, the total number of the subset channel matrices that have to be estimated is $\frac{M}{L_T} \times \frac{N}{L_R} = 4$, which may be seen from the structure of the virtual full channel matrix in Fig. 4.25. However, due to the limited number of available RF chains, the RF chains have to be reused in order to estimate this virtual full channel matrix. To be more explicit, an actual MIMO system is associated with the

subset channel matrix $\mathbf{H}^{(i,j)} \in \mathbb{C}^{2 \times 2}$, which is constructed with the aid of the available RF chains of Fig. 4.24, and the estimated subset channel matrix $\widehat{\mathbf{H}}^{(i,j)} \in \mathbb{C}^{2 \times 2}$ is obtained by the TBCE scheme, for $i \in \{1, 2\}$ and $j \in \{1, 2\}$. After four-fold RF chain reuse, four subset channel matrices are estimated, and the estimated full channel matrix $\widehat{\mathbf{H}} \in \mathbb{C}^{4 \times 4}$ can readily be formed according to Eq. (4.17).

For CSTSK MIMO systems, the TBCE scheme relaying on RF chain reuse is exactly the same as given above, except for that the training data for estimating $\mathbf{H}^{(i,j)}$ are given by

$$\mathbf{Y}_{tM_T}^{(i,j)} = \left[\mathbf{Y}^{(i,j)}(1) \ \mathbf{Y}^{(i,j)}(2) \ \dots \ \mathbf{Y}^{(i,j)}(M_T) \right], \quad (4.18)$$

$$\mathbf{S}_{tM_T}^{(i,j)} = \left[\mathbf{S}^{(i,j)}(1) \ \mathbf{S}^{(i,j)}(2) \ \dots \ \mathbf{S}^{(i,j)}(M_T) \right], \quad (4.19)$$

where $\mathbf{Y}^{(i,j)}(q) \in \mathbb{C}^{L_R \times T}$ is the received signal matrix corresponding to the transmitted symbol matrix $\mathbf{S}^{(i,j)}(q) \in \mathbb{C}^{L_T \times T}$ for $1 \leq q \leq M_T$, and T is the number of time slots occupied by the CSTSK signal block.

4.3.1.2 Simulation Results

This section provides the simulation results of using the TBCE scheme to aid the NBJTRAS algorithm. The simulation setup used in this section was the same as the setup employed in Section 4.2.2. In particular, an independent Rayleigh block fading environment was considered, and two types of MIMO were considered, which were the uncoded CSTSK MIMO system and the three-stage serial-concatenated turbo coded SDM/V-BLAST MIMO system. Two metrics were used for assessing the achievable performance, namely, the BER and the MCEE of the channel estimator. The MCEE for NBJTRAS aided MIMO systems is defined by

$$J_{\text{MCEE}}(\widehat{\mathbf{H}}_{\text{sub}}) = \frac{\|\mathbf{H}_{\text{sub}} - \widehat{\mathbf{H}}_{\text{sub}}\|^2}{\|\mathbf{H}_{\text{sub}}\|^2}, \quad (4.20)$$

where $\mathbf{H}_{\text{sub}} \in \mathbb{C}^{L_R \times L_T}$ denotes the true channel matrix of the activated MIMO system and $\widehat{\mathbf{H}}_{\text{sub}}$ its estimate. All the results were averaged over 100 channel realisations. We have summarized the system parameters of uncoded NBJTRAS aided CSTSK MIMO system in Table 4.3 and of the three-stage serial-concatenated turbo coded and NBJTRAS aided SDM/V-BLAST MIMO system of Fig. 4.24 in Table 4.4.

4.3.1.2.1 TBCE for NBJTRAS Aided Uncoded CSTSK Systems

We first applied the conventional TBCE scheme relaying on RF chain reuse, presented in Fig. 4.24 of Section 4.3.1.1, to NBJTRAS aided uncoded CSTSK MIMO systems. For the NBJTRAS aided CSTSK(4, 4; 2, 2; 2, 4, QPSK) system of Fig. 4.24 associated with the AS loading factor $f_{\text{AS}}(4, 4) = 2$ and a system's normalized throughput of $R = 2$ bits/symbol, the achievable BER performance is shown in Fig. 4.26, where it may be seen that as the number of CSTSK training

Table 4.3: System parameters of the TBCE aided NBJTRAS assisted CSTSK system of Fig. 4.24 and the TTCE aided NBJTRAS assisted CSTSK system of Fig. 4.32.

Number of Tx antennas	M
Number of Rx antennas	N
Number of Tx RF chains	L_T
Number of Rx RF chains	L_R
Symbol durations per block	T
Number of dispersion matrices	Q
Modulation	\mathcal{L} -QAM or \mathcal{L} -PSK
AS loading factor	$f_{AS}(M, N)$ of Eq. (4.12)
Number of training blocks	M_T
Number of signal blocks per frame	$\tau = 250$
Pilot overhead	O_p of Eq. (3.7)
Channels	Frequency-flat Rayleigh fading
Detector	ML detector of Eq. (2.19)
Number of CE iterations	I_{ce}

blocks increases, i.e. have a higher PO, the BER performance is improved due to the improved CE accuracy. When the number of training blocks is increased to $M_T = 30$ ($O_p = 12\%$), the SNR gap between the BER curve of the perfect CSI based system and that of the CE based system becomes smaller than 0.1 dB. Additionally, it is worth mentioning that for a NBJTRAS aided MIMO system, the CE error may cause two errors, namely, the AS error due to the inaccurate CE used by the NBJTRAS and the detection error owing to the inaccurate CE used by the MIMO data detector. The combination of these two errors leads to the overall performance degradation. However, it is widely recognized that the data detector is much more sensitive to the CE error.

Fig. 4.27 compares the MCEE performance of the TBCE scheme for the NBJTRAS aided CSTSK(4,4;2,2;2,4,QPSK) system system of Fig. 4.24 given the AS factor of $f_{AS}(4,4) = 2$ and a system's normalized throughput of $R = 2$ bits/symbol with those of the TBCE scheme for the conventional CSTSK(2,2;2,2;2,4,QPSK) operating without AS, obtained given different POs. It can be seen from Fig. 4.27 that for the cases of $O_p = 0.8\%$ ($M_T = 2$) and $\text{SNR} < -1$ dB as well as $O_p = 2\%$ ($M_T = 5$) and $\text{SNR} < -5$ dB, the MCEE of the training based NBJTRAS aided CSTSK system is slightly worse than that of the training based conventional CSTSK system operating without AS. Note that for the non-AS based conventional CSTSK system, the MCEE is purely the CE error, but for the NBJTRAS aided CSTSK system, the MCEE also includes the AS error. However, despite the fact that the CE error may degrade the performance of the NBJTRAS, the MCEE of the TBCE scheme for the NBJTRAS aided CSTSK is significantly lower than the MCEE of the TBCE scheme for the conventional non-AS CSTSK in general. More specifically,

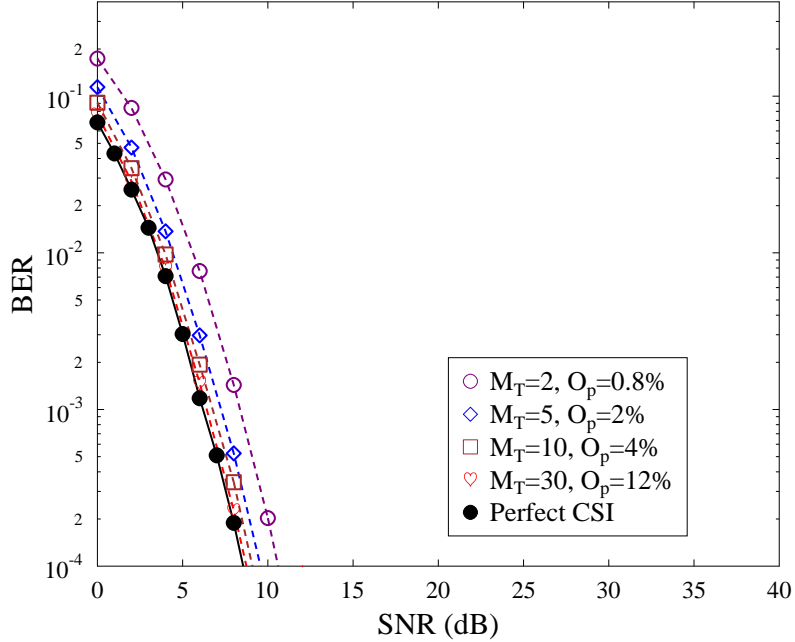


Figure 4.26: BER performance of the TBCE scheme assisted and the NBJTRAS aided CSTSK(4,4;2,2;2,4,QPSK) system of Fig. 4.24 associated with $f_{AS}(4,4) = 2$ and a system's normalized throughput of $R = 2$ bits/symbol. The number of CSTSK training blocks is $M_T = 2, 5, 10$ and 30 and the corresponding POs are $O_p = 0.8\%, 2\%, 4\%$ and 12%, respectively. The BER performance is compared to that of the NBJTRAS aided CSTSK(4,4;2,2;2,4,QPSK) system of Fig. 4.7 based on perfect CSI. All other system parameters were summarized in Table 4.3.

with $\text{SNR} > -1 \text{ dB}$ and $O_p < 4\% (M_T < 5)$ as well as with $O_p > 4\% (M_T > 5)$ for all the range of SNR values, the TBCE for the NBJTRAS aided CSTSK(4,4;2,2;2,4,QPSK) significantly outperforms the TBCE for the conventional non-AS aided CSTSK(2,2;2,2;2,4,QPSK). This clearly demonstrates that with the aid of the NBJTRAS scheme, the CE accuracy is significantly enhanced, which is remarkable considering the fact that both the channel estimators employ the same number of training blocks and rely on the same CE scheme.

It has been mentioned in the discussion for the results of Fig. 4.26 that the overall performance degradation of the TBCE assisted NBJTRAS-MIMO system from the optimal perfect CSI based performance bound is caused by the two error sources, the AS error and the data detection error due to an inaccurate CE. In order to quantify the effects of these two errors, we designed a simulation study where the NBJTRAS was based on the perfect CSI, and the TBCE scheme with M_T training blocks was only used to estimate the selected subset channel matrix which was then used in data detection. The performance degradation of such a perfect NBJTRAS aided MIMO system from the perfect CSI bound was purely due to the data detection error caused by an inaccurate CE. Fig. 4.28 shows the BER performance comparison between this perfect NBJTRAS aided CSTSK(4,4;2,2;2,4,QPSK) system and the TBCE based NBJTRAS aided CSTSK(4,4;2,2;2,4,QPSK) system, given the two different numbers of CSTSK training blocks,

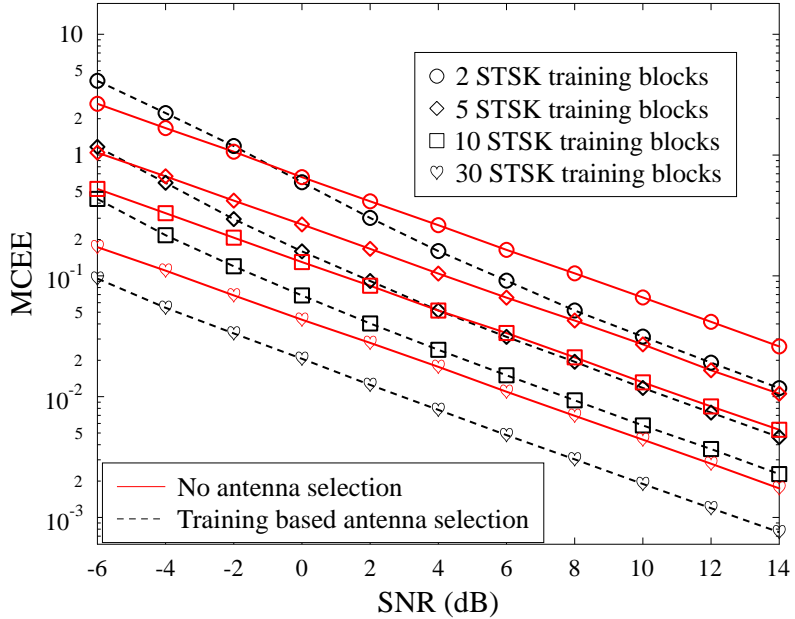


Figure 4.27: MCEE performance of the TBCE scheme assisted and the NBJTRAS aided CSTSK(4,4;2,2;2,4,QPSK) system of Fig. 4.24 associated with $f_{AS}(4,4) = 2$ and a system's normalized throughput of $R = 2$ bits/symbol. The number of CSTSK training blocks is $M_T = 2, 5, 10$ and 30 and the corresponding POs are $O_p = 0.8\%, 2\%, 4\%$ and 12%, respectively. The MCEE performance is compared to that of the TBCE scheme for the conventional CSTSK(2,2;2,2;2,4,QPSK) system of Fig. 2.17 operating without AS. All other system parameters were summarized in Table 4.3.

$M_T = 2$ and 10, associated with the corresponding POs of $O_p = 0.8\%$ and 4%. It may be seen from Fig. 4.28 that in the case of $O_p = 0.8\%$ ($M_T = 2$), there exists an SNR gap of about 0.4 dB between the imperfect and perfect NBJTRAS scenarios, which quantifies the effect of the AS error. Since the TBCE based NBJTRAS aided CSTSK(4,4;2,2;2,4,QPSK) has a 2 dB performance degradation from the perfect CSI performance bound, the effect of the data detection error caused by the inaccurate CE accounts for about 1.6 dB SNR degradation. This confirms that AS is less sensitive to the CE error than MIMO data detection is. Moreover, when the PO is increased to $O_p = 4\%$ ($M_T = 10$), the BER performance of the imperfect NBJTRAS aided system converges to the perfect NBJTRAS aided system, implying that the AS error becomes negligibly small.

Fig. 4.29 compares the achievable MCEE performance of the TBCE scheme for the imperfect TBCE based NBJTRAS aided CSTSK(4,4;2,2;2,4,QPSK) system with those of the TBCE scheme for the perfect CSI based NBJTRAS aided CSTSK(4,4;2,2;2,4,QPSK) system, given different POs. Again for the latter, the TBCE scheme is only used to estimate the selected subset channel matrix. It can be seen that as the SNR increases, the MCEE of the imperfect TBCE based NBJTRAS converges to that of the perfect NBJTRAS system, implying that increasing the SNR is capable of reducing the AS error. Additionally, increasing the number of CSTSK training blocks also reduces the performance gap between the imperfect training based NBJTRAS and the perfect

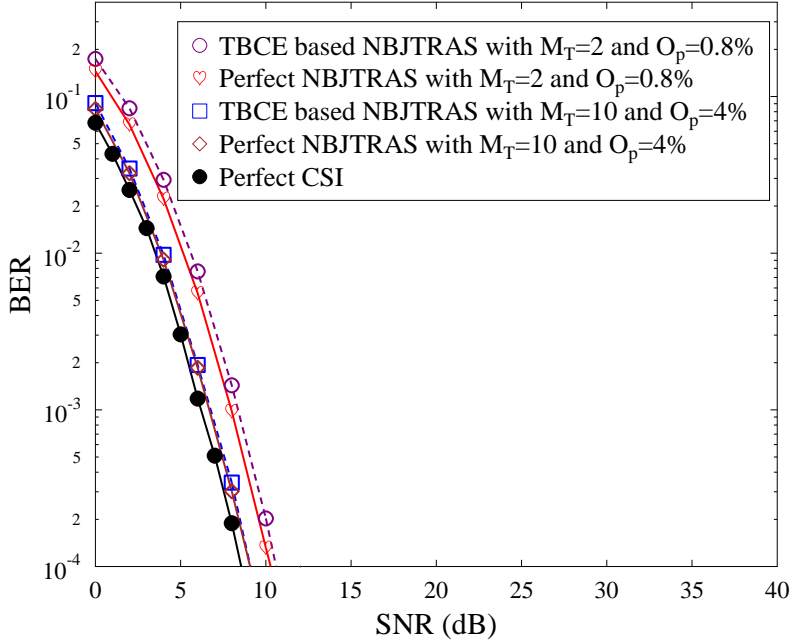


Figure 4.28: BER performance comparison between the imperfect TBCE based NBJTRAS and the perfect NBJTRAS for the CSTSK(4,4;2,2;2,4,QPSK) system of Fig. 4.24 associated with $f_{AS}(4,4) = 2$ and a system's normalized throughput of $R = 2$ bits/symbol, given the numbers of CSTSK training blocks $M_T = 2$ and 10 and the corresponding POs are $O_p = 0.8\%$, 2%, 4% and 12%. The optimal perfect CSI based BER performance bound is included as the benchmark. All other system parameters were summarized in Table 4.3.

NBJTRAS. For example, at the SNR = -6 dB, the MCEE performance gap between these two systems is approximately 4.0 for the case of $O_p = 0.8\%$ ($M_T = 2$), while the MCEE gap is reduced to as small as 0.2 for the case of $O_p = 4\%$ ($M_T = 10$). This corresponds to the BER performance shown in Fig. 4.28, where there exists a clear SNR gap in the case of $O_p = 0.8\%$ ($M_T = 2$), while in the case of $O_p = 4\%$ ($M_T = 10$) there exists a negligible performance loss. Additionally, from Fig. 4.29 it may be seen that with $O_p = 12\%$ ($M_T = 30$), the MCEE of the imperfect training based NBJTRAS converges to the MCEE of the perfect NBJTRAS system, with a MCEE gap of 0.02 at the SNR = -6 dB.

4.3.1.2.2 TBCE for NBJTRAS Aided Three-Stage Turbo Coded SDM/V-BLAST Systems

The three-stage serial-concatenated turbo coded SDM/V-BLAST MIMO system was considered using the MIMO configuration of MIMO(8,4;4,2;4-QAM) system of Fig. 4.24 associated with an AS factor of $f_{AS}(8,4) = 2$ and a throughput of $R = 8$ bits/symbol. The BER performance of the TBCE scheme assisted and NBJTRAS aided MIMO(8,4;4,2;4-QAM) is depicted in Fig. 4.30, using the optimal performance bound associated with the perfect CSI based NBJTRAS aided MIMO(8,4;4,2;4-QAM) as the benchmark. It can be seen from Fig. 4.30 that when

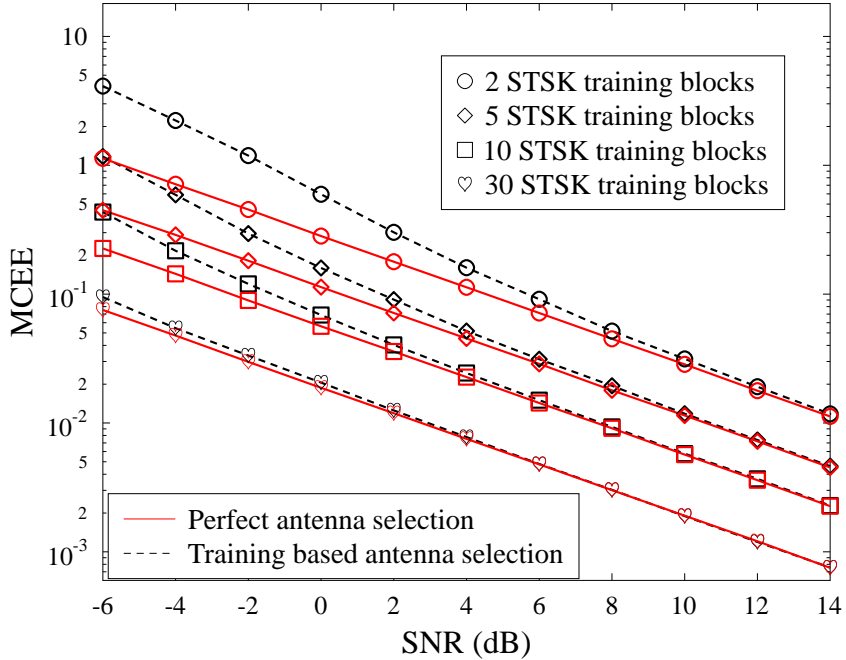


Figure 4.29: MCEE performance comparison between the imperfect TBCE based NBJTRAS and the perfect NBJTRAS for the CSTSK(4,4;2,2;2,4,QPSK) system of Fig. 4.24 associated with $f_{AS}(4,4) = 2$ and a system's normalized throughput of $R = 2$ bits/symbol, given the numbers of CSTSK training blocks $M_T = 2$ and 10 and the corresponding POs are $O_p = 0.8\%$, 2%, 4% and 12%. The optimal perfect CSI based BER performance bound is included as the benchmark. All other system parameters were summarized in Table 4.3.

PO is $O_p = 0.04\%$ ($M_T = 8$) is employed by the TBCE scheme, the system's BER converges to a vanishingly low value at the SNR value of 5 dB, while an infinitesimally low BER is attained at the SNR of 4.6 dB, when the PO increases to $O_p = 0.06\%$ ($M_T = 12$). When the CE utilizes the PO of $O_p = 0.15\%$ ($M_T = 30$), it becomes capable of assisting the NBJTRAS aided MIMO(8,4;4,2;4-QAM) scheme to achieve a vanishingly low BER at the SNR value of 2.1 dB, but there still exists a performance gap of approximately 0.7 dB with respect to the benchmark associated with perfect CSI. Evidently, the NBJTRAS aided MIMO system assisted by the standard TBCE scheme having a PO up to $O_p = 0.15\%$ is incapable of approaching the performance bound of the idealised NBJTRAS aided MIMO system associated with perfect CSI.

We further investigated the achievable MCEE performance of the standard TBCE scheme, when assisting the NBJTRAS aided MIMO system as well as when assisting the conventional MIMO system operating without AS. The MCEE results obtained for the both systems are compared in Fig. 4.31, where the POs were set to $O_p = 0.04\%$ ($M_T = 8$), 0.06% ($M_T = 12$) and 0.15% ($M_T = 30$), respectively. It can readily be seen from Fig. 4.31 that the MCEE of the training based CE for the NBJTRAS aided MIMO(8,4;4,2;4-QAM) scheme associated with $f_{AS}(8,4) = 2$ is approximately 3 dB lower than the MCEE of the same training based CE for the conventional

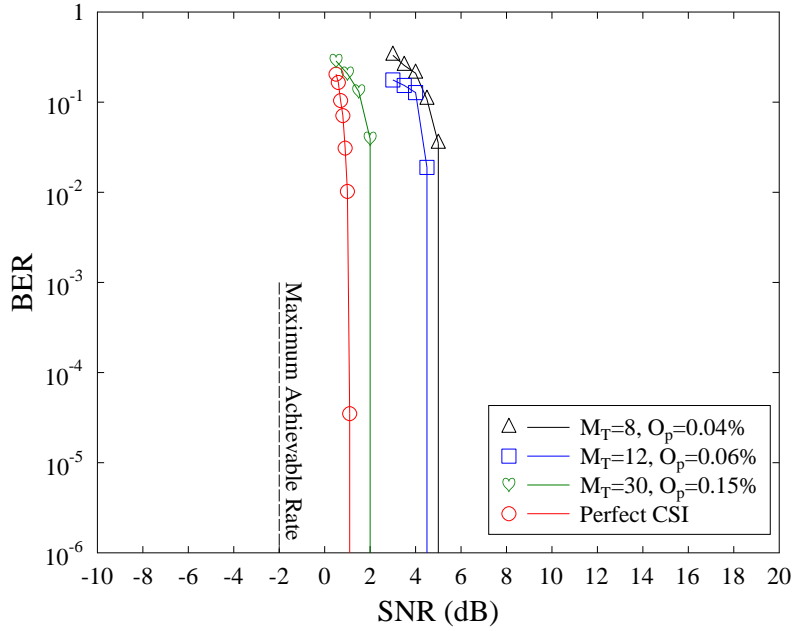


Figure 4.30: BER performance of the TBCE scheme assisted and the NBJTRAS aided three-stage turbo coded MIMO(8,4;4,2;4-QAM) system of Fig. 4.24 associated with $f_{AS}(8,4) = 2$ and a throughput of $R = 8$ bits/symbol, given different POs, in comparison with the perfect CSI based performance bound. All other system parameters were summarized in Table 4.4.

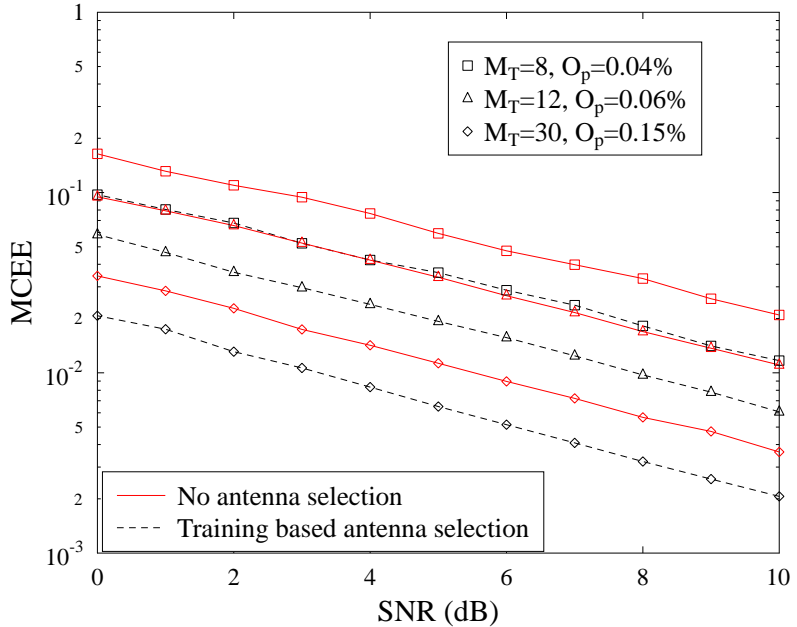


Figure 4.31: MCEE performance of the TBCE scheme for the NBJTRAS aided three-stage turbo coded MIMO(8,4;4,2;4-QAM) system of Fig. 4.24 associated with $f_{AS}(8,4) = 2$ and a throughput of $R = 8$ bits/symbol, given different POs, in comparison to the MCEE performance of the TBCE scheme for the conventional MIMO(4,2;4,2;4-QAM) of Fig. 2.7 operating without AS. All other system parameters were summarized in Table 4.4.

Table 4.4: System parameters of the TBCE and TTCE based three-stage serial-concatenated turbo coded and NBJTRAS aided SDM/V-BLAST MIMO systems of Fig. 4.24 and Fig. 4.32, respectively.

Number of Tx antennas	M
Number of Rx antennas	N
Number of Tx RF chains	L_T
Number of Rx RF chains	L_R
Modulation	\mathcal{L} -QAM or \mathcal{L} -PSK
AS loading factor	$f_{AS}(M, N)$ of Eq. (4.12)
Number of training blocks	M_T
Number of selected reliable MIMO symbol blocks	$M_{sel} = 500$
Number of signal blocks per frame	$\tau = 20,000$
Pilot overhead	O_p of Eq. (3.7)
Channels	Frequency-flat Rayleigh fading
Detector	ML MIMO soft-demapper of Eq. (2.6)
Interleaver blocklength	160,000 bits
Outer channel code	Half-rate RSC
Generator polynomials	$(G_{RSC}^r, G_{RSC}) = (7, 5)_8$
Precoder	URC
Number of inner iterations	I_{in}
Number of outer iterations	I_{out}

MIMO(4, 2; 4, 2; 4-QAM) operating without AS. This clearly demonstrates that the proposed NBJTRAS scheme is capable of improving the TBCE accuracy, which supports a widely recognised observation that AS is generally beneficial in terms of enhancing the accuracy of TBCE.

4.3.2 TTCE for NBJTRAS

In Section 4.3.1, we have discussed the conventional TBCE for assisting the NBJTRAS aided MIMO system, where it has been found that a low PO may be sufficient for AS operation since it is relatively insensitive to CE errors. However, unlike AS operation, data detection is relatively more sensitive to CE errors, and the coarse CE obtained by the TBCE scheme based on a low PO is insufficiently accurate for the system to attain the optimal ML performance associated with perfect CSI. To obtain an accurate estimate of the MIMO CSI based on a TBCE scheme would impose a substantial PO and hence would erode the system's effective throughput quite considerably. Therefore, the challenge here is to design a CE scheme for NBJTRAS aided MIMO systems, which is capable of approaching the optimal MIMO performance bound associated with perfect

CSI, without increasing the training overhead and the associated computational complexity. These two considerations motivate the design of our novel TTCE scheme, illustrated in Fig. 4.32, for assisting the NBJTRAS aided MIMO system.

4.3.2.1 System Description

The equivalent system diagram of our proposed TTCE scheme for NBJTRAS aided MIMO systems is described in Fig. 4.32, where it can be seen that differing from the conventional TBCE scheme for NBJTRAS depicted in Fig. 4.24, the proposed TTCE scheme consists of two parts or two tiers. The first part or tier one, which is in fact the conventional TBCE scheme of Fig. 4.24, generates an initial estimate of the full channel matrix utilizing only a low number of training blocks. The rough initial estimate of the full channel matrix is used for NBJTRAS, and the selected subset channel estimate is then used in initial data detection. The motivation for this tier-one arrangement is based on the fact that AS operation is less sensitive to CE errors, and the conventional TBCE scheme employing a few training blocks is sufficient for AS operation to select a near optimal antenna combination according to the NBAS optimisation criterion of Eq. (4.2). The second part or tier two includes a DDCE scheme to assist iterative joint channel estimation and data detection. The motivation for this tier-two arrangement is based on our novel joint channel estimation and turbo detection scheme for MIMOs, detailed in Section 3.4, which is capable of approaching the optimal ML performance bound associated with perfect CSI, while only relying on a low training overhead and without increasing computational complexity.

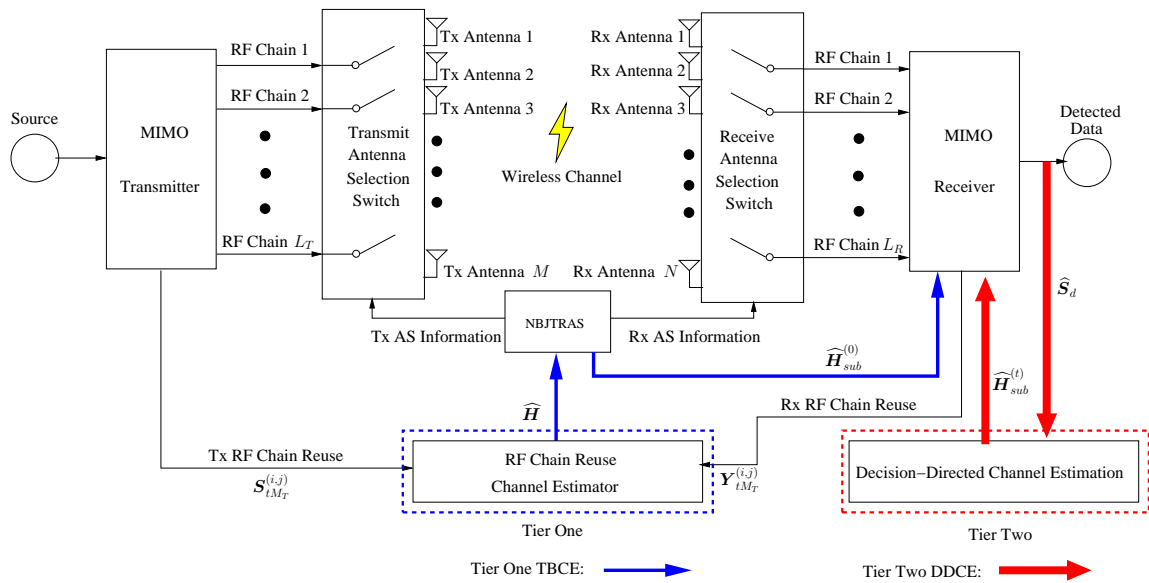


Figure 4.32: Proposed two-tier channel estimation scheme for NBJTRAS aided MIMO systems.

4.3.2.1.1 Tier One

Now let us first recap the operation of tier one. By completing the RF chain reuse based TBCE in tier one, as detailed in Section 4.3.1.1, we have the initial coarse channel estimate of the full channel matrix as $\hat{\mathbf{H}} \in \mathbb{C}^{N \times M}$. Based on this coarse estimate, we perform the NBJTRAS to select the specific subset MIMO system over which the actual data transmission will take place. This process also yields the coarse estimate $\hat{\mathbf{H}}_{sub} \in \mathbb{C}^{L_R \times L_T}$ of the actual subset channel matrix $\mathbf{H}_{sub} \in \mathbb{C}^{L_R \times L_T}$ for data transmission. Additionally, the coarse estimate of the subset channel matrix $\hat{\mathbf{H}}_{sub}$ will be used for both initial data detection and further CE refinement in tier two.

4.3.2.1.2 Tier Two

It has been demonstrated previously that even though an inaccurate channel estimate delivered by the conventional TBCE relying only on a small training overhead may not have significant impact on AS operation, it affects data detection seriously. Therefore, the coarse estimate $\hat{\mathbf{H}}_{sub}$ is insufficient for the receiver detector to attain an adequate performance, not to say to approach the optimal performance bound associated with perfect CSI. In tier two, a CE scheme that is capable of improving the CE accuracy is necessary, and such a CE estimation can only be a blind one or based on decision-directed updating. One straightforward and efficient way of achieving this purpose is to employ the Decision-Directed SBCE (DDSBCE) scheme introduced in Chapter 3.

We are now ready to provide the details of tier two in the proposed TTCE scheme. Generally, given the initial CE of the subset channel matrix obtained in the tier one, we may perform the DDSBCE to further refine it in an iterative joint CE and data detection process. To be more explicit, for the uncoded MIMO system, the SBCE scheme introduced in Section 3.3 of Chapter 3 can be invoked. Moreover specifically, given the initial estimate of the subset channel matrix as $\hat{\mathbf{H}}_{sub} \in \mathbb{C}^{L_R \times L_T}$, let the observation data be

$$\mathbf{Y}_{d\tau} = [\mathbf{Y}(1) \ \mathbf{Y}(2) \cdots \mathbf{Y}(\tau)] \quad (4.21)$$

for the STSK MIMO, or

$$\mathbf{y}_{d\tau} = [\mathbf{y}(1) \ \mathbf{y}(2) \cdots \mathbf{y}(\tau)] \quad (4.22)$$

for the SDM/V-BLAST MIMO, where τ is referred to as the number of received data blocks in one frame. Assuming the maximum number of CE iterations to be I_{ce} , the semi-blind iterative CE algorithm consists of Steps 1 to 4 described in Section 3.3 of Chapter 3.

Furthermore, for near-capacity MIMO systems, the joint CE and three-stage turbo detection schemes introduced in Sections 3.4 and 3.5 of Chapter 3 can be employed. More explicitly, for the near-capacity CSTSK MIMO system of Fig. 2.28, the joint BBSBCE scheme discussed in Section 3.4.2 can be invoked, while for the SDM/V-BLAST MIMO system of Fig. 2.7, the soft-decision aided BBSBCE scheme introduced in Section 3.5.1 can be employed.

We summarize the above discussions in Table 4.5.

Table 4.5: TTCE arrangements for various MIMO systems.

NBJTRAS Aided System	Tier One	Tier Two
Uncoded MIMO System	Conventional TBCE	SBCE (Section 3.3.1 of Chapter 3)
Near-Capacity CSTSK	Conventional TBCE	BBSBCE (Section 3.4.2 of Chapter 3)
Near-Capacity SDM/V-BLAST	Conventional TBCE	BBSB-SCE (Section 3.5.1 of Chapter 3)

4.3.2.2 Simulation Results and Discussions

This section provides the simulation results of the proposed TTCE scheme for NBJTRAS aided MIMO systems of Fig. 4.32. The simulation setup was as given in Section 4.2.2. Specifically, independent Rayleigh block fading environment was considered. Two MIMO systems considered were the uncoded CSTSK and the three-stage serial-concatenated turbo coded SDM/V-BLAST MIMO system. Two metrics were used for assessing the achievable performance, namely, the BER and the MCEE of the channel estimator. All the results were averaged over 100 channel realisations.

4.3.2.2.1 TTCE for NBJTRAS Aided Uncoded CSTSK System

For the NBJTRAS assisted uncoded CSTSK(4, 4; 2, 2; 2, 4, QPSK) system of Fig. 4.32 associated with $f_{AS}(4, 4) = 2$ and a normalized throughput of $R = 2$ bits/symbol, the achievable BER performance of the proposed TTCE scheme associated with a PO of $O_p = 2\%$ ($M_T = 5$) is shown in Fig. 4.33, in comparison to the performance of the conventional TBCE scheme of Fig. 4.24 given POs of $O_p = 2\%$ ($M_T = 5$) and 4% ($M_T = 10$). It may be seen that in the low SNR region of $\text{SNR} < 3$ dB, the TTCE assisted system fails to converge to the perfect CSI bound. However, for the SNR range of $\text{SNR} > 3$ dB, the BER of the TTCE assisted system is capable of converging to the perfect CSI based performance. The results of Fig. 4.33 also indicates that the conventional TBCE assisted NBJTRAS aided CSTSK system with $O_p = 4\%$ ($M_T = 10$) is unable to attain the BER performance bound associated with perfect CSI.

Fig. 4.34 shows the MCEE convergence behaviour of the proposed TTCE scheme given different SNRs, where it can be seen that $I_{ce} = 3$ iterations are sufficient for the TTCE scheme of Fig. 4.32 to reach the convergence state. Fig. 4.35 depicts the MCEE performance comparison between the TTCE scheme and the conventional TBCE scheme when assisting the NBJTRAS aided uncoded CSTSK(4, 4; 2, 2; 2, 4, QPSK) system. As expected, with a PO of $O_p = 2\%$ ($M_T = 5$), the conventional TBCE scheme has the same performance as the initial CE performance of the proposed TTCE scheme which also employs $O_p = 2\%$. When PO increases to $O_p = 4\%$ ($M_T = 10$), in the extremely low SNR range of $\text{SNR} < -4$ dB, the conventional TBCE scheme is capable of outperforming the proposed TTCE. This agrees with the BER performance comparison shown in

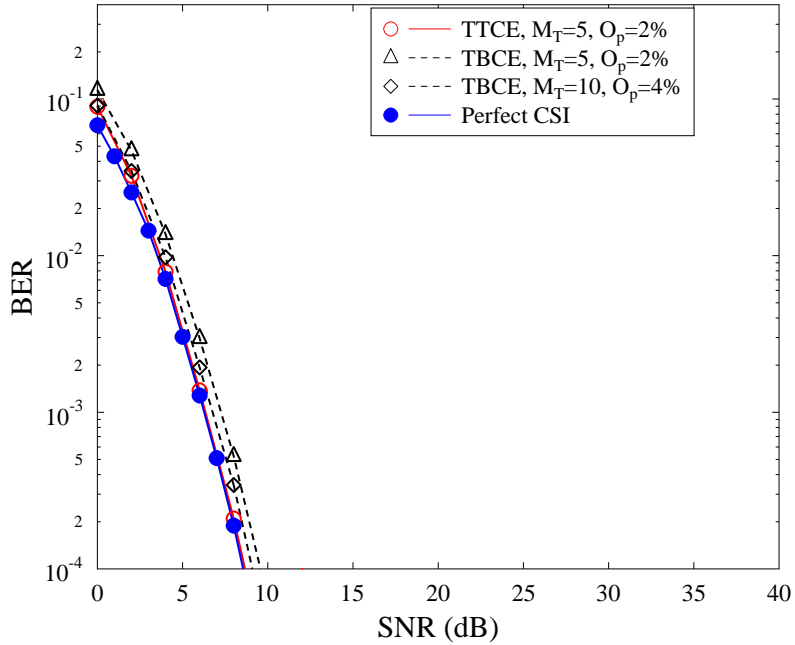


Figure 4.33: BER performance of the proposed TTCE based NBJTRAS aided uncoded CSTSK(4,4;2,2;2,4, QPSK) system of Fig. 4.32 given $M_T = 5$ initial training blocks and a PO of $O_p = 2\%$, in comparison to those of the conventional TBCE assisted NBJ-TRAS aided uncoded CSTSK(4,4;2,2;2,4, QPSK) system of Fig. 4.24 given POs of $O_p = 2\%$ ($M_T = 5$) and 4% ($M_T = 10$). The systems' normalized throughput is $R = 2$ bits/symbol. All other system parameters were summarized in Table 4.3.

Fig. 4.33. However, as SNR increases, the TTCE scheme is capable of refining the channel estimate and outperforming the conventional TBCE scheme.

Fig. 4.35 also provides the MCEE performance of the conventional TBCE scheme of Fig. 4.24 associated with a PO of $O_p = 100\%$ ($M_T = 250$) as a performance bound for the proposed TTCE scheme. This is because in our simulation, each frame contains 250 CSTSK symbol blocks. If the symbol decisions are correct, the proposed TTCE should be able to converge to this performance bound. It can be seen from Fig. 4.35 that in the region of $\text{SNR} < 6$ dB, a performance degradation from this performance bound exists due to the relatively high BER. However, when $\text{SNR} > 6$ dB, the BER becomes lower than 10^{-3} and the decisions becomes reliable, which may be used for significantly refining the channel estimates. In another word, these decisions may be equivalently seen as training blocks. Therefore, the proposed TTCE scheme with $\tau = 250$ blocks per frame is capable of approaching the performance bound of the conventional TBCE with $M_T = \tau$ CSTSK training blocks in the high SNR range which corresponds to $\text{SNR} > 6$ dB in this example.

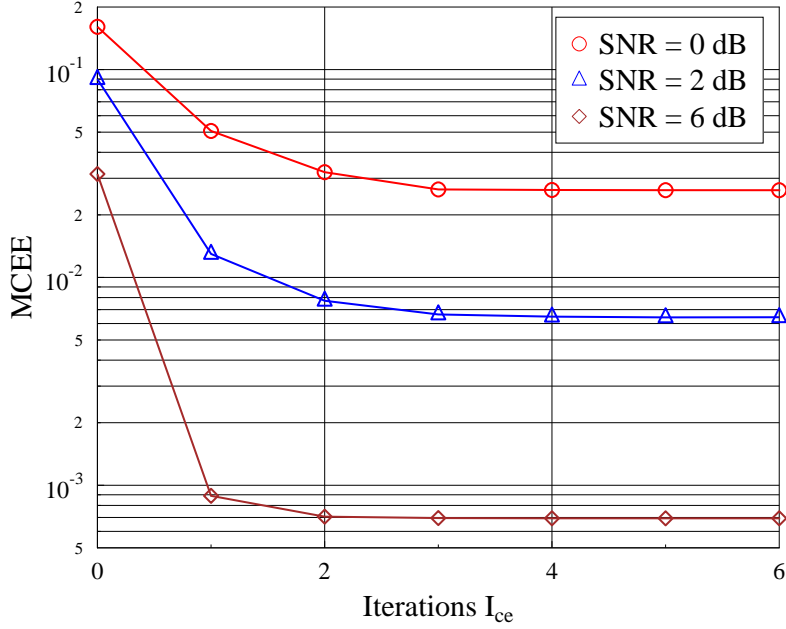


Figure 4.34: MCEE convergence performance of the proposed TTCE scheme for the NBJ-TRAS aided uncoded CSTSK(4,4;2,2;2,4, QPSK) system of Fig. 4.32 associated with $f_{AS}(4,4) = 2$ and given $M_T = 5$ training blocks and a PO of $O_p = 2\%$, at different SNR values of 0 dB, 2 dB and 6 dB. The systems' normalized throughput is $R = 2$ bits/symbol. All other system parameters were summarized in Table 4.3.

4.3.2.2.2 TTCE for NBJTRAS Aided Three-Stage Turbo Coded SDM/V-BLAST MIMO System

Now we are ready to present the achievable performance of our proposed TTCE assisted NBJTRAS aided near-capacity three-stage turbo coded MIMO(8,4;4,2;4-QAM) system of Fig. 4.32 having a throughput of $R = 8$ bits/symbol and employing $f_{AS}(8,4) = 2$. According to Table 4.5, for near-capacity SDM/V-BLAST MIMO systems, the tier-two DDSBCE scheme is the BBSB-SCE scheme given in Section 3.5.1 of Chapter 3. The maximum number of the selected symbol blocks invoked for the DDSBCE scheme in the tier two of the TTCE was set to $M_{sel} = 500$ blocks, and we tested the effects of $M_T = 12$ and 30 MIMO training blocks, corresponding to POs of $O_p = 0.06\%$ and $O_p = 0.15\%$. The achievable BER performance of the TTCE assisted NBJTRAS aided three-stage turbo coded MIMO(8,4;4,2;4-QAM) scheme is shown in Fig. 4.36 as solid curves, in comparison to those of the standard TBCE assisted same MIMO(8,4;4,2;4-QAM) arrangement, which are depicted as dashed curves in Fig. 4.36. The optimal performance bound of the idealised NBJ-TRAS aided near-capacity MIMO(8,4;4,2;4-QAM) associated with perfect CSI is also included in Fig. 4.36 as a benchmark. It can be seen from Fig. 4.36 that the proposed TTCE assisted NBJ-TRAS aided MIMO(8,4;4,2;4-QAM) system is capable of achieving an infinitesimally low BER at $\text{SNR} \approx 1.9$ dB, given $O_p = 0.06\%$ ($M_T = 12$). Hence it outperforms the standard TBCE assisted NBJTRAS aided MIMO system by approximately 2.7 dB in the SNR. This clearly demon-

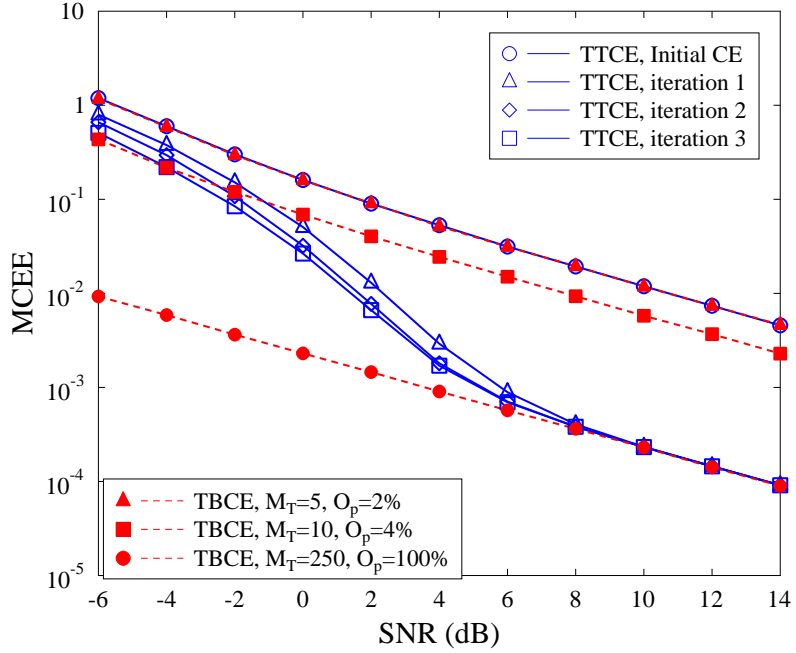


Figure 4.35: MCEE performance of the proposed TTCE scheme for the NBJTRAS aided uncoded CSTSK(4, 4; 2, 2; 2, 4, QPSK) system of Fig. 4.32 given $M_T = 5$ initial training blocks and a PO of $O_p = 2\%$, in comparison to those of the conventional TBCE assisted NBJTRAS aided uncoded CSTSK(4, 4; 2, 2; 2, 4, QPSK) system of Fig. 4.24 given POs of $O_p = 2\%$ ($M_T = 5$), 4% ($M_T = 10$) and 100% ($M_T = 250$). The systems' normalized throughput is $R = 2$ bits/symbol. All other system parameters were summarized in Table 4.3.

strates the power of the tier-two DDSBCE scheme in improving the accuracy of the MIMO CE. Additionally, we note that there exists a small SNR gap of approximately 0.5 dB between the TTCE aided MIMO system using $O_p = 0.06\%$ ($M_T = 12$ initial training data blocks) and the perfect CSI performance bound. The reason for this performance degradation can be explained as follows. The CE error of the tier-one TBCE scheme has two effects. Firstly, the full channel matrix estimate \hat{H} contains the CE error which in turn will cause AS errors. Secondly, the initial estimate \hat{H}_{sub} of the selected subset MIMO system used for actual communication also contains the CE error. Even though the effects of the CE error in the initial estimate \hat{H}_{sub} on the system's achievable performance will be completely eliminated by the tier-two DDSBCE scheme, the effects of the AS error cannot be dealt with by the tier-two DDSBCE scheme. Given a low number of initial training data, such as in the case of $M_T = 12$ ($O_p = 0.06\%$), the AS error will be noticeable, and this leads to a slight degradation of the overall performance observed in Fig. 4.36. By increasing the number of initial training data, we will be able to reduce the AS error and consequently to mitigate this performance loss. Observe in Fig. 4.36 that the TTCE assisted NBJTRAS aided MIMO system is capable of closely approaching the the optimal performance bound associated with perfect CSI with the aid of $M_T = 30$ ($O_p = 0.15\%$) initial training data blocks.

The effects of the block-of-bits selection threshold T_h on the achievable BER performance of the BBSB-SCE were also investigated by varying the value of T_h in the set $\{0.01, 0.03, 0.05, 0.1\}$ under the same system configuration. The corresponding results are shown in Fig. 4.37, where it can be seen that for $T_h = 0.03$ and 0.05 , the same system performance is attained with the aid of the BBSB-SCE scheme. However, for a threshold value of $T_h = 0.01$, a performance degradation occurs, since the number of the decision blocks selected for CE is probably insufficient for such a low threshold. On the other hand, given a high value of $T_h = 0.1$, some unreliable decision blocks may have been selected for CE and this may lead to a performance degradation. The results of Fig. 4.37 clearly confirm that as long as the threshold value is not chosen to be too high or too low, the performance of the BBSB-SCE scheme remains insensitive to the actual value of T_h . Indeed, there exists a range of values for T_h , which allow the BBSB-SCE scheme to attain its full performance potential. For this system, values in the interval $T_h \in [0.03, 0.05]$ are all appropriate.

Fig. 4.38 characterizes the MCEE convergence performance of the proposed TTCE assisted NBJTRAS aided MIMO(8, 4; 4, 2; 4-QAM) system of Fig. 4.32 given $M_T = 12$ initial training blocks ($O_p = 0.06\%$) and a throughput of $R = 8$ bits/symbol. Additionally, the MCEE performance of the standard TBCE scheme based NBJTRAS aided MIMO(8, 4; 4, 2; 4-QAM) given

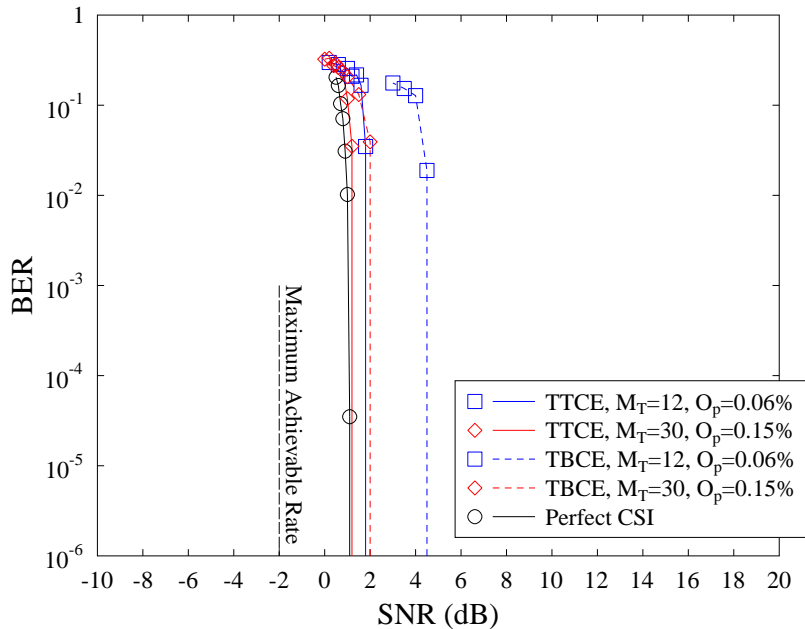


Figure 4.36: Achievable BER performance of the proposed TTCE assisted NBJTRAS aided three-stage turbo coded MIMO(8, 4; 4, 2; 4-QAM) system of Fig. 4.32 associated with $M_T = 12$ and 30 initial training blocks and POs of $O_p = 0.06\%$ and $O_p = 0.15\%$, in comparison to those of the standard TBCE scheme assisted NBJTRAS aided three-stage turbo coded MIMO(8, 4; 4, 2; 4-QAM) system of Fig. 4.24 associated with the same POs. The systems' normalized throughput is $R = 8$ bits/symbol. All other system parameters were summarized in Table 4.4.

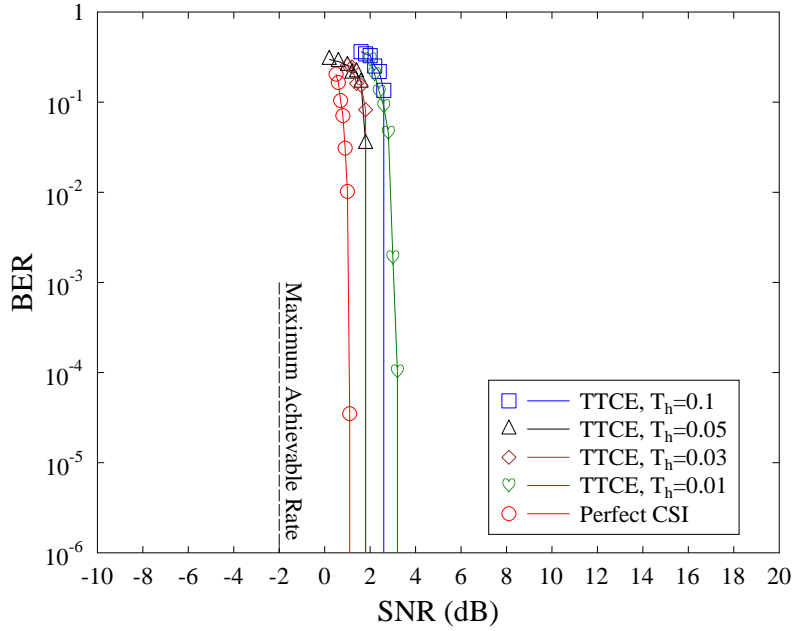


Figure 4.37: Effects of the block-of-bits selection threshold T_h to the achievable performance of the TTCE assisted NBJTRAS aided three-stage turbo coded MIMO(8, 4; 4, 2; 4-QAM) system of Fig. 4.32 associated with $M_T = 12$ initial training blocks and a PO of $O_p = 0.06\%$. The system's normalized throughput is $R = 8$ bits/symbol. All other system parameters were summarized in Table 4.4.

$M_T = 12$ ($O_p = 0.06\%$) and 500 ($O_p = 2.5\%$) training blocks are also presented in Fig. 4.38 for comparison. From the results shown in Fig. 4.38, it can be seen that the tier-two BBSB-SCE scheme is capable of substantially improving the accuracy of the CE by approximately 15 dB, and its MCEE converges in 5 iterations from the initial MCEE of the TBCE scheme associated with $M_T = 12$ ($O_p = 0.06\%$) training data to that of the TBCE scheme with the aid of $M_T = 500$ ($O_p = 2.5\%$) training data for $\text{SNR} > 1.8$ dB. This is because in our simulations the BBSB-SCE scheme selects no more than $M_{\text{sel}} = 500$ high-quality data blocks per frame for the DDCE and, furthermore, with the aid of the tier-two BBSB-SCE scheme, our TTCE assisted and NBJTRAS aided MIMO(8, 4; 4, 2; 4-QAM) arrangement attains a vanishingly low BER at the SNR value of 1.8 dB, as shown in Fig. 4.36. Therefore, under the operational conditions of $\text{SNR} > 1.8$ dB the selected data symbols are all correct and they are as “good” as the training data symbols.

4.4 Chapter Summary and Conclusions

In Section 4.1, we reviewed the concept of AS and in Section 4.2 we proposed a simple yet efficient AS algorithm, referred to as the NBJTRAS. Moreover, we proposed a novel TTCE scheme for NBJTRAS aided MIMO systems in Section 4.3.2, which was demonstrated to be capable of achieving both high CE accuracy and high system throughput, while maintaining a low computational complexity.

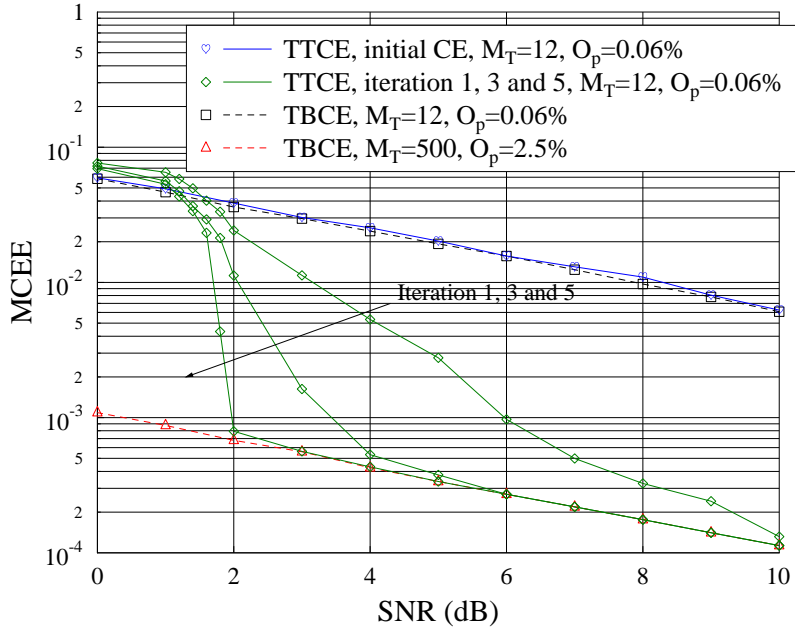


Figure 4.38: Achievable MCEE performance of the proposed TTCE assisted NBJTRAS aided three-stage turbo coded MIMO(8, 4; 4, 2; 4-QAM) system of Fig. 4.32 given $M_T = 12$ training blocks ($O_p = 0.06\%$), in comparison to those of the standard TBCE scheme assisted NBJTRAS aided three-stage turbo coded MIMO(8, 4; 4, 2; 4-QAM) system of Fig. 4.24 given $M_T = 12$ and 500 training blocks, corresponding to POs of $O_p = 0.06\%$ and 2.5%. The systems' normalized throughput is $R = 8$ bits/symbol. All other system parameters were summarized in Table 4.4.

A general introduction of AS and CE schemes for AS was provided in Section 4.1. To be more explicit, a pair of popular AS optimization criteria were discussed in Section 4.1.1, namely, the CBAS optimization of Fig. 4.1 and NBAS optimization of Fig. 4.2. It was pointed out that the main idea of CBAS was to select the specific antenna combination that maximizes the MIMO system's channel capacity. The optimal exhaustive search based process was illustrated in Fig. 4.1. However, it was widely recognized that the exhaustive search over all the possible subsets of the full channel matrix may imposed an excessive system complexity and it became impractical for systems having a large number of Tx and/or Rx antennas. Therefore, another popular AS optimization criterion – the NBAS was introduced in Section 4.1.1.2, where the main idea was to select the particular subset channel matrix combination that captures the maximum channel power or equivalently maximizes the system's SNR, so as to attain a better BER performance. As it was also demonstrated that in contrast to the CBAS algorithms of Section 4.1.1.1, the NBAS algorithms of Section 4.1.1.2 were capable of approaching the performance of CBAS, while imposing a reduced AS complexity. Hence this chapter mainly focused on the NBAS criterion. Section 4.1.2 further discussed three types of AS, namely, the TxAS of Fig. 4.3, RxAS of Fig. 4.6 and JTRAS. Since TxAS and RxAS can be regarded as special cases of JTRAS, we mainly considered JTRAS. Additionally, since the full CSI was required for AS aided MIMO systems, in Section 4.1.3 we briefly introduced the

relevant background of CE schemes in a depth necessary for AS.

Section 4.2 provided the system description and simulation results for the proposed simple yet efficient NBJTRAS algorithm conceived for MIMO systems, assuming that the full channel matrix was available. More specifically, the system description was given in Fig. 4.7 of Section 4.2.1, where an example was provided for illustrating the NBJTRAS algorithm. Additionally, the complexity analysis of our proposed NBJTRAS algorithm was given in Section 4.2.1.3, while the AS loading factor was defined in Section 4.2.1.4. Our simulation results characterizing NBJTRAS aided MIMO systems were presented in Section 4.2.2, where both uncoded CSTSK and three-stage turbo coded SDM/V-BLAST MIMO systems were considered. It was found from the simulation results depicted in Fig. 4.10, Fig. 4.11, Fig. 4.12, Fig. 4.13, Fig. 4.14, Fig. 4.15, Fig. 4.17 and Fig. 4.21 that the NBJTRAS was indeed capable of improving both the BER and throughput performance of MIMO systems, compared to the conventional MIMO systems utilizing the same number of RF chains operating without AS. Additionally, apart from the independent Rayleigh flat fading environment, we also considered the spatially correlated fading environment for the simulation of three-stage turbo coded SDM/V-BLAST MIMO systems in Fig. 4.18, Fig. 4.19, Fig. 4.22 and Fig. 4.23,. The results obtained demonstrated that at a low spatial correlation level, the NBJTRAS aided MIMO system was capable of achieving the same performance gain over the conventional MIMO system operating without AS as in the independent fading environment, while in a highly correlated channel environment, the NBJTRAS aided MIMO was still capable of outperforming the conventional MIMO without AS, but providing a smaller performance gain than in the independent fading environment. We have summarized the performance of NBJTRAS aided MIMO system of Fig. 4.7 in Table 4.6 under independent fading channel environments, and in Table 4.7 under spatially correlated fading environment, including the throughput, AS loading factor $f_{AS}(M, N)$, required SNR for achieving $BER = 10^{-4}$ and AS complexity order.

Our detailed discussions of CE schemes designed for aiding the proposed NBJTRAS algorithm were included in Section 4.3, where it was pointed out that generally, a TBCE scheme was preferred due to its simplicity. Therefore, we first developed the RF chain reused-based TBCE aided NBJTRAS systems of Fig. 4.24 in Section 4.3.1, where it was shown in Fig. 4.26 and Fig. 4.28 that since the AS operation was relatively insensitive to the CE error, conventional TBCE relying on a low number of training blocks is adequate for the purpose of obtaining an estimate of the full channel matrix to carry out AS. However, since the CE error has a more significant impact on the attainable data detection performance, there may exist considerable performance gap between the TBCE aided NBJTRAS system and the perfect CSI based scenario, if the PO is insufficiently high. In order to eliminate this performance gap without imposing a high PO, in Section 4.3.2 we proposed the novel TTCE scheme , which consists of two tiers. More specifically, tier one adopts the TBCE scheme only utilizing a low number of training blocks for generating a rough estimate of the full channel matrix for NBJTRAS, while the tier two adopts the DDSBCE for refining the accuracy of the selected subset CE for data detection. In this way, a low training overhead and hence a high

Table 4.6: Performance summary of NBJTRAS aided uncoded CSTSK and three-stage turbo coded SDM/V-BLAST MIMO systems of Fig. 4.7 under independent fading environments at $\text{BER} = 10^{-4}$. Their AS complexity is on the order of $C_{\text{NBJTRAS}} \approx \mathcal{O}\left((M \cdot (L_R + 1) + 1) \cdot \mathbf{C}_N^{L_R}\right)$.

MIMO Scheme	Throughput [bits/symbol]	$f_{AS}(M, N)$	SNR [dB]	Figure	C_{NBJTRAS}
CSTSK(2, 2; 2, 2; 2, 4, QPSK)	2	1	14.5	Fig. 4.10	N/A
CSTSK(4, 4; 2, 2; 2, 4, QPSK)	2	2	8.5	Fig. 4.10	96
CSTSK(6, 6; 2, 2; 2, 4, QPSK)	2	3	7.0	Fig. 4.10	360
CSTSK(40, 4; 2, 2; 2, 4, QPSK)	2	11	5.6	Fig. 4.10	960
CSTSK(4, 2; 4, 2; 2, 4, QPSK)	2	1	13.5	Fig. 4.12	N/A
CSTSK(8, 4; 4, 2; 2, 4, QPSK)	2	2	10	Fig. 4.12	192
CSTSK(12, 6; 4, 2; 2, 4, QPSK)	2	3	9	Fig. 4.12	720
CSTSK(60, 6; 4, 2; 2, 4, QPSK)	2	11	7.2	Fig. 4.12	3600
CSTSK(4, 4; 4, 4; 2, 4, 16-QAM)	3	1	12.5	Fig. 4.14	N/A
CSTSK(8, 8; 4, 4; 2, 4, 16-QAM)	3	2	9.6	Fig. 4.14	3360
CSTSK(12, 12; 4, 4; 2, 4, 16-QAM)	3	3	8.6	Fig. 4.14	35640
CSTSK(80, 8; 4, 4; 2, 4, 16-QAM)	3	11	7.6	Fig. 4.14	5040
MIMO(2, 2; 2, 2; BPSK)	2	1	-3	Fig. 4.17	N/A
MIMO(4, 4; 2, 2; BPSK)	2	2	-6.6	Fig. 4.17	96
MIMO(6, 6; 2, 2; BPSK)	2	3	-7.7	Fig. 4.17	360
MIMO(8, 8; 2, 2; BPSK)	2	4	-8.3	Fig. 4.17	896
MIMO(36, 4; 2, 2; BPSK)	2	10	-9.1	Fig. 4.17	864
MIMO(4, 2; 4, 2; 4-QAM)	8	1	4	Fig. 4.21	N/A
MIMO(8, 4; 4, 2; 4-QAM)	8	2	1.4	Fig. 4.21	192
MIMO(12, 6; 4, 2; 4-QAM)	8	3	0.2	Fig. 4.21	720
MIMO(16, 8; 4, 2; 4-QAM)	8	4	-0.4	Fig. 4.21	1792
MIMO(52, 8; 4, 2; 4-QAM)	8	10	-1.5	Fig. 4.21	5824

system throughput is maintained, while the accuracy of CE and hence the system's achievable BER performance is significantly enhanced. The extensive simulation results of Fig. 4.33 and Fig. 4.36 showed that with only a small training overhead, the system's achievable BER performance of this novel TTCE aided NBJTRAS scheme was capable of converging to the perfect CSI based performance bound. We have summarized the performance of TBCE aided NBJTRAS assisted MIMO system of Fig. 4.24 and TTCE aided NBJTRAS assisted MIMO system of Fig. 4.32 in Table 4.8, including the throughput, AS loading factor $f_{AS}(M, N)$, required SNR for achieving $\text{BER} = 10^{-4}$

Table 4.7: Performance summary of NBJTRAS aided uncoded CSTSK and three-stage turbo coded SDM/V-BLAST MIMO systems of Fig. 4.7 under spatially correlated fading environments at $\text{BER} = 10^{-4}$. Their AS complexity is on the order of $C_{\text{NBJTRAS}} \approx \mathcal{O}((M \cdot (L_R + 1) + 1) \cdot \mathbf{C}_N^{L_R})$.

MIMO Scheme	Throughput [bits/symbol]	ρ	$f_{AS}(M, N)$	SNR [dB]	Figure
MIMO(2, 2; 2, 2; BPSK)	2	0	1	-3	Fig. 4.18
	2	0.3	1	-1	
	2	0.6	1	-0.1	
	2	0.9	1	3.3	
MIMO(4, 4; 2, 2; BPSK)	2	0	2	-6.6	Fig. 4.18
	2	0.3	2	-4.2	
	2	0.6	2	-2.2	
	2	0.9	2	1.7	
MIMO(8, 8; 2, 2; BPSK)	2	0	4	-8.2	Fig. 4.19
	2	0.3	4	-5.8	
	2	0.6	4	-3.5	
	2	0.9	4	1.5	
MIMO(4, 2; 4, 2; 4-QAM)	8	0	1	4	Fig. 4.22
	8	0.3	1	7.1	
	8	0.6	1	8.6	
	8	0.9	1	13.8	
MIMO(8, 4; 4, 2; 4-QAM)	8	0	2	1.4	Fig. 4.22
	8	0.3	2	4.5	
	8	0.6	2	6.8	
	8	0.9	2	12	
MIMO(16, 8; 4, 2; 4-QAM)	8	0	4	-0.1	Fig. 4.23
	8	0.3	4	3.2	
	8	0.6	4	5.9	
	8	0.9	4	11.5	

and AS complexity order.

This chapter focused on the concept of AS for MIMO systems. It was shown that AS techniques were capable of efficiently achieving the advantages of MIMO systems with an affordable number of RF chains. Therefore, this promising concept was deemed to be capable of finding wide employment in future mobile communication systems, particularly in massive MIMOs and millimetre-wave communications. However, it has been recognised by researchers that due to the

Table 4.8: Performance summary of TBCE and TTCE aided NBJTRAS assisted uncoded CSTSK and three-stage turbo coded SDM/V-BLAST MIMO systems of Fig. 4.24 and Fig. 4.32, respectively, at $\text{BER} = 10^{-4}$. Their AS complexity is on the order of $C_{\text{NBJTRAS}} \approx \mathcal{O}((M \cdot (L_R + 1) + 1) \cdot \mathbf{C}_N^{L_R})$.

MIMO Scheme	Throughput [bits/symbol]	CE Scheme	PO	$f_{AS}(M, N)$	SNR [dB]	Figure
CSTSK(4, 4; 2, 2; 2, 4, QPSK)	2	TBCE	0.8%	2	10.5	Fig. 4.26
	2	TBCE	2%	2	9.5	
	2	TBCE	4%	2	9	
	2	TBCE	12%	2	8.6	
	2	TTCE	2%	2	8.5	
MIMO(8, 4; 4, 2; 4-QAM)	8	TBCE	0.04%	2	5.1	Fig. 4.30
	8	TBCE	0.06%	2	4.6	
	8	TBCE	0.15%	2	2.1	
	8	TTCE	0.06%	2	1.9	Fig. 4.36
	8	TTCE	0.15%	2	1.4	

limited size of mobile handsets, it is impractical to accommodate a relatively large number of AEs. In this case, MIMO-aided transmit diversity in the mobile uplink becomes difficult to realize. Against this background, the more recent concept of cooperative communications is advocated for the sake for allowing the nodes to assist each other by forwarding messages to the destination. The diversity gain of cooperative communications is achieved by forming a VAA for each node in a cooperative communication network, where several single-antenna-aided nodes (users) cooperatively share their antennas. As a benefit, their random locations will result in mutually uncorrelated Rayleigh fading. Therefore, in the next chapter, we will focus our attention on cooperative virtual MIMO systems and propose a Differential STSK (DSTSK) aided and successive relaying assisted cooperative multi-user system.

Multiple-Symbol Differential Sphere Detection Aided Differential Space-Time Shift Keying

5.1 Introduction

5.1.1 Differential MIMO Systems

The MIMO systems discussed in Chapters 2, 3 and 4 are coherent MIMO schemes, which generally require CSI for performing data detection or antenna selection. In this case, the accuracy of CE has a significant impact on the performance of coherently detected MIMO systems. Since CE techniques [43, 45–47] exploit the fact that the consecutive time-domain samples of each of the CIR taps are correlated, obeying a correlation that is commensurate with the velocity of the vehicle, both the pilot symbol overhead and the CE complexity increase commensurately, as the vehicular speed increases. This implies having more rapidly fluctuating CIR taps. Additionally, for a MIMO system associated with M Tx antennas and N Rx antennas, a total of $(M \times N)$ MIMO channels have to be estimated, which may also lead to increasingly high CE complexity, as the number of Tx and Rx antennas increases.

In contrast to classic coherent detectors, the family of differentially encoded non-coherent detectors requires no CSI at the receivers, hence they constitute an attractive design alternative [104, 105]. Furthermore, since non-coherent receivers usually suffer from the well-known 3 dB SNR penalty, the MSDD algorithm [91] can be applied for mitigating the associated performance degradation, albeit at the cost of an exponentially increased complexity upon extending the MSDD detection window size N_w on the order of $C_{MSDD} = \mathcal{L}^{(N_w-1)}$. The concept of MSDSD was proposed by Lampe *et al.* [98] for reducing the detection complexity to an order of $C_{MSDSD} = \mathcal{L} \cdot (N_w - 1)$, while enhancing the attainable BER performance. As a further advance, the SISO-

MSDSD is capable of achieving substantial iteration gains [99].

5.1.2 Cooperative Communication Systems

It has been widely recognised that in order to achieve a diversity gain, the distance between multiple AEs of MIMO systems has to be sufficiently high for the sake of experiencing independent fading. However, due to the critical limitation of physical size and hardware cost, it may become hard to accommodate co-located antennas on mobile devices. Additionally, these co-located antennas may experience spatially correlated fading, which may lead to the erosion of diversity gain.

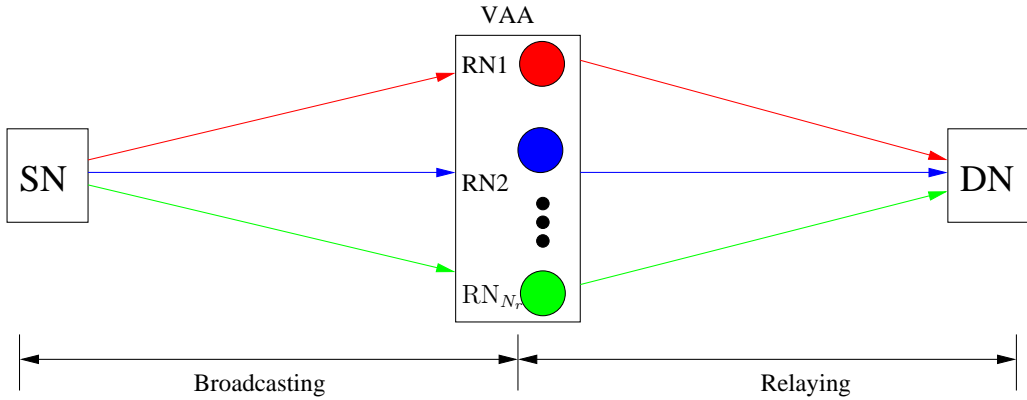


Figure 5.1: Block diagram of cooperative communication system.

As a more recent concept, cooperative communication systems were proposed [109–113] for allowing the RNs (or mobile nodes) to assist each other by forwarding messages from the SN to the DN. Fig. 5.1 illustrates the block diagram of a cooperative communication system, where it may be seen that in cooperative systems, a number of RNs that are sufficiently far apart may be selected to form a VAA [117]. In this way, a distributed MIMO system may be constructed relying on the spatially distributed single antennas of the mobile devices. Since the correlation between AEs can be avoided, “cooperative diversity” may be realized. Additionally, the operation of a conventional cooperative communication system is based on a two-phase principle, namely, the broadcasting phase followed by the relaying phase. To be more explicit, the SN transmits its source information to the RNs in the broadcasting phase and then the RNs forward the information to the DN during the relaying phase. However, it may be observed that in conventional two-phase cooperative communication systems [112, 113, 158, 159], a 50% multiplexing loss is encountered due to the half-duplex transmit and receive constraint of practical transceivers. Therefore, the concept of successive relaying was proposed in [160] for recovering the half-duplex multiplexing loss.

Generally, the cooperative protocols may be classified as the AF protocol [104, 114, 115] and the DF protocol [105, 116, 161, 162]. In AF cooperative communications, the noisy signals transmitted from the SN are amplified by the RNs and then forwarded to the DN, while in a DF relaying

network, the noisy source signals are first decoded and re-encoded at the RNs, and then they are forwarded to the DN. As it has been discussed before, coherently detected MIMO systems have to estimate the CSI and this may become impractical, because firstly, in cooperative communication systems, the number of wireless links may be significantly increased, which may lead to an excessive CE complexity. Secondly, it is unrealistic to expect that the RNs dedicate precious battery power to the complex CE operations in addition to the relaying task. Therefore, differential MIMO schemes might be preferred in cooperative communication systems, since no CSI is required.

5.1.3 Novel Contributions

Against the above background, in this chapter, we will first briefly review the MSDSD aided DSTSK system. Then we will propose a DSTSK aided MUSRC system. By exploiting the flexibility of the DSTSK concept, our system becomes capable of supporting different number of users by appropriately adjusting the constellation size of the PSK modulation scheme employed by DSTSK, and we opt for using BPSK, QPSK, 8-PSK, etc., in conjunction with a variable number of dispersion matrices. Additionally, our system is capable of activating a different number of relays by adjusting the dimensions of each dispersion matrix. Since we apply the successive relaying philosophy of [160] in our system, the 50% throughput loss of conventional two-phase relaying is recovered at the cost of supporting less users. Finally, the DS-CDMA concept is adopted for suppressing the MAI.

The rest of this chapter is organized as follows. The discussion of MSDSD aided DSTSK systems is provided in Section 5.2, while the proposed DSTSK aided MUSRC system is detailed in Section 5.3. Our chapter summary and conclusions are presented in Section 5.4.

5.2 MSDSD for DSTSK

Again, the CDD schemes usually suffer from a 3 dB SNR penalty compared to their coherently detected MIMO counterparts associated with perfect CSI in case of a low Doppler frequency, i.e. slow fading. Additionally, when the fading channel fluctuates rapidly due to a high vehicular speed, an error-floor may be formed by CDD. In order to combat these problems, MSDD was proposed, which makes joint decisions based on $N_w - 1 (> 1)$ information symbols/blocks, where N_w is referred to as detection window size [92, 93, 95–97, 107, 108]. In this way, the effects of fading channels may be readily mitigated and the performance degradation compared to coherent schemes may be compensated. However, a major problem faced by MSDD is the exponentially increased detection complexity associated with an increased window size N_w . For example, in an \mathcal{L} -DPSK scheme, MSDD has to detect $\mathcal{L}^{(N_w-1)}$ legitimate combinations of $(N_w - 1)$ information symbols. As a remedy, MSDSD was proposed for reducing the detection complexity to $\mathcal{L} \cdot (N_w - 1)$ while retaining the system performance with the aid of sphere detection [98]. In this section, we will briefly review

the MSDSD aided DSTSK philosophy.

5.2.1 DSTSK Transmitter Structure

We consider a Rayleigh fading environment. The DSTSK system employing \mathcal{L} -PSK is denoted as DSTSK(M, N, T, Q, \mathcal{L}), where M and N are the numbers of Tx and Rx antennas, respectively, while $T = M$ is the number of time slots occupied by the DSTSK signal block and Q is the number of dispersion matrices employed.

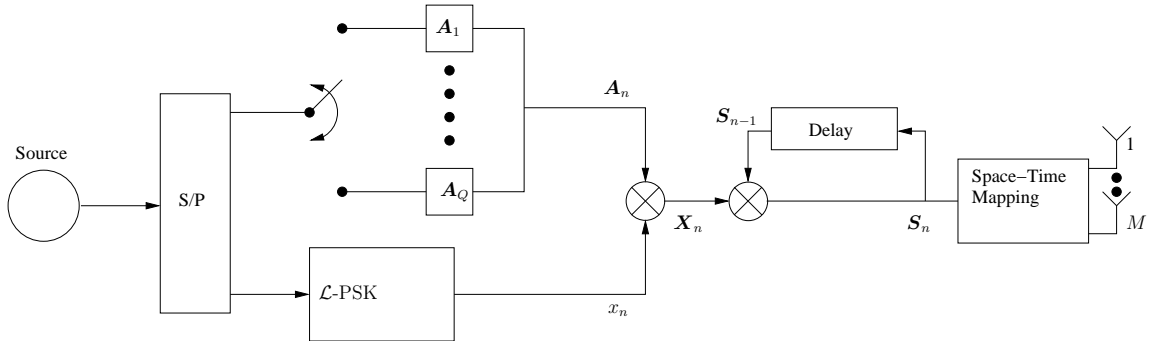


Figure 5.2: Transmitter structure of the DSTSK based MIMO scheme.

Fig. 5.2 illustrates the transmitter structure of a DSTSK MIMO system, which is similar to that of the CSTSK scheme shown in Fig. 2.17, except for the differential encoding operation invoked for DSTSK. More specifically, in the DSTSK scheme, the information bit sequence is firstly converted to a number of blocks with the number of BPB given by $\text{BPB} = \log_2(Q) + \log_2(\mathcal{L})$. The first $\log_2(Q)$ bits of the n th block are used for selecting a specific dispersion matrix A_n from the Q pre-assigned dispersion matrices $\{A_q \in \mathbb{C}^{T \times T}, 1 \leq q \leq Q\}$, while the remaining $\log_2(\mathcal{L})$ bits are mapped to the complex-valued \mathcal{L} -PSK symbol $s_n \in \{s_l, 1 \leq l \leq \mathcal{L}\}$ [5]. In this way, a total of BPB source bits are mapped to a unitary¹ DSTSK signal block $X_n \in \mathbb{C}^{T \times T}$ as

$$X_n = s_n A_n. \quad (5.1)$$

Given the condition that in DSTSK systems the number of transmit antennas and the number of time slots should be identical [5], i.e. we have $M = T$, the signal blocks are differentially encoded as

$$S_n = \begin{cases} I_T, & n = 0, \\ X_n S_{n-1}, & n > 0, \end{cases} \quad (5.2)$$

where $S_n \in \mathbb{C}^{T \times T}$ is the DSTSK transmission matrix. The corresponding received signal block $Y_n \in \mathbb{C}^{T \times N}$ can be expressed as [5]

$$Y_n = S_n H_n + V_n, \quad (5.3)$$

¹The dispersion matrices A_q are designed to be unitary in order to ensure X_n to be unitary matrices [124].

where $\mathbf{H}_n \in \mathbb{C}^{M \times N}$ is the MIMO channel matrix, whose elements are generated according to Clarke's fading model [163] of zero-mean and unit variance, while each element of the AWGN matrix $\mathbf{V}_n \in \mathbb{C}^{N \times T}$ obeys the complex-valued Gaussian distribution of $\mathcal{CN}(0, N_0)$ with N_0 being the AWGN power.

5.2.2 Hard-Decision Aided MSDSD

Since MSDSD relies on a sliding-window model associated with a window size of $N_w > 2$, the N_w received MSDSD signal blocks of Eq. (5.3) may be formulated as

$$\mathbf{Y} = \mathbf{S} \mathbf{H} + \mathbf{V}, \quad (5.4)$$

where we have $\mathbf{Y} = [\mathbf{Y}_n^T \mathbf{Y}_{n-1}^T \cdots \mathbf{Y}_{n-N_w+1}^T]^T$, $\mathbf{S} = \text{diag}\{\mathbf{S}_n, \mathbf{S}_{n-1}, \dots, \mathbf{S}_{n-N_w+1}\}$, $\mathbf{H} = [\mathbf{H}_n^T \mathbf{H}_{n-1}^T \cdots \mathbf{H}_{n-N_w+1}^T]^T$ and $\mathbf{V} = [\mathbf{V}_n^T \mathbf{V}_{n-1}^T \cdots \mathbf{V}_{n-N_w+1}^T]^T$. Based on the N_w -symbol signal blocks of \mathbf{Y} , we detect the $(N_w - 1)$ transmitted DSTSK signal blocks $\{\mathbf{X}_n, \mathbf{X}_{n-1}, \dots, \mathbf{X}_{n-N_w+2}\}$.

According to the differential encoding process of Eq. (5.2), it may be seen that each transmission matrix $\mathbf{S}_{(n+1)-i}$ for $1 \leq i \leq N_w$ contains a common multiplier $\mathbf{S}_{(n+1)-N_w}$ which is the oldest transmission matrix in the observation window. In order to avoid the effects of the common multiplier $\mathbf{S}_{(n+1)-N_w}$, we define an accumulated information matrix of

$$\mathbf{D}_i = \mathbf{S}_{(n+1)-i} \mathbf{S}_{(n+1)-N_w}^H = \begin{cases} \prod_{j=i}^{N_w-1} \mathbf{X}_{(n+1)-j}, & 1 \leq i < N_w \\ \mathbf{I}_T, & i = N_w. \end{cases} \quad (5.5)$$

Then the equivalent baseband received MSDSD signal blocks of Eq. (5.4) may be rewritten as

$$\mathbf{Y} = \mathbf{D} \bar{\mathbf{S}}_{N_w} \mathbf{H} + \mathbf{V}, \quad (5.6)$$

where the accumulated information block-diagonal matrix $\mathbf{D} = \text{diag}\{\mathbf{D}_1, \mathbf{D}_2, \dots, \mathbf{D}_{N_w}\}$, and the common multiplier block-diagonal matrix $\bar{\mathbf{S}}_{N_w} = \text{diag}\{\mathbf{S}_{(n+1)-N_w}, \mathbf{S}_{(n+1)-N_w}, \dots, \mathbf{S}_{(n+1)-N_w}\}$. Note that both $\bar{\mathbf{S}}_{N_w}$ and \mathbf{D} are unitary matrices since we have $\bar{\mathbf{S}}_{N_w} \bar{\mathbf{S}}_{N_w}^H = \mathbf{I}_{TN_w}$ and $\mathbf{D} \mathbf{D}^H = \mathbf{I}_{TN_w}$.

The MSDSD aims for maximizing the *a posteriori* probability of [92]

$$\Pr(\mathbf{Y}|\mathbf{S}) = \frac{\exp\left(-N_R \cdot \text{tr}\left\{\mathbf{Y}^H (\mathbf{R}_{YY})^{-1} \mathbf{Y}\right\}\right)}{(\pi^{N_w} \det(\mathbf{R}_{YY}))^{N_R}}, \quad (5.7)$$

where the correlation matrix \mathbf{R}_{YY} is expressed as

$$\mathbf{R}_{YY} = \mathbb{E}\left\{\mathbf{Y} \cdot \mathbf{Y}^H\right\} = \mathbf{D} \mathbf{R}_{HH} \mathbf{D}^H + \mathbf{R}_{VV} = \mathbf{D} \mathbf{C} \mathbf{D}^H, \quad (5.8)$$

where $\mathbf{C} = \mathbf{I}_T \otimes (\mathbf{R}_{HH} + \mathbf{R}_{VV}) = \mathbf{I}_T \otimes \bar{\mathbf{C}}$ is also a correlation matrix, and the fading channel's correlation matrix \mathbf{R}_{HH} is given by

$$\mathbf{R}_{HH} = \begin{bmatrix} \rho_0 & \rho_1 & \cdots & \rho_{N_w-1} \\ \rho_1 & \rho_0 & \cdots & \rho_{N_w-2} \\ \vdots & \vdots & \ddots & \vdots \\ \rho_{N_w-1} & \rho_{N_w-2} & \cdots & \rho_0 \end{bmatrix}, \quad (5.9)$$

whose elements constituted by the correlation factors may be obtained by the temporal fading correlation function defined in Clarke's fading model as $\rho_k = J_0(2\pi k f_d)$ [163], while the correlation matrix of the equivalent AWGN matrix is given by

$$\mathbf{R}_{VV} = N_0 \cdot \mathbf{I}_{N_w}. \quad (5.10)$$

Then the trace operation of the *a posteriori* probability based decision metric of in Eq. (5.7) can be further formulated as

$$\text{tr} \left\{ \mathbf{Y}^H (\mathbf{R}_{YY})^{-1} \mathbf{Y} \right\} = \text{tr} \left\{ \mathbf{Y}^H (\mathbf{D} \mathbf{C} \mathbf{D}^H)^{-1} \mathbf{Y} \right\}. \quad (5.11)$$

Since \mathbf{D} is a unitary matrix, we have $\mathbf{D}^{-1} = \mathbf{D}^H$. Let \mathbf{L} denote the lower triangular matrix, which is created by decomposing the inversion of the channel's correlation matrix, namely, by $\mathbf{C}^{-1} = \mathbf{L} \mathbf{L}^H$, we may then reformulate the trace operation in Eq. (5.11) as

$$\text{tr} \left\{ \mathbf{Y}^H (\mathbf{R}_{YY})^{-1} \mathbf{Y} \right\} = \text{tr} \left\{ \mathbf{Y}^H \mathbf{D} \mathbf{C}^{-1} \mathbf{D}^H \mathbf{Y} \right\} = \left\| \mathbf{L}^H \mathbf{D}^H \mathbf{Y} \right\|^2, \quad (5.12)$$

where $\mathbf{L} \in \mathbb{C}^{TN_w \times TN_w}$ is a block lower triangular matrix taking the form of

$$\mathbf{L} = \begin{bmatrix} \mathbf{L}_{1,1} & 0 & \cdots & 0 \\ \mathbf{L}_{2,1} & \mathbf{L}_{2,2} & \cdots & 0 \\ \vdots & \vdots & \ddots & \vdots \\ \mathbf{L}_{N_w,1} & \mathbf{L}_{N_w,2} & \cdots & \mathbf{L}_{N_w,N_w} \end{bmatrix}, \quad (5.13)$$

with each sub-matrix $\mathbf{L}_{i,j}$, $1 \leq i \leq N_w$ and $1 \leq j \leq N_w$ having a size of $(T \times T)$. Furthermore, each $\mathbf{L}_{i,i}$ is a lower triangular matrix. Then the decision metric of Eq. (5.12), which is a part of Eq. (5.7) can be rewritten as

$$\left\| \mathbf{L}^H \mathbf{D}^H \mathbf{Y} \right\|^2 = \sum_{i=1}^{N_w} \left\| \sum_{j=i}^{N_w} \mathbf{L}_{j,i} \mathbf{D}_j^H \mathbf{Y}_{(n+1)-j} \right\|^2. \quad (5.14)$$

Note that maximizing Eq. (5.7) is equivalent to minimizing Eq. (5.14) which is a "shortest vector problem" [108]. In this case, we may invoke MSDSD for examining the accumulated information matrices $\{\mathbf{D}_i\}_{i=1}^{N_w}$ of Eq. (5.5) that lie within the sphere radius of R_{SD} , which is given as

$$\sum_{i=1}^{N_w} \left\| \sum_{j=i}^{N_w} \mathbf{L}_{j,i} \mathbf{D}_j^H \mathbf{Y}_{(n+1)-j} \right\|^2 \leq R_{SD}^2. \quad (5.15)$$

Note that the accumulated information matrices $\{\mathbf{D}_i\}_{i=1}^{N_w-1}$ contain the transmitted DSTSK signal blocks $\{\mathbf{X}_{(n+1)-i}\}_{i=1}^{N_w-1}$ to be detected in the current observation window, while we have $\mathbf{D}_{N_w} = \mathbf{I}_T$.

Additionally, if we define $\bar{\mathbf{C}}^{-1} = \bar{\mathbf{L}} \bar{\mathbf{L}}^H$, we have the $(N_w \times N_w)$ -element lower triangular matrix

$$\bar{\mathbf{L}} = \begin{bmatrix} l_{1,1} & 0 & \cdots & 0 \\ l_{2,1} & l_{2,2} & \cdots & 0 \\ \vdots & \vdots & \ddots & \vdots \\ l_{N_w,1} & l_{N_w,2} & \cdots & l_{N_w,N_w} \end{bmatrix}, \quad (5.16)$$

then we have the relationship of

$$\mathbf{L} = \mathbf{I}_T \otimes \bar{\mathbf{L}} \quad (5.17)$$

and the MSDSD of Eq. (5.15) may be further simplified to

$$\sum_{i=1}^{N_w} \left\| \sum_{j=i}^{N_w} l_{j,i} \mathbf{D}_j^H \mathbf{Y}_{(n+1)-j} \right\|^2 \leq R_{SD}^2. \quad (5.18)$$

Let us now define the Partial Euclidean distance (PED) of Eq. (5.18) as

$$d_i^2 = \sum_{t=i}^{N_w} \left\| \sum_{j=t}^{N_w} l_{j,t} \mathbf{D}_j^H \mathbf{Y}_{(n+1)-j} \right\|^2 = d_{i+1}^2 + \delta_i, \quad (5.19)$$

for $i = N_w - 1, N_w - 2, \dots, 1$, where the PED increment δ_i can be expressed as

$$\begin{aligned} \delta_i &= d_i^2 - d_{i+1}^2 = \left\| \sum_{j=i}^{N_w} l_{j,i} \mathbf{D}_j^H \mathbf{Y}_{(n+1)-j} \right\|^2 = \left\| l_{i,i} \mathbf{D}_i^H \mathbf{Y}_{(n+1)-i} + \sum_{j=i+1}^{N_w} l_{j,i} \mathbf{D}_j^H \mathbf{Y}_{(n+1)-j} \right\|^2 \\ &= \left\| l_{i,i} \mathbf{X}_{(n+1)-i}^H \mathbf{Y}_{(n+1)-i} + \mathbf{D}_{i+1} \left(\sum_{j=i+1}^{N_w} l_{j,i} \mathbf{D}_j^H \mathbf{Y}_{(n+1)-j} \right) \right\|^2. \end{aligned} \quad (5.20)$$

Based on the PED increment of Eq. (5.20), the hard-decision aided MSDSD may be implemented by the SD algorithm of [98] to examine the set of candidates $\{\mathbf{X}_{(n+1)-i}\}_{j=1}^{N_w-1}$ that lie within the decoding sphere radius R_{SD} . Additionally, it may be seen from Eq. (5.20) that in the MSDSD, for a specific index i , all the previously tested accumulated symbol blocks $\{\mathbf{D}_j\}_{j=i+1}^{N_w}$ have been determined and, therefore, only the current symbol block of $\mathbf{X}_{(n+1)-i}$ has to be tested. For further details please refer to [98].

5.2.3 Soft-Decision Aided MSDSD

For the sake of achieving a near-capacity performance in this section, the soft-decision aided MSDSD principle is introduced. In order to assist the MSDSD receiver to accept soft information, the *a priori* probability of the N_w -block-diagonal accumulation matrix \mathbf{D} may be expressed as

$$\ln(\Pr\{\mathbf{D}\}) = \sum_{i=1}^{N_w-1} \ln(\Pr\{\mathbf{X}_{(n+1)-i}\}), \quad (5.21)$$

where the “probabilities” of $\ln(\Pr\{\mathbf{X}_{(n+1)-i}\})$ for $1 \leq i \leq N_w - 1$ may be calculated from the *a priori* LLRs and the corresponding binary bit combinations. Similar to the hard-decision aided MSDSD, the soft-decision aided MSDSD aims for minimizing the Euclidean distance of

$$\sum_{i=1}^{N_w} \left\| \sum_{j=i}^{N_w} l_{j,i} \mathbf{D}_j^H \mathbf{Y}_{(n+1)-j} \right\|^2 - \sum_{i=1}^{N_w-1} \ln(\Pr\{\mathbf{X}_{(n+1)-i}\}) \leq R_{SD}^2. \quad (5.22)$$

If we define the PED of the soft-decision MSDSD as

$$d_i^2 = \sum_{t=i}^{N_w} \left\| \sum_{j=t}^{N_w} l_{j,t} \mathbf{D}_j^H \mathbf{Y}_{(n+1)-j} \right\|^2 - \sum_{i=1}^{N_w-1} \ln(\Pr\{\mathbf{X}_{(n+1)-i}\}) = d_{i+1}^2 + \delta_i, \quad (5.23)$$

then the PED increment is given by

$$\delta_i = \left\| l_{i,i} \mathbf{X}_{(n+1)-i}^H \mathbf{Y}_{(n+1)-i} + \mathbf{D}_{i+1} \left(\sum_{j=i+1}^{N_w} l_{j,i} \mathbf{D}_j^H \mathbf{Y}_{(n+1)-j} \right) \right\|^2 - \sum_{i=1}^{N_w-1} \ln (\Pr\{\mathbf{X}_{(n+1)-i}\}). \quad (5.24)$$

Note that the corresponding hard-decision-based formulae can be seen in Eq. (5.20). By obtaining the PED of Eq. (5.23) and the PED incremental of Eq. (5.24), the SD algorithm of hard-decision aided MSDSD may be invoked to get the soft-decisions which can further be incorporated with the powerful near-capacity three-stage serial-concatenated turbo coding scheme of Fig. 2.7 discussed in Chapter 2.

5.2.4 Simulation Results

The achievable performance of both the uncoded hard-decision aided and of the three-stage turbo coded soft-decision aided MSDSD for DSTSK MIMO systems of Fig. 5.2 were investigated in frequency-flat Rayleigh fading environments, where the normalized Doppler frequency was chosen as $f_d = 0.01$ for simulating a relatively slow fading environment and $f_d = 0.03$ for a fast fading environment. The average transmitted symbol power was normalised to unity and, therefore, the SNR was $\frac{1}{N_0}$, with N_0 being the AWGN power. A pair of DSTSK MIMO systems, DSTSK(2, 1, 2, 4, QPSK) and DSTSK(2, 2, 2, 4, QPSK), were considered, which have a normalized throughput of $R = 2$ bits/symbol. The system parameters of the uncoded MSDSD aided DSTSK scheme of Fig. 5.2 are summarized in Table 5.1.

Table 5.1: System parameters of the uncoded hard-decision MSDSD aided DSTSK scheme of Fig. 5.2.

Number of Tx antennas	M
Number of Rx antennas	N
Symbol durations per block	T
Number of dispersion matrices	Q
Modulation	\mathcal{L} -PSK
Channels	Frequency-flat Rayleigh fading
Normalized Doppler frequency	f_d
Detector	MSDSD
Detection window size	N_w

5.2.4.1 Uncoded Hard-Decision aided MSDSD for DSTSK

DSTSK(2, 2, 2, 4, QPSK) associated with $R = 2$ bits/symbol

We first consider the hard-decision aided MSDSD for DSTSK(2, 2, 2, 4, QPSK) scheme of Fig. 5.2 under the normalized Doppler frequency of $f_d = 0.01$. The system's normalized throughput is $R = 2$ bits/symbol. The achievable BER performance is shown in Fig. 5.3, in comparison to the benchmark BER performance of the CSTSK(2, 2, 2, 4, QPSK) scheme of Fig. 2.17 based on the perfect CSI as well as the BER of the CDD scheme associated with $N_w = 2$. It may be seen that at $f_d = 0.01$, the CDD BER curve falls below 10^{-6} at just over SNR = 23 dB, while the CSTSK scheme reached the same BER level at about SNR = 20 dB, where the characteristic 3 dB SNR penalty of CDD is clearly observed. However, when the MSDSD associated with a window size of $N_w = 4$ is considered, the performance of the DSTSK is slightly improved, while increasing the window size to $N_w = 6$ shows no further performance improvement.

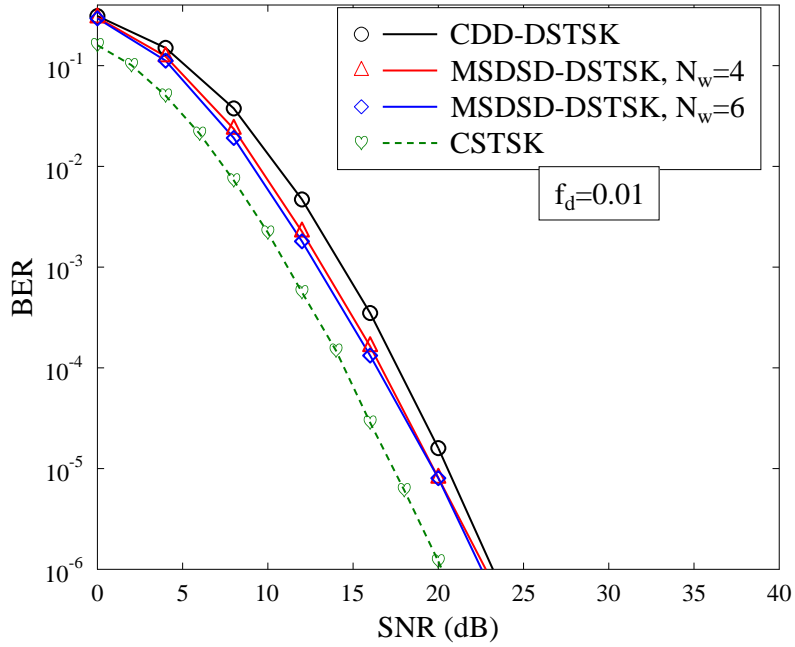


Figure 5.3: Achievable BER performance of the hard-decision aided MSDSD for the DSTSK(2, 2, 2, 4, QPSK) system of Fig. 5.2 under fading condition of $f_d = 0.01$, in comparison to that of the CDD aided DSTSK(2, 2, 2, 4, QPSK) and CSTSK(2, 2, 2, 4, QPSK) of Fig. 2.17. The system's normalized throughput is $R = 2$ bits/symbol. All other system parameters were summarized in Table 5.1.

We further show the achievable BER performance of MSDSD for the DSTSK(2, 2, 2, 4, QPSK) scheme of Fig. 5.2 under the normalized Doppler frequency of $f_d = 0.03$ in Fig. 5.4, in comparison to the performance of the CDD and the CSTSK. It may be seen that as the fading rate increases, resulting in more rapidly fluctuating CIR taps, the CDD experiences an error-floor at about BER of 10^{-5} . By contrast, the MSDSD does not exhibit such an error-floor. Furthermore, the MSDSD

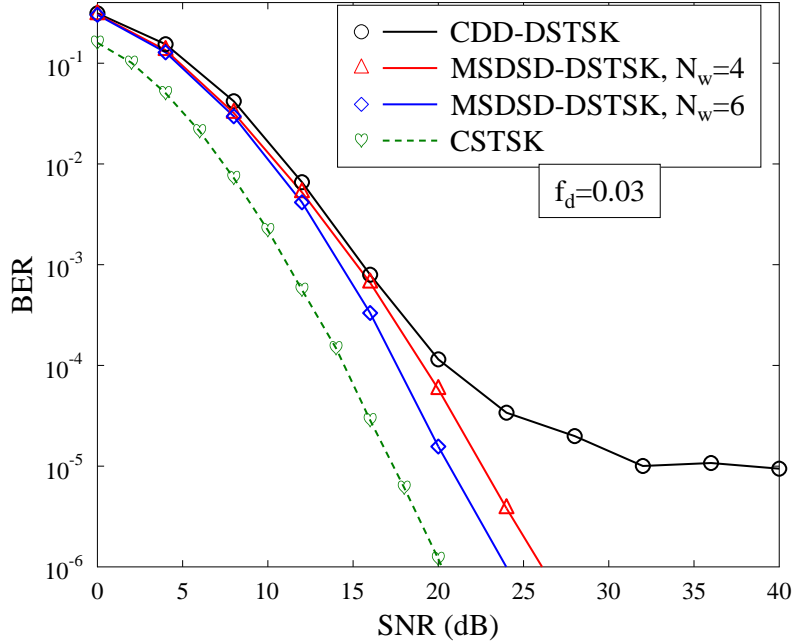


Figure 5.4: Achievable BER performance of the hard-decision aided MSDSD for the DSTSK(2, 2, 2, 4, QPSK) system of Fig. 5.2 under fading condition of $f_d = 0.03$, in comparison to that of the CDD aided DSTSK(2, 2, 2, 4, QPSK) and CSTSK(2, 2, 2, 4, QPSK) of Fig. 2.17. The system's normalized throughput is $R = 2$ bits/symbol. All other system parameters were summarized in Table 5.1.

associated with the window size of $N_w = 4$ achieves the BER of 10^{-6} at about $\text{SNR} = 26$ dB, while the MSDSD associated with the window size of $N_w = 6$ achieves the same BER at about $\text{SNR} = 24$ dB, where a SNR gain of about 2 dB is attained by increasing the widow size from 4 to 6. Note that this is different from the BER performance under $f_d = 0.01$ depicted in Fig. 5.3, where no further performance gain is achieved upon increasing the window size.

It may be concluded from the above discussion that as the normalized Doppler frequency increases, the CDD experiences an irreducible error-floor, while the MSDSD is capable of mitigating this error-floor. Secondly, in a relatively slow-fading environment, no obvious performance gain can be achieved by increasing the detection window size of the MSDSD, but in a relatively fast fading environment, a performance gain can be attained by expanding the window size.

DSTSK(2, 1, 2, 4, QPSK) associated with $R = 2$ bits/symbol

We also considered the hard-decision aided MSDSD for the DSTSK(2, 1, 2, 4, QPSK) system of Fig. 5.2 under the normalized Doppler frequencies of $f_d = 0.01$ and 0.03 . The system's normalized throughput is $R = 2$ bits/symbol. The corresponding achievable BER performance of the case $f_d = 0.01$ are depicted in Fig. 5.5, where it may be seen that firstly, unlike the case of the CDD aided DSTSK(2, 2, 2, 4, QPSK), the CDD aided DSTSK(2, 1, 2, 4, QPSK) experienced an error-

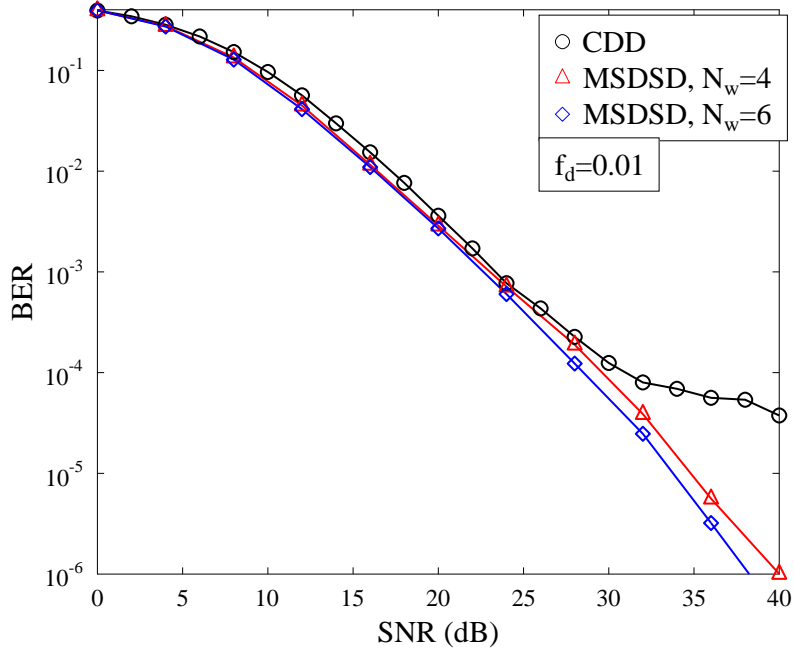


Figure 5.5: Achievable BER performance of the hard-decision aided MSDSD for the DSTSK(2, 1, 2, 4, QPSK) system of Fig. 5.2 under fading condition of $f_d = 0.01$, in comparison to that of the CDD aided DSTSK(2, 1, 2, 4, QPSK). The system's normalized throughput is $R = 2$ bits/symbol. All other system parameters were summarized in Table 5.1.

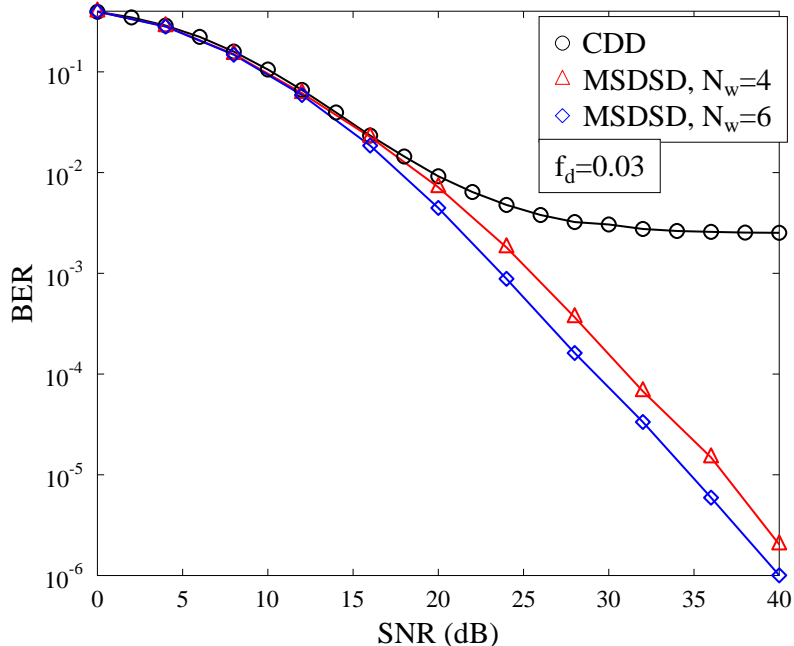


Figure 5.6: Achievable BER performance of the hard-decision aided MSDSD for the DSTSK(2, 1, 2, 4, QPSK) system of Fig. 5.2 under fading condition of $f_d = 0.03$, in comparison to that of the CDD aided DSTSK(2, 1, 2, 4, QPSK). The system's normalized throughput is $R = 2$ bits/symbol. All other system parameters were summarized in Table 5.1.

floor. This implies that increasing the number of receive antennas is capable of reducing the error-floor. Additionally, it may be seen from Fig. 5.5 that again, with the aid of MSDSD, the error-floor experienced by CDD may be mitigated. The achievable BER performance of the MSDSD aided DSTSK(2, 1, 2, 4, QPSK) under $f_d = 0.03$ are depicted in Fig. 5.6, where it may be seen that the error-floor of the CDD scheme tends to become higher upon increasing the normalized Doppler frequency, while the MSDSD only experiences a modest performance loss and no error-floor is observed.

5.2.4.2 Soft-Decision aided MSDSD for DSTSK

The achievable BER performance of the soft-decision MSDSD aided three-stage turbo coded DSTSK systems of Fig. 5.2 was investigated. An interleaver length of 10,000 bits was used by the three-stage serial-concatenated turbo encoder/decoder. The generator polynomials of the RSC encoder represented in a binary format were $G_{RSC} = [1, 0, 1]_2$ and $G_{RSC}^r = [1, 1, 1]_2$, while those of the URC encoder were $G_{URC} = [1, 0]_2$ and $G_{URC}^r = [1, 1]_2$. The numbers of inner iterations and outer iterations were $I_{in} = 2$ and $I_{out} = 4$. The system parameters of the soft-decision MSDSD aided three-stage turbo coded DSTSK scheme of Fig. 5.2 are summarized in Table 5.2.

Table 5.2: System parameters of the soft-decision MSDSD aided three-stage turbo coded DSTSK scheme of Fig. 5.2.

Number of Tx antennas	M
Number of Rx antennas	N
Symbol durations per block	T
Number of dispersion matrices	Q
Modulation	\mathcal{L} -PSK
Channels	Frequency-flat Rayleigh fading
Normalized Doppler frequency	f_d
Detector	MSDSD
Detection window size	N_w
Interleaver blocklength	10,000 bits
Outer channel code	Half-rate RSC
Generator polynomials	$(G_{RSC}^r, G_{RSC}) = (7, 5)_8$
Precoder	URC
Number of inner iterations	$I_{in} = 2$
Number of outer iterations	$I_{out} = 4$

We first considered the DSTSK(2, 2, 2, 4, QPSK) system of Fig. 5.2 associated with $f_d = 0.01$. The system's normalized throughput is $R = 2$ bits/symbol. The corresponding BER performance

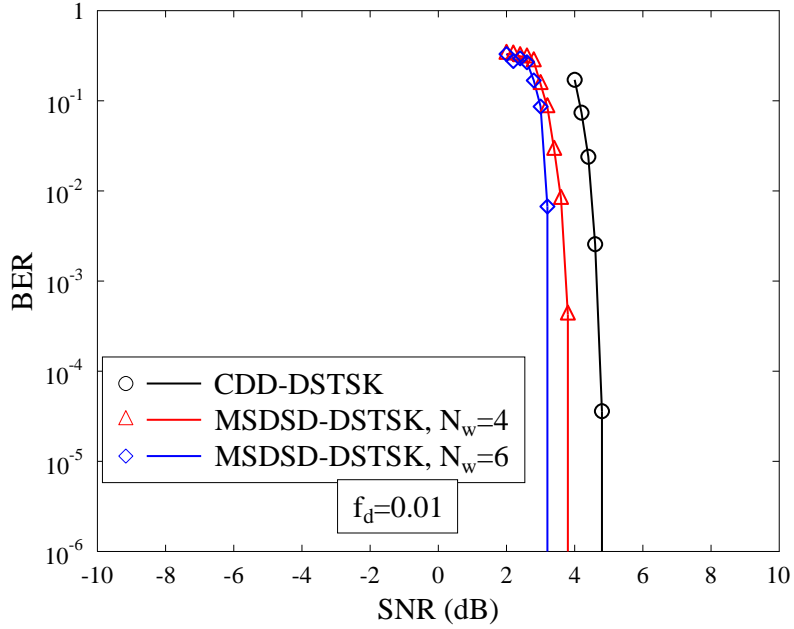


Figure 5.7: Achievable BER performance of the soft-decision MSDSD aided three-stage turbo coded DSTSK(2,2,2,4,QPSK) system of Fig. 5.2 under fading condition of $f_d = 0.01$. The system's normalized throughput is $R = 2$ bits/symbol. All other system parameters were summarized in Table 5.2.

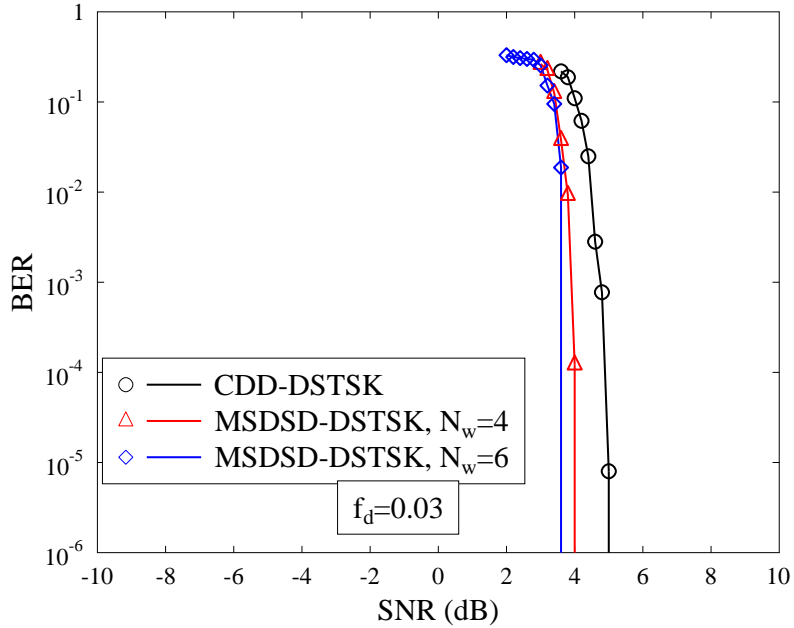


Figure 5.8: Achievable BER performance of the soft-decision MSDSD aided three-stage turbo coded DSTSK(2,2,2,4,QPSK) system of Fig. 5.2 under fading condition of $f_d = 0.03$. The system's normalized throughput is $R = 2$ bits/symbol. All other system parameters were summarized in Table 5.2.

is depicted in Fig. 5.7, where it can be seen that the MSDSD is capable of improving the performance of the DSTSK system relying on the CDD. For example, a “near-error-free” performance is achieved by the CDD at $\text{SNR} = 4.9$ dB, while the MSDSD associated a window size of $N_w = 4$ is

capable of achieving an infinitesimally low BER at $\text{SNR} = 3.9 \text{ dB}$. Moreover, it may also be seen that by employing the SISO-MSDSD and three-stage turbo coding scheme of Fig. 2.7, the BER performance of DSTSK is significantly improved, compared to the uncoded BER performance shown in Fig. 5.3. Additionally, we also considered the DSTSK(2, 2, 2, 4, QPSK) system associated with $f_d = 0.03$. Recall that $f_d = 0.03$ represents a relatively fast-fading environment, therefore an error-floor may exist in the case of CDD, as seen from the BER performance recorded for the uncoded DSTSK(2, 1, 2, 4, QPSK) shown in Fig. 5.4. By contrast, it may be observed from Fig. 5.8 that there is no visible error-floor, implying that the irreducible error-floor experienced by the CDD can be mitigated by employing the three-stage turbo codes architecture of Fig. 2.7.

5.3 DSTSK aided MUSRC System

In the previous section, we have introduced the MSDSD for DSTSK systems. It has also been mentioned previously that in cooperative communication systems, differential schemes are preferred since no CSI is required. Against this background, we propose a DSTSK aided and successive relaying assisted multi-user DF cooperative system. We employ low-complexity non-coherent detection, which does not require any CSI, neither at the RNs nor at the DN. Specifically, the SNs employ differentially encoded PSK modulation, while the RNs perform SISO-MSDSD based DF relaying during the relaying phase. Similarly, DSTSK transmission is employed at the RNs, which is detected with the aid of the SISO-MSDSD at the DN. More explicitly, three-stage serial-concatenated turbo encoding/decoding is employed throughout the system in order to enhance the attainable performance. Additionally, the MMBCS algorithm introduced in Section 2.3.5 of Chapter 2 is employed to select the optimal DSTSK configuration for supporting a specific number of users. Moreover, we adopt a successive relaying architecture for recovering the conventional 50% half-duplex relaying-induced throughput loss, at the cost of supporting less users.

5.3.1 System Model

Let us now focus on the system model of the proposed MUSRC system whose schematic is depicted in Fig. 5.9, where the two-phase relaying network consists of K SNs (users), $2N_r$ RNs and a DN. Due to the limited size of the shirt-pocket mobile devices, the SNs and RNs are all limited to have a single antenna. By contrast, the number of antenna elements at the DN depends on the configuration of the DSTSK scheme adopted. DS-CDMA is adopted as the multiple access technique [11]. Since two-phase successive relaying is employed, the number of VAAs in the network is $N_{VAA} = 2$. The number of RNs in each of the two VAA groups is $N_r = 2$.

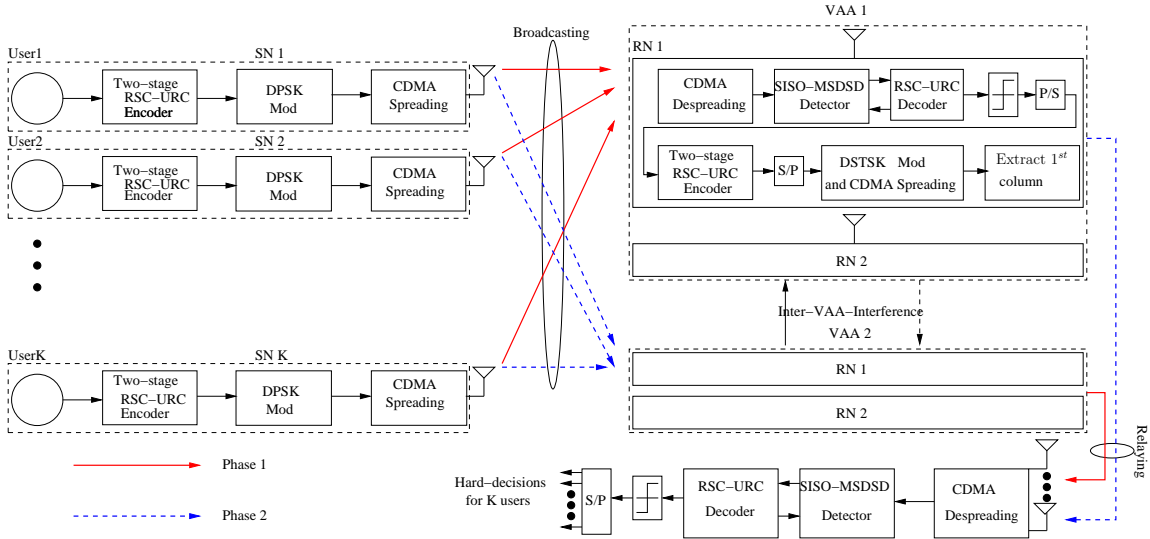


Figure 5.9: Block diagram of the DSTSK aided MUSRC system, which implements the two-phase successive relaying with the aid of two virtual antenna arrays. In this example, the number of RNs in each VAA is $N_r = 2$.

5.3.1.1 System Operation Overview

The operation of our MUSRC system is based on a two-phase (*Phase 1* and *Phase 2*) alternating principle, where each operating phase contains two concurrent transmissions referred to as broadcasting and relaying transmissions, which are outlined as follows.

1) Phase 1

The operation of *Phase 1* is represented in Fig. 5.9 by the solid-line arrows. During the broadcast phase, the information bits of each of the K SNs are firstly channel encoded by the two-stage serial-concatenated RSC-URC encoder of Fig. 5.10 at the SNs. The channel coded bits are mapped to the DPSK constellation symbols for generating K differentially encoded symbol sequences, which are spread by the K user-specific spreading codes. The CDMA-spread signals are transmitted from each of the K SNs to the first VAA (VAA1), which is formed by N_r RNs. At the RNs of VAA1, the signals received from the SNs are firstly de-spread, and then decoded by the three-stage serial-concatenated decoder of Fig. 5.10, generating the K decoded signals of the K users.

During the relaying transmission, the decoded users' signals, which are acquired from the most recent broadcast slot, are encoded by the two-stage RSC-URC encoder of Fig. 5.10 at the VAA2, which are further modulated by the DSTSK modulator before being spread by the VAA-specific spreading codes, and finally transmitted to the DN. At the DN, the signal received from the VAA2 is de-spread and then decoded by the three-stage serial-concatenated decoder of Fig. 5.10. Finally, the hard decisions are generated for the K users to complete *Phase 1*.

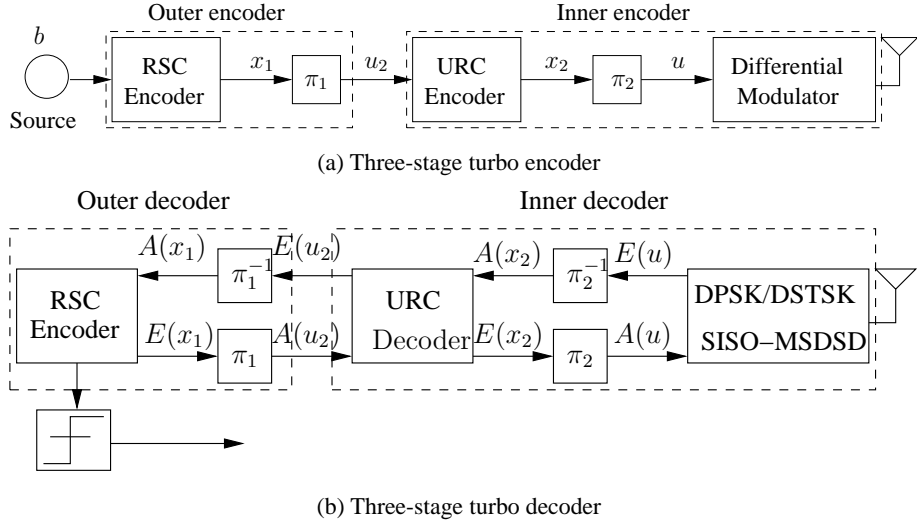


Figure 5.10: Structure of three-stage serial-concatenated turbo encoder/decoder.

2) Phase 2

The operations of *Phase 2* are depicted in Fig. 5.9 by the dashed-line arrows, which are exactly identical to those in *Phase 1*, except for the roles of the VAA1 and VAA2, which are swapped. More explicitly, in *Phase 2*, the VAA2 is in the broadcast mode, while the VAA1 is in the relaying transmission mode. In this way, the successive relaying becomes capable of recovering the conventional 50% throughput loss.

In order to suppress the successive relaying-induced Inter-VAA-Interference (IVI), the classic DS-CDMA technique is adopted at the RNs, where each VAA is assigned a specific spreading code, which implies that N_{VAA} spreading codes will be adopted by the VAAs in the network. As a result, the number of users supported is reduced by N_{VAA} , albeit in reality only the users roaming at the cell-edge will rely on relaying.

5.3.1.2 Relay Architecture Overview

We assume that the proposed MUSRC has a symmetric topology as illustrated in Fig. 5.11. By exploiting the fact that the RNs in each VAA are geometrically close to each other, and the distances between them are significantly smaller than the distances from the SNs to RNs and from the RNs to DN, we can reasonably assume that the distances from the SNs to the RNs in a VAA are equal and the distances spanning from the RNs in a VAA to the DN are also equal, which are denoted as D_{sr} and D_{rd} , respectively. Then the average path-loss reduction of the source-to-relay (SR) links and relay-to-destination (RD) links can be expressed as

$$G_{sr} = \left(\frac{D_{sd}}{D_{sr}} \right)^\alpha \quad \text{and} \quad G_{rd} = \left(\frac{D_{sd}}{D_{rd}} \right)^\alpha,$$

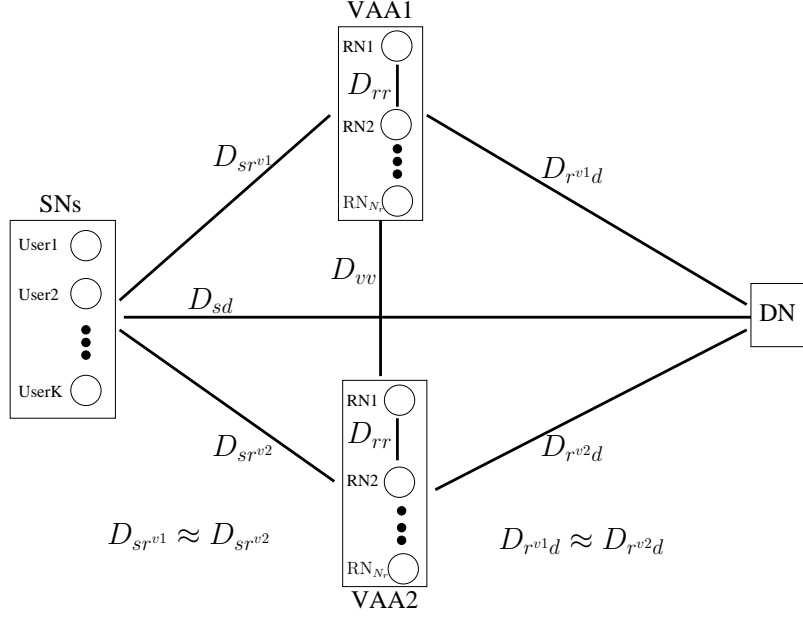


Figure 5.11: Topology of the proposed MUSRC system. The system is symmetric in the sense that the distance from the SNs to the VAA1 is approximately equal to the distance from the SNs to the VAA2, while the distance between the VAA1 and the DN is approximately equal to the distance between the VAA2 and the DN.

respectively, where D_{sd} is the distance between the SNs and DN, which is normalized to unity. Additionally, the average path-loss reduction between the two VAAs is denoted as

$$G_{vv} = \left(\frac{D_{sd}}{D_{vv}} \right)^\alpha,$$

where D_{vv} is the distance between the two VAAs. Throughout this paper, the path-loss exponent is given by $\alpha = 3$, which represents a typical urban area. Naturally, the above assumptions do not affect the general applicability of our analysis.

Since the direct signals transmitted from the SNs to the DN are attenuated by the pathloss, especially in high-carrier-frequency mobile broadband systems, such as millimetre-wave communication and free-space optical mobile systems [164, 165], we only consider the SR and RD transmissions. For the SR transmission, we adopt the DPSK signalling (e.g. DBPSK and DQPSK), while for the RD transmission, we adopt the DSTSK($N_r, N, T, Q, \mathcal{L}$) system associated with $N_r = T$. Naturally, increasing T improves the achievable BER performance at the cost of reducing the system throughput, while imposing a higher complexity in forming a VAA [5]. Having a higher complexity is due to the fact that, since $N_r = T$, the designer has to choose more RNs and the synchronisation of the RNs also becomes more of a challenge. Therefore, we limit the number of the time slots to $T = 2$ and mainly consider two configurations, namely, the DSTSK(2, 1, 2, Q, \mathcal{L}) and DSTSK(2, 2, 2, Q, \mathcal{L}), associated with $N = 1$ and $N = 2$ receive antennas at the DN, respectively.

Since no CSI is required by our MUSRC, no CSI is available for selecting RNs. Hence the selection of RNs can only be based on their geometric location information [117]. Referring to

Fig. 5.11, let us now discuss how to select the RNs and how to arrange the selected RNs into the two VAAs, based on the RNs' geometric location information. It is plausible that having a symmetric topology as illustrated in Fig. 5.11 is reasonable, because the two VAAs may be treated identically. In this symmetric topology, we can denote the distance from the SNs to each of the two VAAs as D_{sr} , while denoting the distance between each of the two VAAs and the DN as D_{rd} . In order to benefit from collaborative relaying, we have

$$D_{sr} < D_{sd} \text{ and } D_{rd} < D_{sd}. \quad (5.25)$$

The distance between any pair of RNs in a VAA, which is denoted as D_{rr} , satisfies

$$D_{rr} \ll D_{sr} \text{ and } D_{rr} \ll D_{rd}. \quad (5.26)$$

Furthermore, we should have $D_{rr} \geq 10 \times \lambda$, where λ is the carrier's wavelength, in order to ensure that we fully exploit the spatial diversity, but this condition is usually automatically met for the mobile relays. Regarding how to divide the selected RNs into two VAAs, we note that the distance between the two VAAs, which is denoted as D_{vv} , should be sufficiently large, so that the inter-VAA interference is minimised. On the other hand, D_{vv} should not be excessive so that the condition Eq. (5.25) is satisfied. Lastly, the question arises, whether we should place a VAA closer to the SNs or closer to the DN. Since the RD links employ DSTSK, which has an inherent diversity capability and it is more powerful than the DPSK scheme employed by the SR links, therefore, we may appoint a VAA closer to the SNs, for the sake of achieving a balance of performance for the SR and RD links. This would also mitigate the error propagation inflicted by the DF scheme. More explicitly, we arrange for

$$D_{sr} < D_{rd}. \quad (5.27)$$

Let us now detail the operations involved in SNs, RNs and DN.

5.3.1.3 Source Nodes

During the broadcast interval, the information bit sequence \mathbf{b}^k of the k^{th} user is encoded by the two-stage serial-concatenated channel encoder of Fig. 5.10, and the encoded bit sequence \mathbf{u}^k is mapped to a PSK symbol sequence $\mathbf{x}^k = \{x_n^k\}$, which is then differentially encoded according to

$$s_n^k = \begin{cases} 1, & n = 0, \\ x_n^k \cdot s_{n-1}^k, & n > 0. \end{cases} \quad (5.28)$$

The system employs a set of spreading codes $\{\mathbf{c}^k\}_{k=1}^{K+N_{VAA}}$, each having a spreading factor of L_s , where $N_{VAA} = 2$ is the number of VAAs. The first K spreading codes are used for supporting the K users, and the spreading operation at the k^{th} SN is expressed as

$$\mathbf{e}_n^k = \frac{1}{\sqrt{L_s}} s_n^k \mathbf{c}^k, \quad 1 \leq k \leq K. \quad (5.29)$$

5.3.1.4 Relay Nodes

We assume that the CDMA up-link is synchronized, so that all the signals arrive at a RN with the same delay and hence the near-zero cross-correlation property of the DS-CDMA system may be exploited for reducing the multi-user interference (MUI). Additionally, the Rayleigh fading channel is considered to be quasi-static, yielding a constant fading envelope and phase within an L_s -chip transmission period. Let the two VAAs be denoted by V_1 and V_2 , respectively. In the sequel, column vector based notation will be adopted.

1) Decoding

The signal received at the m^{th} RN of the VAA V_1 may be expressed as

$$\mathbf{y}_{nV_1}^m = \sqrt{G_{sr}} \sum_{k=1}^K \mathbf{e}_n^k h_{nV_1}^{km} + \sqrt{G_{vv}} \{ \text{first-}L_s\text{-elements} (\mathbf{P}_{V_2} \mathbf{H}_{V_2}^m) \} + \bar{\mathbf{v}}_{nV_1}^m, \quad (5.30)$$

where $\mathbf{y}_{nV_1}^m \in \mathbb{C}^{L_s \times 1}$, $h_{nV_1}^{km} \in \mathbb{C}$ is the n^{th} Rayleigh distributed channel coefficient between the k^{th} SN and the m^{th} RN of the VAA V_1 , while $\mathbf{P}_{V_2} \in \mathbb{C}^{TL_s \times N_r}$ is the received CDMA-spread DSTSK signal block from the VAA V_2 . Furthermore, $\mathbf{H}_{V_2}^m \in \mathbb{C}^{N_r \times 1}$ is the equivalent channel matrix between the VAA V_2 and the m^{th} RN of the VAA V_1 , while $\bar{\mathbf{v}}_{nV_1}^m \in \mathbb{C}^{L_s \times 1}$ is the equivalent AWGN vector. De-spreading $\mathbf{y}_{nV_1}^m$ for the k^{th} user yields

$$\begin{aligned} r_{nV_1}^{km} &= \frac{\sqrt{G_{sr}}}{\sqrt{L_s}} (\mathbf{c}^k)^T \mathbf{y}_{nV_1}^m \\ &= \frac{\sqrt{G_{sr}}}{\sqrt{L_s}} (\mathbf{c}^k)^T \mathbf{e}_n^k h_{nV_1}^{km} + \eta_{nV_1}^{km} + \bar{\mathbf{v}}_{nV_1}^{km} \\ &= \sqrt{G_{sr}} s_n^k h_{nV_1}^{km} + \eta_{nV_1}^{km} + \bar{\mathbf{v}}_{nV_1}^{km}, \end{aligned} \quad (5.31)$$

where $\eta_{nV_1}^{km}$ denotes the MUI and IVI term, which may be substantially reduced as a benefit of the near-orthogonality of the spreading code family employed [11], and $\bar{\mathbf{v}}_{nV_1}^{km}$ is the noise term having a zero mean and a variance of $N_0/2$ per dimension. When considering a detection window of N_w received samples, Eq. (5.31) may be expressed as

$$\mathbf{r} = \sqrt{G_{sr}} \text{diag}\{\mathbf{s}\} \mathbf{h} + \mathbf{v} = \sqrt{G_{sr}} \mathbf{S} \mathbf{h} + \mathbf{v}, \quad (5.32)$$

where $\mathbf{r} = [r_{nV_1}^{km} \ r_{(n-1)V_1}^{km} \ \dots \ r_{(n-N_w+1)V_1}^{km}]^T$ includes the N_w consecutive signals received within the detection window of N_w samples, $\mathbf{s} = [s_n^k \ s_{n-1}^k \ \dots \ s_{n-N_w+1}^k]^T$ is the corresponding differentially encoded symbol vector, and $\mathbf{S} = \text{diag}\{\mathbf{s}\}$, while $\mathbf{h} \in \mathbb{C}^{N_w \times 1}$ is the Rayleigh fading channel vector and $\mathbf{v} \in \mathbb{C}^{N_w \times 1}$ the AWGN vector. Note that \mathbf{S} is a unitary matrix, and any small residual MUI and IVI term in Eq. (5.31) is assumed to be included in \mathbf{v} . For notational simplification, we omit the user index k in the sequel.

The SISO-MSDSD is based on the Log-MAP algorithm [1], where given the window size of N_w , the multiple-symbol decisions for $x_n, x_{n-1}, \dots, x_{n-N_w+2}$ depend on the conditional probabil-

ity density function (PDF) $p(\mathbf{r}|\mathbf{s})$, which satisfies the following relation [99]

$$-\ln(p(\mathbf{r}|\mathbf{s})) \propto \mathbf{r}^H \mathbf{R}_{rr}^{-1} \mathbf{r}. \quad (5.33)$$

Define the channel's correlation matrix as $\mathbf{R}_{hh} = \mathbb{E}\{\mathbf{h}\mathbf{h}^H\}$, the noise correlation matrix as $\mathbf{R}_{vv} = \mathbb{E}\{\mathbf{v}\mathbf{v}^H\}$ and the combined correlation matrix $\mathbf{C} = \mathbf{R}_{hh} + \frac{1}{G_{sr}}\mathbf{R}_{vv}$. Then the power normalized conditional correlation matrix \mathbf{R}_{rr} of the received signal vector \mathbf{r} in Eq. (5.33) is given by

$$\mathbf{R}_{rr} = \frac{1}{G_{sr}} \mathbb{E}\{\mathbf{r}\mathbf{r}^H\} = \mathbf{S}\mathbf{R}_{hh}\mathbf{S}^H + \frac{1}{G_{sr}}\mathbf{R}_{vv} = \mathbf{S}\mathbf{C}\mathbf{S}^H. \quad (5.34)$$

Upon applying the Cholesky factorisation, we have $\mathbf{C}^{-1} = \mathbf{L}\mathbf{L}^H$, where \mathbf{L} is a lower triangular matrix. By defining the upper triangular matrix of

$$\mathbf{U} = \left(\frac{1}{\sqrt{G_{sr}}} \mathbf{L}^H \text{diag}\{\mathbf{r}\} \right)^*, \quad (5.35)$$

we arrive at

$$-\ln(p(\mathbf{r}|\mathbf{s})) \propto \|\mathbf{U}\mathbf{s}\|^2. \quad (5.36)$$

Note that the common phase shift s_{n-N_w+1} in all the first $N_w - 1$ elements of the differential symbol vector \mathbf{s} has no effect on the ML metric of Eq. (5.36). If we define the accumulated differential symbol as [166]

$$\begin{aligned} a_i &= s_{(n+1)-i} \cdot s_{(n+1)-N_w}^* = \begin{cases} \prod_{j=i}^{N_w-1} x_{(n+1)-j}, & 1 \leq i \leq N_w - 1, \\ 1, & i = N_w, \end{cases} \\ &= \begin{cases} x_{(n+1)-i} \cdot a_{i+1}, & 1 \leq i \leq N_w - 1, \\ 1, & i = N_w, \end{cases} \end{aligned} \quad (5.37)$$

the following relationship is obtained

$$-\ln(p(\mathbf{r}|\mathbf{s})) \propto \|\mathbf{U}\mathbf{a}\|^2, \quad (5.38)$$

where $\mathbf{a} = [a_1 \ a_2 \ \dots \ a_{N_w-1} \ a_{N_w}]^T$ is the accumulated differential symbol vector. Sphere Decoding (SD) examines the set of candidates $\{x_{(n+1)-j}\}_{j=1}^{N_w-1}$ that lie within the decoding sphere radius R , i.e. within

$$\|\mathbf{U}\mathbf{a}\|^2 \leq R^2. \quad (5.39)$$

The SISO-MSDSD accepts the *a priori* soft information from the URC decoder of Fig. 5.10 and produces the corresponding soft outputs. Assuming that the symbols $\{x_{(n+1)-j}\}_{j=1}^{N_w-1}$ are independent, their *a priori* information may be expressed as

$$\ln(\Pr\{\mathbf{a}\}) = \sum_{j=1}^{N_w-1} \ln(\Pr\{x_{(n+1)-j}\}). \quad (5.40)$$

By defining

$$\mathbf{U} = \begin{bmatrix} u_{1,1} & u_{1,2} & \cdots & u_{1,N_w} \\ 0 & u_{2,2} & \cdots & u_{2,N_w} \\ \vdots & \ddots & \ddots & \vdots \\ 0 & \cdots & 0 & u_{N_w,N_w} \end{bmatrix}. \quad (5.41)$$

we may further modify Eq. (5.39) to yield:

$$\|\mathbf{U}\mathbf{a}\|^2 - \ln(\Pr\{\mathbf{a}\}) = \sum_{j=1}^{N_w-1} \left(\left| \sum_{l=j}^{N_w-1} u_{j,l} a_l \right|^2 - \ln(\Pr\{x_{(n+1)-j}\}) \right) \leq R^2. \quad (5.42)$$

The partial-Euclidean-distance (PED) contribution is then defined as

$$d_i^2 = \sum_{j=i}^{N_w-1} \left(\left| \sum_{l=j}^{N_w-1} u_{j,l} a_l \right|^2 - \ln(\Pr\{x_{(n+1)-j}\}) \right) = d_{i+1}^2 + \Delta_i^2, \quad (5.43)$$

where the PED increment is expressed as

$$\Delta_i^2 = \left| u_{i,i} a_{i+1} x_{(n+1)-i} + \sum_{l=i+1}^{N_w-1} u_{i,l} a_l \right|^2 - \ln(\Pr\{x_{(n+1)-i}\}). \quad (5.44)$$

The *a posteriori* probability of the bit of interest b_n can then be calculated by the Max-Log-MAP algorithm [1], which is expressed as

$$\begin{aligned} L_p(b_n|\mathbf{r}) &= \ln \left(\frac{\Pr\{b_n = 1|\mathbf{r}\}}{\Pr\{b_n = 0|\mathbf{r}\}} \right) \\ &\approx -\|\mathbf{U}\mathbf{a}_{MAP}^{b_n=1}\|^2 + \ln(\Pr\{x_{MAP}^{b_n=1}\}) + \|\mathbf{U}\mathbf{a}_{MAP}^{b_n=0}\|^2 - \ln(\Pr\{x_{MAP}^{b_n=0}\}) \\ &= d_{MAP}^{b_n=1} - d_{MAP}^{b_n=0}, \end{aligned} \quad (5.45)$$

where the subscript MAP indicates the MAP solution obtained by the SD, while the superscripts $b_n=1$ and $b_n=0$ indicate the associated solutions obtained with the bit of interest b_n set to 1 and 0, respectively. Furthermore, $d_{MAP}^{b_n=1}$ and $d_{MAP}^{b_n=0}$ denotes the minimum PEDs estimated by the SD when the bit of interest b_n is set to 1 and 0, respectively.

The *extrinsic* information of b_n may be calculated by subtracting the *a priori* information of Eq. (5.40) from the *a posteriori* probability of Eq. (5.45), which can then be fed to the URC decoder to form an decoding inner loop, as portrayed in Fig. 5.10. Finally, after the termination of the three-stage MSDSD-URC-RSC turbo decoding process depicted in Fig. 5.10, the hard-decision outputs of the three-stage turbo decoder recover the bit sequences of the K users at the m^{th} RN, each having the length L_f , to form the decision matrix $\widehat{\mathbf{B}}^m = [\widehat{\mathbf{b}}^{1m} \widehat{\mathbf{b}}^{2m} \cdots \widehat{\mathbf{b}}^{Km}]$, where $m \in \{1, \dots, N_r\}$ in our system. The details of the three-stage turbo decoding process can be found in [1].

2) Forwarding

In order to perform the three-stage serial-concatenated RSC-URC-DSTSK encoding, as illustrated in Fig. 5.10, the decision matrix $\widehat{\mathbf{B}}^m \in \mathbb{C}^{L_f \times K}$ is firstly parallel-to-serial (P/S) converted to form

the decision vector $\hat{\mathbf{b}}_{vec}^m \in \mathbb{C}^{KL_f \times 1}$. Then this decision vector is encoded by the half-rate RSC-URC encoder to generate a coded sequence $\hat{\mathbf{u}}^m \in \mathbb{C}^{2KL_f \times 1}$, which is then serial-to-parallel (S/P) converted to the coded matrix $\hat{\mathbf{U}}^m \in \mathbb{C}^{2L_f \times K}$ and then transmitted by the DSTSK modulator [124].

In order to support K users, the number of bits conveyed by each DSTSK signal block and the number of users have to meet the following condition

$$K = \log_2(Q) + \log_2(\mathcal{L}), \quad (5.46)$$

where $\log_2(Q)$ bits are used for choosing a specific dispersion matrix $\mathbf{A}_n \in \mathbb{C}^{T \times N_r}$ from the set of Q dispersion matrices and $\log_2(\mathcal{L})$ bits are adopted to unambiguously represent a specific constellation point s_n of the conventional \mathcal{L} -PSK modulation scheme. To elaborate a little further, supporting different numbers of users can be realized by appropriately modifying the values of Q and \mathcal{L} , without changing the system configuration. For example, we may have $Q = 2$ and $\mathcal{L} = 2$ for a system supporting $K = 2$ users, while we may opt for the values of $Q = 4$ and $\mathcal{L} = 4$ for supporting $K = 4$ users. Additionally, given a specific number of users, various combinations of Q and \mathcal{L} may be used, provided that the relation Eq. (5.46) is satisfied, which are summarised in Table 5.3 for different values of K . The most beneficial DSTSK combination selection is detailed in Section 5.3.2.

After obtaining the dispersion matrix \mathbf{A}_n and the corresponding conventional \mathcal{L} -PSK symbol s_n , the DSTSK signal block is generated as

$$\mathbf{X}_n^m = s_n \mathbf{A}_n. \quad (5.47)$$

The number of transmit antennas and the number of time slots should be identical for the DSTSK scheme [5], i.e. $N_r = T$. With this constraint, the DSTSK symbol block is given by

$$\mathbf{S}_n^m = \begin{cases} \mathbf{I}_T, & n = 0, \\ \mathbf{X}_n^m \mathbf{S}_{n-1}^m, & n > 0, \end{cases} \quad (5.48)$$

which is spread by the spreading code \mathbf{c}_{V_1} of the VAA V_1 to yield

$$\mathbf{P}_{V_1}^m = \frac{1}{\sqrt{L_s}} \mathbf{S}_n^m \otimes \mathbf{c}_{V_1}, \quad (5.49)$$

where the spread DSTSK signal block obeys $\mathbf{P}_{V_1}^m \in \mathbb{C}^{TL_s \times N_r}$. Since in our proposed MUSRC system N_r RNs form a VAA, if we denote the equivalent signal block transmitted by the VAA V_1 to the DN as $\mathbf{P}_{V_1} \in \mathbb{C}^{TL_s \times N_r}$, then the m^{th} column of \mathbf{P}_{V_1} is contributed by the m^{th} column of $\mathbf{P}_{V_1}^m$. To be more specific, the m^{th} column of $\mathbf{P}_{V_1}^m$ is transmitted by the corresponding m^{th} RN to the DN. This corresponds to the system block diagram shown in Fig. 5.9, where for example, the first RN in the VAA1 extracts and transmits the first column of the DSTSK modulated and spread signal block matrix formulated in Eq. (5.49). Note that the allocation of the total transmission power to the RNs in a VAA is performed automatically. This is because every dispersion matrix \mathbf{A}_n is designed to have the same constant power [5] and, therefore, every equivalent signal matrix \mathbf{P}_{V_1} has the same constant power. Since the m^{th} RN transmits the m^{th} column of \mathbf{P}_{V_1} , where $1 \leq m \leq N_r$, the transmit powers of all the N_r RNs add up to the total transmit power.

5.3.1.5 Destination Node

All the RNs are assumed to be perfectly synchronized, implying that during the T time slots, the N_r RNs in a specific VAA group transmit their signal blocks simultaneously. Furthermore, the Rayleigh fading channel is assumed to be quasi-static so that the fading envelope and phase remain constant within the time duration of $L_s T$. The de-spread signal block received at the DN with the aid of N receive antennas over T time slots may be expressed as [5]

$$\mathbf{R}_n = \sqrt{G_{rd}} \mathbf{S}_n \mathbf{H}_n + \mathbf{V}_n, \quad (5.50)$$

where $\mathbf{R}_n \in \mathbb{C}^{T \times N}$, and $\mathbf{S}_n \in \mathbb{C}^{T \times N_r}$ is the equivalent differential signal block received from the transmitting VAA, whose m^{th} column is identical to the m^{th} column of \mathbf{S}_n^m , while $\mathbf{H}_n \in \mathbb{C}^{N_r \times N}$ denotes the fading channel matrix between the transmitting VAA and the DN, while $\mathbf{V}_n \in \mathbb{C}^{T \times N}$ is the corresponding AWGN matrix. Note the “similarity” between Eq. (5.50) and Eq. (5.31), where the scalar elements in Eq. (5.31) are replaced by matrices in Eq. (5.50). Unlike Eq. (5.31), however, there exists no MUI or IVI in Eq. (5.50). Note that Eq. (5.50) has the same form of Eq. (5.3).

Similar to the RNs, the three-stage MSDSD-URC-RSC turbo decoder detects the signal blocks received at the DN. More explicitly, the URC and RSC decoders of Fig. 5.10 used at the DN are exactly identical to the ones employed in the RNs, while the SISO-MSDSD of the RNs is extended for detecting the DSTSK signal blocks. In particular, over the N_w DSTSK signal blocks, Eq. (5.50) can be expressed as

$$\overline{\mathbf{R}} = \sqrt{G_{rd}} \overline{\mathbf{S}} \overline{\mathbf{H}} + \overline{\mathbf{V}}, \quad (5.51)$$

where we have $\overline{\mathbf{R}} = [\mathbf{R}_n^T \mathbf{R}_{n-1}^T \cdots \mathbf{R}_{n-N_w+1}^T]^T$, $\overline{\mathbf{S}} = \text{diag}\{\mathbf{S}_n, \mathbf{S}_{n-1}, \dots, \mathbf{S}_{n-N_w+1}\}$, $\overline{\mathbf{H}} = [\mathbf{H}_n^T \mathbf{H}_{n-1}^T \cdots \mathbf{H}_{n-N_w+1}^T]^T$ and $\overline{\mathbf{V}} = [\mathbf{V}_n^T \mathbf{V}_{n-1}^T \cdots \mathbf{V}_{n-N_w+1}^T]^T$. Then the MSDSD for DSTSK systems introduced in Section 5.2 may be invoked for generating the bit decisions for the K users.

5.3.2 DSTSK Configuration Selection

It has been demonstrated in Section 2.3.5 of Chapter 2 that the choice of the number of dispersion matrices Q and the conventional PSK constellation size \mathcal{L} is important for achieving a fixed throughput. Therefore, the MMBCS algorithm was proposed. Similarly, in our proposed DSTSK aided MUSRC scheme, the novel MMBCS algorithm may also be invoked for selecting the optimal combination of Q and \mathcal{L} .

It has been mentioned in Section 5.3.1.4 that the proposed MUSRC system is capable of supporting the same number of users by different DSTSK configurations. To be more explicit, according to Eq. (5.46), for a given number of users K , we may opt for different combinations of Q and \mathcal{L} . For example, if we have $K = 4$ users, the possible combinations of Q and \mathcal{L} are $(Q, \mathcal{L}) = (2, 8)$, $(Q, \mathcal{L}) = (4, 4)$ and $(Q, \mathcal{L}) = (8, 2)$. Detailed DSTSK configuration list is shown in Table 5.3. Since different configurations (Q, \mathcal{L}) for the same number of users K may

Table 5.3: Combinations of Q and \mathcal{L} for supporting different numbers of users K and the corresponding lower bound complexity N_c [98] associated with $N_w = 4$, DBPSK at SNs and $N = 1$ receive antenna at DN.

$K = 2$	$K = 3$	$K = 4$	$K = 5$
$Q = 2, \mathcal{L} = 2$ ($N_c = 180$)	$Q = 2, \mathcal{L} = 4$ ($N_c = 200$)	$Q = 2, \mathcal{L} = 8$ ($N_c = 250$)	$Q = 2, \mathcal{L} = 16$ ($N_c = 360$)
N/A	$Q = 4, \mathcal{L} = 2$ ($N_c = 200$)	$Q = 4, \mathcal{L} = 4$ ($N_c = 250$)	$Q = 4, \mathcal{L} = 8$ ($N_c = 360$)
N/A	N/A	$Q = 8, \mathcal{L} = 2$ ($N_c = 250$)	$Q = 8, \mathcal{L} = 4$ ($N_c = 360$)
N/A	N/A	N/A	$Q = 16, \mathcal{L} = 2$ ($N_c = 360$)

have different $d_{\max-\min}(Q, \mathcal{L})$, the resultant BERs may be different as well. The most appropriate DSTSK configuration is obviously the one that yields the lowest BER. The maximum minimum-determinant values of $d_{\max-\min}(Q, \mathcal{L})$ for various DSTSK configurations (Q, \mathcal{L}) are listed in Table 5.4 for the system with the DBPSK at the SNs and $N = 1$ receive antenna at the DN as well as for the system with the DQPSK system at the SNs and $N = 2$ receive antennas at the DN. Then according to the MMBCS algorithm, we arrive at the optimal DSTSK configurations $(Q_{\text{opt}}, \mathcal{L}_{\text{opt}})$ to support various number of users K , which are summarized in Table 5.5. In the following simulation study, we will demonstrate that the most appropriate DSTSK configuration selected by our proposed MMBCS algorithm is capable of outperforming other DSTSK configurations, in terms of their maximum achievable rate.

5.3.3 Simulation Results

A Rayleigh fading environment having a normalized Doppler frequency $f_d = 0.01$ was considered, and an interleaver length of 10,000 bits was used by the three-stage serial-concatenated turbo encoder/decoder. The generator polynomials of the RSC encoder were $G_{\text{RSC}} = [1, 0, 1]_2$ and $G'_{\text{RSC}} = [1, 1, 1]_2$, while the generator polynomials of the URC encoder were $G_{\text{URC}} = [1, 0]_2$ and $G'_{\text{URC}} = [1, 1]_2$, where G'_{RSC} and G'_{URC} are the feedback polynomials of the RSC and URC encoders, respectively. The numbers of inner iterations and outer iterations were $I_{\text{in}} = 2$ and $I_{\text{out}} = 4$, respectively. Unless otherwise stated², the distance between the two VAAs was $D_{vv} = \frac{1}{4}$. $N_r = 2$ RNs were employed in each of the two VAA groups, leading to a total of $2N_r = 4$ relays. Since the transmit signal powers of all the simulated systems (SNs to RNs and RNs to DN) were normalized to unity, the equivalent SNR of the overall system was defined as $\frac{1}{N_0}$, with N_0 being the equivalent

²Normally, the closer the two VAAs, the stronger IVI and the poorer the achievable system performance.

Table 5.4: The maximum minimum-determinant $d_{\max-\min}(Q, \mathcal{L})$ for different combinations of (Q, \mathcal{L}) for the system with the DBPSK at the SNs and $N = 1$ receive antenna at the DN as well as for the system with the DQPSK system at the SNs and $N = 2$ receive antennas at the DN.

DBPSK at SNs and $N = 1$ receive antenna at DN				
	$Q = 2$	$Q = 4$	$Q = 8$	$Q = 16$
$\mathcal{L} = 2$	$d_{\max-\min}(2, 2) = 1.99846$	$d_{\max-\min}(4, 2) = 1.41065$	$d_{\max-\min}(8, 2) = 0.47171$	$d_{\max-\min}(16, 2) = 0.092138$
$\mathcal{L} = 4$	$d_{\max-\min}(2, 4) = 1.21914$	$d_{\max-\min}(4, 4) = 0.75919$	$d_{\max-\min}(8, 4) = 0.21126$	N/A
$\mathcal{L} = 8$	$d_{\max-\min}(2, 8) = 0.58578$	$d_{\max-\min}(4, 8) = 0.40317$	N/A	N/A
$\mathcal{L} = 16$	$d_{\max-\min}(2, 16) = 0.15224$	N/A	N/A	N/A
DQPSK at SNs and $N = 2$ receive antennas at DN				
	$Q = 2$	$Q = 4$	$Q = 8$	$Q = 16$
$\mathcal{L} = 2$	$d_{\max-\min}(2, 2) = 1.99822$	$d_{\max-\min}(4, 2) = 1.41172$	$d_{\max-\min}(8, 2) = 0.42625$	$d_{\max-\min}(16, 2) = 0.10477$
$\mathcal{L} = 4$	$d_{\max-\min}(2, 4) = 1.36047$	$d_{\max-\min}(4, 4) = 0.80871$	$d_{\max-\min}(8, 4) = 0.20731$	N/A
$\mathcal{L} = 8$	$d_{\max-\min}(2, 8) = 0.58579$	$d_{\max-\min}(4, 8) = 0.42085$	N/A	N/A
$\mathcal{L} = 16$	$d_{\max-\min}(2, 16) = 0.15224$	N/A	N/A	N/A

Table 5.5: Optimal combinations $(Q_{\text{opt}}, \mathcal{L}_{\text{opt}})$ for supporting different numbers of users K , associated with DBPSK or DQPSK at SNs and $N = 1$ or 2 receive antennas at DN.

$K = 2$	$K = 3$	$K = 4$	$K = 5$
$(Q_{\text{opt}}, \mathcal{L}_{\text{opt}}) = (2, 2)$	$(Q_{\text{opt}}, \mathcal{L}_{\text{opt}}) = (4, 2)$	$(Q_{\text{opt}}, \mathcal{L}_{\text{opt}}) = (4, 4)$	$(Q_{\text{opt}}, \mathcal{L}_{\text{opt}}) = (4, 8)$

system's AWGN power. Taking into account the path losses in Eqs. (5.31) and (5.50), the noise power at a RN was set to N_0/G_{sr} while the noise power at the DN was given by N_0/G_{rd} . The set of $(K + 2)$ non-orthogonal random codes with the spreading factor $L_s = 256$ was used to support multiple K users and the two VAAs. The system parameters of the three-stage turbo coded DSTSK aided MUSRC system of Fig. 5.9 are summarized in Table 5.6.

Table 5.6: System parameters of the three-stage turbo coded DSTSK aided MUSRC system of Fig. 5.9.

Number of RNs in a VAA	N_r
Number of Rx antennas	N
Symbol durations per block	$T = N_r$
Number of dispersion matrices	Q
Distance between two VAAs	D_{vv}
Distance between SN and RNs	D_{sr}
Spreading factor	$L_s = 256$
Number of users	K
Modulation	\mathcal{L} -PSK
Channels	Frequency-flat Rayleigh fading
Normalized Doppler frequency	$f_d = 0.01$
Detector	MSDSD
Detection window size	N_w
Interleaver blocklength	10,000 bits
Outer channel code	Half-rate RSC
Generator polynomials	$(G_{RSC}^r, G_{RSC}) = (7, 5)_8$
Precoder	URC
Number of inner iterations	$I_{in} = 2$
Number of outer iterations	$I_{out} = 4$

5.3.3.1 DBPSK for SR transmission and DSTSK($2, 1, 2, Q, \mathcal{L}$) for RD transmission

We first considered the proposed DSTSK aided MUSRC system of Fig. 5.9 employing DBPSK for the SR transmission and a DSTSK scheme of DSTSK($2, 1, 2, Q, \mathcal{L}$) for the RD transmission, associated with $N_r = 2$ relays in each of the two VAA groups and a DN equipped with $N = 1$ receive antenna. Various number of Q dispersion matrices and \mathcal{L} -PSK constellations may be adopted by the DSTSK scheme at the RNs, depending on the number of users K , as listed in Table 5.3. The most appropriate or optimal combination $(Q_{\text{opt}}, \mathcal{L}_{\text{opt}})$ can be determined using the proposed MMBCS algorithm as presented in Section 5.3.2. The optimal combinations $(Q_{\text{opt}}, \mathcal{L}_{\text{opt}})$ corresponding to various K can be found in Table 5.5. Therefore, we commenced our investigations with the aid of the maximum achievable rate to verify the facts that the different combinations of (Q, \mathcal{L}) lead to different system performances and the optimal combination $(Q_{\text{opt}}, \mathcal{L}_{\text{opt}})$ found by the MMBCS algorithm indeed offers the optimal performance. The simulation results obtained are shown in Fig. 5.12, where the DSTSK aided MUSRC systems supporting $K \in \{3, 4\}$ users were considered, in conjunction with an MSDSD window size of $N_w = 4$. The normalized source-to-relay distance was chosen as $D_{sr} = 0.51$, which will be shown to be the optimal distance for the system configurations used in this example later in this section.

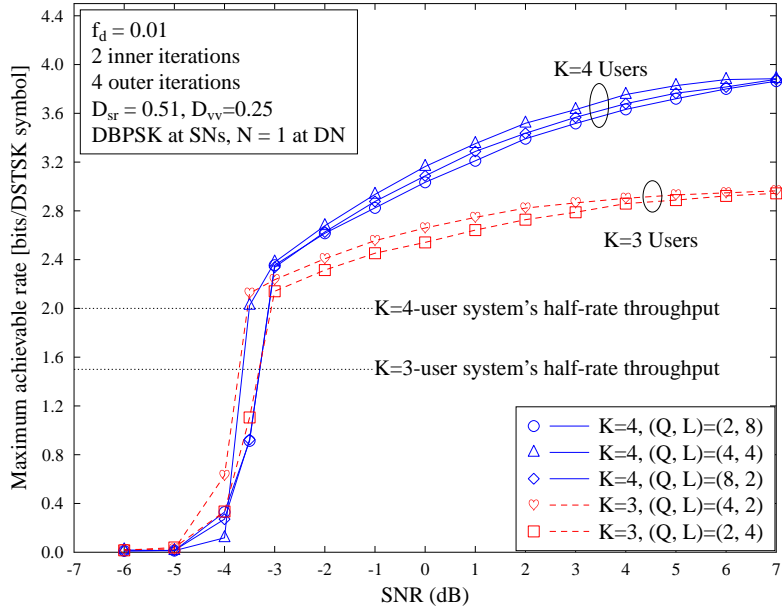


Figure 5.12: Maximum achievable rates of DSTSK($2, 1, 2, Q, \mathcal{L}$) aided MUSRC scheme of Fig. 5.9 using different combinations of (Q, \mathcal{L}) for supporting $K = 3$ and 4 users, associated with DBPSK at SNs and $N = 1$ receive antenna at DN. All other system parameters were summarized in Table 5.6.

It can be seen from Table 5.3 that for $K = 3$ users, there are two legitimate combinations of $(Q, \mathcal{L}) = (4, 2)$ and $(Q, \mathcal{L}) = (2, 4)$. The corresponding maximum achievable rates of these two configurations are shown in Fig. 5.12 as two dashed curves, where it is seen that both these two DSTSK combinations are capable of achieving the system throughput of 3 bits/symbol at ap-

proximately $\text{SNR} = 7$ dB. However, based on the fact that for near-capacity systems, a vanishingly low BER may occur a few dBs beyond the system's capacity, as exemplified latter by the BER simulation results of Fig. 5.15, we may focus our attention on the system's capacity point and its immediate vicinity. It can be seen that the combination of $(Q, \mathcal{L}) = (4, 2)$ reach the half-rate throughput of 1.5 bits/symbol at $\text{SNR} = -3.8$ dB, while the combination of $(Q, \mathcal{L}) = (2, 4)$ reach the half-rate throughput at $\text{SNR} = -3.4$ dB. Beyond this point, the combination $(Q, \mathcal{L}) = (4, 2)$ still outperforms the other combination $(Q, \mathcal{L}) = (2, 4)$. Clearly, the combination $(Q, \mathcal{L}) = (4, 2)$ is the most appropriate configuration based on the system's maximum achievable rate. This agrees with the results produced by the proposed MMBCS algorithm as listed in Table 5.5, which also confirms that $(Q_{\text{opt}}, \mathcal{L}_{\text{opt}}) = (4, 2)$ is the best configuration for supporting $K = 3$ users.

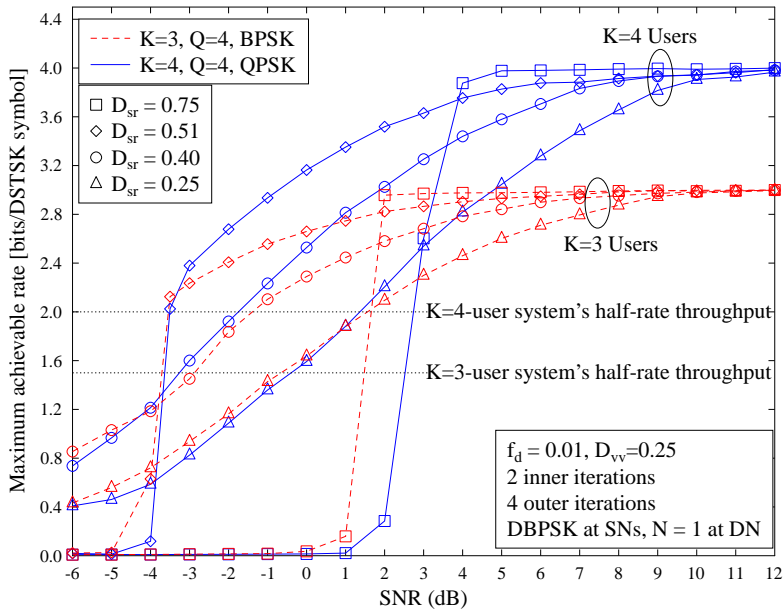


Figure 5.13: Effects of different SR distances on the system's maximum achievable rate for the systems $(Q_{\text{opt}}, \mathcal{L}_{\text{opt}}) = (4, 2)$ and $(Q_{\text{opt}}, \mathcal{L}_{\text{opt}}) = (4, 4)$ to support $K = 3$ and $K = 4$ users, respectively. All other system parameters were summarized in Table 5.6.

The three maximum achievable rates for the system with $K = 4$ users are shown in Fig. 5.12 as solid curves, where we observe that the combination $(Q, \mathcal{L}) = (4, 4)$ reaches the half-rate throughput point at approximately $\text{SNR} = -3.7$ dB, while the other two combinations require about $\text{SNR} = -3$ dB. Additionally, beyond its half-rate SNR point, the combination $(Q, \mathcal{L}) = (4, 4)$ outperforms the other two combinations, in terms of the maximum achievable rate. Therefore, $(Q, \mathcal{L}) = (4, 4)$ can be regarded as the optimal combination, which again agrees with the results of Table 5.5, provided by the proposed MMBCS algorithm. It is worth pointing out that all the legitimate DSTSK configurations (Q, \mathcal{L}) associated with the same number of users K have the same system complexity. According to the operational principle of our SISO-MSDSD invoked for DSTSK, the size of the search-set is determined by the product $Q \cdot \mathcal{L}$, which in fact depends on the number of users K . Note that all the combinations have the same product $Q \cdot \mathcal{L}$, as $\log_2(Q \cdot \mathcal{L}) = K$. In other words, given the number of users K , the lower-bounded complexity of our

SISO-MSDSD aided cooperative system is determined. This lower-bounded complexity is given in Table 5.3 as N_c , where the complexity is quantified in terms of the number of complex additions, multiplications and absolute value calculations per user.

Fig. 5.13 shows the effects of the different SR distances D_{sr} on the maximum achievable rate for the DSTSK systems $(Q_{\text{opt}}, \mathcal{L}_{\text{opt}}) = (4, 2)$ to support $K = 3$ users and $(Q_{\text{opt}}, \mathcal{L}_{\text{opt}}) = (4, 4)$ to support $K = 4$ users, respectively, where the SR distances are chosen as $D_{sr} \in \{0.25, 0.40, 0.51, 0.75\}$. The maximum achievable rates associated with the system of $K = 3$ users are shown as dashed curves, where it can be seen that even though the curve of $D_{sr} = 0.51$ exhibits a lower throughput in the low-SNR region, it reaches the half-rate throughput point at $\text{SNR} = -3.8$ dB, which is smaller than the SNR values required by the other three SR distances. Additionally, the $D_{sr} = 0.51$ scenario outperforms the others beyond its half-rate SNR point and up to about $\text{SNR} = 2$ dB, where a vanishingly low BER is achieved as will be seen in Fig. 5.15. The four solid curves in Fig. 5.13 correspond to the maximum achievable rates associated with the four SR distances D_{sr} for the system of $K = 4$ users. It can be seen that similar to the 3-user system, in the low-SNR region, the curve of the $D_{sr} = 0.51$ case for the 4-user system is relatively low, but it reaches the half-rate point at $\text{SNR} = -3.7$ dB, which is earlier than the other three SR distance cases. Furthermore, the $D_{sr} = 0.51$ scenario outperforms the other three cases up to $\text{SNR} = 3$ dB. Therefore, we can conclude that the SR distance $D_{sr} = 0.51$ is optimal for this system configuration to support both $K = 3$ and 4 users, in terms of the system maximum achievable rate.

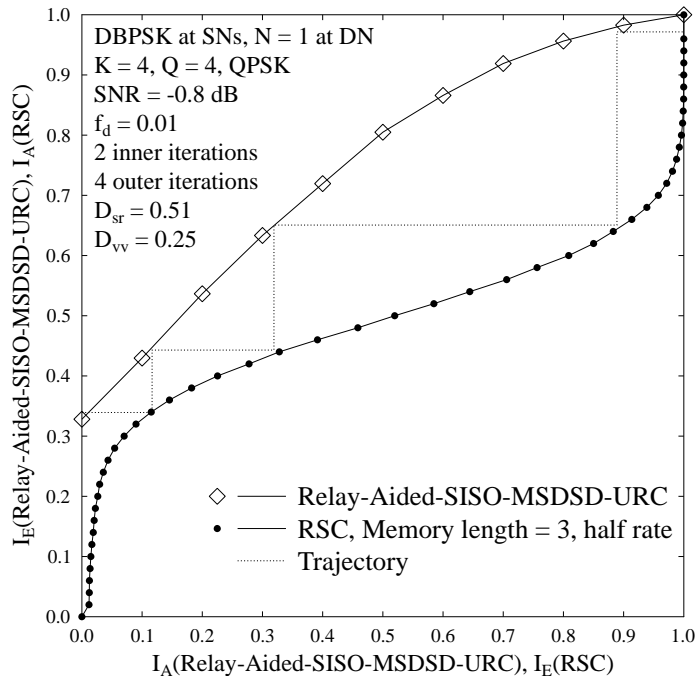


Figure 5.14: The EXIT characteristics and the corresponding decoding trajectory of the proposed cooperative system $(Q_{\text{opt}}, \mathcal{L}_{\text{opt}}) = (4, 4)$ for the given number of $K = 4$ users at $\text{SNR} = -0.8$ dB. All other system parameters were summarized in Table 5.6. The corresponding BER curves are seen in Fig. 5.15.

Fig. 5.14 portrays the EXIT chart [1] of the DSTSK aided MUSRC system $(Q_{\text{opt}}, \mathcal{L}_{\text{opt}}) = (4, 4)$ supporting $K = 4$ users and relying on a detection window size of $N_w = 4$. It can be seen that an open tunnel exists between the EXIT curves of the inner MSDSD-URC decoder and of the outer RSC decoder at $\text{SNR} = -0.8$ dB. The Monte-Carlo simulation based stair-case shaped decoding trajectory, which closely matched the EXIT curves, is also provided at $\text{SNR} = -0.8$ dB. This trajectory shows that the point of perfect convergence at $(1.0, 1.0)$ is reached with the aid of $I_{\text{out}} = 4$ iterations, implying that our system supporting $K = 4$ users and relying on an MSDSD detection window size of $N_w = 4$ is capable of achieving a vanishingly low error probability beyond the point of $\text{SNR} = -0.8$ dB, as is confirmed by the BER curves of the $K = 4$ -user system characterized in Fig. 5.15.

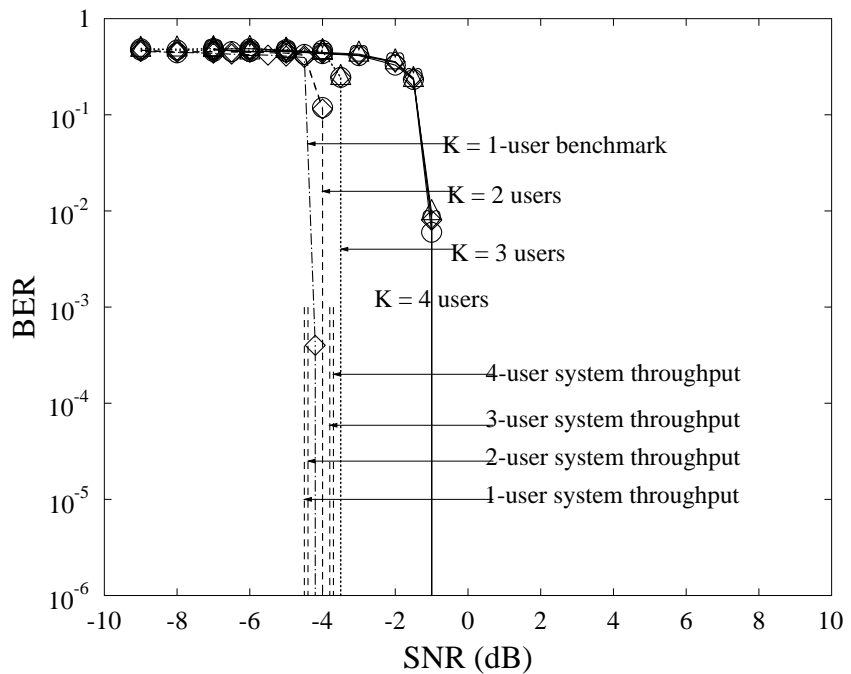


Figure 5.15: BER performance of the proposed cooperative system of Fig. 5.9 supporting $K = 1, 2, 3$ and 4 users and the corresponding system capacity. The system employs DBPSK at SNs and $N = 1$ receive antenna at DN. All other system parameters were summarized in Table 5.6. The corresponding EXIT chart is seen in Fig. 5.14.

In a multi-user system exhibiting fairness, the BER performance should be identical for each user. We plot the BER performance of the individual users in Fig. 5.15 for the cases of $K = 2, 3$ and 4 . The BER curve group indicated by “ $K = 4$ users” contains the four individual users’ BERs, while the BER curve group of “ $K = 3$ users” represents the three individual users’ BERs. Finally, the two BER curves of the two-user system as well as of the single-user benchmark are grouped under the labels of “ $K = 2$ users” and “ $K = 1$ -user benchmark”, respectively. It can be seen from Fig. 5.15 that for the system supporting $K \in \{2, 3, 4\}$ users, all the users in each case share the same BER performance, implying that the same QoS is guaranteed for each of the K users. Additionally, the system throughput for each of the $K = 1, 2, 3$ and 4 scenarios are also plotted in Fig. 5.15, where

it can be seen that the differences between the capacity lines and “Turbo cliffs” are usually less than 3 dB, implying that our proposed DSTSK aided MUSRC scheme is indeed capable of achieving near-capacity performance with the aid of three-stage serial-concatenated coding scheme.

Table 5.7: Comparison of the complexity bounds N_c [98] for the DSTSK aided MUSRC system and the conventional DPSK aided MUSRC system, both associated with $N_w = 4$, DBPSK at SNs and $N = 1$ receive antenna at DN. The DSTSK aided system employs 2 RNs per VAA and the conventional DPSK based system has a single RN per VAA.

Users	$K = 2$	$K = 3$	$K = 4$	$K = 5$
DSTSK aided MUSRC ($N_r = 2$ per VAA)	$N_c = 180$	$N_c = 200$	$N_c = 250$	$N_c = 360$
DPSK aided MUSRC ($N_r = 1$ per VAA)	$N_c = 35$	$N_c = 46$	$N_c = 70$	$N_c = 150$

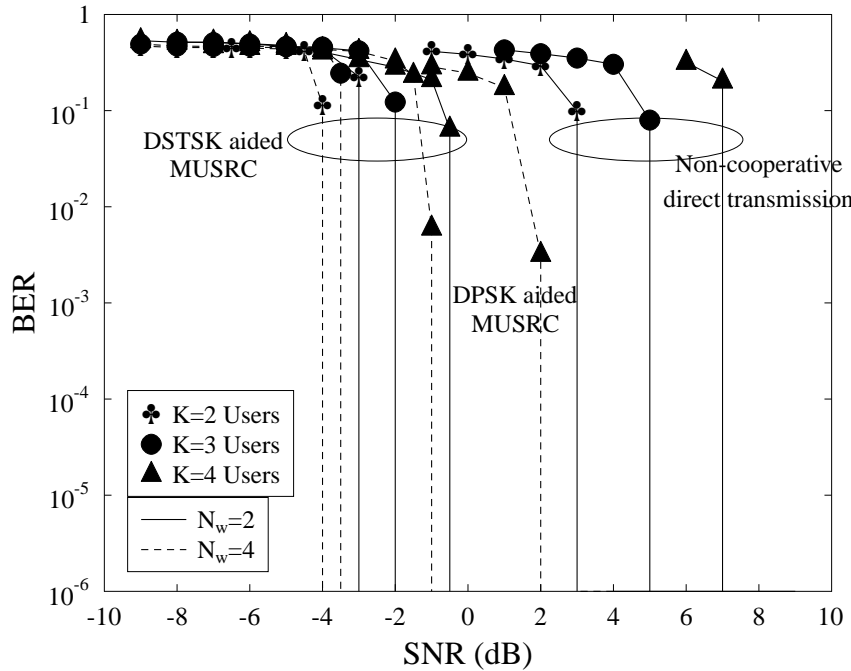


Figure 5.16: Effects of MSDSD window size N_w on the BER performance of the proposed DSTSK aided MUSRC system, which employs DBPSK at SNs and $N = 1$ receive antenna at DN, as well as the BER performance comparison with the DSTSK non-cooperative direct transmission system and the conventional DPSK aided MUSRC system. All other system parameters were summarized in Table 5.6.

Fig. 5.16 shows the effects of the MSDSD detection window size N_w on the attainable BER performance of our proposed system supporting $K \in \{2, 3, 4\}$ users. It can be seen from the results shown in Fig. 5.16 that the BER performance is improved as the window size increases from $N_w = 2$ to 4, at the cost of a higher complexity. However, the complexity of the proposed MSDSD scheme does not increase exponentially, hence the system’s complexity remains acceptable for a detection window size of $N_w = 4$. The BER performances of non-cooperative three-stage serial-concatenated turbo coding aided DSTSK schemes relying on an MSDSD window size of $N_w = 4$

are also included in Fig. 5.16 for the comparison with our proposed DSTSK aided MUSRC system. Observe in Fig. 5.16 that the proposed DSTSK aided MUSRC system significantly outperforms the non-cooperative DSTSK scheme. We also simulated a DPSK aided MUSRC system, where the DSTSK scheme based on $N_r = 2$ RNs per VAA invoked for relaying in our proposed DSTSK aided MUSRC was replaced by the conventional DPSK based relaying relying on a single RN per VAA. The performance of this DPSK aided MUSRC system supporting $K = 4$ users and with an MSDSD window size of $N_w = 4$ is also included in Fig. 5.16. Observe from Fig. 5.16 that the proposed DSTSK aided MUSRC offers a performance gain of about 3 dB over this DPSK aided MUSRC, which is achieved at the cost of imposing a slightly higher complexity than the DPSK aided MUSRC system, as confirmed by the complexity bounds N_c of the two MUSRC systems given in Table 5.7.

5.3.3.2 DQPSK for SR transmission and DSTSK(2, 2, 2, Q, \mathcal{L}) for RD transmission

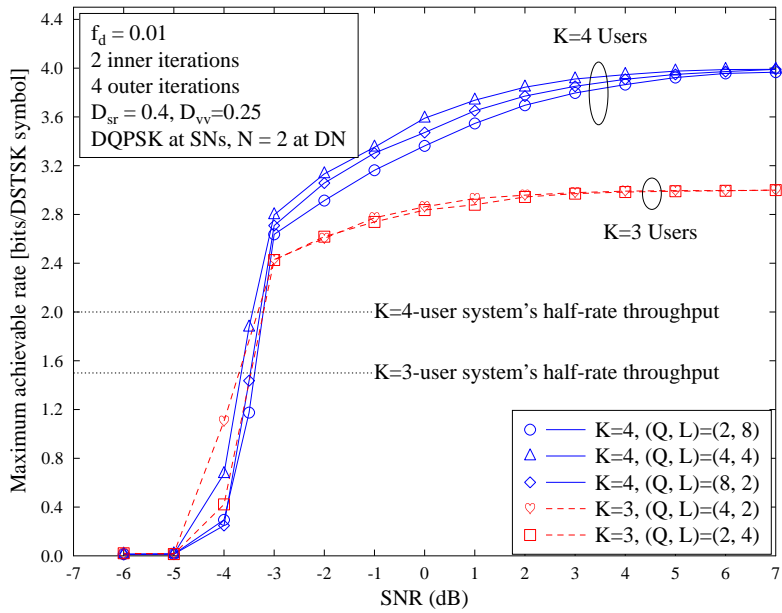


Figure 5.17: Maximum achievable rates of DSTSK(2, 2, 2, Q, \mathcal{L}) aided MUSRC scheme of Fig. 5.9 using different combinations of (Q, \mathcal{L}) for supporting $K = 3$ and 4 users, associated with DQPSK at SNs and $N = 2$ receive antenna at DN. All other system parameters were summarized in Table 5.6.

We also considered the proposed DSTSK aided MUSRC system of Fig. 5.9 employing DQPSK for the SR transmission and a DSTSK scheme of DSTSK(2, 2, 2, Q, \mathcal{L}) for the RD transmission, associated with $N_r = 2$ relays in each of the two VAA groups and a DN equipped with $N = 2$ antennas. We first quantified the maximum achievable rates for all the legitimate DSTSK configurations (Q, \mathcal{L}) supporting $K \in \{3, 4\}$ users, respectively, in conjunction with an MSDSD window size of $N_w = 4$. The SR distance was chosen as $D_{sr} = 0.4$, which will be shown to be the optimal distance for this DSTSK aided MUSRC system. The simulation results obtained are

shown in Fig. 5.17, where the maximum achievable rates of the two DSTSK configurations supporting $K = 3$ users are depicted as dashed curves, while the maximum achievable rates of the three DSTSK configurations supporting $K = 4$ users are shown as solid curves. The results of Fig. 5.17 demonstrate that the configuration $(Q, \mathcal{L}) = (4, 2)$ is optimal for the 3-user system while the configuration $(Q, \mathcal{L}) = (4, 4)$ is optimal for the 4-user system, in terms of the maximum achievable rate. This observation agrees with the results provided by the proposed MMBCS algorithm listed in Table 5.5, which again demonstrates the power of the MMBCS algorithm in selecting the optimal DSTSK configuration $(Q_{\text{opt}}, \mathcal{L}_{\text{opt}})$ for the given number of users K .

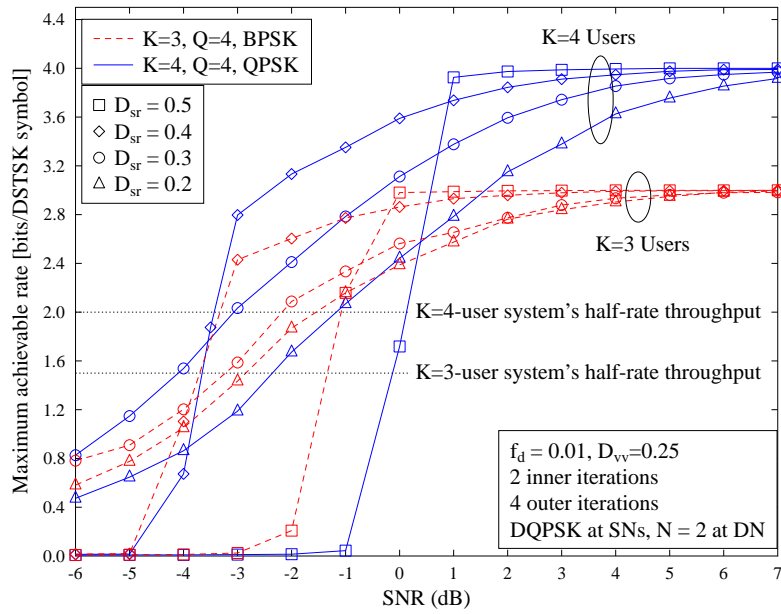


Figure 5.18: Effects of different SR distances on the system's maximum achievable rate for the systems $(Q_{\text{opt}}, \mathcal{L}_{\text{opt}}) = (4, 2)$ and $(Q_{\text{opt}}, \mathcal{L}_{\text{opt}}) = (4, 4)$ to support $K = 3$ and $K = 4$ users, respectively. All other system parameters were summarized in Table 5.6.

The effects of SR distances D_{sr} on the maximum achievable rate of the proposed cooperative system for the optimal combinations of $(Q_{\text{opt}}, \mathcal{L}_{\text{opt}}) = (4, 2)$ and $(Q_{\text{opt}}, \mathcal{L}_{\text{opt}}) = (4, 4)$ supporting $K \in \{3, 4\}$ users, respectively, are portrayed in Fig. 5.18, where the SR distances chosen for our simulation were $D_{sr} \in \{0.2, 0.3, 0.4, 0.50\}$. The four dashed curves in Fig. 5.18 depict the maximum achievable rates for the $K = 3$ -user scenario, where it can be seen clearly that the $D_{sr} = 0.4$ scenario outperforms the other three distances. The four maximum achievable rates for the $K = 4$ -user system are illustrated in Fig. 5.18 as solid curves, and it is clearly that the case of $D_{sr} = 0.4$ outperforms the other three cases. Hence, for the DSTSK aided MUSRC system employing the DQPSK for the SR transmission and a DSTSK scheme of DSTSK(2, 2, 2, Q, \mathcal{L}) for the RD transmission, the SR distance of $D_{sr} = 0.4$ is optimal.

Fig. 5.19 portrays the EXIT chart for the DSTSK aided MUSRC system $(Q_{\text{opt}}, \mathcal{L}_{\text{opt}}) = (4, 4)$ supporting $K = 4$ users and relying on a detection window size of $N_w = 4$. It can be seen that an open tunnel exists at $\text{SNR} = -2.4$ dB. The Monte-Carlo simulation based stair-case shaped decoding trajectory shows that the point of perfect convergence at $(1.0, 1.0)$ is reached with the

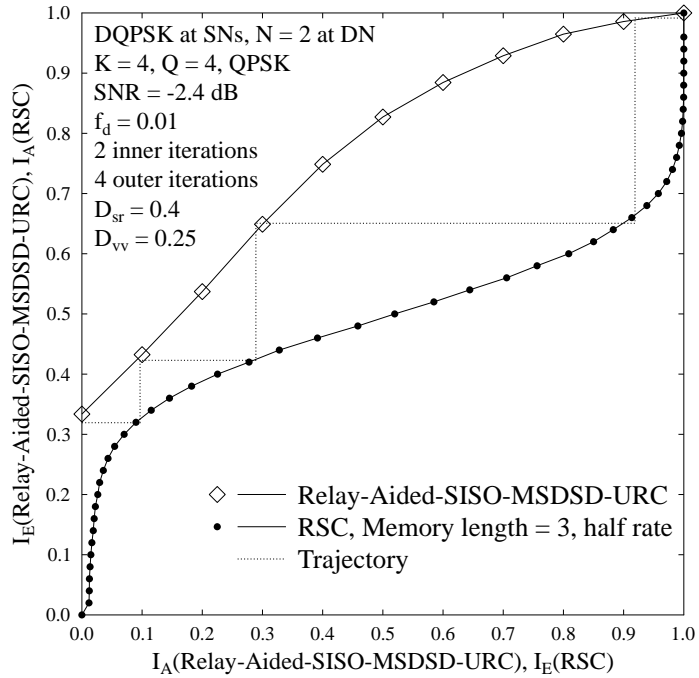


Figure 5.19: The EXIT characteristics and the corresponding decoding trajectory of the proposed cooperative system $(Q_{\text{opt}}, \mathcal{L}_{\text{opt}}) = (4, 4)$ for the given number of $K = 4$ users at $\text{SNR} = -2.4$ dB. All other system parameters were summarized in Table 5.6. The corresponding BER curves are seen in Fig. 5.20.

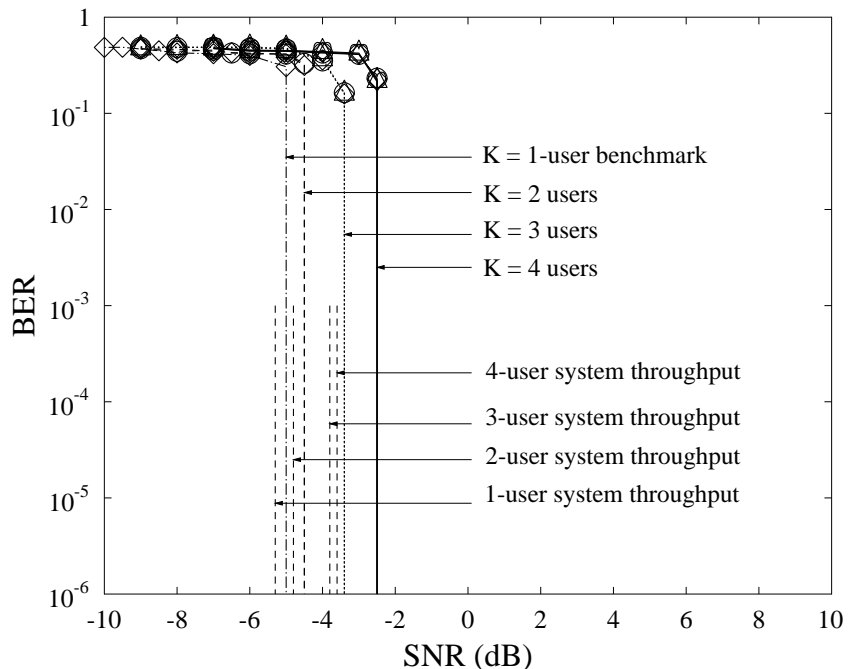


Figure 5.20: BER performance of the proposed cooperative system of Fig. 5.9 supporting $K = 1, 2, 3$ and 4 users and the corresponding system capacity. The system employs DQPSK at SNs and $N = 2$ receive antenna at DN. All other system parameters were summarized in Table 5.6. The corresponding EXIT chart is seen in Fig. 5.19.

aid of $I_{out} = 4$ iterations. Hence our system supporting $K = 4$ users with an MSDSD detection window size of $N_w = 4$ is capable of achieving a vanishingly low error probability beyond the point of $\text{SNR} = -2.4$ dB, which is also confirmed by the BER curves of the $K = 4$ -users system provided in Fig. 5.20. In Fig. 5.20, we plot the BER performance of the individual users for the systems supporting $K = 2, 3$ and 4 users, respectively, where it can be seen clearly that all the users in each system exhibit an identical BER performance, indicating that the same QoS is guaranteed for each of the K users. The $K = 1$ user performance is included as a benchmark. By comparing the BER “Turbo cliffs” with their corresponding capacity lines in Fig. 5.20, we observe that our DSTSK aided MUSRC scheme is capable of achieving near-capacity performance with the aid of three-stage serial-concatenated coding scheme.

5.4 Chapter Summary and Conclusions

In Section 5.2, we first introduced the MSDSD aided DSTSK system and demonstrated that the MSDSD was capable of mitigating the error-floor in differential MIMO systems, while maintaining a lower computational complexity than its coherent-detection-assisted counterpart. Additionally, based on the MSDSD assisted DSTSK system, we proposed the MUSRC system of Fig. 5.9 in Section 5.3.

Specifically, the general introduction of differential MIMO systems and cooperative communication systems was provided in Section 5.1. To be more explicit, it was pointed out in Section 5.1.1 that unlike coherent MIMO schemes, differential MIMO schemes do not require CSI for performing data detection. As a result, high-complexity CE schemes may be avoided, which is advantageous, especially when number of antennas or the fading rate is high. However, it was also mentioned that CDD assisted differential schemes usually suffer from a characteristic 3 dB SNR penalty. Against this background, the MSDD philosophy of Section 5.1.1 was introduced for compensating this performance loss. However, due to the exponentially increased computational complexity of an increased window size N_w , the value of N_w has to remain moderate. Then the novel concept of MSDSD was proposed for the sake of reducing the detection complexity, compared to MSDD, while enhancing the achievable BER performance. Section 5.1.2 generally discussed the concept of cooperative communications, where differential schemes may be applied, since no CSI is required. Two major types of cooperation were considered in the literature, namely the AF and DF relaying protocols. Additionally, it was also mentioned in Section 5.1.2 that the conventional two-phase operation of relaying systems suffer from a 50% throughput loss. Therefore, the concept of successive relaying systems may be invoked in conjunction with the DS-CDMA technique for recovering this throughput loss.

Section 5.2 reviewed the family of MSDSD aided DSTSK systems. More explicitly, the differential encoding transmitter structure of DSTSK was described in Fig. 5.2 of Section 5.2.1. Then the hard-decision and soft-decision MSDSD aided DSTSK systems were introduced in Sec-

tions 5.2.2 and 5.2.3, respectively. The corresponding simulation results of MSDSD aided DSTSK were shown in Section 5.2.4. More specifically, it was found from the simulations of Fig. 5.4, Fig. 5.5 and Fig. 5.6 that the MSDSD was capable of mitigating the error-floor of CDD based DSTSK schemes, especially when the fading rate is high, e.g. given the normalized Doppler frequency of $f_d = 0.03$. Additionally, it was seen from Fig. 5.4, Fig. 5.6, and Fig. 5.8 that in a relatively fast fading environment, the performance of the MSDSD might be enhanced by expanding the window size at the cost of an increased computational complexity. Moreover, it was also found from the comparison between Fig. 5.3 and Fig. 5.5 that employing MIMO techniques helped in reducing the error-floor due to their increased diversity gain. Finally, it was shown in Fig. 5.7 and Fig. 5.8 that the three-stage serial concatenated turbo coding scheme of Fig. 5.10 could be invoked for the sake of significantly improving the system's performance. We have summarized the performance of MSDSD aided DSTSK systems of Fig. 5.2 in Table 5.8, including the throughput, required SNR for achieving $\text{BER} = 10^{-6}$ and complexity order.

Table 5.8: Performance summary of MSDSD aided DSTSK(2,2,2,4,QPSK) and DSTSK(2,1,2,4,QPSK) systems of Fig. 5.2 at $\text{BER} = 10^{-6}$. The corresponding systems' normalized throughput is $R = 2$ bits/symbol. Their MSDSD complexity lower bound is on the order of $C_{MSDSD} = Q \cdot \mathcal{L}(N_w - 1)$.

MIMO Scheme	f_d	N_w	SNR (Uncoded) [dB]	SNR (Coded) [dB]	C_{MSDSD}	Figure
DSTSK(2,2,2,4,QPSK)	0.01	2	23	4.9	16	Fig. 5.3 and Fig. 5.7
		4	22.5	3.9	48	
		6	22.5	3.3	80	
	0.03	2	Error-floor	5.1	16	Fig. 5.4 and Fig. 5.8
		4	26	4.1	48	
		6	24	3.6	80	
DSTSK(2,1,2,4,QPSK)	0.01	2	Error-floor		16	Fig. 5.5
		4	40		48	
		6	38		80	
	0.03	2	Error-floor		16	Fig. 5.6
		4	42		48	
		6	40		80	

The DSTSK aided MUSRC system of Fig. 5.9 was proposed in Section 5.3. To be more explicit, the two-phase alternating operation principle was introduced in Section 5.3.1.1, where it was shown that by adopting the successive relaying, the conventional 50% throughput loss could be recovered. The relay architecture was introduced in Section 5.3.1.2, while the operations of the

SNs, RNs and DN were described in Sections 5.3.1.3, 5.3.1.4 and 5.3.1.5, respectively. In Section 5.3.2, the MMBCS proposed in Chapter 2 was employed for the DSTSK scheme to select the optimal configuration for the MUSRC system. The corresponding simulation results investigation were provided in Fig. 5.12 to Fig. 5.20 of Section 5.3.3, where it was shown that the proposed DSTSK aided MUSRC system was capable of achieving a near-capacity performance, while maintaining a low complexity. We have summarized the performance of the proposed MUSRC systems of Fig. 5.9 in Table 5.9, including the number of supported users K , required SNR for achieving $\text{BER} = 10^{-6}$ and complexity order.

Table 5.9: Performance summary of DSTSK aided MUSRC systems of Fig. 5.9 at $\text{BER} = 10^{-6}$. The MSDSD complexity lower bound is on the order of $C_{MSDSD} = Q \cdot \mathcal{L}(N_w - 1)$.

Cooperatie Scheme	f_d	N_w	K	SNR [dB]	C_{MSDSD}	Figure
DBPSK and DSTSK($2, 1, 2, Q, \mathcal{L}$)	0.01	4	1	-4.1	12	Fig. 5.15
			2	-3.9	24	
			3	-3.4	42	
			4	-0.8	72	
DBPSK and DSTSK($2, 1, 2, Q, \mathcal{L}$)	0.01	2	2	-2.4	8	Fig. 5.16
			3	-1.9	14	
			4	-0.4	24	
			1	-4.9	18	Fig. 5.20
DQPSK and DSTSK($2, 2, 2, Q, \mathcal{L}$)	0.01	4	2	-4.4	36	
			3	-3.3	60	
			4	-2.4	96	

Conclusions and Future Research

In this concluding chapter, we will provide the overall summary and conclusions of this treatise in Section 6.1. Design guidelines for the MIMO systems discussed in this thesis will be listed in Section 6.2. Then several promising topics will be briefly discussed as future research directions in Section 6.3.

6.1 Summary and Conclusions

- **Chapter 2:** In Chapter 2, we briefly reviewed a pair of MIMO systems, namely the SDM/V-BLAST and STSK. The system model and performance investigation of uncoded SDM/V-BLAST were detailed in Section 2.1. More specifically, the system model of uncoded SDM/V-BLAST was introduced in Section 2.1.1, where the optimal ML detection rule was formulated in Eq. (2.5). Additionally, it was also pointed that the optimal ML solution of SDM/V-BLAST might impose excessive detection complexity, as the total number of Tx antennas was increased. In this case, the family of linear detectors, such as the MMSE and ZF detectors may be employed for the sake of achieving a lower complexity, at the expense of a performance loss. The corresponding simulation results based on optimal ML detection of uncoded SDM/V-BLAST were provided in Fig. 2.2, Fig. 2.3, Fig. 2.4, Fig. 2.5 and Fig. 2.6 of Section 2.1.2, where it was demonstrated that the system's throughput might be improved by either employing higher order modulations or by increasing the number of Tx antennas, while owing to the lack of transmit diversity, a diversity gain could only be achieved by employing multiple AEs at the receiver side. For the sake of achieving a near-capacity performance, the powerful three-stage serial-concatenated turbo coded SDM/V-BLAST MIMO system of Fig. 2.7 was introduced in Section 2.2, where it was pointed out that a URC may be employed to beneficially spread the *extrinsic* information across the iterative decoder components to avoid the well-known error-floor exhibited by the conventional turbo schemes. This was confirmed by the BER performance characterized in Section 2.2.2, as exemplified by the

Sections	Contributions
Section 2.1	Reviewed the system model and performance of uncoded SDM/V-BLAST system, pointing out that the optimal ML solution might impose an exponentially increased detection complexity, while the low-complexity linear detectors might experience a performance loss. Our simulation results demonstrated that a diversity gain can only be achieved at the receiver side.
Section 2.2	Conceived a three-stage turbo coded SDM/V-BLAST MIMO system for the sake of eliminating the potential error-floor and for achieving a near-capacity performance.
Section 2.3	Introduced the novel concept of STSK systems and detailed its system design, computational complexity, maximum achievable diversity, as well as its dispersion matrix design. Proposed a MMBCS algorithm for selecting the most appropriate STSK configurations.
Section 2.4	Developed a three-stage serial-concatenated turbo coding aided CSTSK MIMO system for the sake of achieving a near-capacity performance.

Table 6.1: Summary of contributions of Chapter 2.

results shown in Fig. 2.9, Fig. 2.13, etc. Additionally, EXIT charts were adopted as a tool for predicting the convergence behaviour of the iterative decoder, as shown in Fig. 2.8 and Fig. 2.10.

As a more recent MIMO concept, CSTSK modulation scheme of Fig. 2.17 was introduced in Section 2.3, in terms of its system model, computational complexity, maximum achievable diversity order and dispersion matrix generation. More specifically, Section 2.3.1 gave an overview of the system design of the novel STSK scheme. A four-step STSK encoding procedure was shown in Fig. 2.17, where it may be seen that in each symbol block, $\log_2(Q)$ information bits were encoded by activating one out of Q dispersion matrices, while another $\log_2(\mathcal{L})$ bits were modulated by the conventional \mathcal{L} -PSK/QAM modulations. In this way, an extra $\log_2(Q)$ bits may be encoded by the STSK scheme, leading to an improved system throughput formulated in Eq. (2.9). Due to the elimination of ICI, facilitated low-complexity single-antenna-based ML detection, which was expressed in Eq. (2.20), associated with the corresponding computational complexity detailed in Eq. (2.21) and (2.22) for fast and slow fading, respectively. The maximum achievable diversity order of the CSTSK systems was characterized in Eq. (2.25) as $N \cdot \min(M, T)$, implying that solely increasing M beyond T or increasing T beyond M made no further contribution to the attainable diversity gain. The generation of dispersion matrices was detailed in Section 2.3.4, where a random search algorithm was adopted for optimizing the PSEP formulated in Eq. (2.27). We also proposed a

novel MMBCS algorithm in Section 2.3.5, which was demonstrated to be capable of selecting the most appropriate STSK configuration, while avoiding the time-consuming Monte-Carlo simulation based approach. The uncoded CSTSK MIMO system's performance was then intensively investigated in Fig. 2.18, Fig. 2.19, Fig. 2.20, Fig. 2.21, Fig. 2.22, Fig. 2.23, Fig. 2.24, Fig. 2.25, Fig. 2.26 and Fig. 2.27 of Section 2.3.6 based on various CSTSK configurations. By analysing the results obtained from the above-mentioned simulation figures, it was concluded that the proposed CSTSK scheme was capable of striking a flexible tradeoff between the MIMO's diversity and multiplexing gains, while again, facilitating the low-complexity single-antenna-based ML detection owing to the elimination of ICI. Finally, the three-stage serial-concatenated turbo coding aided CSTSK MIMO system of Fig. 2.28 was developed in Section 2.4 for the sake of achieving a near-capacity performance, where it was demonstrated that with the aid of three-stage turbo codes, CSTSK was capable of achieving an infinitesimally low BER and a near-capacity performance, as demonstrated by the BER results depicted in Fig. 2.30 and Fig. 2.32.

We have summarised the major contributions of Chapter 2 in Table 6.1.

- **Chapter 3:** Chapter 3 mainly focused on the CE schemes conceived for the coherently detected MIMO systems discussed in Chapter 2. To be more specific, the system model of conventional TBCE constructed for CSTSK systems of Fig. 3.1 was introduced in Section 3.2.1, and the corresponding performance investigation was provided in Fig. 3.2, Fig. 3.3, Fig. 3.4, Fig. 3.5, Fig. 3.6, Fig. 3.7, Fig. 3.8 and Fig. 3.9 of Section 3.2.2 based on the CSTSK MIMO system, under both uncoded and three-stage serial-concatenated turbo coded scenarios. Two metrics, namely the BER and the MCE have been adopted for assessing the performance of the CE based schemes. As expected, the simulation results of Fig. 3.2, Fig. 3.4, Fig. 3.6, Fig. 3.8 and Fig. 3.9 confirmed that in order for the TBCE based scheme to approach the perfect CSI benchmark, a high PO (a large number of training blocks) was required, hence substantially reducing the system's effective throughput. For example, from the BER performance of TBCE shown in Fig. 3.2, it may be seen that as PO increased, the BER performance was improved, and when the PO became $O_p = 12\%$ ($M_T = 30$), the BER curve of TBCE approached that of the perfect CSI case. Additionally, in order to solve the throughput loss problem faced by TBCE, SBCE schemes were introduced in Fig. 3.10 of Section 3.3, in which the detected bits and training symbol blocks were used jointly for further DDCE. The corresponding simulation results were presented in Fig. 3.11, Fig. 3.12, Fig. 3.13, Fig. 3.14, Fig. 3.15, Fig. 3.16, Fig. 3.17 and Fig. 3.18 of Section 3.3.2 in terms of the BER and MCE metrics. The BER results shown in Fig. 3.11, Fig. 3.13, Fig. 3.14, Fig. 3.16, and Fig. 3.17 demonstrated that the SBCE based schemes were capable of approaching the performance of the perfect CSI scenario with the aid of a low PO, substantially outperforming the TBCE scheme utilizing the same PO. Additionally, from the MCE simulations depicted in Fig. 3.12, Fig. 3.15 and Fig. 3.18, it might be clearly seen that typically as

few as $I_{ce} = 5$ iterations were sufficient for the MCE to converge, and over a certain SNR threshold range, the SBCE based scheme was capable of reaching the ultimate performance bound associated with perfect CSI.

Based on the concept of SBCE introduced in Section 3.3, our novel BBSBCE scheme designed for the three-stage turbo coded CSTSK regime of Fig. 3.20 was proposed in Section 3.4. Firstly, the conventional arrangements of CE and turbo detection MIMO schemes of Fig. 3.19 were discussed in Section 3.4.1 and two major limitations were recognized. Firstly, the conventional turbo coded CE scheme utilizing the entire detected data frame for DDCE introduces an extra CE loop, leading to a significant increase in computational complexity. Secondly, the detected frame contains erroneous decisions, leading to potentially serious error propagation, which may degrade the system's achievable performance. In order to overcome these limitations, the efficient yet low-complexity BBSBCE based scheme of Fig. 3.20 and Fig. 3.21 was detailed in Section 3.4.2. A high system throughput was maintained, since the proposed scheme only utilized a low PO for generating an initial CE. Most significantly, unlike the existing methods, the proposed BBSBCE scheme did not require an extra iterative loop between the CE and the turbo detector-decoder, since the BBSB iterative CE was naturally embedded into the original iterative three-stage demapping-decoding turbo loop. Furthermore, since only high-confidence decision blocks are selected in the BBSBCE based scheme, the error propagation problem exhibited by conventional SBCE schemes was mitigated. In this way, the complexity order of BBSBCE seen in Table 3.7 became close to that of the idealised three-stage turbo demapping-decoding scheme associated with perfect CSI. Additionally, the CRLB was introduced in Section 3.4.3, which was capable of characterizing the best attainable performance of our proposed BBSBCE algorithm. The performance of the proposed BBSBCE algorithm was extensively investigated in Fig. 3.24, Fig. 3.25, Fig. 3.26, Fig. 3.27, Fig. 3.28, Fig. 3.29, Fig. 3.30, Fig. 3.31, Fig. 3.32 and Fig. 3.33 of Section 3.4.4. More specifically, it was confirmed in Fig. 3.26 and Fig. 3.31 that the proposed semi-blind BBSBCE and three-stage turbo demapping-decoding scheme was capable of approaching the near-capacity performance bound of the idealised three-stage turbo detector-decoder at the same number of turbo iterations. Additionally, Fig. 3.28 and Fig. 3.33 confirmed that the proposed BBSBCE was capable of approaching the CRLB associated with the specific number of training sequence length related to the frame length.

In Section 3.5, the BBSBCE algorithm was improved by incorporating the concept of soft-decision based CE scheme for the sake of further reducing the effects of erroneous decisions in our SBCE scheme, namely in the BBSB-SCE arrangement. More specifically, we firstly demonstrated that the soft-decision aided CE was inappropriate for the STSK MIMO system. Then a novel semi-blind joint BBSB-SCE and three-stage turbo detection-decoding scheme was proposed for near-capacity SDM/V-BLAST MIMO systems in Section 3.5.1. The soft symbol estimation invoked for soft-decision based CE was first reviewed in Section 3.5.1.1.

Then the system model of the BBSB-SCE aided scheme seen in Fig. 3.40 was detailed in Section 3.5.1.2. The corresponding simulation results were provided in Section 3.5.2, where it was confirmed in Fig. 3.43 that with the aid of selecting ‘just-sufficient’ number of reliable decision blocks and by employing the soft-decision based CE, the proposed BBSB-SCE based scheme was capable of approaching the optimal ML performance bound associated with perfect CSI, while maintaining a high system effective throughput and without imposing an excessive computational complexity. Additionally, the BBSB-SCE operating in time varying environments was also considered, where it was pointed out that there was a trade-off between the time-varying channel’s estimator’s (TVCE) performance and the turbo channel decoder’s performance, as shown in Fig. 3.48.

We have summarised the major contributions of Chapter 3 in Table 6.2.

Sections	Contributions
Section 3.2	Reviewed the system model and the performance of the TBCE scheme of Fig. 3.1 for MIMO systems, and confirmed that TBCE was capable of obtaining accurate CSI at the expense of reducing system’s overall throughput.
Section 3.3	Introduced the system model of Fig. 3.10 and characterized the performance of SBCE scheme invoked for MIMO systems, confirming that SBCE was capable of obtaining accurate CSI with the aid of a small PO, hence maintaining a high system throughput.
Section 3.4	Proposed a novel BBSBCE algorithm, which reduced the effects of error propagation imposed on SBCE schemes by selecting only high-quality decisions. Additionally, the CE loop was embedded in a turbo loop of Fig. 3.20, leading to further complexity reduction.
Section 3.5	Incorporated the BBSBCE of Fig. 3.20 in Section 3.4 with soft CE for the sake of further reducing the effects of error propagation.

Table 6.2: Summary of contributions of Chapter 3.

- **Chapter 4:** Chapter 4 mainly focused on the AS schemes designed for MIMO systems. This is motivated by the fact that MIMO systems utilize multiple RF chains, hence their power consumption and hardware costs tend to be substantial. Moreover, for massive MIMO systems and particularly for millimetre-wave based MIMO systems, the number of available antenna array elements increases massively, while in practice the number of available RF chains is typically limited. As a remedy, AS offers a low-cost, low-complexity technique of reducing the number of RF chains utilized at the transmitter and/or receiver, while retaining the significant advantages of MIMO systems. Section 5.1 briefly introduced the concept of AS for MIMO systems. More specifically, two popular AS optimization criteria were

discussed in Section 4.1.1, namely the CBAS and NBAS. Then three AS arrangements were introduced in Section 4.1.2 as TxAS, RxAS and JTRAS. Additionally, since CSI is required for AS aided MIMO systems, we briefly introduced the background of CE schemes for AS in Section 4.1.3.

Sections	Contributions
Section 4.1	Briefly introduced the concept of AS for MIMO systems. Two popular AS criteria (CBAS and NBAS), three arrangements (TxAS, RxAS and JTRAS) were reviewed.
Section 4.2	Proposed a simple yet efficient NBJTRAS algorithm for MIMO systems, which was demonstrated to be capable of improving the MIMO system's BER and throughput.
Section 4.3	Further proposed a novel TTCE scheme for NBJTRAS aided MIMO systems by exploiting the fact that AS was less sensitive to CE errors than data detection.

Table 6.3: Summary of contributions of Chapter 4.

In Section 4.2 we proposed a simple yet efficient NBJTRAS algorithm for MIMO systems. More specifically, the system description was provided in Section 4.2.1 based on perfectly known CSI. An example was provided to clearly show the process of the proposed NBJTRAS algorithm in Fig. 4.8. Section 4.2.1.3 analysed the complexity of our proposed NBJTRAS algorithm, where it was shown that the complexity of NBJTRAS was significantly lower than that of an exhaustive search, especially when the number of Tx/Rx antennas was high. The corresponding simulation results of NBJTRAS aided MIMO systems were presented in Section 4.2.2 based on perfect CSI. The NBJTRAS designed for uncoded CSTSK systems was firstly investigated in Section 4.2.2.1 in an independently fading environment, where Fig. 4.10, Fig. 4.12 and Fig. 4.14 confirmed that NBJTRAS was capable of improving the BER performance of MIMO systems compared to the conventional MIMO systems utilizing the same number of RF chains. By contrast, Fig. 4.11, Fig. 4.13 and Fig. 4.15 showed that the attainable MIMO channels' throughput performance was also improved by employing NBJTRAS. Then the performance of NBJTRAS invoked for three-stage turbo coded SDM/V-BLAST systems was investigated in Section 4.2.2.2 under both independent and spatially correlated fading environments, where it was found that at a low spatial correlation level, the NBJTRAS aided MIMO system was capable of achieving the same performance gain over the conventional MIMO system using no AS, as in the independent fading environment, while in the highly correlated channel environment, the NBJTRAS aided MIMO was still capable of outperforming the conventional MIMO, but provided a lower performance gain.

Since CSI is usually needed in AS aided MIMO systems, we investigated CE schemes con-

ceived for the proposed NBJTRAS algorithm in Section 4.3. More specifically, we first introduced the simple TBCE scheme designed for NBJTRAS in Section 4.3.1 based on the RF chain reuse scheme of Fig. 4.25. It was found from the simulation results of Fig. 4.26 and Fig. 4.28 that due to the reason that AS operation was relatively insensitive to the CE errors, conventional TBCE associated with a low PO was adequate for AS. However, since the CE errors had a more significant impact on the data detection performance, there still existed a certain performance gap between the TBCE aided NBJTRAS system and the perfect CSI scenario. In order to circumvent this problem, we proposed the novel TTCE scheme of Fig. 4.32 in Section 4.3.2, which included TBCE of Fig. 4.24 for AS and initial data detection. It also included DDCE of Fig. 3.10 for further CE refinement and data detection. The corresponding BER performance shown in Fig. 4.33 and the MCE convergence performance depicted in Fig. 4.34, confirmed that with only a low PO, the BER performance of TTCE aided NBJTRAS was capable converging to the perfect CSI based performance.

We have summarised the major contributions of Chapter 4 in Table 6.3.

- **Chapter 5:** Chapter 5 mainly focused on the MSDSD aided DSTSK system for the sake of avoiding complex CE. Section 5.1 gave a brief introduction to both differential detection and to cooperative communications. More specifically, it was pointed out in Section 5.1.1 that differential detection did not require CSI and therefore, complex CE could be avoided. However, it was also observed that the conventional CDD experiences the well-known 3 dB performance loss and that an irreducible error-floor may be formed in the presence of fast fading channels. Then MSDD was proposed for solving the problems of CDD and MSDSD was further developed for the sake of reducing the excessive complexity imposed by MSDD. Section 5.1.2 introduced the concept of cooperative communications, where differential MIMO techniques are attractive, since no CSI was needed.

The system description of Fig. 5.2 and performance results of MSDSD aided DSTSK were detailed in Section 5.2, where both hard-decision and soft-decision aided MSDSD were discussed. The corresponding simulation results were provided in Fig. 5.3, Fig. 5.4, Fig. 5.5, Fig. 5.6, Fig. 5.7 and Fig. 5.8 of Section 5.2.4. As it was confirmed in Fig. 5.3 and Fig. 5.4, in relatively fast fading environments that CDD might exhibit an irreducible error floor, while the MSDSD was capable of mitigating the error-floor. The DSTSK aided cooperative communication system of Fig. 5.9 was proposed in Section 5.3, namely the MUSRC. More specifically, DSTSK transmission was employed at the RNs, which was detected with the aid of SISO-MSDSD at the DN. Additionally, the MMBCS algorithm introduced in Section 2.3.5 was employed to select the optimal DSTSK configuration for supporting a specific number of users. Moreover, we adopted a successive relaying architecture for recovering the conventional 50% half-duplex relaying-induced throughput loss, albeit at the cost of supporting less users.

Sections	Contributions
Section 5.1	Briefly introduced the differential detection philosophy and the concept of cooperative communications.
Section 5.2	Investigated the family of MSDSD aided DSTSK systems.
Section 5.3	Proposed the MUSRC system of Fig. 5.9 based on MSDSD aided DSTSK.

Table 6.4: Summary of contributions of Chapter 5.

Coherent Versus Differential MIMOs: In this thesis, coherent versus differential MIMO systems have been discussed. Naturally, coherent MIMO systems require CSI for performing data detection. In this case, accurate yet efficient CE schemes are desired. We have introduced three major types of CE techniques, namely the TBCE, BCE and SBCE of Section 1.2. It has been demonstrated in Fig. 3.2 that the conventional TBCE scheme is capable of achieving accurate CE at the cost of significantly reduced throughput loss. BCE does not reduce the system's throughput, but it is widely recognized that the BCEs impose a high complexity and slow convergence, whilst suffering from unavoidable estimation and decision ambiguities. This potentially limits the applications of BCE schemes. Against this background, in Section 3.3 SBCE schemes were proposed for achieving accurate CE without significantly reducing the system's throughput. Moreover, in Section 3.4.2, we proposed a BBSBCE scheme for three-stage turbo coded near-capacity coherent MIMO systems, which has been demonstrated to be capable of approaching the optimal performance obtained by perfect CSI.

As a counterpart of coherent MIMO systems, differential MIMO systems were discussed in Chapter 5, where no CSI is required for performing data detection. However, compared to coherent MIMOs, differential MIMOs may have a lower design flexibility since transmitted data blocks have to rely on unitary matrices. More importantly, CDD invoked for differential MIMOs experiences 3 dB performance loss and the Doppler frequency also affects the performance of CDD schemes. To be more explicit, when the Doppler frequency increases, the system performance will be significantly degraded, leading to an error floor in CDD schemes. MSDD schemes lead to a lower performance discrepancy between the coherent and differential schemes. However, the detection complexity increases exponentially with the detection window size N_w . In order to conceive low-complexity ML-MSDD for Rayleigh fading channels, the MSDSD of Section 5.2 was proposed, which introduces the concept of SD into MSDD schemes for the sake of reducing the computational complexity.

From the above discussion, it may be concluded that even though CSI is required for coherent MIMOs, they are attractive due to their capability of providing a higher design flexibility compared to their differential counterparts. Additionally, with the aid of the proposed low-complexity BB-

SBCE scheme, the system's performance may be capable of approaching the perfect CSI bound. On the other hand, with the aid of MSDSD, differential MIMOs are capable of reducing the performance gap compared to its coherent counterpart and may find its applications in the case that obtaining CSI is impractical, i.e. in cooperative communication systems. The comparison between coherent and differential MIMOs are summarized in Table 6.5.

Table 6.5: Coherent versus differential MIMO systems.

MIMO Types	Coherent MIMO	Differential MIMO
CSI	Required, may be obtained by TBCE, BCE or SBCE, etc	Not required
Design flexibility	High	Low
Detectors	ML, MMSE, ZF, etc	CDD, MSDD, MSDSD, etc
Applications	Wide range of applications when CE is practical	Preferred when CE becomes impractical

6.2 Design Guidelines

Improving the overall quality of wireless systems in terms of striving for a better compromise amongst the conflicting design constraints of, i.e. BER, effective throughput, coding rate, etc., are the basic motivation of our designs. These efforts led to the design guidelines listed below:

- Compared to the conventional single-antenna aided systems, MIMO systems are capable of providing spatial diversity and/or multiplexing gains. Accordingly, for the sake of achieving MIMO advantages, we may opt for invoking two types of MIMOs – SDM/V-BLAST and novel STSK systems.
- However, the performance of MIMOs heavily relies on the accuracy of CE, which may become a crucial component in coherent MIMO communication systems. Conventional TBCE schemes of Fig. 3.1 is capable of acquiring accurate CSI by employing a high PO, which may substantially reduce the system's effective throughput. The BCE techniques have attracted significant attention. However, it is well-known that blind methods not only impose a high complexity, while exhibiting a slow convergence, but also suffer from inherent estimation and decision ambiguities.
- The SBCE scheme of Fig. 3.10 is proposed for solving the above-mentioned problems of TBCE and BCE, which is capable of significantly improving the CE accuracy, while employing only a low PO, hence maintaining a high system throughput. Additionally, the joint CE and turbo detection/decoding philosophy of Fig. 3.19 is attractive, since the turbo detector/decoder is capable of feeding back more reliable detected signals to assist the DDCE and

likewise, more accurate channel estimates will result in an increasingly more accurate turbo detector/decoder output.

- However, there are two major limitations of conventional joint CE and turbo detection schemes of Fig. 3.19. Firstly, the conventional turbo coded CE scheme utilizing the entire detected data frame for DDCE introduces an extra CE loop, hence leading to a significant increase in computational complexity. Secondly, the detected frame contains erroneous decisions, potentially leading to serious error propagation, which may degrade the system's achievable performance.
- For the sake of avoiding the above-mentioned limitations of conventional joint CE and turbo detection schemes of Fig. 3.19, we may use a low-complexity joint BBSBCE and three-stage iterative demapping/decoding scheme of Fig. 3.20 for near-capacity CSTSK systems, which does not impose an extra iterative loop between the channel estimator and the three-stage turbo detector. Additionally, only the “high quality” or “more reliable” blocks-of-bits are selected for further DDCE, for the sake of reducing both the error propagation and the CE complexity.
- Additionally, in order to further mitigate the effects of “bad” decisions to certain extent and to improve the system's performance, we opt for using a novel BBSB-SCE scheme in Section 3.5.
- Even though the above-mentioned CE schemes may help to efficiently realize the “MIMO advantages”, it may also be realized that since MIMO systems utilize multiple RF chains both at transmitter and receiver, their power consumption and hardware costs are substantial. Moreover, for massive MIMO systems and particularly for millimetre-wave based MIMO systems, the number of available antenna array elements increases massively, while in practice the number of available RF chains is typically limited.
- For the sake of removing the above-mentioned barriers of MIMOs, we may introduce the concept of AS into MIMO systems, which offers a low-cost, low-complexity technique of reducing the number of RF chains utilised at the transmitter and/or receiver, while retaining the significant advantages of MIMO systems.
- Generally, two popular optimization criteria can be used for AS algorithms, namely the CBAS and NBAS of Sections 4.1.1.1 and 4.1.1.2. The optimal CBAS may be achieved by a complex full-search, while sub-optimal algorithms may lead to certain performance loss. Moreover, it has been demonstrated that NBAS algorithms are capable of approaching the performance of CBAS techniques, while imposing a lower AS complexity.
- Against this background, we may opt for using the low-complexity yet efficient NBJTRAS algorithm of Section 4.2 in MIMO systems, which is capable of significantly improving the attainable MIMO performance. Additionally, the proposed NBJTRAS aided MIMO system

is capable of achieving an extra diversity gains over that of the conventional MIMO system relying on the same number of RF chains and operating without AS, albeit this gain is achieved at the cost of employing more AEs than the latter.

- In the AS aided MIMO systems of Fig. 4.7, CSI is usually required for performing both AS and data detection. The TBCE scheme of Fig. 4.24 is often preferred due to its simplicity. However, the conventional TBCE schemes are capable of generating accurate MIMO CSI only at the cost of imposing a potentially excessive PO, which significantly erodes the system's throughput, while simultaneously imposing an excessive CE complexity.
- Additionally, it has been shown in Fig. 4.28 that for AS aided MIMO systems, AS requires a less accurate CSI, while data detection must rely on a very accurate channel estimate.
- Against this background, we may employ TTCE scheme proposed in Section 4.3.2 relying on a low PO for assisting the NBJTRAS aided MIMO system, which maintains a high system throughput, while imposing a low computational complexity. To be more explicit, in tier one of the proposed TTCE scheme of Fig. 4.32, a low-complexity yet low-pilot-overhead based TBCE scheme relying on RF chain reuse generates a coarse initial estimate of the full MIMO channel matrix using only a low number of training symbol blocks. Then NBJTRAS is carried out based on this rough CE, and the selected TAs and RAs are activated for actual data transmission. In tier two of the proposed scheme, a SBCE scheme is employed. As seen in of Fig. 4.32, this scheme relies on the selected subset channel matrix, obtained in the tier-one NBJTRAS stage, as the initial MIMO CE for activating the decoding process invoked for detecting the data as well as for refining the CE.
- From all the above discussion, it may be concluded that realizing the potential MIMO advantages requires the AEs to be sufficiently far apart. This becomes impractical due to the physical size of mobile devices. Fortunately, we may rely on the concept of a distributed MIMO techniques, namely on cooperative communications, where the individual single-antenna based mobile devices may for a VAA for the sake of achieving spatial diversity.
- Due to the dual-phase operations, conventional cooperative communications typically experiences a 50% throughput loss. In order to make up for the throughput loss of conventional half-duplex cooperation, we may opt for invoking a successive relying protocol, where the main idea is to utilize a pair of VAAs, so that the signals arriving from the SNs may be received by one of the pair of VAA and concurrently transmitted by another one. Additionally, in successive relaying system IVI may exist. Therefore, the classic DS-CDMA technique may be invoked for the sake of suppressing the interference.
- Moreover, in coherent distributed MIMO systems, multiple wireless channels have to be estimated. This may not only reduce the system's throughput efficiency, but also impose an

excessive CE complexity. Against this background, we may opt for invoking the family of differential MIMO schemes for the sake of avoiding CE.

- Conventional CDD imposes the well-known 3 dB performance loss and an irreducible error-floor may be formed in the presence of rapidly fading channels. Then MSDD philosophy is then proposed for solving the problems of CDD, at the expense of imposing an excessive computational complexity. As a remedy, we may opt for using MSDSD for the sake of reducing the excessive complexity imposed by MSDD.

6.3 Future Research

In this section, we will briefly discuss a number of future research ideas.

6.3.1 Particle Swarm Optimisation for Antenna Selection Schemes

It has been mentioned in Chapter 4 that for the CBAS schemes of Fig. 4.1, optimal performance may be achieved by exhaustive search, while imposing increasingly high computational complexity. Against this background, a near-optimal yet low complexity AS algorithm is desired. As an efficient population-based stochastic search algorithm, the concept of the PSO proposed by Kennedy and Eberhart in 1995 [167] may be invoked for AS schemes [168, 169]. More specifically, the PSO algorithm relies on a group of random particles, where each particle represents a potential solution to the clustering problem. Then the best value of the objective function (i.e. Eq. (4.1) of CBAS) may be found by keeping a particle moving towards its locally best and the globally best particle. In this way, PSO may be employed to find the near-optimal solution for AS schemes [168].

Apart from the potential ability of reducing the computational complexity, PSO may also be invoked for improving the performance of AS in spatially correlated fading channel environments. Generally, in the research on AS, usually an independent fading environment is assumed, implying that no correlation exists between the Tx/Rx antennas. However, in practice, the correlation between the antennas is unavoidable, especially when the physical size of the mobile devices is limited. It has been demonstrated in Section 4.2.2.2 that in the presence of spatial correlation, the performance of AS may be degraded. One way of solving this problem is to classify the antennas into several groups according to their correlations [169], where PSO may be invoked. More specifically, if we select L_T out of M antennas, we may first employ PSO to classify M antennas into L_T groups. Note that AEs within a group may experience a higher correlation, while AEs from different groups are considered to have lower or zero correlation. Then we select the best antenna in each class, and in this way, a total of L_T antennas may be selected, which have lower spatial correlation, hence resulting in an improved performance of the AS schemes.

6.3.2 Antenna and Relay Selection in Cooperative Communications

As it has been demonstrated in Chapter 5 that cooperative communications are capable of enhancing both the throughput and reliability of wireless communications by employing multiple relays to form a distributed MIMO system. However, in cooperative communications, the number of relays employed is usually limited due to the increased system complexity. Against this background, relay selection (RS) has become an attractive concept due to its capability of efficiently using power and bandwidth resources and owing to its simplicity of implementation [170–176]. As a result, we may further introduce the concept of RS in conjunction with AS into our proposed MUSRC system discussed in Chapter 5. More specifically, in the broadcast phase, RS may be invoked for selecting the best receiving relays according to their channel conditions, i.e. the channels associated with a higher norm. Meanwhile, in the relaying phase, AS takes place at destination to further enhance the performance of the relaying transmission. In this way, the performance of MUSRC may be further improved, while maintaining a low system complexity.

6.3.3 Millimetre-Wave Mobile Broadband Systems

Rapid evolutionary changes have been seen in mobile communications systems every decade since the 1970s. The First generation (1G) cellular systems introduced in 1970s were based on analogue technologies, while the Second generation (2G) systems introduced in the 1980s were digital systems. Both of these two generations of wireless communication systems were mainly designed for providing voice-oriented services. However, due to the fast expansion of multimedia traffic, higher access speeds are required. The International Mobile Telecommunications 2000 (IMT-2000) concept was introduced at the beginning of the 21st century as the Third generation (3G) cellular systems, which could provide 2 Mb/s and 144 kb/s in indoor and vehicular environments. However, this will not be the end of evolution. Researchers have shown their great interests in the future generations of mobile communications, including the Fourth generation (4G) and Fifth generation (5G) systems [177–179].

Nowadays, almost all commercial radio communications including AM/FM radio, high-definition TV, cellular, satellite communications, GPS and Wi-Fi have been confined to a relatively narrow band of RF spectrum in the 300 MHz-3 GHz band. However, the specific portion of RF spectrum above 3 GHz has hardly been explored for commercial wireless communication applications [164, 180]. The Millimetre-wave Mobile Broadband (MMB) systems spanning from 30 GHz to 300 GHz are capable of achieving multiGigabit data rates and beginning to find its potential applications in mobile communication systems. For example, a hybrid *MMB + 4G* system was proposed in [181], where the system's primary information, control channel, and feedback channels are transmitted through a 4G system, while utilizing the MMB for high data rate communications. This is expected to improve the user experience. Additionally, millimetre-wave wireless communication systems may also be applied in high-speed indoor wireless communications [182], railway

communications [183] and soldier-to-soldier communications [184].

Since MMB systems have been considered as a promising solution to the future generation mobile communications, in the next stage of research, we may opt for some of these topics. Additionally, since the wavelengths of the MMB range from 1mm to 10mm, the concept of massive MIMOs [185] may be applied in MMB systems. This may be a promising research topic as well.

Bibliography

- [1] L. Hanzo, O. R. Alamri, M. El-Hajjar, and N. Wu, *Near-Capacity Multi-Functional MIMO Systems: Sphere-Packing, Iterative Detection and Cooperation*. John Wiley & Sons: Chichester, UK, 2009.
- [2] P. W. Wolniansky, G. J. Foschini, G. D. Golden, and R. A. Valenzuela, “V-BLAST: an architecture for realizing very high data rates over the rich-scattering wireless channel,” in *IEEE Proceedings of 1998 URSI International Symposium on Signals, Systems, and Electronics*, pp. 295–300, September 1998.
- [3] R. Mesleh, H. Haas, C. W. Ahn, and S. Yun, “Spatial modulation - a new low complexity spectral efficiency enhancing technique,” in *IEEE Proceedings of First International Conference on Communications and Networking (CHINACOM)*, pp. 1–5, October 2006.
- [4] S. Alamouti, “A simple transmit diversity technique for wireless communications,” *IEEE Journal on Selected Areas in Communications*, vol. 16, pp. 1451–1458, October 1998.
- [5] S. Sugiura, S. Chen, and L. Hanzo, “Coherent and differential space-time shift keying: A dispersion matrix approach,” *IEEE Transactions on Communications*, vol. 58, pp. 3219–3230, November 2010.
- [6] L. Hanzo, M. El-Hajjar, and O. Alamri, “Near-capacity wireless transceivers and cooperative communications in the MIMO era: Evolution of standards, waveform design, and future perspectives,” *Proceedings of the IEEE*, vol. 99, pp. 1343–1385, October 2011.
- [7] A. Goldsmith, S. Jafar, N. Jindal, and S. Vishwanath, “Capacity limits of MIMO channels,” *IEEE Journal on Selected Areas in Communications*, vol. 21, pp. 684–702, June 2003.
- [8] N. Chiurto, B. Rimoldi, and E. Telatar, “On the capacity of multi-antenna Gaussian channels,” in *IEEE Proceedings of 2001 International Symposium on Information Theory*, p. 53, June 2001.
- [9] B. Sklar, *Digital Communications: Fundamentals and Applications*. Publishing House of Electronics Industry, 2 ed., 2006.

- [10] M. B. Pursley and J. S. Skinner, "Adaptive coding for frequency-hop transmission in mobile ad hoc networks with partial-band interference," *IEEE Transactions on Communications*, vol. 57, pp. 801–811, March 2009.
- [11] L. Hanzo, L.-L. Yang, E.-L. Kuan, and K. Yen, *Single- and Multi-carrier DS-CDMA: Multi-User Detection, Space-Time Spreading, Synchronisation, Networking and Standards*. John Wiley and IEEE Press, 2003.
- [12] M. K. Simon and M. S. Alouini, *Digital communications over fading channels*. John Wiley, New York, 2000.
- [13] A. Wittneben, "Base station modulation diversity for digital simulcast," in *IEEE Proceedings of Vehicular Technology Conference (VTC1991-Spring)*, pp. 848–853, May 1991.
- [14] V. Tarokh, N. Seshadri, and A. R. Calderbank, "Space-time codes for high data rate wireless communication: performance criterion and code construction," *IEEE Transactions on Communications*, vol. 44, pp. 744–765, March 1998.
- [15] B. Hassibi and B. M. Hockwald, "High-rate codes that are linear in space and time," *IEEE Transactions on Information Theory*, vol. 48, pp. 1804–1824, July 2002.
- [16] B. Hassibi and B. M. Hockwald, "Cayley differential unitary space-time codes," *IEEE Transactions on Information Theory*, vol. 48, pp. 1485–1503, June 2002.
- [17] R. Y. Mesleh, H. Hass, S. Sinanovic, C. W. Ahn, and S. Yun, "Spatial modulation," *IEEE Transactions on Vehicular Technology*, vol. 57, pp. 2228–2241, July 2008.
- [18] J. Jeganathan, A. Ghayeb, and L. Szczecinski, "Spatial modulation: Optimal detection and performance analysis," *IEEE Communications Letters*, vol. 12, pp. 545–547, August 2008.
- [19] J. Jeganathan, A. Ghayeb, L. Szczecinski, and A. Ceron, "Space shift keying modulation for MIMO channels," *IEEE Transactions on Wireless Communications*, vol. 8, pp. 3692–3703, July 2009.
- [20] M. D. Renzo, H. Haas, A. Ghayeb, S. Sugiura, and L. Hanzo, "Spatial modulation for generalized MIMO: challenges, opportunities and implementation," *Proceedings of the IEEE*, vol. 102, pp. 56–103, January 2014.
- [21] S. Sugiura, S. Chen, and L. Hanzo, "Generalized space-time shift keying designed for flexible diversity-, multiplexing- and complexity-tradeoffs," *IEEE Transactions on Wireless Communications*, vol. 10, pp. 1144–1153, April 2011.
- [22] D. G. Brennan, "Linear diversity combining techniques," *Proceedings of the IRE*, vol. 47, pp. 1075–1102, June 1959.

- [23] C. Xu, S. Sugiura, S. X. Ng, and L. Hanzo, "Spatial modulation and space-time shift keying: Optimal performance at a reduced detection complexity," *IEEE Transactions on Communications*, vol. 61, pp. 206–216, January 2013.
- [24] M. I. Kadir, S. Sugiura, S. Chen, and L. Hanzo, "Unified MIMO-multicarrier designs: A space-time shift keying approach," *IEEE Communications Surveys & Tutorials*, pp. 1–31, November 2014.
- [25] G. J. Foschini, "Layered space-time architecture for wireless communication in a fading environment when using multiple antennas," *Bell Labs Technical Journal*, vol. 1, pp. 41–59, 1996.
- [26] A. Benjebbour, H. Murata, and S. Yoshida, "Comparison of ordered successive receivers for space-time transmission," in *IEEE Vehicular Technology Conference (VTC2001-Fall)*, pp. 2053–2057, October 2001.
- [27] M. O. Damen, H. E. Gamal, and G. Caire, "On maximum-likelihood detection and the search for the closest lattice point," *IEEE Transactions on Information Theory*, vol. 49, pp. 2389–2402, October 2003.
- [28] J. Ward and R. T. Compton, "High throughput slotted ALOHA packet radio networks with adaptive arrays," *IEEE Transactions on Communications*, vol. 41, pp. 460–470, March 1993.
- [29] J. Blogh and L. Hanzo, *Third-generation systems and intelligent wireless networking: smart antennas and adaptive modulation*. New York: Wiley, 2002.
- [30] B. D. V. Veen and K. M. Buckley, "Beamforming: a versatile approach to spatial filtering," *IEEE ASSP Magazine*, vol. 5, pp. 4–24, April 1988.
- [31] S. Chen, S. Sugiura, and L. Hanzo, "Semi-blind joint channel estimation and data detection for space-time shift keying systems," *IEEE Signal Processing Letters*, vol. 17, pp. 993–996, December 2010.
- [32] P. Zhang, I. Dey, S. Sugiura, and S. Chen, "Semi-blind joint channel estimation and data detection for space-time shift keying systems," in *IEEE Proceedings of Vehicular Technology Conference (VTC2011-Spring)*, pp. 993–996, May 2011.
- [33] M. Biguesh and A. B. Gershman, "Training-based MIMO channel estimation: A study of estimator tradeoffs and optimal training signals," *IEEE Transactions on Signal Processing*, vol. 54, pp. 884–893, March 2006.
- [34] E. Bjornson and B. Ottersten, "A framework for training-based estimation in arbitrarily correlated Rician MIMO channels with Rician disturbance," *IEEE Transactions on Signal Processing*, vol. 58, pp. 1807–1820, March 2010.

- [35] C. Fragouli, N. Al-Dhahir, and W. Turin, "Training-based channel estimation for multiple-antenna broadband transmissions," *IEEE Transactions on Wireless Communications*, vol. 2, pp. 384–391, March 2003.
- [36] C. R. Murthy, A. K. Jagannatham, and B. D. Rao, "Training-based and semiblind channel estimation for MIMO systems with maximum ratio transmission," *IEEE Transactions on Signal Processing*, vol. 54, pp. 2546–2558, July 2006.
- [37] J. K. Cavers, "An analysis of pilot symbol assisted modulation for Rayleigh fading channels," *IEEE Transactions on Vehicular Technology*, vol. 40, pp. 686–693, November 1991.
- [38] X. Ma, G. B. Giannakis, and S. Ohno, "Optimal training for block transmissions over doubly selective wireless fading channels," *IEEE Transactions on Signal Processing*, vol. 51, pp. 1351–1366, May 2003.
- [39] T. L. Marzetta, "BLAST training: estimating channel characteristics for high capacity space-time wireless," in *Proceedings of 37th Annual Allerton Conference on Communication, Control and Computing*, pp. 1–9, September 1999.
- [40] Y. Li, "Optimum training sequences for OFDM systems with multiple transmit antennas," in *Proceedings of 2000 IEEE Global Communications Conference (GLOBECOM-2000)*, vol. 3, pp. 1478–1482, November 2000.
- [41] S. Sugiura and L. Hanzo, "Effects of channel estimation on spatial modulation," *IEEE Signal Processing Letters*, vol. 19, pp. 805–808, October 2012.
- [42] A. A. Nasir, H. M. ehrpouyan, S. Durrani, S. D. Blostein, and R. A. Kennedy, "Antenna selection algorithms for MEA transmission systems," in *IEEE Proceedings of 2014 International Workshop on Signal Processing Advances in Wireless Communications*, pp. 1–5, June 2014.
- [43] L. Tang, R. W. Liu, V. C. Soon, and Y. F. Huang, "Indeterminacy and identifiability of blind identification," *IEEE Transactions on Circuits and Systems*, vol. 38, pp. 499–509, May 1991.
- [44] P. Stoica and G. Ganesan, "Space-time block codes: Trained, blind and semi-blind detection," in *IEEE Proceedings of 2002 International Conference on Acoustics, Speech, and Signal Processing (ICASSP)*, pp. 1609–1612, May 2002.
- [45] S. Shahbazpanahi, A. B. Gershman, and J. H. Manton, "Closed-form blind MIMO channel estimation for orthogonal space-time block codes," *IEEE Transactions on Signal Processing*, vol. 53, pp. 4506–4517, December 2005.
- [46] C. Shin, R. W. Heath, and E. J. Powers, "Blind channel estimation for MIMO-OFDM systems," *IEEE Transactions on Vehicular Technology*, vol. 56, pp. 670–685, March 2007.

- [47] X. Liu, M. E. Bialkowski, S. Lu, and H. Hui, "A novel blind channel estimation algorithm for a MIMO system," in *IEEE Proceedings of Vehicular Technology Conference (VTC2008-Spring)*, pp. 1113–1117, May 2008.
- [48] S. Shahbazpanahi, A. B. Gershman, and G. B. Giannakis, "Blind and semiblind channel and carrier frequency-offset estimation in orthogonally space-time block coded MIMO systems," *IEEE Transactions on Signal Processing*, vol. 56, pp. 702–711, February 2008.
- [49] E. Carcalho and D. T. M. Slock, "Blind and semi-blind FIR multichannel estimation: (global) identifiability conditions," *IEEE Transactions on Signal Processing*, vol. 52, pp. 1053–1064, April 2004.
- [50] A. Medles and D. T. M. Slock, "Semiblind channel estimation for MIMO spatial multiplexing systems," in *IEEE Proceedings of Vehicular Technology Conference (VTC2001-Fall)*, pp. 1240–1244, October 2001.
- [51] S. Buzzi, M. Lops, and S. Sardellitti, "Performance of iterative data detection and channel estimation for single-antenna and multiple-antennas wireless communications," *IEEE Transactions on Vehicular Technology*, vol. 53, pp. 1085–1104, July 2004.
- [52] M. Abuthinien, S. Chen, and L. Hanzo, "Semi-blind joint maximum likelihood channel estimation and data detection for MIMO systems," *IEEE Signal Processing Letters*, vol. 15, pp. 202–205, January 2008.
- [53] H. R. Palally, S. Chen, W. Yao, and L. Hanzo, "Partical swarm optimisation aided semi-blind joint maximum likelihood channel estimation and data detection for MIMO systems," in *IEEE Proceedings of 15th Workshop on Statistical Signal Processing (SSP09)*, pp. 309–312, August 2009.
- [54] H. Li, S. M. Betz, and H. V. Poor, "Performance analysis of iterative channel estimation and multiuser detection in multipath DS-CDMA channels," *IEEE Transactions on Signal Processing*, vol. 55, pp. 1981–1993, May 2007.
- [55] M. Jiang, J. Akhtman, and L. Hanzo, "Iterative joint channel estimation and multi-user detection for multiple-antenna aided OFDM systems," *IEEE Transactions on Wireless Communications*, vol. 6, pp. 2904–2914, August 2007.
- [56] P. S. Rossi and R. R. Müller, "Joint twofold-iterative channel estimation and multiuser detection for MIMO-OFDM systems," *IEEE Transactions on Wireless Communications*, vol. 7, pp. 4719–4729, November 2008.
- [57] J. Ylioinas and M. Juntti, "Iterative joint detection, decoding, and channel estimation in turbo-coded MIMO-OFDM," *IEEE Transactions on Vehicular Technology*, vol. 58, pp. 1784–1796, May 2009.

- [58] J. Zhang, S. Chen, X. Mu, and L. Hanzo, "Joint channel estimation and multi-user detection for SDMA/OFDM based on dual repeated weighted boosting search," *IEEE Transactions on Vehicular Technology*, vol. 60, pp. 3265–3275, September 2011.
- [59] J. Zhang, S. Chen, X. Mu, and L. Hanzo, "Turbo multi-user detection for OFDM/SDMA systems relying on differential evolution aided iterative channel estimation," *IEEE Transactions on Communications*, vol. 60, pp. 1621–1633, June 2012.
- [60] P. Zhang, S. Chen, and L. Hanzo, "Reduced-complexity near-capacity joint channel estimation and three-stage turbo detection for coherent space-time shift keying," *IEEE Transactions on Communications*, vol. 61, pp. 1902–1912, May 2013.
- [61] P. Zhang, S. Chen, and L. Hanzo, "Embedded iterative semi-blind channel estimation for three-stage-concatenated MIMO-aided QAM turbo-transceiver," *IEEE Transactions on Vehicular Technology*, vol. 63, pp. 439–446, January 2014.
- [62] S. Abdallah and N. Psaromiligkos, "Semi-blind channel estimation with superimposed training for OFDM-based AF two-way relaying," *IEEE Transactions on Wireless Communications*, vol. 13, pp. 2468–2477, May 2014.
- [63] F. Rusek, D. Persson, B. K. Lau, E. G. Larsson, T. L. Marzetta, O. Edfors, and F. Tufvesson, "Scaling up MIMO: Opportunities and challenges with very large arrays," *IEEE Signal Processing Magazine*, vol. 30, pp. 40–60, January 2013.
- [64] K. C. Huang and Z. Wang, "Terahertz terabit wireless communication," *IEEE Microwave Magazine*, vol. 12, pp. 108–116, June 2011.
- [65] T. S. Rappaport, S. Sun, R. Mayzus, H. Zhao, Y. Azar, K. Wang, G. N. Wong, J. K. Schulz, M. Samimi, and F. Gutierrez, "Millimeter wave mobile communications for 5G cellular: It will work!," *IEEE Access*, vol. 1, pp. 335–349, May 2013.
- [66] K. C. Huang and Z. Wang, "Millimeter-wave circular polarized beamsteering antenna array for Gigabit wireless communications," *IEEE Transactions on Antennas and Propagation*, vol. 54, pp. 743–746, February 2006.
- [67] F. Khan and Z. Pi, "mmwave mobile broadband (MMB): Unleashing the 3-300 GHz spectrum," in *IEEE Proceedings of 34th Sarnoff Symposium*, pp. 1–6, May 2004.
- [68] S. Sanaye and A. Norsratinia, "Antenna selection in MIMO systems," *IEEE Communications Magazine*, vol. 42, pp. 68–73, October 2004.
- [69] A. Gorokhov, "Antenna selection algorithms for MEA transmission systems," in *IEEE Proceedings of 2002 ICASSP*, vol. 3, pp. 2857–2860, May 2002.
- [70] M. G-Alkhansari and A. B. Gershman, "Fast antenna subset selection in MIMO systems," *IEEE Transactions on Signal Processing*, vol. 52, pp. 339–347, February 2004.

- [71] A. S. Hiwale, A. A. Ghatol, and S. D. Bhad, “Performance analysis of space-time trellis codes with receive antenna selection,” in *IEEE Proceedings of WCSN 2008*, pp. 148–152, December 2008.
- [72] D. Liu and D. K. C. So, “Performance based receive antenna selection for V-BLAST systems,” *IEEE Transactions on Wireless Communications*, vol. 8, pp. 214–225, January 2009.
- [73] Z. Xu, S. Sfar, and R. S. Blum, “Analysis of MIMO systems with receive antenna selection in spatially correlated Rayleigh fading channels,” *IEEE Transactions on Vehicular Technology*, vol. 58, pp. 251–262, January 2009.
- [74] W. A. Al-Hussaibi and F. H. Ali, “Receive antenna selection for uplink multiuser MIMO systems over correlated Rayleigh fading channels,” in *IEEE Proceedings of International Symposium on Wireless Personal Multimedia Communications*, pp. 1–5, October 2011.
- [75] L. Yang and Z. Lin, “BER analysis of multiuser relaying networks with receive antenna selection,” in *Proceedings of 2013 International Conference on Wireless Communications & Signal Processing (WCSP)*, pp. 1–4, October 2013.
- [76] R. G. Stephen, C. R. Murthy, and M. Coupechoux, “A Markov decision theoretic approach to pilot allocation and receive antenna selection,” *IEEE Transactions on Wireless Communications*, vol. 12, pp. 3813–3823, August 2013.
- [77] R. W. Heath, S. Sandhu, and A. Paulraj, “Antenna selection for spatial multiplexing systems with linear receivers,” *IEEE Communications Letters*, vol. 5, pp. 142–144, March 2013.
- [78] R. Rajashekhar, K. S. Hari, and L. Hanzo, “Antenna selection in spatial modulation systems,” *IEEE Communications Letters*, vol. 17, pp. 521–524, March 2013.
- [79] W. H. Chung and C. Y. Hung, “Multi-antenna selection using space shift keying in MIMO systems,” in *IEEE Proceedings of Vehicular Technology Conference (TVC2012-Spring)*, pp. 1–5, May 2012.
- [80] S. Kim, M. Shin, and C. Lee, “Transmit antenna selection scheme for iterative receivers in MIMO systems,” *IEEE Signal Processing Letters*, vol. 14, pp. 916–919, December 2007.
- [81] S. Sanayei and A. Nosratinia, “Capacity maximizing algorithms for joint transmit-receive antenna selection,” in *IEEE Proceedings of Asilomar Conference on Signals, Systems and Computers*, pp. 1773–1776, November 2004.
- [82] H. S. Kim and Y. S. Byun, “Near-optimal selection of joint transmit-receive antennas for MIMO channel based on maximizing channel capacity,” in *IEEE Proceedings of APCC-2006*, pp. 1–5, August 2006.

[83] Y. R. Wei and M. Z. Wang, "Capacity-based efficient joint transmit and receive antenna selection schemes in MIMO systems," in *IEEE Proceedings of 2006 International Conference on Information & Communication Technologies: From Theory to Applications (ICTTA-2006)*, pp. 2125–2129, April 2006.

[84] R. S. Blum, Z. Xu, and S. Sfar, "A near-optimal joint transmit and receive antenna selection algorithm for MIMO systems," in *IEEE Proceedings of Radio and Wireless Symposium 2009*, pp. 554–557, January 2009.

[85] M. Naeem and D. C. Lee, "Near-optimal selection of transmit and receive antennas for MIMO systems," in *IEEE Proceedings of The 9th International Symposium on Communication and Information Technologies (ISCIT-2009)*, pp. 572–577, September 2009.

[86] T. Gucluoglu and T. M. Duman, "Space-time coded systems with joint transmit and receive antenna selection," in *Proceedings of 2007 International Conference on Communications (ICC-2007)*, pp. 5305–5310, June 2007.

[87] A. Yilmaz and O. Kucur, "Error performance of joint transmit and receive antenna selection in two hop amplify-and-forward relay system over Nakagami-m fading channels," in *IEEE Proceedings of International Symposium on Personal Indoor and Mobile Radio Communications*, pp. 2198–2203, September 2010.

[88] T. Gucluoglu and T. M. Duman, "Performance analysis of transmit and receive antenna selection over flat fading channels," *IEEE Transactions on Wireless Communications*, vol. 7, pp. 3056–3065, August 2008.

[89] J. M. Chakravarti and Y. N. Trivedi, "Performance analysis of Alamouti transmit diversity with a sub-optimum joint transmit-receive antenna selection scheme," in *IEEE Proceedings of 2013 National Conference on Communications (NCC-2013)*, pp. 1–5, February 2013.

[90] P. Zhang, S. Chen, and L. Hanzo, "Two-tier channel estimation aided near-capacity MIMO transceivers relying on norm-based joint transmit and receive antenna selection," *IEEE Transactions on Wireless Communications*, vol. 14, pp. 122–137, January 2015.

[91] D. Divsalar and M. K. Simon, "Multiple-symbol differential detection of MPSK," *IEEE Transactions on Communications*, vol. 38, pp. 300–308, March 1990.

[92] P. Ho and D. Fung, "Error performance of multiple-symbol differential detection of PSK signals transmitted over correlated Rayleigh fading channels," *IEEE Transactions on Communications*, vol. 40, pp. 1566–1569, October 1992.

[93] D. Divsalar and M. Simon, "Maximum-likelihood differential detection of uncoded and trellis coded amplitude phase modulation over AWGN and fading channels-metrics and performance," *IEEE Transactions on Communications*, vol. 42, pp. 76–89, January 1994.

- [94] K. Mackenthun, "A fast algorithm for multiple-symbol differential detection of MPSK," *IEEE Transactions on Communications*, vol. 42, pp. 1471–1474, April 1994.
- [95] P. Fan, "Multiple-symbol detection for transmit diversity with differential encoding scheme," *IEEE Transactions on Consumer Electronics*, vol. 47, pp. 96–100, February 2001.
- [96] M. K. Simon and M.-S. Alouini, "Multiple symbol differential detection with diversity reception," *IEEE Transactions on Communications*, vol. 49, pp. 300–308, August 2001.
- [97] R. Schober and L. Lampe, "Noncoherent receivers for differential space-time modulation," *IEEE Transactions on Communications*, vol. 50, pp. 768–777, May 2002.
- [98] L. Lampe, R. Schober, V. Pauli, and C. Windpassinger, "Multiple-symbol differential sphere decoding," *IEEE Transactions on Communications*, vol. 53, pp. 1981–1985, December 2005.
- [99] V. Pauli, L. Lampe, and R. Schober, "Turbo DPSK" using soft multiple-symbol differential sphere decoding," *IEEE Transactions on Information Theory*, vol. 52, pp. 1385–1398, April 2006.
- [100] V. Pauli and L. Lampe, "On the complexity of sphere decoding for differential detection," *IEEE Transactions on Information Theory*, vol. 53, pp. 1595–1603, April 2007.
- [101] C. Xu, L. Wang, S. X. Ng, and L. Hanzo, "Multiple-symbol differential sphere detection aided differential space-time block codes using QAM constellations," *IEEE Signal Processing Letters*, vol. 18, pp. 497–500, September 2011.
- [102] P. Zhang, S. Chen, and L. Hanzo, "Differential space-time shift keying-aided successive-relaying-assisted decode-and-forward cooperative multiuser CDMA," *IEEE Transactions on Vehicular Technology*, vol. 62, pp. 2156–2169, January 2013.
- [103] M. I. Kadir, S. Chen, K. Hari, K. Giridhar, and L. Hanzo, "OFDM-aided differential space-time shift keying using iterative soft multiple-symbol differential sphere decoding," *IEEE Transactions on Vehicular Technology*, vol. 63, pp. 4102–4108, October 2014.
- [104] L. Wang and L. Hanzo, "The amplify-and-forward cooperative uplink using multiple-symbol differential sphere-detection," *IEEE Signal Processing Letters*, vol. 16, pp. 913–916, October 2009.
- [105] S. Sugiura, S. Chen, H. Haas, P. M. Grant, and L. Hanzo, "Coherent versus non-coherent decode-and-forward relaying aided cooperative space-time shift keying," *IEEE Transactions on Communications*, vol. 59, pp. 1707–1719, June 2011.
- [106] V. Fung, T. S. Rappaport, and B. Thoma, "Bit error simulation for $\pi/4$ DQPSK mobile radio communications using two-ray and measurement-based impulse response models," *IEEE Journal on Selected Areas in Communications*, vol. 11, pp. 393–405, April 1993.

[107] C. Gao, A. M. Haimovich, and D. Lao, “Multiple-symbol differential detection of MPSK space-time block codes: Decision metric and performance analysis,” *IEEE Transactions on Communications*, vol. 54, pp. 1502–1510, August 2006.

[108] L. Hanzo, Y. Akhtman, L. Wang, and M. Jiang, *MIMO-OFDM for LTE, WIFI and WIMAX: Coherent versus Non-Coherent and Cooperative Turbo-Transceivers*. John Wiley & Sons, 2010.

[109] A. Sendonaris, E. Erkip, and B. Aazhang, “User cooperation diversity-part I:system description,” *IEEE Transactions on Communications*, vol. 51, pp. 1927–1938, November 2003.

[110] A. Sendonaris, E. Erkip, and B. Aazhang, “User cooperation diversity-part II: Implementation aspects and performance analysis,” *IEEE Transactions on Communications*, vol. 51, pp. 1939–1948, November 2003.

[111] Y. Fan, C. Wang, H. V. Poor, and J. S. Thompson, “Cooperative multiplexing: toward higher spectral efficiency in multiple-antenna relay networks,” *IEEE Transactions on Information Theory*, vol. 55, pp. 3909–3926, September 2009.

[112] H. J. An and H. K. Song, “Cooperative communication in SIMO systems with multiuser-OFDM,” *IEEE Transactions on Consumer Electronics*, vol. 53, pp. 339–343, May 2007.

[113] C. Xu, E. Ternon, S. Sugiura, S. X. Ng, and L. Hanzo, “Multiple-symbol differential sphere decoding aided cooperative differential space-time spreading for the asynchronous CDMA uplink,” in *IEEE Proceedings of IEEE Global Communications Conference (GLOBECOM-2011)*, pp. 1–5, September 2011.

[114] T. Issariyakul and V. Krishnamurthy, “Amplify-and-forward cooperative diversity wireless networks: Model, analysis, and monotonicity properties,” *IEEE Transactions on Networking*, vol. 17, pp. 225–238, February 2009.

[115] J. Tian, Q. Zhang, and F. Yu, “Non-coherent detection for two-way AF cooperative communications in fast Rayleigh fading channels,” *IEEE Transactions on Communications*, vol. 59, pp. 2753–2762, October 2011.

[116] S. Lee, W. Su, S. Batalama, and J. D. Matyas, “Cooperative decode-and-forward ARQ relaying: Performance analysis and power optimization,” *IEEE Transactions on Wireless Communications*, vol. 9, pp. 2632–2642, August 2010.

[117] M. Dohler, A. Gkelias, and H. Aghvami, “A resource allocation strategy for distributed MIMO multi-hop communication systems,” *IEEE Communications Letters*, vol. 8, pp. 99–101, February 2004.

[118] D. Tse and P. Viswanath, *Fundamentals of Wireless Communication*. Cambridge University Press, 2005.

- [119] J. Wang, S. X. Ng, A. Wolfgang, L.-L. Yang, S. Chen, and L. Hanzo, "Near-capacity three-stage MMSE turbo equalization using irregular convolutional codes," in *IEEE Proceedings of Turbo-Coding-2006*, pp. 1–6, April 2006.
- [120] Z. Guo and P. Nilsson, "Algorithm and implementation of the K-best sphere decoding for MIMO detection," *IEEE Journal on Selected Areas in Communications*, vol. 24, no. 3, pp. 491–503, 2006.
- [121] L. Wang, L. Xu, S. Chen, and L. Hanzo, "Apriori-LLR-threshold-assisted K-best sphere detection for MIMO channels," in *Proceedings of Vehicular Technology Conference (VTC2008-Spring)*, pp. 867–871, May 2008.
- [122] C. Xu, S. Sugiura, S. X. Ng, and L. Hanzo, "Spatial modulation and space-time shift keying: Optimal performance at a reduced detection complexity," *IEEE Transactions on Communications*, vol. 61, pp. 206–216, January 2013.
- [123] I. Land, P. A. Hoeher, and S. Gligorević, "Computation of symbol-wise mutual information in transmission systems with logAPP decoders and application to EXIT charts," in *Proceedings of 5th International ITG Conference on Source and Channel Coding (SCC)*, pp. 195–202, January 2004.
- [124] C. Xu, S. Sugiura, S. X. Ng, and L. Hanzo, "Reduced-complexity noncoherently detected differential space-time shift keying," *IEEE Signal Processing Letters*, vol. 18, pp. 153–156, March 2011.
- [125] R. W. Heath and A. J. Paulraj, "Linear dispersion codes for MIMO systems based on frame theory," *IEEE Transactions on Signal Processing*, vol. 50, pp. 2429–2441, October 2002.
- [126] C. Cozzo and B. L. Hughes, "Joint channel estimation and data detection in space-time communications," *IEEE Transactions on Communications*, vol. 51, pp. 1266–1270, August 2003.
- [127] M. Sandell, C. Luschi, P. Strauch, and R. Yan, "Iterative channel estimation using soft decision feedback," in *Proceedings of IEEE Global Communications Conference (GLOBECOM-1998)*, pp. 3728–3733, IEEE, November 1998.
- [128] S. Song, A. C. Singer, and K. Sung, "Soft input channel estimation for turbo equalization," *IEEE Transactions on Signal Processing*, vol. 52, no. 10, pp. 2885–2894, 2004.
- [129] B. Hu, A. Kocian, R. Piton, A. Hviid, B. H. Fleury, and L. K. Rasmussen, "Iterative joint channel estimation and successive interference cancellation using a SISO-SAGE algorithm for coded CDMA," in *Proceedings of 38th Asilomar Conference on Signals, Systems and Computers*, pp. 622–626, November 2004.

- [130] Y. Wu, X. Zhu, and A. K. Nandi, "Soft-input turbo channel estimation for single-carrier multiple-input-multiple-output systems," *IEEE Transactions on Vehicular Technology*, vol. 58, no. 7, pp. 3867–3873, 2009.
- [131] W. Haselmayr, D. Schellander, and A. Springer, "Iterative channel estimation and turbo equalization for time-varying channels in a coded OFDM-LTE system for 16-QAM and 64-QAM," in *Proceedings of 21st IEEE International Symposium on Personal, Indoor and Mobile Radio Communications*, pp. 614–618, September 2010.
- [132] M. Loncar, R. Muller, J. Wehinger, and T. Abe, "Iterative joint detection, decoding, and channel estimation for dual antenna arrays in frequency selective fading," in *Proceedings of 5th IEEE International Symposium Wireless Personal Multimedia Communications*, pp. 125–129, October 2002.
- [133] M. Loncar, R. Muller, J. Wehinger, C. F. Mecklenbrauker, and T. Abe, "Iterative channel estimation and data detection in frequency-selective fading MIMO channels," *European Transactions on Telecommunications*, vol. 15, no. 5, pp. 459–470, 2004.
- [134] H. Li, S. M. Betz, and H. V. Poor, "Performance analysis of iterative channel estimation and multiuser detection in multipath DS-CDMA channels," *IEEE Transactions on Signal Processing*, vol. 55, no. 5, pp. 1981–1993, 2007.
- [135] M. Qaisrani and S. Lambotharan, "An iterative (turbo) channel estimation and symbol detection technique for doubly selective channels," in *IEEE Proceedings of Vehicular Technology Conference (VTC2007-Spring)*, pp. 2253–2256, April 2007.
- [136] M. Sellathurai and S. Haykin, "Turbo-BLAST for wireless communications: Theory and experiments," *IEEE Transactions on Signal Processing*, vol. 50, no. 10, pp. 2538–2546, 2002.
- [137] M. Nicoli, S. Ferrar, and U. Spagnolini, "Soft-iterative channel estimation: methods and performance analysis," *IEEE Transactions on Signal Processing*, vol. 55, no. 6, pp. 2993–3006, 2007.
- [138] S. M. Kay, *Fundamentals of Statistical Signal Processing: Estimation Theory*. NJ: Prentice-Hall, 1993.
- [139] J. Zhang, L. Hanzo, and X. Mu, "Joint decision-directed channel and noise-variance estimation for MIMO OFDM/SDMA systems based on expectation-conditional maximization," *IEEE Transactions on Vehicular Technology*, vol. 60, pp. 2139–2151, June 2011.
- [140] A. Scherb, V. Kühn, and K. D. Kammeyer, "Cramer-Rao lower bound for semiblind channel estimation with respect to coded and uncoded finite-alphabet signals," in *Proceedings of IEEE 38th Asilomar Conference on Signals, Systems, and Computers*, pp. 2193–2197, November 2004.

- [141] T.-H. Pham, Y.-C. Liang, and A. Nallanathan, "A joint channel estimation and data detection receiver for multiuser MIMO IFDMA systems," *IEEE Transactions on Communications*, vol. 57, pp. 1857–1865, June 2009.
- [142] T.-H. Pham, Y.-C. Liang, and A. Nallanathan, "Joint channel estimation and data detection for multi-input multi-output single carrier cyclic-prefix (MIMO-SCCP) systems," in *Proceedings of IEEE International Conference on Communications (ICC 2008)*, pp. 594–598, May 2008.
- [143] S. Wang and A. Abdi, "Low-complexity optimal estimation of MIMO ISI channels with binary training sequences," *IEEE Signal Processing Letters*, vol. 13, pp. 657–660, November 2006.
- [144] M. Biguesh and A. B. Gershman, "Training-based MIMO channel estimation: A study of estimator tradeoffs and optimal training signals," *IEEE Transactions on Signal Processing*, vol. 54, no. 3, pp. 884–893, 2006.
- [145] M. C. Valenti and B. D. Woerner, "Iterative channel estimation and decoding of pilot symbol assisted turbo codes over flat-fading channels," *IEEE Journal on Selected Areas in Communications*, vol. 19, pp. 1697–1705, September 2001.
- [146] J. Hua, L. Meng, X. Xu, D. Wang, and X. You, "Novel scheme for joint estimation of SNR, Doppler, and carrier frequency offset in double-selective wireless channels," *IEEE Transactions on Vehicular Technology*, vol. 58, pp. 1204–1217, March 2009.
- [147] J. Hua, L. Meng, G. Li, D. Wang, B. Sheng, and X. You, "Joint estimation of channel parameters for very low signal-to-noise ratio environment in mobile radio propagations," *Radio Science*, vol. 45, August 2010.
- [148] A. Dogandzic and B. Zhang, "Estimating Jakes' Doppler power spectrum parameters using the whittle approximation," *IEEE Transactions on Signal Processing*, vol. 53, pp. 987–1005, March 2005.
- [149] T. Abe and T. Matsumoto, "Space-time turbo equalization in frequency-selective MIMO channels," *IEEE Transactions on Vehicular Technology*, vol. 52, pp. 469–475, May 2003.
- [150] W. M. Gifford, M. Z. Win, and M. Chiani, "Diversity with practical channel estimation," *IEEE Transactions on Wireless Communications*, vol. 4, pp. 1935–1947, July 2005.
- [151] Q. Ma and C. Tepedelenlioglu, "Antenna selection for space-time coded systems with imperfect channel estimation," *IEEE Transactions on Wireless Communications*, vol. 6, pp. 710–719, February 2007.

- [152] A. B. Narasimhamurthy and C. Tepedelenlioglu, "Antenna selection for MIMO-OFDM systems with channel estimation error," *IEEE Transactions on Wireless Communications*, vol. 58, pp. 2269–2278, June 2009.
- [153] V. Kristem, N. B. Mehta, and A. F. Molisch, "A novel, balanced, and energy-efficient training method for receive antenna selection," *IEEE Transactions on Wireless Communications*, vol. 9, pp. 2742–2752, September 2010.
- [154] S. Kashyap and N. B. Mehta, "Joint antenna selection and frequency-domain scheduling in OFDMA systems with imperfect estimates from dual pilot training scheme," *IEEE Transactions on Wireless Communications*, vol. 12, pp. 3473–3483, July 2013.
- [155] R. Ertel and J. Reed, "Generation of two equal power correlated Rayleigh fading envelopes," *IEEE Communications Letters*, vol. 2, pp. 276–278, October 1998.
- [156] N. Beaulieu, "Generation of correlated Rayleigh fading envelopes," *IEEE Communications Letters*, vol. 3, pp. 172–172, June 1999.
- [157] T. Gucluoglu and E. Panayirci, "Performance of transmit and receive antenna selection in the presence of channel estimation errors," *IEEE Signal Communications Letters*, vol. 12, pp. 371–373, May 2008.
- [158] C. Kotchasarn, "Cooperative diversity for synchronous uplink DS-CDMA transmission over Rayleigh frequency flat fading channel," in *Proceedings of 2009 IEEE Student Conference on Research and Development (SCoReD 2009)*, pp. 53–56, November 2009.
- [159] W. Fang, L.-L. Yang, and L. Hanzo, "Single-user performance of uplink DS-CDMA using relay-assisted diversity," in *Proceedings of 17th IEEE International Symposium on Personal, Indoor and Mobile Radio Communications (PIMRC'06)*, pp. 1–5, September 2006.
- [160] Y. Fan, C. Wang, J. Thompson, and H. V. Poor, "Recovering multiplexing loss through successive relaying using repetition coding," *IEEE Transactions on Wireless Communications*, vol. 6, pp. 4484–4493, December 2007.
- [161] J. N. Laneman, D. N. C. Tse, and G. W. Wornell, "Cooperative diversity in wireless networks: efficient protocols and outage behavior," *IEEE Transactions on Information Theory*, vol. 50, pp. 3062–3080, December 2004.
- [162] P. Zhang, J. Yuan, J. Chen, and J. Yang, "Analyzing amplify-and-forward and decode-and-forward cooperative strategies in Wyner's channel model," in *IEEE Proceedings of 2009 Wireless Communications and Networking Conference*, pp. 1–5, April 2009.
- [163] R. H. Clarke, "A statistical theory of mobile radio reception," *Bell Labs Technical Journal*, vol. 47, pp. 957–1000, 1968.

[164] Z. Pi and F. Khan, "An introduction to millimeter-wave mobile broadband systems," *IEEE Communications Magazine*, vol. 49, pp. 101–107, June 2011.

[165] T. Kamalakis, I. Neokosmidis, A. Tsipouras, S. Pantazis, and I. Andrikopoulos, "Hybrid free space optical/millimeter wave outdoor links for broadband wireless access networks," in *Proceedings of IEEE International Symposium on Personal, Indoor and Mobile Radio Communications (PIMRC'07)*, pp. 1–5, September 2007.

[166] C. Xu, S. X. Ng, and L. Hanzo, "Near-capacity irregular convolutional coded cooperative differential linear dispersive codes using multiple-symbol differential detection," *IEEE Signal Processing Letters*, vol. 18, pp. 173–176, March 2011.

[167] J. Kennedy and R. Eberhart, "Particle swarm optimization," in *Proceedings of IEEE International Conference on Neural Networks*, pp. 1942–1948, November 1995.

[168] M. Sinaie, M. S. Tohidi, and P. Azmi, "Particle swarm optimization for energy efficient antenna selection in MIMO broadcasting channel," in *Proceedings of 21st IEEE Iranian Conference on Electrical Engineering (ICEE)*, pp. 1–4, May 2013.

[169] J. Dai and M. Chen, "Improved particle swarm optimization - based antenna selection scheme for correlated MIMO channels," in *Proceedings of 12th IEEE International Conference on Communication Technology (ICCT)*, pp. 512–515, November 2010.

[170] Y. Jing and H. Jafarkhani, "Single and multiple relay selection schemes and their achievable diversity orders," *IEEE Transactions on Wireless Communications*, vol. 8, pp. 1414–1423, March 2009.

[171] D. S. Michalopoulos, H. A. Suraweera, G. K. Karagiannidis, and R. Schober, "Amplify-and-forward relay selection with outdated channel estimates," *IEEE Transactions on Communications*, vol. 60, pp. 1278–1290, May 2012.

[172] Y. Luo and J. Zhang, "Relay selection for energy harvesting cooperative communication systems," in *Proceedings of 2013 IEEE Global Communications Conference (GLOBECOM-2013)*, pp. 2514–2519, IEEE, December 2013.

[173] Y. Li, Q. Yin, W. Xu, and H. Wang, "On the design of relay selection strategies in regenerative cooperative networks with outdated CSI," *IEEE Transactions on Wireless Communications*, vol. 10, pp. 3086–3097, September 2011.

[174] I. Krikidis, T. Charalambous, and J. S. Thompson, "Buffer-aided relay selection for cooperative diversity systems without delay constraints," *IEEE Transactions on Wireless Communications*, vol. 11, pp. 1957–1967, May 2012.

[175] R. Madan, N. B. Mehta, A. F. Molisch, and J. Zhang, “Energy-efficient cooperative relaying over fading channels with simple relay selection,” *IEEE Transactions on Wireless Communications*, vol. 7, pp. 3013–3025, August 2008.

[176] A. Ikhlef, D. S. Michalopoulos, and R. Schober, “Max-max relay selection for relays with buffers,” *IEEE Transactions on Wireless Communications*, vol. 11, pp. 1124–1135, March 2012.

[177] J. Wells, “Faster than fiber: The future of multi-G/s wireless,” *IEEE Microwave Magazine*, vol. 10, pp. 104–112, May 2009.

[178] S. Ohmori, Y. Yamao, and N. Nakajima, “The future generations of mobile communications based on broadband access technologies,” *IEEE Communications Magazine*, vol. 38, pp. 134–142, December 2000.

[179] L. Hanzo, H. Haas, S. Imer, D. O’Brien, M. Rupp, and L. Gyongyosi, “Wireless myths, realities, and futures: From 3G/4G to optical and quantum wireless,” *Proceedings of the IEEE*, vol. 100, pp. 1853–1888, May 2012.

[180] F. Khan and Z. Pi, “mmWave mobile broadband (MMB): Unleashing the 3300GHz spectrum,” in *Proceedings of 2013 IEEE Sarnoff Symposium 2011*, pp. 1–6, May 2011.

[181] Z. Pi and F. Khan, “System design and network architecture for a millimeter-wave mobile broadband (MMB) system,” in *Proceedings of 2013 IEEE Sarnoff Symposium 2011*, pp. 1–6, May 2011.

[182] D. Dardari and V. Tralli, “High-speed indoor wireless communications at 60 GHz with coded OFDM,” *IEEE Transactions on Communications*, vol. 47, pp. 1709–1721, November 1999.

[183] H. Meinel, A. Plattner, and G. Reinhold, “A 40 GHz railway communication system,” *IEEE Journal On Select Areas in Communications*, vol. 1, pp. 615–622, September 1983.

[184] S. L. Cotton, W. G. Scanlon, and B. K. Madahar, “Millimeter-wave soldier-to-soldier communications for covert battlefield operations,” *IEEE Communications Magazine*, vol. 47, pp. 72–81, October 2009.

[185] J. Hoydis, S. Brink, and M. Debbah, “Massive MIMO: How many antennas do we need?,” in *Proceedings of 49th IEEE Annual Allerton Conference on Communication, Control, and Computing*, pp. 545–550, September 2011.

Subject Index

Symbols

1G	232
2G	232
3G	232
4G	232
5G	232

A

ACO.....	15
AEs.....	1
AF.....	18
AS.....	11
ASCs.....	14
AWGN	43

B

BBSB.....	89
BBSB-SCE.....	12
BBSBCE.....	12
BCE	8
BCH.....	36
BER	2
BLAST	6
BLER.....	14
BPB	25
BPSK.....	20
BS	3

C

CBAS	15
CDD.....	16

CE.....	8
CIR.....	7
COAS	14
CRLB	95
CSI	4
CSTSK.....	11, 41

D

D-BLAST.....	6
DD-LSCE.....	19
DDCE	19
DDSBCE	172
DF	18
DLDC	4
DN	18
DPSK.....	18
DS-CDMA.....	11
DSTM	17
DSTSK.....	17, 183

E

EDAS	14
EGC	3
EXIT	24

F

FEC	2
FH.....	2
FIM	97

I

IAS	4
-----------	---

ICI	4	PO	22		
IMT-2000	232	PSAM	8		
ISSA	15	PSEP	46		
IVI	199	PSK	20		
J					
JTRAS	12	PSO	11		
L					
LDCs	4	Q			
LLRs	31	QoS	1		
LS	8	QPSK	20		
LS-MIMO	132	R			
LSCE	9	RAs	15		
M					
MAI	20	RF	11		
MCEE	70	RLS	108		
MIMO	1	RNs	18		
ML	4	RSC	19		
ML-MSDD	18	RWBS	11		
MMB	232	Rx	24		
MMBCS	21	RxAS	12		
MMSE	6	S			
MRC	3	SBCE	8		
MSDD	17	SC	3		
MSDSD	18	SD	18		
MSE	96	SDM	6		
MUSRC	17	SDMA	7		
N					
NBAS	15	SIMO	3		
NBJTRAS	20	SISO-MSDSD	18		
O					
OF	46	SM	4		
OFDM	8	SN	18		
OFDMA	139	SNR	3		
P					
PED	190	SSK	4		
PEP	16	STBC	3		
T					
TAs	15	STC	3		
TB-LSCE	101	STSK	4		
STTCs	3	SwC	3		

TBCE.....	8
TTCE.....	139
TVCE	125
Tx.....	24
TxAS	12

U

URC.....	19
----------	----

V

V-BLAST	6
VAA.....	18

Z

ZF.....	6
---------	---

Author Index

A

Aazhang, B. [109] 18, 185
Aazhang, B. [110] 18, 185
Abdallah, S. [62] 12
Abdi, A. [143] 96
Abe, T. [149] 127
Abe, T. [132] 87
Abe, T. [133] 87
Abuthinien, M. [52] 10–12, 67, 77
Aghvami, H. [117] 19, 185, 200
Ahn, C.W. [3] 1, 4, 5
Ahn, C.W. [17] 4
Akhtman, J. [55] 10–12, 67, 77, 87, 89, 90
Akhtman, Y. [108] 17, 186, 189
Al-Dhahir, N. [35] 8, 9, 67
Al-Hussaibi, W.A. [74] 13, 14, 138
Alamouti, S. [4] 1, 3, 5, 19
Alamri, O.R. [1] 1, 2, 11, 15, 31, 33, 34, 59,
64, 89, 99, 112, 116, 125, 133, 134,
146, 202, 204, 213
Alamri, O. [6] 1–3, 6, 7, 18, 35
Ali, F.H. [74] 13, 14, 138
Alouini, M.-S. [96] 17, 18, 186
Alouini, M.S. [12] 3
An, H.J. [112] 18, 185
Azar, Y. [65] 11, 133

B

Batalama, S. [116] 18, 185
Beaulieu, N. [156] 151
Benjebbour, A. [26] 6

Bernard Sklar, [9] 2, 3, 36
Berthold Thoma, [106] 17
Betz, S.M. [54] 10, 11, 67, 77
Betz, S.M. [134] 87
Bhad, S.D. [71] 13, 14, 138, 139
Bialkowski, M.E. [47] 10, 16, 67, 184
Biguesh, M. [33] 8, 67
Biguesh, M. [144] 101
Bjornson, E. [34] 8, 67
Blogh, J. [29] 7
Blostein, S.D. [42] 9
Blum, R.S. [84] 15
Blum, R.S. [73] 13, 14, 138
Brennan, D.G. [22] 5, 13
Buckley, K.M. [30] 7
Buzzi, S. [51] 10, 12, 67, 77
Byun, Y.S. [82] 15

C

Caire, G. [27] 6, 18, 26
Calderbank, A.R. [14] 3, 5
Carcalho, E. [49] 10, 67, 77
Cavers, J.K. [37] 8, 9
Ceron, A. [19] 4, 5
Chakravarti, J.M. [89] 15
Chen, S. [31] 8, 10–12, 19, 67, 77, 88
Chen, J. [162] 185
Chen, S. [60] 12
Chen, S. [32] 8–12, 67, 77
Chen, S. [58] 10, 11, 67, 77, 87, 89, 90
Chen, S. [59] 10, 11, 67, 77, 87, 89, 90

Chen, S. [105] 16, 18, 184, 185
Chen, S. [103] 17
Chen, S. [90] 15
Chen, S. [102] 17
Chen, S. [52] 10–12, 67, 77
Chen, S. [53] 10–12, 67, 77
Chen, S. [21] . 4, 5, 19, 24, 42, 43, 46, 58, 59
Chen, S. [24] 5, 89
Chen, S. [5]1, 3–5, 19, 24, 42–47, 49, 58, 88,
109, 187, 200, 205, 206

Chen, S. [121] 32
Chen, S. [119] 31
Chen, S. [61] 12
Chiani, M. [150] 139
Chiurtu, N. [8] 1
Chung, W.H. [79] 14, 136, 139
Clarke, R.H. [163] 188, 189
Compton, R.T. [28] 7
Coupechoux, M. [76] 13
Cozzo, C. [126] 67, 77

D

Damen, M.O. [27] 6, 18, 26
Dey, I. [32] 8–12, 67, 77
Divsalar, D. [91] 17, 184
Divsalar, D. [93] 17, 186
Dogandzic, A. [148] 125
Dohler, M. [117] 19, 185, 200
Duman, T.M. [86] 15, 16, 135, 138, 139
Duman, T.M. [88] 15, 16
Durrani, S. [42] 9

E

Edfords, O. [63] 11, 133
El-Hajjar, M. [1] . 1, 2, 11, 15, 31, 33, 34, 59,
64, 89, 99, 112, 116, 125, 133, 134,
146, 202, 204, 213
El-Hajjar, M. [6] 1–3, 6, 7, 18, 35
Erkip, E. [109] 18, 185
Erkip, E. [110] 18, 185

Ertel, R. [155] 151

F

Fan, P. [95] 17, 186
Fan, Y. [111] 18, 185
Fan, Y. [160] 185, 186
Fang, W. [159] 185
Ferrar, S. [137] 87
Fleury, B.H. [129] 68, 87, 108
Foschini, G.J. [25] 6
Foschini, G.J. [2] 1, 6, 24
Fragouli, C. [35] 8, 9, 67
Fung, D. [92] 17, 186, 188
Fung, V. [106] 17

G

G-Alkhansari, M. [70] . 13–15, 135, 138, 139
Gamal, H.E. [27] 6, 18, 26
Ganesan, G. [44] 10, 12
Gao, C. [107] 17, 186
Gershman, A.B. [45] 10, 16, 184
Gershman, A.B. [70] . 13–15, 135, 138, 139
Gershman, A.B. [33] 8, 67
Gershman, A.B. [144] 101
Gershman, Alex B. [48] 10, 67, 77
Ghatol, A.A. [71] 13, 14, 138, 139
Ghrayeb, A. [18] 4, 44
Ghrayeb, A. [20] 4
Ghrayeb, A. [19] 4, 5
Giannakis, G.B. [38] 8, 9
Giannakis, Georgios B. [48] 10, 67, 77
Gifford, W.M. [150] 139
Giridhar, K. [103] 17
Gkelias, A. [117] 19, 185, 200
Gligorević, S. [123] 33
Golden, G.D. [2] 1, 6, 24
Goldsmith, A. [7] 1
Gorokhov, A. [69] 13
Grant, P.M. [105] 16, 18, 184, 185
Gucluoglu, T. [157] 161

Gucluoglu, T. [86] 15, 16, 135, 138, 139
Gucluoglu, T. [88] 15, 16
Guo, Z. [120] 32
Gutierrez, F. [65] 11, 133

H

Haas, H. [105] 16, 18, 184, 185
Haas, H. [3] 1, 4, 5
Haas, H. [20] 4
Haimovich, A.M. [107] 17, 186
Hanzo, L. [6] 1–3, 6, 7, 18, 35
Hanzo, L. [104] 16, 18, 184, 185
Hanzo, L. [60] 12
Hanzo, L. [29] 7
Hanzo, L. [159] 185
Hanzo, L. [11] 2, 197, 202
Hanzo, L. [31] 8, 10–12, 19, 67, 77, 88
Hanzo, L. [55] 10–12, 67, 77, 87, 89, 90
Hanzo, L. [58] 10, 11, 67, 77, 87, 89, 90
Hanzo, L. [59] 10, 11, 67, 77, 87, 89, 90
Hanzo, L. [113] 18, 185
Hanzo, L. [139] 96
Hanzo, L. [105] 16, 18, 184, 185
Hanzo, L. [124] 46, 187, 205
Hanzo, L. [103] 17
Hanzo, L. [108] 17, 186, 189
Hanzo, L. [166] 203
Hanzo, L. [101] 17, 18
Hanzo, L. [90] 15
Hanzo, L. [102] 17
Hanzo, L. [1] 1, 2, 11, 15, 31, 33, 34, 59,
64, 89, 99, 112, 116, 125, 133, 134,
146, 202, 204, 213
Hanzo, L. [52] 10–12, 67, 77
Hanzo, L. [53] 10–12, 67, 77
Hanzo, L. [41] 9
Hanzo, L. [20] 4
Hanzo, L. [21] 4, 5, 19, 24, 42, 43, 46, 58, 59
Hanzo, L. [23] 5

Hanzo, L. [24] 5, 89
Hanzo, L. [5] 1, 3–5, 19, 24, 42–47, 49, 58,
88, 109, 187, 200, 205, 206
Hanzo, L. [78] 14, 136, 139
Hanzo, L. [121] 32
Hanzo, L. [119] 31
Hanzo, L. [122] 32
Hanzo, L. [61] 12
Hari, K.S. [78] 14, 136, 139
Hari, K. [103] 17
Haselmayr, W. [131] 68, 87
Hass, H. [17] 4
Hassibi, B. [16] 4
Hassibi, B. [15] 4
Haykin, S. [136] 87, 109, 113, 117
Heath, R.W. [125] 46
Heath, R.W. [77] 14
Heath, R.W. [46] 10, 16, 184
Hiwale, A.S. [71] 13, 14, 138, 139
Ho, P. [92] 17, 186, 188
Hockwald, B.M. [16] 4
Hockwald, B.M. [15] 4
Hoehler, P.A. [123] 33
Hu, B. [129] 68, 87, 108
Hua, J. [146] 125
Hua, J. [147] 125
Huang, K.C. [66] 11, 133
Huang, K.C. [64] 11, 133
Huang, Y.F. [43] 10, 16, 184
Hughes, B.L. [126] 67, 77
Hui, H. [47] 10, 16, 67, 184
Hung, C.Y. [79] 14, 136, 139
Hviid, A. [129] 68, 87, 108

I

I.Andrikopoulos, [165] 200
Issariyakul, T. [114] 18, 185

J

Jafar, S. [7] 1

Jagannatham, A.K. [36] 8, 10, 67, 77
Jeganathan, J. [18] 4, 44
Jeganathan, J. [19] 4, 5
Jiang, M. [55] 10–12, 67, 77, 87, 89, 90
Jiang, M. [108] 17, 186, 189
Jindal, N. [7] 1
Juntti, M. [57] 10, 11, 67, 77, 87, 89, 90

K

Kü, V. [140] 96
Kadir, M.I. [103] 17
Kadir, M.I. [24] 5, 89
Kamalakis, T. [165] 200
Kashyap, S. [154] 139
Kay, S.M. [138] 95–97
Kennedy, R.A. [42] 9
Khan, F. [67] 11, 133
Khan, F. [164] 200
Kim, H.S. [82] 15
Kim, S. [80] 14, 136
Kocian, A. [129] 68, 87, 108
Kotchasarn, C. [158] 185
Krishnamurthy, V. [114] 18, 185
Kristem, V. [153] 139
Kuan, E.-L. [11] 2, 197, 202
Kucur, O. [87] 15, 16, 135, 138, 139

L

Lambotharan, S. [135] 87
Lampe, L. [97] 17, 186
Lampe, L. [100] 17, 18
Lampe, L. [99] 17, 18, 185, 203
Lampe, L. [98] 17, 18, 184, 187, 190, 207, 214
Land, I. [123] 33
Laneman, J.N. [161] 185
Lao, D. [107] 17, 186
Larsson, E.G. [63] 11, 133
Lau, B.K. [63] 11, 133
Lee, C. [80] 14, 136
Lee, D.C. [85] 15
Lee, S. [116] 18, 185
Li, G. [147] 125
Li, H. [54] 10, 11, 67, 77
Li, H. [134] 87
Li, Y. [40] 8, 9
Liang, Y.-C. [141] 96
Liang, Y.-C. [142] 96
Lin, Z. [75] 13
Liu, D. [72] 13, 14, 138, 139
Liu, R.W. [43] 10, 16, 184
Liu, X. [47] 10, 16, 67, 184
Loncar, M. [132] 87
Loncar, M. [133] 87
Lops, M. [51] 10, 12, 67, 77
Lu, S. [47] 10, 16, 67, 184
Luschi, C. [127] 68, 87, 108

M

M.ehrpouyan, H. [42] 9
Mü, R.R. [56] 10, 11, 67, 77, 87, 89, 90
Ma, X. [38] 8, 9
Ma, Q. [151] 139, 161
Mackenthun, K. [94] 17
Manton, J.H. [45] 10, 16, 184
Marzetta, T.L. [39] 8, 9
Marzetta, T.L. [63] 11, 133
Matsumoto, T. [149] 127
Matyjas, J.D. [116] 18, 185
Mayzus, R. [65] 11, 133
Mecklenbrauker, C.F. [133] 87
Medles, A. [50] 10, 12, 67, 77
Mehta, N.B. [153] 139
Mehta, N.B. [154] 139
Meng, L. [146] 125
Meng, L. [147] 125
Mesleh, R.Y. [17] 4
Mesleh, R. [3] 1, 4, 5
Molisch, A.F. [153] 139

Mu, X. [58] 10, 11, 67, 77, 87, 89, 90
Mu, X. [59] 10, 11, 67, 77, 87, 89, 90
Mu, X. [139] 96
Muller, R. [132] 87
Muller, R. [133] 87
Murata, H. [26] 6
Murthy, C.R. [76] 13
Murthy, C.R. [36] 8, 10, 67, 77

N

Naeem, M. [85] 15
Nallanathan, A. [141] 96
Nallanathan, A. [142] 96
Nandi, A.K. [130] 68, 87, 106
Narasimhamurthy, A.B. [152] 139, 161
Nasir, A.A. [42] 9
Neokosmidis, I. [165] 200
Ng, S.X. [113] 18, 185
Ng, S.X. [124] 46, 187, 205
Ng, S.X. [166] 203
Ng, S.X. [101] 17, 18
Ng, S.X. [23] 5
Ng, S.X. [119] 31
Ng, S.X. [122] 32
Nicoli, M. [137] 87
Nilsson, P. [120] 32
Norsatinia, A. [68] 12, 14, 15, 133, 135, 136, 138, 139
Norsatinia, A. [81] 15, 16

O

Ohno, S. [38] 8, 9
Ottersten, B. [34] 8, 67

P

Palally, H.R. [53] 10–12, 67, 77
Panayirci, E. [157] 161
Pantazis, S. [165] 200
Pauli, V. [100] 17, 18
Pauli, V. [99] 17, 18, 185, 203
Pauli, V. [98] 17, 18, 184, 187, 190, 207, 214
Paulraj, A.J. [125] 46
Paulraj, A. [77] 14
Persson, D. [63] 11, 133
Pham, T.-H. [141] 96
Pham, T.-H. [142] 96
Pi, Z. [164] 200
Pi, Z. [67] 11, 133
Piton, R. [129] 68, 87, 108
Poor, H.V. [54] 10, 11, 67, 77
Poor, H.V. [111] 18, 185
Poor, H.V. [134] 87
Poor, H.V. [160] 185, 186
Powers, E.J. [46] 10, 16, 184
Psaromiligkos, N. [62] 12
Pursley, M.B. [10] 2

Q

Qaisrani, M. [135] 87

R

Rajashekhar, R. [78] 14, 136, 139
Rao, B.D. [36] 8, 10, 67, 77
Rappaport, T.S. [106] 17
Rappaport, T.S. [65] 11, 133
Rasmussen, L.K. [129] 68, 87, 108
Reed, J. [155] 151
Renzo, M.D. [20] 4
Rimoldi, B. [8] 1
Rossi, P.S. [56] 10, 11, 67, 77, 87, 89, 90
Rusek, F. [63] 11, 133

S

Samimi, M. [65] 11, 133
Sanayeи, S. [81] 15, 16
Sanayeи, S. [68] 12, 14, 15, 133, 135, 136, 138, 139
Sandell, M. [127] 68, 87, 108
Sandhu, S. [77] 14
Sardellitti, S. [51] 10, 12, 67, 77

Schellander, D. [131] 68, 87
Scherb, A. [140] 96
Schober, R. [97] 17, 186
Schober, R. [99] 17, 18, 185, 203
Schober, R. [98] 17, 18, 184, 187, 190, 207, 214
Schulz, J.K. [65] 11, 133
Sellathurai, M. [136] 87, 109, 113, 117
Sendonaris, A. [109] 18, 185
Sendonaris, A. [110] 18, 185
Seshadri, N. [14] 3, 5
Sfar, S. [84] 15
Sfar, S. [73] 13, 14, 138
Shahbazpanahi, S. [45] 10, 16, 184
Shahram Shahbazpanahi, [48] 10, 67, 77
Sheng, B. [147] 125
Shin, C. [46] 10, 16, 184
Shin, M. [80] 14, 136
Simon, M.K. [12] 3
Simon, M.K. [96] 17, 18, 186
Simon, M.K. [91] 17, 184
Simon, M. [93] 17, 186
Sinanovic, S. [17] 4
Singer, A.C. [128] 68, 87, 108
Skinner, J.S. [10] 2
Slock, D.T.M. [49] 10, 67, 77
Slock, D.T.M. [50] 10, 12, 67, 77
So, D.K.C. [72] 13, 14, 138, 139
Song, H.K. [112] 18, 185
Song, S. [128] 68, 87, 108
Soon, V.C. [43] 10, 16, 184
Spagnolini, U. [137] 87
Springer, A. [131] 68, 87
Stephen, R.G. [76] 13
Stoica, P. [44] 10, 12
Strauch, P. [127] 68, 87, 108
Su, W. [116] 18, 185
Sugiura, S. [41] 9
Sugiura, S. [31] 8, 10–12, 19, 67, 77, 88
Sugiura, S. [32] 8–12, 67, 77
Sugiura, S. [113] 18, 185
Sugiura, S. [105] 16, 18, 184, 185
Sugiura, S. [124] 46, 187, 205
Sugiura, S. [20] 4
Sugiura, S. [21] 4, 5, 19, 24, 42, 43, 46, 58, 59
Sugiura, S. [23] 5
Sugiura, S. [24] 5, 89
Sugiura, S. [5] 1, 3–5, 19, 24, 42–47, 49, 58, 88, 109, 187, 200, 205, 206
Sugiura, S. [122] 32
Sun, S. [65] 11, 133
Sung, K. [128] 68, 87, 108
Szczecinski, L. [18] 4, 44
Szczecinski, L. [19] 4, 5

T

Tang, L. [43] 10, 16, 184
Tarokh, V. [14] 3, 5
Telatar, E. [8] 1
Tepedelenlioglu, C. [151] 139, 161
Tepedelenlioglu, C. [152] 139, 161
Ternon, E. [113] 18, 185
Thompson, J.S. [111] 18, 185
Thompson, J. [160] 185, 186
Tian, J. [115] 18, 185
Trivedi, Y.N. [89] 15
Tse, D.N.C. [161] 185
Tse, D. [118] 26
Tsiopoulos, A. [165] 200
Tufvesson, F. [63] 11, 133
Turin, W. [35] 8, 9, 67

V

Valenti, M.C. [145] 111
Valenzuela, R.A. [2] 1, 6, 24
Veen, B.D.V. [30] 7
Vishwanath, S. [7] 1
Viswanath, P. [118] 26

W

Wang, J. [119] 31
Wang, L. [104] 16, 18, 184, 185
Wang, L. [121] 32
Wang, S. [143] 96
Wang, C. [111] 18, 185
Wang, C. [160] 185, 186
Wang, D. [146] 125
Wang, D. [147] 125
Wang, K. [65] 11, 133
Wang, L. [108] 17, 186, 189
Wang, L. [101] 17, 18
Wang, M.Z. [83] 15
Wang, Z. [66] 11, 133
Wang, Z. [64] 11, 133
Ward, J. [28] 7
Wehinger, J. [132] 87
Wehinger, J. [133] 87
Wei, Y.R. [83] 15
Win, M.Z. [150] 139
Windpassinger, C. [98] 17, 18, 184, 187, 190, 207, 214
Wittneben, A. [13] 3, 5
Woerner, B.D. [145] 111
Wolfgang, A. [119] 31
Wolniansky, P.W. [2] 1, 6, 24
Wong, G.N. [65] 11, 133
Wornell, G.W. [161] 185
Wu, Y. [130] 68, 87, 106
Wu, N. [1] 1, 2, 11, 15, 31, 33, 34, 59, 64, 89, 99, 112, 116, 125, 133, 134, 146, 202, 204, 213

X

Xu, C. [113] 18, 185
Xu, C. [101] 17, 18
Xu, C. [122] 32
Xu, C. [124] 46, 187, 205
Xu, C. [166] 203

Xu, C. [23] 5
Xu, L. [121] 32
Xu, X. [146] 125
Xu, Z. [84] 15
Xu, Z. [73] 13, 14, 138

Y

Yan, R. [127] 68, 87, 108
Yang, J. [162] 185
Yang, L.-L. [159] 185
Yang, L.-L. [11] 2, 197, 202
Yang, L.-L. [119] 31
Yang, L. [75] 13
Yao, W. [53] 10–12, 67, 77
Yen, K. [11] 2, 197, 202
Yilmaz, A. [87] 15, 16, 135, 138, 139
Ylioinas, J. [57] 10, 11, 67, 77, 87, 89, 90
Yoshida, S. [26] 6
You, X. [146] 125
You, X. [147] 125
Yu, F. [115] 18, 185
Yuan, J. [162] 185
Yun, S. [3] 1, 4, 5
Yun, S. [17] 4

Z

Zhang, P. [60] 12
Zhang, P. [61] 12
Zhang, B. [148] 125
Zhang, J. [58] 10, 11, 67, 77, 87, 89, 90
Zhang, J. [59] 10, 11, 67, 77, 87, 89, 90
Zhang, J. [139] 96
Zhang, P. [162] 185
Zhang, P. [32] 8–12, 67, 77
Zhang, P. [90] 15
Zhang, P. [102] 17
Zhang, Q. [115] 18, 185
Zhao, H. [65] 11, 133
Zhu, X. [130] 68, 87, 106